

Acta Geodaetica, Geophysica et Montanistica Hungarica

VOLUME 21, NUMBERS 1-2, 1986

EDITOR-IN-CHIEF

A TÁRCZY-HORNOCH

F MARTOS

ASSOCIATE EDITOR

J SOMOGYI

EDITOR

J VERŐ

EDITORIAL BOARD

**A ÁDÁM, GY BARTA, P BIRÓ, S DOLESCHALL,
L KAPOLYI, F KOVÁCS, A MESKÓ, F STEINER,
J ZÁMBÓ**



Akadémiai Kiadó, Budapest

AGGM 21 (1-2) 1-240 (1986) HU ISSN 0236-5758

ACTA GEODAETICA, GEOPHYSICA et MONTANISTICA HUNGARICA

A Quarterly Journal of the Hungarian Academy of Sciences

Acta Geodaetica, Geophysica et Montanistica (AGGM) publishes original reports on geodesy, geophysics and minings in English.

AGGM is published in yearly volumes of four numbers by

AKADÉMIAI KIADÓ

Publishing House of the Hungarian Academy of Sciences
H-1054 Budapest, Alkotmány u. 21.

Manuscripts and editorial correspondence should be addressed to

AGGM Editorial Office
H-9401 Sopron P.O. Box 5

Subscription information

Orders should be addressed to

KULTURA Foreign Trading Company
H-1389 Budapest P.O. Box 149

INSTRUCTIONS TO AUTHORS

Manuscripts should be sent to the editors (MTA Geodéziai és Geofizikai Kutató Intézet, AGGM Editorial Office, H-9401 Sopron, P.O.Box 5, HUNGARY). Only articles not submitted for publication elsewhere are accepted.

Manuscripts should be typewritten in duplicate, double-spaced, 25 lines with 50 letters each. The papers generally include the following components, which should be presented in the order listed.

1. Title, name of author(s), affiliation, dateline, abstract, keywords
2. Text, acknowledgements
3. References
4. Footnotes
5. Legends
6. Tables and illustrations

1. The *affiliation* should be as concise as possible and should include the complete mailing address of the authors. The *date of receipt* of the manuscript will be supplied by the editors. The abstract should not exceed 250 words and should clearly and simply summarize the most important methods and results. 5–10 significant expressions describing the content are used as *keywords*. Authors may recommend these keywords.

2. The *text* should be generally in English and as short and clear as possible. From Hungarian authors papers are also accepted in Hungarian.

The section heading should *not* be underlined or in capitals.

Please note that underlining denotes special types:

- single underlining: italics
- double underlining: bold-face roman

**ACTA GEODAETICA,
GEOPHYSICA et MONTANISTICA
HUNGARICA**

A Quarterly Journal of the Hungarian Academy of Sciences

EDITOR-IN-CHIEF

F Martos

ASSOCIATE EDITOR

J Somogyi

EDITOR

J Verő

EDITORIAL BOARD

A Ádám, Gy Barta, P Biró, S Doleschall, L Kapolyi
F Kovács, A Meskó, F Steiner, J Zámbo

VOLUME 21



Akadémiai Kiadó, Budapest
1986

CONTENTS

Application of statistical methods in the interpretation of the study of surface movements — <i>Detrekői Á</i>	3
New results in Earth tides research — <i>Bartha G</i> and <i>Varga P</i>	13
An intelligent digital data acquisition system for recording the tidal signal — <i>Mentes Gy</i>	21
Time variation in geopotential in spherical harmonics — <i>Biró P</i> and <i>Thöng N C</i>	31
Optimum Doppler positioning — <i>Bányai L</i>	41
Laboratory test of capacitive pendulums — <i>Mentes Gy</i>	55
Digital surface model on a triangular base — <i>Kalmár J</i>	71
Effect of surface topography on magnetotelluric measurements (H-polarization) — <i>Tavartkiladze S A</i>	81
Effect of surface topography on magnetotelluric measurements (E-polarization) — <i>Tavartkiladze S A</i>	93
The Dunaharaszti earthquake, January 12, 1956 — <i>Szeidovitz Gy</i>	109
Problem of direct task in nuclear magnetism logging — <i>Szemerédy P</i>	127
Super-high-latitude maximum of Pc2-4 intensity — <i>Plyasova-Bakounina T A</i> , <i>Troitskaya V A</i> , <i>Münch J W</i> , <i>Gauler H F</i>	143
On the possible effect of environmental factors on the occurrence of traffic accidents — <i>Střešitk J</i> and <i>Prigančová A</i>	155
Approximative solution of the direct problem of magnetotellurics for two-layered, three- dimensional structures — <i>Takács E</i> and <i>Turai E</i>	167
Physical modeling of the adjustment distance — <i>Ádám A</i> and <i>Szarka L</i>	177
Three phases of post-storm events in ionospheric absorption — <i>Márcz F</i>	201
Seismic activity in Hungary — <i>Zsiros T</i> and <i>Mónus P</i>	209
Perspectives on electromagnetic deep sounding in ore prognostication — <i>Ádám A</i> , <i>Paarma H</i> and <i>Pospišil L</i>	215
Professor István Hazay — 85years — <i>Biró P</i>	229
 <i>Book reviews</i>	
Erdbeben und Erdbebengefährdung, Hurlig E and Stiller H eds. — <i>Verő J</i>	231
Phosphate Minerals, Nriagu J O and Moore P B eds — <i>Tomschey O</i>	231
Angewandte Geophysik. Band I, Gravimetrie und Magnetik, Millitzer H and Weber F eds — <i>Verő J</i>	232
Bibliographie der in der DDR 1977-1982 zur Geschichte der Geologie, Mineralogie, Geophysik und Paläontologie vorgelegten Arbeiten — <i>Verő J</i>	232
Plateau Uplift. The Rhenish Shield — A Case History, Fuchs K, von Gehlen K, Mälzer H, Murawski H, Semmel A eds — <i>Ádám A</i>	233
Digital Filtering. Applications in Geophysical Exploration for Oil, Meskó A — <i>Verő J</i>	233
Pyroclastic Rocks, Fisher G V and Schmincke H U — <i>Póka T</i>	234

Dynamics of the Middle Atmosphere. Advances in Earth and Planetary Sciences, Holton J R and Matsuno T eds — <i>Bencze P</i>	234
Ásványi nyersanyagok története Magyarországon (History of mineral resources in Hungary), Fülöp J — <i>Verő J</i>	235
Rock Mechanics. Fundamentals of Economic Construction of Underground Excavations, Wittke W — <i>Janositz J</i>	236
Mineral Deposits of the Alps and the Alpine Epoch in Europe, Schneider H J ed. — <i>Kisházi P</i> .	236
Geochemical Aspects of Radioactive Waste Disposal, Brookins D G — <i>Pécsi-Donáth É</i>	237
Quantitative Aspects of Magnetospheric Physics. Geophysics and Astrophysics Monographs, Lyons L R and Williams D J — <i>Verő J</i>	237
Historical Events and People in Geosciences, Schröder W ed. — <i>Verő J</i>	238
Developments and Applications of Geomorphology, Costa JE and Fleischer P Jay eds — <i>Lóczy D</i>	238
Patterns of Change in Earth Evolution, Holland HD and Trendall A F eds — <i>Verő J</i>	239
Das Phänomen des Polarlichts, Schröder W — <i>Verő J</i>	240
Equations of motion of vertically thrown and falling particles for Newton's drag law — <i>Pethő Sz</i>	241
Some questions of the economic evaluation of natural resources — <i>Faller G</i> and <i>Tóth M</i>	259
On the statistical resonance in vibratory screens and conveyors — <i>Pethő Sz</i>	265
Energy of fluid-bearing porous systems — <i>Zoltán Gy</i>	297
Energy value of changes of mass and state in porous reservoirs — <i>Zoltán Gy</i>	315
Rock model based on pore structure — <i>Bauer K</i> and <i>Balla L</i>	345
Flocculation of the Visonta lingite sludges by polyacrylamides — <i>Mrs Lakatos Szabó J</i> and <i>Lakatos I</i>	355
A new method to calculate heat- and vapour absorption of mine air — <i>Janositz J</i>	367
Frequency of endogen mine fires as a function of coal loss and rate of advance — <i>Kovács F</i> ...	389
On the deep electrical conductivity of the central part of Caucasus Minor on base of MTS data — <i>Demidova T A</i>	405
High-pressure elastic wave velocities in Armenian granitoids of different age and origin — <i>Volarovich M P</i> , <i>Yefimova G A</i> , <i>Balasanyan V S</i>	415
High-pressure changes of remanent rock magnetization — <i>Lebedev T S</i> , <i>Savenko B Ya</i>	423
Zonality of the elastic parameter distribution under regional PT conditions in the Earth's crust — <i>Lebedev T S</i> , <i>Korchin V A</i> , <i>Burtny P A</i>	431
Change of acoustic rock properties due to deformation under complex states of stress — <i>Bayuk E I</i> , <i>Dyaur N I</i>	449
<i>Book reviews</i>	
Angewandte Geophysik. Band II. Geoelektrik — Geothermik — Radiometrie — Aerogeophysik, Miltzer H and Weber F eds — <i>Verő J</i>	457
Fundamentals of mining engineering, Zambó J — <i>Martos F</i>	457
Principles of sedimentary basin analysis, Miall A D — <i>Ádám A</i>	459
Introduction to potential theory, Sigl R — <i>Somogyi J</i>	459
Optimization and design of geodetic networks, Grafarend E W and Sanso F eds — <i>Somogyi J</i> .	460
The geometry of geodetic inverse linear mapping and non-linear adjustment, Teunissen P J G — <i>Somogyi J</i>	461
In memoriam Professor Antal Tarczy-Hornoch — <i>Somogyi J</i>	463

AUTHOR INDEX

- Ádám A 177, 215, 233, 459
 Balasanyan V S 415
 Balla L 345
 Bányai L 41
 Bartha G 13
 Bauer K 345
 Bayuk E I 449
 Bencze P 234
 Bíró P 31, 229
 Brookins D G 237
 Burtny P A 431
 Costa J E 238
 Demidova T A 405
 Detrekői Á 3
 Dyaur N I 449
 Fallér G 259
 Fisher G V 234
 Fleisher P Ya 238
 Fuchs K 233
 Fülöp J 235
 Gauler H F 143
 Grafarend E W 460
 Hazay I 229
 Holland H D 239
 Holton J R 234
 Hurtig E 231
 Janositz J 236, 367
 Kalmár J 71
 Kisházi P 236
 Korchin V A 431
 Kovács F 389
 Lakatos I 355
 Lakatos Szabó J 355
 Lebedev T S 423, 431
 Lóczy D 238
 Lyons L R 237
 Mälzer H 233
 Márcz F 201
 Martos F 457
 Matsuno T 234
 Mentés Gy 21, 55
 Meskó A 233
 Miall A D 459
 Millitzer H 232, 457
 Mónus P 209
 Moore P B 231
 Münch J W 143
 Murawski H 233
 Nriagu J O 231
 Paarma H 215
 Pécsi-Donáth É 237
 Pethő Sz 241, 265
 Plyasova-Bakounina T A 143
 Póka T 234
 Pospisil L 215
 Prigancová A 155
 Sanso F 460
 Savenko B Ya 423
 Schmincke H U 234
 Schneider H J 236
 Schröder W 238, 240
 Semmel A 233
 Sigl R 459
 Somogyi J 459, 460, 461, 463
 Stiller H 231
 Šteřtík J 155
 Szarka L 177
 Szeidovitz Gy 109
 Szemerédy P 127
 Takács E 167
 Tavartkiladze S A 81, 93
 Teunissen P J G 461
 Thông N C 31
 Tomschey O 231
 Tóth M 259
 Trendall A F 239
 Troitskaya V A 143
 Turai E 167
 Verő J 231, 232, 233, 235, 237, 238, 239, 240, 457
 Volarovich M P 415
 von Gehlen K 233
 Weber F 232, 457
 Witke W 236
 Yefimova G A 415
 Zambó J 457
 Zoltán Gy 297, 315
 Zsiros T 209

KEYWORD INDEX

- absorption 201, 367
- acceleration 265
- acoustic properties of rocks 449
- adjustment 3
- adjustment distance 177
- advance 389
- amplitude of elastic waves 449
- angle of impact 265
- angle of throo 265
- anionic polymers 355
- anomaly 215
- Armenia 415
- atmospheric electricity 155
- biometeorological typification 155
- boundary value problem 31
- bridging mechanism 355
- Broadcast Ephemeris 41
- capacitive pendulum 21, 55
- capillary pressure 297, 315
- Caucasus Minor 405
- change of state 297
- coagulate 355
- coal loss 389
- coal mines 367, 389
- coloured minerals 415
- compressibility 315
- conductivity 405
- conductivity anomaly 215
- conveyor 265
- co-sedimentation 241
- costs 259
- crapaudine 55
- crust 431
- data acquisition 21
- deep fractures 215
- degree of hydrolysis 355
- dewatering 355
- digital surface model 71
- digital terrain model 71
- Doppler Calibration Campaign 41
- Doppler positioning 41
- drag force 241
- drag law 241
- Dunaharaszti earthquake 109
- earthquake 109, 209
- earthquake intensity 209
- Earth tides 13
- economic evaluation 259
- elastic properties 415, 431
- elastic properties of rocks 431
- elastic waves 449
- electrical conductivity 405
- electric conductivity anomaly 215
- endogen mine fires 389
- energy 297
- environment 155
- E-polarization 93
- equations of motion 241
- expenditure 259
- filtering 21
- finite element interpolation 71
- Finkey's constant 241
- fire hazard 389
- floc 355
- flocculation 355
- fluid-bearing reservoir 297
- fluid index 127
- formation pressure 315
- fractures 215, 449
- free fluid index 127
- frequency response 55
- gas storage 297
- geodynamics 13
- geomagnetic activity 155
- geomagnetic array 143
- geomagnetic disturbances 201
- geomagnetic pulsations 143, 155
- geomagnetism 143
- geopotential 31
- granitoides 415
- gravity field 31
- Graz-Lustbühel observatory 41
- heat absorption 367
- high latitude geomagnetism 143
- historical earthquakes 209
- horizontal pendulum 13
- H-polarization 81
- Hungary 109, 209
- hydrolysis 355
- hydrostatic pressure 423, 449
- impact 265
- impulse response 55
- inhomogeneity 13
- initial velocity 241, 265
- integral equations 81, 93, 167
- intelligent data acquisition 21

interfacial energy 297
interfacial tension 297, 315
interpolation 71
ionospheric absorption 201
kinematic parameters 241
laboratory test 55
lateral inhomogeneity 13
least squares method 3
length of stay 265
lignite sludge 355
lineament 177, 215
linear prediction 21
linearity 55
logging 127
longwalls 389
loss 389
magnetic changes of rocks 423
magnetism 127
magnetization 423
magnetotellurics 81, 93, 167, 177
magnetotelluric sounding 405
mathematical modeling 3, 81, 93, 167
Mecsek coal mines 389
metallogenesis 215
mine air 367
mine fires 389
mineral resources 259
minerals 415
model 71, 167, 345
modeling 3, 81, 93, 167, 177
Newton's drag law 241
nuclear magnetism logging 127
observatory 41
Odra-line 215
optimum production 259
ore 215
ore prospecting 215
particle size 241
Pc 2-4 143
Penc observatory 41
pendulum 13, 21, 55
Periadriatic lineament 177
permeability 345
phase exchange 297
physical modeling 177
polarization 81, 93
polyacrylamide 355
polyelectrolyte 355
polymers 355
pore structure 345
porosity 345
porous reservoir 315
porous system 297
positioning 41
post-storm event 201
pressure 297, 315, 423, 449
production 259
properties of rocks 449
proton precession 127
pulsations 143, 155
rate of advance 389
ratio of co-sedimentation 241
relative acceleration 265
remanent rock magnetization 423
reservoir 297, 315
resonance 265
resources 259
rock fracture 449
rock magnetization 423
rock model 345
rocks 423, 431, 449
Ruhr coal mines 367
saturation 315
screen 265
secular variation 31
sedimentation 241, 355
seismic damages 109
seismicity 109, 209
sensitivity 55
settling 241
settling velocity 241
shield 431
sludge 355
solar wind-control 143
Sopron-Alomhegy observatory 41
sorption 355
sounding 405
specific costs 259
spherical harmonics of geopotential 31
statistical resonance 265
step correction 21
storm 201
surface model 71
surface movement 3, 31
suspension 355
tension 297, 315
terrain model 71
terminal settling velocity 241
3-D models 167
throw 265
tides 13
topographic effect 81, 93
transcontinental lineament 215
triangular coverage 71
typification 155
Ukrainian rocks 423
Ukrainian shield 431
underground gas storage 297
uniaxial pressure 423
unit-step response 55
vapour absorption 355
velocity 241, 265
velocity of elastic waves 449
vertically thrown particles 241
vibratory conveyor 265
vibratory screen 265
waves 449
well logging 127
wettability 297, 315
zonality in the crust 431

CONTENTS

Application of statistical methods in the interpretation of the study of surface movements — <i>Detrekői Á</i>	3
New results in Earth tides research — <i>Bartha G</i> and <i>Varga P</i>	13
An intelligent digital data acquisition system for recording the tidal signal — <i>Mentes Gy</i>	21
Time variation in geopotential in spherical harmonics — <i>Biró P</i> and <i>Thông N C</i>	31
Optimum Doppler positioning — <i>Bányai L</i>	41
Laboratory test of capacitive pendulums — <i>Mentes Gy</i>	55
Digital surface model on a triangular base — <i>Kalmár J</i>	71
Effect of surface topography on magnetotelluric measurements (H-polarization) — <i>Tavartkiladze S A</i>	81
Effect of surface topography on magnetotelluric measurements (E-polarization) — <i>Tavartkiladze S A</i>	93
The Dunaharaszti earthquake, January 12, 1956 — <i>Szeidovitz Gy</i>	109
Problem of direct task in nuclear magnetism logging — <i>Szemerédy P</i>	127
Super-high-latitude maximum of Pc2-4 intensity — <i>Plyasova-Bakounina T A, Troitskaya V A, Münch J W, Gauler H F</i>	143
On the possible effect of environmental factors on the occurrence of traffic accidents — <i>Strěštitk J</i> and <i>Prigancová A</i>	155
Approximative solution of the direct problem of magnetotellurics for two-layered, three-dimensional structures — <i>Takács E</i> and <i>Turai E</i>	167
Physical modeling of the adjustment distance — <i>Ádám A</i> and <i>Szarka L</i>	177
Three phases of post-storm events in ionospheric absorption — <i>Márcz F</i>	201
Seismic activity in Hungary — <i>Zsiros T</i> and <i>Mónus P</i>	209
Perspectives on electromagnetic deep sounding in ore prognostication — <i>Ádám A, Paarma H</i> and <i>Pospišil L</i>	215
Professor István Hazay — 85 years — <i>Biró P</i>	229

Book reviews

Erdbeben und Erdbebengefährdung, <i>Hurtig E</i> and <i>Stiller H</i> eds. — <i>Verő J</i>	231
Phosphate Minerals, <i>Nriagu J O</i> and <i>Moore P B</i> eds — <i>Tomschey O</i>	231
Angewandte Geophysik. Band I, Gravimetrie und Magnetik, <i>Millitzer H</i> and <i>Weber F</i> eds — <i>Verő J</i>	232
Bibliographie der in der DDR 1977-1982 zur Geschichte der Geologie, Mineralogie, Geophysik und Paläontologie vorgelegten Arbeiten — <i>Verő J</i>	232

Plateau Uplift. The Rhenish Shield — A Case History, Fuchs K, von Gehlen K, Mälzer H, Murawski H, Semmel A eds — <i>Ádám A</i>	233
Digital Filtering. Applications in Geophysical Exploration for Oil, Meskó A — <i>Verő J</i>	233
Pyroclastic Rocks, Fisher G V and Schmincke H U — <i>Póka T</i>	234
Dynamics of the Middle Atmosphere. Advances in Earth and Planetary Sciences, Holton J R and Matsuno T eds — <i>Bencze P</i>	234
Ásványi nyersanyagok története Magyarországon (History of mineral resources in Hungary), Fülöp J — <i>Verő J</i>	235
Rock Mechanics. Fundamentals of Economic Construction of Underground Excavations, Wittke W — <i>Janositz J</i>	236
Mineral Deposits of the Alps and the Alpine Epoch in Europe, Schneider H J ed. — <i>Kisházi P</i> .	236
Geochemical Aspects of Radioactive Waste Disposal, Brookins D G — <i>Pécsi-Donáth É</i>	237
Quantitative Aspects of Magnetospheric Physics. Geophysics and Astrophysics Monographs, Lyons L R and Williams D J — <i>Verő J</i>	237
Historical Events and People in Geosciences, Schröder W ed. — <i>Verő J</i>	238
Developments and Applications of Geomorphology, Costa JE and Fleischer P Jay eds — <i>Lóczy D</i>	238
Patterns of Change in Earth Evolution, Holland HD and Trendall A F eds — <i>Verő J</i>	239
Das Phänomen des Polarlichts, Schröder W — <i>Verő J</i>	240

APPLICATION OF STATISTICAL METHODS IN THE INTERPRETATION OF THE STUDY OF SURFACE MOVEMENTS

Á DETREKŐI¹

[Manuscript received January 20, 1984]

Author takes in his paper as starting point the general characteristics of the mathematical models of surface-movement measurements. The usual conditions imposed on the points studied, on the co-ordinate system applied and on the characterization of the stochastic properties of the measurements are shown.

In the next part of the paper the processing of the measured results are discussed, starting with problems of the least square adjustment, followed by the choice of the quantities suitable to characterize the movements. Finally, the interpretation of the results are dealt with in detail. Here at first the special problems of the hypothesis-study for describing the immobility, and then the methods of function definition are discussed.

Keywords: adjustment; least squares method; mathematical modeling; surface movement

The aim of the study of surface movements is always the characterization of the movement of bodies and of the deformations occurring during the movements. Geodetic methods can be very well used to this purpose. In the present paper a short review is given on the methods of mathematical statistics used in the processing of geodetic measurements of movement studies, with special emphasis on surface movements.

Both the movement of bodies and its measurement are complicated physical processes. To describe them in a mathematical form it is inevitable to accept a model which properly reflects the physical, geometrical and stochastic characteristics of movement and measurement. The same movement and measurement can be characterized by different models. The choice of a proper model is the precondition of the successful solution of the problem of a movement study.

When constructing a model of movements it is advisable to deal separately with the physical characteristics of the model and with the mathematical model of geodetic measurements. The two sides of the model are not independent of each other. The definition of the physical characteristics is the task of miners, geophysicists, geologists and civil engineers using the results of movement studies. The model of geodetic measurements is determined by the geodesists.

¹ Institute for Photogrammetry of the Technical University Budapest, Műegyetem rakpart 3, H-1111 Budapest

The process of constructing a model for a surface-movement study can be summarized in the following—of course simplified—form:

The aim of a movement study is to describe the change of a surface defined by the function $F(X, Y, Z)$. The description can be done as a function of time, or of force (or of a quantity proportional to the force). In the first case one speaks about a description with a kinematic aim, in the second case about a description with a kinetic aim. For the sake of simplicity in the followings movement studies with kinetic aims are discussed, since they are usual in case of surface movements. The change on $F(X, Y, Z)$ can be written in this case in the form $F[X(t), Y(t), Z(t)]$.

As first step of the model construction, the surface $F(X, Y, Z)$ is substituted by its selected geometric elements; the movements of the elements are measured and from them the movement of the total surface is concluded. Selected elements can be points or distinkted lines. The surface studied is substituted most frequently—mainly in case of high precision requirements—by its distinkted points (Pelzer 1971). This is the method, e.g. in case of vertical crustal movement networks. At lower precision requirements the studied geometric element can be a level line of given height, too.

This step of model establishment can be regarded as the substitution of the function $F[X(t), Y(t), Z(t)]$ by n functions of the type $X_i(t), Y_i(t), Z_i(t)$ ($i = 1, 2, \dots, n$). This step of model construction is illustrated in Fig. 1.

In the second step of modeling, the functions $X_i(t), Y_i(t), Z_i(t)$ which describe the paths of the different points studied are substituted by the points $X_i(t_j), Y_i(t_j), Z_i(t_j)$ ($j = 1, 2, \dots, s$) assigned to the different measurement epochs. This substitution is illustrated in Fig. 2.

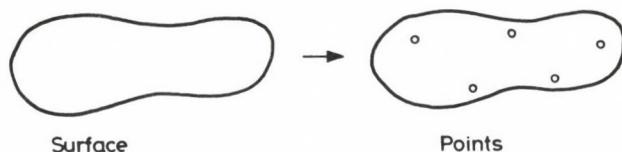


Fig. 1

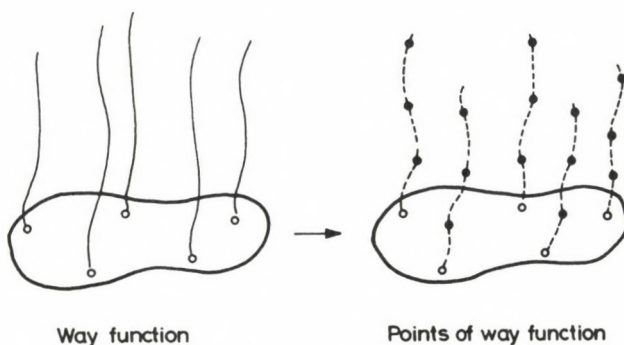


Fig. 2

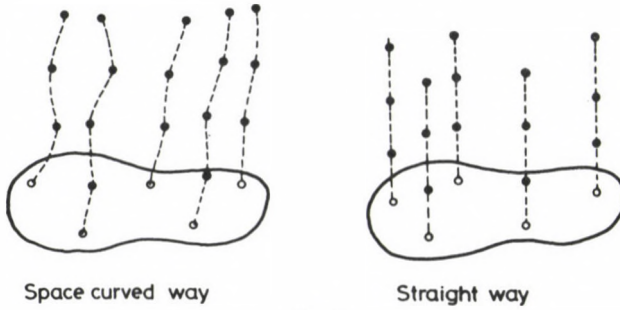


Fig. 3

In case of the solution of practical tasks it is often sufficient to study the projection of the movement in a certain direction. In this case it is assumed that the other two projections are constant. The study of vertical movement is an example for the latter case (Fig. 3).

The path of the points and the function describing it has been discussed so far. It has not yet been dealt with the co-ordinate system in which the equation of the path is defined. The suppositions in regard of the co-ordinate system is the next step of model establishment. At a surface movement of local character (e.g. landslide) it can be supposed that the geodetic base-points with a very stable permanent marking outside of the movement zone and the position of the co-ordinate system defined by them is immobile and can be regarded as an inertial system. In case of the movement study of greater areas the definition of the proper co-ordinate system is more difficult.

The steps discussed so far are connected to the physical part of the model. The geodetic part of it is connected to the geometry of the network used, and to its stochastic characteristics. The latter was described in the last decade usually by stochastic processes (Detrekői 1974, Niemeier 1980) and divided into parts in the following way:

$$y(t) = d(t) + s(t) + h(t), \quad (1)$$

where

$y(t)$ = the stochastic process of measurements,

$d(t)$ = the deterministic part of the measurements,

$s(t)$ = the stochastic process characterizing the so-called signal,

$h(t)$ = the stochastic process characterizing the so-called noise.

Function $d(t)$ characterizes the assumed equations of the paths of measured points, function $s(t)$ the stochastic deviation due to unevennesses in the movement, i.e. the difference between the assumed and actual path, $h(t)$ the errors of the measurement. Figure 4 illustrates the three quantities in case of the co-ordinates of a single point Z .

Of course, the values of the mentioned functions are only given at moments t_1, t_2, \dots, t_s of the measurements or can be estimated for them.

The aim of the processing of the data measured at the moments t_1, t_2, \dots, t_s is to determine the movement paths on the basis of them.

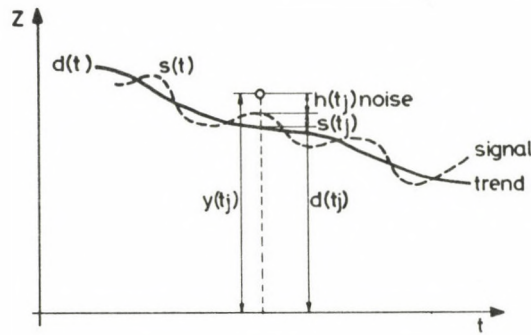


Fig. 4

The task can be solved in one step by means of collocation based on the method of least squares (Moritz 1975). In the practice, however, it is solved in several steps.

On one hand the characterization of the motion having occurred till a certain measurement epoch t_j can be needed, therefore one does not wait till the last measurement has been carried out.

On the other hand a joint determination of the results of more measurements and the characterization of the functions describing the motion need vast computation work, and therefore the point of view of computation technics has also a role in separating the task into parts.

The measurements of movement studies are mostly processed in the following steps:

1. The joint adjustment of the geodetic measurements assigned to the different t_j measurement epochs.
2. Determination of the characteristics of the displacement between two measurement epochs.
3. Determination of the functions describing the paths of the different points on the basis of the data measured at more or all measurement epochs.

The methods of mathematical statistics have an important role in the solution of all three steps. Steps 1 and 2 are often carried out jointly (Hazay 1967).

In the nomenclature of geodesy a joint processing of geodetic measurements carried out at different epochs is called the adjustment of the network determined by the points and measurements. At the adjustment of surface motion studies—and generally of movement studies—the following special problems occur:

- a) Which method should be followed if no basis point is at disposal that can be regarded as immobile?
- b) What to do if the measurement at the epoch t_j cannot be regarded as independent of earlier (or later) measurements?

It is relatively easy to answer the first question from a formal point of view. If there is no immobile point in the network, then it is a so-called free network. Several methods of the adjustment of free networks can be found in the literature; nowadays the

most frequently applied one is the adjustment with pseudo-inverses. The application of pseudo-inverses—or of any other methods developed for the adjustment of free networks—is only a solution of problems of computation-technics, (first of all the difficulties of the solution of normal equations having a matrix with singular coefficients is eliminated). It does not help, however, to determine the paths of the points by the co-ordinates obtained at the different measurement times (Detrekői 1977b, Heck 1981). The lack of immobile basis points means namely that there is no immobile co-ordinate system, in which the paths could be determined. The movement can be characterized in such a case by means of special quantities, i.e. by functions of the co-ordinates invariant to a shift or rotation of the co-ordinate system. The distance between two points is e.g. such a function.

The second problem refers to how to take into account the connection between the results obtained at different measurement epochs. If the measured data obtained at different times are not independent, then theoretically a joint processing is necessary. Nevertheless, if they are processed separately—as occurs many times at the solution of practical tasks—than both the adjusted quantities (co-ordinates, measurement results) and their covariance matrices will be distorted. An unfounded assumption of the independence can—according to literature data—considerably distort first of all the elements of the covariance matrices, and makes the further processing more difficult (Schüler 1973).

The next task is to determine the characteristics of the movement between two measurement epochs. As a first step of the processing it is usually controlled whether there happened a movement between the two measurement epochs, or the change in co-ordinates and measured results is only the consequence of the inevitable errors of measurements. In the last one and a half decade statistical probes have been applied with a special preference to decide the immobility, if the movements had the same order of magnitude as the scattering of the measurements (Wolfram 1970, Pelzer 1971, Storozenko 1972, Detrekői 1974, 1977a). In Hungary the application of statistical probes were already applied from 1969 on—internationally among the first—at the movement studies of engineering objects. When statistical probes are applied a zero hypothesis H_0 expressing the immobility is used in general and its acceptance is decided by proper statistical functions on a certain probability level. Probes for deciding the immobility are used in two steps. In the first step several quantities are jointly examined (e.g. the co-ordinates of all basis points are regarded as immobile), in the second these quantities are individually checked (Pelzer 1971). For the joint examination of more quantities mostly the F -probes are used. In this case the quadratic difference characterizing jointly the variations of the different quantities and the equality of the variances obtained from the adjustment are regarded as zero hypotheses. If a movement occurs, the quadratic difference is greater than the variance obtained from the adjustment. In case of a special arrangement of the points (e.g. in case of points seated beside a dyke or bank) the sign-probe or the t -probe, in other cases the Wilcoxon probe can be well used.

For individual testing of the quantities, the u - and t -probes became frequent. Here the zero hypothesis expresses the equality of the values obtained at different times. If the results of several earlier measurements are at disposal for the same quantity, then the probe developed for the correlation coefficient can also be applied, thereby the zero hypothesis referring to the zero velocity can be investigated in fact.

An important question of the application of statistical probes is the probability level on which the acceptance or rejection of the zero hypothesis is decided. In books on mathematical statistics mostly the level of $p=0.95$ is recommended. At this probability level, however, the probability of the so-called second-type error can be rather big. The second-type error means that one accepts a zero hypothesis for an epoch, when it does not hold. In our case the zero hypothesis means the immobility, consequently the result of the second-type error is that an existing movement is not indicated. It can have serious consequences, first of all in cases of local surface movements as e.g. the slide of a splay. Therefore it is reasonable to choose a lower p -value. Favourable experiences have been got with the so-called inverse probes in case of engineering constructions. In case of several times repeated measurements the acceptance of the zero hypothesis is not decided on a constant probability level, but the minimum probabilities p_{\min} are determined one by one at which the zero hypothesis is yet acceptable. If a considerably higher p_{\min} value is obtained as before than an immobility cannot be assumed (Detrekői 1979).

Statistical probes are advantageously applicable for the control of the immobility of basis points, too.

Having adjusted the results of the different measurement epochs, the next step of processing is to determine the characteristics of the movement. This can be done

for points,
for lines,
for surfaces.

In case of a processing for points the starting basis is in general the co-ordinate changes X_i, Y_i, Z_i of the points in the directions X, Y, Z between two measurements. At the solution of practical tasks the graphical representation of the displacement is mostly made by its horizontal projection

$$r_i^2 = X_i^2 + Y_i^2 \quad (2)$$

and by the quoted projection of the height value Z_i (Fig. 5). A processing from point to point is not suitable for the characterization of the connection between the movements of different points.

In case of a processing from line to line it is concluded from the changes of the points situated along the line to the changed form of the line. For example, the characteristics of a sinking depression should be determined from the sinking of the points situated along a straight line. This task can be considered as the determination of a function.

If the characteristic of the changed line is known—as e.g. the equation of Martos in case of the previous example (Hoványi 1968)—then the problem is to determine the unknown parameters of a known function. Since the function in question has only two variables, the computation can easily be made by the least squares method, by the method of minimax or by an other method. If the connection between the points should also be taken into account, then the measured results referring to the different points cannot be regarded as independent. A theoretically correct way of solution can be assured then by collocation based on the method of least squares.

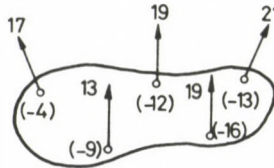


Fig. 5

If the function character is unknown, then either the proper function type can be chosen by means of a graphic representation or, after having computed with several different functions, the best function can be selected on the basis of an objective criterion. The determination index can be advantageously used as criterion.

A representation from line to line already characterizes the connection between the points along the line, too, however, it gives no information on connections in a direction perpendicular to the lines.

A further possibility is to process the points jointly for surfaces. If a projection of the movement of the points can be given in the form of a closed function—e.g. an originally plane surface is deformed into a cylindric one—the task is again to determine the function. For this the same holds that has been discussed in connection with the processing for lines. In case of surface movements, however, such functions cannot be found. The joint processing of the points is reduced now to the determination of the iso-lines of the places of identical displacement (Fig. 6).

Approved methods for this purpose are interpolations based on the method of least squares or filtering. Recently, successful experiments have been made in this direction with the method of finite elements.

A further task of processing is the joint processing of the results of several measurements made at different times. This is often reduced to the repeated processing of the results of two measurements. For example, the results of the measurements t_s are jointly processed with those of t_1 and t_{s-1} . This way one gets on the basis of the period $t_s - t_1$ information on the total displacement of the points and on the basis of the period $t_s - t_{s-1}$ information on the velocity of points. The principle is represented for the case of the Z co-ordinate of one single point in Fig. 7.

A joint processing of more measurements in different epochs can also be made by points, by lines and by surfaces. A processing from point to point means the

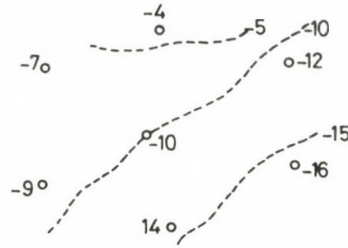


Fig. 6

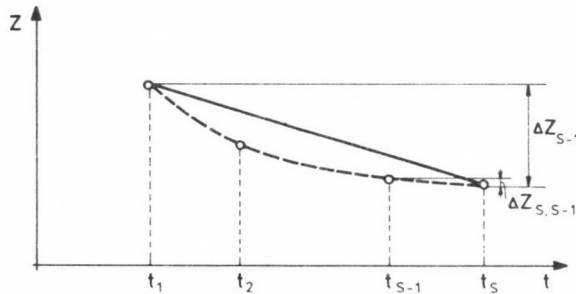


Fig. 7

determination of the paths of points. If the task is divided into co-ordinates, then the aim is to determine the functions $X_i(t)$, $Y_i(t)$, $Z_i(t)$ of the point P_i from the results assigned to the measurement epochs t_1, t_2, \dots, t_s . The task can be very important not only for the characterization of the movement so far, but also for the prediction of an expectable movement. A prediction of movements has exceptional economical importance in certain cases. In respect of the mathematical solution of the problem the previously said are valid.

If the processing is made along a line, the surface defined by the line must be determined. Finally in case of processing for a surface, the aim is to determine the function $F[X(t), Y(t), Z(t)]$ having been the basis in the discussion of the model.

In this paper I dealt with the processing of the results of geodetic measurements carried out for the determination of surface movements and hereby I started from the mathematical model. The discussed principles—as statistical methods in general—can be successfully applied if measurements in required number are at disposal. This condition is fulfilled in case of measurements made at different epochs both for local and regional surface movements. The number of epochs, however, is high enough only for statistical processing at the movement studies aimed for mining survey or civil engineering survey. In national and continental networks there are not enough measurements made at different epochs which would allow to determine the characteristics of the time variations by means of the methods of mathematical statistics.

References

- Detrekői Á 1974: Application of the methods of mathematical statistics for the measurement of displacements and deformations (in Hungarian). *Geodézia és Kartográfia*, 5, 365—375.
- Detrekői Á 1977a: Über das stochastische Modell ingenieurgeodätischer Deformationsmessungen. XV. FIG Kongress, Stockholm, Band 6.
- Detrekői Á 1977b: Netzausgleichung bei ingenieurgeodätischen Deformationsmessungen. *Periodica Polytechnica, Civil Engineering*, 21, 23—47.
- Detrekői Á 1979: Zur Anwendung mathematisch-statistischer Tests bei ingenieurgeodätischen Deformationsmessungen. *Vermessungstechnik*, 27, 207—208.
- Hazay I 1967: Adjustment of networks of vertical crustal movements (in Hungarian). *Geodézia és Kartográfia*, 19, 321—324.
- Heck B 1981: Die Verwendung relativer Fehlerellipsen zur Analyse von Deformationsmessungen. Beiträge zum II. Int. Symp. über Deformationsmessungen. Verlag Konrad Wittwer, Stuttgart
- Hoványi L 1968: Surveying of mines (in Hungarian). Műszaki Könyvkiadó, Budapest
- Joó I, Detrekői Á 1983: Deformation measurements. Akadémiai Kiadó, Budapest
- Moritz H 1975: Elements of Collocations B. I. Wissenschaftsverlag, Mannheim, Wien, Zürich
- Niemeier W 1980: Zur Auswertung geodätischer Messreihen. *Allgemeine Vermessungsnachrichten*, 1, 41—59.
- Pelzer H 1971: Analyse von Deformationsmessungen. Veröffentlichung der Deutschen Geodätischen Kommission Reihe C. 136. München
- Schüler K 1973: Korrelationsänderungen und scheinbare Punktverschiebungen im Trialterationsnetz. Mitteilungen aus dem Institut für Theoretische Geodäsie der Universität Bonn. Nr. 19.
- Storozenko A F 1972: Method analiza ustojchirosthi reperov. *Geodézia i Aerofotoszjemka*, 3, 41—45.
- Welsch H 1981: Gegenwärtiger Stand der geodätischen Analyse und Interpretation geometrischer Deformationen. *Allgemeine Vermessungsnachrichten*, 88, 41—51.
- Wolfram O 1970: Deformationsmessungen an einem Wohngebäude. *Allgemeine Vermessungsnachrichten*, 9, 370—373.

NEW RESULTS IN EARTH TIDES RESEARCH

G BARTHA¹ and P VARGA²

[Manuscript received September 5, 1984]

The following aspects are included in the paper: principle of Earth tides; importance of tidal investigations in global and local geodynamics illustrated by some foreign and Hungarian results. It is concluded that tidal measurements—especially with horizontal pendula—seem to be useful means in the search for lateral inhomogeneities. At the same time the big tectonical structures have no considerable influence upon the tidal measurements.

Keywords: Earth tides; geodynamics; horizontal pendulum; lateral inhomogeneity

Earth tides

The phenomenon of Earth tides exerted by the Moon and the Sun consists of the deformation of the solid Earth and of a periodical change in its gravitational field. The origin of the tidal force F_t is shown in Fig. 1. The centrifugal force F_{cf} produced by the relative motion of two celestial bodies is balanced by their mutual gravitational force F_{gr} , but the equilibrium is only true at the centre of Earth's mass. On the surface, there appears a difference between them ($F_t = F_{gr} - F_{cf}$), it is called tidal force. The potential function of the tidal force can be expressed by the well known series

$$W = \frac{mf}{R} \sum_{n=2}^{\infty} P_n(\cos \Theta), \quad (1)$$

where m is the mass of the perturbing celestial body (Moon or Sun), f the gravitation constant, $P_n(\cos \Theta)$ the spherical harmonics and R , Θ are shown in Fig. 1. If the Earth would be a rigid body, merely a periodical change in the gravity field would be produced by this force. However, there is a nearly elastic deformation, too. Its magnitude is determined mainly by the geographical latitude, but also by the physical structure of the Earth. The vertical deformation at the latitude of 47° is 35—40 cm and the changes of the gravity vector are about 200 μgal in magnitude and about 30 msec in direction (1 msec = 0.001").

¹ Geodetic and Geophysical Research Institute of the Hungarian Academy of Sciences, H-9400 Sopron, Múzeum u. 6—8

² Hungarian State Loránd Eötvös Geophysical Institute Budapest, H-1145 Budapest, Columbus u. 17—23

Very close relations exist between the Earth tides and other geodynamic phenomena, as summarized in Table I. The following three important geodynamic phenomena are included in the table:

- the free motion of the rotation axis,
- the forced motion of the rotation axis and
- the Earth tides.

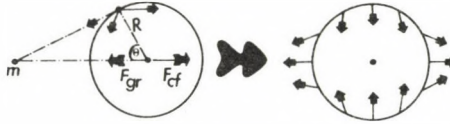


Fig. 1. Tidal effect

Table I. Geodynamic phenomena

Phenomenon	Exerting force	Coordinate system	Rigid model	Elastic model	Elastic-viscous model
free motion of the rotation axis	—	Earth fixed	Euler wobble	Chandler wobble	—
forced motion of the rotation axis	lunisolar	inertial	precession nutation	—	—
Earth tides	lunisolar	Earth fixed	theoretical tides	static tides	static-viscous tides

The forced motion of the rotation axis (precession and nutation) as well as the Earth tides are exerted by the same lunisolar perturbation, but they are treated in different coordinate systems (inertial system and Earth fixed system) (Melchior 1966). Three Earth models appear in Table I: the rigid, the elastic and the elastic-viscous model. The last of them is the best approximation of the real Earth. The differences between these models are well emphasized by the values related to the free motion of the axis (polar motion). The length of the polar motion period is 305 days for the rigid model (Euler period) and 433 days for the elastic model, what coincides with the measured period (Chandler period).

In the rigid model the Earth tidal phenomenon is highly idealized, i.e. there are no deformations and changes are only possible in the gravitational field of the Earth (theoretical tides). In the elastic model deformations are possible and the theoretical tides are disturbed by them. According to Love's theory this disturbance in the gravity change, i.e. the Earth tides in the elastic model can be expressed as a product of the theoretical tides and the amplitude factor K . This amplitude factor K is the ratio between the tides of the rigid and the elastic body. A better approximation of the real effect can be reached by permitting a phase lag in the model, what is done in the elastic-

viscous model. Thus the complete lunisolar effect can be interpreted as a sum of several periodical tides and it is written in the following form:

$$\text{lunisolar effect} = \sum_{i=1}^n K_i T_i(\omega_i t + \varphi_i + \kappa_i) \quad (2)$$

where K_i is the amplitude factor of tide T_i with frequency ω_i , φ_i is the tide phase at $t = 0$ and κ_i is the phase lag.

The primary aim of the tidal investigation is to determine the factors K_i which gives information about the elastic properties of our planet. Since the theoretical tides can be computed with great accuracy, the reliability of the obtained data is determined by the accuracy of the observations, strictly speaking by the instruments and the observational conditions.

The instruments of tidal observations are: recording gravimeters, horizontal pendula and extensometers. In this paper the results of gravimeters and pendula will be dealt with. The changes in the magnitude and in the direction of the gravity vector can be recorded by gravimeters and pendula, respectively. The recorded curves are composed from three components:

$$\text{Record} = \text{lunisolar effect} + \text{local effect} + \text{instrumental drift}. \quad (3)$$

The amplitude factors K_i in the lunisolar part (usually denoted by δ at gravimeters and by γ at pendula) are in a simple connection with the so-called Love numbers h , k characterizing the elasticity of the Earth and they can be deduced from different Earth models by:

$$\begin{aligned} \delta &= 1 + h - \frac{3}{2}k \\ \gamma &= 1 + k - h. \end{aligned} \quad (4)$$

The task of evaluation is to separate the components of a record as well as to determine the factors K_i and the phase lags κ_i . For this purpose some special methods based on harmonical analysis were developed, which are applicable only since the introduction of large computers.

Results of the tidal investigation

The components of a tidal record comprise—with except of the instrumental drift—important geodynamical informations. Let us discuss at first the lunisolar part. Earlier the amplitude factors computed from the lunisolar part were used to test the Earth models based on different idealizations of the structure of the Earth. The mean values of the amplitude factors obtained at different stations were compared with the values computed from different models. The value of amplitude factor depends, however, only slightly on the change of the model parameters. As the physical structure of the Earth is nowadays rather well-known from seismological data, the “test role” has

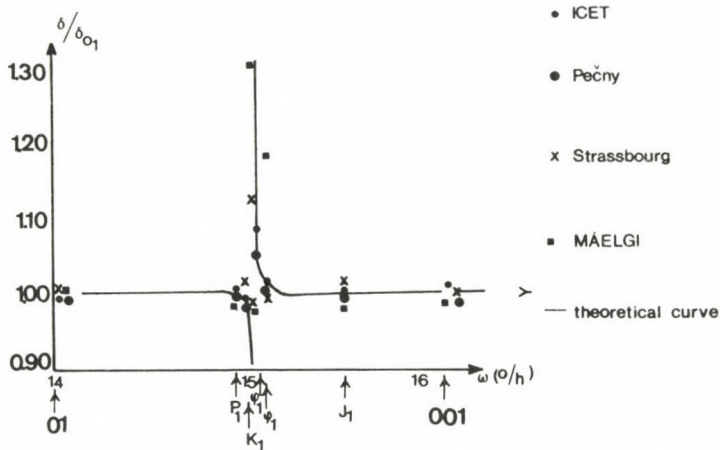


Fig. 2. Liquid core resonance effect based on results of ICET of the Geod. Topographic Inst. in Czechoslovakia, Pečny, of the Strassbourg observatory and of MÄELGI

only a secondary importance, unless the accuracy of the observation could be greatly improved. At the same time the lunisolar part comprises information about the Earth's core. It has been theoretically proved already at the end of the last century that if the Earth's core is liquid, then a wobble of nearly one day period should exist besides the Chandler wobble which has a very small amplitude not measurable directly. However, its detection would mean an important proof of the liquid state of core and further details about the condition of the core could also be expected from it. Jeffreys (1949), later Molodensky (1953) revealed that this nearly diurnal oscillation gets into resonance with the diurnal part of the lunisolar tidal effect, thus transforming the amplitude factors. This is the so-called resonance effect of the liquid core and it is well demonstrated in Fig. 2 by the measured amplitude factors, where the relative amplitude factors (obtained factors/factor of tide O_1) are shown in the neighbourhood of the resonance frequency. By using relative factors the instrumental calibration problems can be eliminated.

Concerning the information comprised in the lunisolar part it should be mentioned that the values of the amplitude factors depend not only on the global structure of the Earth (i.e. on the radial inhomogeneity) but also on deeper lateral inhomogeneities. Investigations in this direction will be dealt with below. German scientists (Bonatz et al. 1983) recorded with Askania borehole tiltmeters along a profile crossing a SW—NE striking fault in the Hunsrück Hills located northwestward from Frankfurt am Main. The ocean loading and meteorologic effects were eliminated from the observed data. The results obtained from this observation campaign are shown in Figs 3a and 3b. In the figures the relative amplitude factors are demonstrated for the big tides. The global amplitude factors for these tides have been taken as 100% and the observed values are related to them. The observation sites are denoted by black

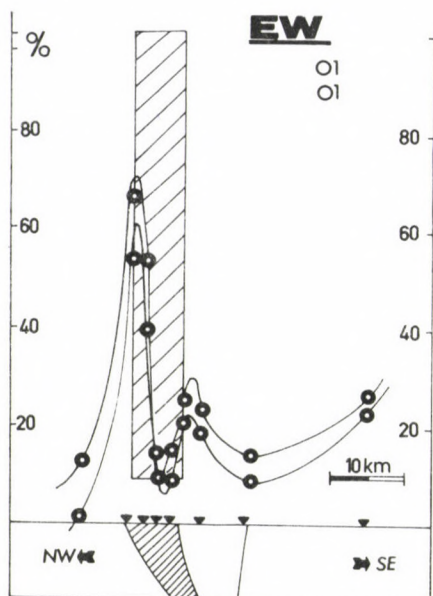


Fig. 3a. Profile crossing fault in Hunsbrück Hills

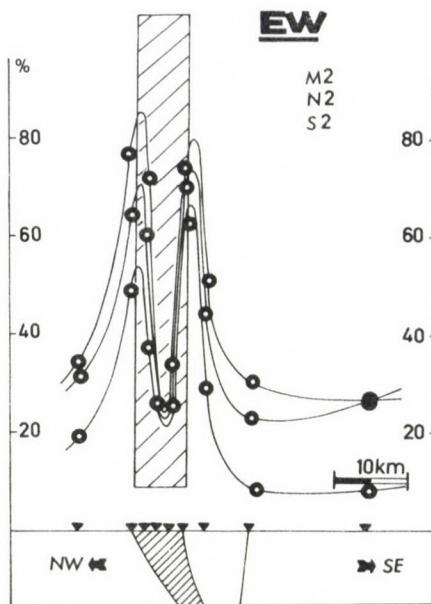


Fig. 3b. Profile crossing fault in Hunsbrück Hills

Table II. Gravimetric tidal results (Varga 1982, Dittfeld et al. 1981)

Station	Observed ampl. factors		Observed phase lags		Ampl. factors with eliminated ocean loading	
	O_1	M_2	O_1	M_2	O_1	M_2
Observations in Hungary						
Tihany	1.155	1.187	$0^{\circ}.06$	$0^{\circ}.09$	1.161	1.161
Budapest	1.156	1.189	$0^{\circ}.18$	$0^{\circ}.63$	1.160	1.159
Penc	1.158	1.191	$-0^{\circ}.27$	$-0^{\circ}.30$	1.164	1.167
Pécs	1.155	1.210	$0^{\circ}.52$	$0^{\circ}.68$	1.162	1.180
Observations in other countries						
Bonn	1.158	1.197	$-0^{\circ}.55$	$1^{\circ}.92$	1.165	1.160
Potsdam	1.156	1.191	$0^{\circ}.06$	$1^{\circ}.36$	1.162	1.164
Pečny	1.159	1.181	$-0^{\circ}.73$	$1^{\circ}.23$	1.165	1.154
Graz	1.163	1.188	$0^{\circ}.17$	$1^{\circ}.20$	1.169	1.162
Observation of Soviet Academic Institute						
Sofia	1.145	1.175	$-0^{\circ}.84$	$-0^{\circ}.40$	1.150	1.156

triangles. The structure of the fault zone is well reflected in the results and this method seems to be a great promise for the investigation of the lateral inhomogeneities.

At the same time from Hungarian observations carried out in international cooperation, no direct connection seems to exist between the tidal parameters and the big tectonic structures. A tidal observation campaign with gravimeters was carried out by the Hungarian Eötvös Loránd Geophysical Institute (MÁELGI) at different stations. The results are summarized in Table II. Parallel with MÁELGI's instrument, other recording gravimeters were working at each station, too, in order to receive more reliable results. The results in Table II are very homogeneous in spite of great distances between some stations. It must be mentioned, however, that the instrument of the Institute of Earth's Physics of the Soviet Academy of Sciences—which was compared several times with MÁELGI's instrument—produced a somewhat deviating result in Sofia.

In connection with the investigations of great tectonics, pendulum observations carried out in cooperation by the Geodetic and Geophysical Research Institute of the

Table III. Pendulum results (Bartha 1976)

Station	Observed ampl. factors		Observed phase lags	
	O_1	M_2	O_1	M_2
Sopron	0.707	0.742	4.57	-0.27
Graz	0.687	0.738	4.78	4.74

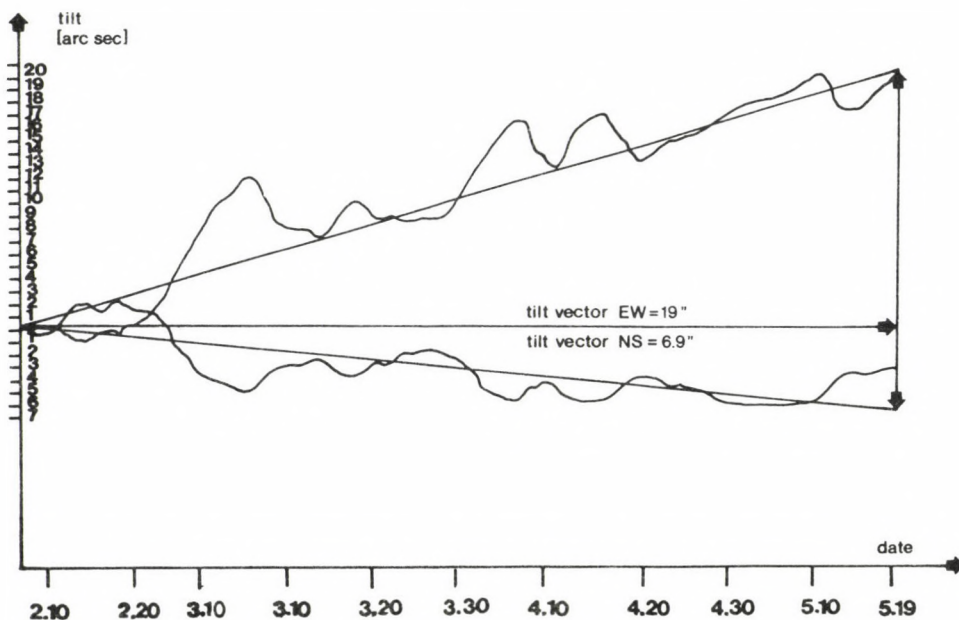


Fig. 4. Local tilts in a still-standing pit in Pécs, Hungary

Hungarian Academy of Sciences (GGKI) and the Technical University Graz, are worth being mentioned (Bartha 1976). The results obtained are summed up in Table III. The amplitude ratio γ was nearly the same both in Sopron and Graz. This is a remarkable result, because the records of horizontal pendula are generally different from site to site due to the strong influence of observational conditions and local tectonic effects.

As mentioned previously, the local component, too, carries geodynamic informations besides the lunisolar part. This will be illustrated with an example. A horizontal pendulum recording was carried out by GGKI in a still-standing pit near to Pécs, in the southern part of Hungary. The recorded tilts were by some orders higher than the tidal effect itself (Fig. 4). These records included obviously local informations and awoke the interest of mining experts.

Conclusions

The investigation of Earth tides represents an important part of the geodynamic research. The investigation of the resonance effect of the liquid core means an important improvement for the research of the physical structure of the Earth. The lateral inhomogeneities indicated by Earth tides parameters may be indications of structural units of the Earth in great depths not detectable by the conventional methods of geophysics and geodesy. Tidal instruments—first of all pendula and extensometers—can play an important role in the observation of local movements caused by local tectonic effects or industrial activities.

The improvement of the instrumental accuracy is a very important factor of development in tidal research. It is the precondition for a more reliable testing of the Earth models by tidal results. The present instrumentation, however, also reveals possibilities for an advancement in geodynamic research. Parallel observations (more instruments at each stations, and coordinated simultaneous observations at different stations), and more tidal observatories could yield better geodynamic informations than we have at present.

References

- Bartha G 1976: Parallel Earth tide registrations in Sopron and Graz. *Acta Geod. Geoph. Mont. Hung.*, 11, 203–228.
- Bonatz M, Gerstenecker C, Kistermann R, Zschah J 1983: Tilt measurements across a deep fault zone. Proc. of the 9th International Symposium on Earth Tides. Schweizerbart'sche Verlagsbuchhandlung, Stuttgart
- Dittfeld H J, Simon Z, Varga P, Vendikov A, Volkov V A 1981: Global analysis of Earth tide observations in Obninsk, Potsdam, Pečny, Tihany and Sofia. Study of the Earth tides. *Bulletin No. 4*, 4–94.
- Jeffreys H 1949: Dynamic effects of a liquid core. *Monthly Not. R. Astr. Soc.* 109, No. 6, 670–687.
- Melchior P 1966: The Earth Tides. Pergamon Press Oxford
- Molodensky M S 1953: Elastic tides free nutation and some questions relating to the Earth's structure (in Russian). *Trudi Geofiziceseskogo Instituta*, 19/146.
- Varga P 1982: Earth tide observations with recording gravimeter BN-07 (GS-11, No. 190). *Geophysical Transactions*, 28/2, 19–32.

AN INTELLIGENT DIGITAL DATA ACQUISITION SYSTEM FOR RECORDING THE TIDAL SIGNAL

GY MENTES¹

[Manuscript received December 4, 1984]

The construction and the operation principle of an intelligent digital data acquisition system is presented that can be programmed for recording different geodynamic phenomena. A filtering method is described that prefilters the tidal data measured digitally with a high sampling rate thus the hourly tidal values are recorded. A procedure is also given to program the system for recording signals being different from the tidal ones.

Keywords: capacitive pendulum; filtering; intelligent data acquisition; linear prediction; step correction

Introduction

The properties of the tidal signals (microseismic oscillations, spikes, steps superposed on the curve and gaps) cause a lot of problems when digitizing. There are two ways to digitize the output signal of a tidal measuring instrument. An analog record e.g. a photorecord made on a photodrum or a record made by an electric strip chart recorder can be digitized by means of a curve digitizer (indirect digitizing) and then processed directly by a computer. In this case the irregularities of the record can be manually smoothed out what is a very subjective and tiresome work. Moreover, this method has another disadvantage, namely the digital data contain the error of the analog recorder of about 0.5—2%, too. By sampling the output signal of the tidal instruments by means of a simple digitizer at the hourly time marks, the error of the digitization can be very high because of the above mentioned properties of the tidal signal. In this case an analog record is always needed to verify the digital data. There are some attempts to solve this problem by applying a high sampling rate and making program systems which are able to preprocess the densely sampled tidal data (Jentzsch 1981, Plag and Jahr 1983). However, this method considerably increases the number of data to be stored.

The development of the microprocessor and microcomputer technique enables the construction of intelligent digital data acquisition systems which combine the

¹ Geodetic and Geophysical Research Institute of the Hungarian Academy of Sciences, Sopron, Hungary, H-9401, P.O.B. 5

advantages of the digital data recording and the manual evaluation of an analog record. Such an intelligent system can prefilter and preprocess the measured tidal data and yields correct hourly tidal data without tiresome manual work and need no large storage capacity for tidal recording (Asch 1983).

In many cases e.g. when recording the free oscillations of the Earth all data obtained with a high sampling rate are needed, else we need the preprocessed data or sometimes only the results. Therefore an intelligent digital data acquisition system must be programmable for different tasks. Presently such systems can already be constructed at reasonable prices.

The electric construction of the intelligent digital data acquisition system

Figure 1 shows the block diagram of the data acquisition system. It is controlled by a microprocessor MC 6802 from MOTOROLA. The controller program is stored in the EPROM memory. The RAM memory is used for calculations and temporary storage of data as a buffer memory. When the buffer memory is full, the sampled or preprocessed data can be transferred in blocks into the exchangeable non-volatile semiconductor memory which may be exchanged as a cassette, or into the cassette unit,

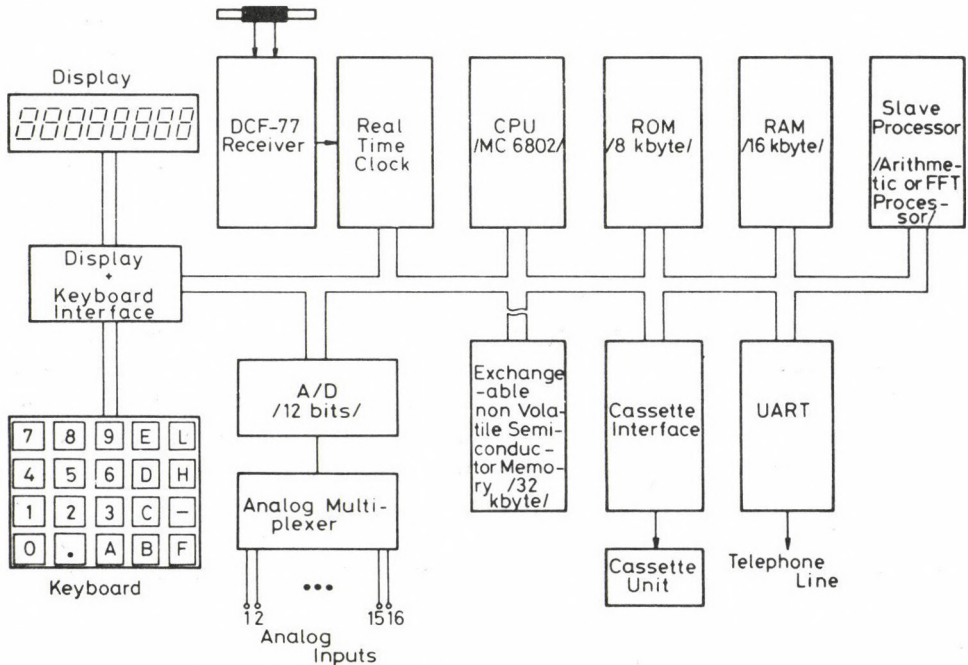


Fig. 1

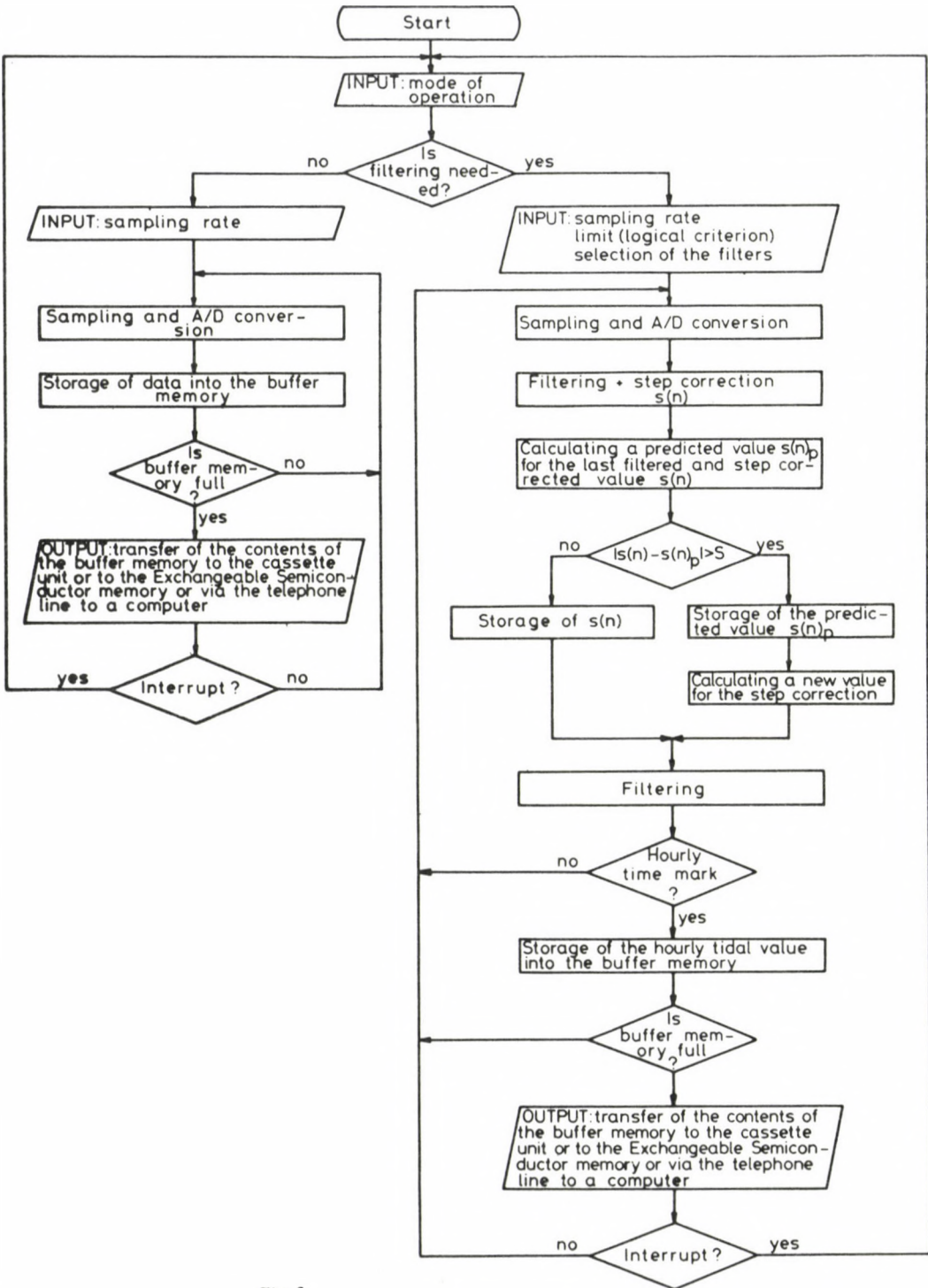


Fig. 2

or the data can be directly transferred via telephone line into a large computer. The exchangeable semiconductor memory is more reliable under conditions of an Earth tides observatory than the cassette unit which contains moving mechanical parts. The storage capacity of the exchangeable semiconductor memory is sufficient for about 15 days to store the prefiltered hourly values of tidal data measured e.g. by a pair of horizontal pendulums including the records of environmental parameters, too. The digital recorder system has 16 analog input channels, an analog multiplexer and a 12 bits analog to digital converter. The sampling and converting of the analog channels is controlled by the master processor. The exact time is given by the realtime clock which can be synchronized by means of a DCF—77 receiver. The speed of the system can be increased applying a slave processor which is a high speed arithmetic or an FFT processor depending on the desired filtering algorithm.

The data acquisition system has keyboard and a display too, for the manual control of its operation and for input and display parameters needed for data sampling and filtering.

The operation of the system is given in Fig. 2. The filter program shown in the flow chart is written for prefiltering of tidal data measured by a capacitive pendulum.

The description of the filter algorithm

There are always self-swingings, steps and spikes superposed on the tidal curve. It is the duty of the filter program to remove these undesired signals from the tidal curve, similarly to the manual evaluation of the analog records. The filtering cannot be solved solely by mathematical filters with the desired accuracy, as even if such filters decrease the amplitude of spikes significantly, nevertheless they smudge the spike over the whole curve after its appearance. By inserting logical decisions into the filter program this problem can be eliminated.

It is assumed in the filtering algorithm described hereafter that the sampling period is less than the half of the eigenperiod of the self-swinging and the hourly time mark is an integral multiple of the sampling period.

Let us suppose that the sampled tidal data are

$$a_1, a_2, a_3, \dots, a_i, \dots$$

a_i is an extreme end value, if

$$a_{i-1} < a_i > a_{i+1} \quad \text{or} \quad a_{i-1} > a_i < a_{i+1}$$

then

$$\begin{aligned} b_j &= b_{j+1} & j &= 1, 2, 3, \dots, m-1, \\ b_m &= a_i \end{aligned}$$

where the n th point of the smoothed curve $s(n)$ will be calculated from m extreme end values by the Fox-Schuler averaging method:

$$s(n) = \frac{1}{2^{m-1}} \sum_{j=1}^m \binom{m-1}{j-1} b_j + C, \quad (1)$$

where

C = the value of the step correction calculated at the previous point.

The predicted value for $s(n)$ from the previous p smoothed values is

$$s(n)_p = \sum_{k=1}^p \alpha_k s(n-k), \quad k = 1, 2, \dots, p, \quad (2)$$

where

α_k = linear predictive coefficients.

If

$$|s(n)_p - s(n)| > S, \quad (3)$$

where S is a prefixed limit for the presence of a step in the curve, then

$$C = C + s(n)_p - s(n)$$

$$u_l = u_{l+1}$$

$$u_r = s(n)_p, \quad l = 1, 2, \dots, r-1$$

otherwise

$$u_l = u_{l+1}$$

$$u_r = s(n), \quad l = 1, 2, \dots, r-1.$$

The tidal value at the hourly time mark is:

$$y = \frac{1}{2^{r-1}} \sum_{l=1}^r \binom{r-1}{l-1} u_l, \quad (4)$$

where the average value is calculated from r smoothed and step-corrected values.

A method for determination of the linear predictive coefficients

The above described procedure can be adapted besides Earth tides recording for recording of other signals, too. In this case the sampling rate and the linear predictive coefficients should be chosen properly. For this the character of the signal must be known. The linear predictive coefficients α_i in the basic relationship of the linear prediction

$$s(n)_p = \sum_{i=1}^p \alpha_i s(n-i); \quad i = 1, 2, \dots, p$$

are determined so that the error of the prediction

$$E = \sum_{n=n_0}^{n_1} \left[s(n) - \sum_{i=1}^p \alpha_i s(n-i) \right]^2$$

should be a minimum.

By applying the notations: $\alpha_0 = -1$ and

$$\Phi(i, j) = \sum_{n=n_0}^{n_1} s(n-i)s(n-j) = \Phi(j, i)$$

we get

$$E = \sum_{i=0}^p \sum_{j=0}^p \alpha_i \Phi(i, j) \alpha_j.$$

Minimizing E with respect to the coefficients α_i the latter yield the best results for the prediction and can be obtained by solving the simultaneous equations

$$\sum_{i=1}^p \alpha_i \Phi(i, k) = \varphi(k); \quad k = 1, 2, \dots, p,$$

where

$$\varphi(k) = \Phi(0, k).$$

The values of $\Phi(i, j)$ can be calculated in knowledge of the signal to be measured.

A fast Fox-Schuler averaging algorithm for microprocessors

In the practice we need to calculate the Fox-Schuler average from different number of extreme end values. When we calculate the average directly by formula (4) we have to use different formula at different number of extreme end values used for filtering. Therefore the direct programming of the formula (4) is inconvenient and moreover the calculation is slow. Using the algorithm described below, we need no different formulas depending on the number of measured values involved in the filtering. Let us suppose that the local maximum and minimum values of the sampled data are:

$$y_1, y_2, y_3, \dots$$

then we can calculate the Fox-Schuler average as seen in Fig. 3, where:

$$\begin{aligned} Y_2 &= \frac{y_1 + y_2}{2}; & Y'_3 &= \frac{y_2 + y_3}{2} \dots \\ Y_3 &= \frac{Y_2 + Y'_3}{2} & Y''_4 &= \frac{Y'_3 + Y'_4}{2} \dots, \\ & \vdots & & \end{aligned}$$

and Y_2, Y_3, Y_4, \dots are averages obtained from 2, 3, 4, ... extreme end values respectively.

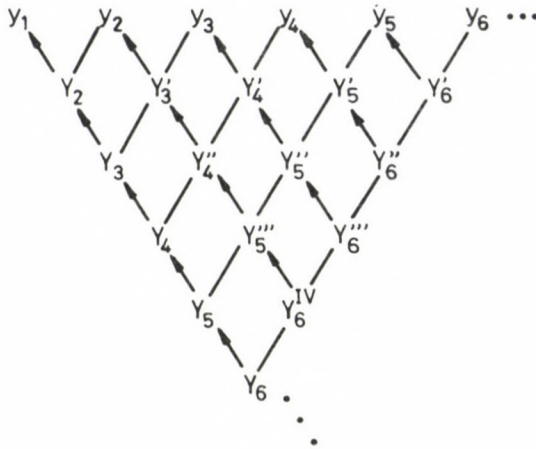


Fig. 3

The lines show the two values from which the average value is obtained and the arrows show the values in place of which the latest calculated average value can be written back into the memory. Only as many storage registers are needed in the memory as many extreme end values are used for filtering and we need no constant registers for storage of the filter coefficients. We have to enter only one parameter for running the program, namely the number of the extreme end values which the average is calculated from. The algorithm is very fast because it consists only of addition and shifting sequences.

Testing of the filtering algorithm

The above described filtering method gives acceptable results for Earth tide record even if we use only three values for the Fox-Schuler averaging and only two previous values for the linear prediction.

In this case

$$s(n) = (b_1 + 2b_2 + b_3)/4, \quad y = (u_1 + 2u_2 + u_3)/4$$

and

$$\alpha_1 = 2, \quad \alpha_2 = -1.$$

It means that the microprocessor can calculate very quickly the averages and the linear prediction by shifting registers instead of multiplication and division algorithms which would require several hundred machine cycles.

Because some parts of the system are still under construction, the filter method was tested on a computer. Figure 4 shows the simulated input signal. The eigenperiod of the "simplified" tidal signal (a sinus wave of one day period) was 50 s, the spikes and steps had amplitudes half of the signal. The accuracy of the method depends on the quality of the linear prediction, on the gain of the system, on the sampling rate and on

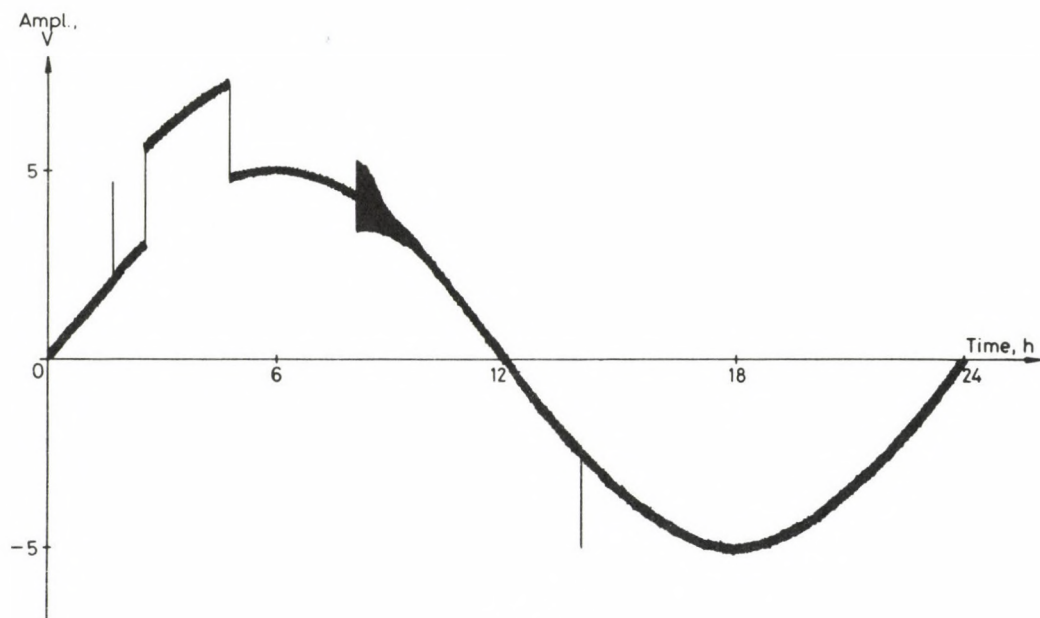


Fig. 4

Table I

Limit [S]	Sampling period [s]	Average error of the filtering in percentage of amplitude with RMS error			
		1	5	10	20
0.1	5	1.10 ± 3.60	4.02 ± 4.24	0.29 ± 0.32	0.15 ± 0.16
	10	26.1 ± 28.1	0.36 ± 0.38	0.72 ± 0.75	0.12 ± 0.15
	20	23.9 ± 26.0	1.94 ± 2.14	1.94 ± 2.14	295.0 ± 457.0
0.05	5	80.67 ± 97.56	0.30 ± 0.33	0.48 ± 0.51	0.26 ± 0.27
	10	81.20 ± 98.07	0.72 ± 0.76	0.08 ± 0.08	0.13 ± 0.15
	20	2.0 ± 2.1	1.94 ± 2.14	0.33 ± 0.40	295.0 ± 457.0
0.02	5	4.0 ± 4.2	0.40 ± 0.40	0.19 ± 0.07	65.5 ± 68.0
	10	0.36 ± 0.40	0.08 ± 0.104	0.07 ± 0.08	65.4 ± 68.0
	20	1.90 ± 2.1	295.0 ± 456.8	0.57 ± 0.63	64.6 ± 67.0
0.01	5	0.8 ± 0.8	0.50 ± 0.52	0.37 ± 0.11	42.0 ± 43.0
	10	1.8 ± 1.8	0.36 ± 0.36	0.25 ± 0.10	42.0 ± 43.0
	20	1.2 ± 1.3	0.68 ± 0.84	0.60 ± 0.42	41.0 ± 43.0

the limit S . Table I shows the method for different parameters. From Table I it follows that both the sampling rate and the limit S have an optimum at a given gain. The most important point is to choose properly the limit. When the limit is lower or nearly as low as the errors obtained from the A/D conversion and calculations, the error of the filter program will be very high because the program always substitutes the measured value for the predicted value. If the limit is too high the program will not find small steps in the input signal.

It turned out during the calculations that the accuracy of the method is depending on the shape of the signal, too. The best parameters obtained from the theoretical calculations do not give always the best results in the practice. For this reason the optimum of the parameters must be determined by experimentation at the beginning of recording the signal.

Conclusion

An intelligent digital data acquisition system on the one hand diminishes the manual work for preprocessing of tidal data on the other it increases the accuracy of the measurement. The method eliminates the subjective errors. A high dynamic range of the analog to digital converter and properly chosen parameters of the filter program enable to achieve a higher accuracy than with other recording methods.

The above described intelligent digital data acquisition system and data collection algorithm is suitable for recording of other physical phenomena besides the Earth tides.

References

- Asch G 1983: Digital data acquisition and preprocessing of tidal data. *BIM*, 89, 5742–5748.
Jentsch G 1981: Automatic treatment and preprocessing of tidal data recorded at 1 min intervals. *BIM*, 85, 5415–5428.
Plag H P, Jahr T 1983: On processing of Earth tidal data. *BIM*, 89, 5759–5786.

TIME VARIATION IN GEOPOTENTIAL IN SPHERICAL HARMONICS

P BIRÓ¹ and N C THÔNG¹

[Manuscript received March 1, 1985]

Time variations of the earth's gravity field can mathematically be described by the variation in geopotential. This latter is determined by the solution of the third boundary value problem of potential theory for time variations if observed variations in gravity and in height are available at surface stations. A possible way to solve this problem is presented by using spherical harmonic expansion. The solution results in the determination of the time variation of the fully normalized spherical harmonic coefficients of the geopotential. After having numerically determined the spherical harmonic expansion of the variation in geopotential its geodetic effects such as the variation in geoid undulation and in direction of the local vertical can be computed. Numeric experiences of model computations are demonstrated. The determination of the variation in geopotential enables us to compute the true surface movements if repeated observations of the natural coordinates of stations will be available.

Keywords: boundary value problem; gravity field; secular variation; spherical harmonics of geopotential; surface movements

Time variation of the earth's gravity field will be mathematically described by the variation δW in geopotential. This latter can be determined by the solution of the third boundary value problem of the potential theory for time variations if boundary values of the variation δg^* in gravity and δH in height of stations in a world-wide net are known. One kind of the solutions of this problem is that by the appropriate use of Stokes' integral formula as it has been shown by several authors.

Now, we are going to demonstrate another kind of solution of the problem mentioned before, using spherical harmonics.

It will be assumed that time variations in geopotential in relatively short time (in several decades) are induced merely by a rearrangement of the earth's masses and the effect of the secular variation in the angular velocity of the earth's rotation can be neglected. (For longer periods this latter can separately be regarded.)

In this case the variation δW in geopotential is the change in gravitational potential of the earth's masses and therefore Laplace's equation

$$\operatorname{div} \operatorname{grad} \delta W = \Delta \delta W = \frac{\partial^2}{\partial x^2} \delta W + \frac{\partial^2}{\partial y^2} \delta W + \frac{\partial^2}{\partial z^2} \delta W = 0 \quad (1)$$

is valid for the outer space. This means δW to be a harmonic function.

¹ Department of Geodesy, Institute of Geodesy, Surveying and Photogrammetry, Technical University of Budapest, H-1521 Budapest

The general solution of this homogeneous, linear, partial differential equation of second order can be constructed by the difference in the spherical harmonic expansions of the gravitational potential V at the epochs t and $t + \delta t$ as

$$\begin{aligned} \delta W(r, \vartheta, \lambda) &= V(r, \vartheta, \lambda)_{t+\delta t} - V(r, \vartheta, \lambda)_t = \\ &= \frac{kM}{r} \sum_{n=2}^{\infty} \left(\frac{a}{r}\right)^n \sum_{m=0}^n (\overline{\delta C}_{nm} \cos m\lambda + \overline{\delta S}_{nm} \sin m\lambda) \overline{P}_{nm}(\cos \vartheta) \end{aligned} \quad (2)$$

being r, ϑ, λ the spherical coordinates, kM the geocentric gravitational constant, a the semimajor axis of the earth, $\overline{P}_{nm}(\cos \vartheta)$ the fully normalized associated Legendre function of degree n and order m , $\overline{\delta C}_{nm}$ and $\overline{\delta S}_{nm}$ are the time variations of the fully normalized spherical harmonic coefficients of the geopotential.

These latter indicate the rearrangement of the earth's masses. If the mass displacements inside of the earth body are known (as for example in model computations) the time variations of the normalized harmonic coefficients can be computed by

$$\begin{aligned} \overline{\delta C}_{no} &= \frac{1}{\sqrt{2n+1}} \frac{1}{Ma^n} \left\{ \left[\iiint_{\text{earth}} (r')^n P_n(\cos \vartheta') dm \right]_{t+\delta t} - \right. \\ &\quad \left. - \left[\iiint_{\text{earth}} (r')^n P_n(\cos \vartheta') dm \right]_t \right\} \end{aligned} \quad (3a)$$

and

$$\begin{aligned} \left[\frac{\overline{\delta C}_{nm}}{\overline{\delta S}_{nm}} \right] &= \sqrt{\frac{(n+m)!}{2(2n+1)(n-m)!}} \cdot \frac{(n-m)!}{(n+m)!} \cdot \frac{2}{Ma^n} \cdot \\ &\quad \cdot \left\{ \left[\iiint_{\text{earth}} (r')^n P_{nm}(\cos \vartheta') \begin{bmatrix} \cos m\lambda' \\ \sin m\lambda' \end{bmatrix} dm \right]_{t+\delta t} - \right. \\ &\quad \left. - \left[\iiint_{\text{earth}} (r')^n P_{nm}(\cos \vartheta') \begin{bmatrix} \cos m\lambda' \\ \sin m\lambda' \end{bmatrix} dm \right]_t \right\} \end{aligned} \quad (3b)$$

being r', ϑ', λ' the spherical coordinates of the mass element dm of the earth's body.

The more general case is if the coefficients are to be determined by observations at a limited number of stations at the earth's surface.

For the sake of the numeric determination of the unknown coefficients $\overline{\delta C}_{nm}$ and $\overline{\delta S}_{nm}$ the boundary condition

$$\frac{\partial}{\partial r} \delta W + \frac{2}{r} \delta W = -(\delta g^* + \frac{2g}{r} \delta H) \quad (4)$$

for the displaced equipotential surface of the earth's gravity field (Bíró 1983: 245.8) or the same in spherical harmonics

$$\delta g^* + \frac{2g}{r} \delta H = \frac{1}{r} \sum_{n=0}^{\infty} (n-1) \left(\frac{R}{r}\right)^{n+1} \delta W_n(\vartheta, \lambda) \quad (5)$$

can be constructed disregarding the horizontal gravity gradient, being R the earth's mean radius and $\delta W_n(\vartheta, \lambda)$ Laplace's surface harmonic of degree n . This latter can be taken from the surface spherical harmonic expansion of δW for the sphere with radius R being

$$\delta W(\vartheta, \lambda) = \frac{kM}{R} \sum_{n=2}^{\infty} \sum_{m=0}^n (\overline{\delta C}_{nm} \cos m\lambda + \overline{\delta S}_{nm} \sin m\lambda) P_{nm}(\cos \vartheta) \quad (6)$$

with the approximation $a \doteq R$. In fact this is the spherical harmonic expansion of the variation in potential at the geoid.

Let us replace the term of degree n of the spherical harmonic expansion (6) for $\delta W_n(\vartheta, \lambda)$ in (5) then the following result is obtained:

$$\delta g^* + \frac{2g}{r} \delta H = \frac{kM}{r^2} \sum_{n=2}^{\infty} (n-1) \left(\frac{R}{r}\right)^n \sum_{m=0}^n (\overline{\delta C}_{nm} \cos m\lambda + \overline{\delta S}_{nm} \sin m\lambda) \overline{P}_{nm}(\cos \vartheta). \quad (7)$$

Having a finite number of *observed variations* δg^* and δH at the earth surface equations as (7) can serve as *observation equations* for the determination of a finite number of unknowns. The system of equations can be solved for the coefficients $\overline{\delta C}_{nm}$ and $\overline{\delta S}_{nm}$.

Replacing the computed fully normalized harmonic coefficients into the observation equations (7), a mean square error of the process can be determined.

The numeric values of the fully normalized harmonic coefficients determined by this way can be replaced in (2) or in (6) and the time variation δW in geopotential can be computed for the earth's surface or for the geoid.

With known changes in geopotential the *geodetic effects* of the time variation of the earth's gravity field can be computed.

The vertical displacement δN of the equipotential surfaces (or the variation in geoid undulation) can be determined by using Bruns' formula for time variations with the approximation $a \doteq r \doteq R$ as

$$\delta N = \frac{\delta W}{g} \doteq R \sum_{n=2}^h \sum_{m=0}^n (\overline{\delta C}_{nm} \cos m\lambda + \overline{\delta S}_{nm} \sin m\lambda) P_{nm}(\cos \vartheta) \quad (8)$$

with h a finite number of degree.

The change $\delta \Theta$ in direction of the local vertical can be determined in meridian and in prime vertical components as derivatives of the variation (8) in geoid undulation

as

$$\delta\Theta = \begin{bmatrix} \delta\Theta_\Phi \\ \delta\Theta_A \end{bmatrix} = \begin{bmatrix} \frac{1}{gR} \frac{\partial}{\partial\vartheta} \delta W \\ -\frac{1}{gR \sin\vartheta} \frac{\partial}{\partial\lambda} \delta W \end{bmatrix} \quad (9)$$

or in spherical harmonic expansions as

$$\delta\Theta_\Phi = \delta\Phi \doteq \sum_{n=2}^h \sum_{m=0}^n (\overline{\delta C}_{nm} \cos m\lambda + \overline{\delta S}_{nm} \sin m\lambda) \frac{\partial}{\partial\vartheta} P_{nm}(\cos\vartheta) \quad (10a)$$

$$\delta\Theta_A = \delta A \cos\Phi \doteq -\frac{1}{\sin\vartheta} \sum_{n=2}^h \sum_{m=0}^n m(\overline{\delta S}_{nm} \cos m\lambda - \overline{\delta C}_{nm} \sin m\lambda) P_{nm}(\cos\vartheta) \quad (10b)$$

with Φ , A and $\delta\Phi$, δA the astronomic (natural) coordinates and their time variations.

In lack of practical observations, *model computations* have been carried out. The geodynamic model by Barta (1985) has been used. He has expressed the vertical shift of the equipotential surface at a height of 6000 km above sea level as the effect of the displacing deep inhomogenities of the earth's masses by the sum of two simple zonal spherical harmonic expansions of degree 8 with the poles P_1 , P_2 and he has computed the harmonic coefficients A_n , B_n and the coordinates of the poles as well.

By using Barta's results, a formula for the *time variation δg of the gravity at sea level* has been constructed as

$$\delta g^*(\vartheta, \lambda) = \frac{kM}{R^3} \sum_{n=2}^8 (n-1) \left(\frac{r}{R}\right)^{n-1} \{A_n [P_n(\cos\beta_1)_{t+\delta t} - P_n(\cos\beta_1)_t] + B_n [P_n(\cos\beta_2)_{t+\delta t} - P_n(\cos\beta_2)_t]\} \quad (11)$$

being $R=6371$ km the earth's radius, $r=12371$ km, β_1, β_2 the polar angles of the arbitrary point $P(\vartheta, \lambda)$ referring to the actual location of the poles P_1 and P_2 at the epochs t and $t+\delta t$ (Thông 1985, Biró et al. 1985).

Gravity variations (per year) at the geoid computed by (11) as simulated observations in a $10^\circ \times 10^\circ$ grid net (in 612 stations) served as one kind of input data for our further computations.

As the other kind of input data the *variation in height $\delta H=0$* has been accepted for the geoid.

By using this set of input data as simulated observations totally 612 *observation equations* as

$$\delta g^* = \frac{kM}{R^2} \sum_{n=2}^h (n-1) \sum_{m=0}^n (\overline{\delta C}_{nm} \cos m\lambda + \overline{\delta S}_{nm} \sin m\lambda) \overline{P}_{nm}(\cos\vartheta) \quad (12)$$

Table I

n	m	$\overline{\delta C}_{nm}$	$\overline{\delta S}_{nm}$
2	0	0.65254967D-23	—
2	1	0.51429758D-10	-0.36684490D-10
2	2	-0.15710007D-07	-0.16997998D-07
3	0	0.21977910D-25	—
3	1	0.62191859D-09	-0.98039896D-08
3	2	-0.10146989D-07	-0.34938885D-08
3	3	0.19475958D-07	-0.94606601D-08
4	0	-0.34623425D-24	—
4	1	0.44074349D-09	-0.31437928D-09
4	2	-0.76079794D-09	-0.11631648D-08
4	3	-0.45227171D-09	-0.15268437D-08
4	4	0.63150282D-08	-0.17146898D-08
5	0	-0.41136190D-24	—
5	1	-0.43445608D-09	-0.13220028D-08
5	2	-0.22327063D-08	-0.76878244D-09
5	3	0.36076027D-08	0.87585393D-09
5	4	-0.29678435D-08	0.37986664D-08
5	5	-0.15588383D-07	0.25592368D-08
6	0	-0.61042083D-24	—
6	1	0.43764657D-11	-0.31217027D-11
6	2	-0.54579955D-09	-0.58406191D-09
6	3	-0.49245867D-11	-0.16625126D-10
6	4	0.17191991D-08	0.11745744D-09
6	5	-0.31024969D-10	-0.13545794D-11
6	6	-0.26680969D-08	0.21132485D-08
7	0	0.46187405D-24	—
7	1	-0.16635772D-09	-0.74603694D-10
7	2	-0.48088797D-09	-0.16558301D-09
7	3	0.52056510D-09	0.49333513D-09
7	4	-0.72024088D-09	0.92186628D-09
7	5	-0.84714069D-09	0.26157156D-09
7	6	0.10904541D-08	0.16791520D-08
7	7	0.96953556D-11	0.58789215D-09
8	0	0.11008136D-24	—
8	1	-0.19723299D-09	0.14068493D-09
8	2	0.53473322D-09	0.25161090D-09
8	3	0.23837326D-09	0.80473464D-09
8	4	0.16281761D-09	-0.58648604D-09
8	5	0.17532292D-08	0.76547639D-10
8	6	0.21792097D-09	-0.49842479D-09
8	7	0.10992945D-08	-0.27907217D-08
8	8	0.27316658D-08	0.87194817D-10

for the geoid have been constructed. They have been solved by the method of the least squares for the unknown variations in fully normalized harmonic coefficients $\overline{\delta C}_{nm}$, $\overline{\delta S}_{nm}$ in several variants.

As Variant 1 77 unknown coefficients to degree and order $n=m=8$ have been computed. The results are given in Table I.

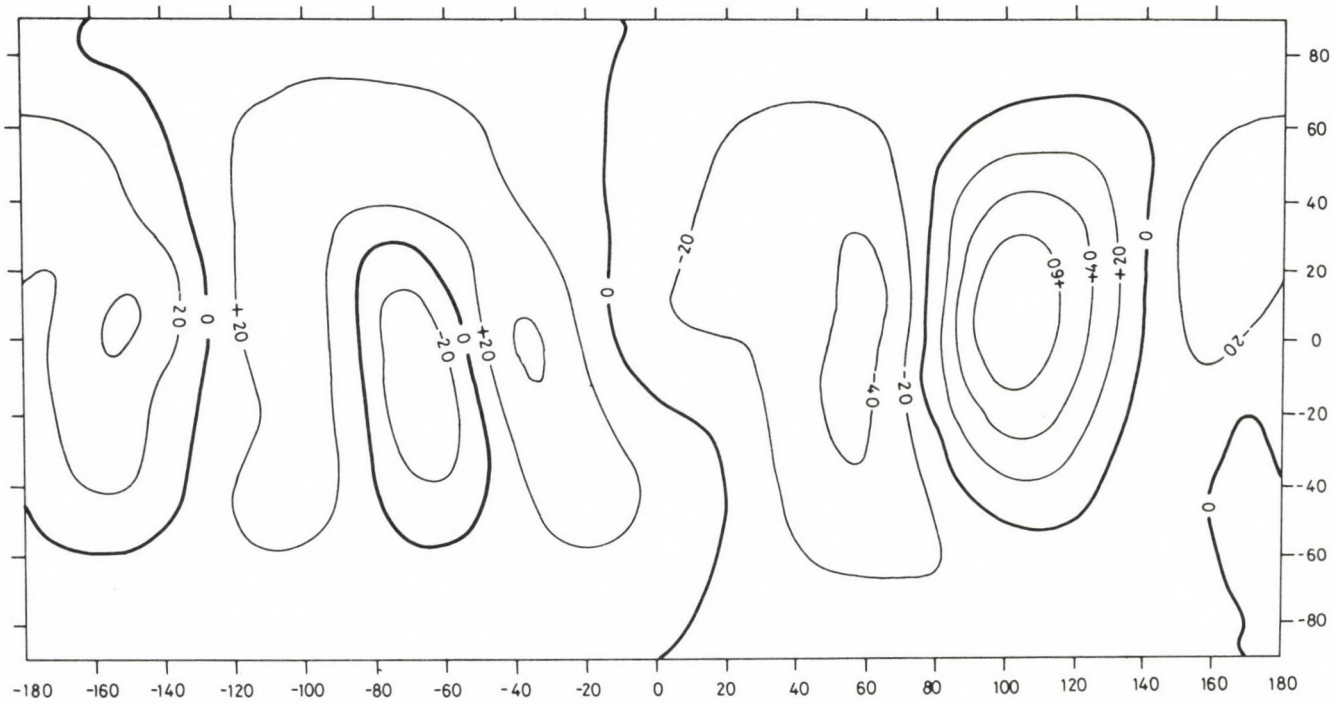


Fig. 1. The global distribution of the variation δN in geoid undulation as computed by the model. Contour intervals are 20 cm/a

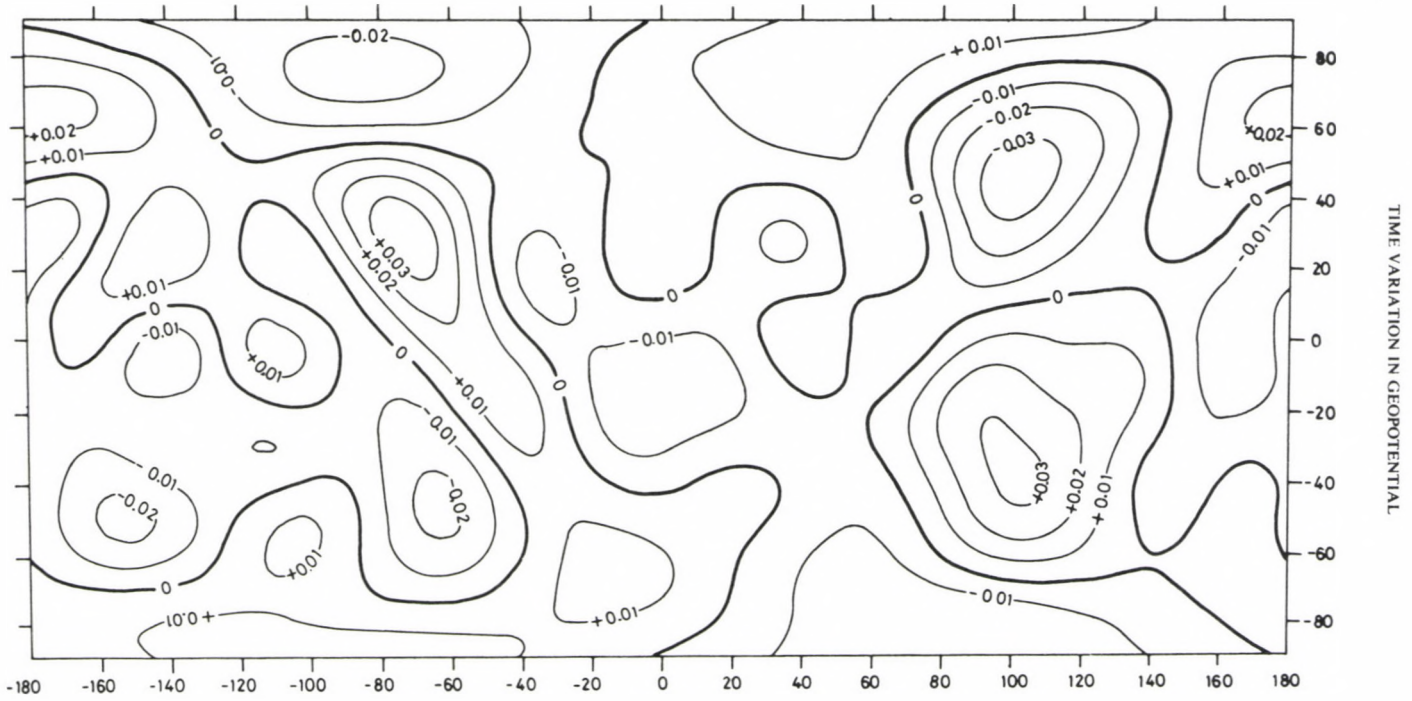


Fig. 2. The global distribution of the meridian component $\delta\Theta_{\phi}$ of the variation in the direction of the local vertical as computed by the model. Contour intervals are 10^{-2} arcseconds/a

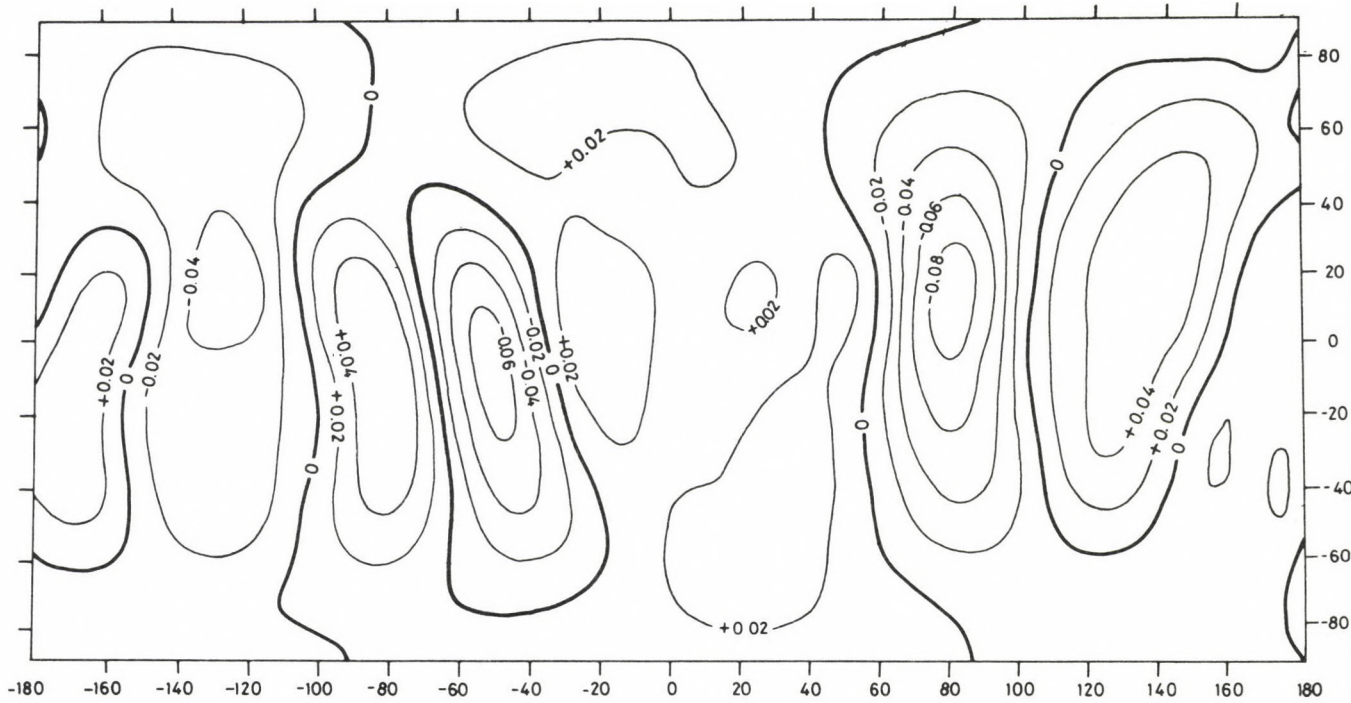


Fig. 3. The global distribution of the East-West component $\delta\theta_A$ of the variation in direction of the local vertical as computed by the model. Contour intervals are 2×10^{-2} arcseconds/a

The variations of the harmonic coefficients of order $m=0$ (the zonal harmonic coefficients) are in fact zeros because of the inner structure of the model (i. e. mass displacements are assumed around the axis of earth's rotation).

The computed variations in the normalized harmonic coefficients have been replaced into the observation equations (12) and the root mean square error of the spherical harmonic expansion $m_{\delta g} = \pm 5.5$ microgals/year (i.e. in $10^{-8} \text{ ms}^{-2}/\text{a}$) has been computed.

By replacing the harmonic coefficients $\overline{\delta C_{nm}}$ and $\overline{\delta S_{nm}}$ into (8), (10) and (11) the *geodetic effects*, i.e. the variations δN in geoid undulation and $\delta\Theta_\phi, \delta\Theta_A$ in direction of the local vertical could be computed. Their global distributions are demonstrated in Figs 1, 2 and 3.

Variations δN in geoid undulation computed by (8) could be compared with that of the model given by Barta (1985) and a root mean square deviation $m_{\delta N} = \pm 2 \text{ cm/a}$ has been got.

For the variation $\delta\Theta$ in direction of the local vertical there have been no computations before, therefore our results could not be compared with any standard. The result of our computations by formulae (10) in Variant 1 has been accepted as the standard for comparison of the result of calculations in other variants.

The model computations have been repeated in several other variants with less number of simulated observations and to lower degree and order of the spherical harmonic expansion. In all variants also the root mean square deviations $m_{\delta g}, m_{\delta N}, m_{\delta\Theta_\phi}$ and $m_{\delta\Theta_A}$ from the standard have been computed. The results are tabulated in Table II.

The results in Table II demonstrate that 162 stations in $20^\circ \times 20^\circ$ distribution (Variant 2) are as sufficient as even more ones for the spherical harmonic expansion to degree and order 8,8. An acceptable global distribution of the geodetic effects of the time variation of the earth's gravity field can be determined by using 36 observations in $60^\circ \times 30^\circ$ distribution around the earth (Variant 7). Rather good numeric results can be achieved by a world-wide gravity net of 84 stations in $30^\circ \times 30^\circ$ distribution and a spherical harmonic expansion to degree and order 6,6 (Variant 6).

Table II

Serial number	n, m	Density	Number of coefficients	Number of stations	$m_{\delta g}$ 10^{-8} ms^{-2}/a	$m_{\delta N}$ cm/a	$m_{\delta\Theta_\phi}$ 10^{-3} arcsec/a	$m_{\delta\Theta_A}$ 10^{-3} arcsec/a
1	8.8	$10^\circ \times 10^\circ$	77	612	5.5	2.0	—	—
2	8.8	$20^\circ \times 20^\circ$	77	162	5.5	2.0	—	—
3	8.8	$30^\circ \times 20^\circ$	77	126	6.5	2.0	0.95	0.64
4	7.7	$40^\circ \times 20^\circ$	60	90	42.3	7.8	—	—
5	6.6	$40^\circ \times 20^\circ$	45	90	42.8	6.5	8.0	9.2
6	6.6	$30^\circ \times 30^\circ$	45	84	38.8	5.6	4.9	9.2
7	5.5	$60^\circ \times 30^\circ$	32	36	46.3	9.1	7.9	11.4
8	4.4	$60^\circ \times 40^\circ$	21	27	84.8	17.2	11.6	23.3

A comparison of the results of our recent model computation with that of Weisz (1985) (Biró et al. 1984) the results for variation δN in geoid undulation as computed by spherical harmonic expansion seem to be significantly more accurate than those computed by the appropriate use of Stokes' integral formula using the same number of simulated observations.

After having repeatedly observed the stations of the *International Absolute Gravity Base Network* formulae (7), (8) and (10) enable us to determine the *true surface displacements* of earth's surface stations in which the variations $\delta\Phi^*$, δA^* and δH in natural coordinates will have been observed as

$$\overline{\delta v} = \begin{bmatrix} \delta x_1 \\ \delta x_2 \\ \delta x_3 \end{bmatrix} = \begin{bmatrix} R & 0 & 0 \\ 0 & R & 0 \\ 0 & 0 & 1 \end{bmatrix} \begin{bmatrix} \delta\Phi^* - \delta\Theta_\phi \\ \delta A^* \cos \Phi - \delta\Theta_A \\ \delta H + \delta N \end{bmatrix} \quad (13)$$

with $\delta\Phi^* = \Phi(t + \delta t) - \Phi(t)$, $\delta A^* = A(t + \delta t) - A(t)$ and $\delta H = H(t + \delta t) - H(t)$ the differences in observed natural coordinates of the station in the epochs t and $t + \delta t$. (The effect of the polar motion must be regarded in Φ and A .)

The resultant

$$\overline{\delta s} = \begin{bmatrix} \delta x_1 \\ \delta x_2 \end{bmatrix} \quad (14)$$

of the first and second components of (13) indicate the *true horizontal displacement* of the station and the component δx_3 represents the *true vertical surface movement*.

References

- Barta Gy 1985: Some properties of the Earth's core looked upon on the basis of investigations of the force fields of the Earth. *Acta Geod. Geoph. Mont. Hung.* 20, 29–60.
- Biró P 1983: Time variation of height and gravity. *Sammlung Wichmann*, Vol. 14, Wichmann, Karlsruhe and Akadémiai Kiadó, Budapest
- Biró P, Thõng N C, Weisz E 1984: A contribution to the network design of the International Absolute Gravity Base Net. Circular letter to the members of the SSG 3.87 IAG. Budapest
- Biró P, Thõng N C, Weisz E 1985: Modeling of secular variations in gravity and in geoidal undulations. *Periodica Polytechnica C.E.* (in press)
- Heiskanen W A, Moritz H 1967: *Physical geodesy*. Freeman and Co., San Francisco and London
- Thõng N C 1985: Modellszámítások a nehézségi erõtér idõbeli változására (Modeling of secular gravity variation). *Geodézia és Kartográfia*, 37, 94–100.
- Torge W 1980: *Geodesy*. Walter de Gruyter, Berlin, New York
- Weisz E 1985: Modellszámítások a valódi függõleges felszínmozgások meghatározására (Modeling of true vertical surface movements). *Geodézia és Kartográfia*, 37, 101–105.

OPTIMUM DOPPLER POSITIONING

L BÁNYAI¹

[Manuscript received April 9, 1985]

Based on features of the GEODOP-III program and of Broadcast Ephemeris, a new data processing concept is presented. According to this method the receiver parameters or their differences are estimated from the Doppler observations providing an optimum multipoint solution in a relative sense.

Processing the observations of the 2nd Doppler Calibration Campaign at the Satellite Geodetic Observatory Penc and the observations between the Observatory Graz-Lustbühel and the Geodynamic Station Sopron-Alomhegy, the method proved to be an effective tool for receiver comparison and optimum relative Doppler positioning.

Keywords: Broadcast Ephemeris; Doppler Calibration Campaign; Doppler positioning; Graz-Lustbühel observatory; Penc observatory; Sopron-Alomhegy observatory

1. Introduction

According to one of the usual procedures in the satellite Doppler positioning the Broadcast or Precise Ephemeris is relaxed at the specified level in the semi-short-arc data reduction programs.

In this method the accuracy of point positioning and the coordinate system are defined by the used observations and by the ephemeris system. Experiences from permanent observations show that the geocentric coordinates can be derived with an accuracy better than ± 1 m and ± 3 m using Precise and Broadcast Ephemeris, respectively (Schluter et al. 1982, Ádám 1982).

Accuracy of coordinate differences higher by one order of magnitude can be achieved using multipoint solution where the simultaneous observations of different stations are evaluated in a common adjustment. In a relative sense a great part of orbit errors are eliminated from the solution and the accuracy depends on the proper knowledge of receiver parameters included in the reduction program.

Recently some papers were published dealing with receiver investigations based on different ideas (Archinal 1982, Rinner and Pesec 1982, Mihály et al. 1982, Fejes 1983, Dietrich and Lehmann 1984).

In the following another method will be summarized which is based on features of GEODOP-III program and on the special statistical treatment of suitable Broadcast passes (Bányai 1984a, 1984b).

¹ Geodetic and Geophysical Research Institute of the Hungarian Academy of Sciences H-9400 Sopron P.O.B. 5.

2. Principle of the method

2.1 Theoretical background

The GEODOP-III program (Kouba and Boal 1976) can be regarded as “condition adjustment” and the adjusted quantities are obtained as

$$Z_a = Z_0 + \zeta$$

where Z_0 is the approximate value and ζ is the random walk variable. In the adjustment an *a priori* weight

$$P = \frac{1}{\sigma^2}$$

can be assigned to each quantity where σ is the variance of the variable ζ .

If the different approximate values and weights are known and a great number of suitable passes have been observed, it can be supposed before the adjustment according to the central limit theorem that ζ is an independent random walk variable with normal distribution and its expected value is zero:

$$N(0, \sigma).$$

Using the series of the random walk variables realized by the adjustment as statistical samples, the mean (\bar{x}) and standard deviation ($\bar{\sigma}$) can be computed as an estimation of the expected values and variances. Based on the parameters

$$N(0, \sigma) \quad \text{and} \quad N(\bar{x}, \bar{\sigma})$$

different tests of fit can be used to investigate the distribution of adjusted quantities.

The aim is to determine the *a priori* approximate values and weights having real physical meanings, so that they can assure a normal distribution of the investigated quantities at least at a probability level of 99 percent.

The independence of parameters are expressed by diagonal weight matrices. The intermittently integrated Doppler counts as basic quantities observed with precise oscillators can be approximated by a diagonal weight matrix (Kouba 1983).

In this approach the distribution of used passes, through the distribution of orbit bias parameters assigned to Broadcast Ephemeris in the adjustment, has a basic importance. Therefore, to reduce the influence of systematic orbit errors (to make it random-like) and to satisfy the preliminary statistical expectations the following selection principles should be taken:

- a) very noisy passes should be rejected,
- b) elevations of closest approach point should be over 15 degrees (tropospheric effect),
- c) elevations of closest approach points should be less than 80 degrees (ill condition of normal equation in the single point solution),
- d) only one pass should be taken from one ephemeris injection (relative independence of passes),

e) a great number of well-balanced passes with respect to the four principal directions NW, NE, SW, SE and to the elevation angles have to be taken. According to the number of simultaneous passes available, the conditions *d* and *e* may be reduced by the same number of passes in the opposite directions NE-SW, NW-SE or by the same number of south-going and north-going passes.

For practical application of this concept the simultaneous observations of different stations are evaluated in the single point solutions using the series of preliminary approximate values and weights chosen between realistic limits. Comparing the results of the statistical investigations the most suitable values can be found and the relevant receiver parameters can be estimated according to the next procedure.

2.2 Sequence of processing steps

When preparing the investigations, preliminary receiver parameters and program options are chosen, the observations are selected, and the preliminary station coordinates are determined. Based on these values, a cleaned and merged input data file is used in the following steps as usual in GEODOP data processing.

In the first step the weights of receivers are investigated. If the different receivers are weighted properly in the single point solutions the μ_0 standard deviations of unit weight and the μ estimations of range rate standard deviation (Archinal 1982) should be nearly equal and should assure the normal distribution of Doppler count residuals at the specified level.

The next investigated receiver parameter is the delay as an approximate value. In the GEODOP single point solution the delay cannot be distinguished from the orbit along-track bias. Their systematic effects are apportioned according to the assigned weights only. Therefore, from the investigation of the functional relation between the preliminary delay and the sample mean of orbit along-track bias the delay differences can be estimated. In the choice of absolute values, one of them can be fixed or the functional relation between the preliminary delay and corresponding statistics of the test of fit for Doppler count residual may help.

The receiver frequency offset as approximate value is still determined which can be obtained accurately from the GEODOP-III itself. The frequency drift can be estimated from the post processing of frequency offsets only.

If the estimated receiver parameters are far from the preliminary ones, the procedure should be iterated.

2.3 Separation of receivers

Besides the theoretical limiting factors, the effectiveness of this method depends on the separation of investigated receivers. From this point of view two different arrangements can be distinguished.

The first is the so-called calibration arrangement where the receivers are installed together at a suitable site near a geodetic control (0–100 m, short baseline

translocation). The geometric relations between the receivers and the used passes, the ionospheric and tropospheric conditions are practically the same, consequently (apart from the possible disturbing ground reflection) the differences of observations besides the separation come from the receivers themselves. Using the geodetic control measurements as errorfree centering elements, the receiver antenna phase center characteristics can also be investigated.

In the second arrangement the observations of sufficiently separated stations (50–200 km) are analyzed where the benefits of simultaneity are still considerable. While the results contain the influence of different external circumstances at different stations and the receiver conditions in the observation period, the limiting factor is the station separation. However, the estimated parameters in the multipoint solutions can give the optimum solution best fitting to the used observations.

3. Practical investigations

In order to test the effectiveness of the presented method both separation arrangements were investigated by using the observations of the 2nd Doppler Calibration Campaign at the Satellite Geodetic Observatory Penc (DCCP-2) Hungary Sept. 26–Oct. 1, 1983 and the simultaneous observations between the Observatory Graz-Lustbühel and the Geodynamic Station Sopron-Alomhegy from day 219 till 247 in 1979 (Bányai 1984a). In the following the results of this investigation will be summarized.

3.1 Calibration measurements

The description of the investigated receivers of DCCP-2 is presented in Table I.

Due to the relatively short observation period, the limiting factor of this investigation stems from the statistical weakness of the simultaneous passes available. Therefore, in the rigorous selection principle the conditions d and e have been reduced to the same number of passes in the opposite directions NE-SW and NW-SE. The configuration of 24 selected passes (4 days of observations) is shown in Fig. 1.

Table I. Description of the investigated receivers 2nd Doppler Calibration Campaign Penc, 1983

Type	Ser. No.	Owner	Site	Centering elements referring to 6 S (m)		
				ΔN	ΔE	ΔH
JMR 4A	No. 159	GEOCART POLAND	6 SW	0.00	2.00	-0.62
JMR 4A	No. 293	GEOCART POLAND	6SE	0.00	-2.00	-0.62
JMR 4A	No. 294	GEOCART POLAND	6S	0.00	0.00	-0.62
JMR 1A	No. 547	SGO HUNGARY	6	-2.00	0.00	-0.62

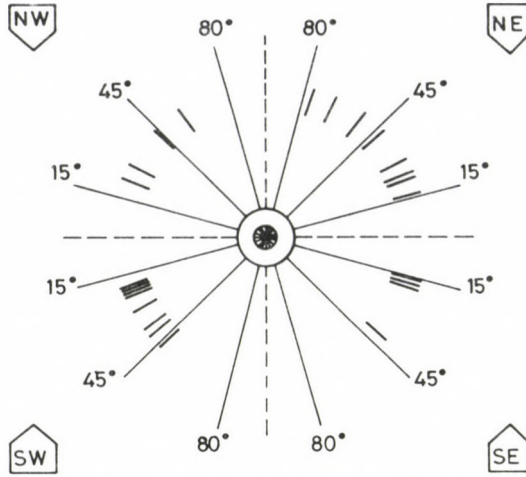


Fig. 1. Configuration of passes with respect to principal directions and elevation angles

In this investigation the results of Bányai (1984b) are treated as preliminary ones and the cleaned and merged input data file is used as described in Chapter 1.2.

The results of the weight investigation are summarized in Fig. 2a, b, c. The statistics of the Kolmogorov test of fit for the Doppler count residual $[K(v)]$ further the values μ_0^2 and μ^2 are plotted *vs.* receiver weight P . In case of the chosen weights 39, 45, 51, 50 the values μ^2 are equal and the values μ_0^2 are similar. The Doppler count residuals have a normal distribution at a probability level of 95 percent and the variances 0.160, 0.149, 0.140, 0.141 count corresponding to these weights are realistic ones.

The results of the delay investigation are summarized in Fig. 3a, b. The sample means of orbit along-track bias $[\bar{x}(\text{ALG})]$ and the statistics of the Kolmogorov test of fit for Doppler count residual $[K(v)]$ are plotted in function of delay (DLY). According to the estimated delay differences (ΔDLY) the absolute values 730, 460, 450, 310 μs have been chosen.

The *a priori* variances (constraints) of adjusted quantities, the estimated receiver weights, the delays and frequency offsets as approximate values and the statistics of the single point runs are summarized in Table II. The comparison of the statistics shows that the same kind of parameters have a similar statistical behaviour at different receivers.

To investigate the antenna phase differences, the phase centre coordinates coming from the multipoint solution using the estimated receiver parameters were centred to the site 6S as usual in geodetic practice. The coordinate differences from the mean (as from the most probable value) and their transformations into a topocentric (i.e. local) coordinate system (N, E, H) can be found in Table III.

Receiver pairs No. 159—No. 294 and No. 293—No. 547 have practically the same phase centre height but there is a significant difference between the two pairs. A phase centre exentricity in the coordinate E can be recognized for receiver No. 547. The

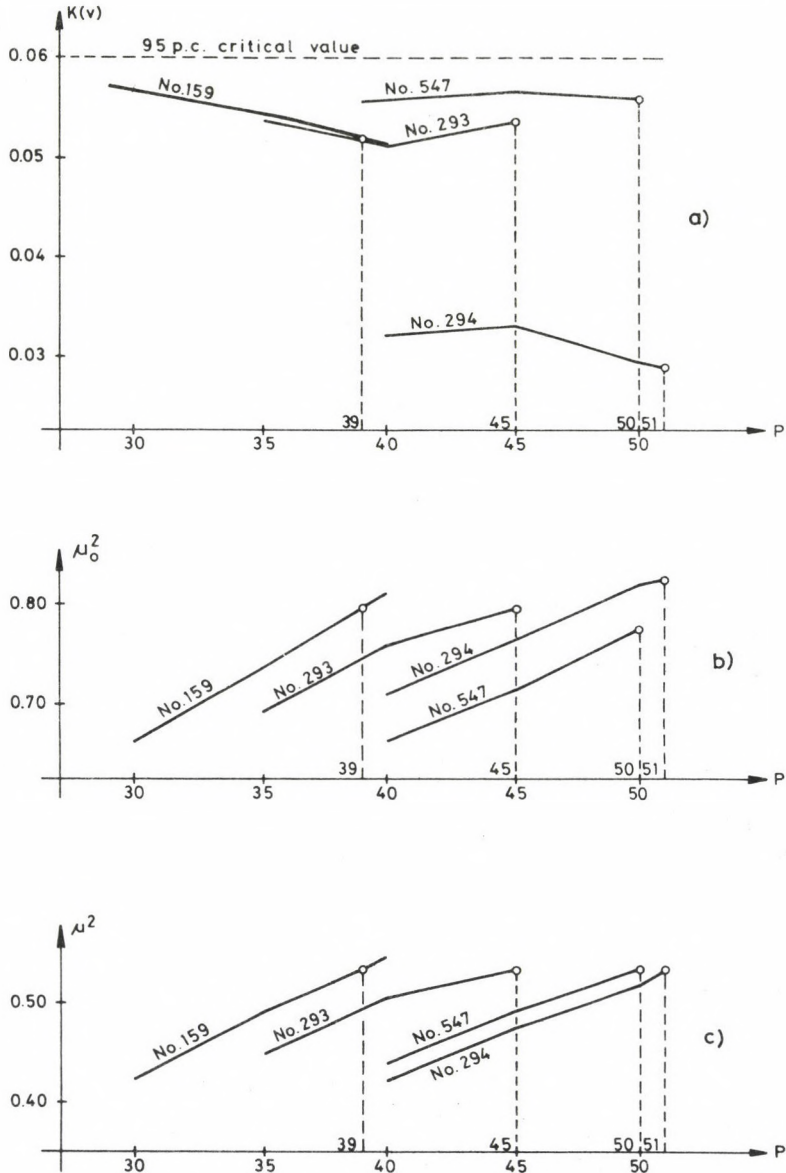


Fig. 2. Investigation of the receiver weight

investigation without this receiver (Table IV) shows clearly the uncertainty of mean phase centre realisation higher by one order of magnitude in the height component than in the *N, E* plane.

This investigation was repeated without receiver investigation where the receivers were weighted equally ($P=25$) and the main delay ($600 \mu s$) was used as usual

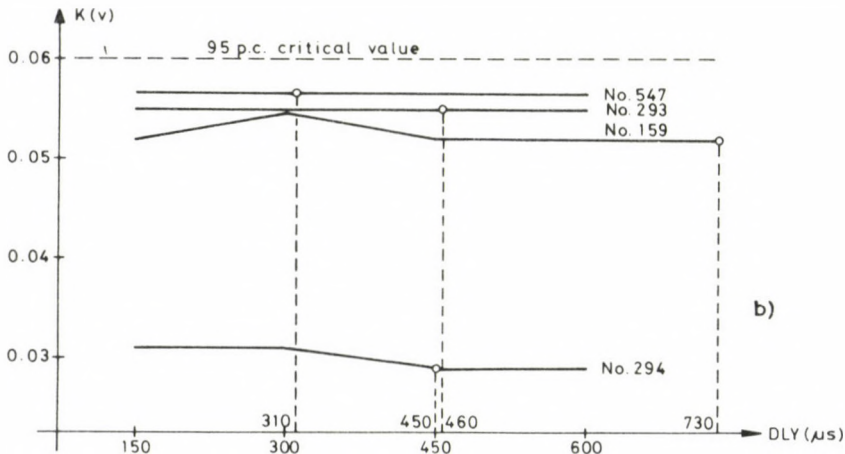
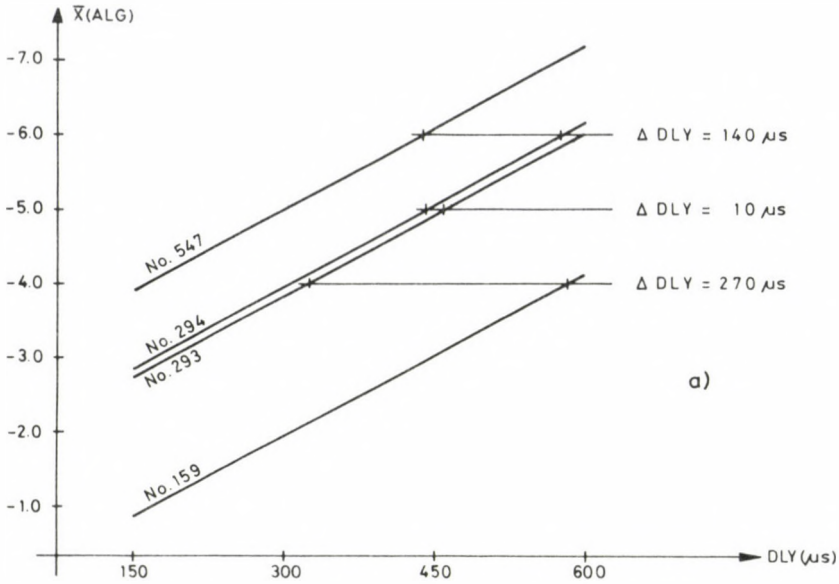


Fig. 3. Investigation of the receiver delay

when there was no sufficient knowledge about the receiver parameters (Table V). Besides the phase centre investigation, the geodetic distances between the receivers were compared in all combinations to the Doppler ones with and without receiver investigations (Table VI). The conclusions of this investigations prove the effectiveness of the method.

Table II. Parameters and statistics of single point runs

		<i>a priori</i> $\mu_0^2 = 1.4 \text{ count}^2$			σ coordinates = 3 m		
		$\sigma_{\text{ALG}} = 26.0 \text{ m}$ $\sigma_{\text{FRQ}} = 1.0 \text{ Hz}$		$\sigma_{\text{ACR}} = 5.0 \text{ m}$ $\sigma_{\text{DLY}} = 1.0 \cdot 10^{-4} \text{ s}$		$\sigma_{\text{OUT}} = 10.0 \text{ m}$ $\sigma_{\text{TRP}} = 10.0\%$	
REC.	No. 159	No. 293	No. 294	No. 547			
P	39 ($\sigma = 0.160 \text{ count}$)	45 ($\sigma = 0.149 \text{ count}$)	51 ($\sigma = 0.140 \text{ count}$)	50 ($\sigma = 0.141 \text{ count}$)			
DLY ₀	730 μs	460 μs	450 μs	310 μs			
FRQ ₀	-5.91 Hz	1.96 Hz	2.25 Hz	9.28 Hz			

Kolmogorov test of fit $N(\bar{x}, \bar{\sigma})$												
	\bar{x}	$\bar{\sigma}$	95%									
ALG	-5.08	10.91	Y	-5.09	12.05	Y	-5.07	11.83	Y	-5.04	11.92	Y
ACR	1.74	2.65	Y	1.86	2.95	Y	1.98	2.78	Y	2.00	3.00	Y
OUT	-4.75	9.33	Y	-4.85	9.46	Y	-4.72	9.39	Y	-4.91	9.57	Y
DLY	-0.56	1.24	Y	-0.65	1.53	Y	-0.62	1.36	Y	-0.78	1.55	Y
FRQ	0.00	0.14	Y	0.00	0.21	Y	0.00	0.16	Y	0.00	0.11	Y
TRP	8.69	15.35	Y	8.83	14.88	Y	10.98	16.27	Y	7.32	13.54	Y
V	0.00	0.12	Y	0.00	0.11	Y	0.00	0.10	Y	0.00	0.10	Y

$\mu_0 = 0.89$	$\mu = 0.73$	$\mu_0 = 0.89$	$\mu = 0.73$	$\mu_0 = 0.91$	$\mu = 0.73$	$\mu_0 = 0.88$	$\mu = 0.73$
----------------	--------------	----------------	--------------	----------------	--------------	----------------	--------------

abbreviations can be found in Table VII.

Table III. Phase centre differences (cm)

Rec. No	ΔX	ΔY	ΔZ	ΔN	ΔE	ΔH
No. 159	11	-5	16	5	-8	18
No. 293	-9	-7	-14	-1	-3	-18
No. 294	15	5	11	-4	0	19
No. 547	-15	7	-14	0	12	-18
r.m.s	15	7	16	4	9	21

Table IV. Phase centre differences (cm)

Rec. No	ΔX	ΔY	ΔZ	ΔN	ΔE	ΔH
No. 159	5	-3	12	5	-4	11
No. 293	-15	-5	-18	-1	0	-24
No. 294	9	7	7	-4	4	12
No. 547	-	-	-	-	-	-
r.m.s	13	6	16	4	3	21

Table V. Phase centre differences (cm) without receiver investigation

Rec. No	ΔX	ΔY	ΔZ	ΔN	ΔE	ΔH
No. 159	0	-34	34	31	-32	18
No. 293	-9	-5	-15	-2	-2	-18
No. 294	10	9	3	-7	5	11
No. 547	-1	30	-23	-22	29	-11
r.m.s	8	27	25	22	25	17

Table VI. Comparison of distances (m)

Distances	Geod.	with rec. inv.		without rec. inv.	
		Doppler	G-D	Doppler	G-D
6 SW-6 S	2.00	1.92	0.08	1.65	0.35
6 SW-6 SE	4.00	3.97	0.03	3.71	0.29
6 SE-6 S	2.00	2.07	-0.07	2.10	-0.10
6*-6 SW	2.83	2.75	0.08	2.89	-0.06
6*-6 S	2.00	2.00	0.00	2.17	-0.17
6*-6 SE	2.83	2.93	-0.10	3.18	-0.35

* phase centre excentricity

3.2 Determination of the traverse GRAZ—SOPRON

For the optimum determination of the traverse GRAZ—SOPRON by Doppler observations, the presented method has been applied, too. In that case there was no sufficient preliminary knowledge on receiver parameters because no common calibration measurement was made so far with the CMA-722B receiver in Graz and with the CMA-751 in Sopron.

While the separation between the two stations is a limiting factor, the great number of simultaneous observations available made possible the rigorous selection described in Chapter 2.1. The configuration of the 112 selected passes is shown in Fig. 4. The same procedure was applied as in the case of calibration. Here the results are only summarized.

The *a priori* variances (constraints) of adjusted quantities, the preliminary station coordinates, the estimated receiver weights, the delays and frequency offsets as approximate values and the statistics of the single point runs are summarized in Table VII. For the comparison of the statistics, the same kind of parameters show a similar statistical behaviour at the two stations.

The Doppler derived traverses coming from the single point and multipoint solutions using the estimated and the mean ($P=25$, $DLY_0=600 \mu s$) receiver parameters were compared to the traverse of $105\,335.81 \pm 0.06$ m derived between the two stations with precise geodetic measurements (Rinner 1981). The results are

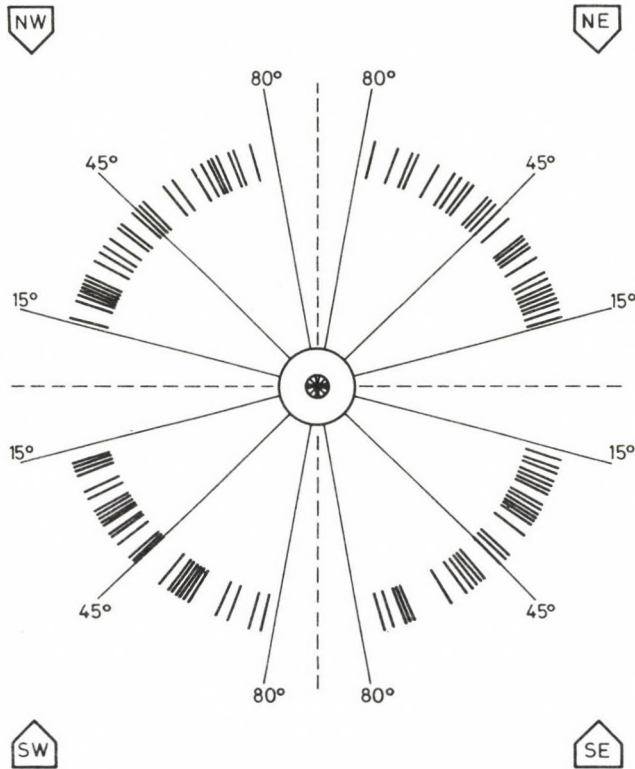


Fig. 4. Configuration of passes with respect to principal directions and elevation angles

summarized in Table VIII. The use of the estimated receiver parameters eliminated a great part of systematic errors and the traverses from single point and multipoint runs are practically the same as the geodetic traverse.

The trend of geodetic and Doppler traverse differences from different runs and the significantly higher consistency of the geodetic traverse prove the effectiveness of the method.

4. Conclusions

Summarizing the results of the investigations presented it is evident that the need for optimum network determinations by multipoint solution requires the proper knowledge of receiver parameters included in the reduction programs.

Using the calibration arrangement based on a relatively short observation period, different kinds of receivers can be compared without Precise Ephemeris and special observation arrangement. Preliminary receiver parameters can be estimated, and the receivers with significantly unic behaviour can be detected before the network observation.

Table VII. Parameters and statistics of single point runs

GRAZ	SOPRON
$X_0 = 4\,194\,433.0$ $\sigma = 3$ m	$X_0 = 4\,123\,990.0$ $\sigma = 3$ m
$Y_0 = 1\,162\,687.0$ $\sigma = 3$ m	$Y_0 = 1\,226\,072.0$ $\sigma = 3$ m
$Z_0 = 4\,647\,247.0$ $\sigma = 3$ m	$Z_0 = 4\,693\,249.0$ $\sigma = 3$ m
FRQ ₀ = 37.79 Hz	FRQ ₀ = -4.46 Hz
DLY ₀ = 310 μ s	DLY ₀ = 350 μ s
$P = 35$ ($\sigma = 0.169$ count)	$P = 45$ ($\sigma = 0.149$ count)

same values: *a priori* $\mu_0^2 = 1.4$ count²

$\sigma_{\text{ALG}} = 26.0$ m	$\sigma_{\text{ACR}} = 5.0$ m	$\sigma_{\text{OUT}} = 10.0$ m
$\sigma_{\text{FRQ}} = 1.0$ Hz	$\sigma_{\text{DLY}} = 1.0 \cdot 10^{-4}$ s	$\sigma_{\text{TRP}} = 10.0\%$

Kolmogorov test of fit

GRAZ CMA-722B						SOPRON CMA-751						
$N(0, \sigma)$		\bar{x}	$\bar{\sigma}$	$N(\bar{x}, \bar{\sigma})$		$N(0, \sigma)$		\bar{x}	$\bar{\sigma}$	$N(\bar{x}, \bar{\sigma})$		
95%	99%			95%	99%	95%	99%			95%	99%	
ALG	N	N	-4.00	23.51	Y	Y	N	N	-4.04	22.93	Y	Y
ACR	N	N	0.72	2.61	Y	Y	N	N	0.81	2.54	Y	Y
OUT	Y	Y	1.08	9.55	Y	Y	Y	Y	-0.05	7.47	Y	Y
DLY	N	N	-0.43	2.61	Y	Y	N	N	-0.45	2.50	Y	Y
FRQ	N	N	0.00	0.21	Y	Y	N	N	0.00	0.12	Y	Y
TRP	Y	Y	2.28	10.73	Y	Y	Y	Y	1.11	8.94	Y	Y
V	N	N	0.00	0.14	N	Y	N	N	0.00	0.12	N	Y
$\mu_0 = 0.96$ $\mu = 0.85$						$\mu_0 = 0.92$ $\mu = 0.83$						

abbreviations:

X, Y, Z	station coordinates	(m)
ALG	orbit along-track bias	(m)
ACR	orbit across-track bias	(m)
OUT	orbit out-of-plane bias	(m)
DLY	receiver delay	(10^{-4} s)
FRQ	receiver frequency offset	(Hz)
TRP	tropospheric bias	(%)
V	Doppler count residual	(count)
Y, N	data have a normal distribution (Y) or not (N) at the specified probability level	

The final processing of the network observations, using the procedure presented and the calibration results as preliminary values can give the optimum solution in a relative sense best fitting to the observations and to the external conditions of the observation sites.

Table VIII. Investigation of Doppler derived traverses

		$P=25$ DLY ₀ = 600 μ s	$P=25$ DLY ₀ = 600 μ s			
		GRAZ	SOPRON	GRAZ—SOPRON	TRAVERSE	G-D
SP	X	4 194 431.89 \pm 1.13	4 123 991.14 \pm 1.00	70 440.75 \pm 1.51	105 335.96 \pm 2.87	-0.15
	Y	1 162 686.61 \pm 0.79	1 226 070.77 \pm 0.69	-63 384.16 \pm 1.05		
	Z	4 647 245.76 \pm 0.96	4 693 248.09 \pm 0.83	-46 002.33 \pm 1.27		
MP	X	4 194 431.57 \pm 0.80	4 123 991.21 \pm 0.79	70 440.36 \pm 0.13	105 335.86 \pm 0.33	-0.05
	Y	1 162 686.82 \pm 0.66	1 226 070.86 \pm 0.65	-63 384.04 \pm 0.18		
	Z	4 647 245.58 \pm 0.68	4 693 248.45 \pm 0.69	-46 002.87 \pm 0.12		

		$P=35$ DLY ₀ = 310 μ s	$P=45$ DLY ₀ = 350 μ s			
		GRAZ	SOPRON	GRAZ—SOPRON	TRAVERSE	G-D
SP	X	4 194 431.86 \pm 1.23	4 123 991.38 \pm 1.18	70 440.48 \pm 1.70	105 335.79 \pm 3.25	0.02
	Y	1 162 686.64 \pm 0.86	1 226 070.74 \pm 0.81	-63 384.10 \pm 1.18		
	Z	4 647 245.76 \pm 1.05	4 693 248.21 \pm 0.99	-46 002.45 \pm 1.44		
MP	X	4 194 431.59 \pm 0.86	4 123 991.16 \pm 0.85	70 440.43 \pm 0.14	105 335.82 \pm 0.34	-0.01
	Y	1 162 687.01 \pm 0.74	1 226 070.91 \pm 0.73	-63 383.90 \pm 0.19		
	Z	4 647 245.71 \pm 0.73	4 693 248.59 \pm 0.75	-46 002.88 \pm 0.12		

abbreviations:

- X, Y, Z station coordinates (m)
 SP single point solution
 MP multipoint solution
 G-D geodetic-Doppler traverse

References

- Ádám J 1982: Statistical analysis of the Doppler coordinates derived at the SGO (in Hungarian). *Geodinform*, 13, 36—46.
- Archinal B 1982: A comparison of geodetic Doppler satellite receivers. Reports of the Department of Geodetic Science and Surveying, Report No. 340. The Ohio State University
- Bányai L 1984a: Investigation of receiver parameters in satellite Doppler positioning. In: *Proceedings of the International Symposium on Space Techniques for Geodynamics*. Sopron, Hungary, 253—264.
- Bányai L 1984b: Calibration of Doppler receivers. Presented at the INTERCOSMOS-COSPAR Conference, Karlovy Vary, Czechoslovakia
- Dietrich R, Lehmann K 1984: Interferometric analysis of Doppler measurements for differential receiver calibration. Presented at the INTERCOSMOS-COSPAR Conference Karlovy Vary, Czechoslovakia
- Fejes I 1983: The "Cross Doppler Count" method for comparison of Doppler receiver performances. *Bull. Geod.*, 57, 365—373.
- Kouba J 1983: A review of geodetic and geodynamic satellite Doppler positioning. *Reviews of Geophysics and Space Physics*, 21, 27—40.
- Kouba J, Boal J 1976: Program GEODOP. Manual Series Survey and Mapping Branch. Department of Energy, Mines and Resources Canada
- Mihály Sz, Fejes I, Ádám J, Bányai L, Varga M, Lehmann K, Raush E, Zubinskij V, Sergienko V 1982: The Doppler Calibration Campaigne Penc. Presented at the Intercosmos Scientific Conference of Section 6, Suzdal, USSR

- Rinner K 1981: Geodätische Verbindung der Observatorien Graz-Lustbühel und Sopron-Alomhegy. Österreichische Akademie der Wissenschaften. Mathematisch-naturwissenschaftliche Klasse. In: *Sitzungsberichte*, 446—467.
- Rinner K, Pesec P 1982: Über die Doppler-Kampagne TESTDOC im Testnetz Steiermark. *Österreichische Zeitschrift für Vermessungswesen und Photogrammetrie*, 70, 4—28.
- Schluter W, Blenski G, Herzberger K, Muller W, Stoger R 1982: Results from permanent Doppler observations at Wettzell using broadcast and precise ephemeris. In: *Proceedings of the Third International Geodetic Symposium on Satellite Doppler Positioning*. Physical Science Laboratory of the New Mexico State University

LABORATORY TEST OF CAPACITIVE PENDULUMS

GY MENTES¹

[Manuscript received April 12, 1985]

Horizontal pendulums, especially the capacitive ones, have an important role in tidal recording, in measurements of local deformations and lately in recording of the eigenvibrations of the Earth. Therefore, it is necessary to know the static and dynamic behaviour of the pendulums. The paper describes a fast laboratory test method for testing newly-made capacitive pendulums.

Keywords: capacitive pendulum; crapaudine; frequency response; impulse response; laboratory test; linearity; sensitivity; unit-step response

Introduction

The horizontal pendulums are calibrated automatically from time to time during the recording. Therefore, the aim of the test is not to calibrate the pendulum, but to control its parameters:

1. the sensitivity of the pendulum in the whole measuring range,
2. the linearity of the capacitive transducer,
3. the amplification factor of the electronics,
4. the damping factor,
5. the functions describing dynamic properties of the pendulums (frequency response, unit-step response, impulse response).

By measuring these listed parameters one can be assured if a newly-made pendulum works properly or it does not.

The construction of the tested pendulum

The tested pendulum type CP1 was developed in the Geodetic and Geophysical Research Institute of the Hungarian Academy of Sciences. It is a metal pendulum with Zöllner-type suspension and has metal suspension wires. Figure 1 shows a sketch of the pendulum from left and above. The pendulum consists of a very rigid base plate (1) which stands on a fixed foot (L) and on two levelling screws (L_1 , L_2) in the corners of a right-angled triangle. L_1 is the "sensitivity screw" and L_2 is the "drift screw". A fine adjusting screw (4, 19) belongs to each of the levelling screws, too. A bracket (8) with

¹ Geodetic and Geophysical Research Institute, Hungarian Academy of Sciences, Sopron, Hungary, H-9401, P.O.B.5

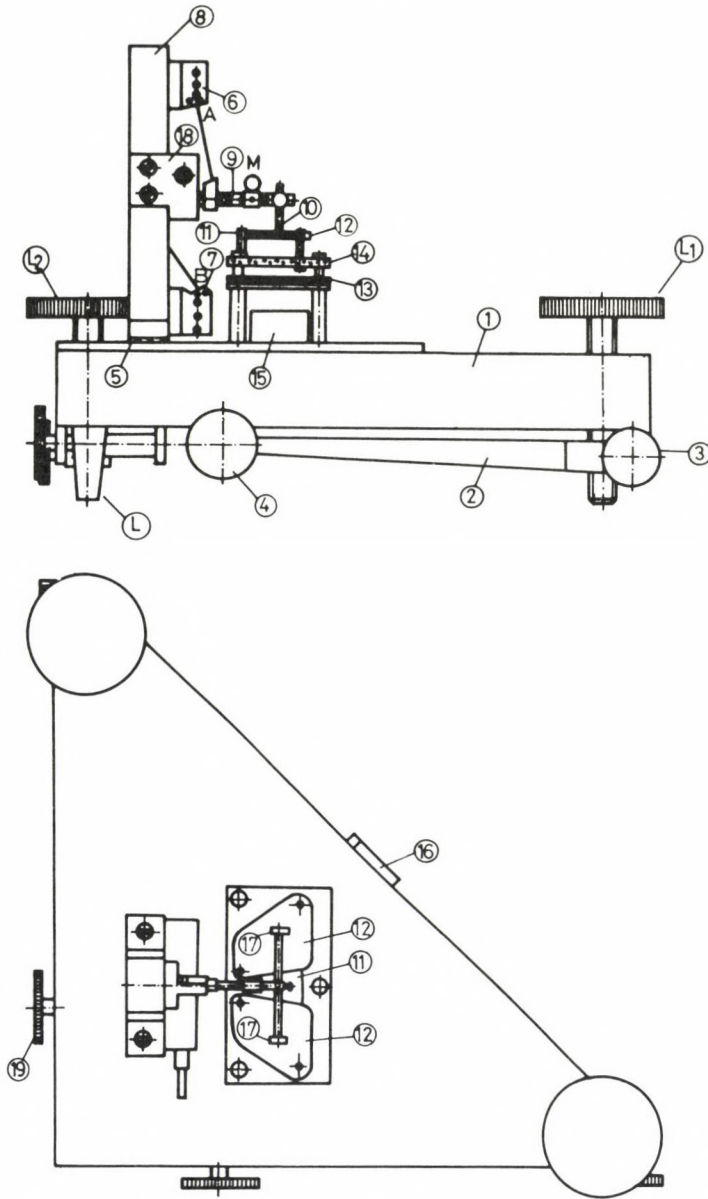


Fig. 1. The construction of the capacitive pendulum

clamps (6, 7) is on the base plate for the suspension wires (A, B) which hold the pendulum beam (9). The moving plate of the differential condenser (11) is fixed to the extremity of the pendulum beam. The connection is made metallicly, so the wires and the bracket form the lead-out of the capacitive transducer and therefore, the bracket must be insulated from the base plate by means of a glass plate (5).

The position of the standing plates (12) of the differential condenser which are also insulated from each other and from the base plate by means of a glass plate (14) can be adjusted by an adjustable console (13).

The capacitive transducer is connected to a bridge circuit which is supplied by a sine wave oscillator. The output voltage of the bridge after amplification is rectified by a phase-sensitive rectifier and recorded analogously (Mentes 1979, Mentes 1981).

The test method

Horizontal pendulums are very sensitive instruments, which makes it difficult to test them in laboratory. Figure 2 shows the cross-section of our laboratory for testing geodetic instruments. A large concrete block separated from the walls and the floor is swimming on sand, therefore, the swingings caused by the environment are effectively damped. This place is stable enough to measure the parameters of the pendulums with an accuracy of about 1—2% being sufficient in the practice.

To avoid the mechanical instabilities, the capacitive pendulum is placed directly on the concrete pillar and the pendulum is tilted by means of a dilatable crapaudine, placed under the drift screw. The movements of the pendulum beam are recorded electrically on a strip-chart recorder and at the same time the turning points of the eigenswingings of the pendulum beam are read on a scale by means of a light beam reflected of a mirror placed in the pendulum beam. The measurement is made as follows:

At first a low sensitivity is set at the pendulum by means of the "sensitivity screw" and then the same tilt ($\varphi = 0.06746$ secs of arc) is given to the pendulum by the crapaudine at different points of the moving range of the pendulum beam. The rotation angle of the pendulum beam arising from the tilting is measured in each point optically and electrically. The pendulum beam has been moved from one position to another by the "drift screw". So it can be measured in one sensitivity range at 8—10 positions of the pendulum beam. The measurement is repeated at different sensitivities. Figure 3 shows

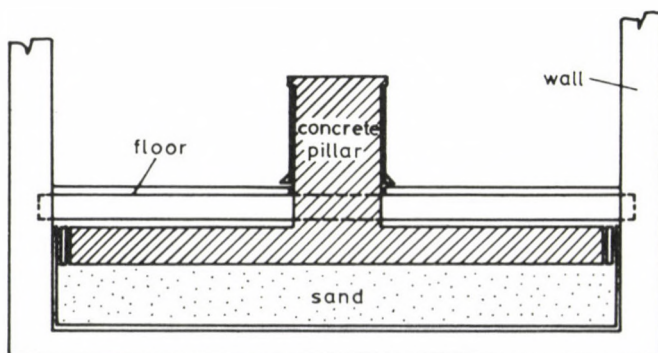


Fig. 2. The concrete pillar for testing horizontal pendulums

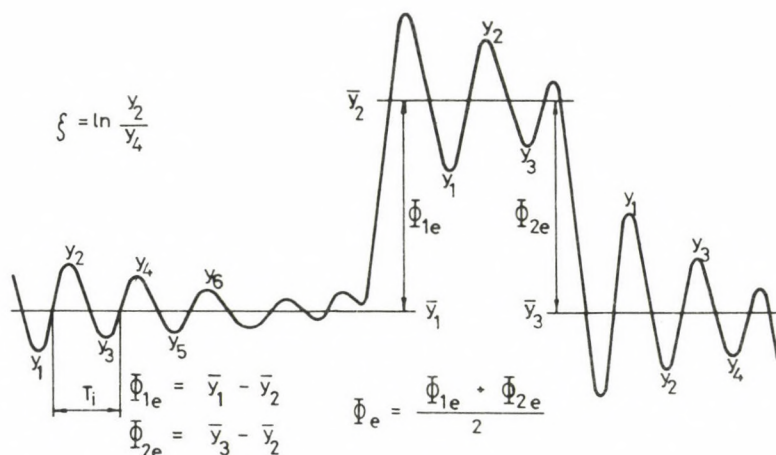


Fig. 3. Electric record of a tilting of the pendulum

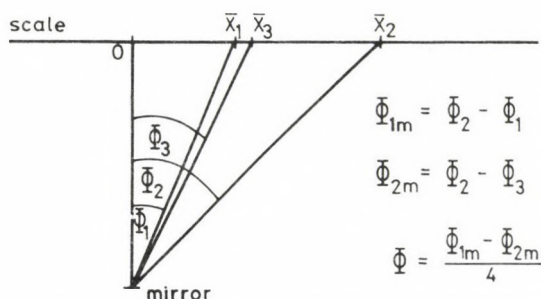


Fig. 4. Determining the angle deviation of the pendulum beam by means of a scale

how the Φ_e electrically measured angle deviation of the pendulum beam due to a tilting φ can be obtained from the electrical record.

The centre lines of the eigenswingings \bar{y}_k can be determined from the y_i amplitudes (turning-points) by a Fox—Schuler averaging method:

$$\bar{y}_k = \frac{1}{2^{n-1}} \sum_{i=1}^n \binom{n-1}{i-1} y_i, \quad k=1, 2, 3 \quad (1)$$

where n = the number of amplitudes involved in the calculations. Because of the hysteresis of the crapaudine Φ_e is the average of Φ_{e1} and Φ_{e2} caused by lifting and lowering of the mercury reservoir of the crapaudine.

The direct angle deviation of the pendulum beam Φ can be obtained from the optically observed \bar{x}_i turning-points, measured simultaneously with y_i . Figure 4 illustrates the method of the calculations. The mean values \bar{x}_k can be determined

Table I

	Measured values				Calculated values		
	Position of the pendulum beam V	Eigen-period T_i s	Deviation of the pendulum beam measured		Mechanical gain K_1	Electrical gain $K_2 \cdot 10^4$ V/sec of arc	Deviation of values K_1 from the fitted parabola
			optically Φ sec of arc	electrically Φ_e V			
Sensitivity stage 1.	0.686	31.0	408.7	0.127	6 058.5	3.110	35.4
	1.315	33.5	469.7	0.146	6 962.6	3.122	-12.8
	1.535	32.9	449.1	0.140	6 657.3	3.125	-70.4
	2.308	32.3	431.0	0.135	6 388.9	3.130	-95.7
	2.898	33.1	452.9	0.141	6 713.6	3.120	-96.2
	3.825	33.2	456.9	0.142	6 772.9	3.108	-78.0
	4.568	31.5	422.8	0.130	6 267.4	3.075	100.0
Average \pm mean square error		32.5 \pm 0.9	441.6 \pm 21.4	0.137 \pm 0.007	6 545.9 \pm 317.7	3.113 \pm 0.018	
Sensitivity stage 2.	4.109	39.0	601.7	0.181	8 919.4	3.008	-534.4
	3.510	41.0	687.1	0.208	10 185.3	3.027	-262.9
	2.925	41.4	705.1	0.215	10 452.1	3.053	-201.1
	2.293	42.0	728.1	0.221	10 793.1	3.042	-171.1
	1.650	42.5	746.3	0.226	11 062.9	3.030	-163.9
	1.073	41.7	737.6	0.225	10 933.9	3.078	125.8
	0.545	43.9	767.4	0.230	11 375.6	2.997	-603.0
Average \pm mean square error		41.6 \pm 1.5	710.5 \pm 54.7	0.215 \pm 0.017	10 531.8 \pm 811.4	3.034 \pm 0.027	
Sensitivity stage 3.	4.476	48.0	931.1	0.279	13 802.3	3.007	-518.3
	2.938	49.1	989.4	0.298	14 666.5	3.012	-318.0
	3.770	50.5	1031.1	0.310	15 284.6	3.006	-566.5
	2.868	50.7	1032.2	0.312	15 300.3	3.018	-676.6
	2.464	51.4	1061.2	0.320	15 730.8	3.016	-690.4
	2.000	52.2	1103.2	0.330	16 353.4	2.995	-532.9
	1.365	54.0	1194.2	0.360	17 702.3	3.014	-422.2
	0.709	57.5	1326.4	0.398	19 662.0	3.001	-888.1
Average \pm mean square error		51.7 \pm 3.0	1083.6 \pm 125.1	0.326 \pm 0.037	16 062.8 \pm 1 854.9	3.009 \pm 0.008	
Sensitivity stage 4.	4.081	56.9	1350.5	0.406	20 019.3	3.003	-104.1
	3.688	58.1	1430.7	0.437	21 208.1	3.054	226.9
	3.129	63.1	1697.5	0.519	25 163.1	3.057	415.3
	2.505	65.4	1836.0	0.554	27 216.1	3.020	631.3
	1.630	70.5	2121.1	0.637	31 442.3	3.004	549.6
	1.608	74.3	2387.5	0.711	35 393.1	2.980	1080.4
	0.375	73.8	2320.6	0.695	34 399.6	2.995	541.1
Average \pm mean square error		66.0 \pm 7.1	1877.7 \pm 413.8	0.566 \pm 0.121	27 834.5 \pm 6 134.0	3.016 \pm 0.029	

similarly to \bar{y}_k . The angles Φ_k belonging to the values \bar{x}_k on the scale can be calculated as follows:

$$\Phi_k = \arctan \frac{\bar{x}_k}{d}, \quad k = 1, 2, 3 \quad (2)$$

where d = the distance between the rotation axis of the pendulum beam and the scale.

Φ_{m1} and Φ_{m2} are the rotation angles of the light beam during lifting and lowering of the mercury reservoir. When calculating the mean value of Φ_{m1} and Φ_{m2} it was taken into account by a divisor 4 that the rotation of the reflected light beam is the double of one of the mirrors and therefore of one of the pendulum beams.

The eigenperiod (T_i) and the damping factor (ζ) of the pendulum are determined from the electric record (Fig. 3). The measured values of T_i , Φ , Φ_e belonging together are given in Table I. All the significant parameters and properties of the pendulum can be obtained from the above mentioned values.

The gain of the capacitive pendulum

The gain of the capacitive pendulum is as follows:

$$K = K_1 \cdot K_2, \quad (3)$$

where $K_1 = \frac{\Phi}{\varphi}$ is the mechanical sensitivity of the pendulum and

$K_2 = \frac{\Phi_e}{\Phi}$ the electrical gain.

The values of K_1 and K_2 are given in Table I. K_2 is slightly depending on the mechanical sensitivity of the pendulum because the distance between the moving and the fixed plates of the capacitive transducer changes somewhat by tilting the pendulum by the sensitivity screw. Figure 5 shows that K_2 is constant in a wider moving range of the pendulum beam at a given sensitivity. K_1 is depending on the position of the

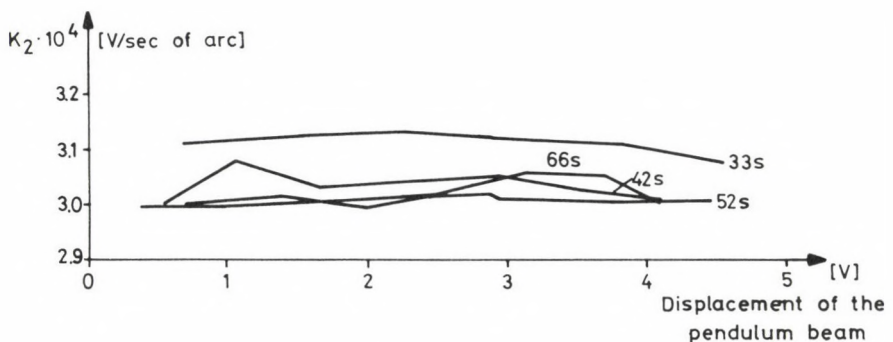


Fig. 5. Electrical sensitivity in the moving range of the pendulum beam

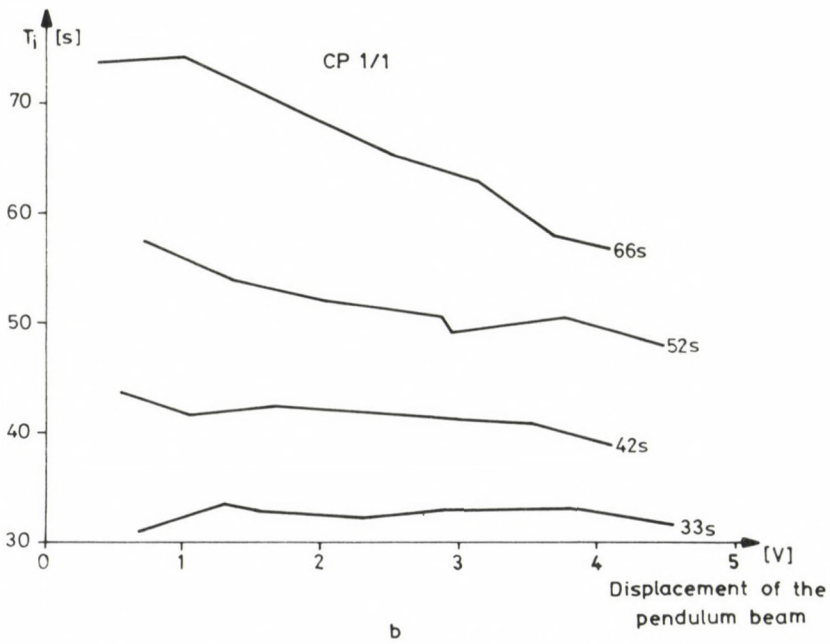
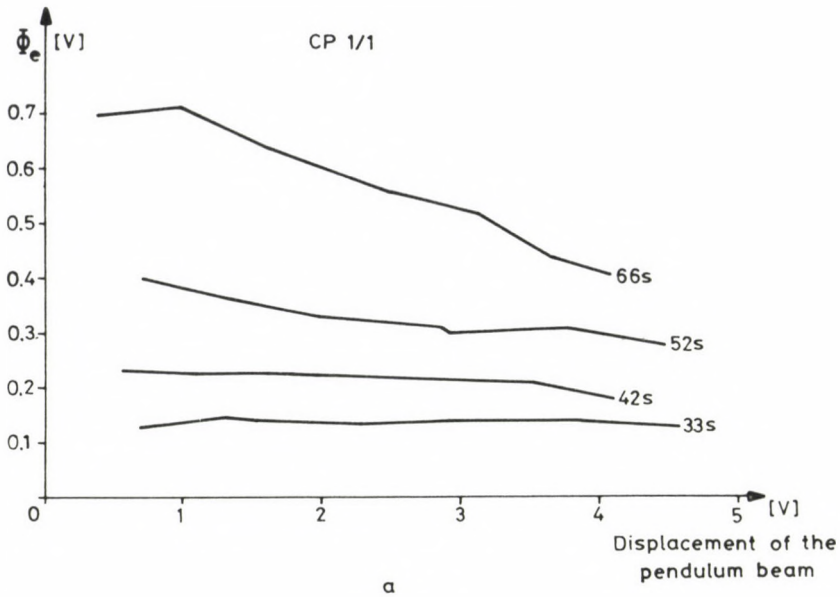


Fig. 6. The change of the sensitivity of the pendulum in the moving range of the pendulum beam

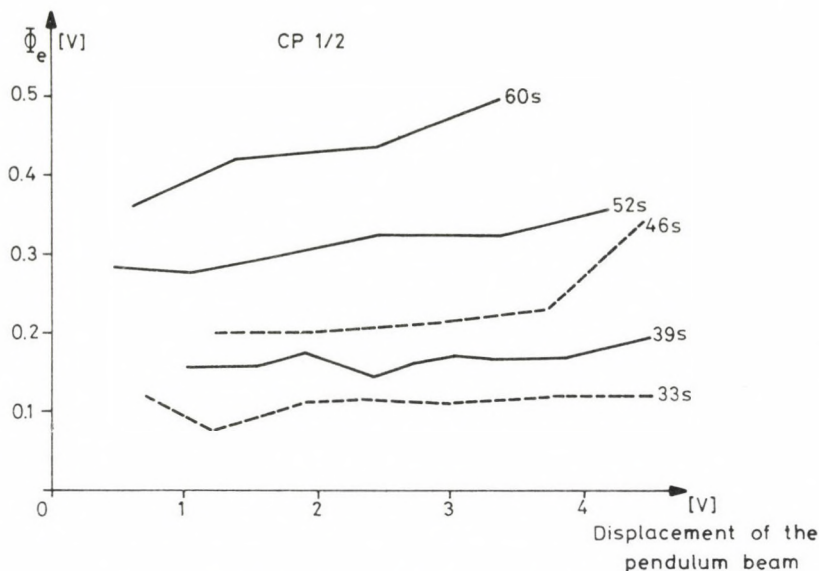


Fig. 7. The change of the sensitivity at different suspensions

pendulum beam. Figure 6 shows Φ_e being proportional to the sensitivity. From the figure we learn that at low sensitivities the sensitivity is constant in the whole moving range, except on the brinks where due to the large deviation of the pendulum beam the angle i , determining the sensitivity of the pendulum increases (Mittelstrass 1966). At higher sensitivities the torsion of the suspension wires plays a growing role in the operation of the pendulum.

According to experiences, the suspension is the better, the higher the sensitivity is at which the sensitivity is constant in the whole moving range. The dotted lines in Fig. 7 shows the change of sensitivity in case of a fully improper suspension. It was impossible to record the Earth tides by the pendulum with this suspension because the drift was very high. The continuous lines show the change of sensitivity after a new, better threading of wires.

The eigenperiod and the damping factor of the pendulum

The mechanical sensitivity is depending on the eigenperiod of the pendulum (Mittelstrass 1966):

$$K_1 = \frac{\Phi}{\varphi} = k \cdot T_i^2, \quad (4)$$

where k = the instrument constant,

T_i = the eigenperiod of the pendulum.

That is why the sensitivity is given by the eigenperiod in the figures.

Similarly to the sensitivity, the eigenperiod is depending on the position of the pendulum beam (Fig. 6), too. Furthermore the eigenperiod is slightly depending on the damping factor.

The instrument constant can be obtained from Eq. (4) by fitting a parabola to the values of T_i and K_1 in Table I. The last column of Table I gives the deviations from the fitted parabola. The deviations are characteristic for the reliability of the measuring method, too. The errors are growing at growing sensitivity because the pendulum is more and more sensitive to the additional tilts caused by the movements of the measuring persons.

Table II

Pendulum	ξ	$\frac{k}{1/s^2}$	$\frac{l_0}{m}$
CP 1/1	0.1890 ± 0.036	6.215	0.0400
CP 1/2	0.1773 ± 0.045	5.507	0.0451

The damping factor of the pendulum is a function of the eigenperiod T_i , the amplitude and the position of the pendulum beam. The deviations from the mean value of the damping factor are so high (Table II) and unsystematic that no unambiguous relationship can be established between the above mentioned values.

The dynamic properties of the capacitive pendulum

During the investigation of the dynamic behaviour of the capacitive pendulum the tiltmeter mode is to be distinguished from the accelerometer mode because in the two modes the operation of the pendulum is somewhat different (Fig. 8).

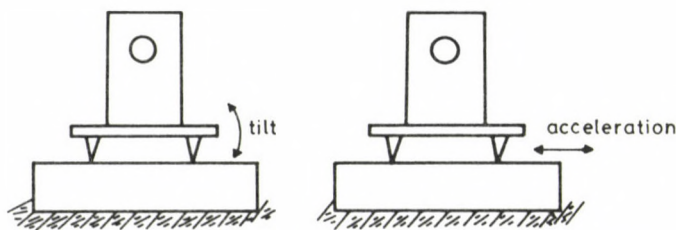


Fig. 8. The tiltmeter and the accelerometer mode of the pendulum

The tiltmeter mode of the capacitive pendulum

The working of the pendulum can be described by the differential equation (Mittelstrass 1966):

$$\Theta \frac{d^2\Phi}{dt^2} + k \frac{d\Phi}{dt} + mgs \sin \Phi + \eta\Phi = mgs \varphi. \quad (5)$$

This differential equation can be written as follows

$$\frac{d^2\Phi}{dt^2} + 2\beta \frac{d\Phi}{dt} + \omega_i^2 \Phi = \frac{g}{l_0} \varphi, \quad (6)$$

where

$$2\beta = \frac{k}{\Theta}; \quad \sin \Phi \approx \Phi; \quad \frac{\Theta}{m \cdot s} = l_0; \quad \omega_i^2 = \frac{g}{l_0} \sin i + \frac{\eta}{\Theta}. \quad (7)$$

From Eq. (6) we obtain by Laplace-transformation:

$$s^2\Phi(s) + 2\beta s \Phi(s) + \omega_i^2 \cdot \Phi(s) = \frac{g}{l_0} \varphi(s) \quad (8)$$

from which the transfer-function of the pendulum is

$$H_1(s) = \frac{\Phi(s)}{\varphi(s)} = \frac{K_1}{1 + 2\xi \tau s + \tau^2 s^2}, \quad (9)$$

where

$$\tau = \frac{1}{\omega_i} \quad \text{the time constant of the pendulum,}$$

$$\xi = \frac{\beta}{\omega_i} \quad \text{the damping factor,}$$

$$K_1 = \frac{g}{l_0 \omega_i^2} \quad \text{the mechanical gain of the pendulum at zero frequency,}$$

$$\omega_i = \frac{2\pi}{T_i} \quad \text{the angle velocity of the eigenswinging of the pendulum.}$$

The transfer function of the electrical amplifier is constant in the frequency range of the Earth tides and other geodynamic phenomena measured by pendulums.

$$H_2(s) = K_2. \quad (10)$$

Therefore, the transfer function of the capacitive pendulum is

$$H(s) = H_1(s) \cdot H_2(s) = \frac{K}{1 + 2\xi \tau \cdot s + \tau^2 s^2} \quad (11)$$

where $K = K_1 \cdot K_2$.

The frequency response of the capacitive pendulum can be derived from Eq. (11) by substituting $s=j\omega$

$$H(j\omega) = \frac{K}{1 + 2\zeta\tau j\omega + (j\omega)^2\tau^2}. \quad (12)$$

The unit-step response of the pendulum can be obtained by inverse Laplace-transformation of $H(s)$. Usually, $\zeta < 1$ at horizontal pendulums and in this case the unit-step response is

$$v(t) = K \left[1 - e^{-\beta t} \left(\cos \omega_\beta t + \frac{\beta}{\omega_\beta} \sin \omega_\beta t \right) \right], \quad (13)$$

where

$$\omega_\beta = \omega_i \sqrt{1 - \zeta^2}$$

$$\beta = \zeta \cdot \omega_i.$$

By differentiation of Eq. (13) the impulse response of the pendulum is obtained:

$$\omega(t) = \frac{K}{\omega_\beta \tau^2} e^{-\beta t} \sin \omega_\beta t. \quad (14)$$

All parameters in Eqs (12—14) can be found by the above described static measurement and therefore the very expensive and hardly accomplishable direct dynamic investigation of the horizontal pendulums can be avoided. Since the eigenperiod and the sensitivity are somewhat depending on the position of the pendulum beam, the above functions have to be calculated by the average values in each sensitivity range given in Table I.

Figures 9—11 show the frequency, unit step and impulse response, respectively, of the CPI/1 capacitive pendulum.

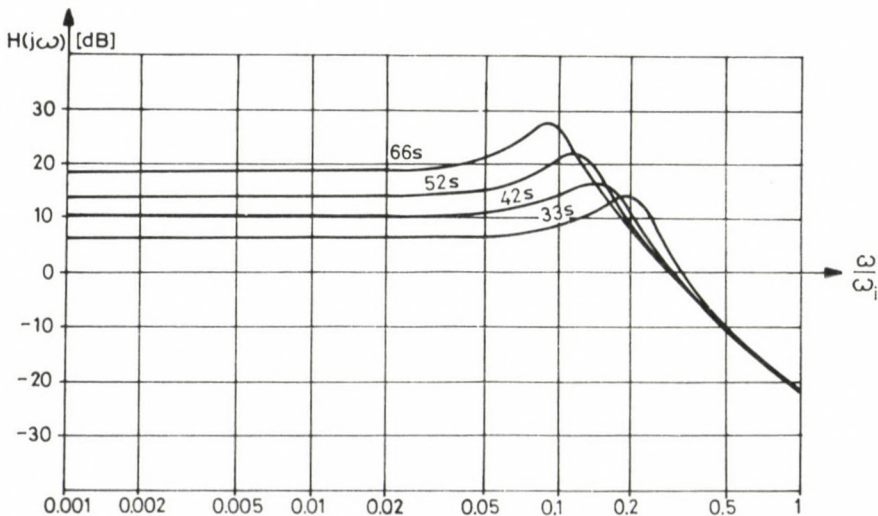


Fig. 9. The frequency response of the pendulum in tiltmeter mode

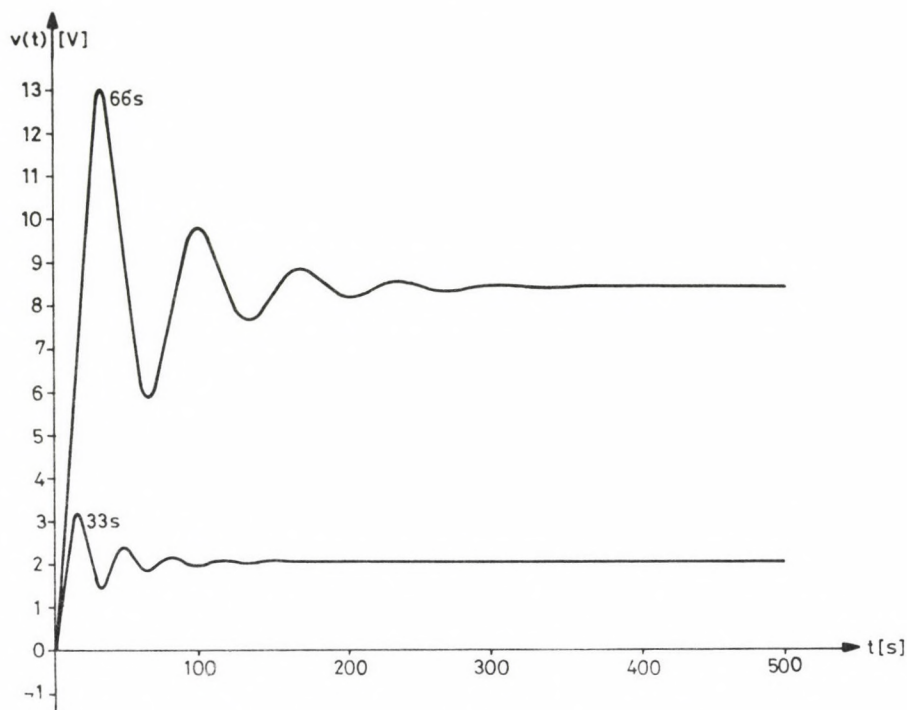


Fig. 10. The unit-step response of the pendulum in tiltmeter mode

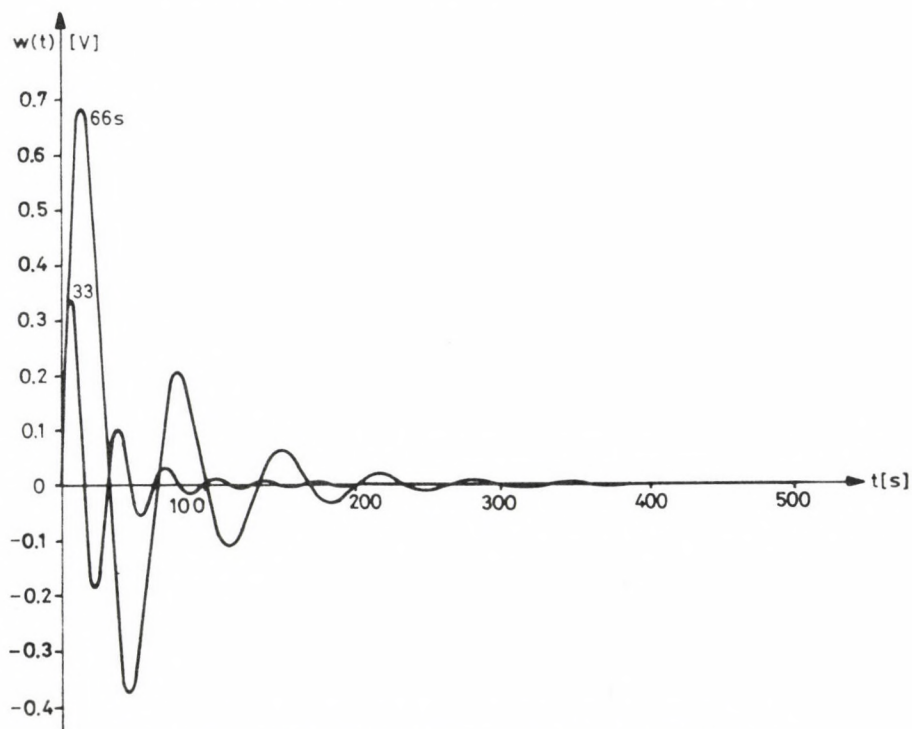


Fig. 11. The impulse-step response of the pendulum in tiltmeter mode

The accelerometer mode of the capacitive pendulum

The operation of the pendulum in an accelerometer mode can be described by the following differential equation:

$$\frac{d^2\Phi}{dt^2} + k \frac{d\Phi}{dt} + mgs \sin i \sin \Phi + \eta \cdot \Phi = ms \frac{d^2x}{dt^2}, \quad (15)$$

where x = the horizontal movement of the pendulum.

Substituting Eq. (7) into Eq. (15) and after Laplace-transformation we obtain the transfer function of the pendulum:

$$H_1(s) = \frac{\Phi(s)}{x(s)} = \frac{1}{l_0} \cdot \frac{s^2 \cdot \tau^2}{1 + 2\xi s\tau + s^2\tau^2}, \quad (16)$$

where

$$l_0 = \frac{g}{4\pi^2 k^2} \text{ the instrument constant}$$

g = the gravity acceleration.

The transfer function of the whole capacitive pendulum is

$$H(s) = H_1(s) \cdot H_2(s) = \frac{K_2}{l_0} \cdot \frac{s^2 \cdot \tau^2}{1 + 2\xi s\tau + s^2\tau^2}, \quad (17)$$

where $H_2(s) = K_2$ the transfer function of the electrical amplifier.

The unit-step response and the impulse response are

$$v(t) = \frac{K_2}{l_0} e^{-\beta t} \cos \omega_\beta t \quad (18)$$

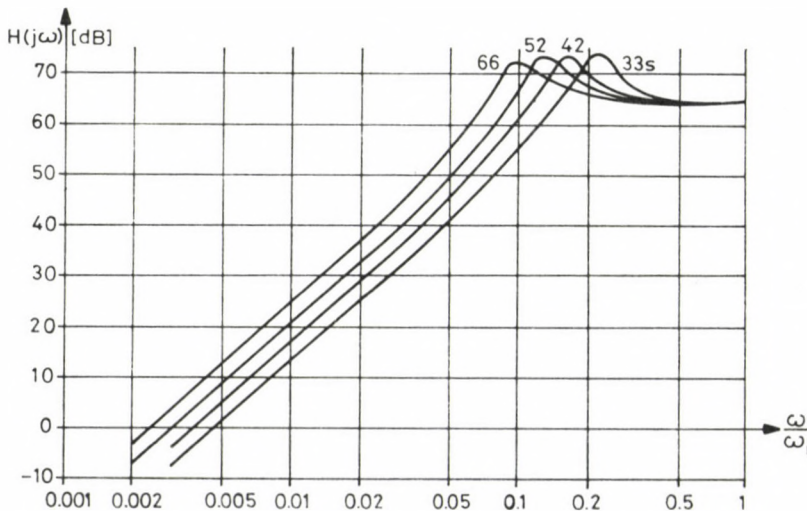


Fig. 12. The frequency response of the pendulum in accelerometer mode

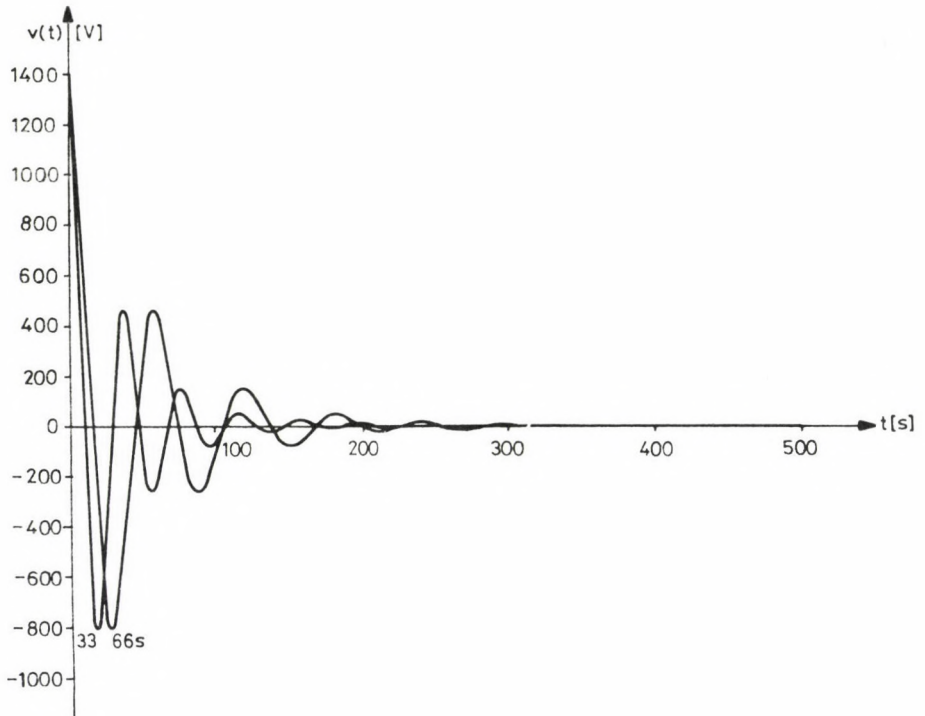


Fig. 13. The unit-step response of the pendulum in accelerometer mode

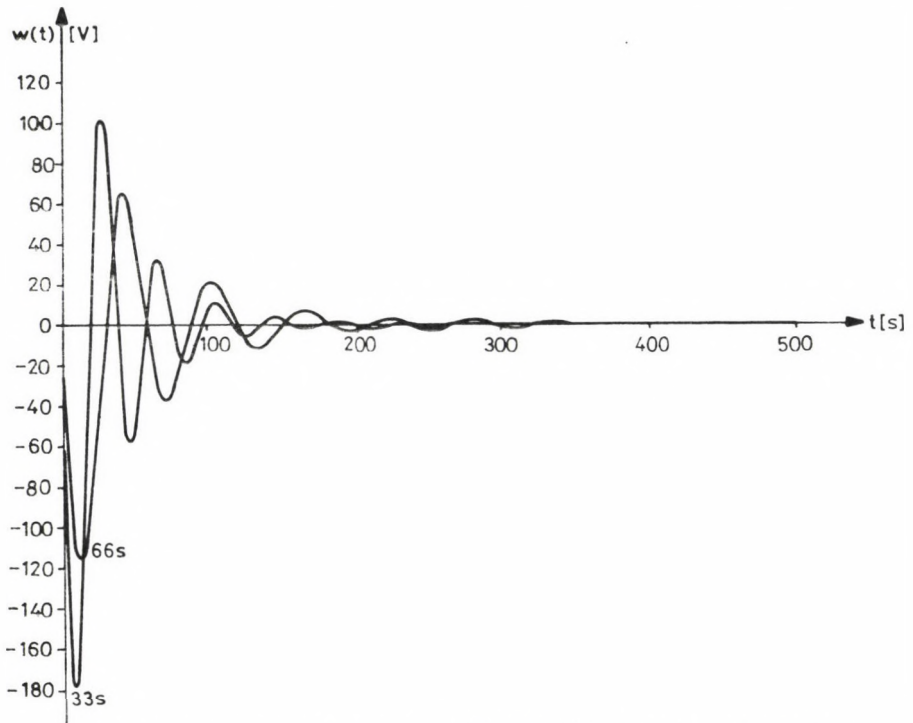


Fig. 14. The impulse-step response of the pendulum in accelerometer mode

and

$$\omega(t) = -\frac{K_2 \beta}{l_0} e^{-\beta t} \cos \omega_\beta t - \frac{K_2 \omega_\beta}{l_0} e^{-\beta t} \sin \omega_\beta t, \quad (19)$$

respectively.

The functions in Eqs (17—19) of the capacitive pendulum CP1/1 calculated on hand of Tables I, II are shown in Figs 12—14.

Conclusions

Horizontal pendulums are by 2—3 orders of magnitude more sensitive instruments than other electric inclinometers, therefore their dynamic investigation on the usual swinging tables (Caspary and Geiger 1979, Eichholz and Schäfler 1982a, 1982b) is nearly impossible. The above described static measurement provides a sufficient accuracy (1—2 percent) for the practice to determine the static and dynamic parameters of a horizontal pendulum. The exact calibration occurs during the Earth tides recording in permanent time intervals. This is necessary because the sensitivity is depending on the position of the pendulum beam, too. By the demonstrated measuring method we can determine the quality of the suspension, the linearity of the transducer and the frequency transfer properties of the capacitive horizontal pendulum in a short time and therefore no long time is needed for observatory records to establish whether the pendulum works properly or not.

References

- Caspary W, Geiger A 1979: Laboruntersuchungen von elektronischen Neigungsmessern. *Zeitschrift für Vermessungswesen*, 9, 410—420.
- Eichholz K, Schäfler R 1982a: Zur Dynamik elektronischer Neigungsmesser (Teil I). *AVN*, 1, 29—45.
- Eichholz K, Schäfler R 1982b: Zur Dynamik elektronischer Neigungsmesser (Teil II). *AVN*, 4, 147—158.
- Mentes Gy 1979: Development of horizontal pendulum recordings. *Acta Geod. Geoph. Mont. Hung.*, 14, 101—109.
- Mentes Gy 1981: Horizontal pendulum with capacitive transducer. *Acta Geod. Geoph. Mont. Hung.*, 16, 269—280.
- Mittelstrass G 1966: Konstruktionsprinzipien von Horizontaleinfachpendeln. *Wissenschaftliche Arbeiten der Lehrstühle für Geodäsie, Photogrammetrie und Kartographie an der Technischen Hochschule Hannover*, Nr. 26.

DIGITAL SURFACE MODEL ON A TRIANGULAR BASE

J KALMÁR¹

[Manuscript received April 10, 1985]

The paper presents one of the methods of surface interpolation, the finite element interpolation on a triangular base, and it discloses its connections to the graph theory.

Keywords: digital surface model; digital terrain model; finite element interpolation; triangular coverage

1. Generally on digital surface models

A digital terrain model is the summary of computation technical methods which enable the quick retrieval of information stored about the surface actually modelled according to the user's special demands. The term surface model limits this interpretation so far that in that case a three-dimensional series of points is stored which represents mathematically a single valued, continuous function known in discrete points:

$$z = f(x, y)$$

where z denotes height in the followings.

The following information types can be deduced from the surface model:

- a) The set of points for a fixed coordinate (x or y or z), i.e. the set of points having a prescribed value of the coordinate and fit to the surface,
- b) For a fixed pair of coordinates (x and y , or x and z , or y and z) the set of points having the actual values of these coordinates and fit to the surface,
- c) The shape of the surface (or of a part of it)
- d) The vector normal to the surface in certain points (if the function is derivable).

2. Surface interpolation on the grid model

Most of the surface models used in the practice suppose that the three-dimensional series of points describing the surface fits to a regular rectangular grid in (x, y) . The so-called random models can be reduced to this case, too, if the points of the

¹ Geodetic and Geophysical Research Institute of the Hungarian Academy of Sciences, Sopron, P.O.B. 5. H-9401

model are densified to a rectangular grid using any method of prediction (e.g. by collocation, Závoti 1982).

It should not be forgotten, however, that in the points of the grid model obtained so the original values of the function do not appear any more but instead values estimated by a certain method, i.e. the grid model deduced by any method from the random set of points cannot be used any more for a rigorous interpolation (nevertheless, such an interpolation is only very seldom necessary).

The grid model can be else treated very easily, its advantages are (Powel 1977):

- a) It is sufficient to store the data z ,
- b) It fits well to automatic data collecting systems,
- c) It can be easily decided for any point in the plane to which rectangular grid element it does belong,
- d) There are numerically stable and rigorous methods for the surface interpolation on a rectangular grid; the continuity along grid lines is warranted already by the bilinear approximation in the rectangles, and by biquadratic or bicubic spline interpolation an approximation continuous in its derivatives can also be reached.

It should be remarked here that the spline interpolation is numerically a method with a high demand for operations, the size of the system of equations for the determination of the coefficients increases linearly with the number of points in the model and the complete system is to be solved in a single run, even if the special form matrix—band matrix—enables certain simplifications.

The above reasons motivated our decision to investigate the possibility for realizing a triangular base finite element interpolation as an alternative for the grid model.

3. Methods of the surface interpolation on a triangular base

It is supposed that a single triangular coverage of the plane is known for which the followings are satisfied:

- a) All model points belong to any of the triangles (i.e. each of the points are the vertices of triangles),
- b) All vertices of the triangles are model points,
- c) The set of triangles covers singly the convex hull of the model points.

According to these the coordinates of all vertices of any chosen triangle are known (as they are model points), therefore a plane can be unambiguously fitted to the three points, being the simplest method of surface fitting. The continuity is already ensured by this as triangles fit to each other along the edges, and the equations of the planes can be deduced without any difficulty:

$$z = f(x, y) = a \cdot x + b \cdot y + c .$$

In the next step some approximative method is used for the computation of the midpoint of the triangle edges. In this case 6 heights are known in the triangle, and a six-

parameter, two-variable polynomial can be fitted to them:

$$z = g(x, y) = a_0 + a_1x + a_2x^2 + a_3y + a_4y^2 + a_5xy.$$

It is valid here, too, that the triangles fit to each other along the triangle edges continuously and it is also true that this polynomial exists for any non-degenerated triangle.

There are interpolation polynomials of even higher degree in the triangle, and the continuous fitting of derivatives can also be ensured, but they suppose even more additional information—value of the function in the gravity centre, partial derivatives in the vertices, partial derivatives in certain directions in the midpoints of the sides (Strang and Fix 1973)—not being contained originally in the model.

4. Generally on the coverage of triangles

The quality of the surface interpolation on a triangle base is basically influenced by the geometry of the triangular network used; from the point of view of the interpolation, such a triangular network is the most advantageous one which is nearly regular, and triangles with very great or very small vertex angles are disadvantageous. The coverage by triangles fulfilling the conditions 3a—c can be easily realized in many ways; on this topic only the following results should be referred here to (e.g. Tomescu 1978):

4.1 *Theorem*: the number of the possible coverages by triangles is in case of an n -angle:

$$\frac{1}{n-1} \binom{2 \cdot n - 4}{n-2}.$$

The basic points of the surface model are not expected to constitute a convex multangle, the situation is generally much more complex, but the order of magnitude of the above result is mostly realistic.

The following results are also interesting from the point of view of coverage by triangles which can be proven by reducing them to Euler's polyhedron-theorem:

4.2 *Theorem*: E is the number of edges in a coverage by triangles, n the number of model points, L the number of triangles, and H the number of points lying on the limit of the convex hull. In such a case one gets:

$$4.21 \quad E = 3(n-1) - H$$

$$4.22 \quad L = 2(n-1) - H.$$

4.3 *Conclusion*: as it is valid that $3 \leq H \leq n$, the following bounds are also valid:

$$4.31 \quad E \leq 3(n-2)$$

$$4.32 \quad L \leq 2(n-2).$$

Conclusion 4.3 enables to estimate the necessary storage capacity for the coverage by triangles: an edge can be stored with its identifier in two words, and a triangle in 3 words, thus a demand of $6(n-2)$ words can be given from both former bounds. Theorem 4.2 can be interpreted so that the coverage by triangles of a set S fulfilling the conditions 3a—c has the same number of edges and triangles, respectively.

5. The algorithm generating the coverage by triangles

Prior to the description of the algorithm, the notion of the Thiessen polygonal (or Dirichlet-cell or Vononoi diagram) is to be introduced.

5.1 *Definition:* the Thiessen polygonal of the points P of the planar set S is the inner hull around P of the perpendicular bisector of the sections between the point P and the other points of S .

For illustration, Fig. 1 shows an example for the determination of the Thiessen polygonal, and Fig. 2 shows the Thiessen polygonal of the points denoted by $+$. Let us now define the notion of the Thiessen neighbourhood.

5.2 *Definition:* The points P and Q of the set S are called Thiessen neighbours then and only then if their Thiessen polygonals have a common edge (a common point is not sufficient).

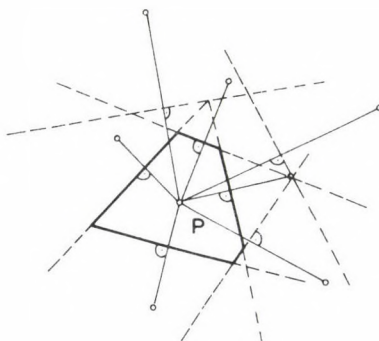


Fig. 1

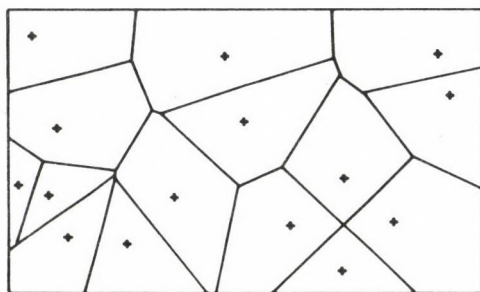


Fig. 2

5.3 *Algorithm*: Let us connect by edges the Thiessen neighbouring points of the set S .

It can be seen that algorithm 5.3 generates with the exception of the following special case an allowed coverage by triangles.

5.4 *Counter-example*: Let us suppose that the points of S lie on a circle. Then the segment connecting any two points of S is a chord of the circle, therefore the perpendicular bisectors intersect each other in one point, i.e. in the centre of the circle. It follows that the connection by edges according to 5.3 results in a polygonal in the circle, i.e. no coverage by triangles is generated. If the neighbourhood would be allowed in 5.2 in case of the existence of a single common point, then any two points should be connected by edges in that case, and intersecting edges would be created, hence the edge-system obtained does not fulfil 3a—c, neither.

Algorithm 5.3 can be specified as an indirect method, as the system of edges generated by them enables the determination of the triangles only after lengthy seeking and the case of the counter-example should be specially considered. Then using the notion of Thiessen neighbourhood should be used for the following method to cover by triangles:

5.5 *Algorithm*: let us find the points of S one by one. The procedure continues in a point P only then, if the triangles fitted to P cover the full angular range in the vicinity of P (if P is an inner point), and the part of the full angular range within the convex hull, respectively.

The definition of a triangle fitted to P is the following: one starts from an edge from P on the left side of which in case of a counter clockwise rotation no triangle is defined; this edge can be already one side of a triangle fitting to P , or if there are not yet any such triangles, then it is the segment between P and the nearest point within S . The latter choice is motivated by the fact that the nearest point to P is surely its Thiessen neighbour.

By starting from the segment chosen in the previous method, let us consider the points of S within an angular range π . The intersection points of the chosen edge—perpendicular bisector and the perpendicular bisector of the segments between the considered points and the point P are then determined; on this basis it can be decided which is the next Thiessen neighbouring point in the counter clockwise sense of rotation—and this will be the third vertex of the new triangle fitted to the chosen edge.

Case 5.4 appears now so that there is no possibility for an unambiguous choice, as several intersection points coincide. In such a case that point is to be selected which gives a greater vertex angle at P .

If there are no points in the angular range considered, then the edge is a bounding edge, and the point P is a boundary point. Let us find in that case the other bounding edge in P and the procedure is to be continued from this edge.

The above is a simplified description of the realized algorithm, as it could be made more rapid by some tricks: e.g. the considered angular range can be made narrower therefore a lower number of points is to be checked, and the angular range

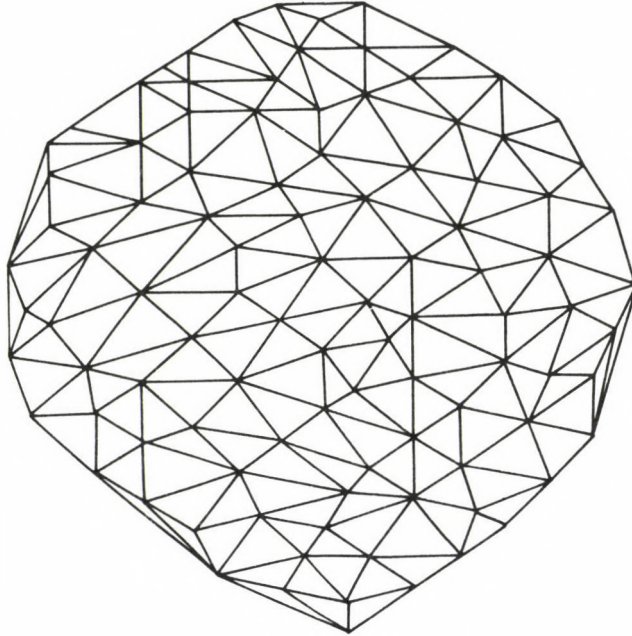


Fig. 3

uncovered can be quicker determined by a multiple storage of the triangles. An example of the triangular coverage created by this algorithm is presented in Fig. 3. The demand on operations needed for the algorithm increases with the square of the model points—it should be reminded to the fact that the demand on operations needed for matrix inversions increases with the cube of the matrix dimension—and for e.g. 1000 model points, the FORTRAN program of the algorithm lasts on a minicomputer of the type HP-1000 E only about 12 minutes. The same computer enables the computation of about 1500 model points with a central memory of 64 kwords using the triangular coverage without any auxiliary store.

There is an important property from the point of view of the graph theory of the system of edges generated by the algorithm 5.3, mentioned already by Brown (1979):

5.6 Theorem: Be S a partial set of the planar points where two arbitrary points are connected by an edge (i.e. it is a complete graph) and the length of the edge should be the Euclidean distance of the two points. Then the set of edges generated by Algorithm 5.3 will contain the minimum spanning tree of the complete graph of S .

It follows from this theorem and from the operation demand of the algorithm generating the triangular coverage that:

5.7 Conclusions: The minimum spanning tree of the complete graph S can be determined by operations whose number is proportional to the square of the number of model points in S .

In order to catch the significance of statement 5.7 it should be reminded that the number of edges in a graph consisting of n points is

$$\binom{n}{2}$$

if it does not contain multiple or loop-edges and no general algorithm is possible to determine the minimum spanning tree where the number of operations increases linearly with the number of edges (Andrásfai 1973).

The coverage by triangles generated by Algorithm 5.3 produces according to our investigations triangular forms being advantageous for the interpolation except of the triangles fitting to the bounding edges but they are bad, i.e. elongated in case of other procedures, too.

On the basis of the coverage by triangles, the approximation of the surface can also be advantageously carried out. The estimation of the height of an unknown point can be given by fitting some surface (mostly a polynomial) on the basis of the least squares to the points in the neighbourhood of the point, and by substituting the coordinates of the given point into the equation of the surface, the height is obtained. This method is very sensitive for the choice of the points when fitting the function, especially if they are not evenly distributed in the neighbourhood of the given point. The principle of the Thiessen-neighbourhood can be exploited in such a case, as it identifies the points which "cover" in all directions as closely as only possible. As the triangular coverage has already been generated the determination of the Thiessen neighbours of a given point can be substituted by two different procedures to select the points in the triangular coverage:

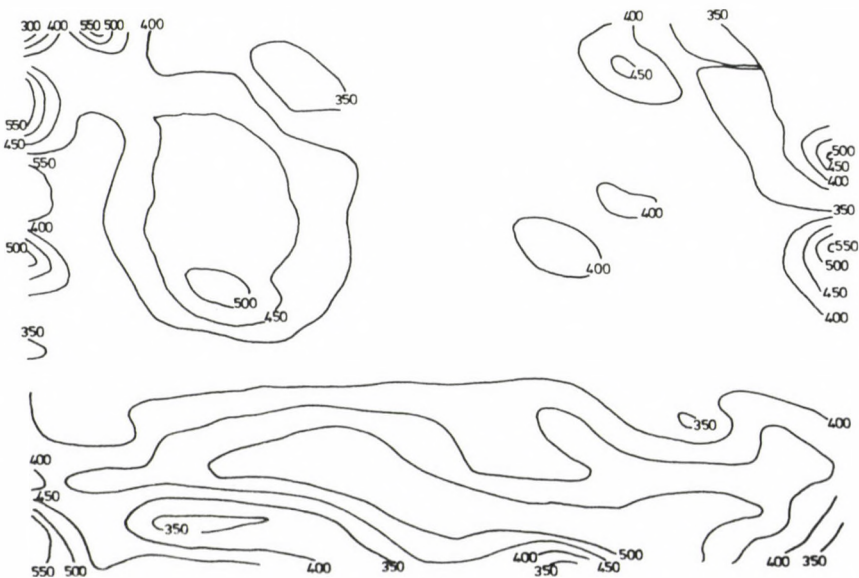


Fig. 4

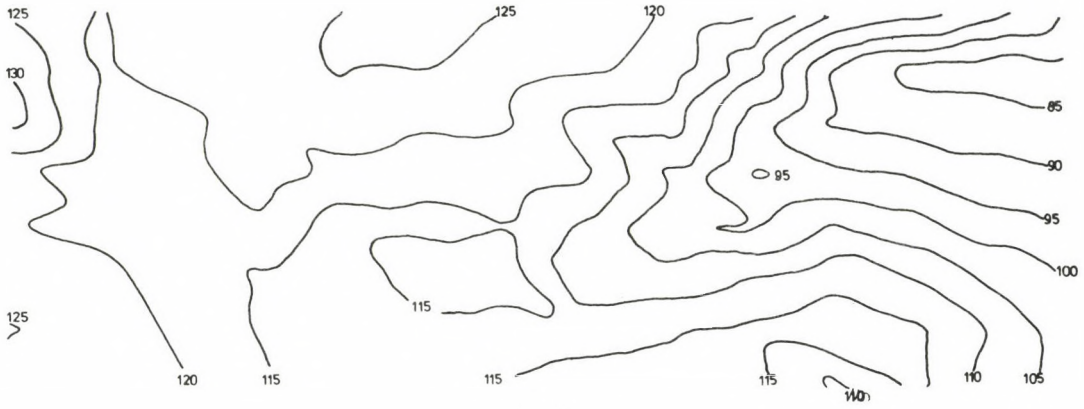


Fig. 5

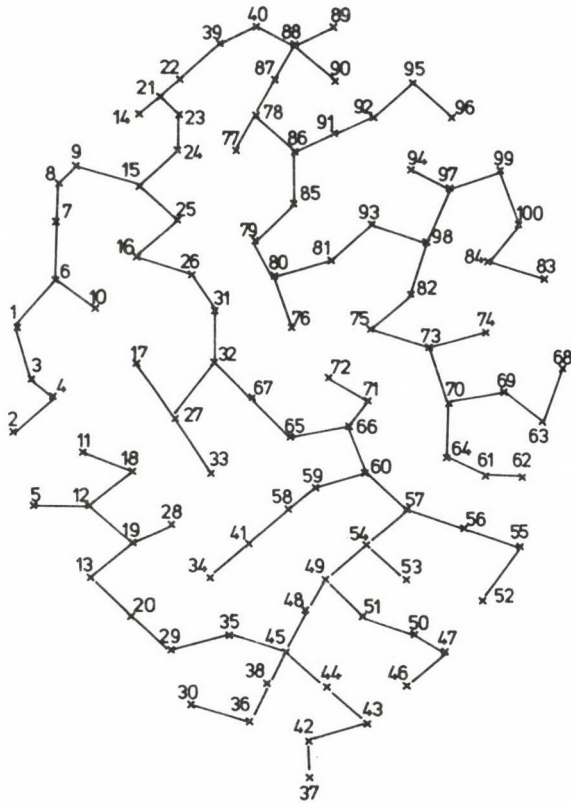


Fig. 6

a) let us find the base point P lying nearest to the point in question and the surface is fitted to it as well as to the points connected by edges with P , or

b) let us determine the triangle whose internal point the point in question is, and the function is fitted to the vertices of that triangle and to the points connected by edges to its vertices.

In the surface models with triangular bases the linear and quadratic interpolations have been both realized triangle by triangle—the height estimation is also solved on both bases, further the plotting of segments and contour lines, too. For the latter, examples are presented in Figs 4 and 5. The heights in the bisecting points of the edges are estimated according to 5b by polynomial-fitting. Using Theorem 5.6, a special program determines the minimum spanning tree of the complete graph on the basis of the coverage by triangles and it is also plotted. An example for this is shown in Fig. 6, where the minimum spanning tree of the edge system in Fig. 3 is presented.

References

- Andrásfai B 1973: Getting acknowledged with the graph theory. (In Hungarian) Tankönyvkiadó Budapest
- Brown K Q 1979: Voronoi Diagrams from Convex Hulls. *Information Processing Letters*, 9, 223—228.
- Chackhva V, Ghare P, Moore J 1979: Applications of Graph Theory Algorithm's. Elsevier North Holland
- Powel M J D 1977: Numerical Methods for Fitting Functions of two Variables. In: *The State of the Art in Numerical Analysis*, D Jacobs ed. Academic Press, 563 —604.
- Rhynsburger D 1973: Analytic Delineation of Thiessen Polygons. *Geographical Analysis* 5, 133—144.
- Strang G, Fix G J 1973: An Analysis of the Finite Element Method, Prentice-Hall Inc., Englewood Cliffs, N. J.
- Tomescu I 1978: Combinatorics and its Applications. (In Hungarian) Műszaki Könyvkiadó, Budapest
- Závoti J 1982: Sopron Surface Modelling by Splines. In: *Proceeding of the Symposium Mathematical Models, Accuracy Aspects and Quality Control*, Helsinki, 540—551.

EFFECT OF SURFACE TOPOGRAPHY ON MAGNETOTELLURIC MEASUREMENTS (H-POLARIZATION)

S A TAVARTKILADZE¹

[Manuscript received March 16, 1984]

The paper presents an effective numerical method to solve the problems about the influence of the earth surface relief on the results of magnetotelluric (MT) investigations in case of a magnetic polarization of the primary electromagnetic field. The uniqueness of the solution is proved, an algorithm is given for the solution and a complete numerical analysis of the given problem is presented which can be extended without violation of generality with some insignificant alterations to a broad class of such type 2-D problems.

The method of the eigenfunctions proved to be a universal numerical method; the computer realization does not imply serious complications.

At first the fundamental distortion factors due to the effect of the surface variations are determined in a wide frequency spectrum on *H*-polarized MTS curves. This enables to elaborate fundamental criteria for interpretation of MT-data in hilly regions for the given polarization.

Keywords: H-polarization; integral equations; magnetotellurics; mathematical modeling; topographic effect

Recently there was a rapid development in the magnetotelluric methods applied to the investigation of the Earth's geological structure. The theory of MT soundings, developed by Tikhonov and Cagniard, presumes that the Earth consists of plane-homogeneous horizontal layers which is certainly an idealization. Big difficulties occur in the interpretation of MT-data within the framework of the 1-D Tikhonov-Cagniard model. In hilly regions the distortion of the curves of MT-soundings is caused in a great extent by variations of the earth surface relief.

This study is denoted to investigate the influence of an elevation of the Earth's surface on the results of deep MT-soundings for the *H*-polarized primary electromagnetic field. A four-layered earth model will be considered, being typical for the deep MTS investigations, namely:

$$\sigma(z) = \begin{cases} \sigma_0 \ll 1 & \text{at } z < f(y) \text{ (air)} \\ \sigma_1 & \text{at } f(y) < z < h_1 \\ \sigma_2 \ll 1 & \text{at } h_1 < z < H \\ \sigma_3 = \infty & \text{at } z > H \end{cases} \quad (1)$$

¹ Geophysical Institute of the Georgian Academy of Sciences, 380 093 Tbilisi, Rukhadze Zoi 1, USSR.

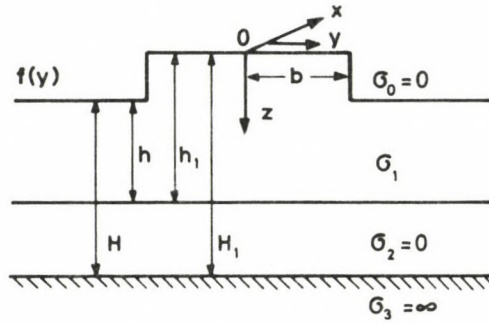


Fig. 1.

in the field of a vertically incident plane electromagnetic wave (a time dependence $e^{i\omega t}$ is assumed). In addition, we suppose that the given medium has a rectangular elevation described by the equation (Fig. 1):

$$Z = f(y) = \begin{cases} 0 & \text{at } |y| < l \\ h_1 - h & \text{at } |y| \geq l. \end{cases} \quad (2)$$

It is assumed that the magnetic permeability is everywhere equal to the magnetic permeability of the vacuum. The specific resistivity of the layers $\rho = 1/\delta$ is measured in mhos, besides the upper half-space $z < f(y)$ and the second layer have infinitely high electrical specific resistivity: $\rho \rightarrow \infty$, and the resistivity of the substratum is infinitely low: $\rho \rightarrow 0$, the medium has a rectangular elevation with a height $\Delta h = h_1 - h$, the half-width of the elevation is l , the thickness of the upper layer is h at $|y| \geq l$ and h_1 at $|y| < l$. The depth to perfectly conducting substratum is H beyond the elevation and H_1 in the region of the elevation. It is supposed that the elevation of the Earth surface is local. The model is excited by a plane electromagnetic wave having the form:

$$H_x^0 = \tilde{H}_{x0} e^{iK_0 z},$$

where $K_0 = \sqrt{-i\omega\mu_0\sigma_0}$, $\text{Re } K_0 \geq 0$; ω — angular frequency. Because the models of the field and the medium satisfy the condition $\partial/\partial x \equiv 0$, the total electromagnetic field breaks up into two independent polarizations: magnetic, H - and electric, E -polarizations.

In this study we shall examine the H -polarized electromagnetic field. Since we solve the MTS problem, we shall be interested in the relative characteristics of the medium and the field. Therefore, without loss of generality, it can be assumed that $\tilde{H}_{x0} = 1$. In this case the constituent components of the electromagnetic field have the form:

$$\vec{H} = \{H_x, 0, 0\} \quad \vec{E} = \{0, E_y, E_z\}.$$

According to Maxwell's equations they are connected by the following relations:

$$E_y = \frac{1}{\sigma_i} \frac{\partial H_x}{\partial z}; \quad E_z = -\frac{1}{\sigma_i} \frac{\partial H_x}{\partial y},$$

where $i = 0, 1, 2$.

The function $H_x(y, z)$ satisfies Helmholtz's equation:

$$\Delta H_x(y, z) + K_1^2 H_x(y, z) = 0 \tag{3}$$

where $\Delta = \frac{\partial^2}{\partial y^2} + \frac{\partial^2}{\partial z^2}$ is the Laplacian operator; the boundary conditions are:

$$\begin{aligned} H_x(y, z) &= 1 && \text{at } z = f(y) \\ H_x(y, z) &= f(h, H, \sigma_1) = e && z = h, |y| \geq l \\ & && z = h_1, |y| < l \end{aligned}$$

and the continuity conditions:

$$[H_x(y, z)] = \left[\frac{1}{\sigma_1} \frac{\partial H_x(y, z)}{\partial z} \right] = 0$$

where square brackets mean the difference between limiting values of functions and their normal derivatives on the opposite sides of a line where the conductivity of the medium has a discontinuity

further the conditions in infinity

$$[H_x(y, z) - H_x^n(y, z)] \rightarrow 0 \quad \text{at } y \rightarrow \pm \infty,$$

where $H_x^n(y, z)$ is the normal field on the surface of the model at $|y| \rightarrow \infty$, $H_x(y, z)$ is a constant quantity at the lower boundary of the top layer and does not depend on the coordinates y, z , but it is a function of the geometric and the electromagnetic parameters of the model. Since the conductivity of the second layer is $\sigma_2 \rightarrow 0$, Neuman's problem is obtained for the determination of the

$$H_x(y, z)|_{z=h}$$

function, its solution is:

$$H_x(y, z)|_{z=h} = \frac{\beta}{\beta \cos K_1 h_1 + K_1 h_1 \sin K_1 h_1},$$

where $\beta = \frac{h_1}{h_1 - H}$.

Consequently, the problem to determine the $H_x(y, z)$ function is fully established. We shall show that the solution of the problem (3) is unique. To this end the function $\tilde{H}_x = H_{x_1} + H_{x_2}$ is introduced, where H_{x_1} and H_{x_2} are arbitrary solutions of the problem (3). Taking into account the previously mentioned properties of the functions $\tilde{H}_x(y, z)$, inside the layer the function \tilde{H}_x will satisfy Helmholtz's equation:

$$\Delta \tilde{H}_x + K_1^2 \tilde{H}_x = 0,$$

the boundary conditions are:

$$\begin{aligned} \tilde{H}_x &= 1 && \text{at } z = f(y) \\ \tilde{H}_x &= f(h, H, \sigma_1) = e && \text{at } \begin{cases} h, |y| \geq l \\ h_1, |y| < l \end{cases} \end{aligned}$$

the continuity conditions:

$$[\tilde{H}_x(y, z)] = \left[\frac{1}{\sigma_1} \frac{\partial H_x(y, z)}{\partial z} \right] = 0,$$

and the conditions for infinity:

$$\frac{\partial \tilde{H}_x(y, z)}{\partial y} \rightarrow 0 \quad \text{at} \quad |y| \rightarrow \infty.$$

Applying Green's second formula to the functions \tilde{H}_x and \tilde{H}_x^* , where \tilde{H}_x^* is the complex conjugate of \tilde{H}_x in the region $V \{ \infty < y < +\infty, f(y) < z < h \}$, it is obtained

$$\iint_V (\tilde{H}_x \Delta \tilde{H}_x^* - \tilde{H}_x^* \Delta \tilde{H}_x) dV = \oint_C \left(\tilde{H}_x^* \frac{\partial \tilde{H}_x}{\partial n} - \tilde{H}_x \frac{\partial \tilde{H}_x^*}{\partial n} \right) dC,$$

where C is the contour of the region V , n is the normal to the contour C . Taking into account that the equations, boundary conditions and conditions for infinity should be satisfied by the functions \tilde{H}_x and \tilde{H}_x^* , we obtain:

$$2K_1^2 \iint_V |\tilde{H}_x|^2 dV = 0.$$

It is known that $K_1^2 = i\omega\mu_0\sigma_1$, $\sigma_1 > 0$, $|\tilde{H}_x|^2 \geq 0$. Therefore, $\tilde{H}_x = 0$ in the region V and the solution of the boundary problem (3) to determine the functions $H_x(y, z)$ is proven to be unique.

It is advantageous to solve the boundary problem (3) by the method of the eigenfunctions. For this it is necessary to transform the homogeneous equation with the inhomogeneous boundary conditions into an inhomogeneous equation with homogeneous boundary conditions. Then the solution is expanded into series. Besides it is obtained an infinite system of normal differential equations with related boundary conditions to determine the coefficients of the expansion. If the region of the determination of the functions $H_x(y, z)$ consists of rectangles in which the solution can be described by known functions and constant coefficients, then an infinite system of linear algebraic equations is obtained for these coefficients. The numerical solution does not imply particular mathematical difficulties.

At first let us separate the normal component of the magnetic field in regions where the thickness of the inhomogeneous surface layer is constant:

$$H_x(y, z) = \frac{\sin K_1(h_1 - z) + C \sin K_1 z}{\sin K_1 h_1} + U(y, z) \quad (4)$$

at $0 < z < h_1; |y| < l$

$$H_x(y, z) = \frac{\sin K_1(h_1 - z) + C \sin K_1 [z - (h_1 - h)]}{\sin K_1 h} + V(y, z) \quad (5)$$

at $h_1 - h < z < h; |y| \geq l$.

To determine the functions $U(y, z)$ and $V(y, z)$ we shall use following boundary problems:

The function $U(y, z)$ satisfies Helmholtz's equation:

$$\Delta U(y, z) + K_1^2 U(y, z) = 0 \quad \text{at} \quad 0 < z < h_1; \quad |y| < l$$

the homogeneous boundary conditions:

$$U(y, z) = 0 \quad \text{at} \quad z = 0 \quad \text{and} \quad z = h_1.$$

The function $V(y, z)$ satisfies Helmholtz's equation, too:

$$\Delta V(y, z) + K_1^2 V(y, z) = 0 \quad \text{at} \quad z = h_1 - h \quad \text{and} \quad z = h, \quad |y| \geq l$$

and the conditions for infinity, which have the following form:

$$V(y, z), \frac{\partial V(y, z)}{y} \rightarrow 0 \quad \text{at} \quad |y| \rightarrow \infty.$$

In addition the functions $U(y, z)$ and $V(y, z)$ have to fit the boundary conditions at $|y| = l$, what follows straightforwardly from the continuity of the components H_x and E_y of the electromagnetic field and have the following form:

at $0 < z < h_1; \quad |y| = l$

$$\frac{\sin K_1(h_1 - z) + e \sin K_1 z}{\sin K_1 h_1} + U(y, z) = \frac{\sin K_1(h_1 - z) + e \sin K_1[z - (h_1 - h)]}{\sin K_1 h} + V(y, z) \quad (6)$$

at $h_1 - h < z < h; \quad |y| \geq l$

$$\frac{\partial U(y, z)}{\partial y} = \frac{\partial V(y, z)}{\partial y}. \quad (7)$$

By the method of the separation of variables, the general solution of the problem is found for the functions $U(y, z)$ and $V(y, z)$ in the following form:

$$U(y, z) = \sum_{n=1}^{\infty} a_n \frac{\text{sh } g_n(h_1)|y|}{\text{ch } g_n(h_1)l} \sin \frac{n\pi z}{h_1},$$

where

$$g_n(h_1) = \sqrt{\left(\frac{n\pi}{h_1}\right)^2 + K_1^2}, \quad \text{Re } g_n(h_1) \geq 0 \quad (8)$$

$$V(y, z) = \sum_{n=1}^{\infty} b_n \exp\{-g_n(h)[|y| - l]\} \sin \frac{n\pi(h-z)}{h}, \quad (9)$$

where

$$g_n(h) = \sqrt{\left(\frac{n\pi}{h}\right)^2 - K_1^2}, \quad \text{Re } g_n(h) \geq 0.$$

The quantities a_n and b_n are the coefficients of the expansion of the functions $U(y, z)$ and $V(y, z)$ into Fourier series at the section $|y|=l$ and can be determined as follows:

$$a_n = \frac{2}{h_1} \int_0^{h_1} U(y, z)|_{|y|=l} \sin \frac{n\pi z}{h_1} dz$$

$$b_n = \frac{2}{h} \int_{h_1-h}^h V(y, z)|_{|y|=l} \sin \frac{n\pi z}{h_1} dz.$$

Substituting expressions (8) and (9) into boundary condition (6) and applying the Fourier transformation in the section $\{|y|=l, 0 < z < h_1\}$ one gets

$$\int_0^{h_1} \frac{\sin K_1(h_1-z) + e \sin K_1 z}{\sin K_1 h_1} \sin \frac{n\pi z}{h_1} dz + \int_0^{h_1} \sum_{n=1}^{\infty} a_n \sin \frac{n\pi z}{h_1} \sin \frac{n\pi z}{h_1} dz =$$

$$= \int_0^{h_1-h} \sin \frac{n\pi z}{h_1} dz + \int_{h_1-h}^{h_1} \frac{\sin K_1(h_1-z) + e \sin K_1[z-(h_1-h)]}{\sin K_1 h} \cdot$$

$$\cdot \sin \frac{n\pi z}{h_1} dz + \int_{h_1-h}^{h_1} b_n \sin \frac{n\pi(h_1-z)}{h} \sin \frac{n\pi z}{h_1} dz. \quad (10)$$

Derivating (8) and (9) with respect to y , then inserting them into the boundary conditions (7) and applying the Fourier transformation in the section $\{|y|=l, h_1-h < z < h\}$, we obtain:

$$\int_{h_1-h}^{h_1} \sum_{n=1}^{\infty} a_n g_n(h_1) \frac{\text{sh } g_n(h_1)l}{\text{ch } g_n(h_1)l} \sin \frac{n\pi z}{h_1} \sin \frac{n\pi z(h_1-z)}{h_1} dz =$$

$$\int_{h_1-h}^h \sum_{n=1}^{\infty} b_n g_n(h) \sin \frac{n\pi(h_1-z)}{h} \sin \frac{n\pi(h_1-z)}{h} dz. \quad (11)$$

Having calculated the integrals occurring in the expressions (10) and (11) an infinite system of linear algebraic equations is obtained to determine the coefficients a and b :

$$a_m = A_m + \sum_{n=1}^{\infty} \alpha_{mn} b_n \quad m = 1, 2, 3, \dots, N_1 \quad (12)$$

$$b_m = \sum_{n=1}^{\infty} \beta_{mn} a_n \quad m = 1, 2, 3, \dots, N_2, \quad (13)$$

where

$$A_m = \frac{2}{h_1} \left[\frac{(-1)^m}{\frac{m^2 \pi^2}{h_1^2} - K_1^2} \left(\frac{m\pi}{h_1} \cot \frac{m\pi h}{h_1} - K_1 \cot K_1 h \sin \frac{m\pi h}{h_1} + \right. \right. \\ \left. \left. + CK_1 \frac{\sin \frac{m\pi h}{h_1}}{\sin K_1 h} \right) - \frac{m\pi/h_1}{\frac{m^2 \pi^2}{h_1^2} - K_1^2} - \frac{(-1)^m h_1}{m\pi} \cos \frac{m\pi h}{h_1} + \frac{h_1}{m\pi} \right] \quad (14)$$

$$\alpha'_{mn} = \begin{cases} -\frac{2}{h_1} \sum_{n=1}^{\infty} \frac{(-1)^{n+m} n \sin \frac{m\pi h}{h_1}}{h\pi \left[\left(\frac{m}{h_1} \right)^2 + \left(\frac{n}{h} \right)^2 \right]} & \text{at } \frac{m}{h_1} \neq \frac{n}{h} \\ (-1)^{m+1} \frac{h}{h_1} & \text{at } \frac{m}{h_1} = \frac{n}{h} \end{cases} \quad (15)$$

$$\beta_{mn} = \begin{cases} \sum_{n=1}^{\infty} \frac{2}{h} \frac{g_n(h_1)}{g_n(h)} \frac{\text{sh } g_n(h_1)l}{\text{ch } g_n(h_1)l} \frac{(-1)^{n+m} m \sin \frac{n\pi h}{h_1}}{h\pi \left[\left(\frac{n}{h_1} \right)^2 - \left(\frac{m}{h} \right)^2 \right]} & \text{at } \frac{n}{h_1} \neq \frac{m}{h} \\ (-1)^n \frac{\text{sh } g_m(h)l}{\text{ch } g_m(h)l} & \text{at } \frac{n}{h_1} = \frac{m}{h} \end{cases} \quad (16)$$

Accordingly the problem to solve the boundary problem for the determination of the functions $H_x(y, z)$ is reduced to the solution of an infinite system of linear algebraic equations the solution of which can be realized on a computer. When numerically realizing the method on a computer, the infinite system is reduced to a finite system of linear algebraic equation.

It follows from the condition to fit the functions $H_x(y, z)$ at the boundaries of divisions of the conductivity $\sigma_1(y)$ that the quantities a_n are the coefficients of the Fourier expansions of the functions having discontinuity in their first derivatives and therefore they vanish as $1/n^2$ at $n \rightarrow \infty$. The quantities b_n are the coefficients of the Fourier expansions of the functions having integrable second derivatives and therefore they vanish as $1/n^3$ at $n \rightarrow \infty$.

From Eqs (12) and (13) it is possible to eliminate a_n or b_n and to get an infinite system of linear algebraic equations concerning a_n or b_n . When solving such a system it is necessary to switch over a finite system of equations the solution of which does not change or changes only slightly when the number of the equations is increased further in the given system. It is necessary to take into account that switching over from the infinite systems (12) and (13) to the finite systems, in the system (12) significantly more

unknowns are to be conversed then in the system (13). Therefore it is more suitable to solve the system (13) with a smaller number of unknowns, for example with N_1 , and then to calculate from (12) the coefficients a_n for a large number $N_2 > N_1$.

It was found at numerical investigations of the given problems that the quantity N_1 should be chosen sufficiently large to obtain an acceptable result in the surroundings of the point $|y|=l$ while on the other hand the results are satisfactory in other points at considerably smaller N_1 values. This fact is very important for the practice. In addition using the symmetry of the problem it is possible to carry out the computation not for each point $-\infty < y < +\infty$, but only for the values $0 \leq y < +\infty$. It should be further remarked that at $H \rightarrow \infty$ the problem for the applied MTS is automatically obtained.

Solving the reduced system and taking into account the above mentioned remarks, we obtain the approximate values of the coefficients a_n and b_n with the given accuracy. Knowing these quantities the function $H_x(y, z)$ can be determined further according to Maxwell's equations also all components of the electromagnetic field and the apparent resistivity of the medium.

The electric field component on the surface of the medium the form

$$E_y(y, z) = \frac{1}{\sigma_1} \frac{\partial H_x(y, z)}{\partial z} \begin{cases} \frac{c - \cos K_1 h}{\sin K_1 h} + \sum_{n=1}^{N_2} \tilde{b}_n \frac{n\pi}{K_1 h} \exp\{-g_n(h)(|y|-l)\} (-1)^{n+1} & \text{at } |y| < l \\ \frac{c - \cos K_1 h_1}{\sin K_1 h_1} + \sum_{n=1}^{N_1} \tilde{a}_n \frac{n\pi}{K_1 h_1} \frac{\operatorname{ch} g_n(h_1)y}{\operatorname{ch} g_n(h_1)l} & \text{at } |y| \geq l. \end{cases}$$

For calculating the impedance we get the following formula.

$$Z = \frac{E_x}{H_x} = \begin{cases} -E_y(y, 0) & \text{at } |y| < l \\ -E_y(y, h_1 - h) & \text{at } |y| \geq l. \end{cases}$$

The relative apparent resistivity equals:

$$\tilde{\rho} = \frac{\rho_k}{\rho_1} = \frac{\sigma_1}{\omega\mu_0} |z|^2 = \begin{cases} \frac{\sigma_1}{\omega\mu_0} |E_y(y, 0)|^2 & \text{at } |y| < l \\ \frac{\sigma_1}{\omega\mu_0} |E_y(y, h_1 - h)|^2 & \text{at } |y| \geq l, \end{cases}$$

where ρ_k = the apparent resistivity of the medium.

According to this algorithm the curves of MTS and the components of the normalized electrical field, $l_y = \frac{E_y}{E_y^0}$ have been calculated by the present author, where

$E_y^0 = E_y(z = h_1 - h, |y| = \infty)$, for normalized parameters of the model:

$$v_1 = \frac{H_1}{h}, \quad v = \frac{H}{h}, \quad \gamma = \frac{\sigma_2}{\sigma_1}, \quad \mu = \frac{h_1}{h}, \quad L = \frac{l}{h}, \quad \lambda = \frac{\Lambda}{h}, \quad d = \frac{y}{h},$$

where Λ = the wavelength in the inhomogeneous upper layer:

$$\Lambda = \frac{R_1 K_1}{2n}.$$

In Figs 2a and 2b the curves of the variations of the amplitude $|E_y|$ — the normalized electrical field — are presented vs. d for different λ values. In Figs 3a and 3b the curves of $\tilde{\rho}$ are presented in different points of the profile d . As it appears from this graphic display the formal interpretation of the MTS curves obtained in a hilly region may give an erroneous geoelectrical section within the framework of the Tikhonov-Cagniard model. It is remarkable that by decreasing the frequencies the distortions do not decay, however, they increase. It is very important for the practice to determine the distance where the distortion can be neglected.

It is apparent from the figures that the effect of the elevation is practically visible up to a distance h (being the thickness of the upper layer at $y \rightarrow \infty$).

We note that the presented numerical method makes possible to solve a large class of 2-D problem of the MTS theory taking into account the variation of the earth surface relief.

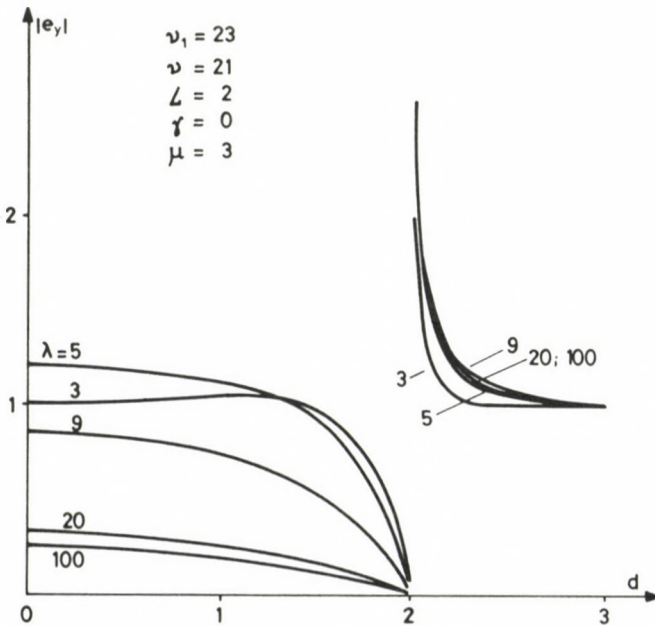


Fig. 2a.

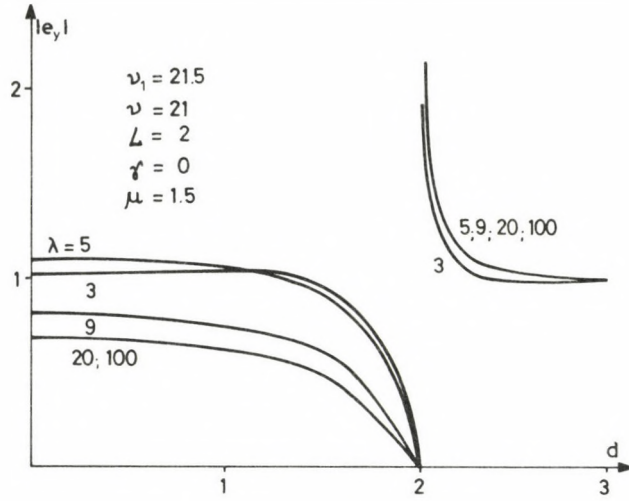


Fig. 2b.

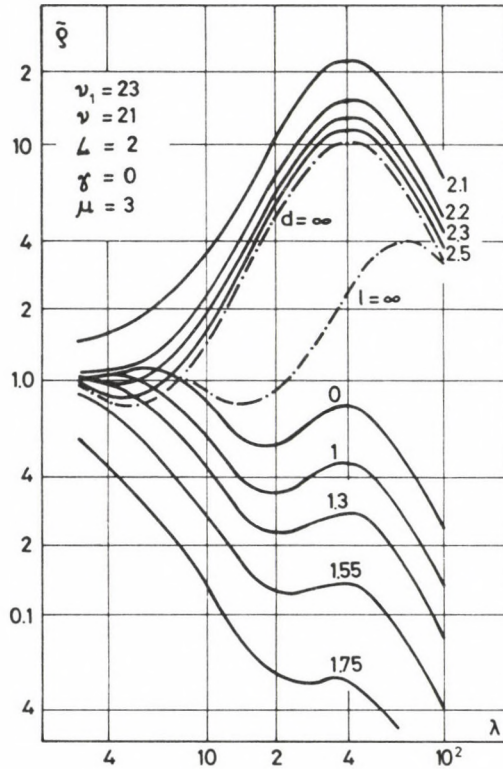


Fig. 3a.

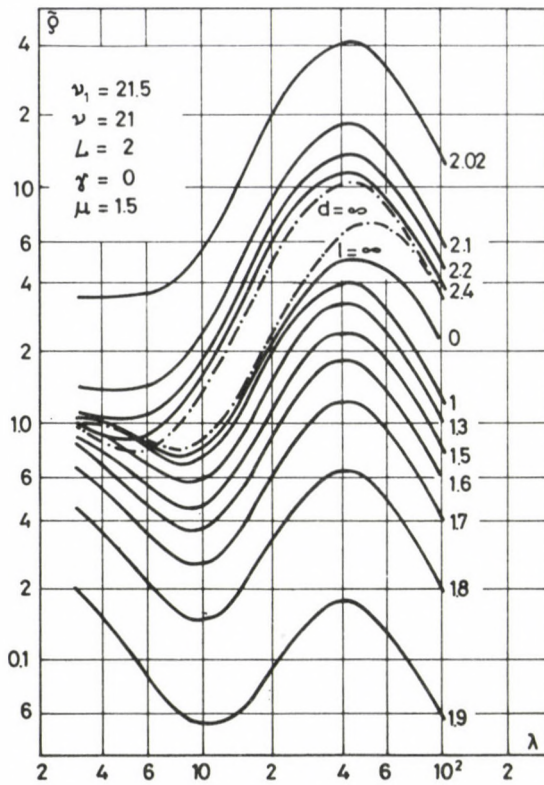


Fig. 3b.

Acknowledgement

Finally I wish to express my gratitude to Prof. V I Dmitriev for his help in the work, his helpful remarks and advices.

References

- Dmitriev V I 1968: Electromagnetic fields in inhomogeneous media (in Russian). Moscow State University
- Tavartkiladze S A 1978: A general mathematical treatment of boundary problems in calculation of the MT fields in inhomogeneous layered media taking into account the variations of the earth surface relief for different polarization of the primary electromagnetic field. In collected paper: "Results of geophysical investigation of the Earth's crust in Caucasus", Tbilisi, Metsnireda
- Tavartkiladze S A 1980: Calculation and analysis of normal and asymptotic curves of the deep magnetotelluric soundings taking into account the variations of the earth surface relief. In collected paper: "Interconnection between the deep structure of Caucasus and some geophysical fields", Tbilisi, Metsnireda

EFFECT OF SURFACE TOPOGRAPHY ON MAGNETOTELLURIC MEASUREMENTS (E-POLARIZATION)

S A TAVARTKILADZE¹

[Manuscript received March 16, 1984]

The paper presents the method of integral equations to investigate the influence of the earth surface relief on the results of MT-measurements in case of the electric polarization of the primary electromagnetic field. The uniqueness of the solution is proved, an algorithm is given for the solution and a numerical investigation of the problem is presented which can be extended without violation of generality with insignificant modifications to a broad class of such type 2-D problems. The essence of the method is the following: the problem of the MTS theory is reduced to a second kind Fredholm type integral equation which conduces to an infinite system of linear algebraic equations and the numerical solution of this system does not imply serious mathematical complications.

The method of integral equations proved to be a convenient numerical method. By the help of this method we succeeded to solve a broad class of MTS problems in inhomogeneous layered media.

At first the characteristics of the distortion effects of the earth surface relief are determined in a wide frequency spectrum on the *E*-polarized MTS curves. This enables to find the fundamental criteria for the interpretation of the magnetotelluric field measurements in hilly regions for the given polarization.

Keywords: *E*-polarization; integral equations; magnetotellurics; mathematical modeling; topographic effect

The present study is devoted to investigate the effect of a rectangular elevation of the earth's surface on the results of deep MT soundings in case of the electrical polarization of the primary electromagnetic field.

A four-layered earth model is considered typical for the deep MT investigations, namely:

$$\sigma(z) = \begin{cases} \sigma_0 \ll 1 & \text{at } z < f(y) \text{ (air)} \\ \sigma_1 & \text{at } f(y) < z < h_1 \\ \sigma_2 \ll 1 & \text{at } h_1 < z < H \\ \sigma_3 \rightarrow \infty & \text{at } z > H \end{cases} \quad (1)$$

in the field of a vertically incident plane electromagnetic wave (a time dependence $e^{i\omega t}$ is assumed). In addition it is supposed that the medium has a rectangular elevation described by the equation (Fig. 1):

$$z = f(y) = \begin{cases} 0 & \text{at } |y| < l \\ h_1 - h & \text{at } |y| \geq l \end{cases}$$

¹ Geophysical Institute of the Georgian Academy of Sciences. 380 093 Tbilisi, Rukhadze Zoi 1. USSR

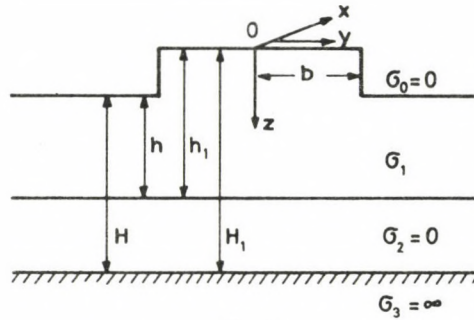


Fig. 1

It is assumed that the magnetic permeability is everywhere equal to the magnetic permeability of the vacuum. The specific resistivity of the layers $\rho = \frac{1}{\sigma}$ is measured in mhos, besides the upper halfspace $z < f(y)$ and the second layer have infinitely high electrical specific resistivity $\rho \rightarrow \infty$ and the resistivity of the substratum is infinitely low $\rho \rightarrow 0$; the medium has a rectangular elevation relief of a height $\Delta h = h_1 - h$, the halfwidth of the elevation is l , the thickness of the upper inhomogeneous layer is equal to h at $|y| \geq l$ and to h_1 at $|y| < l$. The depth to the perfectly conducting substratum is H beyond the elevation and H_1 in the region of the rectangular elevation. It is supposed that the elevation of the surface is local which is important in the numerical realization of the present problem, but it does not restrict its generality. The model is excited by a plane electromagnetic wave having the form:

$$E_x^0 = \tilde{E}_0 e^{ik_0 z},$$

where $k_0 = \sqrt{-i\omega\mu_0\sigma_0}$, $Re k_0 \geq 0$, $\omega =$ angular frequency. Because the models of the electromagnetic field and the inhomogeneous stratified medium satisfy the condition $\partial/\partial x \equiv 0$, the total electromagnetic field breaks up into two independent polarizations: magnetic- H and electric- E polarizations.

In this study the E -polarized electromagnetic field will be examined. Since the MTS problem is to be solved we are interested in the relative characteristics of the medium and the field. Therefore, without loss of generality, it can be assumed that $E_{x_0} = 1$. In this case the components of the electromagnetic field have the form:

$$\vec{E} = \{E_x, 0, 0\}; \quad \vec{H} = \{0, H_y, H_z\}.$$

According to Maxwell's equations they are connected by the following relations:

$$H_y = \frac{1}{i\omega\mu} \frac{\partial E_x}{\partial z}, \quad H_z = -\frac{1}{i\omega\mu} \frac{\partial H_y}{\partial y} \quad \text{where } i=0, 1, 2.$$

The function $E_x(y, z)$ satisfies the Helmholtz equation:

$$\Delta E_x(y, z) + i\omega\mu_0\sigma(z)E_x(y, z) = 0 \tag{2}$$

and the boundary condition:

$$E_x(y, z) = 0 \quad \text{at} \quad z = H.$$

At every border of conductivity divisions, the conditions for continuity of the function $E_x(y, z)$ and its normal derivative are fulfilled:

$$[E_x(y, z)] = \left[\frac{\partial E_x(y, z)}{\partial n} \right] = 0,$$

where n is the normal to the border of conductivity divisions. The condition for infinity is the condition for vanishing the functions:

$$E_x(y, z) - E_x^0(y, z) \rightarrow 0 \quad \text{at} \quad z \rightarrow -\infty,$$

where $E_x^0(y, z)$ is the external field. The displacement currents compared with the conduction currents can be neglected. In this way the problem for determination of the function $E_x(y, z)$ is completely established. It is apparent that one has to determine the function $E_x(y, z)$ in the whole space, therefore the problems to calculate the electromagnetic field for the E -polarization include serious complications.

Before starting to solve the problem the uniqueness of its solution will be proved. For this aim a function is introduced in the following form:

$$\tilde{E}_x = E_{x_1} - E_{x_2},$$

where E_{x_1} and E_{x_2} are two solutions of investigated problem. Then the function \tilde{E}_x satisfies Helmholtz's equation in every layer:

$$\begin{aligned} \Delta \tilde{E}_x + k_0^2 \tilde{E}_x &= 0, & z < f(y) \\ \Delta \tilde{E}_x + k_1^2 \tilde{E}_x &= 0, & h(y) < z < h_1 \\ \Delta \tilde{E}_x + k_2^2 \tilde{E}_x &= 0, & h_1 < z < H, \end{aligned}$$

the boundary condition is $\tilde{E}_x = 0$ at $z = H$. On every border of conductivity (σ) discontinuity the conditions of continuity of the function \tilde{E}_x and its normal derivative are satisfied:

$$[\tilde{E}_x] = \left[\frac{\partial \tilde{E}_x}{\partial n} \right] = 0,$$

n = normal to the border of conductivity discontinuity. The condition for infinity is that the functions $\tilde{E}_x - E_x^0 \rightarrow 0$ vanish at $z \rightarrow -\infty$, where E_x^0 is the external field. (This is because $E_{x_1} = E_x^0 - E_x^1$, $E_{x_2} = E_x^0 - E_x^2$, $\tilde{E}_x = E_{x_1} - E_{x_2}$.)

Inside the layer $h(y) < z < H$ the condition $(\partial \tilde{E}_x / \partial y) \rightarrow 0$ is satisfied at $y \rightarrow \infty$. This condition means that in the infinity the structure presents a horizontally homogeneous medium. Let us consider the complex conjugate function of \tilde{E}_x which equals $\tilde{E}_x^* = E_{x_1}^* - E_{x_2}^*$. Applying the second Green formula to functions \tilde{E}_x and \tilde{E}_x^* in the region:

$$\{z < h(y), \quad h(y) < z < h_1, \quad h_1 < z < H\},$$

it is obtained:

$$\begin{aligned} \iint_{\{z < h(y)\}} (\tilde{E}_x L \tilde{E}_x^* - \tilde{E}_x^* L E_x) d\tau &= \oint_{C_1} \left(\tilde{E}_x^* \frac{\partial \tilde{E}_x}{\partial n} - \tilde{E}_x \frac{\partial \tilde{E}_x^*}{\partial n} \right) dC_1; \\ \iint_{\{h(y) < z < h_1\}} (\tilde{E}_x L \tilde{E}_x^* - \tilde{E}_x^* L \tilde{E}_x) d\tau &= \oint_{C_2} \left(E_x^* \frac{\partial \tilde{E}_x}{\partial n} - \tilde{E}_x \frac{\partial \tilde{E}_x^*}{\partial n} \right) dC_2; \\ \iint_{\{h_1 < z < H\}} (\tilde{E}_x L \tilde{E}_x^* - \tilde{E}_x^* L \tilde{E}_x) d\tau &= \oint_{C_3} \left(\tilde{E}_x^* \frac{\partial E_x}{\partial n} - \tilde{E}_x \frac{\partial \tilde{E}_x^*}{\partial n} \right) dC_3; \end{aligned}$$

where C_1, C_2, C_3 are the contours of the relative regions, $L = (\Delta - k_i^2)$ is Helmholtz's operator and $i = 0, 1, 2$. Summing up the obtained expressions, the contour integrals on the right side of the obtained expressions equal zero to ensure the continuity of the function $E_x(y, z)$ and its normal derivatives and conditions for infinity, therefore it is obtained

$$\begin{aligned} \iint_{\{z < h(y)\}} (\tilde{E}_x L \tilde{E}_x^* - \tilde{E}_x^* L \tilde{E}_x) d\tau + \iint_{\{h(y) < z < h\}} (\tilde{E}_x L \tilde{E}_x^* - \tilde{E}_x^* L \tilde{E}_x) d\tau + \\ + \iint_{\{h_1 < z < H\}} (\tilde{E}_x L \tilde{E}_x^* - \tilde{E}_x^* L \tilde{E}_x) d\tau = 0. \end{aligned}$$

It is known that

$$\Delta \tilde{E}_x - k_i^2 \tilde{E}_x = 0; \quad \Delta \tilde{E}_x^* - k_i^2 E_x^* = 0; \quad \tilde{E}_x \tilde{E}_x^* = |\tilde{E}_x|^2,$$

where $i = 0, 1, 2$. Therefore it is obtained:

$$k_0^2 \iint_{\{z < h(y)\}} |\tilde{E}_x|^2 d\tau + k_1^2 \iint_{\{h(y) < z < h_1\}} |\tilde{E}_x|^2 d\tau + k_2^2 \iint_{\{h_1 < z < H\}} |\tilde{E}_x|^2 d\tau = 0.$$

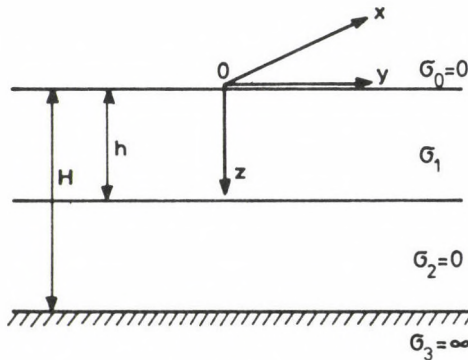


Fig. 2

As $k_i^2 = i\omega \mu \sigma_i$, $\mu = \mu_0 = \text{const}$, $\sigma_i \geq 0$, $|\tilde{E}_x|^2 \geq 0$, the expressions to be integrated are identically equal to zero, that is $\tilde{E}_x \equiv 0$ and $E_{x_1} = E_{x_2}$, which shows after all that the solution of the boundary problem (2) is unique.

Now, we start to solve the problem by the method of integral equations. Reducing the boundary problem (2) to a two-dimensional integral equation, so-called "normal" fields E_x^0 and H_y^0 are needed which correspond to horizontally homogeneous stratified media and the Green function corresponding to the examined problem. Let us examine the model of the horizontally stratified medium illustrated in Fig. 2. From the general solution of the equation

$$\frac{d^2 E_x^0(z)}{dz^2} + k_i^2 E_x^0(z) = 0,$$

where $i=0, 1, 2$, from the boundary condition $E_x^0=0$ at $z=H$ and the condition for infinity which has the form: $E_x - E_x^0 \rightarrow 0$ at $y \rightarrow \infty$, where E_x is the external field, it is obtained:

$$E_x^0(z) = l^{ik_0 z} + \frac{2k_0}{p} [(k_1 + \xi) l^{ik_1 h_1} + (k_1 - \xi) l^{ik_1 h_1}] l^{-ik_0 z} \quad (3)$$

where $0 < z \leq \infty$

$$\xi = \begin{cases} -ik_0 \cot k_0(h_1 - H) & \text{if } k_0 \neq 0; \\ -i \frac{1}{h_1 - H} & \text{if } k_0 = 0. \end{cases} \quad (3a)$$

According to Maxwell's equations for the magnetic field, we find:

$$H_y^0(z) = \frac{1}{i\omega\mu} \cdot \frac{dE_x^0(z)}{dz} = \frac{k_0}{\omega\mu} (l^{ik_0 z} + l^{-ik_0 z}) - \frac{2k_0^2}{\omega\mu p} [(k_1 - \xi) l^{-ik_1 h_1} + l^{ik_1 h_1} (k_1 - \xi)] l^{-ik_0 z}. \quad (4)$$

It is looked for a Green function for the horizontally stratified medium with the boundaries:

$$-\infty < z < 0, \quad z=0, \quad z=h \quad \text{and} \quad z=H,$$

vanishing in the infinity, continuous in its normal derivative at the boundaries $z=0$ and $z=h$, equal to zero at $z=H$, having a logarithmic characteristic for coinciding arguments and satisfying Helmholtz's equation:

$$\Delta_M G(MM_0) + K_1^2 G(MM_0) = -\delta(r_{MM_0}). \quad (5)$$

$$[G(MM_0)]|_{z=0,h} = \left[\frac{\partial G}{\partial n} \right] \Big|_{z=0,h} = 0$$

$$G(MM_0) = 0 \quad \text{at} \quad z = H,$$

$$G(MM_0) \rightarrow 0 \quad \text{at} \quad r_{MM_0} \rightarrow \infty,$$

where $i=0, 1, 2$; $r = \sqrt{(y-y_0)^2 + (z-z_0)^2}$.

For this purpose a Green function is produced in the form of the sum of the general solution corresponding to the homogeneous equation (5) which can be obtained by the method of separation of the variables and by the particular solution of the inhomogeneous equation (5). This particular solution is the function $H_0^{(1)}(K_i r_{MM_0})$ — Hankel's function of zero order and first kind. Using the integral representation of Hankel's functions and the boundary conditions for functions $G(MM_0)$ at $z, z_0 \leq 0$, it is obtained:

$$G(MM_0) = \frac{1}{2\pi} \int_0^{\infty} \cos \lambda(y - y_0) g(z, z_0, \lambda) d\lambda, \quad (6)$$

where

$$g(z, z_0, \lambda) = \frac{l^{\eta_0(z+z_0)}}{p \cdot \eta_0} \left[l^{-2\eta_1 h} (\eta_1 + \zeta) (\eta - \eta_0) - (\eta_1 - \eta_0) (\eta_1 - \zeta) + \frac{1}{\eta_0} l^{-\eta_0 |z - z_0|} \right] \quad (7)$$

$$\zeta = \eta_2 \frac{l^{2\eta_0(h-H)} + 1}{l^{2\eta_0(h-H)} - 1}; \quad \eta_i = \sqrt{\lambda^2 - K_i^2}; \quad \operatorname{Re} \eta_i \geq 0; \quad i = 0, 1, 2 \quad (8)$$

$$p = (\eta_1 + \eta_0) (\eta_1 - \zeta) - (\eta_1 - \eta_0) (\eta_1 + \zeta) l^{-2\eta_1 h}. \quad (9)$$

Now an integral equation is deduced for the function $E_x(y, z)$. For this purpose it is expressed in the following form:

$$E(y, z) = E_x^{(1)}(y, z) + E_x^0(y, z) \quad (10)$$

where E_x^0 expresses the normal, i.e. undisturbed, field in the horizontally stratified homogeneous medium (i.e. at $h_1 = h$). E_x^1 means the anomalous field. Physically this means that the total field is expressed as the sum of the normal and the anomalous fields. The surface at the inhomogeneity is denoted by

$$S = \{|y| < l, \quad 0 < z < h_1 - h\}.$$

The function $E_x(y, z)$ satisfies everywhere Helmholtz's equation:

$$\begin{aligned} \Delta E_x + \tilde{K}^2 E_x &= 0, & z < h(y) \\ \Delta E_x + K_1^2 E_x &= 0, & h(y) < z < h \\ \Delta E_x + K_2^2 E_x &= 0, & h < z < H \end{aligned} \quad (11)$$

where

$$\tilde{K} = \begin{cases} K_0 M \bar{\in} S; \\ K_1 M \in S. \end{cases}$$

Substituting the expression (11) into Eqs (10) they have the following form:

$$\begin{aligned} \Delta E_x^{(1)} + K_0^2 E_x^{(1)} &= \begin{cases} 0 & M \in \bar{S} \\ (K_0^2 - K_1^2) & M \in S \end{cases}, & z < h(y); \\ \Delta E_x^{(1)} + K_1^2 E_x^{(1)} &= 0, & h(y) < z < h; \\ \Delta E_x^{(1)} + K_2^2 E_x^{(1)} &= 0, & h < z < H. \end{aligned} \tag{12}$$

Function $E_x^{(1)}$ satisfies Eqs (12), the boundary condition at $z=H$, the condition of continuity of this function and its normal derivative everywhere at $z < H$ and vanishes in the infinity: $E_x^{(1)} \rightarrow 0$ at $|y| \rightarrow \infty$.

The second Green formula is applied to the functions $E_x^{(1)}$ and $G(MM_0)$, determined by Eq. (6), in the region $\{z < h(y), h(y) < z < h, h < z < H\}$. Summing up the formulae, the summarized field is obtained in the whole halfspace $z < H$. Taking into account the equations, the boundary condition, the continuity conditions and conditions for infinity, which are satisfied by function $E_x^{(1)}$, too, similarly to the proof of the uniqueness of the solution of the boundary problem, and taking into account the peculiarities of the functions $E_x^{(1)}$ and the delta functions, it is obtained after summation:

$$E_x^{(1)}(M_0) + (K_0^2 - K_1^2) \int\int_{z < h(y)} E_x(M) G(MM_0) dS_M + \int\int_{h(y) < z < h} E_x^{(1)}(M) + \int\int_{h < z < H} E_x^{(1)}(M_0) = 0.$$

It is known that:

$$\int\int_{z < h(y)} E_x^{(1)}(M_0) + \int\int_{h(y) < z < h} E_x^{(1)}(M_0) + \int\int_{h < z < H} E_x^{(1)}(M_0) = \int\int_{z < H} E_x^{(1)}(M_0).$$

Therefore we get:

$$E_x^{(1)}(M_0) + (K_0^2 - K_1^2) \int\int_S E_x(M) G(MM_0) dS_M = 0.$$

By adding the function $E_x^0(M_0)$, to the obtained expression it is obtained

$$E_x(M_0) + (K_0^2 - K_1^2) \int\int_S E_x(M) G(MM_0) dS_M = E_x^0(M_0). \tag{13}$$

In this way a two-dimensional Fredholm type integral equation of second kind is obtained on the surface of the rectangular elevation of the earth surface. It should be noted that the obtained integral equation (13) is equivalent to the initial boundary problem for calculating functions $E_x(y, z)$ relatively to the model of the structure of the medium, presented in Fig. 1. It follows from this that the solution of the problem is unique, too.

We normalize the function $E_x(M)$ to $E_x^0(0)$, i.e. a new function is introduced in the following form:

$$U(M) = \frac{E_x(M)}{E_x^0(0)}.$$

Then Eq. (13) is rewritten in the following form:

$$U(M_0) - (K_0^2 - K_1^2) \iint_S U(M) G(MM_0) dS_M = U_0(M_0). \quad (14)$$

The conductivity of the air and of the crystalline basement are equal to zero. It can be shown that the norm of the difference between the solution of Eq. (14) and the solution corresponding to the equation at $K_0 = K_2 = 0$ approaches zero when K_0 and K_2 approach zero, i.e.:

$$\|U - U'\| \rightarrow 0 \quad \text{at } K_0 \rightarrow 0 \quad \text{and } K_2 \rightarrow 0,$$

where U' = the solution of the limit equation. Physically this means that at $\sigma_0/\sigma_1 \ll 1$ and $\sigma_2/\sigma_1 \ll 1$ the conductivities of air and the crystalline basement are extremely small and their effect on the E -polarized MT field can be neglected. Taking into account this circumstance finally, we get

$$U(M_0) + K_1^2 \int_{-l}^{+l} \int_h^{h_1-h} U(M) G(MM_0) dy dz = U_0(M_0). \quad (15)$$

Using the symmetry of the problem along the axis oy , the region can be reduced to its half for which the integral equation is obtained:

$$\begin{aligned} & \int_{-l}^{+l} \int_h^{h_1-h} \{G(-y, z, y_0, z_0) + G(y, z, y_0, z_0)\} U(y, z) dy dz = \\ & = \int_{-l}^0 \int_h^{h_1-h} \{G(-y, z, y_0, z_0) + G(y, z, y_0, z_0)\} U(y, z) dy dz + \int_0^l \int_h^{h_1-h} \{G(-y, z, y_0, z_0) + \\ & + G(y, z, y_0, z_0)\} U(y, z) dy dz = \int_0^l \int_h^{h_1-h} R(MM_0) U(y, z) dy dz, \end{aligned} \quad (16)$$

where $R(MM_0) = \{G(-y, z, y_0, z_0) + G(y, z, y_0, z_0)\}$.

It is noted that at $H \rightarrow \infty$ the equation goes over into the equation of the prospecting variant of the MTS. Taking into account Eqs (15) and (16) the integral equation can be rewritten in the following form:

$$U(M_0) + K_1^2 \int_0^l \int_h^{h_1-h} R(MM_0) U(M) dy dz = U_0(M_0). \quad (17)$$

Integral equation (17) was solved by the method of reduction of the integral operator to a system of linear algebraic equations. Since the model of the structure of the medium, represented in Fig. 1, has an elevation on the surface with rectangular form, thus the kernel of the obtained integral equation can be integrated analytically and this fact definitely simplifies the algorithm of the solution of the problem.

In this way the following system of linear algebraic equations was finally solved:

$$\begin{aligned} U(y_{m+\frac{1}{2}}, z_{n+\frac{1}{2}}) + K_1^2 \sum_{j=0}^{n_2-1} \sum_{i=0}^{n_1-1} U(y_{i+\frac{1}{2}}, z_{j+\frac{1}{2}}) R_{ij}(y_{m+\frac{1}{2}}, z_{n+\frac{1}{2}}) = \\ = U_0(y_{m+\frac{1}{2}}, z_{n+\frac{1}{2}}), \end{aligned} \quad (18)$$

where: $m=0, 1, 2, \dots, n_1-2, n_1-1$; $n=0, 1, 2, \dots, n_2-2, n_2-1$;

$$R_{ij}(y_{m+\frac{1}{2}}, z_{n+\frac{1}{2}}) = \int_{y_i}^{y_{i+1}} \int_{z_j}^{z_{j+1}} R(y, z, y_{m+\frac{1}{2}}, z_{n+\frac{1}{2}}) dy dz =$$

$$= \int_0^\infty Q(y_i, y_{m+\frac{1}{2}}, \lambda) q(\lambda) G(z_j, z_{n+\frac{1}{2}}, \lambda) d\lambda;$$

$$Q(y_i, y_{m+\frac{1}{2}}, \lambda) = \cos \lambda y_{m+\frac{1}{2}} \cos \lambda y_{i+\frac{1}{2}};$$

$$q(\lambda) = \frac{2 \sin \lambda - \frac{\tau_1}{2}}{\lambda};$$

$$G_0(z_j, z_{n+\frac{1}{2}}, \lambda) = \frac{S}{\lambda^2} \left\{ \frac{1}{P} l^{\lambda(z_j+z_{n+\frac{1}{2}})} [l^{-2\eta_1 h} (\eta_1 + \zeta) (\eta_1 + \lambda) - (\eta_1 - \lambda) (\eta_1 - \zeta)] + g_1 \right\};$$

$$g = \begin{cases} l^{-\lambda(z_j - z_{n+\frac{1}{2}})} & \text{at } z_{n+\frac{1}{2}} < z_j; \\ \frac{2}{1 - l^{-\frac{\lambda \tau_2}{2}}} & \text{at } z_j < z_{n+\frac{1}{2}} < z_{j+1}; \\ l^{-\lambda(z_{n+\frac{1}{2}} - z_{j+1})} & \text{at } z_{n+\frac{1}{2}} > z_{j+1}; \\ S = 1 - l^{-\lambda \tau_2}. \end{cases}$$

The functions η, ζ, p are determined by Eqs (8) and (9)

$$U_0(y_{m+\frac{1}{2}}, z_{n+\frac{1}{2}}) = 1 + iK_1 z_{n+\frac{1}{2}} \frac{\alpha - 1}{\alpha + 1}$$

where

$$\alpha = \frac{K_1 + \xi}{K_1 - \xi} l^{-2K_1 h_1}; \quad \xi = -i \frac{1}{h - H}.$$

By solving the system of equations (18) the values of the functions $U(M)$ can be found inside the region of the rectangular elevation.

For convenience of realization of the problem on a computer and of the physical analysis of the obtained numerical material, the electromagnetic and the geometric parameters of the problem are normalized to the corresponding parameters of the first layer: $V_1 = H/h_1$ is the relative depth to the ideally conductive basement outside of the elevation, $\gamma = \sigma_2/\sigma_1$ is the relative conductivity of the second layer, $\mu = h_1/h$, the relative thickness of the elevation, $d = y/h$, the relative distance from the centre of the elevation,

$\lambda = A_1/h_1$, the relative wave number, where A_1 is the wave number in the first layer, $h_y = H_y/H_y^0$, $h_z = H_z/H_y^0$ the components of the relative magnetic field, where $H_y^0 = H_y(z = h_1 - h, d = \infty)$, $\tilde{\rho} = \rho_k/\rho_1$ — the relative apparent resistivity, where $\rho_1 = 1/\sigma_1$, $L = l/h$ — the relative half-width of the elevation.

We make some notes about the system of linear algebraic equations (18). The upper limits for the calculation of the improper integrals which are the coefficients of the system, can be estimated as the integrands vanish in the infinity either exponentially or as $1/\lambda^n$, where $n \geq 3$. The accuracy of the calculation of these improper integrals was determined numerically assuming that the error in the obtained results cannot be more than 0.1%.

The calculated results are shown in a table, calculated for different values of ε being the accuracy of the integration.

Table I

10^{-2}	10^{-3}	10^{-4}	10^{-5}	10^{-6}
11.807	11.808	11.769	11.760	11.760

In Table I $\tilde{\rho}$ is the relative apparent resistivity of the medium. The calculation was made for the following parameters of the model (Fig. 1):

$$\mu = 1.5; \quad V_1 = 21.5; \quad V = 21; \quad L = 2; \quad \lambda = 10; \quad d = 1.$$

Let us investigate further the error of the numerical results, occurring in the reduction of the integral operator to a system of linear algebraic equation. It is noted that the total averaging of the field along the vertical within the rectangular elevation ($n_2 = 1$) substantially shortens the time of the calculation, but this is permissible only for sufficiently low frequencies. Methodical calculations showed that even at high frequencies the number of grid points n_2 can be small (so-called partial averaging of the field). Some numerical results are shown for the following values of the parameters of the model: $\mu = 1.5$; $V_1 = 21.5$; $V = 21$; $L = 2$; $\lambda = 1$; $d = 1$, calculated for different values of n_2 (Table II).

Table II

3	5	8	10
1.012	1.004	1.001	1.000

In addition the number of grid points along the width of the inhomogeneity is constant and equals to $n_1 = 8$. The analysis of Table II shows that although the frequency is sufficiently high ($\lambda = 1$), at not too large values of n_2 the numerical results are totally satisfactory.

In a methodical analysis the effect of the number of grid points along the width of the elevation was also investigated. In Table III the numerical results are presented, as calculated for the same parameters of the model of the medium structure, shown in Fig. 1 as the results in Table II, at fixed values of the grid points along the vertical $n_1 = 4$.

Table III

6	8	10	12	15
1.002	1.004	1.006	1.007	1.008

It is to be noted that the matrix of the system (18) has a quadratic structure with a number of squares n_2^2 . Taking into account that the coefficients depend only on the absolute value of the sum and the difference of the arguments inside the square, it is sufficient to calculate the row and column of the square which considerably reduces the computer time for the calculation. The integrals necessary to form the square, were calculated by series for some points. This circumstance offered a large economy in the computer time because the complicated function G_0 was calculated only once in every point for the whole series of the integrand.

Taking into account all above mentioned remarks, the normalized components of the electromagnetic field have the following form

$$e_x = \frac{E_x(y_0 z_0)}{E_x^0(0)} = U(y_0, z_0), \tag{19}$$

$$h_y = \frac{H_y(y_0 z_0)}{H_y^0(0)} = C \frac{\partial U(y_0, z_0)}{\partial z_0}, \tag{20}$$

$$h_z = \frac{H_z(y_0 z_0)}{H_z^0(0)} = -C \frac{\partial U(y_0, z_0)}{\partial z_0}, \tag{21}$$

where

$$C = \frac{1}{iK_1} \frac{(K_1 + \xi)e^{-iK_1 h} - (K_1 - \xi)e^{iK_1 h}}{(K_1 + \beta)e^{-iK_1 h} + (K_1 - \xi)e^{iK_1 h}}, \quad \xi = -i \frac{1}{h - H} \tag{22}$$

$$U(y_0 z_0) = \begin{cases} 1 + K_1^2 \int_0^l \int_0^{h_1-h} U(M) R(MM_0) |_{z_0=0} dy dz & \text{at } |y| < l \\ \frac{E_x^0(z=h_1-h)}{E_x^0(0)} + K_1^2 \int_0^l \int_0^{h_1-h} U(M) R(MM_0) |_{z_0=h_1-h} dy dz & \text{at } |y| > l \end{cases} \tag{23}$$

$$\frac{\partial U(y_0 z_0)}{\partial z_0} = \begin{cases} \frac{1}{E_x^0(0)} \left[\frac{\partial E_x^0}{\partial z_0} \Big|_{z_0=0} + K_1^2 \int_0^l \int_0^{h_1-h} U(M) \frac{\partial R(MM_0)}{\partial z_0} \Big|_{z_0=0} dy dz \right] & \text{at } |y| < l \\ \frac{1}{E_x^0(0)} \left[\frac{\partial E_x^0}{\partial z_0} \Big|_{z_0=h_1-h} + K_1^2 \int_0^l \int_0^{h_1-h} U(M) \frac{\partial R(MM_0)}{\partial z_0} \Big|_{z_0=h_1-h} dy dz \right] & \text{at } |y| > l \end{cases} \quad (2)$$

$$\frac{\partial U(y_0 z_0)}{\partial y_0} = \begin{cases} \frac{1}{E_x^0(0)} \left[K_1^2 \int_0^l \int_0^{h_1-h} U(M) \frac{\partial R(MM_0)}{\partial y_0} \Big|_{z_0=0} dy dz \right] & \text{at } |y| < l \\ \frac{1}{E_x^0(0)} \left[K_1^2 \int_0^l \int_0^{h_1-h} U(M) \frac{\partial R(MM_0)}{\partial y_0} \Big|_{z_0=h_1-h} dy dz \right] & \text{at } |y| > l \end{cases} \quad (25)$$

where $E_x^0(0), H_y^0(0)$ are the components of the normal electromagnetic field determined by Eqs (3) and (4). The impedance and the apparent resistivity of the medium are determined from the expression:

$$Z = \frac{E_x}{H_y}; \quad \tilde{\rho} = \frac{\rho_k}{\rho_1} = \frac{\sigma_1}{\omega \mu_0} |Z|^2. \quad (26)$$

An analysis of the MTS curves is carried out from the point of view of their interpretation.

In Figs 3, 4 the curves of the variations of the amplitude of the normalized magnetic field components h_z and h_y are presented vs. d for different λ values. As it appears from these curves, the vertical component of the magnetic field, h_z is zero above the centre of the elevation (at $y=0, z=0$). Approaching the boundary of the elevation

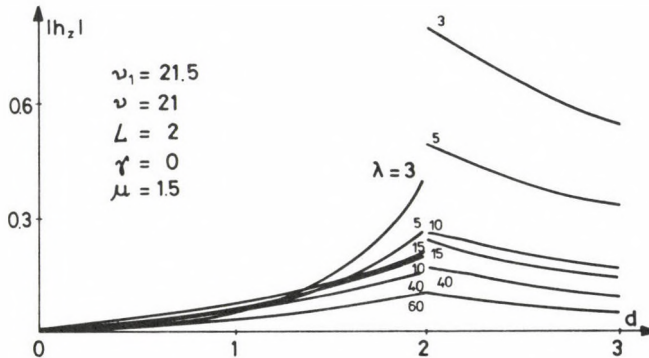


Fig. 3

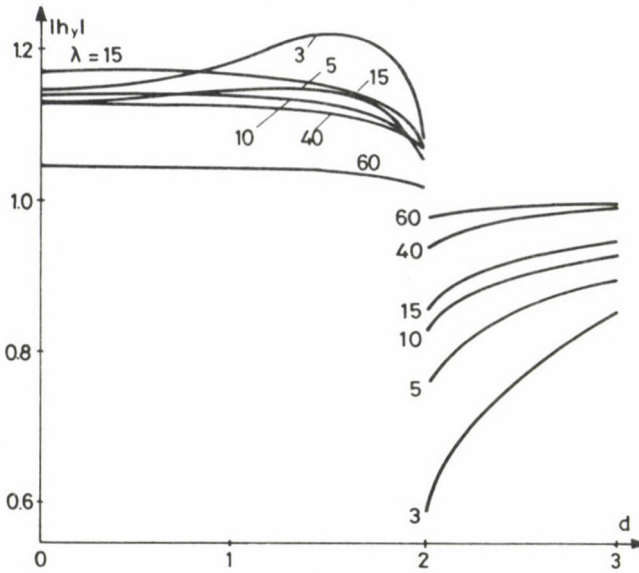


Fig. 4

($|y| = l$), h_z increases almost linearly with the distance, and the quicker the smaller is h_y . For values of λ that are commensurable with the geometric parameters of the inhomogeneous top layer, h_z can have values exceeding the values of the horizontal magnetic component, h_y . With increasing wavelength λ , the amplitude of h_z suitably decreases. The maximum value of h_z appears for the complete set of wavelength values at the boundary of the rectangular elevation ($|y| = l$). When moving away from this boundary ($d \rightarrow \infty$) h_z slowly vanishes.

The character of the variation of the horizontal magnetic field component is more complex. At small values of the wavelength λ approaching from the origin of the system of co-ordinates to the boundary of the inhomogeneity h_y increases to a definite value, exactly on the boundary, at the point $|d| = L$. (In our opinion this is caused by the horizontal skin effect.)

Approaching the boundary of the inhomogeneity from the side of the lowered part of the top layer, h_y increases. For relatively high values of the wavelength λ , the horizontal magnetic field component h_y decreases to a definite value when approaching the boundary of the inhomogeneity, and moving away from it, h_y increases. At $\lambda \rightarrow \infty$ the magnetic field reacts only slightly to the local inhomogeneity of the top layer.

It is noted that the anomaly both in h_z and in h_y increases with increasing width and height of the elevation.

In Figs 5, 6, the curves of the relative apparent resistivity $\tilde{\rho}$ are presented vs. d for different λ values. MTS curves are very strongly deformed in the high frequency range above the elevation. This is connected with the measuring point being above the essential boundary of the conductive medium ($z = h_1 - h$). If the elevation is very

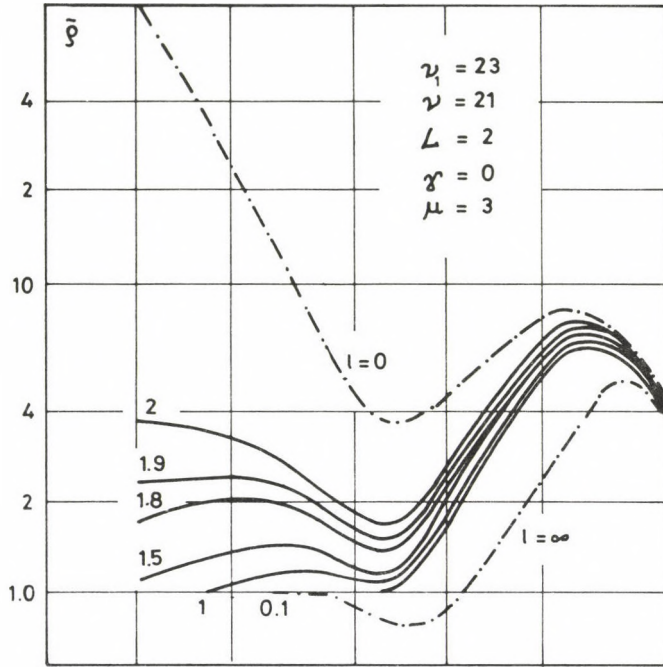


Fig. 5

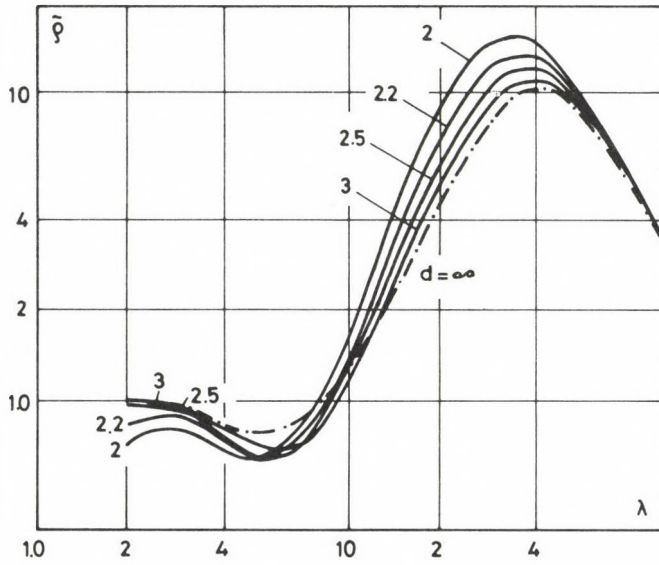


Fig. 6

narrow ($2l \rightarrow 0$), we should get the normal curve of $\tilde{\rho}$ for points being above the Earth's surface. For this curve the high frequency asymptote is not $\tilde{\rho} \rightarrow 1$, but $\tilde{\rho} \rightarrow \infty$. At a finite width of the elevation and at high frequencies, the curve $\tilde{\rho}$ increases at first and then at very high frequencies it begins to converge to 1, i.e. the width of the elevation appears already. At $y < l$ (the region of the elevation) MTS curves have false minima. Increasing the parameter μ at fixed L these minima move to the right. At $y > l$ (out of the elevation) MTS curves are slightly distorted. In this case these distortions become significant only at high values of the parameter μ . In the low frequency range the distortion of the MTS curves decreases gradually and at $\lambda \rightarrow \infty$ they vanish.

From the above said it follows that above the elevation at the E -polarization the MTS curve can have the form of a five-layered curve with the intermediate conductive layer and this can result in false geological structures. In this case the general method to select the distortions is to investigate the dependence of the MTS curve on the distance to the edge of the elevation and the analysis of the distorted magnetic field components.

Acknowledgement

Finally I wish to express my gratitude to Prof. V I Dmitriev for helpful advices and help in the work.

References

- Berdichevsky M N, Dmitriev V I 1976: Distortion of magnetic and electrical fields by near-surface lateral inhomogeneities. *Acta Geod. Geoph. Mont. Hung.*, 12, 447—483.
- Dmitriev V I 1968: Electromagnetic fields in inhomogeneous media (in Russian). Moscow State University
- Tavartkiladze S A 1978: A general mathematical treatment of boundary problems in calculation of the MT fields in inhomogeneous layered media taking into account the variations of the Earth surface relief for different polarization of the primary electromagnetic field. In the collection of papers: "Results of geophysical investigation of the Earth's crust in Caucasus", Tbilisi, Metsniereda

THE DUNAHARASZTI EARTHQUAKE JANUARY 12, 1956

GY SZEIDOVITZ¹

[Manuscript received June 5, 1984]

Existing data are reviewed about the intensity of the Dunaharaszti earthquake which occurred in the immediate vicinity of the Hungarian capital Budapest. The exact intensity values of this earthquake have economical consequences as it was the strongest shock ever recorded in the area, thus it influences earthquake risk prescriptions of buildings. A detailed survey of all existing data leads to a re-evaluation of the intensity data.

Keywords: Dunaharaszti earthquake; earthquake intensity; Hungary; seismic damages; seismicity

An earthquake occurred in the vicinity of the village Dunaharaszti on January 12, 1956 at 06 46 causing severe damages in several villages and a few casualties and more injuries were also recorded. The earthquake occurred in an area where previously in a narrower surrounding ($r = 30$ km) only quakes of intensities $I_0 \leq 5^\circ$ were observed (Fig. 1). Kiss (1958) estimated the epicentral intensity as $I_0 = 7^\circ$ based on the Mercalli—Cancani—Sieberg (MCS) scale. In an unpublished report, Simon (1956) obtained the intensity 7° , too, but when determining the focal depth, he used an epicentral intensity higher by 0.25° , and in a later manuscript (1957) he adopted the intensity 7.5° , while Csomor and Kiss (1962) wrote on a shock of 8° . Bendefy (1956) based on own experiences as well as on works by Láng (1956) and Somogyi (1956) estimated the maximum intensity as $8—9^\circ$.

The focal depth of the earthquake was determined by Simon (1956) in 8 km ($\alpha = 0.003/\text{km}$) based on the Kövesligethy—Cancani equation and the Sponheuer—Ullmann method. He obtained depth values between 4.4 and 10.2 km. The greatest differences belonged to the radii of the isoseists $r_7 = 8.5$ km ($h = 3.4$) and $r_6 = 20$ km ($h = 2.7$ km), for isoseist radii $r_5 = 45$ km, $r_4 = 75$ km, $r_{3.5} = 140$ km the deviations of the focal depths lied within $h = \pm 0.5$ km. Bisztricsány and Csomor (1958) computed 3.31 ± 1.1 km for the focal depth from microseismic data by using the records in Budapest, Kecskemét, Kalocsa, Hurbanovo, Vienna and Campulung. Since the two focal depth determinations by Simon and by Bisztricsány and Csomor resulted in rather different results, the computations have been repeated with both methods used by the mentioned authors. The results will be presented later.

¹ Geodetic and Geophysical Research Institute of the Hungarian Academy of Sciences, Seismological Observatory, Budapest, Meredek u. 18. H-1112

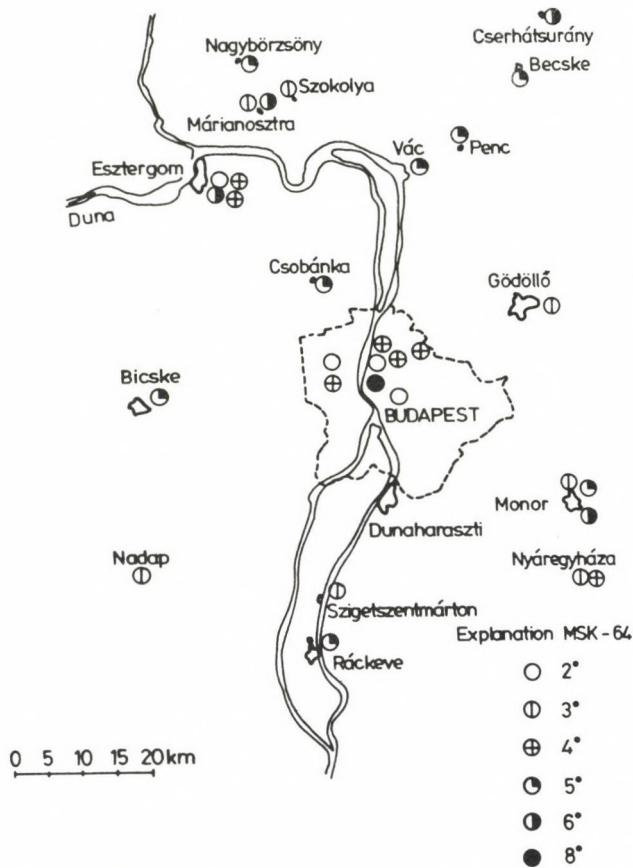


Fig. 1. Map of earthquakes having occurred in the area of Dunaharaszti till 1956

The time of the first arrival on the record of the Wiechert-type pendulum in Budapest differs also at different authors. Kiss (1958) considered 8.5 s as focal time, Simon (1956) 9.3 s. Szilbert and Csomor (1958) 12.8 s, Bisztricsány and Csomor (1958) 12.3 s. The two latter values coincide, as Bisztricsány and Csomor used a loose layer correction of 0.6 s.

The earthquake has been recorded both in Hungary and in the surrounding countries, thus allowing an instrumental determination of the magnitude. The probably most reliable determination of the magnitude was 5.6 based on the Anderson—Wood pendulum in Prague. The Wiechert pendulum in Budapest “unhooked” in consequence of the quake, but the Kalocsa and Szeged pendulums resulted in magnitudes of 5.4 and 5.9, using Bisztricsány’s equation (1974). The difference of 0.5 magnitude may be due to the fact that this magnitude equation can be hardly applied to the Mainka pendulum of the Szeged station.

Simon (1956) determined the magnitude of the earthquake from the epicentral intensity and the focal depth using Gutenberg and Richter’s (1948), Kárnik’s (1968) and

Shebalin's (1959) formulae. He obtained magnitudes between 4.7 and 5.8 and accepted 5 as the most reliable value. All the quoted methods have the common disadvantage that their authors conceived the equations on the basis of extra-Hungarian earthquakes, thus applied to Hungarian shocks they yield less reliable values. The magnitude 5 is anyway too low, and in addition to the already mentioned circumstances it shows the incorrectness of Simon's value of $I_0 = 7.25$.

This short bibliographical survey shows that the main parameters of the earthquake have been determined differently by different authors. In the following, the data about this earthquake will be re-evaluated using the MSK-64 intensity scale (Bisztricsány 1974) and the main parameters will be computed from these results.

This re-evaluation included data not only from the village Dunaharaszti, but also from Taksony and Szigetszentmiklós.

In Dunaharaszti from the existing 3500 buildings 3144 were damaged (reports, insurance minutes). A total of 1207 data could be re-evaluated. Buildings made of adobe and with cob walls having brick chimneys were considered as those belonging to group *A*, houses built of bricks to group *B*, with the remark that a considerable part of the brick buildings cannot be considered as category *B* brick or panel buildings, as they had low-quality fundamentals and mortar. The crowning closing the upper part of the walls was lacking, thus the connection between ceiling and walls was unsatisfactory.

The typical damage is the following: the brick chimney fell down in consequence of the earthquake, it broke through the tile roof and damaged the balks, eventually the ceiling. If brick chimneys fell down, then the damage belongs to the third degree damage type, but if it was not accompanied by other grave damages (deep cracks in the walls, gable fell down), then it was considered as a second degree damage type. As a further criterion of the third degree damage type, deep cracks in the walls were often encountered in adobe and cob wall buildings. A part of the adobe buildings and some brick buildings were damaged so gravely that they had to be demolished. To this group mostly belonged neglected houses. In spite of a complete destruction of the buildings in such cases, it was not considered as a fifth degree damage type, as it did not occur during the earthquake.

Simon (1957) determined the damages of single houses in intensity scale with meticulous work (Fig. 2). This map shows that the most damaged part of the village coincided with the most ancient part of the village called "Alte Haraszti". In 1974 a survey was carried out there to determine the quality of the houses. Some complementary informations from this survey are also presented in Fig. 2. It shows that there is no connection between the earthquake intensity and the damages found in houses 21 years after the earthquake.

All what has been said about Dunaharaszti, refers also to Taksony, where from among 678 damage reports 281 could be re-evaluated. The village had 4170 inhabitants. In Szigetszentmiklós, 56 data could be evaluated. The damages on bouldings are illustrated by some photos made shortly after the earthquake. A part of these photos were found among damage reports to insurance companies, the others were included into Papp's manuscript report (1956). It is regrettable that just photos

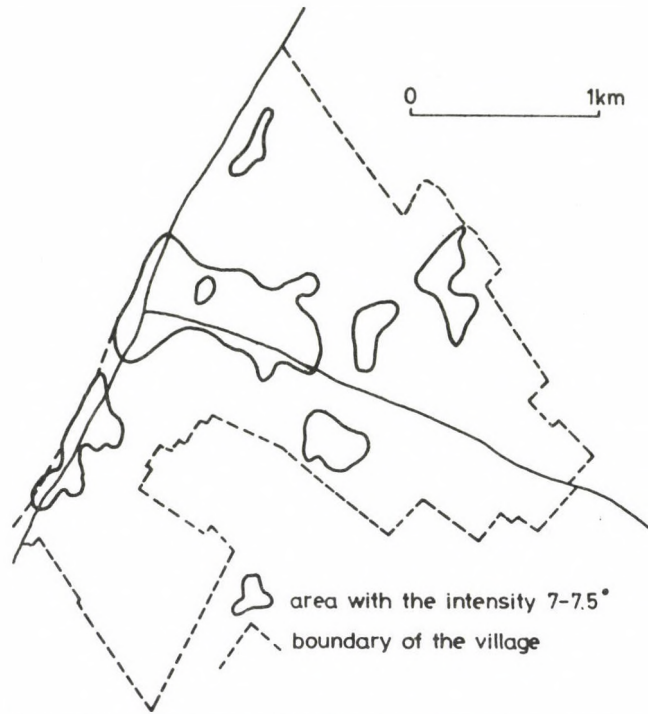


Fig. 2. Most damaged area of the village Dunaharaszti by the earthquake



Fig. 3. Damage in the interior of the church in Taksony



Fig. 4. Szigetszentmiklós, one-layer brick fence destroyed by earthquake



Fig. 5. Dunaharaszti, No. 22, Szőlőhegy Street. Destruction of a cob-wall building by the earthquake



Fig. 6. Cracks on the Council Building of Dunaharaszti, garden front (upper part of the wall)

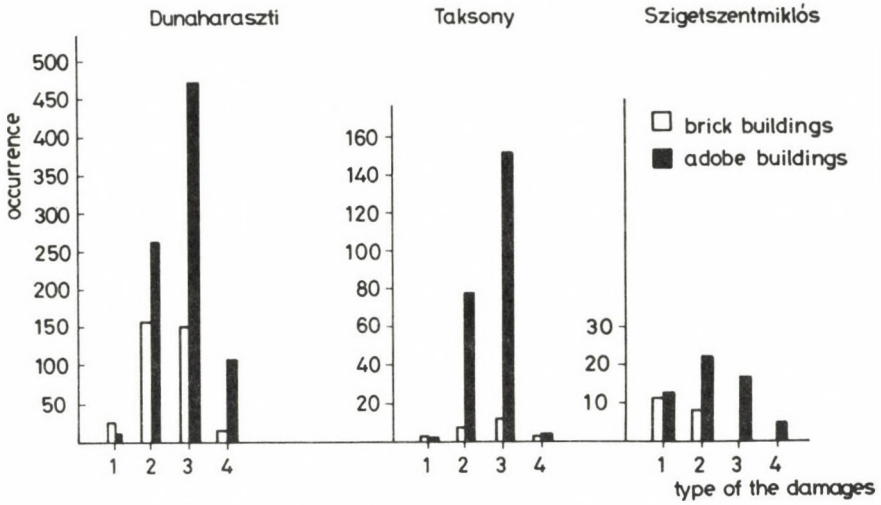


Fig. 7. Occurrence frequencies of different types of damages on brick- and adobe buildings in the epicentral area

Table I

	Type of the buildings								
	ADOBE degree of damages				BRICK degree of damages				
	1	2	3	4	1	2	3	4	
DUNAHARASZTI									
All data	3144								
Evaluated from them	1207	%							
		1.2	31	55.6	12.5	7.1	45.4	43.2	4.2
TAKSONY									
Number of occurrences		2	78	153	6	3	7	11	3
Distribution of the cases in %		0.84	32.6	64	2.5	12.5	29.2	45.8	12.5
SZIGETSZENTMIKLÓS									
Number of occurrences		12	22	17	5	11	7		
Distribution on the cases in %		21	39	30	8.9	61	39		

from the “typical” damages could not be found. Nevertheless, the photos reveal much about the quality and the damages of the buildings, see Figs 3, 4, 5, 6. The connections between the types of the damages, their occurrence frequencies and the type of the buildings is presented in Fig. 7.

The results of this investigation are also summarized in Table I, from where one can see that about 50% of the adobe buildings in Dunaharaszti suffered 3rd degree damages, corresponding to the isoseist 7°. Fourth degree damages were found in about 12.5% of the group A buildings, being just twice as high as that typical for the 7°-

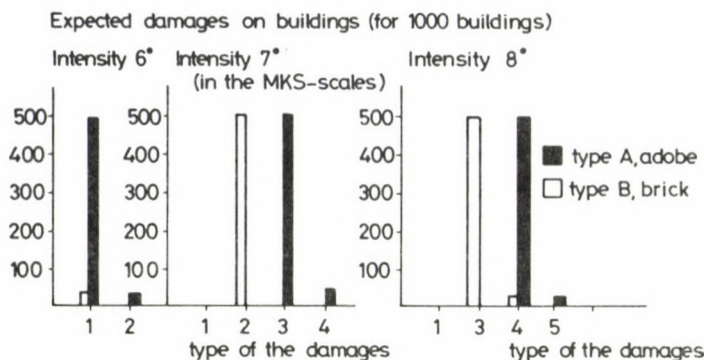


Fig. 8. Damages on buildings at different intensities

iseist. These high damages may be the consequence of the poor quality of the buildings. Similarly, the percentage of group *B* buildings with 3rd degree damages is very high (43.2%). This value approaches already that of a 8°-quake. The 4th degree damages in group *B* buildings also reached a level nearly corresponding to a 8°-shock (4.2%).

Damages on 24 brick buildings could be evaluated in Taksony, and on 18 in Szigetszentmiklós. These are too low values to enable any conclusion about the intensity. In Taksony, 64% of the adobe houses suffered 3rd degree damages, and 2.5% 4th degree damages. The number of 3rd degree damages reaches the 7° intensity level, that of the 4th degree damages does not reach it. In Szigetszentmiklós there were 1820 buildings at the time of the earthquake, and only a small part of them suffered damages. According to the insurance reports, the intensity of the quake did not reach here the intensity 7°. It is somewhat disturbing that Simon evaluated here about 1200 damages on buildings, but he did not construct a map similar to that of Dunaharaszti. Anyway there were less damages in Szigetszentmiklós than in the other two villages. This can be due probably to the fact that the seismic impedance of the subsoil in this village is higher, i.e. its area is less dangerous from a seismic point of view. We should like to add that the buildings in the Budapest suburb Csepel suffered less than those in Soroksár in spite of similar distances from the epicentre of the quake.

The connection between building damages and MSK-intensities can be made more illustrative by representing them graphically (Fig. 8). A comparison of this theoretical distribution of the building damages with those observed in the three villages could result in a conclusion yielding a more accurate estimation of the intensities. Figures 7 and 8 show that the distribution of damages does not correspond to any of the theoretical distributions. The greatest deviation is observed at an intensity of 6°. The empirical distribution in Dunaharaszti and Taksony fits better to the theoretical distribution of intensity 7°. In Szigetszentmiklós, the number of building damages was shifted towards lower values, but at the same time the ratio of the 4th degree damages did not change.

In spite of the uncertainties in these investigations we conclude from an analysis of the building damages in Dunaharaszti that the intensity of the earthquake was there higher than 7°, but it did not reach the intensity of 8°. Thus the problem of the epicentral intensity could not be unambiguously resolved by the analysis of the building damages. It was necessary to ascertain the conclusion by including further data into the study.

A criterion of the intensity 8° is that tombstones fell down in cemeteries. Simon (1956) reported that both in Dunaharaszti and Taksony about 60—80 tombstones fell down. This is apparently a small part of all the tombstones in the corresponding cemeteries. Figure 9 shows that behind the tombstone which fell down there are many others which were not damaged; similarly the rotated tombstone of Fig. 10 is surrounded by undamaged ones. In Szigetszentmiklós, no tombstones fell down, but several were rotated (Fig. 11). Papp (1956) supported Simon's statements, and mentioned that many tombstones fell toward S-SW in the northern part of the cemetery, while in the southern parts, tombstones fell toward North. That does not mean that the epicentre of the earthquake was just below the cemetery, but it means that tombstones fell toward the pit (Fig. 9). In Taksony, a great part of the tombstones was rotated by 9—17° (Fig. 12) and less fell down (Fig. 13).

Papp (1956) mentioned that shallow dug wells got nearly without exception sandy, but in Szigetszentmiklós the hammered Norton wells did not dilapidate (criterion of intensity 7°). In Taksony 3 cm wide cracks were found on the surface and a few mud craters were also observed (Figs 14, 15). These additional observations suggest that the intensity of the shock did not surpass 7° in Szigetszentmiklós, but in Taksony it approximated 8°.

As it has been already mentioned, heaviest damages occurred outside of the epicentral area in Soroksár — in a southern suburb of Budapest. In Csepel, lying nearly in the same epicentral distance, damages were much less. The frequency of damages on buildings in the district of Budapest has been summarized in Figs 16 and 17.

In most districts of Budapest, the number of damage reports did not surpass 50, i.e. the houses were damaged in a ratio of less than 1%. Evidently slight damages occurred on more buildings but being very slight ones they were not reported to the insurance.

It should be mentioned that Papp (1956) investigated the yield of the Budapest warm springs, too, and he found that the effect of the shock was evident in the yield of the springs of the Rudas spa (Fig. 18). Water yields increased immediately after the earthquake, then they diminished to values below the preshock yield. In case of the Gellért spa, the changes did not surpass the usual level. In the deep bored well of the Tétényi street hospital, the quiet water level got higher after the shock. In the spas Császár and Lukács, the springs Török, István and Római showed variations which cannot be unambiguously identified with earthquake effects, as there were building activities in the corresponding areas, and experimental pumping was made.

Up to now reports from the inhabitants as well as damage surveys at the spot have been evaluated. Local damages have been, however, investigated by the village

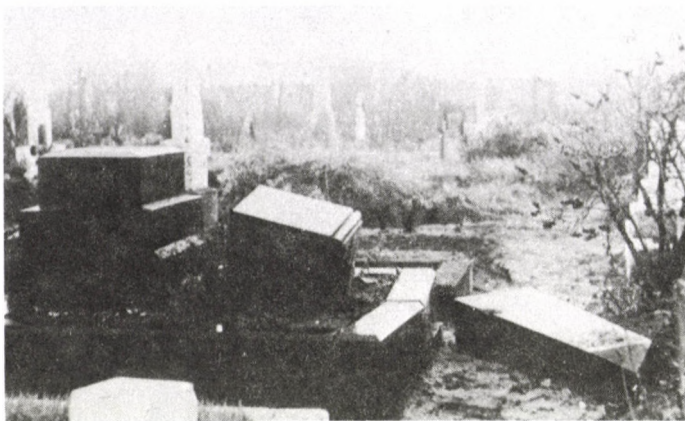


Fig. 9. Cemetery of Dunaharaszti, marble tombstone which fell down toward the pit. In the background standing tombstones



Fig. 10. Cemetery Taksony, tombstone rotated by the earthquake. No tombstone can be seen which fell down

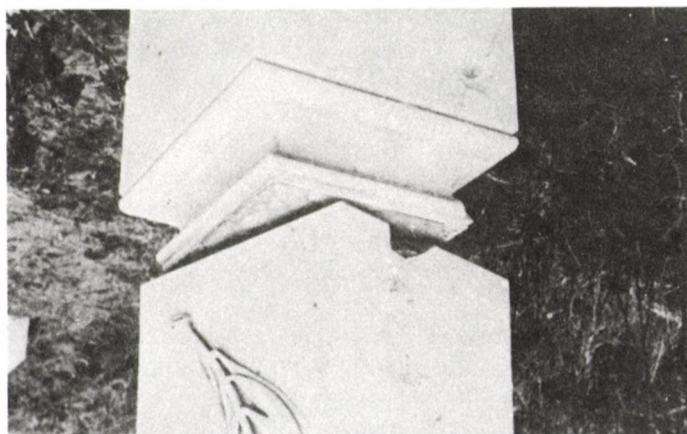


Fig. 11. Cemetery of Szigetszentmiklós. Rotated tombstone. No tombstones can be seen which fell down



Fig. 12. Taksony cemetery. No tombstone can be seen which fell down



Fig. 13. Taksony cemetery. Tombstone fell down. Dunaharaszti earthquake January 12, 1956

and district councils, too (Reports of the District Councils of Budapest 1956), and from the number of the dwelling houses and from the total sum needed for reparations, the damage on an average building can be computed (E_p).

If Budapest is also included into this study then highest caution is to be preserved there as flat houses in the central part of the city cannot be compared to simple adobe



Fig. 14. Sand geysers in Taksony after the earthquake



Fig. 15. Sand geysers in Taksony after the earthquake

buildings in Dunaharaszti. Due to the lack of a better solution, the number of flats was used as a basis in the city houses. In the outskirts of the capital, the districts XX, XV, IV, the average houses did not differ considerably from village houses, and thus it is to be expected that our conclusions are here more reliable. In Fig. 19 a comparison is presented between the values E_p and the intensities determined by Simon (1956). It is surprising that E_p is only slightly correlated with the intensities. E.g. in the districts III, IV, XV, XVIII only slight damages occurred in spite of an estimated intensity 6.5° . It is not to be supposed that official organs kept silent about a certain part of the damages as damaged persons obtained brick- and tile-tickets for the reconstruction. It is also surprising that the villages Szigethalom and Érd have similar intensities of 6° , as the

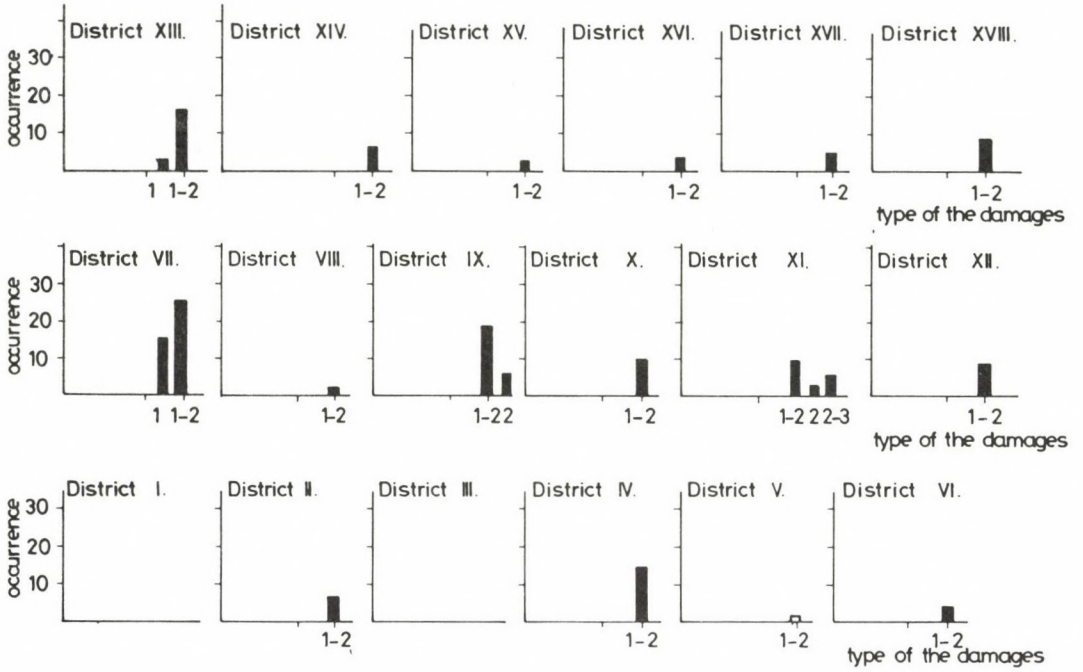


Fig. 16. Types of the damages on buildings and their occurrences in districts of Budapest (a)

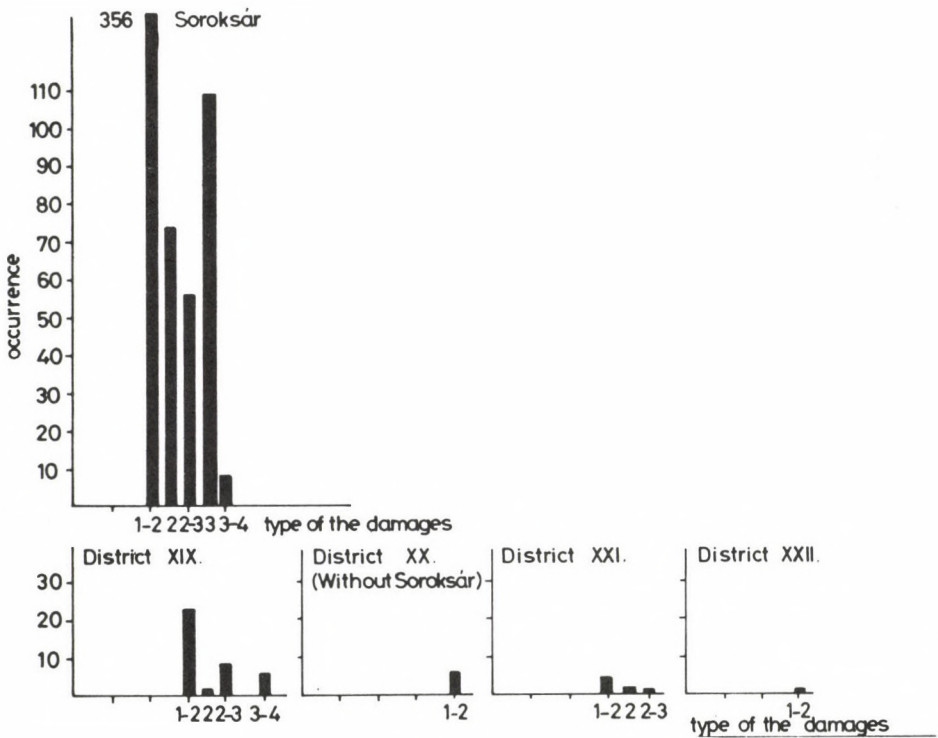


Fig. 17. Types of the damages on buildings and their occurrences in districts of Budapest (b)

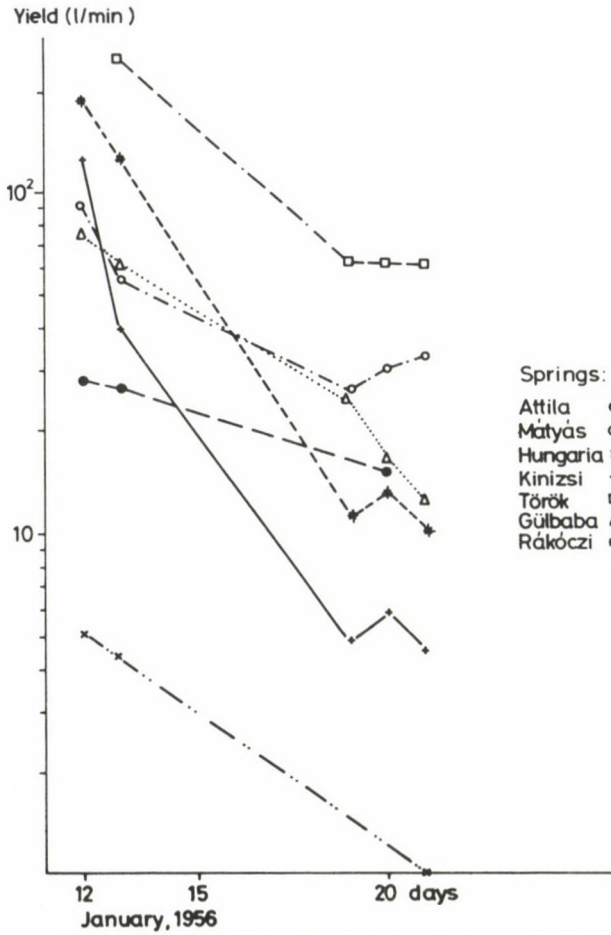


Fig. 18. Water yield of the springs of the Rudas spa after the earthquake

average damage for one building in the latter case was 3.5 Ft, and in the former 671 Ft. In the epicentral area, the average damage is more closely correlated with the intensities. Figure 19 shows both Simon's intensity values and the intensities estimated by us on the basis of the average damage on one house. Both isoseists cover each other in the area of the villages Dunaharaszti, Taksony and Szigetszentmiklós, but we added the village Alsónémedi to this area as the average damage was here rather high, while Simon considered the shock in this village as having an intensity of only 6°. Szigethalom belongs after Simon partially to the area of the isoseist 7°, we accepted this estimation, but take Dunavarsány, too, to the isoseist 7° on the basis of the high average damage. The shape of the area within the isoseist 6° is elliptic, at Simon and also in our estimation, having a major axis in the direction N-S. We considered the western bulge in the northern part of this area as unfounded as the average damage was in the Budapest districts II and XII negligible. In the southern part Simon constructed

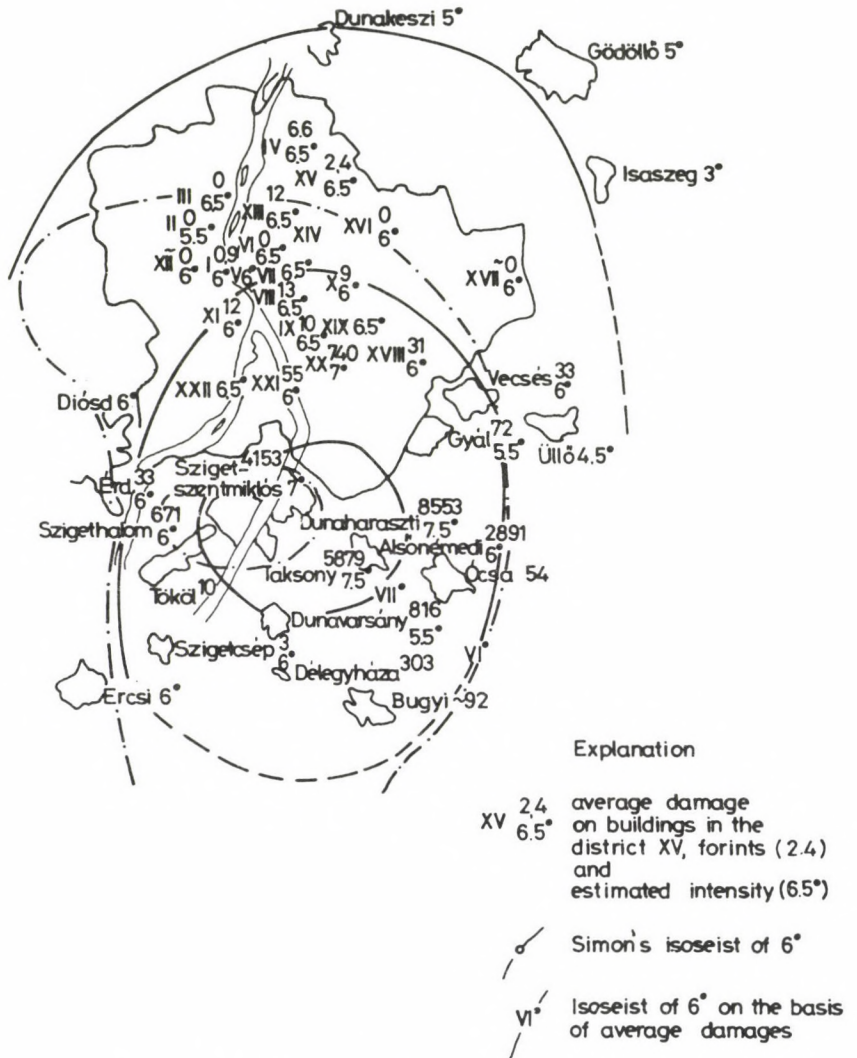


Fig. 19. Isoseists of the January 12, 1956 earthquake of Dunaharaszti

an isoseist parallel to the Danube till Dömös (Fig. 19). The southern boundary of the area accepted by us is represented by the dotted line as no report on damages was obtained from the village councils of this area. It is possible that damages were as slight as the councils did not consider it worth to report. An experiment was also made to determine the isoseist 5° on the basis of the building damages. According to an official report, in the northern districts of Pest, the eastern part of the capital, the damages were slight, thus isoseist 5—6° can be drawn here. According to reports of the inhabitants, the shock reached the intensity 5° in Dunakeszi and Gödöllő. Thus the isoseist 5° can

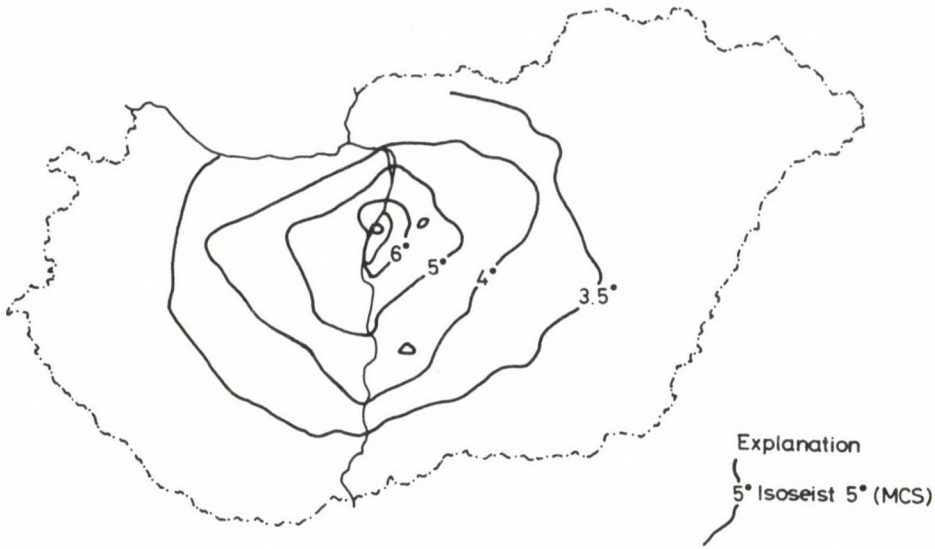


Fig. 20. Isoseists of the Dunaharaszti earthquake in 1956 after Simon (1956)

be drawn roughly parallel to the isoseist 6° through these villages. In the eastern part Isaszeg experienced a shock of 3° what seems to be unexpectedly low. In Úllő the observed intensity was only 4.5° in spite of the vicinity of this village to the epicentral area. Further parts of the isoseist 5° could not be drawn.

Simon constructed also isoseists further away from the epicentre with the radii $r_5 = 45$ km, $r_4 = 75$ km, $r_{3.5} = 110$ km (Fig. 20). In his opinion (Fig. 5) the isoseist 5° has the form of an irregular quadrangle having its longer axis along the Danube-line, the other perpendicularly to it, and their intersection lies in the epicentral area. The isoseist r_4 has a shape rather similar to that of the isoseist r_5 . It seems that both axes have directions of tectonic lines along which the earthquake intensity does not decrease as strongly as otherwise. Naturally such isoseists differing strongly from a circular symmetry do not allow a very accurate determination of the focal depth (Sponheuer).

As it has been already mentioned in the introduction, we repeated the determinations of the local depth due to the very diverging values computed by earlier authors. Taking into account the values $r_7 = 6.3$ km, $r_6 = 16$ km, $r_5 = 34$ km for the isoseist radii, and 7.5° for the epicentral intensity and using the same method as Simon did, the focal depths in Table II were obtained. Supposing an absorption of $\alpha = 0.005$,

Table II

$I_0 - I$	r_0	$h_{1(\alpha=0.05)}$	$h_{2(\alpha=0.01)}$	$h_{3(\alpha=0.005)}$
0.5	6.3	6.5	6.2	5.6
1.5	16.0	8.7	5.7	5.4
2.5	34.0	5.0	6.4	5.7

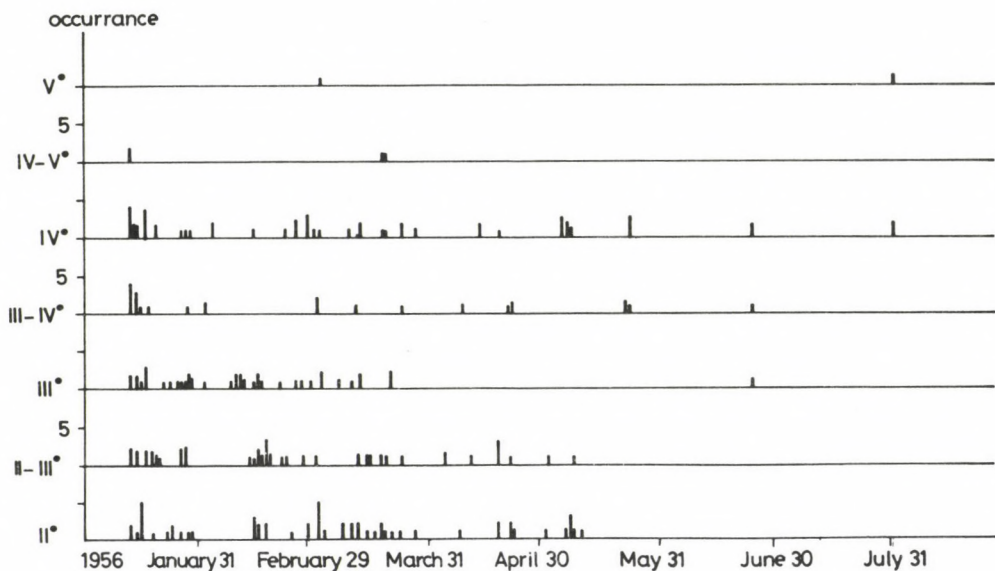


Fig. 21. Distribution of aftershocks with different intensities

the average focal depth is 5.57 km with a mean square error of ± 0.12 km. This focal depth is less than that obtained by Simon but somewhat greater than obtained by Bisztricsány and Csomor from microseismic data. Using their initial data, but neglecting the farther stations (Vienna and Campulung) the focal depth was found to be 5.4 km being in excellent agreement with the focal depth determined from isoseist radii, constructed on the basis of average damages.

The earthquake was followed by many after-shocks but their intensity did not surpass $I_0 = 5^\circ$ (Fig. 21). The activity of the area survived, as 1966, a shock with an intensity $I_0 = 2.5^\circ$ was observed in Dunaharaszti, one of $I_0 = 5^\circ$ 1974 in Törökbálint, and lastly one of 3.5° 1983 in Budaörs.

As a conclusion it can be said that the heaviest shocked area of the 1956 quake included the villages Dunaharaszti and Taksony. Here the intensity reached, or even surpassed slightly the intensity 7.5° on the MSK-scale. In Szigetszentmiklós, the intensity did not reach 7° . The focal depth of the shock was 5–6 km, its magnitude 5.5–5.6.

The earthquake caused damages within Budapest, too, mainly in the suburb Soroksár.

References

- Bendefy L 1956: On the earthquake of January 1956 in the vicinity of the capital (in Hungarian). *Földmérő*, 2, No 2. 1—3.
- Bisztricsány E 1974: Engineering seismology (in Hungarian). Akadémiai Kiadó, Budapest
- Bisztricsány E, Csomor D 1958: Microseismical evaluation of the earthquake of January 12 1956, and the crustal structure of the Hungarian Basin. *Acta Geologica*, 5, 235—244.
- Csomor D, Kiss Z 1962: Seismicity of Hungary Part II (in Hungarian). *Geofizikai Közlemények*, 9, 51—75.
- Gutenberg B, Richter C F 1948: Earthquake magnitude, intensity, energy and acceleration. *BSSA*, 38, 163—191.
- Kárnik V 1968: Seismicity of the European area. Part 1. Czechoslovak Academy of Sciences
- Kiss Z 1958: Macroseismic report on the year 1956 (in Hungarian). Műszaki Könyvkiadó, Budapest
- Láng S 1956: On the earthquake from January 12, 1956, in the vicinity of Budapest (in Hungarian). *Földr. Közl.*, 4, 104—106.
- Map series on architectural geology of Budapest. Map on the technical and economic situation of Dunaharaszti. Published by the Survey Service of Hungary, 1977
- Papp F 1956: Notes about the earthquake of January 12, 1956. Manuscript
- Reports of the District Councils of Budapest on Construction and Traffic 1956. Manuscript
- Shebalin N V 1959: Correlation between magnitude and intensity of earthquakes, asthenosphere. *BCIS, Tr. SC A*, 20, 31—37.
- Simon B 1956: The Dunaharaszti earthquake on January 12, 1956. Manuscript
- Simon B 1957: The effect of the earthquake January 12, 1956 on the village Dunaharaszti. A map with the scale 1:5000. Manuscript
- Somogyi S 1956: Observations in the area affected by the earthquake on January 12, 1956 near Budapest (in Hungarian) *Földrajzi Értesítő*, 5, 129—134
- Szilbert M, Csomor D 1958, 1960, 1961: Rapport Microseismique 1956, 1957, 1958. Műszaki Könyvkiadó, Budapest

PROBLEM OF DIRECT TASK IN NUCLEAR MAGNETISM LOGGING

P SZEMERÉDY¹

[Manuscript received September 3, 1984]

The nuclear magnetism well logging (NML) provides information on the free fluid index (FFI) of a reservoir. In the course of a measurement the value of FFI is estimated from the initial amplitude of the observed proton signal, using an experimentally established relation. The paper deals with the direct task of the NML and presents a theoretical derivation for this empirical function. Only the case of second generation nuclear magnetism logging devices is considered with the assumption that the sonde arrangement is centred and the coil in the tool is long enough as compared to its diameter.

Keywords: free fluid index; nuclear magnetism logging; proton precession; well logging

Introduction

The nuclear magnetism log (NML) shows a considerable promise for obtaining a continuous permeability index of a well, estimating water cut, measuring total porosity in carbonates and determining residual oil saturation. Its concept and basic design principles were published first in 1960 (Brown and Gamson). During the 1960's experiments with the method — not only in the US but in the SU too — have been launched (Akselrod et al., 1963). After initial successes routine use of the NML in formation evaluation was hindered by difficulties in connection with instrumental development and signal processing. With progressing technical conditions a second generation NML equipment suitable for industrial application was elaborated in the US (Herrick et al. 1979).

From the physical point of view the principal phases of the nuclear magnetism logging are as follows:

1. Establishing nuclear magnetic polarization in the fluids present in the formation by means of a strong DC magnetic field;
2. Removing the polarizing magnetic field so that the polarization formed previously should start into precessional motion in the earth's magnetic field;
3. Observation of the precession.

The sensor part of the NML tool is a coil which serves for both producing the magnetic field in the zone adjacent to the borehole and observing the precession after the polarizing field has been removed. During the first phase a strong DC current is sent

¹ Geophysical Department, Eötvös University Budapest

through the coil and in the third one the precessing polarization induces a damped sinusoidal electromotive force in it. This electromotive force can be described as

$$U = V_0 e^{-t/T_2^*} \cos(\omega_0 t + \delta), \quad (1)$$

where ω_0 and T_2^* are the frequency of precession in the earth's magnetic field and transversal relaxation time, respectively. The initial amplitude V_0 is proportional to the quantity of free fluids in the logged formation. The direct aim of a measurement is to determine V_0 and the free fluid index (FFI) can be obtained from the following simple relation: $V_0 = g \cdot \text{FFI}$. The coefficient g depends on several factors: e.g. the hole diameter, the angle between the direction of the earth's magnetic field and the hole axis, and on the way of switching off the polarizing field. Since the influence of these factors on the g coefficient is only qualitatively known the functional relation in question must be determined experimentally.

With increasing importance of the nuclear magnetism logging method an analysis of its empirical moments has become a topical problem. This paper presents the result and summary of a study which aims at theoretically deducing the functional relation between the coefficient g and the relevant factors. Such an analysis assumes deduction of the mathematical expression for V_0 , i.e. determination of the solution of the direct task of the method. The possession of the solution may not only provide a simplification for the calibration of an instrument, but also a possibility for more reliable fixing the optimum working conditions of an NML tool.

Formulation of the problem

The general formula of the AC voltage induced in the coil in the third phase has been published by Praxmayer (1966), Akselrod et al. (1976) and others is:

$$U = \frac{1}{I_p} \int \left\langle \mathbf{H}_p, \frac{d\mathbf{M}}{dt} \right\rangle dv, \quad (2)$$

where $\langle \rangle$ is a symbol for the scalar product; I_p and \mathbf{H}_p are the polarizing current and polarizing magnetic field, respectively. \mathbf{M} denotes the precessing polarization brought about by the polarizing phase and subsequent removal of the polarizing field. The integration is to be performed over the volume of formation.

Figure 1 shows the cross-section of the coil used in nuclear magnetism logging along the longitudinal axis and the axis perpendicular to it.

Owing to the predominant length of the coil the role of the short sides may be neglected in a first approximation, thus the polarizing field produced by the coil can be considered as "two-dimensional". In the u_1, u_2, u_3 coordinate system, shown on Fig. 1, this field has two components:

$$\mathbf{H}_p = (H_{p1}, H_{p2}, 0).$$

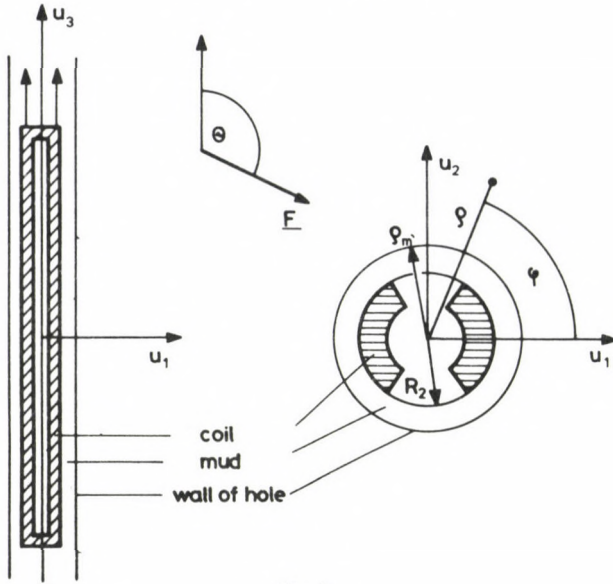


Fig. 1

The NML responds only to fluids with T_2^* times surpassing about 20 ms. By definition such fluids are referred to as free fluids (Brown and Gamson 1960). The switching-off pulse of the polarizing field takes a significantly shorter time than 20 ms, so during the pulse the effect of transversal relaxation may be perfectly neglected. Consequently in Eq. (1) and in Bloch's equations — not cited here — the transversal relaxation time T_2^* can be taken as infinite for the duration of the switching-off pulse. Expressed in terms of the absolute value M of the polarization \mathbf{M} and its unit vector \mathbf{m} this means that M can be considered as a constant for this time.

Furthermore, we have to take into account that within the zone where the bulk contribution to the integral under (2) comes from, the polarizing field H_p is significantly higher than F , the intensity of the earth's magnetic field, \mathbf{F} . Thus the equilibrium polarization established during the polarizing phase can be expressed as: $M = \kappa \cdot H_p$ where κ is the practically equal nuclear magnetic susceptibility of water and oil. Basing on what has been said above as well as taking into account the formulas (1) and (2) it can be demonstrated that the AC voltage induced in the coil immediately after the switching-off pulse satisfies the equation

$$U_0 = FFI \cdot K \int_{R_m}^{\infty} k^2 \langle \mathbf{h}, \mathbf{m}_a \rangle du_1 du_2 = V_0 \cos(\tau + \delta), \quad (3)$$

where

$$K = \frac{\omega_0 I \kappa F^2}{I_p \mu_0}. \quad (4)$$

The notations are as follows:

- F — intensity of the earth's magnetic field (T);
- $\mu_0 = 4\pi \cdot 10^{-7}$ Vs/Am, permeability of vacuum;

- κ – relative nuclear magnetic susceptibility;
 $\omega_0 = \gamma F$, frequency of precession in the earth's magnetic field;
 $\gamma = 2.675127 \cdot 10^8 \text{ Am}^2/\text{Js}$, gyromagnetic ratio of proton;
 R_m – radius of borehole (m);
 l – length of coil (m);
 I_p – intensity of polarizing current (A);
 $\tau = \omega_0 t$;
 \mathbf{m}_a – asymptotic solution of the equation of motion describing the behaviour of the unit polarization \mathbf{m} during the switching-off pulse;
 $\mathbf{h} = \mathbf{H}_p/H_p$, unit vector of the polarizing field.

The explanation of notations should be completed with a few remarks: For the sake of convenience the time variable t is replaced by the angle variable $\tau = \omega_0 t$, and a point denotes the derivation with regard to τ . In Eq. (3) the presence of the factor FFI is obviously necessary since the free fluid fills in only an FFI-part of the formation volume.

Considerations in this paper are confined only to the problem of second generation instruments. On this case the time-dependence of the polarizing field is illustrated in Fig. 2, using strongly distorted dimensions (Herrick et al. 1979).

After the polarizing phase of T_p duration the magnetic field is switched off in two steps. According to the nomenclature used in nuclear magnetic resonance (NMR) investigations the first step is a fast adiabatic process (Lösche 1957, Slichter 1980) lasting up to the instant of the first zero passage of the polarizing field intensity, denoted on the figure by t_v . From this instant t_v the second step commences, which corresponds to a damped oscillation of the magnetic field with ω_0 frequency, the frequency of precession in the earth's magnetic field. In the adiabatic section the polarization turns gradually into the direction of the earth's field and at the end of the rotation its direction will agree with that of the earth's field. Subsequent oscillation of the magnetic field causes the polarization to rotate out of this parallel position and start its

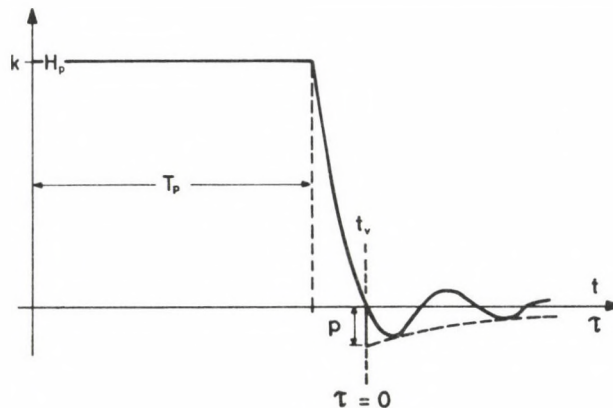


Fig. 2

precessional motion in the earth's field. Thus the outlined second step can be compared with the $\pi/2$ pulse of the spin-echo method (Lösche 1957, Slichter 1980).

According to the previous remarks the first part of the switching-off pulse rotates the unit polarization \mathbf{m} , into the earth's field direction. The effect of its second part upon \mathbf{m} is inherent in the asymptotical solution, \mathbf{m}_a belonging to $\tau \rightarrow \infty$, of the

$$\dot{\mathbf{m}} = \mathbf{m} \times [\mathbf{F}_0 + p\mathbf{h}e^{-b\tau} \sin \tau] \tag{5}$$

normalized gyroscope equation. The normalized form is used only for the sake of convenience and obtained again by the substitution of $\tau = \omega_0 t$. Hence the meaning of the new notations can be at once recognized. Namely, $\mathbf{F}_0 = \mathbf{F}/F$ is the unit vector of the earth's magnetic field, while p corresponds to the momentary relative amplitude of the magnetic field oscillation at $\tau = 0$, as shown in Fig. 2. The initial condition for the solution is evidently given by the circumstance that at $\tau = 0$ the unit polarization is parallel with the unit vector \mathbf{F}_0 .

As a conclusion we can state that, apart from a factor, the determination of the initial amplitude, V_0 , or the solution of the direct task is equivalent to deducing the amplitude of the sinusoidally oscillating function

$$Q(\tau) = \int_{R_m}^{\infty} k^2 \langle \mathbf{h}, \dot{\mathbf{m}}_a(\tau) \rangle du_1 du_2. \tag{6}$$

Also the coefficient g mentioned in the introduction is obtainable in the knowledge of this amplitude.

Solution of the direct task

For the computation of the integral Q we have to know the functions $k(u_1, u_2)$ and $\mathbf{h}(u_1, u_2)$, i.e. the distribution of intensity and the direction of the polarizing field. Also the differential equation (5) includes both functions, because the relative intensity $p(u_1, u_2)$ deviates from the relative intensity k only in a proportionality factor.

Using a suitably constructed coil, the polarizing field approximates well the magnetic field of a dipole line (Akselrod et al. 1976). When the coil axis is identical with the hole axis the integral Q can be written as a sum of a double series and from this sum the amplitude A of the function $Q(\tau)$ can be deduced. The essence of the rather lengthly calculation is summarized in the Appendix. According to this consideration the amplitude A in question is expressible in the following form:

$$A = A(b, p_s, \Theta, \rho_m) = 2\pi R_2^2 k_s^2 P(b, p_s, \Theta, \rho_m), \tag{7}$$

where

$$P = \left\{ \left[\sum_{r=0}^{\infty} a_{2r+1} p_s^{2r+1} \mu'_{2r+1} \right]^2 + \left[\sum_{r=0}^{\infty} b_{2r+1} p_s^{2r+1} \mu'_{2r+1} \right]^2 \right\}^{1/2}. \tag{8}$$

The meanings of the notations are as follows:

R_2 – outer radius of the coil, shown on Fig. 1;

$k_s = H_{ps}/F$, relative intensity of the polarizing field at the outer coil radius R_2 ;

- p_s – relative oscillation amplitude of the magnetic field at the radius R_2 at the moment the oscillation begins;
 b – relative damping coefficient for the oscillating magnetic field;
 Θ – angle between the hole axis and the direction of the earth's field;
 $\rho_{m'}$ = R_m/R_2 , the relative hole radius;
 a_n = $a_n(b, \Theta)$ and
 b_n = $b_n(b, \Theta)$ coefficients which can be computed according to the procedure discussed in the Appendix, furthermore with the
 ρ = r'/R_2 relative polar distance we have

$$\mu'_n = \int_{\rho_{m'}}^{\infty} \frac{d\rho}{\rho^{2n+3}} \quad (9)$$

Supposing a vertically deepened borehole and taking into account a geomagnetic inclination of 63° , typical in Hungary, we have: $\Theta = 153^\circ$. For this case and when choosing a relative damping coefficient of $b = 0.2$ the values of the coefficients a_n and b_n can be found in Table I of the Appendix, up to $n = 21$. (The value $n = 21$ corresponds to $r = 10$ in the formula (8).)

According to what has been told above as well as on the basis of Eqs (3) and (6) the coefficient g under discussion is expressible in the following way:

$$g = g(b, p_s, \Theta, \rho_{m'}) = 2\pi R_2^2 k_s^2 K P(b, p_s, \Theta, \rho_{m'}) \quad (10)$$

Consequently, the coefficient g and so the $V_0 = g \cdot \text{FFI}$ initial amplitude too is proportional to the function P .

In Fig. 3 function P is plotted against the parameter p_s for several fixed values of the hole radius $\rho_{m'}$, with the use of Table I, i.e. when $\Theta = 153^\circ$ and $b = 0.2$. The curves show that to every hole-radius belongs an optimum p_s value, for which the initial amplitude V_0 is an absolute maximum. The existence of these absolute maxima deserves

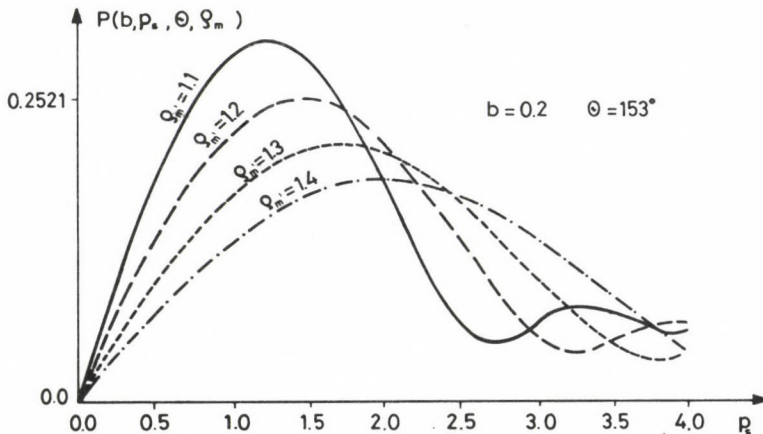


Fig. 3

attention from the point of view of selecting the correct conditions for the nuclear magnetism well logging. Namely, in case of small FFI values the level of the electromotive force induced in the coil is very low, it is comparable with the level of thermal noise. In such a case the gain in signal-to-noise ratio which can be attained by adjusting the optimum p_s value is not negligible.

Conclusion

Up to now there have been no attempts to solve the direct task in the nuclear magnetism logging. This study presents a solution of this problem for the second generation devices in the case of a sufficiently long coil and a sonde arrangement coaxial with the hole axis. It is demonstrated that the solution in question, can be obtained by determining the P function according to Eq. (8). In the knowledge of this function we can expect a more simple calibration of the instrument as well as an increase in the accuracy of measurement. The analysis directs the attention to the circumstance that to every hole radius there belongs a p_s value for which the signal-to-noise ratio of the proton signal is maximum.

Acknowledgements

The author is very much indebted to F Schipp for the valuable discussions in connection with the arising mathematical problems. Thanks are due to A Hajósy for checking some parts of the lengthy calculations. At the same time my gratitude is due to S Molnár, to my companion in performing numerical computations.

Appendix*

Mathematical formulation of the problem

In the u_1, u_2, u_3 rectangular coordinate system, shown on Fig. 1, let us introduce the polar vector: $\mathbf{u} = (u_1, u_2, 0)$. Then the intensity of the "two-dimensional" polarizing field existing around the coil can be characterized by a function of the form $k = k(\mathbf{u})$, while its direction given by a unit vector is: $\mathbf{h} = \mathbf{h}(h_1(\mathbf{u}), h_2(\mathbf{u}), 0)$. In the same coordinate system the unit vector of the earth's magnetic field is: $\vec{\mathbf{F}}_0 = (F_{01}, F_{02}, F_{03})$. The intensity of the oscillating magnetic field at $\tau = 0$ is described by a function $p = p(\mathbf{u})$ which is proportional to $k(\mathbf{u})$. Under such conditions we have the following initial value problem:

$$\begin{aligned} \dot{\mathbf{m}}(\tau) &= \mathbf{m}(\tau) \times [\vec{\mathbf{F}}_0 + p\mathbf{h}e^{-b\tau} \sin \tau], \\ \mathbf{m}(0) &= \vec{\mathbf{F}}_0. \end{aligned} \quad (\text{A-1})$$

The solution of this differential equation with the above initial condition satisfies the equation as follows:

$$Q(\tau) = \int_{|\mathbf{u}| \geq R_m} k^2 \langle \mathbf{h}, \dot{\mathbf{m}}_a(\tau) \rangle du_1 du_2 = A \cos(\tau + \delta), \quad (\text{A-2})$$

* In the Appendix, upper case letters denote the following: $\vec{\mathbf{A}}$ vectors, \mathbf{A} matrices. Lower case letters like \mathbf{m} are vectors, too.

where $\mathbf{m}_0(\tau)$ is the asymptotic solution of the initial value problem, belonging to $\tau \rightarrow \infty$. The value of the coefficient A is to be determined as a function of the free parameters which will be detailed later. Solution of a similar problem has been dealt with in an article by Schipp and Szemerédy (1984). (The study concerns a direct task relevant to the first generation devices, where the initial value problem appears in an other form.)

Solution of the initial value problem

Consider two vectors, $\vec{\mathbf{A}} = (a_1, a_2, a_3)$ and $\vec{\mathbf{B}} = (b_1, b_2, b_3)$, in the Euclidean space and introduce the matrix

$$\mathbf{A} = \begin{bmatrix} 0 & a_3 & -a_2 \\ -a_3 & 0 & a_1 \\ a_2 & -a_1 & 0 \end{bmatrix}. \quad (\text{A-3})$$

The the following relation holds: $\vec{\mathbf{B}} \times \vec{\mathbf{A}} = \mathbf{A} \cdot \vec{\mathbf{B}}$. Thus, applying the correspondence $\vec{\mathbf{F}}_0 \rightarrow \mathbf{F}$ and $\mathbf{h} \rightarrow \mathbf{H}$ the differential equation in (A-1) can be transformed into a matrix differential equation. Using the notation

$$w = \frac{p}{2\sqrt{-1}} = \frac{p}{2i} \quad (\text{A-4})$$

we have

$$\begin{aligned} \dot{\mathbf{M}}(\tau) &= [\mathbf{F} + e^{-b\tau}(w e^{it} + w^* e^{-it})\mathbf{H}]\mathbf{M}(\tau), \\ \mathbf{M}(0) &= \mathbf{E}, \end{aligned} \quad (\text{A-5})$$

where \mathbf{E} is the unit matrix and the asterisk denotes the complex conjugate. In the knowledge of the solution $\mathbf{M}(\tau)$ of the matrix differential equation (A-5) the solution of the initial value problem is expressible as

$$\mathbf{m}(\tau) = \mathbf{M}(\tau)\vec{\mathbf{F}}_0. \quad (\text{A-6})$$

Let us seek the solution of (A-5) in the following form:

$$\begin{aligned} \mathbf{M}(\tau) &= \left[\sum_{m=-\infty}^{\infty} \sum_{n=0}^{\infty} C_{m,n} e^{-nb\tau} e^{im\tau} \right] e^{\mathbf{F}\tau} \mathbf{D}, \\ C_{0,0} &= \mathbf{E} \end{aligned} \quad (\text{A-7})$$

where

$$\mathbf{D} = \left[\sum_{m=-\infty}^{\infty} \sum_{n=0}^{\infty} C_{m,n} \right]^{-1}. \quad (\text{A-8})$$

From Eqs (A-5), (A-7) and (A-8) a recursion formula can be obtained for the $C_{m,n}$ matrices which is as follows:

$$\begin{aligned} C_{m,n} [(im - nb)\mathbf{E} + \mathbf{F}] - \mathbf{F}C_{m,n} &= w\mathbf{H}C_{m-1,n-1} + w^*\mathbf{H}C_{m+1,n-1}, \\ n &= 1, 2, 3, \dots, \\ m &= 0, \pm 1, \pm 2, \dots, \end{aligned} \quad (\text{A-9})$$

where

$$C_{0,0} = \mathbf{E}$$

and

$$C_{m,0} = \mathbf{0}, \quad \text{if } m \neq 0.$$

Note: It can be proved that the solution $\mathbf{M}(\tau)$ is a unitary matrix, i.e.

$$\mathbf{M}^{-1} = \mathbf{M}^\dagger, \quad (\text{A-10})$$

where the matrix \mathbf{M}^\dagger is the adjugate of the matrix \mathbf{M} .

General form of coefficient A contained by equation (A—2)

It is easy to demonstrate that, after a suitable transformation based on Eqs (A—5), (A—6), (A—7) and (A—8) moreover the relations $F^+ = -F$ and $F\vec{F}_0 = \vec{0}$, for the scalar product $S_a(\tau) = \langle \mathbf{h}, \dot{\mathbf{m}}_a \rangle$ in the integral of Eq. (A—2) we have

$$S_a(\tau) = - \sum_{m=-\infty}^{\infty} \sum_{n=0}^{\infty} \langle e^{-F\tau} \mathbf{Fh}, \mathbf{C}_{m,n}^+ \vec{F}_0 \rangle = - \sum_{m=-\infty}^{\infty} \sum_{n=0}^{\infty} S_{m,n}(\tau). \tag{A—11}$$

Applying a suitable unitary transformation the matrix F can be diagonalized. With the unitary matrix U of this transformation we obtain

$$S_{m,n}(\tau) = \langle Ue^{-F\tau}U^+(U\mathbf{Fh}), UC_{m,n}^+ \vec{F}_0 \rangle = \langle e^{-J\tau} \vec{Z}_{0,0}, \vec{X}_{m,n} \rangle, \tag{A—12}$$

where

$$\vec{X}_{m,n} = UC_{m,n}^+ \vec{F}_0, \tag{A—13}$$

$$\vec{Z}_{m,n} = UC_{m,n}^+ (\mathbf{Fh})$$

and $J = UFU^+$ is the diagonalized F matrix. Denoting the vector components by an upper index we get

$$S_{m,n}(\tau) = e^{i\tau} Z_{0,0}^1 (X_{m,n}^1)^* + e^{-i\tau} Z_{0,0}^2 (X_{m,n}^2)^*. \tag{A—14}$$

According to Eq. (A—2) the scalar product $S_a(\tau)$ is real, therefore the coefficients of the exponential functions in the above expression are complex conjugates of each other. Thus, using the denotation

$$W_{m,n} = \int_{|\mathbf{u}| \geq R_m} k^2(\mathbf{u}) Z_{0,0}^1(\mathbf{u}) (X_{m,n}^1(\mathbf{u}))^* d\mathbf{u}_1 d\mathbf{u}_2 \tag{A—15}$$

we can write that

$$Q(\tau) = - \left[\sum_{m=-\infty}^{\infty} \sum_{n=0}^{\infty} W_{m,n} \right] e^{i\tau} - \left[\sum_{m=-\infty}^{\infty} \sum_{n=0}^{\infty} W_{m,n} \right]^* e^{-i\tau}. \tag{A—16}$$

In case we assume that

$$- \sum_{m=-\infty}^{\infty} \sum_{n=0}^{\infty} W_{m,n} = \frac{1}{2} A e^{i\delta} \tag{A—17}$$

the condition (A—2) will be met, i.e.

$$Q(\tau) = A \cos(\tau + \delta). \tag{A—18}$$

Thus the coefficient A can be expressed as

$$A = 2 \left| \sum_{m=-\infty}^{\infty} \sum_{n=0}^{\infty} W_{m,n} \right|. \tag{A—19}$$

Obtaining expressions for the vectors $\vec{X}_{m,n}$ and $\vec{Z}_{m,n}$

Applying the operator U of the unitary transformation to the adjungate of the matrix equation (A—9) and taking into account that $F^+ = -F$ and $H^+ = -H$ we obtain

$$-(im + nb)UC_{m,n}^+ + UC_{m,n}^+ F - JUC_{m,n}^+ = -w^* UC_{m-1,n-1} H - w UC_{m+1,n-1} H. \tag{A—20}$$

Multiplication of this equation from the right side by the vectors \vec{F}_0 , \mathbf{h} and $\mathbf{Fh} = \mathbf{h} \times \vec{F}_0$ one after another provides relations for the vectors $\vec{X}_{m,n}$, $\vec{Z}_{m,n}$ and for an additional vector: $\vec{Y}_{m,n} = U(C_{m,n} \mathbf{h})$. These relations represent linear equation systems of the vector components. On the basis of this equations a recursion formula can be deduced for the $X_{m,n}^1$ series appearing in the integral (A—15). Since $X_{m,n}^1$ can be expressed as a linear combination of the series $Z_{r,s}^1$ it is most practical to write the recursion formula for the series $Z_{m,n}^1$, which will be denoted by $z_{m,n}$.

Recursion formula for the $z_{m,n}$ and $\zeta_{m,n}$ series

The recursion formula obtainable for the series $z_{m,n}$, through solving the previously mentioned equation system, can be simplified by means of the substitution

$$z_{m,n} = p^n z_{0,0} \zeta_{m,n} \quad (\text{A—21})$$

into the connection concerning the $\zeta_{m,n}$ series:

$$\begin{aligned} \zeta_{m,-1} &= 0, & \zeta_{0,0} &= 1, \\ \zeta_{m,n} &= -(\alpha_{m,n} \zeta_{m+1,n-1} + \beta_{m,n} \zeta_{m-1,n-1}) \langle \vec{F}_0, \mathbf{h} \rangle - \\ & - (\gamma_{m,n} \zeta_{m,n-2} + \delta_{m,n} \zeta_{m-2,n-2} + \varepsilon_{m,n} \zeta_{m+2,n-2}), \end{aligned} \quad (\text{A—22})$$

where

$$\begin{aligned} m &= 0, \pm 1, \pm 2, \dots, \\ n &= 0, 1, 2, \dots \quad \text{and} \\ \zeta_{m,n} &= 0, \quad \text{if } m \neq 0. \end{aligned}$$

Meaning of the notations is as follows:

$$\alpha_{m,n} = v R_{m,n} (\lambda_{m,n} + \lambda_{m+1,n-1}), \quad (\text{A—23})$$

$$\beta_{m,n} = v^* R_{m,n} (\lambda_{m,n} + \lambda_{m-1,n-1}), \quad (\text{A—24})$$

$$\gamma_{m,n} = v v^* R_{m,n} (\lambda_{m-1,n-1} + \lambda_{m+1,n-1}), \quad (\text{A—25})$$

$$\delta_{m,n} = v^{*2} R_{m,n} \lambda_{m-1,n-1}, \quad (\text{A—26})$$

$$\varepsilon_{m,n} = v^2 R_{m,n} \lambda_{m+1,n-1}, \quad (\text{A—27})$$

$$R_{m,n} = \frac{\lambda_{m,n}}{1 + \lambda_{m,n}^2}, \quad (\text{A—28})$$

$$\lambda_{m,n} = \frac{1}{i(m-1) + nb} \quad \text{and} \quad (\text{A—29})$$

$$v = \frac{1}{2i}. \quad (\text{A—30})$$

For the quantity $z_{0,0}$ the second equation of (A—13) provides an equation: $Z_{0,0}^1 = z_{0,0} = (\mathbf{U}(\mathbf{Fh}))^1$. After expressing the operator U in the u_1, u_2, u_3 coordinate system we have

$$z_{0,0} = (\mathbf{U}(\mathbf{Fh}))^1 = \frac{1}{\sqrt{2}} [1 - \sin^2 \Theta \cos^2 (\psi - \varepsilon)]^{1/2}. \quad (\text{A—31})$$

The meaning of the angles Θ, ψ and ε is shown on Fig. A—1. From the same figure we can see also the meaning of the scalar product $\langle \vec{F}_0, \mathbf{h} \rangle$ which is as follows:

$$\langle \vec{F}_0, \mathbf{h} \rangle = \sin \Theta \cos (\psi - \varepsilon) = \cos \vartheta. \quad (\text{A—32})$$

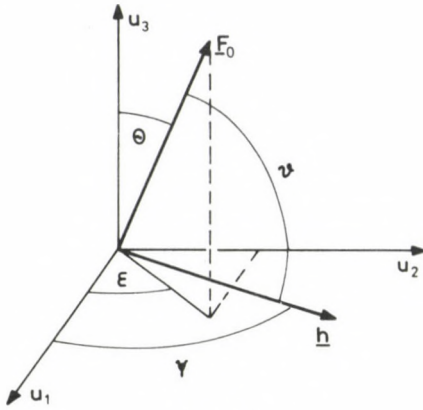


Fig. A-1

Dipole line approximation of the $W_{m,n}$ series

According to Fig. 1 the polar angle, φ , is measured from the u_1 coordinate axis. Besides it seems to be practical to measure the polar distance in $\rho = |u|/R_2$ units related to the outer radius of the coil, R_2 . Thus, if the relative intensity of the polarizing field at a distance of $\rho = 1$ is denoted by k_s , the relative intensity and direction of the polarizing magnetic field is given by the following formulas:

$$k(\rho) = \frac{k_s}{\rho^2}, \tag{A-33}$$

$$h(\varphi) = (\sin 2\varphi, -\cos 2\varphi, 0).$$

Similar equations describe the distribution and direction of the magnetic field in the oscillatory phase of the switching-off pulse

$$p(\rho) = \frac{p_s}{\rho^2}, \tag{A-34}$$

$$h(\varphi) = (\sin 2\varphi, -\cos 2\varphi, 0),$$

where p_s is the relative amplitude of the magnetic field oscillation at $\tau = 0$, existing at the polar distance $\rho = 1$. Then we have

$$\cos \vartheta = \sin \Theta \sin (2\varphi - \varepsilon), \quad \text{respectively} \tag{A-35}$$

$$\psi = 2\varphi - \pi/2. \tag{A-36}$$

In order to introduce cylindrical coordinates, fitting better to the problem, to the integral in Eq. (A-15) we apply the polar transformation

$$u_1 = \rho R_2 \cos \varphi, \tag{A-37}$$

$$u_2 = \rho R_2 \sin \varphi.$$

After performing the transformation and using the following notations

$$\mu'_n = \int_{\rho_m}^{\infty} \frac{d\rho}{\rho^{2n+3}}, \tag{A-38}$$

$$A_{m,n} = \int_0^{2\pi} \zeta_{m,n}(2\varphi - \pi/2 - \varepsilon) \cdot [1 - \sin^2 \Theta \cos^2(2\varphi - \pi/2 - \varepsilon)] d\varphi, \tag{A-39}$$

moreover

$$G_{m,n}^* = \lambda_{m,n}(vA_{m-1,n-1}^* + v^*A_{m+1,n-1}^*), \tag{A-40}$$

for the $W_{m,n}$ series we obtain

$$W_{m,n} = -\frac{1}{2} R_2^2 k_s^2 p_s^2 \mu_n' G_{m,n}^*, \tag{A-41}$$

where $\rho_m = R_m/R_2$ represents the relative borehole radius.

Expressing the $\zeta_{m,n}$ series in the form of a Fourier series

When forming the terms of the series $\zeta_{m,n}$ one after another we can see that $\zeta_{m,n}$ is a trigonometric polynomial of n -th order of the variable $s = 2\varphi - \pi/2 - \varepsilon$, i.e.

$$\zeta_{m,n}(s) = \sum_{j=-n}^n \xi_{m,n}(j) e^{ijs}, \tag{A-42}$$

where

$$\xi_{m,n}(j) = \frac{1}{2\pi} \int_{-\pi}^{\pi} \zeta_{m,n}(s) e^{-ijs} ds = \mathcal{F}[\zeta_{m,n}(s)]_j \tag{A-43}$$

$$j = 0, \pm 1, \pm 2, \dots, \pm n$$

is the j -th Fourier coefficient of the function $\zeta_{m,n}(s)$. This property of the terms in the $\zeta_{m,n}$ series can be utilized to construct a recursion formula for the Fourier coefficients, $\xi_{m,n}(j)$, themselves. After taking the Fourier transform of Eq. (A-22) and using the relation

$$\mathcal{F}[\zeta_{m,n}(s) e^{\pm is}]_j = \xi_{m,n}(j \mp 1), \tag{A-44}$$

we obtain

$$\begin{aligned} \xi_{m,n}(j) = & -\alpha_{m,n} [\xi_{m+1,n-1}(j-1) + \xi_{m+1,n-1}(j+1)] \frac{\sin \Theta}{2} - \\ & -\beta_{m,n} [\xi_{m-1,n-1}(j-1) + \xi_{m-1,n-1}(j+1)] \frac{\sin \Theta}{2} - \\ & -[\gamma_{m,n} \xi_{m,n-2}(j) + \delta_{m,n} \xi_{m-2,n-2}(j) + \varepsilon_{m,n} \xi_{m+2,n-2}(j)], \end{aligned} \tag{A-45}$$

where

$$\begin{aligned} n &= 1, 2, 3, \dots, \\ m &= 0, \pm 1, \pm 2, \dots \quad \text{and} \\ j &= 0, \pm 1, \pm 2, \dots \end{aligned}$$

under the conditions that

$$|j| \leq n \quad \text{and} \quad |m| \leq n.$$

For the values of $n < 0$, and if these conditions are not met: $\xi_{m,n}(j) = 0$. Furthermore, we have $\zeta_{0,0}(0) = 1$.

Expressing the series $A_{m,n}$ and $G_{m,n}$

In Eq. (A—39) the part of the integrand in square brackets is a second order trigonometric polynomial, i.e

$$1 - \sin^2 \Theta \cos^2 s = \sum_{j=-1}^1 a'_{2j} e^{2ijs}, \tag{A—46}$$

where

$$a'_0 = \left(1 - \frac{\sin^2 \Theta}{2} \right), \tag{A—47}$$

$$a'_{-2} = a'_{-2} = - \frac{\sin^2 \Theta}{2}. \tag{A—48}$$

The integrand in Eq. (A—39) is a periodical function of φ of π periode. Thus using Eqs (A—42) and (A—46) the integral can be written in the form of

$$A_{m,n} = 2\pi \sum_{j=-1}^1 a'_{2j} \hat{\zeta}_{m,n}(2j). \tag{A—49}$$

After introducing the notation

$$G'_{m,n} = \lambda_{m,n}^* \sum_{j=-1}^1 a'_{2j} [v^* \hat{\zeta}_{m-1,n-1}(2j) + v \hat{\zeta}_{m+1,n-1}(2j)] \tag{A—50}$$

and taking into account Eqs (A—40) and (A—49) we have

$$G_{m,n} = 2\pi G'_{m,n}. \tag{A—51}$$

As a consequence of the conditions imposed on the Fourier coefficients $\hat{\zeta}_{m,n}(j)$ we have that $G_{m,0} = G'_{m,0} = 0$ for all values of m .

Formula for the coefficient A to be determined

From Eqs (A—19), (A—41) and (A—51) we can see that

$$A = 2 \left| \sum_{m=-\infty}^{\infty} \sum_{n=0}^{\infty} W_{m,n} \right| = 2 \left| \sum_{m=-\infty}^{\infty} \sum_{n=0}^{\infty} W_{m,n}^* \right| = 2\pi R_2^2 k_2^2 \left| \sum_{n=1}^{\infty} \left\{ \mu'_n \left[\rho_s^n \sum_{m=-n}^n G'_{m,n} \right] \right\} \right|. \tag{A—52}$$

It is to be emphasized that the absolute value in the above expression is a function of the free parameters Θ , b , p_s and ρ_m :

$$P(b, p_s, \Theta, \rho_m) = \left| \sum_{n=1}^{\infty} \left\{ \mu'_n(\rho_m) \left[p_s^n \sum_{m=-n}^n G'_{m,n}(b, \Theta) \right] \right\} \right|. \tag{A—53}$$

Thus, with the help of the so defined P function we have

$$A = A(b, p_s, \Theta, \rho_m) = 2\pi R_2^2 k_2^2 P(b, p_s, \Theta, \rho_m). \tag{A—54}$$

Structure of the recursions given by the formulàs (A—22) and (A—45)

Terms of the $\zeta_{m,n}$ series take up non-zero values only for the value pairs (m, n) marked with x on the Figure A—2. The same holds for the Fourier coefficients $\hat{\zeta}_{m,n}(j)$, too. However, the recursion of the last ones proceeds no more in the (m, n) "plane", but in the (m, n, j) three dimensional space. Equation (A—50) shows that the $G'_{m,n}$ series involves only the Fourier coefficients of even order. On the other hand the Fourier coefficients of even order are different from zero only when $n-1$ is also even. From this it follows that if n is even then $G'_{m,n} = 0$ for all values of m .

Note

It is convenient to denote separately the real and imaginary part of the sum in Eq (A—53):

$$a_n = \operatorname{Re} \left[\sum_{m=-n}^n G'_{m,n} \right],$$

$$b_n = \operatorname{Im} \left[\sum_{m=-n}^n G'_{m,n} \right].$$
(A—55)

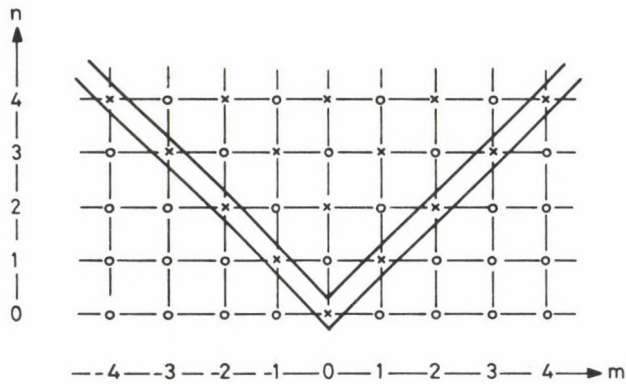


Fig. A-2

Using these and taking into consideration that $G'_{m,n}$ is different from zero only for odd values of n , we can write the formula (A—53) as follows:

$$P = \left\{ \left[\sum_{r=0}^{\infty} a_{2r+1} p_s^{2r+1} \mu'_{2r+1} \right]^2 + \left[\sum_{r=0}^{\infty} b_{2r+1} p_s^{2r+1} \mu'_{2r+1} \right]^2 \right\}^{1/2}. \quad (\text{A—56})$$

Example for the a_n and b_n coefficients

On the territory of Hungary the geomagnetic inclination is approximately 63° , which means that for a vertically deepened borehole $\Theta = 153^\circ$. Table I presents for this Θ value and for a relative damping coefficient $b = 0.2$ the values of non-zero a_n and b_n coefficients up to $n = 21$. (From $r = 0$ to $r = 10$.) To avoid an accumulation of numerical errors the iteration given by the formula (A—45) has been carried out by means of a double precision complex algorithm. Table I shows that the coefficients decrease rapidly with growing n . Due to this circumstance the series appearing in Eq. (A—56) are satisfactorily well convergent in that value domain of the variables p_s and ρ_m , which may be important from the point of view of the present investigation.

Table I

n	a_n	b_n
1	-0.22875655 E+00	0.22875652 E+01
3	0.10226023 E+00	-0.19800816 E+01
5	-0.23025848 E-01	0.46834612 E+00
7	0.24595594 E-02	-0.49602900 E-01
9	-0.14491106 E-03	0.28947056 E-02
11	0.51419502 E-05	-0.10166797 E-03
13	-0.10620977 E-06	0.20730085 E-05
15	0.64786643 E-09	-0.11993755 E-07
17	0.37452888 E-10	-0.75008888 E-09
19	-0.16212257 E-11	0.32018818 E-10
21	0.38843732 E-13	-0.76518821 E-12

References

- Akselrod S M, Danevich V I, Melik-Shakhnazarov A M 1963: To the theory of nuclear-magnetic logging (in Russian). *Izv.vuzov. Ser.Neft' i gaz*, No. 4, 93—98.
- Akselrod S M, Danevich V I, Zaporozhets V M, Evdokimov A F, Melik-Shakhnazarov, A M, Neretin V D, Orlov G L 1976: Nuclearmagnetic methods of borehole logging (in Russian). NEDRA, Moskva
- Brown R J S, Gamson B W 1960: Nuclear magnetism logging. *Trans., AIME.*, 219, 201—219.
- Herrick R C, Couturie S H, Best D L 1979: An improved nuclear magnetism logging system and its application to formation evaluation. Paper SPE 8361 presented at the 1979 SPE Annual Technical Conference and Exhibition, Las Vegas
- Lösche A 1957: Kerninduktion. VEB Deutscher Verlag der Wissenschaften, Berlin
- Praxmayer T 1966: On the amplitude of the nuclear magnetic logging signal. *Acta Geophys. Pol.*, 14, 301—314.
- Schipp F, Szemerédy P 1984: Mathematical model for a problem of nuclear magnetism well logging. *Teubner-Texte zur Mathematik, Leipzig*, 64, 275—285.
- Slichter C P 1980: Principles of magnetic resonance. Springer Verlag, Berlin

SUPER-HIGH-LATITUDE MAXIMUM OF Pc2-4 INTENSITY

T A PLYASOVA-BAKOUNINA,¹ V A TROITSKAYA¹

J W MÜNCH,² H F GAULER²

[Manuscript received October 25, 1984]

The investigation of the distribution of Pc2-4 intensities along a meridian using an array of stations at latitudes from 53° to 77° (9 stations) clearly demonstrated that the location of the main maximum of intensity is definitely different for different classes of micropulsations in the period band of Pc2-4. The main maximum is located: at latitudes from 74° to 77° for Pc2-4_{sw} (solar wind-controlled micropulsations) and at latitudes lower than 65° for Pc2-4_{mg} (magnetospheric ones).

A final conclusion was drawn about the localization of the sources of the two types of the pulsations in the period band of Pc2-4.

Keywords: geomagnetic array; geomagnetic pulsation; high latitude geomagnetism; Pc2-4; solar wind-control

Information about the distribution of Pc2-4 intensities is very important in the investigation of Pc2-4 generation, in particular in the localization of their sources.

Investigations of the intensity distribution in subauroral and middle latitudes have shown (Kopitenko et al. 1969, Stening and Gupta 1971) that the location of the maximum Pc3 intensities is at $L \sim 4$, and of Pc4 ones is at $L < 4$ (Samson and Rostoker 1972). An analysis of Pc4 intensities at a network of stations ($L = 2.4 \div 3.8$) (Green 1976) has shown that the maximum intensity moves to lower latitudes with decreasing period of the oscillations. Orr and Webb (1975), analysing data from stations with $L = 3.1 \div 6.6$, have also remarked that the position of the intensity maximum both for Pc3 or for Pc4 is at $L > 3$, while only the Pc3 maximum of intensity exists for latitudes with $L < 3$.

Analyses of multiple frequency signals observed on a latitudinal network of stations showed that Pc3-5 frequencies can vary between stations but at the same time each station has a peak at an identical frequency (Stuart and Usher 1966, Herron and Heitzler 1966, Stuart et al. 1971, Samson et al. 1971). Therefore the investigation of the intensity distribution on a latitudinal array of stations showed for identical frequencies different results.

Namely, Baransky et al. (1969) have shown that the position of the middle latitude maxima both for Pc3 or for Pc4 coincide with each other in contrast to e.g.

¹ Institute of Physics of the Earth, Moscow D-242, B. Grouzinskaya 10, USSR

² Siegen University, Siegen, FRG

Green (1976) and Samson and Rostoker (1972). A similar investigation of the Pc2-4 intensity on an extensive meridional array of stations (latitudes from 0° to 74°) demonstrated the existence in addition to the above mentioned middle latitude maximum (57°) also of two other maxima: a subauroral ($\sim 64^\circ$) and a high-latitude ($\sim 70^\circ$) one (Baransky et al. 1973, Sobolev et al. 1977). It was found that the position of these maxima is stable both for Pc3 or for Pc4.

Beside the mechanism of Pc2-4 generation internal to the magnetosphere such as drift mirror instability (Hasegawa 1969), drift instability (Kozhevnikov et al. 1976), or bounce resonance (Southwood et al. 1969), several extramagnetospheric mechanisms were proposed in the literature: generation by protons coming from the bow shock (Gul'elmi 1974, Kovner et al. 1976); magnetosheath waves generated at the quasi-parallel portion of the bow shock (Greenstadt 1973); Kelvin—Helmholz instability at the magnetopause (Sen 1965, Dungey and Southwood 1970, Southwood 1968, Golikov et al. 1980, Pu and Kivelson 1983, Mishin 1981). Without a comparative analysis of each of the discussed external mechanisms, it is evident that for each of them, even if the magnetopause itself is not a source of the oscillations, in any case it is the region of conversion of one type of waves into another one, i.e. it can be considered as a secondary source. Hence any of the external mechanisms is supposed as a consequence of a maximum in the ground Pc2-4 intensity in the region of the projection of the magnetopause to the surface (latitudes higher than 74°).

Baransky et al. (1973) and Sobolev et al. (1977) have confirmed however, that Pc3-4 intensity is reduced North of 70° for the majority of events. This fact contradicts to the localization of Pc2-4 sources at the magnetopause and consequently to an external origin of Pc2-4. As Pc2-4 intensity has not been investigated at latitudes higher than 74° (except Bolshakova and Troitskaya 1984), we supposed that apparently a new enhancement of the intensity or even a maximum of Pc2-4 intensity exists in the region higher than 74° .

The present work was performed for testing this idea.

Following Plyasova-Bakounina et al.'s (1983) suggestion that the Pc2-4 class could be divided into two groups in accordance with the type of pulsations sources (internal and external ones), the present analysis was carried out separately for each group: for magnetospheric pulsations (Pc2-4_{mg}) and for solar wind-controlled pulsations (Pc2-4_{sw}).

Data and analysis

The main characteristic of the present study is the use of Pc2-4 micropulsation intensities from a meridian chain of stations, including high latitudes up to 77° .

The data of two meridional chains of stations were analyzed (see Fig. 1 and Table I). The first one is ($\lambda \sim 120^\circ$): Borok ($\Phi = 53^\circ$), Andenes ($\Phi = 65^\circ$), Bear Island ($\Phi = 71^\circ$), Heiss ($\Phi = 74^\circ$), Ny Alesund ($\Phi = 76^\circ$) and Mirny (conjugated point, in Antarctica) ($\Phi = 77^\circ$). The maximum longitudinal difference between stations of this chain is less than 30° . In addition, data of a more western chain were analyzed, too

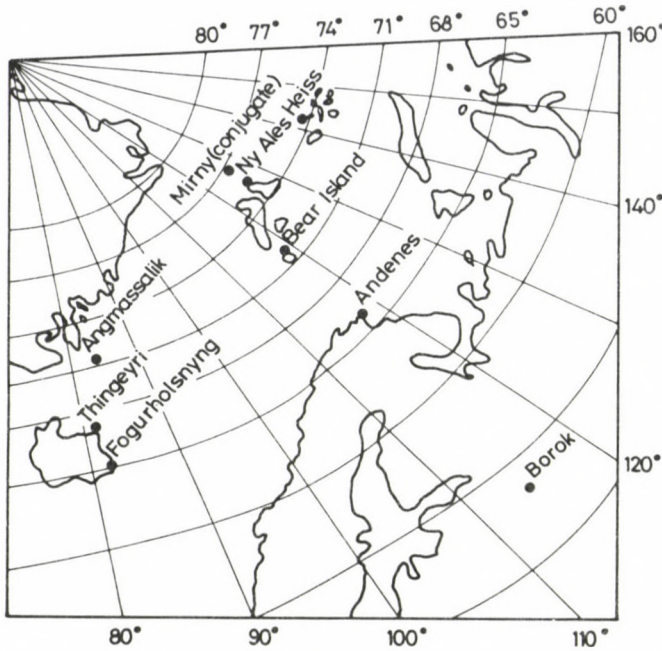


Fig. 1. Location of the 9 geomagnetic stations: 6 German ones (Ny Alesund, Bear Island, Andenes and Angmagssalik, Thingeyri, Fogurholsnyng) operated by the Siegen University and 3 Soviet ones (Borok, Heiss, Mirny) operated by IFZ of the Soviet Academy of Sciences

Table I

Stations	Φ	Λ	L
Mirny (conjugate) (M)	77°	122°	
Ny Alesund (NA)	75° 84'	127°	16.7
Heiss (H)	74°	144°	13.8
Bear Island (BI)	71° 12'	119°	9.5
Angmagssalik (ANG)	70° 61'	85°	
Thingeyri (TH)	68° 23'	85°	
Andenes (A)	66° 32'	119°	6.2
Fogurholsnyng (F)	65° 07'	85°	
Borok (B)	53°	115°	2.8

($\Lambda \sim 85^\circ$): Fogurholsnyng ($\Phi = 66^\circ$), Thingeyri ($\Phi = 68^\circ$), Angmagssalik ($\Phi = 70^\circ$). The longitudinal difference between the two chains is about 30° .

The fluxgate magnetometer of the Soviet stations (chart records) were run at speeds of 15 mm/min; the German stations yielded digital magnetometer data (tape records). For the sake of a convenient processing of the common data, the German data were transformed to chart records with the same chart speed, as Soviet data. AFR (Amplitude Frequency Response) was taken into account for both sets of data. The

interval processed is August—October 1978 (IMS experiment) restricted to 05-14 LT and requiring also that Interplanetary Magnetic Field Data be available (King 1979; ISEE-J Data).

Only events ("wave packets") exhibiting harmonic structure were chosen. It means that the mean pulsation periods during each event were estimated with an accuracy of $\pm 10\%$. The time intervals of such events change from 10 min up to one hour. 22 events were recorded at all 9 stations and 76 events were recorded only at three Soviet stations (Borok—Heiss—Mirny).

For each event the following parameters were visually estimated: 1. average period T for both horizontal components H and D ; 2. maximum amplitude A^{\max} . A^{\max} was calculated using the two components H and D : $A^{\max} = (A_H^{\max 2} + A_D^{\max 2})^{1/2}$. The set of T and A^{\max} data was split into two parts. The criterium for the selection was the condition: T coincides (does not coincide) with the calculated T_c , where $T_c = 160/B$, B is the average magnitude of the IMF for each event.

We attributed events to the two groups as follows:

1. to solar wind-controlled micropulsations Pc_{sw} , if $T = T_c$;
2. to magnetospheric micropulsations Pc_{mg} , if $T \neq T_c$.

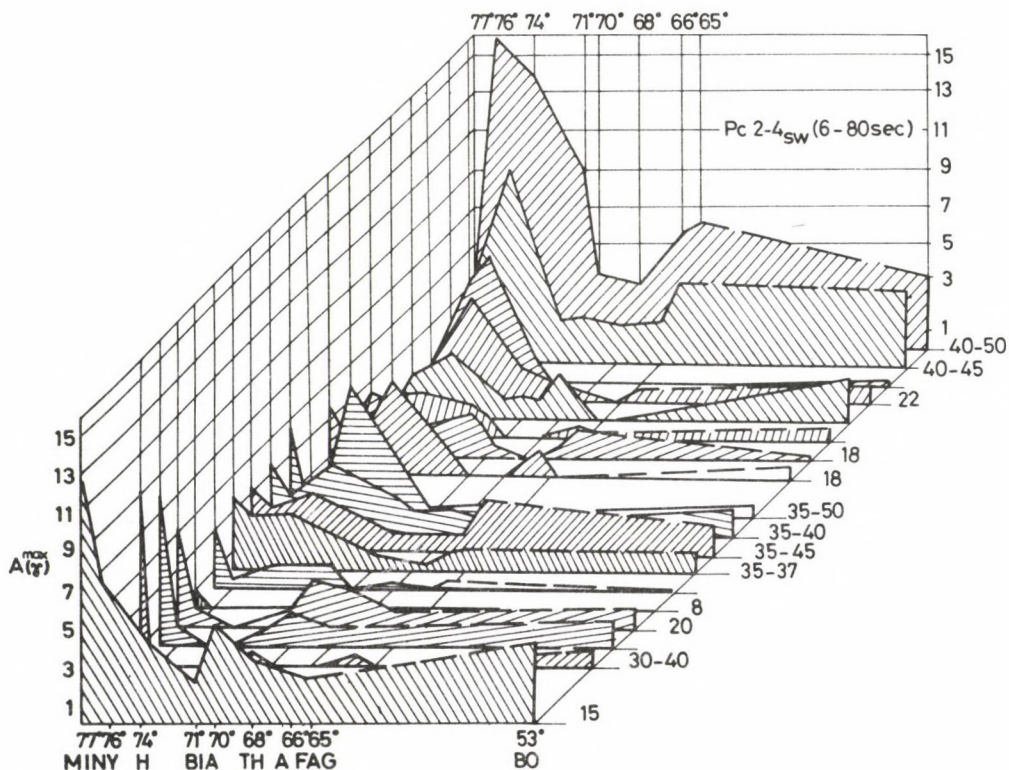


Fig. 2. The dependence of the amplitude of the solar wind-controlled pulsations $Pc_{2-4_{sw}} A^{\max}$ on latitude, the X-axis is the latitude with Soviet and German stations are marked. The Y-axis is the amplitude in nT. Each curve illustrates separate pulsation events recorded at the network of stations

Results

With neglecting latitudinal differences among stations the data of the two chains of stations were combined and considered as a single one.

Examples of the dependence A^{max} on the latitude for Pc_{sw} pulsations are shown in Fig. 2. Each curve corresponds to a separate event, "wave packet" with a constant period over the network of stations. The pulsation intensity is sharply reduced with decreasing latitude of the observation point. A super-high-latitude (SHL) maximum of the intensity is evident in the region of latitudes over 74° . It exists both for Pc2 and Pc3-4 (periods 6—80 s). Its position changes from one event to another in a latitude range from 74° to 77° . The well known high-latitude maximum at 70° is comparatively small for the majority of events. The earlier also known auroral maximum (64°) can be discovered here by an enhancement of the intensity of pulsations near stations An and F. The middle latitude maximum (57°) is naturally absent from these graphs because there are no observation points in appropriate latitudes (from 65° to 53°).

Figures 3 and 4 show the dependence of the location of the SHL maximum of $Pc_{2-4_{sw}}$ intensity at different times of the day and at different magnetic activities ($K_p=1-2$ in Fig. 3, $K_p > 2$ in Fig. 4).

The SHL maximum is located at higher latitudes in the morning hours than afternoon; it seems that it does not depend on the level of magnetic activity. A similar

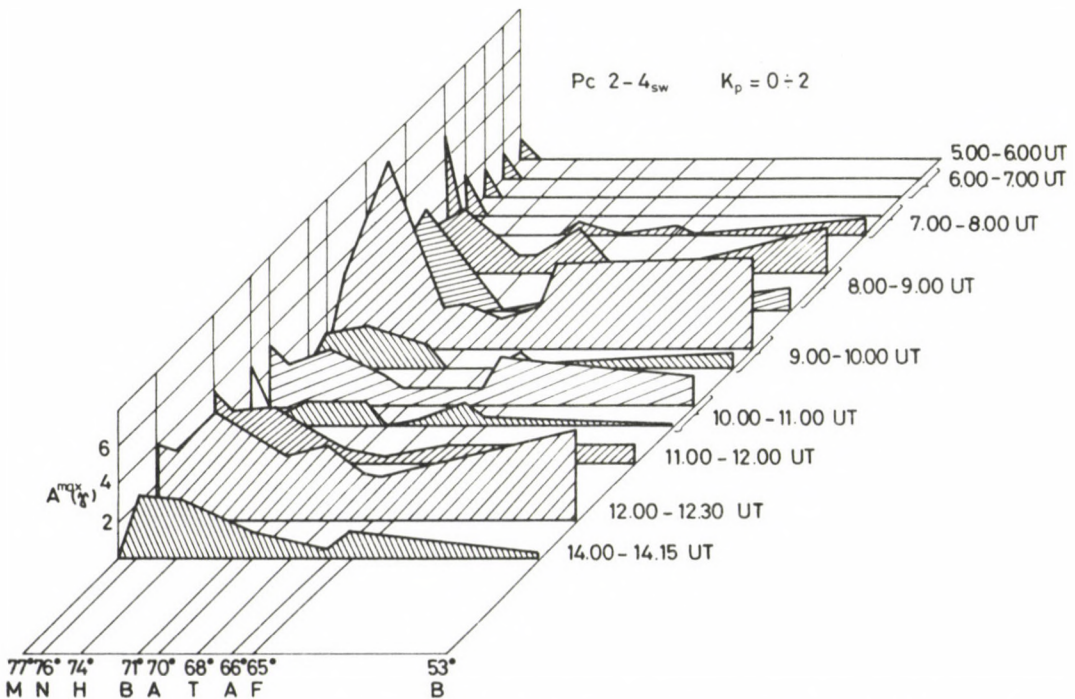


Fig. 3. Dependence of the amplitude A^{max} of $Pc_{2-4_{sw}}$ on latitude for low magnetic activity $K_p=0-2$

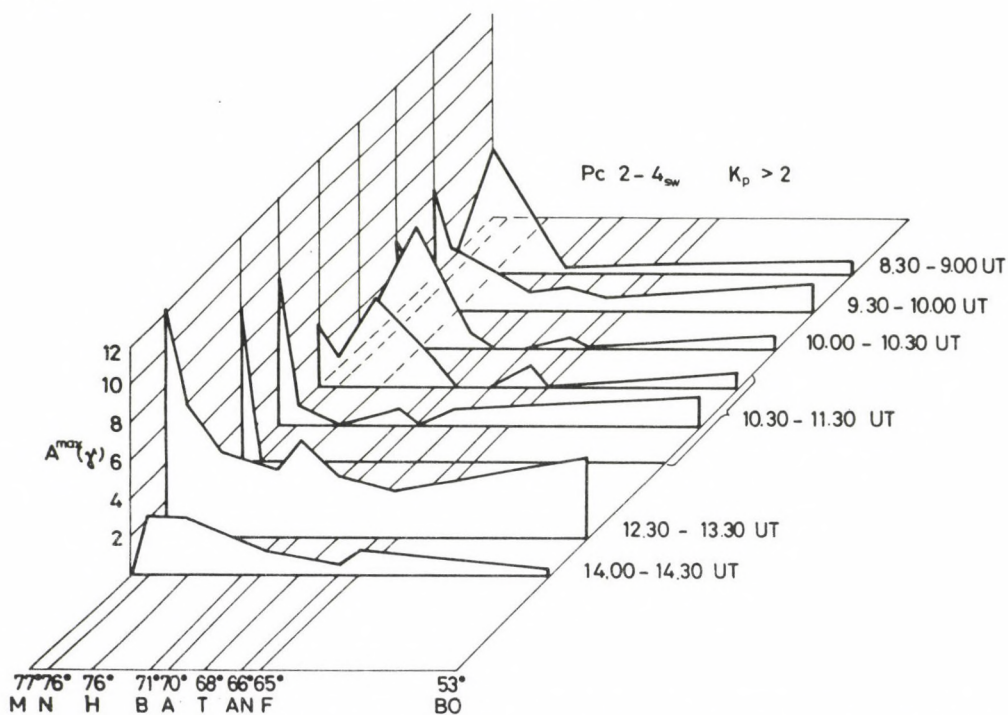


Fig. 4. Dependence of the amplitude A^{\max} of Pc2-4_{sw} on latitude for high magnetic activity $K_p > 2$

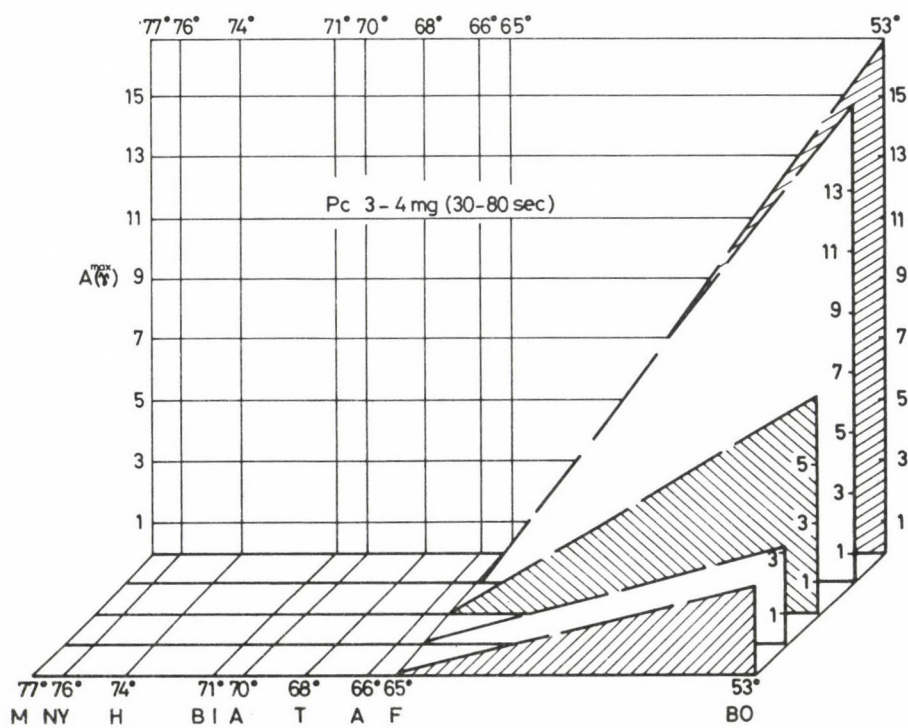


Fig. 5. Dependence of the amplitude A^{\max} of the magnetospheric pulsations Pc2-4_{mg} on latitude

dependence on local time exists for the location of the southern boundary of the dayside cusp. Without additional statistics however, no definite conclusion can be made about the connection between dayside cusp location and position of the SHL maximum.

Figure 5 shows a set of curves on the dependence of A^{\max} on Φ for Pc_{mg} pulsations. The figure is constructed analogously to Fig. 2. The intensity of Pc_{mg} sharply increases with decreasing latitude. Characteristic for this figure is not only the absence of the SHL maximum, but also the absence of any activity of these pulsations at latitudes higher than 65° . One can conclude, that the intensity maximum of magnetospheric oscillations is situated apparently at middle and low latitudes. It should be noted that in contrast to Fig. 2, a similar form of the amplitude decrease with increasing latitudes exists only for pulsations in the period band 30–80 s.

Table II
St. Borok ($L=2.8$)

T, s	Class	N	N _{mg} /N _{sw}
6–20	mg	0	0
	sw	36	
20–40	mg	1	0.02
	sw	44	
40–80	mg	8	1
	sw	9	

This fact is illustrated by Table II which was constructed for the station Borok ($L=2.8$). Table II shows the number of events; solar wind-controlled micropulsations ($N_{Pc2-4_{sw}}$) and magnetospheric ones ($N_{Pc2-4_{mg}}$) and their ratio for different bands of periods (6–20 s, 20–40 s, 40–80 s). The table shows that the group of magnetospheric micropulsations appears more seldom as compared to solar windcontrolled ones at $L=2.8$. Namely, there is about an equal number of events in both groups in the Pc4 band, but there are practically no magnetospheric pulsation events in the Pc3 and Pc2 period bands.

Discussion

Figure 6 shows two schemes (the upper one is adopted from Fukunishi and Lanzerotti 1974) which illustrate the shape of the attenuation of pulsation amplitudes with latitude, if their source is located at the magnetopause (top) and inside the magnetosphere, here e.g. at the plasmopause (bottom). The source power distributions with latitude for the two types of the sources (external and internal ones) are

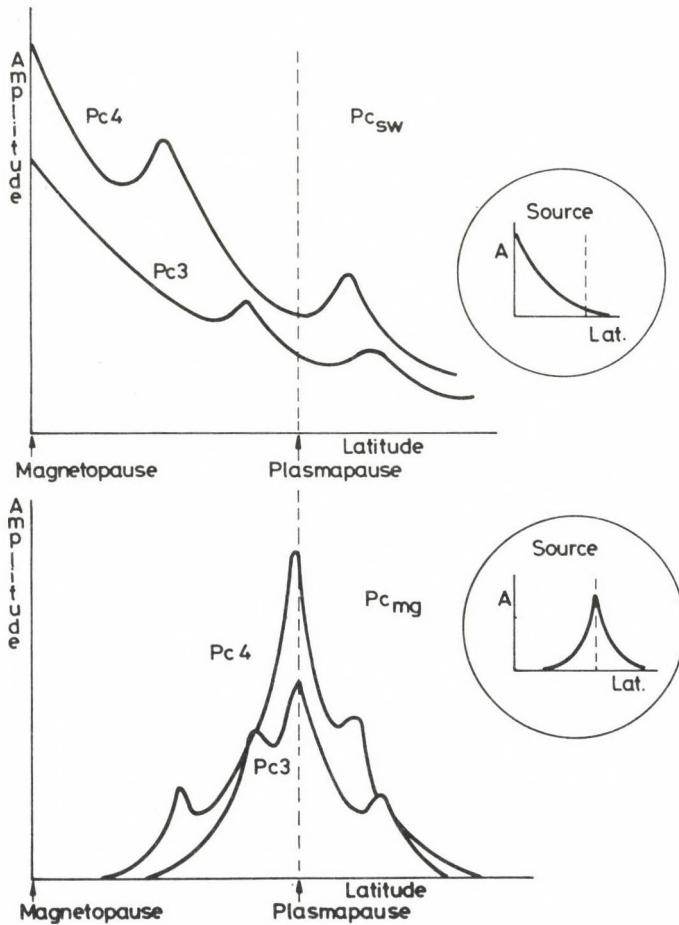


Fig. 6. Schematic form of the dependence of the amplitude of pulsations generated at the magnetopause (top) and at the plasmopause (bottom) on latitude

represented separately in circles. One can suppose that the external source is a surface wave on the magnetopause with amplitude A which is damped exponentially with increasing distance inside the magnetosphere toward low latitudes. The internal source is a surface wave on the plasmopause (see Kovner et al. 1976a) with amplitude A which is also damped exponentially with increasing distance to both sides of the plasmopause—toward low latitudes and toward high latitudes.

If we take into account the field line resonance as a mechanism of amplification of Pc2-4 (Chen and Hasegawa 1974) considering the propagation of these signals in the magnetosphere, then the power distribution of the pulsations with latitude both for external and for internal sources will be changed so as the schemes show. The positions of the maxima correspond roughly to the regions of amplification of oscillations for two frequency ranges (Pc3 and Pc4) (Orr and Mathew 1971, Hughes and Bellow 1979).

Comparing the schemes with experimental results (Fig. 2) for Pc2-4_{sw} one sees common features with the top one:

- a) the position of the main maximum of intensity coincide with each other, it corresponds to the region of the dayside cusp;
 - b) the intensity decreases with latitude in both cases analogously (exponentially).
- Such an analogy with the scheme indicates that the source of the solar wind-controlled pulsations (Pc2-4_{sw}) is situated outside of the magnetosphere.

No additional maxima are visible in Fig. 2 near to the plasmopause in contrast to Fig. 6 (top), due to a lack of observations at corresponding latitudes. But, it should be noted that even their presence (or absence) would be consistent with the location of Pc2-4_{sw} sources outside the magnetosphere. On the contrary, the absence of the super-high-latitude maximum eliminates the possibility of an external source.

Comparing the schemes with the experimental results for Pc2-4_{mg} (Fig. 5) common features can be seen with the bottom one:

1. lack of SHL maximum corresponding to the magnetopause,
2. lack of any activity at latitudes higher than 65°,
3. higher amplitudes of pulsations at middle latitudes not far from the plasmopause.

Such a similarity with the scheme indicates that the source of Pc2-4_{mg} is by no means located at the magnetopause. The location of their sources seems to correspond to inner regions of magnetosphere—deeper than $L = 6$. The possible location of this source could be either the plasmopause (Kovner et al. 1976a) or the region of the ring current. According to Pokhotelov et al. (1984), just in the region of the ring current the development of the drift anisotropy instability is possible which leads to the generation of the compressive Alfvén waves (CAW). It is important that the increment of CAW is essentially higher than the increment of both the drift instability (Kozhevnikov et al. 1976) and of the drift-mirror one (Hasegawa 1969). It is also significant that the frequencies of CAW have to be lower than the drifts Larmer frequency which corresponds according to estimations to the Pc4 period band ($T > 60$ s). Thus it can be explained that the majority of Pc_{sw} at middle latitudes belong to the frequency band of Pc2-3.

If the magnetospheric pulsations are generated by any other mechanisms with a wide frequency band then the experimental fact of the lack of Pc2-3_{mg} on $L = 2.8$ could be explained, e.g. as an amplification by local field line resonance. Since the field line tube at $L = 2.8$ is appropriate for the amplification of 50–60 s pulsations (Orr and Mathew 1971, Hughes and Bellow 1979), just these oscillations will dominate there.

The lack of Pc2-3_{mg} at low latitudes ($L < 2$) is an additional evidence in favour of internal source of Pc_{mg} generating waves within a limited frequency range (long period waves, Pc4-5), in particular in favour of Pc_{mg} generation by compressive Alfvén waves. But, the investigation of the polarization characteristics of Pc3 (20–25 s) pulsations at low latitude stations ($L = 2.0$ –1.8) has shown that some results are inconsistent with the excitation of these waves by external sources (Lanzerotti et al. 1981). It is an argument rather in favour of some part of low-latitude Pc3 belonging to the subclass of Pc3_{mg}. Nevertheless, this problem needs a special analysis.

As a next step a more detailed analysis of the position of the intensity maxima should be performed for both types of pulsations by increasing the statistics and by adding to the present chain of stations new stations at latitudes from 64° to 53° and lower.

Conclusion

The analysis of Pc2-4 intensities along the meridian led to the discovery of new dependences by dividing the Pc2-4 class of pulsations into two sub-classes: *a*) solar wind-controlled pulsations Pc2-4_{sw} and *b*) magnetospheric ones Pc2-4_{mg}. It was shown for the first time that the main maximum of Pc2-4_{sw} intensity is found within the region of the southern boundary of dayside cusp. Further the intensity of Pc2-4_{sw} is reduced toward low latitudes exponentially.

These results have removed the earlier contradiction between the idea about the location of the Pc2-4 sources external to the magnetosphere and the experimental result about the location of the main maximum of Pc2-4 intensity inside the magnetosphere at 70° (e.i. at $L=8-10$).

The meridional distribution of the Pc2-4_{mg} intensity shows that the source of these pulsations is located inside the magnetosphere deeper than $L=6$. The ring current region or the plasmopause are possible candidates as regions of Pc2-4_{mg} generation.

References

- Baransky L N, Bolshakova O V, Geller L A, Kazak B N 1969: Latitude dependence of the period and amplitude of stable Pc3-4 pulsations. *Geomagn. Aeron.*, 9, 917.
- Baransky L N, Plyasova-Bakounina T A, Ramanudzhachari P R, Sobolev L A, Selivanov I V 1973: Distribution of the intensity of Pc3-4 pulsations along the geomagnetic meridian. *Geomagn. Aeron.*, 13, 924.
- Bolshakova O V, Troitskaya V A 1984: The relationship between high-latitude maximum of Pc3 intensity and dayside cusp. *Geomagn. Aeron.* (in press)
- Chen L, Hasegawa A 1974: A theory of long-period magnetic pulsations. 1. Steady-state excitation of field line resonances. *J. Geophys. Res.*, 79, 1024.
- Dungey J W, Southwood D J 1970: Ultra-low frequency waves in the magnetosphere. *Sp. Sci. Rev.*, 10, 672.
- Fukunishi H, Lanzerotti L J 1974: ULF pulsations evidence of the plasmopause. 1. Spectral studies of Pc3 and Pc4 pulsations near $L=4$. *J. Geophys. Res.*, 79, 142.
- Golikov Yu V, Plyasova-Bakounina T A, Troitskaya V A, Chernikov A A, Pustovalov V V, Hedgecock P C 1980: Where do solar wind-controlled micropulsations originate. *Planet. Space Sci.*, 28, 535.
- Green C A 1976: The longitudinal phase variations at Pc3-4 micropulsations. *Planet. Space Sci.*, 24, 79.
- Greenstadt E 1973: Field-determined oscillations in the magnetosheath: a possible source of medium period daytime micropulsations, in Proceedings of Conference in Solar Terrestrial Relations. D Venkstesan ed. University of Calgary, Calgary, Alta
- Gul'elmi A V 1974: Diagnostics of the magnetosphere and interplanetary medium by means of pulsations. *Space Sci. Rev.*, 16, 337.
- Hasegawa A 1969: Drift mirror instability in the magnetosphere. *Phys. Fluids*, 12, 2642.
- Herron T J, Heitzler J R 1966: Latitude-period dependency of geomagnetic micropulsations. *Nature*, 210, 361.
- Hughes W J, Bellow W 1979: Geomagnetic pulsations. Proceeding of the Air Force Geophysics Laboratory Workshop on geomagnetism. Special Report, No. 233. 29. Massachusetts, U.S.A.

- King J H 1979: Interplanetary Medium Data Book, Supplement 1. NASA Goddard Space Flight Center, Greenbelt, Md. Rep. NSSDC 79-08.
- Kovner M S, Kusnetzowa V A, Lebedev V V, Plyasova-Bakounina T A, Troitskaya V A 1976a: On low frequency oscillation in the near-earth plasma. *Annales de Geophysique*, 32, 3, 189.
- Kovner M S, Lebedev V V, Plyasova-Bakounina T A, Troitskaya V A 1976b: On the generation of low-frequency waves in the solar wind in the front of the bow shock. *Planet. Space Sci.*, 24, 261.
- Kopitenko Yu A, Raspopov O M, Van Chi F 1969: The relationship between the geomagnetic pulsations and the magnetosphere parameters. *Kosmicheskie issledovaniya*, 7, 266.
- Kozhevnikov A A, Michailovsky A B, Pochotelov O A 1976: The role of protons of the radiation belts in the generation of Pc3-5. *Planet. Sp. Sci.*, 24, 465.
- Lanzerotti L J, Medford L V, MacLennan C C, Hasegawa T 1981: Polarisation characteristics of hydromagnetic waves at low geomagnetic latitudes. *J. Geophys. Res.*, 86, 5500.
- Mishin V V 1981: On the MHD instability of the Earth's magnetopause and its geophysical effects. *Planet. Space Sci.*, 29, 359.
- Orr D, Mathew J A D 1971: The variation of geomagnetic micropulsation period with latitude and the plasmopause. *Planet. Space Sci.*, 19, 897.
- Orr D, Webb D C 1975: Statistical studies of geomagnetic pulsations with period between 10 and 70 sec and their relationship to the plasmopause region. *Planet. Space Sci.*, 23, 1169.
- Plyasova-Bakounina T A, Stuart W F, Troitskaya V A, Charchenko I P 1983: How to select solar wind-controlled micropulsations? Theses reports. EGU Meeting, Budapest, 1980; In: *Issledovaniya po geomagnetizmu i aeronomie i fizike Solntsa*, Irkutsk
- Pokhotelov O A, Pelipenko V A, Amato E 1984: Drift anisotropy instability of a fine-B magnetospheric plasma, Preprint IFSI Lonsiglio Nazionale della Ricerche 00044 Frascati IFSI-84-12
- Pu Z Y, Kivelson M 1983: Kelvin-Helmholz instability at the magnetopause: solution for compressible plasmas. *J. Geophys. Res.*, 88, 841.
- Samson J G, Rostoker G 1972: Latitude-dependent characteristics of high-latitude Pc4 and Pc5 micropulsations. *J. Geophys. Res.*, 6133.
- Samson J C, Jacobs J A, Rostoker G 1971: Latitude-dependent characteristics of long period geomagnetic micropulsations. *J. Geophys. Res.*, 76, 3675.
- Sen A K 1965: Effects of compressibility of Kelvin-Helmholz instability in plasmas. *Physics Fluids*, 7, 1293.
- Sobolev A V, Barkova E S, Danilov A A, Solovjev S I 1977: To the question about the latitude dependence of the Pc3 intensity. Symposium on Physics of the Magnetosphere, Theses reports, Irkutsk
- Southwood D J 1968: The hydromagnetic stability of the magnetospheric boundary. *Planet. Space Sci.*, 16, 587.
- Southwood D J 1974: Some features of field line resonances in the magnetosphere. *Planet. Space Sci.*, 22, 483.
- Southwood D J, Dungey J W, Etherington R C 1969: Bounce resonance interaction between pulsations and trapped particles. *Planet. Space Sci.*, 17, 349.
- Stening R J, Gupta J C 1971: Amplitude and periods of geomagnetic pulsations in the Pc3, 4 range at Canadian observatories. *Geophys. J.* 23, 379.
- Stuart W F, Usher M J 1966: An investigation of micropulsations at middle latitudes. *Geophys. J. R. astr. Soc.*, 12, 1.
- Stuart W F, Sherwood V E, MacIntosh S M 1971: An analysis of micropulsation spectra (Pc) obtained from U.K. Observatories. *J. Atmos. Terr. Phys.*, 33, 869.

ON THE POSSIBLE EFFECT OF ENVIRONMENTAL FACTORS ON THE OCCURRENCE OF TRAFFIC ACCIDENTS

J STŘEŠTÍK¹ and A PRIGANCOVÁ²

[Manuscript received December 28, 1984]

The paper is devoted to the analysis of occurrence of traffic accidents in Bratislava in the years 1979—81 and in individual regions of Slovakia in the years 1980—82. The weekly and daily variations of the traffic accident rates are presented, as well as the cross correlation of the occurrence of accidents in separate territorial units. Relation to meteorological factors, i.e. pressure and relative atmospheric humidity, biometeorological typification of the weather, as well as to electromagnetic effects, i.e. atmospheric electricity and geomagnetic activity, is investigated. The dependence on geomagnetic activity is discussed with a view to the relation between geomagnetic activity and the occurrence of geomagnetic pulsations. The part played by geomagnetic pulsations in the mechanism of the effect of the variable magnetic field on the human organism is demonstrated. It is pointed out that the close dependence of this mechanism observed on the pulsation period plays a part in synchronization with bioactive periods.

Keywords: atmospheric electricity; biometeorological typification; environment; geomagnetic activity; geomagnetic pulsations

Introduction

In recent decades, the research into the effects of the physical properties of the environment on biological processes has developed into an important interscience discipline. Scientists, working in various fields of science, are joining their forces in an effort to solve this problem. A summary of a number of results can be found, e.g. in Gnevyshev and Ol' (1971).

By physical properties of the environment one understands meteorological parameters, together with solar activity and the variations of the geomagnetic field (GMF), as well as of the electric field of the Earth's atmosphere. It was found that the biosphere reacts sensitively to the changes of the parameters mentioned. This is reflected in various biological processes, among others also in the activity of the nervous central system of man. If this activity is disturbed for some reason, the general psychic condition of man deteriorates and an inadequate reaction to an external stimulus may follow. Certain social indexes of human activity serve as the measure of this inadequate reaction.

¹ Geophysical Institute of the Czechoslovak Academy of Sciences, Boční II, 141 31 Praha 4, Czechoslovakia

² Geophysical Institute of the Slovak Academy of Sciences, Dúbravská cesta, 842 28 Bratislava, Czechoslovakia

In this paper, the authors have concentrated on analysing the traffic accident rate. Most traffic accidents are caused by the incorrect reaction of the driver to a traffic situation. The capability of reacting correctly may, for example, be influenced by some external factors. The presented results of the analysis of the dynamics of the traffic accident rate are evidence that these ideas are justified.

Traffic accident data

The traffic accident data refer to the years 1979—81. Data on the number of traffic accidents, which occurred on the territory of the town of Bratislava in the individual three-hour intervals UT of each day, are available. The numbers of accidents thus refer to the same intervals as the published *K*-indices of geomagnetic activity. By adding up the values for the eight intervals, one obtains the data for each day. The numbers of traffic accidents with regard to the administrative division of Slovakia, i.e. by regions (West Slovakian, Central Slovakian and East Slovakian region), related to the years 1980—82, are also available. The capital of Slovakia, Bratislava, is considered to be an independent region in this respect.

Variation of the traffic accident rate

Since data covering a period of only three years were used for the analysis, annual variations were not investigated and the authors restricted themselves to studying the weekly and daily variation of the traffic accident rate.

Weekly variation

The traffic accident rate depends very substantially on the traffic density. The changes in density are then reflected in the accident rate. The marked weekly variation for Bratislava is shown in Fig. 1. The daily occurrence of traffic accidents is expressed as

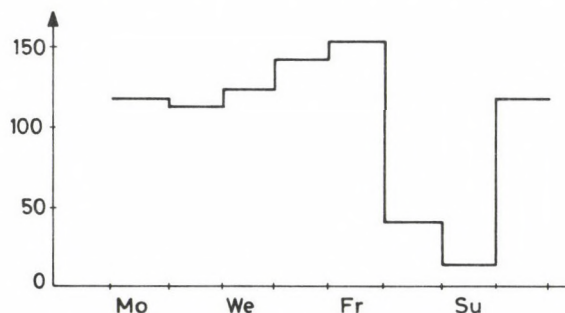


Fig. 1. Weekly variation of the traffic accident rate in Bratislava in 1979—81. Vertical axis: percentage of the daily number of accidents averaged for a week

a percentage of the average daily number of accidents in the whole. The differences between the individual working days are small, however, on Saturday and Sunday the number of accidents drops to one half. On free days there is no business traffic and individual traffic of a recreational nature is transferred beyond the city limits. On Fridays both types of traffic tend to cumulate and, consequently, the number of accidents on this day is the highest. In constructing the graph in Fig. 1, the different working-hour pattern around holidays was taken into account. The weekly variations of the traffic accident rate in the individual regions of Slovakia displays a similar pattern, but has a smaller amplitude. On free days, the number of accidents is about 80 percent of the number on working days, and this applies to all three regions. The reason for this is that recreational traffic is not transferred outside the limits of the region.

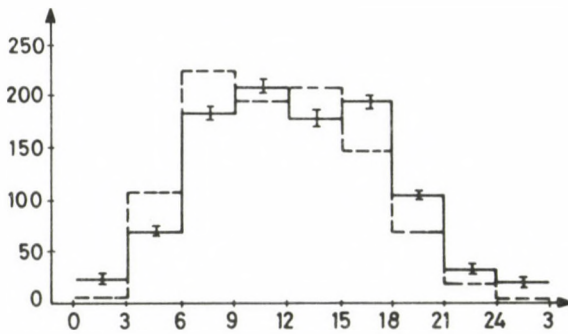


Fig. 2. Daily variation of the traffic accident rate in Bratislava in 1979—81. Horizontal axis: time UT. Vertical axis: percentage of the three-hour-interval number of accidents averaged for a day (also applies to Fig. 3). Solid line refers to free days (Saturday and Sunday), dashed line to working days (Monday to Friday). For the sake of clarity of the figure, the mean errors are shown only in the holiday graph; on working days they are roughly half

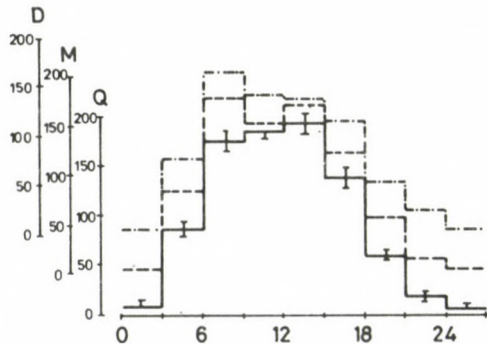


Fig. 3. Daily variation of the traffic accident rate in Bratislava in 1979—81 separately for days with different levels of geomagnetic activity. Solid line refers to quiet days (Q, $A_p < 8$), dashed line to medium disturbed days (M, $8 \leq A_p \leq 25$), and dot-dashed line to disturbed days ($A_p > 25$). Separate vertical axes for Q-, M- and D-days. For sake of clarity of the figure, the mean errors are only given in the solid-curve graphs; for the other graphs their values are roughly the same (this also applies to Figs 5 and 6)

Daily variation

The traffic accident rate also displays a conspicuous daily variation which, just like the weekly variation, is due to the difference in the traffic density. Figure 2 refers to Bratislava. The daily variations on working and free days differ, as can be seen from Fig. 2. On free days, the maximum is displaced to later times of the day, roughly by one interval, in accordance with the shift of the daily regime. Apart from this, an increase can be observed in the afternoon on free days.

The effect of the level of the total geomagnetic activity on the shape of the daily variation curve can be admitted, as shown in Fig. 3. On geomagnetically quiet days ($\Sigma K < 16$), there is one maximum in the daily variation between 12 and 15 hrs UT (Graph Q). If the activity is higher, another maximum will appear in the interval between 6 and 9 hrs UT (Graph M) which will predominate if the level $\Sigma K > 24$ (Graph D).

Territorial dependence of the traffic accident rate

Apart from the general traffic rules, the variation of the traffic accident rate in the individual territorial units also depends on other objective, namely on environmental factors. These may be the same or they may differ. By analysing the correlation of the traffic accident rate in the individual regions of Slovakia, we are also investigating the effect of certain common factors on which we shall concentrate below. The correlation coefficients between the daily number of accidents for the individual pairs of regions are the following: 0.49 for West Slovakia *vs.* Central Slovakia, 0.35 for West Slovakia *vs.* East Slovakia and 0.57 for Central Slovakia *vs.* East Slovakia. As expected, the correlation is lowest between the two most distant regions. This may be due to different

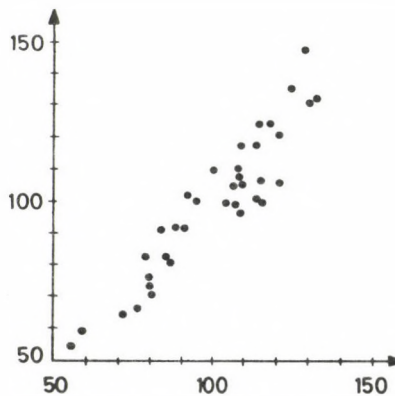


Fig. 4. Cross correlation of values of monthly sums of traffic accidents between the Central Slovakian region (horizontal axis) and East Slovakian region (vertical axis). The monthly sums are in percent of the mean value

meteorological situations in the regions being considered. The correlation is depicted in Fig. 4 for the Central Slovakian *vs.* the East Slovakian region, based on the monthly averages of the traffic accident rates.

Possible effect of natural factors on the traffic accident rate

Meteorological factors

Meteorological data from the observatory of the Charles University in Prague—Karlovy were used in this study. They do not reflect the meteorological situation in Bratislava, or in Slovakia as a whole, particularly well, however, they can be used to determine certain tendencies.

The most important biometeorological factor is the atmospheric pressure. Figure 5 shows the traffic accident rate in Bratislava on days when the atmospheric pressure was within the indicated interval. One can clearly see that, on days when the pressure was lower, the accident rate was higher. The dashed line in Fig. 5 represents the dependence with a shift of one day, since the changes in weather usually tend to move from west to east. The dependence is practically the same. The relations, constructed for the individual regions of Slovakia, are the same. Moreover, one can see that, with increasing distance from Prague, the curve becomes flatter and more undulated because the values, observed in Prague, are a poorer representation of the actual situation in a more distant region.

Another important meteorological factor is the relative atmospheric humidity. However, this displays a considerable annual variation: it is higher in winter than in summer. That is why deviations of the long-term standard, determined from humidity observations over 200 years (published together with the values of the relative

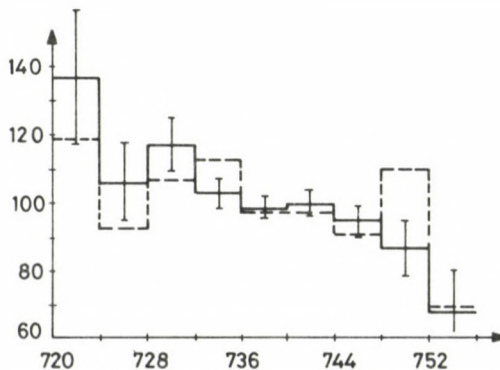


Fig. 5. Traffic accident rate in Bratislava in 1979—81 *vs.* atmospheric pressure in Prague. Horizontal axis: pressure in mm Hg. Vertical axis: percentage of the daily number of accidents averaged for a whole period (also applies to Figs 6 to 8). Solid line: data for the same day; dashed line: accident rate related to the atmospheric pressure on the previous day

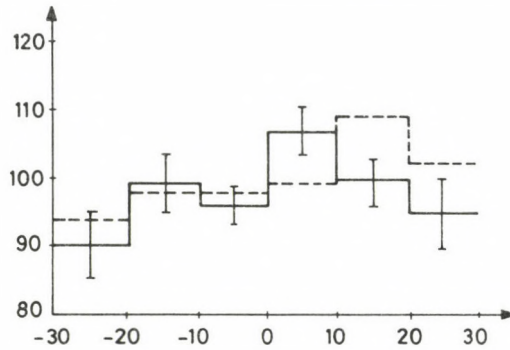


Fig. 6. Traffic accident rate in Bratislava in 1979—81 vs. deviation of relative humidity from long-term average. Horizontal axis: deviation as percentage of long-term average; the same as in Fig. 5 applies to the solid and dashed lines

humidity) were used. Figure 6 shows the traffic accident rate in Bratislava on the days on which these deviations were within the set limits. Although the dependence is not as unambiguous as in the case of atmospheric pressure, one can see that the traffic accident rate increased on days when the deviation was positive, i.e. the humidity was higher than usual in the given time of year. A similar dependence, shifted by one day, is also shown as a dashed line in this case. The same that was said about the atmospheric pressure applies to these relations produced for the individual regions of Slovakia.

In this investigation (as well as further on) the whole data set is divided into several subsets based on the values of the determined parameters. Care was taken to have a proportional representation of working and free days in each subset, i.e. to avoid the weekly variation affecting the results. This determined the number and size of the individual subsets; if division into more groups were to be considered, the condition of proportional representation would no longer be satisfied.

Various methods of biometeorological typification of the weather have been developed to provide a comprehensive description of the meteorological situation with regard to their biotropic effects. For our purposes, we shall use the biometeorological typification data (Biowetter) published by the Institut für Meteorologie und Geodynamik in Vienna. The data are suitable for describing the weather in Bratislava with a view to the small distance. According to the Biowetter method, the individual days are marked with the symbols A, B, C, D, E, depending on the meteorological situation. It was found that the results of some groups do not differ very much. For our purposes, it is sufficient to combine the days marked A, B, E (favourable days) into one group, and those marked C and D (unfavourable days) into another. On unfavourable days, the number of traffic accidents increases by about 18 percent as compared to the favourable days. This is valid for Bratislava; in the other regions, the increase is slightly smaller and it decreases with increasing distance from Vienna, because the typification, determined there, is less representative of the weather in the particular region. For example, in the East Slovakian region the difference between favourable and unfavourable days is only 10 percent.

Atmospheric electricity

Among the important factors of the environment is also atmospheric electricity. The values of the gradient of the electrostatic potential were obtained from the Nagycenk Observatory near Sopron in Hungary. With a view to the small distance, they can be considered as satisfactory for describing the electric field in Bratislava. The values of the gradient are given for each hour together with the daily average. However, the values frequently ran off the scale of the recording device (most frequently impulses in the electric field) and, consequently, the value of the gradient for the appropriate hourly interval is not given (it has been replaced by the symbol +S or -S depending on the sense of the deviation). The daily average is, of course, lacking, too. There were about 40 percent of days in the period investigated on which the gradient of the electric field displayed extreme values. A higher traffic accident rate was observed in Bratislava on these days, 14 percent on an average, as compared to the other days when the values of the potential gradient were within the limits of the recording instrument (normal electric field) for the whole day. Since atmospheric electricity is a variable phenomenon as regards position, in very much the same way as meteorological factors, the accident rate in the individual regions displays a dependence on atmospheric electricity which decreases with increasing distance from the point of measurement.

Geomagnetic activity

Apart from the factors we have already discussed, also geomagnetic factors come to bear in the complex of external influences. The effect of the variable magnetic field on the human organism in various walks of human life is now being intensively studied. In this study, we shall use the *K*-indices from the Niemegk Observatory in the GDR (or rather their daily sums ΣK). As opposed, e.g. to meteorological factors, the field of geomagnetic variations changes only little with position and, therefore, the distance from the observatory is of no particular importance.

In our data sample, we divided the days into groups based on the values of ΣK : $\Sigma K < 8$, $8 \leq \Sigma K < 16$, $16 \leq \Sigma K < 24$, $24 \leq \Sigma K < 32$, and $\Sigma K \geq 32$. The traffic accident rate for each of these groups is shown in Fig. 7. Most accidents occur on days with medium geomagnetic activity and on days with very high activity. Consequently, the dependence of the number of accidents on the level of geomagnetic activity is not linear. The pattern of this dependence is preserved even if other external effects are eliminated. The bold line in Fig. 7 applies to all data, the dot-dashed line at the top applies to days referred to as meteorologically unfavourable (Groups C and D according to Biowetter), and the dashed line at the bottom to meteorologically favourable days (Groups A, B, E according to Biowetter). At the same time, the figure documents the increase of the number of accidents on meteorologically unfavourable days and illustrates the interval in which the accident rate may fluctuate, when favourable or, on the contrary, unfavourable effects cumulate. A similar situation is

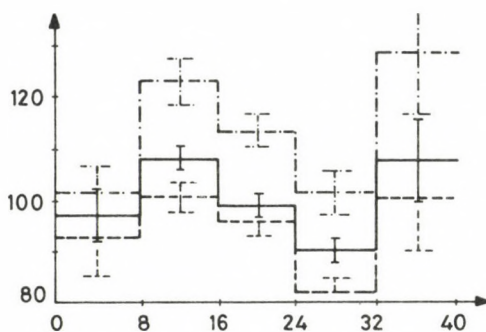


Fig. 7. Traffic accident rate in Bratislava in 1979—81 vs. level of geomagnetic activity as recorded at the Niemegek Observatory. Horizontal axis: values of ΣK . Solid line: all data, dashed line (at the bottom): data for meteorologically favourable days; dot-dashed line (at the top): data for meteorologically unfavourable days. The mean errors are given for all graphs provided this is not to the detriment of the graph's clarity. In some places, therefore, they have only been plotted to one side of the mean value (this also applies to Fig. 8)

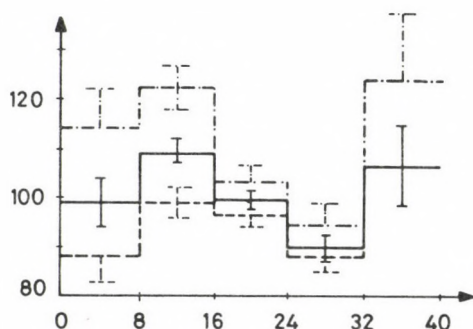


Fig. 8. The same as in Fig. 7. Solid line: all data; dashed line (at the bottom): data for days on which the values of the potential gradient of the electric field were within the limits of the recording instrument; dot-dashed line (at the top): data for days with extreme values of the gradient

depicted in Fig. 8 where the solid line is identical with the solid line in Fig. 7, the dot-dashed line refers to days with extreme values of the potential gradient of atmospheric electricity, and the dashed line to days on which the values of this gradient did not exceed the limits of the record. The relation of the accident rate to geomagnetic activity remains the same in all cases, and the other factors only caused the whole pattern to be displaced upwards or downwards.

Figures 7 and 8 do not indicate the number of days which fall into each interval on the horizontal axis. This distribution may vary from period to period, e.g. with the solar cycle, more days with higher geomagnetic activity occurring in the solar cycle maximum years. If the dependence of the number of traffic accidents on geomagnetic activity were to be expressed by a straight line (although this dependence is not linear) the run of the line would be affected considerably by the number of days in the individual intervals. This may be one of the reasons why the trends of the dependence of some phenomena on geomagnetic activity frequently differ considerably.

Discussion

The statistical t -test was applied to the results. As regards the significance test of the difference between two samples, it holds that $t = d/s_d$, where $d = |x_1 - x_2|$ can be determined from the mean values, and $s_d = (s_1^2 + s_2^2)^{\frac{1}{2}}$ from the appropriate mean errors for both samples. For the so-called zero hypothesis (i.e. the assumption that the difference being investigated is insignificant) to be rejected with a 95 percent probability, it is necessary for $t > 1.96$; if the hypothesis is to be rejected with a 99 percent probability, $t > 2.58$. In dividing the sample of traffic accidents into two groups on the basis of biometeorological typification, one finds that $t = 4.41$, and this is quite sufficient to assume the phenomenon to actually exist. Similarly, in dividing the sample into two groups on the basis of the data on atmospheric electricity, $t = 4.08$, and this is again quite satisfactory.

In constructing the graphs in Figs 5—8, the sample was divided into a number of parts, and the mean error s was given for each of the parts in the figures. If the t -test is applied to two neighbouring groups, one usually does not obtain a sufficiently large t because a large effect cannot be expected, if the change of the parameter is small. However, if the groups are more remote to each other, the value of t tends to be sufficiently large. For example, in comparing the groups at the margin and in the middle of the graph in Fig. 5, t is in the interval of 1.9 to 2.5. As regards the dependence on ΣK , the decrease of the traffic accident rate in the middle part of the graph (between the second and fourth groups), where $t = 3.83$, is statistically significant. The decrease for the lowest values is not sufficiently ensured ($t = 1.45$) which also applies to the increase for the highest activity values ($t = 1.34$), where the small number of days with activity $\Sigma K > 32$ is reflected. The data refer to the solid curves in Figs 7 and 8. The dependences represented by the dashed and dot-dashed curves were tested separately with the same result: t between 1.9 and 3.2 corresponds to the decrease in the middle part of the graph and $t = 1.2$ —1.5 to pattern at the margins of the graph.

The relation between the traffic accident rate and ΣK was also persistence tested. If the dependence determined for a particular sample is to be realistic, this dependence must also hold for the individual parts of the sample, obtained either by random division, or as a result of some criterion which is independent of the factor being studied. Biometeorological typification and atmospheric electricity can be considered independent of ΣK . The results are shown in Figs 7 and 8 as dashed and dot-dashed curves and indicate that the behaviour is the same in all cases. The persistence test also requires the same dependence to hold also for the data from another region, or from another period. The relation between ΣK and the traffic accident rate in the separate regions of Slovakia for the years 1980—1982 is the same as the graphs in Figs 7 and 8, and is therefore not shown. These results were also t -tested, and it was found that the values of t are within the same interval as for the Bratislava data.

Whereas the geomagnetic activity ΣK is a parameter independent of the meteorological quantities, the same cannot be said of the relations between the

individual meteorological quantities. A higher relative air humidity (to be more precise, the deviation from a long-term normal) usually corresponds to a lower atmospheric pressure, the cloudiness is larger as well as the partial pressure of water vapours, the values of the electrostatic potential are higher, and these frequently exceed the recording range of the instrument; if one restricted oneself to the summer months, also the air temperature would be lower. Although the correlation coefficients are not large (atmospheric pressure *vs.* relative humidity — 0.19, relative humidity *vs.* pressure of water vapours 0.37, relative humidity *vs.* cloudiness 0.34, atmospheric pressure *vs.* cloudiness — 0.46, etc.), the result is that a certain quantity, e.g. the traffic accident rate in this case, displaying a statistically significant correlation with a particular meteorological quantity, will also cause this correlation to appear with the other meteorological quantities. It needs special methods to decide what part can be ascribed to the effect of the given meteorological quantity and what part is due to the correlation of this quantity with another; it is far outside the scope of this study. The most convenient solution seems to be a complex characteristic of the meteorological situation using one of the methods of biometeorological typification, in which the contingent influences of all factors are summarily taken into account. Let us mention, however, that there is a number of methods of typification, that they are being developed constantly, and that at this time, it is impossible to decide which is the most suitable with regard to the study of meteorological effects on man's psyche.

The relation, illustrated in Figs 7 and 8, agrees well with the results of Srivastava and Saxena (1980). They investigated the occurrence of cardiac infarcts and, to a lesser extent, also of traffic accidents, and found that their occurrence in both cases was more frequent on days with medium geomagnetic activity. However, their maximum lies roughly one interval closer to higher activity.

The non-linear variation of the accident rate with geomagnetic activity indicates that there may be yet another factor in the geomagnetic field which affects the traffic accident rate, whose influence is strongest under medium geomagnetic activity. It is interesting that the occurrence of geomagnetic pulsations is indeed most frequent

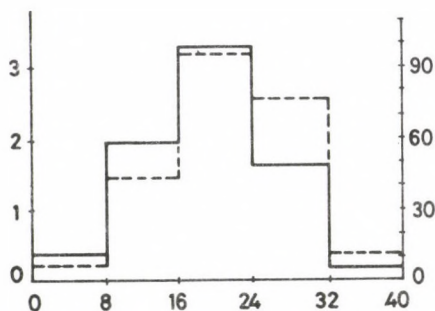


Fig. 9. Dependence of the Hurbanovo geomagnetic pulsation parameters on the level of geomagnetic activity. Horizontal axis: values of ΣK . Dashed line: mean pulsations amplitudes; left-hand scale in nT; solid line: product of mean amplitudes with pulsation duration; right-hand scale in nT. min

under these very conditions. The relation between these pulsations and geomagnetic activity is illustrated in Fig. 9, which shows the mean pulsation amplitude, as well as the product of the amplitude with pulsation duration for each activity interval; this expresses the magnitude of the pulsation field energy better. The pulsation data are from the Hurbanovo Observatory in southern Slovakia and refer to the period 1979—82. All Pc 3 pulsations were used. For narrower frequency bands, we would observe the dependence of the position of the maximum on the period: for pulsations with a shorter period the maximum would be displaced towards higher geomagnetic activity. The dependence of the pulsation period on the total geomagnetic activity is known and has been graphically represented, e.g. by Jacobs (1970).

We shall now compare the dependence between the pulsation period and geomagnetic activity, on the one hand, and the traffic accident rate in Figs 7 and 8, on the other. The first maximum ($8 \leq \Sigma K < 16$, i.e. $K = 1-2$) corresponds to a level of activity at which the conditions are most favourable for the occurrence of pulsations with periods of about 50 s. The next maximum ($\Sigma K \geq 32$, i.e. $K \geq 4$) corresponds to activity at which the conditions are most favourable for the occurrence of pulsations with periods of 20 s and less. This result is remarkable if one considers that the bioactive frequencies of the human organisms correspond to these periods (Breithaupt 1979).

Direct observations of geomagnetic pulsations would have to be considered if this problem is to be studied in more detail. Srivastava and Saxena (1980) took some steps in this direction and found a positive correlation. However, the currently published geomagnetic pulsation data are usually not the most suitable initial material and do not yield good results. The reason for this is the selectivity of the effect of the individual periods. It is, therefore, necessary to distinguish carefully between pulsations with different periods. Some pulsation index methods, which also take the periods into account, are well suited to this purpose. The first attempts in this respect have already been made. The preliminary results have proved positive correlation between the traffic accident rate and the occurrence of geomagnetic pulsations with periods of about 50 and 20 s. This positive correlation was not observed for pulsations whose periods are in other frequency bands. This rule applies to the Bratislava data as well as the data from the other regions of Slovakia.

The results mentioned indicate the possible mechanism by which the variable geomagnetic field acts on the human organism. It involves the low-frequency background (geomagnetic pulsations) of the changes of the geomagnetic field, whose variations may be transmitted via the information channel of the interaction of the human organism with the environment. Increased attention will have to be devoted to geomagnetic pulsations, in particular to their periods. This is also related to establishing a suitable method of numerical pulsation characteristics which would provide information about the amount of energy transferred in the narrow frequency bands. In solving the problem of this mechanism, it will be necessary to exploit the results of laboratory measurements of the effects of variable magnetic fields on biological objects, especially in the neighbourhood of bioactive frequencies, or to orient these measurements directly towards solving this problem.

References

- Breithaupt H 1979: Biological Rhythms and Communication. In: *Electromagnetic Bio-Information*, Proceedings of the Symposium, Marburg, Sept. 5, 1977. Edited by F A Popp et al., Urban & Schwarzenberg, München—Wien—Baltimore
- Gnevyshev M N, Ol' A I 1971: Effects of Solar Activity on the Earth's Atmosphere and Biosphere (in Russian). Izd. Nauka, Moscow. Translated from Russian under Israel Programme for scientific translations, 1977.
- Jacobs J A 1970: Geomagnetic Micropulsations. *Physics and Chemistry in Space*, 1. Springer Verlag Berlin, Heidelberg, New York
- Srivastava B J, Saxena S 1980: Geomagnetic-Biological Correlations: Some New Results. *Indian Journal of Radio and Space Physics*, 9, 121—126.

APPROXIMATIVE SOLUTION OF THE DIRECT PROBLEM OF MAGNETOTELLURICS FOR TWO-LAYERED, THREE-DIMENSIONAL STRUCTURES

E TAKÁCS¹ and E TURAI¹

[Manuscript received January 21, 1985]

The paper presents an approximative method with integral equations for the determination of electromagnetic fields of plane waves in two-layered, three-dimensional structures. The effect of subsurface boundaries is taken into account by current- and charge densities and the secondary fields due to them are determined by the Stratton-Chu formula. The surface current- and charge densities can be given with the field intensities reflected at the boundary, and the latter can be computed in case of plane waves inciding downwards for single surface elements by the reflection coefficients. The method takes only first reflections into account. The application of the method is presented by examples which lead to conclusions about the conditions of its application and about the characteristics of the computational procedure.

Keywords: integral equations; magnetotellurics; mathematical modeling; 3-D models

The behaviour of the MT field above 3-D structures needs further investigation. For this purpose the application of approximate numerical methods—which can be used only for modeling of relatively simple structures—is therefore justified. In order to illustrate complicated physical processes, these methods deserve attention from a didactical point of view, too.

The present paper presents a method which enables the approximate solution of the direct problem of the magnetotelluric field for two-layered, 3-D structures.

The MT field on the surface of the Earth can be regarded as the superposition of the primary field incident from upwards and of the secondary field originating from the subsurface boundary. The secondary field is from the boundary reflected and many times reverberated field. The approximation in case of the method presented here means that

- only the first reflexion is considered;
- the subsurface boundary is supposed to be set up from plane elements;
- approximate numerical methods are used in the computations.

The components of the secondary field from the lower boundary are given at the Earth's surface by the vectorial Huyghens-principle which defines surface current and charge densities at the lower boundary as sources of the secondary field and they are given by the components reflected there. The secondary field at the surface is then given by the Stratton-Chu formulas.

¹ Technical University for Heavy Industry, Miskolc, Hungary, H-3515

Let us translate the process above into a mathematical formalism. The magnetic and electric components of the primary field being incident from above on the Earth's surface with a time variation $\exp(j\omega t)$ are on the surface \mathbf{H}_0 and \mathbf{E}_0 . By setting $|\mathbf{E}_0| = 1$ for the electric field

$$\mathbf{H}_0 = -\frac{k_1}{\mu_1 \omega} [\mathbf{e} \times \mathbf{E}_0],$$

where

— $\mathbf{e} = \frac{\mathbf{E}_0 \times \mathbf{H}_0}{|\mathbf{E}_0| \cdot |\mathbf{H}_0|}$ is a unit vector in the direction of the wave propagation,

— $k_1 = \sqrt{\frac{\omega \mu_1 \sigma_1}{2}} (j-1)$ the wave number in the upper layer,

— ω is the angular frequency,

— μ_1 the magnetic permeability

— σ_1 the specific conductivity of the upper layer.

The incident field components in a point A of the subsurface boundary are:

$$\mathbf{E}_i = \mathbf{E}_0 \exp [jk_1(\mathbf{r}_A - \mathbf{r}_0)] \quad (1)$$

$$\mathbf{H}_i = \mathbf{H}_0 \exp [jk_1(\mathbf{r}_A - \mathbf{r}_0)],$$

where

— $\mathbf{r}_A - \mathbf{r}_0$ is the vector from the surface to the point A , and

— $\mathbf{k}_1 = k_1 \mathbf{e}$.

If the neighbourhood of the point A of the lower boundary is supposed to be plane, the reflected field components \mathbf{E}_r and \mathbf{H}_r can be computed from the incident field components. Decomposing the incident and reflected wave into components perpendicular to and parallel with the plane of incidence—defined by the unit vectors \mathbf{e} —and by the unit vector of the normal of the plane surface element, the components $E_{r\perp}$, $E_{r\parallel}$, $H_{r\perp}$, $H_{r\parallel}$, can be computed from the equations

$$\begin{bmatrix} E_{r\perp} & H_{r\parallel} \\ E_{r\parallel} & H_{r\perp} \end{bmatrix} = \begin{bmatrix} D_E & 0 \\ 0 & D_H \end{bmatrix} \begin{bmatrix} E_{i\perp} & H_{i\parallel} \\ E_{i\parallel} & H_{i\perp} \end{bmatrix} \quad (2)$$

using the components $E_{i\perp}$, $E_{i\parallel}$, $H_{i\perp}$, $H_{i\parallel}$ of the incident wave, where

$$D_E = -\frac{\sqrt{\sigma_2/\sigma_1 + n_z^2 - 1} + n_z}{\sqrt{\sigma_2/\sigma_1 + n_z^2 - 1} - n_z}$$

and

$$D_H = -\frac{\sigma_1/\sigma_2 \sqrt{\sigma_2/\sigma_1 + n_z^2 - 1} + n_z}{\sigma_1/\sigma_2 \sqrt{\sigma_2/\sigma_1 + n_z^2 - 1} - n_z}$$

are the reflexion coefficients valid for the plane wave if the incident wave propagates in the direction z and

$$\mu_1 \cong \mu_2 \cong \mu_0 = 4\pi \cdot 10^{-7} \text{ Vs/Am},$$

— n_z is the component in the direction z of the normal unit vector, further

$$\begin{aligned} E_{i\perp} &= (\mathbf{E}_i \cdot \mathbf{e}_\perp), & E_{i\parallel} &= (\mathbf{E}_i \cdot \mathbf{e}_\parallel), \\ H_{i\perp} &= (\mathbf{H}_i \cdot \mathbf{e}_\perp), & H_{i\parallel} &= (\mathbf{H}_i \cdot \mathbf{e}_\parallel), \\ \mathbf{e}_\perp &= \frac{\mathbf{e} \times \mathbf{n}}{\sqrt{1 - (\mathbf{e}\mathbf{n})^2}}, & \mathbf{e}_\parallel &= \mathbf{e} \times \mathbf{e}_\perp. \end{aligned}$$

Using Cartesian coordinates and expressing the reflected components by the surface primary components using Eqs (1) and (2) the components of the reflected field are in point A of the lower boundary

if $|n_z| \neq 1$

$$H_r(A)_x = \frac{D_H n_y (n_y H_{0x} - n_x H_{0y}) + D_E n_x (1 - 2n_z^2) (n_x H_{0x} + n_y H_{0y})}{1 - n_z^2} \exp [jk_1 z]$$

$$H_r(A)_y = \frac{D_H n_x (n_x H_{0y} - n_y H_{0x}) + D_E n_y (1 - 2n_z^2) (n_x H_{0x} + n_y H_{0y})}{1 - n_z^2} \exp [jk_1 z]$$

$$H_r(A)_z = 2D_E n_z (n_x H_{0x} + n_y H_{0y}) \exp [jk_1 z]$$

$$E_r(A)_x = \frac{D_E n_y (n_y E_{0x} - n_x E_{0y}) + D_H n_x (1 - 2n_z^2) (n_x E_{0x} + n_y E_{0y})}{1 - n_z^2} \exp [jk_1 z]$$

$$E_r(A)_y = \frac{D_E n_x (n_x E_{0y} - n_y E_{0x}) + D_H n_y (1 - 2n_z^2) (n_x E_{0x} + n_y E_{0y})}{1 - n_z^2} \exp [jk_1 z]$$

$$E_r(A)_z = 2D_H n_z (n_x E_{0x} + n_y E_{0y}) \exp [jk_1 z],$$

if $|n_z| = 1$

$$H_r(A)_x = -D_E H_{0x} \exp [jk_1 z], \quad E_r(A)_x = D_E E_{0x} \exp [jk_1 z],$$

$$H_r(A)_y = -D_E H_{0y} \exp [jk_1 z], \quad E_r(A)_y = D_E E_{0y} \exp [jk_1 z],$$

$$E_r(A)_z = H_r(A)_z = 0.$$

According to the vectorial Huyghens-principle (Simonyi 1967) electric and magnetic surface current densities— \mathbf{K}_e , \mathbf{K}_m —and charge-densities— σ_e , σ_m —can be defined in each point of the lower reflecting surface (S) which substitute the effect of this surface, and are defined as:

$$\mathbf{K}_e = \mathbf{n} \times \mathbf{E}_r, \quad \mathbf{K}_m = -\mathbf{n} \times \mathbf{H}_r,$$

$$\sigma_e = |\mathbf{n}\mathbf{E}_r|, \quad \sigma_m = |\mathbf{n}\mathbf{H}_r|.$$

These current and charge densities produce the following secondary field components in a surface point P using the Stratton—Chu formulas:

$$E_r(P)_x = \frac{1}{4\pi} \int_S [-j\omega\mu_0 (nH)_x + g_1 ((nE)_y Z - (nE)_z Y) + g_1 (\mathbf{n}\mathbf{E}_r)_X] \psi_1 \, dS$$

$$\begin{aligned}
 E_r(P)_y &= \frac{1}{4\pi} \int_S [-j\omega\mu_0(nH)_y + g_1((nE)_z X - (nE)_x Z) + g_1(\mathbf{nE}_r) Y] \psi_1 \, dS \\
 E_r(P)_z &= \frac{1}{4\pi} \int_S [-j\omega\mu_0(nH)_z + g_1((nE)_x Y - (nE)_y X) + g_1(\mathbf{nE}_r) Z] \psi_1 \, dS \\
 H_r(P)_x &= \frac{1}{4\pi} \int_S [\sigma_1(nE)_x + g_1((nH)_y Z - (nH)_z Y) + g_1(\mathbf{nH}_r) X] \psi_1 \, dS \\
 H_r(P)_y &= \frac{1}{4\pi} \int_S [\sigma_1(nE)_y + g_1((nH)_z X - (nH)_x Z) + g_1(\mathbf{nH}_r) Y] \psi_1 \, dS \\
 H_r(P)_z &= \frac{1}{4\pi} \int_S [\sigma_1(nE)_z + g_1((nH)_x Y - (nH)_y X) + g_1(\mathbf{nH}_r) Z] \psi_1 \, dS
 \end{aligned} \tag{3}$$

where

- $(nE)_{x,y,z}$ and $(nH)_{x,y,z}$ are the Cartesian components of the vectorial products, $(\mathbf{n}(A) \times \mathbf{E}_r(A))$ and $(\mathbf{n}(A) \times \mathbf{H}_r(A))$
- $X = \sin \Theta \cos \varphi$, $Y = \sin \Theta \sin \varphi$, $Z = \cos \Theta$,
- $g_1 = jk_1 - \frac{1}{r}$.
- $\psi_1 = \exp(j\mathbf{k}_1 \cdot \mathbf{r})/r$ (Green's function)
- φ, Θ, r spherical coordinates (origin in P and the axes $\varphi = 0$ and $\Theta = 0$ coincide to the axes x and z).

The Stratton—Chu formulas in the form given by Eq (3) is already suitable to carry out the modeling. The formulas are really the sums of surface integrals of the type $\int_S f_1(A) f_2(A) \, dS$, where dS is the surface element, $f_1(A)$ is the function yielding the values of some reflected field components on the surface S , and $f_2(A)$ is a weight-function.

The secondary components are determined on the Earth's surface by numerical integration. For this the reflecting surface S is approximated by N plane surface elements (ΔS) and

$$\int_S f_1(A) \cdot f_2(A) \, dS \approx \sum_{i=1}^N \int_{\Delta S_i} f_1(A) \cdot f_2(A) \, dS = \sum_{i=1}^N J$$

where

$$J = f_1^d \cdot f_2^d \Delta S_i,$$

and f_1^d, f_2^d are the values of $f_1(A)$ and $f_2(A)$ in a point of the surface element.

The resulting field is at the surface of the Earth:

$$\mathbf{E}(P) = \mathbf{E}_0 + \mathbf{E}_r(P)$$

$$\mathbf{H}(P) = \mathbf{H}_0 + \mathbf{H}_r(P).$$

Using them, input impedances and apparent specific resistivities can be determined for selected frequencies.

The algorithm presented here results in evidently approximate values. Therefore the validity of the approximation should be investigated prior to any application.

A possibility for this is given by the modelling a horizontally stratified half-space. In that case the result is omitting the deduction of the formulas:

$$Z = \frac{E_x}{H_y} = \frac{\omega\mu_1}{k_1} \frac{1 + D_E \exp(jk_1 2h_1)}{1 - D_E \exp(jk_1 2h_1)}. \quad (4)$$

Here h_1 is the thickness of the top layer. Equation 4 yields a solution being identical with the usual solution by differential equations in spite only a single reflection at the lower boundary is regarded. For the horizontally stratified case further reflections can also be easily taken into account which result, however, in deviations from the exact values. This deviation diminishes below a limit of 1% in the range $\lambda_1/h_1 = (1 \div 20)$, if at least ten multiple reflections are taken into account (Fig. 1). That is by no means in

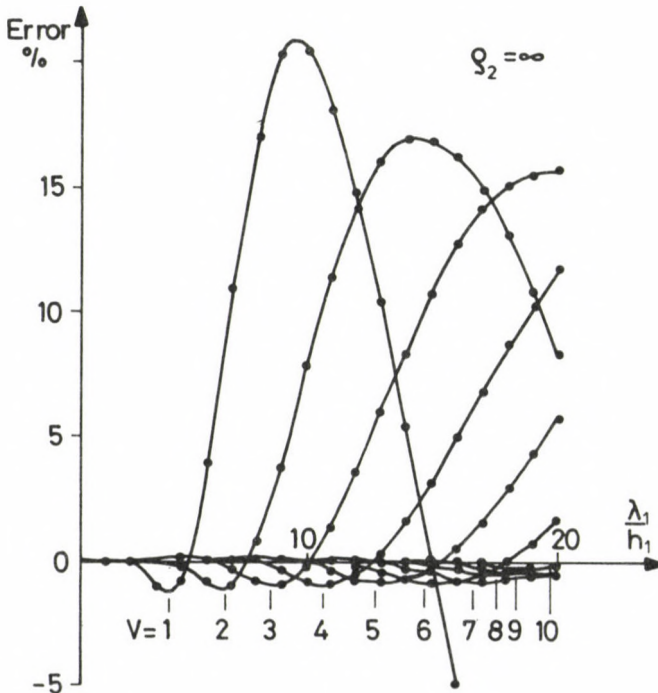


Fig. 1. Errors of the normed apparent specific resistivities computed by taking into account the multiple reflections for a horizontal layer boundary. The parameter V of the curves is the number of reflections

contradiction to the fact that Eq. (4) yields an exact solution for the horizontally stratified half-space, as Eq. (4) is essentially the formula for the sum of the geometric sequence corresponding to the multiple reflections.

The physical background of this results is that in an 1-D case the electromagnetic field remains plane wave even after multiple reflections.

It is to be expected that the range of the applicability of the approximative formula depends on the amplitude of the relief of the reflecting surface in the laterally inhomogeneous case. In order to collect information for this case, the method has been applied for the model of the known 2-D step for which unfortunately only the results of the H -polarization are available (Dmitriev and Kokodushkin 1971). The results are compared on Fig. 2, where the solid lines represent data from Dmitriev and Kokodushkin's album, and points mean data calculated with the present method. y_p is the distance of the measurement point from the surface projection of the step. The values calculated in the case $h_2/h_1 = 1.25$ by the approximate method coincide quite closely for all frequencies with the data in the album. As the height of the step increases the range of congruence diminishes. This comparison enables conclusions on the allowed range of the depth change of the basement.

In spite of the above limitations some actual problems of practical MT measurements can be studied by the present method.

It is an interesting problem for the practice to find the volume of rocks for a given basement depth and frequency from which the geological information comes. With this

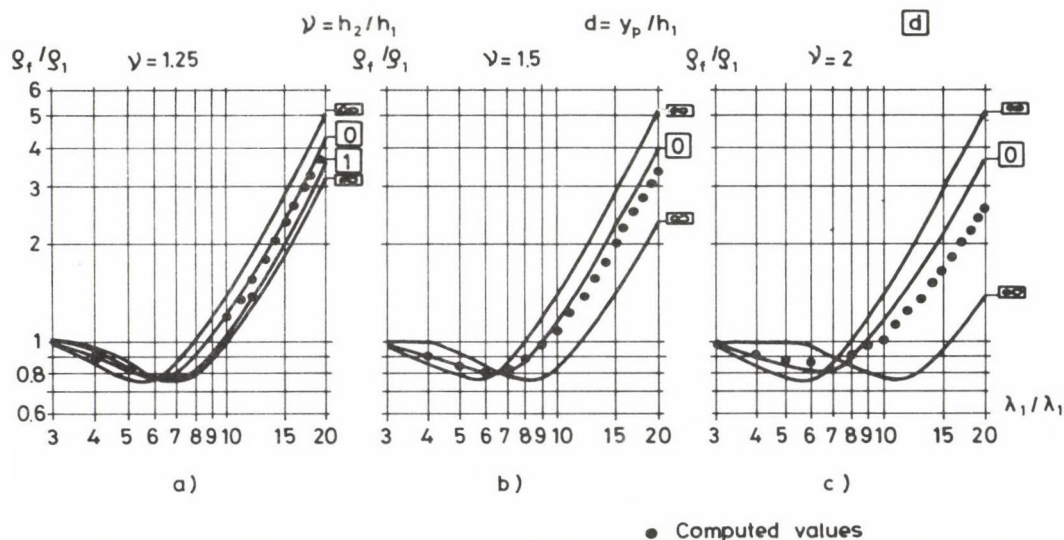


Fig. 2. A comparison between normed apparent specific resistivities computed by the present method for the step-model (points) and the frequency sounding curves published by Dmitriev and Kokodushkin (1971).

h_1 and h_2 : depths of the upper and lower edges of step,

$$\gamma = h_2/h_1,$$

y_p : distance of the point computed from the surface projection of the step,

$d = y_p/h_1$, the parameter of the curves

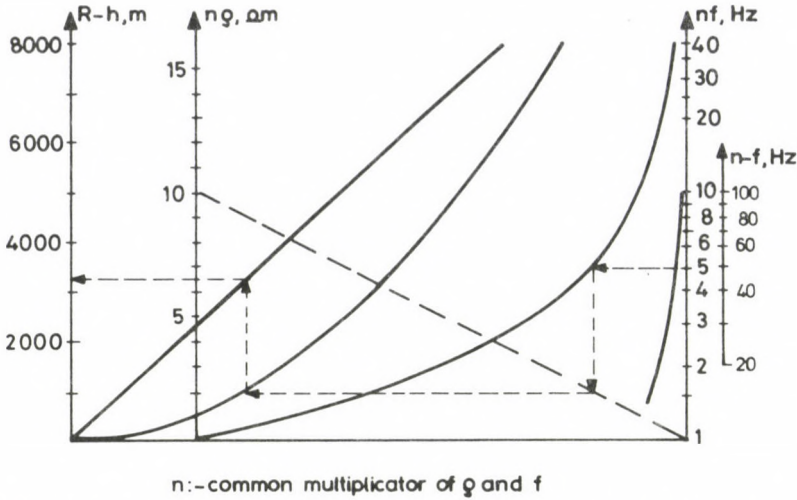


Fig. 3. Nomogram for the determination of the radius R of the reflecting circular plate necessary to reach an error of 1 percent in $\rho_a(f)/\rho_1$ in case of $\rho_2 = \infty$, one-dimensional case

aim in the mind it was determined which area the surface should have in a 1-D case from which the reflexions must be taken into account to reach an accuracy of 1% in the apparent specific resistivity. For the case $\rho_2 = \infty$, Fig. 3 shows a nomogramme to determine the radius R of the circular plate to be taken into account for the reflexions in function of ρ_1 and h_1 . Using the equation

$$\text{error [\%]} = \frac{[\rho_a(f)/\rho_1]_R - \rho_a(f)/\rho_1}{\rho_a(f)/\rho_1} \cdot 100$$

theoretical error functions can be determined, where $[\rho_a(f)/\rho_1]_R$ is the normed specific apparent specific resistivity taking into account the finite reflecting surface. Figure 4 shows these error functions for $\rho_2 = \infty$. The figure enables the conclusion that the radius of the finite reflecting surface should be chosen equal to the wavelength in the first layer ($R = \lambda_1$), in which case the error is 0.1% being sufficient for practical demands. This connection can be also used for planning the numerical and even the analogue multidimensional modeling.

In addition to the previous it can also be decided what length should a structure have in the strike direction to allow its treatment as a 2-D structure. For all measurement points a radius R can be determined for any accuracy level so that in a direction the structure does not change within an interval of $[-R, R]$, then choosing this direction as the direction of the strike, the structure can be treated as a 2-D one within the given error limit.

The approximate numerical modeling solves further the question of the lateral resolution power of the MT-measurements. Figure 5 shows e.g. that the 3-D structures

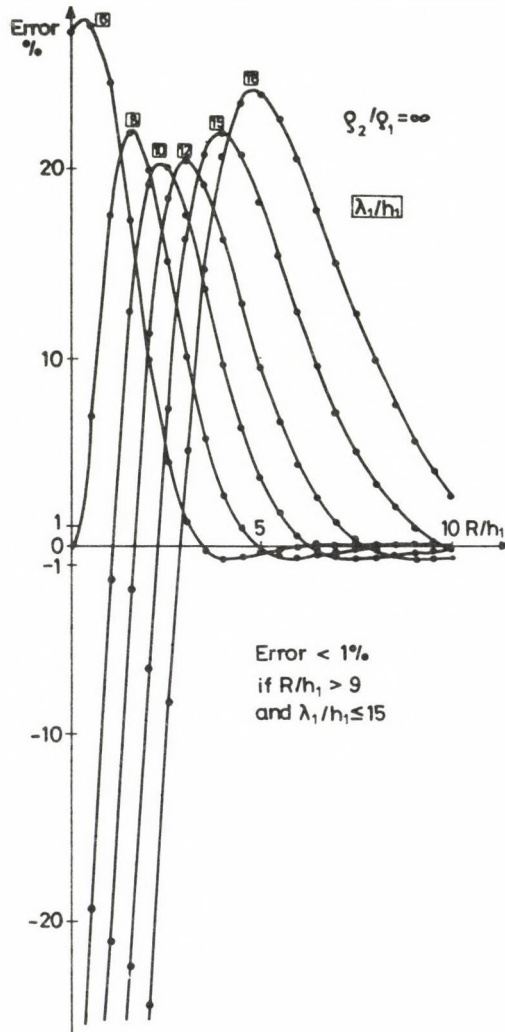


Fig. 4. The error of the normed apparent specific resistivities computed by taking into account the finite reflecting surface in function of R/h_1 .

h_1 : thickness of the cover,

λ_1 : wave length in the cover,

λ_1/h_1 : parameter of the curves,

R : the radius of the circular plate taken into account in the computations

with the given dimensions yield separate anomalies at a frequency of 1 Hz, both on the curves of the apparent specific resistivity and of the H_z -values.

It is an important question for the practical exploration which differences occur between 2-D and 3-D structures for a given elongation. An example for this problem is presented in Figs 6 and 7. The horizontal dimension of the 3-D body is in this case 1000×1000 m.

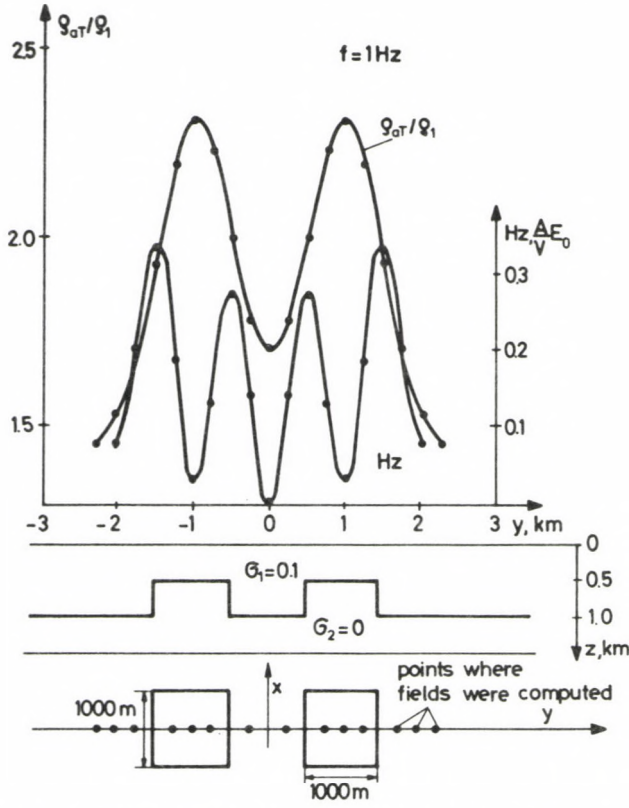


Fig. 5. Normed apparent specific resistivities (ρ_{aT}/ρ_1) and the vertical magnetic field component (H_z) computed above two horsts lying near to each other at $f = 1 \text{ Hz}$.

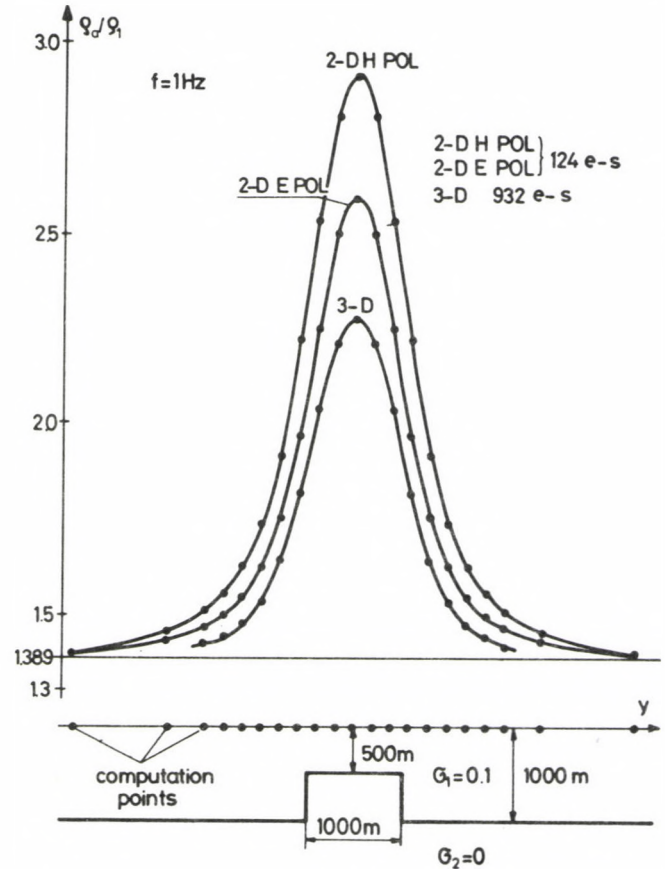


Fig. 6. Normed apparent specific resistivities (ρ_a/ρ_1) computed above a horst (3-D) and a (2-D H-pol, 2-D E-pol) ridge for $f = 1 \text{ Hz}$.

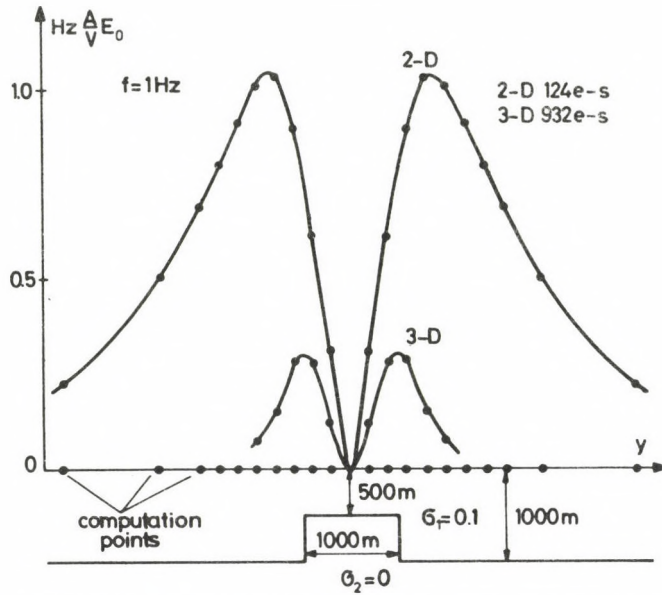


Fig. 7. Vertical magnetic field components (H_z) computed above a horst (3-D) and a 2-D ridge (2-D) for the E polarized case at $f=1$ Hz

References

- Simonyi K 1967: Theoretical electricity, Budapest (in Hungarian)
 Dmitriev V I, Kokodushkin G A 1971: Albom paletok dlya magnitotelluricheskogo zondirovaniya v neodnorodnykh sredakh, Moscow University

PHYSICAL MODELING OF THE ADJUSTMENT DISTANCE

A ÁDÁM¹ and L SZARKA¹

[Manuscript received February 1, 1985]

Some magnetotelluric sounding curves in polarization H show a steep rise of the apparent resistivity vs. period over great tectonic lines, such as the Periadriatic lineament in the Alps. This distortion is due to the buildup of electric charges on conductivity discontinuities and it comes to an end in the "adjustment distance" from the discontinuity.

From this point of view the character of this distortion and the adjustment distance of graphite dykes were studied by physical modeling in the field of an electric dipole between 0.01—5 MHz in different transmitter-receiver arrangements. An approximation of the magnetotelluric field enabled to compare the features of MT curves in polarization H to the controlled source MT or frequency sounding curves, with the latter more emphasizing the transmitter effect. The values of adjustment distances measured in MT fields are near to the numerical values of Rangayanaki and Madden (1980) in case of thin dykes.

Keywords: adjustment distance; magnetotellurics; Periadriatic lineament; physical modeling

1. Introduction

Some (ρ_{\max}) magnetotelluric frequency sounding curves in polarization H measured in the Alps along the Periadriatic lineament show a very steep rise (more than 63.5°) being on the contrary to the theory and have unlikely high values ($\rho > 10^5$ ohm) at large periods (Ádám et al. 1984). ρ_{\max} curves measured in the Gail-valley in Schlanitzen and Sittmoos are presented as examples in Fig. 1.

The Periadriatic lineament (as a significant tectonic zone) represents an elongated highly conductive quasi-two-dimensional structure. The crystalline rock is cracked in it due to several times renewed mechanical effects and thus it has an enlarged porosity. The "overrise" of the H polarized ρ_{\max} curves measured perpendicularly to the fracture zone can be attributed to charges at resistivity interfaces as it has been described by Price (1973) for a vertical discontinuity (Fig. 2).

The effect of buildup of charges is known from different numerical modelings (e.g. the curve ρ_{\max} shows a similar overrise over the edge of a high conducting half layer as it has been calculated by Tátrallyay 1977, using the finite difference method). Praus (1976) referred to the fact that the apparent resistivity is distorted over resistivity interfaces, and reaches the real value of ρ only after a so-called "recovery zone".

¹ Geodetic and Geophysical Research Institute of the Hungarian Academy of Sciences, H-9401 Sopron, P.O.B. 5.

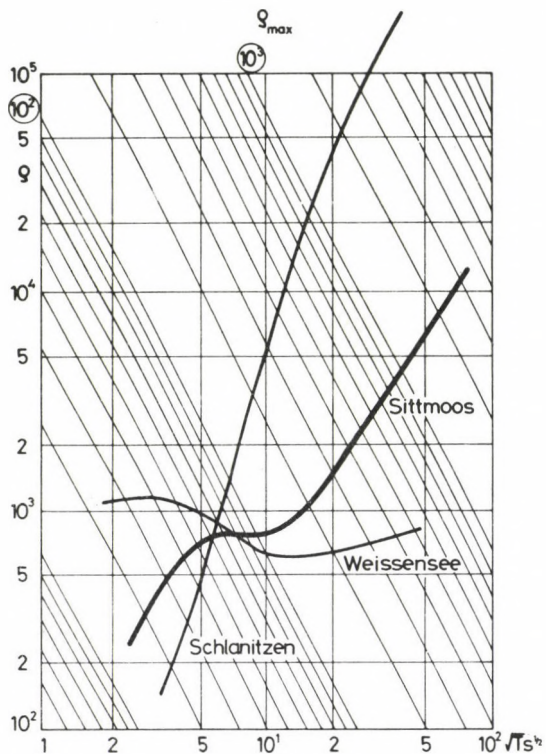


Fig. 1. Sounding curves ρ_{\max} (polarization H) along the Periadriatic lineament in the Gail-valley according to Ádám et al. (1984)

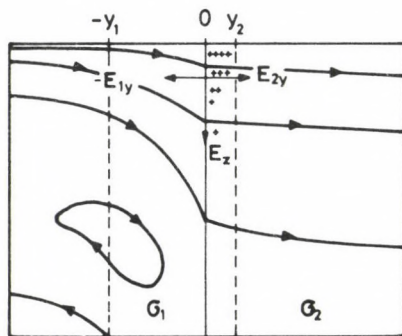


Fig. 2. Distribution of current lines and surface electric charges on the boundary of a vertical conductivity contrast (according to Price 1973)

This phenomenon must be taken into account in MT interpretation, as noted by several authors (e.g. Flores et al. 1985): When the layered structure is interpreted from H polarization curves the resistivity values are overestimated on the side with higher resistivity.

It is necessary to determine for different resistivity contrasts the zone in which the distortion of MT curves must be taken into account.

This phenomenon is frequency-dependent: The longer the period of the MT field is the larger is the "recovery zone". Thus the "disturbance field" determines the behavior of the electromagnetic field in larger and larger areas. The buildup of charges is exclusively an H polarization effect.

This phenomenon is related also to the problem of current channeling (Jones 1983).

In current channeling the terms "adjustment distance" or "equilibrium distance" are used instead of the "recovery zone".

Jones' review (1983) deals with the current channeling from several points of view. In his introduction one sentence points out its connection to the present problem: "... the problem of current channeling is directly related to the buildup of charges on conductivity discontinuities, hence it may be expected intuitively that the important physical parameter term is the gradient of the scalar electrostatic potential of those charges."

According to Le Mouel and Menvielle (1982) the electric field can be divided into a normal (n) and an abnormal part (a):

$$\mathbf{E} = \mathbf{E}_n + \mathbf{E}_a. \quad (1)$$

The local induction can be neglected if $\frac{\partial \mathbf{A}_a}{\partial t} \ll \text{grad } \varphi$, where \mathbf{A}_a is the vectorpotential of the abnormal part, φ is the scalar potential due to the buildup of charges. Thus the relation (1) can be simplified into

$$\mathbf{E} = \mathbf{E}_n + \text{grad } \varphi.$$

This is the basic relation of the current channeling. According to the above authors this relation is valid if

$$\delta^2 \gg S$$

where δ is the penetration depth in the material where anomalous currents are flowing, S is a characteristic cross-section of the anomalous flow of currents.

In the current channeling the potential of charges has a role within the adjustment distance characterizing just the disturbance zone of the MT measurements, too.

In this paper we do not want to take sides in the problem of current channeling which is a difficult structure- and frequency-dependent phenomenon.

Recently several authors deny its validity — mainly in the short period range — (Fischer 1984, Thera and Dupis 1983, McKirdy and Weaver 1983) referring to the fact,

that the phenomena observed by the French group in the Pyrénées and in the Rhine graben can be described by the MT theory, without supposing any injected currents.

Our aim is to study the characteristics of the "adjustment distance".

After describing the modeling equipment similarities between MT and dipole-generated frequency sounding (FRS) curves are discussed. On the basis of theoretical considerations and model experiments a good approximation of the MT field could be made with a special model arrangement over 2-D structures. This is the so-called 2.5-D FRS modeling. Then quasi MT and FRS curves are compared in polarization H over 2-D graphite dykes and adjustment distances are studied in more details.

A qualitative period dependence of the adjustment distance is determined and ratios H_z/H_y are also presented in the boundary zones.

2. Description of the modeling equipment

The electromagnetic modeling laboratory in the Geodetic and Geophysical Research Institute of the Hungarian Academy of Sciences, in Sopron can be applied to model electromagnetic field anomalies generated by finite electric and magnetic dipoles.

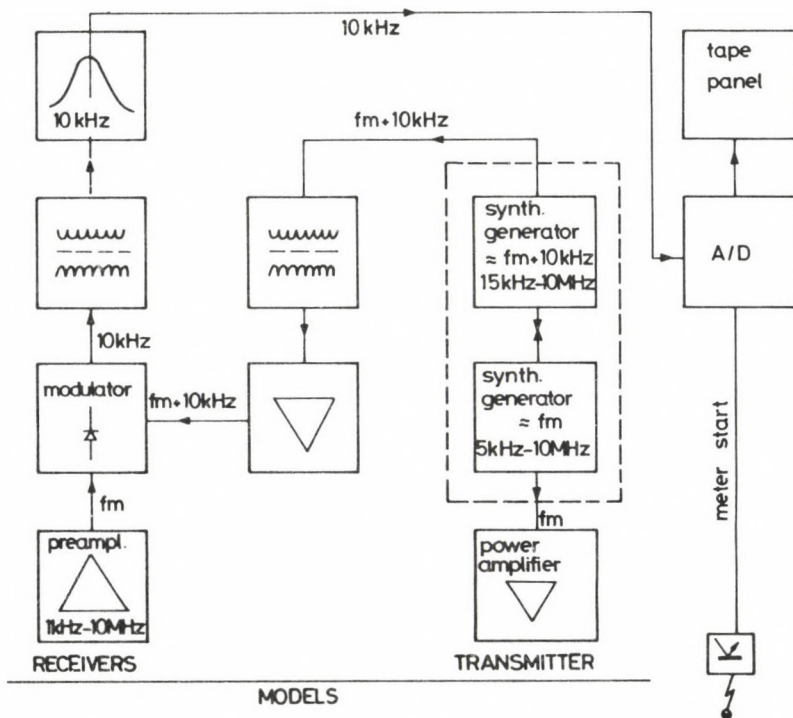


Fig. 3. Block diagram of the analogue modeling equipment

The new version of the transmitting and receiving circuits were developed following Moroz (1984) as it can be seen in Fig. 3. (The first version is described by Ádám et al. 1981, the latest one by Márcz et al. 1985.)

The measuring frequency f_m in the range 20 kHz—5 MHz is produced by a synthesizer generator. The output current is of nearly constant intensity due to a power amplifier. The voltage related to different field components is amplified in a wide-band preamplifier of low noise just above the measuring dipoles. Then, in a modulator the signal of frequency f_m is modulated with an other signal of frequency $f_m + 10$ kHz, coming directly from the second synthesizer generator and thus a signal of low intermediate frequency (10 kHz) is produced. The modeled electromagnetic field is determined by the amplitude and phase of this signal.

Measured data — after an analogue-digital conversion — are punched on tape or get immediately at a computer. Sampling is controlled by an optical starting unit.

Measurements are carried out in a large tank made of poliester resin with the dimensions 4 m × 3 m × 0.5 m.

3. Similarity of magnetotelluric and artificial frequency sounding (FRS) curves over two layered half spaces having high conductivity basement

It was shown by Ádám et al. (1983) that in case of high conductivity basement and large enough r/h_1 ratio (where r is the distance between the receiver and the transmitter, h_1 is the depth of the high conductivity basement) the electromagnetic field generated by a horizontal electric dipole is similar to the magnetotelluric field. A quite good agreement can be reached in modeling circumstances: it was shown both theoretically and experimentally that $r/h_1 = 3$ is large enough to reach a difference of 3% between the corresponding ρ values.

To model the MT field, two layouts were used: an equatorial and an axial position. For polarizations E and H these two layouts can be combined in four different ways (Fig. 4).

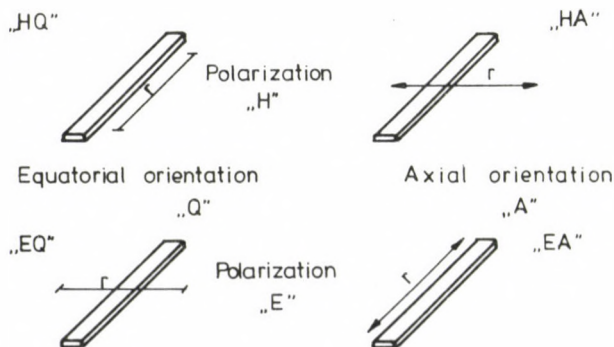


Fig. 4. Positions of transmitter and receiver in modelings of conductive dykes (Ádám et al. 1983)

There are two main effects which may cause significant distortions in the MT field:

a) The receiver indicates a field anomaly not only when it lies over a lateral inhomogeneity, but it shows a secondary effect in consequence of a direct "interaction" between the transmitter and the inhomogeneity. This distortion is different in different transmitter-receiver configurations: the largest distortion can be found in position HQ . The distortion effect is less in case of positions HA and EQ (see Figs 14—15 in Ádám et al. 1983), but they are not symmetrical because of the transmitter effect. Despite of this distortion effect, certain profile sections are very similar to the MT case.

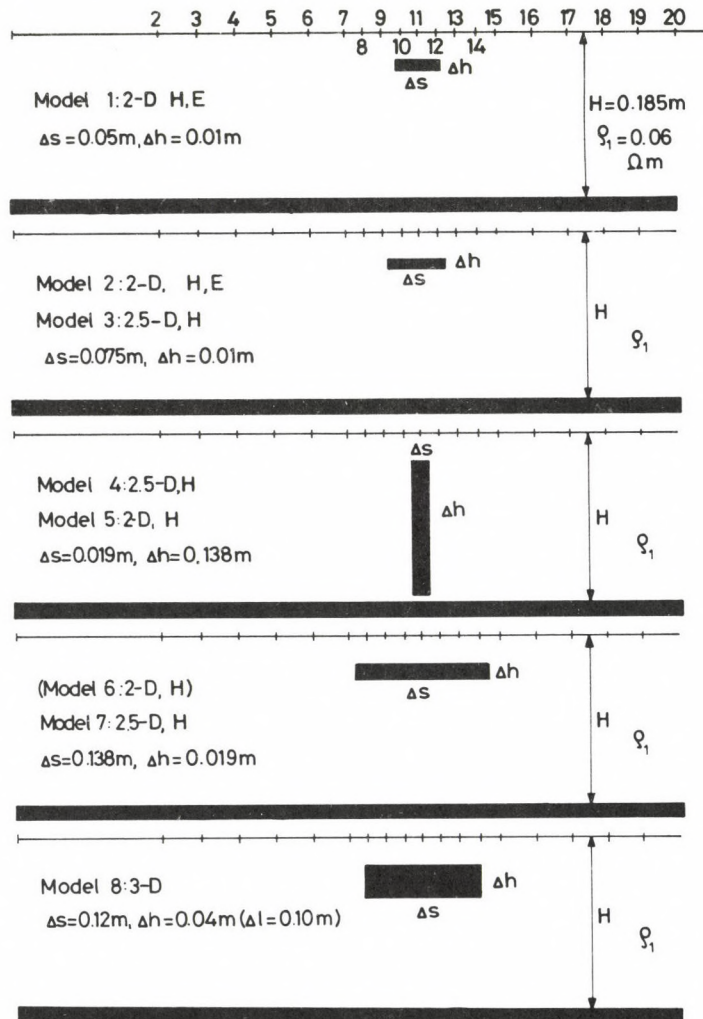


Fig. 5. Dyke structures modeled by horizontal electric dipoles. Numbers 1—20 show the measuring points.

H : polarization H , E : polarization E .

2-D: shown in Fig. 6a. 2.5-D: shown in Fig. 6b

b) In position Q (dipole equatorial configuration) also a vertical magnetic field component exists, on the contrary to magnetotellurics. (In the positions A that is in axial configurations, the situation in this respect is more similar to MT.)

In the position EQ the profiles H_z and H_z/H_y are similar to MT profiles (see Fig. 17a in Ádám et al. 1983), but coming closer to the dyke the difference increases. H_z differs from zero both over the dyke and far from it. In contrast with to the H polarization magnetotellurics, the electric dipole-generated EM field in positions HQ and HA has a vertical magnetic component, too.

2.5-D measuring arrangement

It was aimed with further experiments over models shown in Fig. 5 to overcome the above mentioned difficulties of measurements in polarization H .

In case of an undistorted magnetotelluric H polarization the magnetic field parallel to the strike should be constant

$$\frac{\partial H_y}{\partial x} = 0.$$

A new quasi MT arrangement of less distortion was to be elaborated on the basis of this relation using FRS technique.

If the former 2-D graphite model is limited between the transmitter and the receiver so that the transmitter is outside of the dyke, and the receiver is over it (see Fig. 6) then the variation of H_y along the profile x is much less as shown in Fig. 7.

Thus — on the basis of this relation — this “2.5-D” FRS model is similar to a 2-D magnetotelluric one. According to the measurements, the optimum value of d is approximately $r/3$. In this case the variation of H_y is not more than 3%. (It must be remarked that the name “2.5-D” does not follow the mathematical modeling nomenclature.)

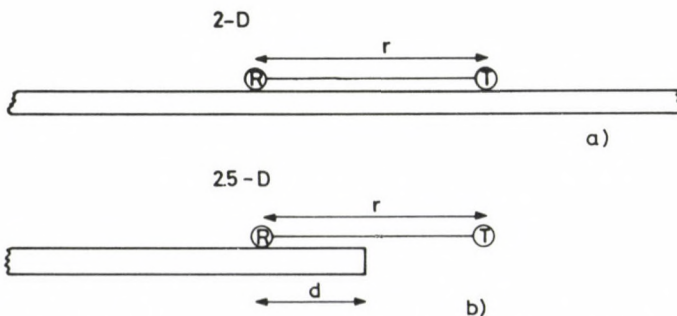


Fig. 6. a) 2-D FRS position which corresponds to a 2-D MT position, distorted by the transmitter effect, b) 2.5-D FRS position which correspond to a 2-D MT position, being less distorted by the transmitter effect

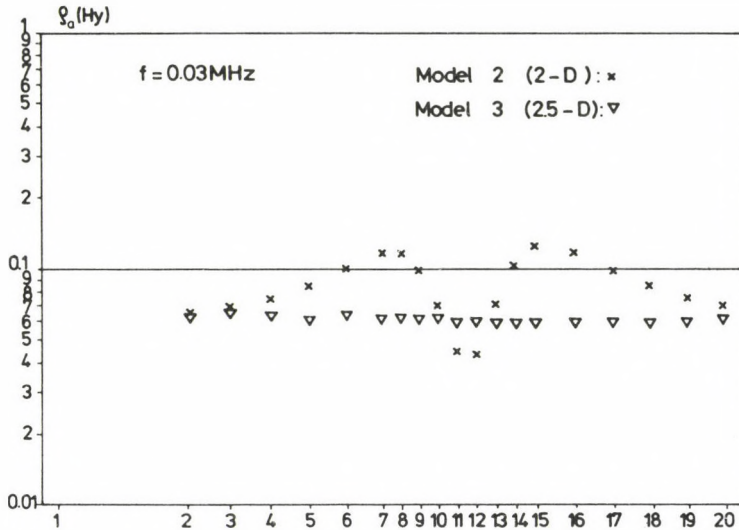


Fig. 7. Profiles H_y measured in dip direction in field of a horizontal electric transmitting dipole
 x: 2-D FRS position, where H_y has significant changes (corresponding to Fig. 6a),
 ∇ : 2.5-D FRS position, where H_y is nearly constant (corresponding to Fig. 6b)

The distortion of electric field was also studied in polarization H over a 2.5-D graphite dyke by a fixed horizontal electric dipole.

Figure 8 shows the horizontal electric field distributions due to electric dipoles placed parallel and perpendicular to the graphite dyke.

Without the graphite dyke in these two cases the electric vectors would be orthogonal. That means that the less the angle is between the vectors, the larger is the distortion. The direction of the electric field around the dyke is perpendicular to the strike. Thus a transmitting electric dipole placed perpendicular to the strike, forms really a quasi H polarization EM field in the vicinity of high conductivity structures.

Taking into account that the transmitting dipole is also moving, the approximation of the MT field is even better than indicated in Fig. 8.

Figure 9 shows profiles over 2-D and 2.5-D models measured by a moving transmitter-receiver arrangement.

Electric field directions are nearer to a position perpendicular to the strike of the graphite model than they were using a fixed transmitting dipole.

The 2.5-D situation is closer to the magnetotelluric H polarization, although some E polarization effects (which are antiparallel on the two sides of the model) also appear.

In magnetotellurics, a component H_z appears only over lateral inhomogeneities in case of polarization E . In an electric dipole-generated field, in case of a dipole-equatorial position, H_z is not zero even over a 1-D layered half space. Additionally, in case of polarization H , H_z values are not constant, as it is shown by a profile H_z/H_y in

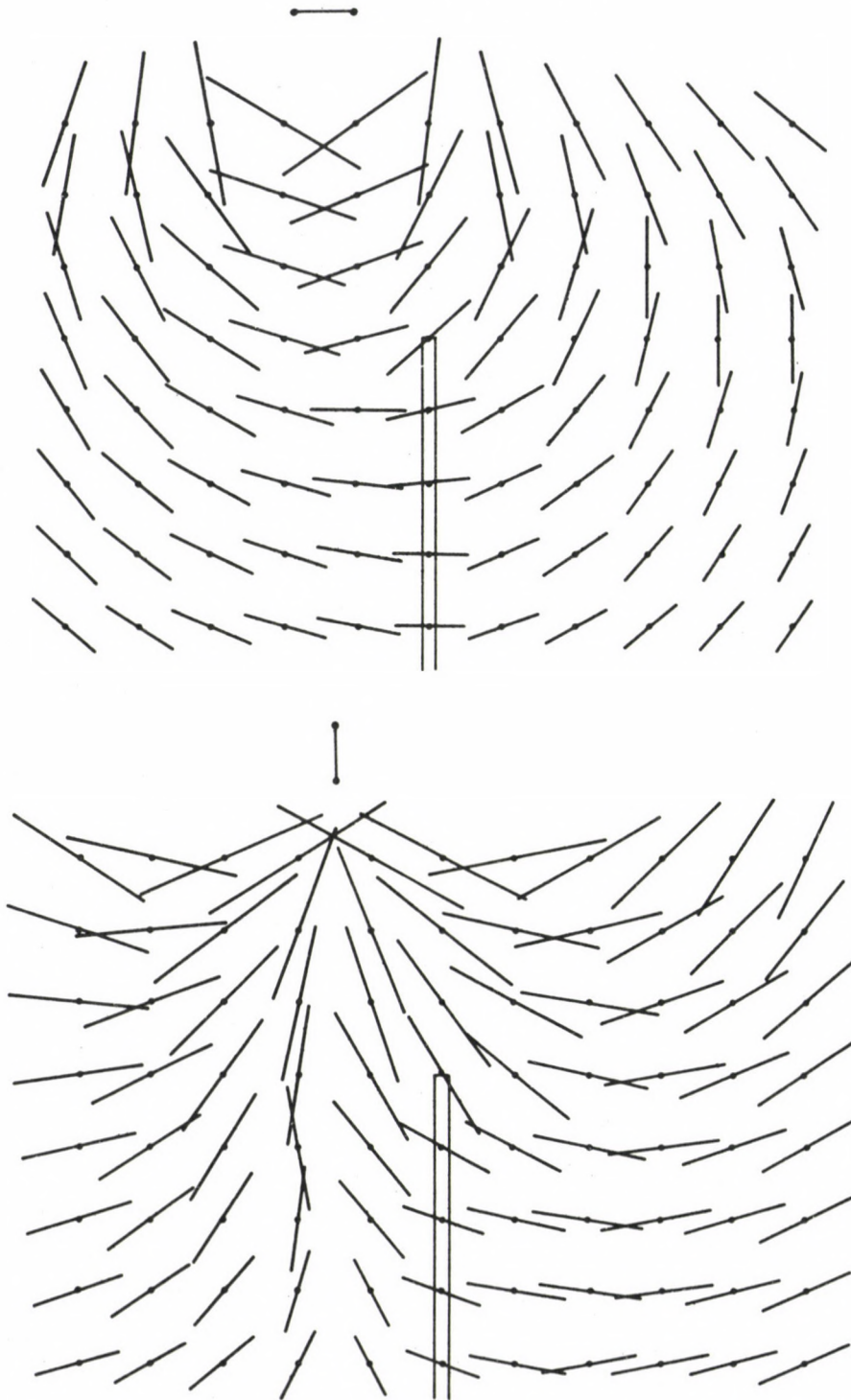


Fig. 8. Distortion of the electric field around a graphite dyke in field of a fixed horizontal electric dipole. The lengths of vectors is proportional to the logarithm of the field

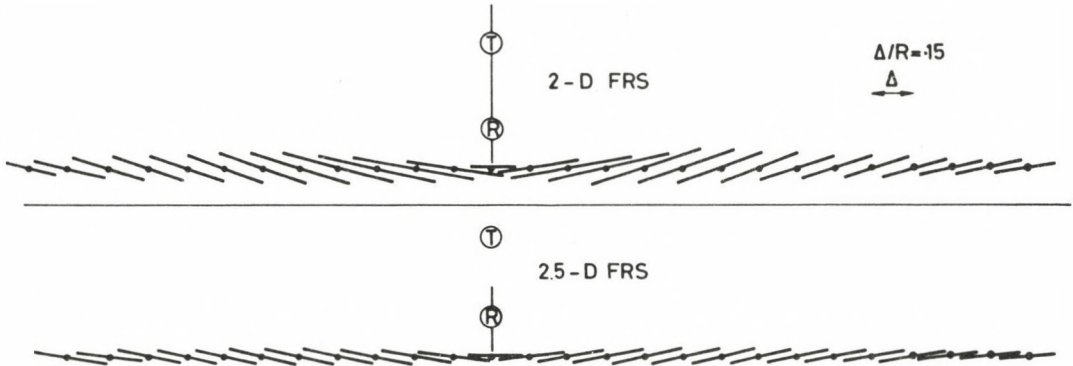


Fig. 9. Electric field vectors measured by a moving transmitter-receiver arrangement in polarization H over 2-D FRS (upper row) and 2.5-D FRS (lower row) profiles. R : distance between the transmitter (T) and receiver (R)

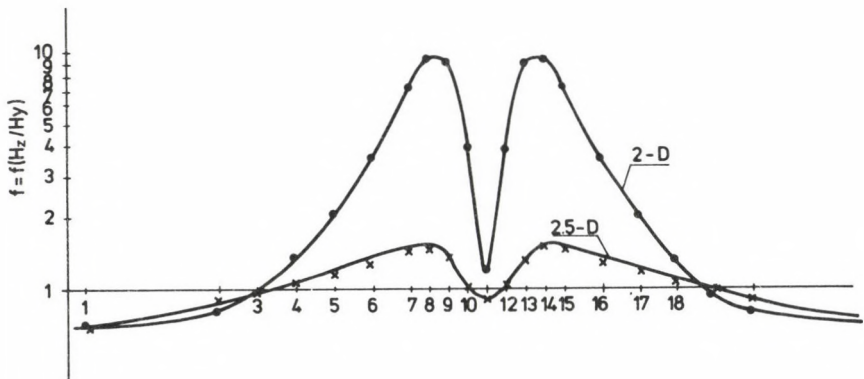


Fig. 10. Profiles H_z/H_y in field of horizontal electric dipole in dip direction.

●: 2-D FRS position,
×: 2.5-D FRS position

Fig. 10 for 2-D and 2.5-D models. A H_z anomaly is due to a small E polarization effect of the position HQ .

Therefore this new 2.5-D FRS modeling does not satisfy the condition of a perfect MT modeling with respect to the H_z component.

Ratios H_z/H_y as geomagnetic induction parameters will not be dealt with in this paper. They will be treated only as a special case of FRS.

4. FRS model measurements over 2-D graphite dykes

Sounding curves over models No. 1 and 2 in polarization E are summarized in Figs 11 and 12. 2-D FRS cases (distorted 2-D MT cases) for polarization H are shown in Figs 13—15.

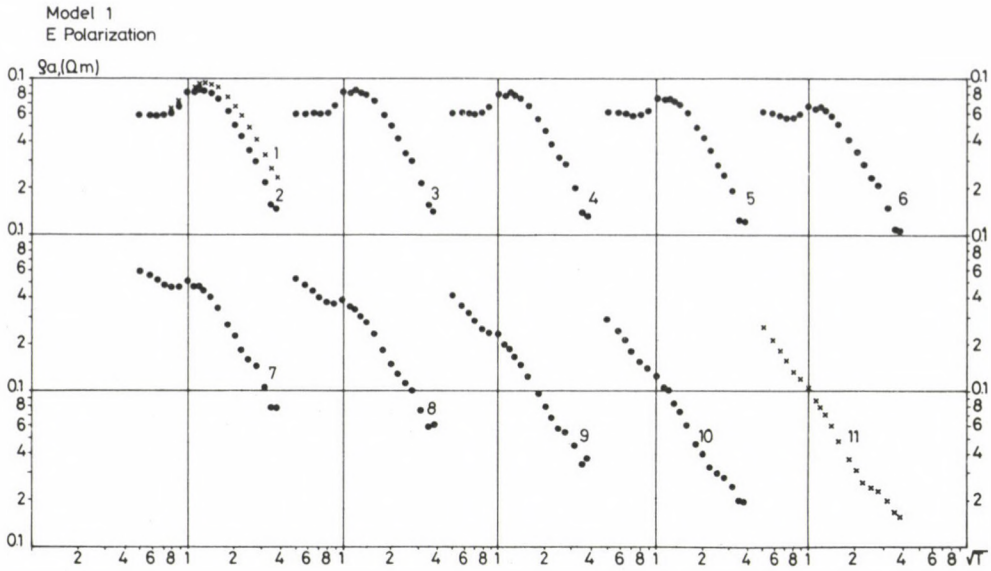


Fig. 11. Sounding curves ρ_{E_x/H_y} over model 1 shown in Fig. 5 at points 1—11. Measuring points are denoted by numbers as shown in Fig. 5. Point 1 is far from the dyke, point 11 is just over the centre of the model structure (E-polarization)

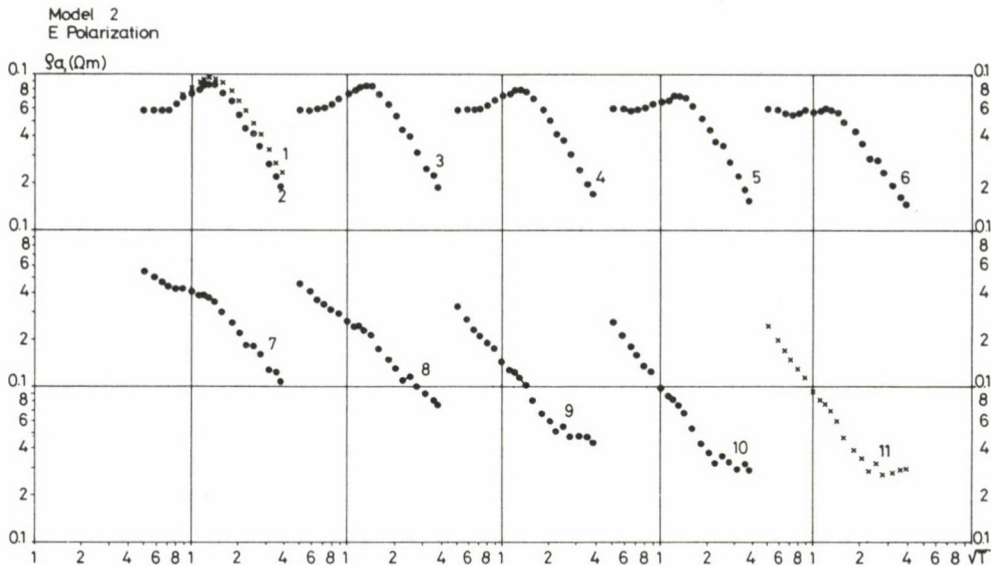


Fig. 12. Sounding curves ρ_{E_x/H_y} over model 2 shown in Fig. 5 at points 1—11. Measuring points are denoted by numbers as shown in Fig. 5. Point 1 is far from the dyke, point 11 is just over the centre of the model structure (E-polarization)

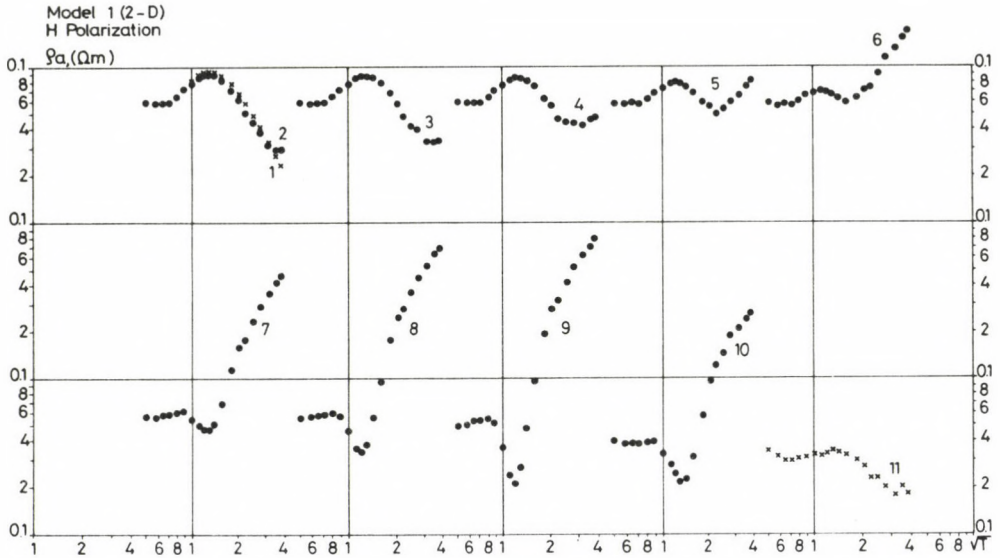


Fig. 13. Sounding curves ρ_{E_x/H_y} over model 1 shown in Fig. 5 at points 1—11. Measuring points are denoted by numbers as shown in Fig. 5. Point 1 is far from the dyke, point 11 is just over the centre of the model structure (*H*-polarization)

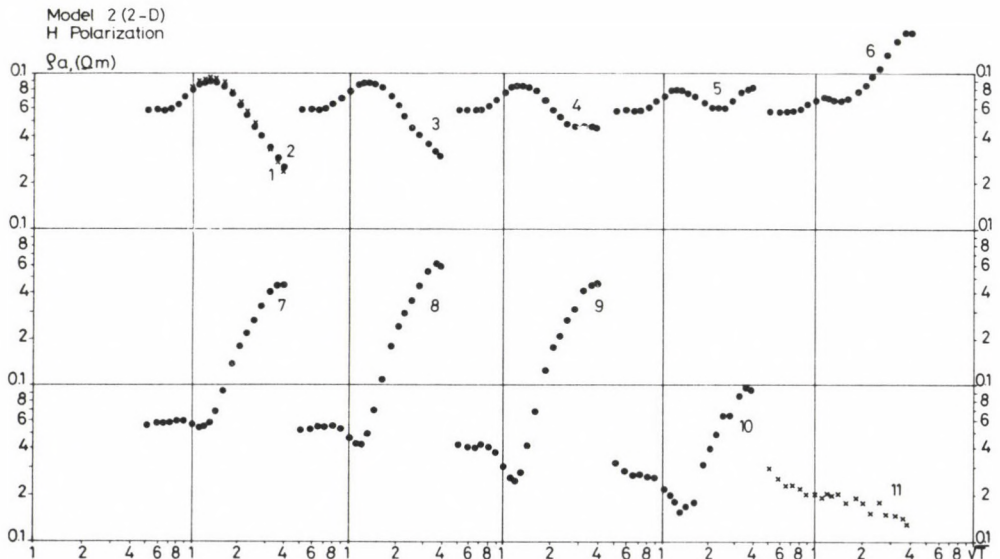


Fig. 14. Sounding curves ρ_{E_x/H_y} over model 2 shown in Fig. 5 at points 1—11. Measuring points are denoted by numbers as shown in Fig. 5. Point 1 is far from the dyke, point 11 is just over the centre of the model structure (*H*-polarization)

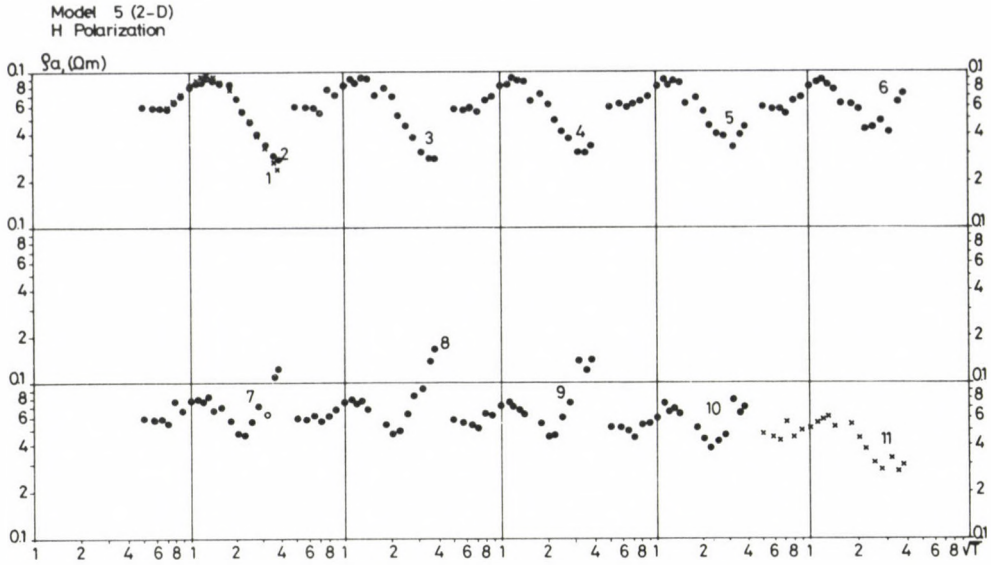


Fig. 15. Sounding curves ρ_{E_x/H_y} over model 5 shown in Fig. 5 at points 1—11. Measuring points are denoted by numbers as shown in Fig. 5. Point 1 is far from the dyke, point 11 is just over the centre of the model structure (H-polarization)

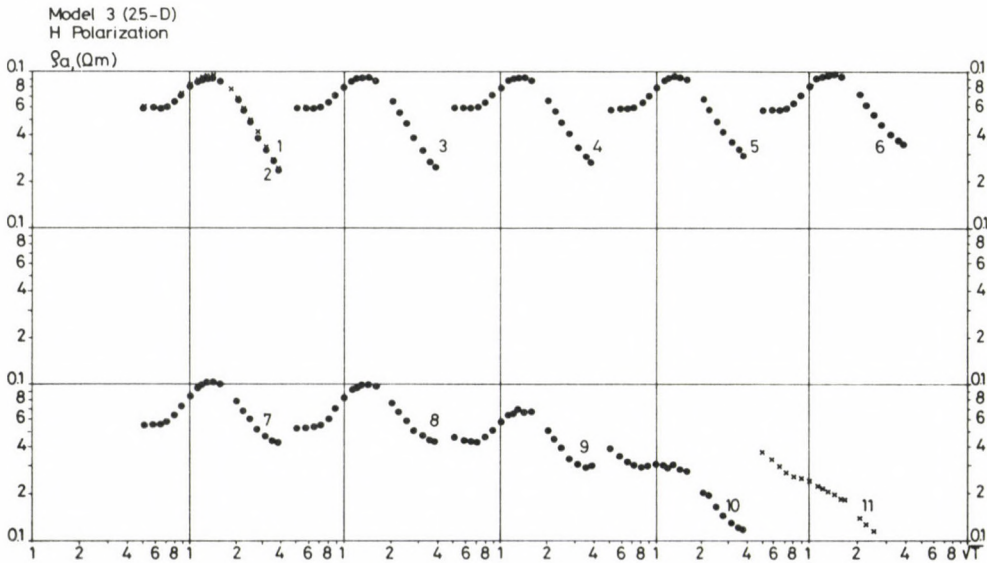


Fig. 16. Sounding curves ρ_{E_x/H_y} over model 3 shown in Fig. 5 at points 1—11. Measuring points are denoted by numbers as shown in Fig. 5. Point 1 is far from the dyke, point 11 is just over the centre of the model structure (H-polarization)

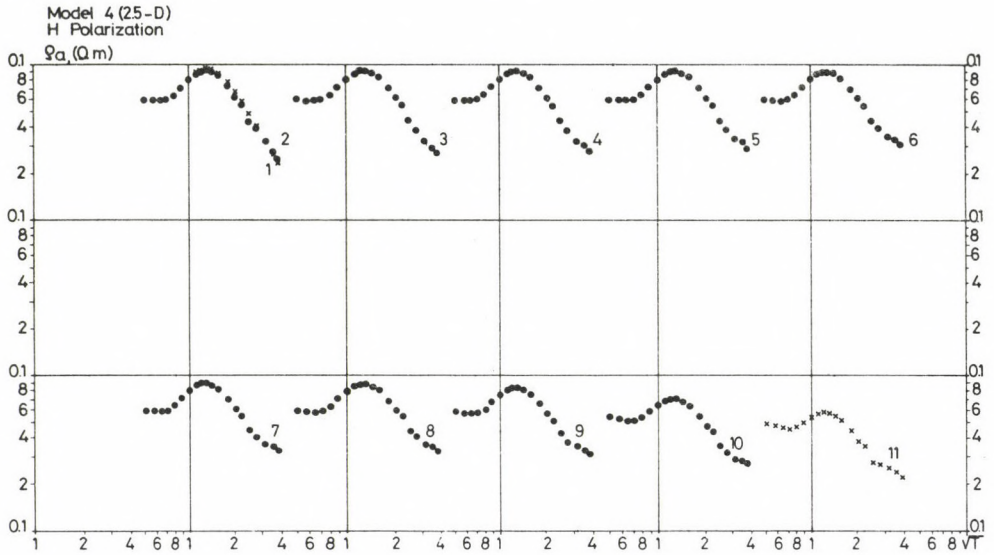


Fig. 17. Sounding curves ρ_{E_x/H_y} over model 4 shown in Fig. 5 at points 1—11. Measuring points are denoted by numbers as shown in Fig. 5. Point 1 is far from the dyke, point 11 is just over the centre of the model structure (H-polarization)

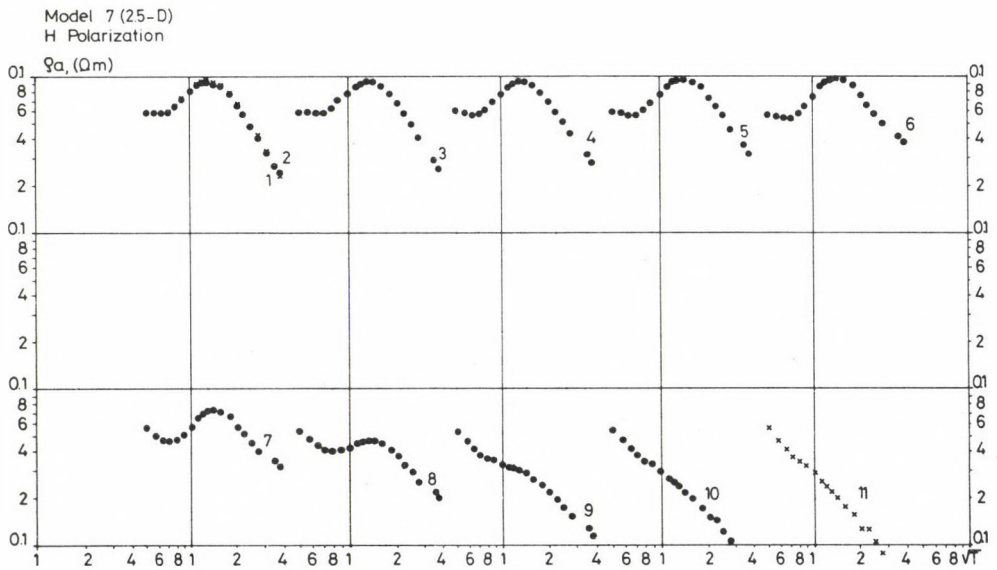


Fig. 18. Sounding curves ρ_{E_x/H_y} over model 7 shown in Fig. 5 at points 1—11. Measuring points are denoted by numbers as shown in Fig. 5. Point 1 is far from the dyke, point 11 is just over the centre of the model structure (H-polarization)

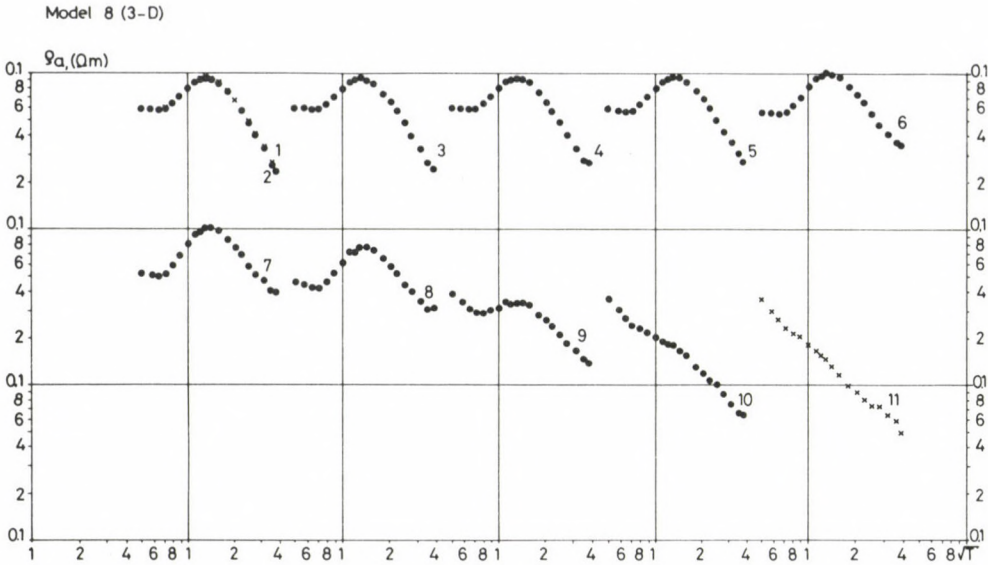


Fig. 19. Sounding curves ρ_{E_x/H_y} over model 8 shown in Fig. 5 at points 1—11. Measuring points are denoted by numbers as shown in Fig. 5. Point 1 is far from the dyke, point 11 is just over the centre of the model structure (H -polarization)

Figures 16—18 show sounding curves for 2.5-D FRS models in polarization H , while a 3-D model is presented in Fig. 19.

A comparison between Figs 13—15 and Figs 16—18 gives a possibility to compare MT anomalies with FRS ones in polarization H . (A comparison of sounding curves in polarization E can be found in the paper by Ádám et al. 1983.)

In polarization H , in case of both measuring arrangements (namely in case of both 2-D and 2.5-D FRS measurements which correspond to FRS and MT) the effect of the resistivity contrast at the lowest frequency can be detected already in point 2. Coming closer to the edge of the dyke, this effect appears also at higher frequencies. Specially in 2-D FRS position (this is the FRS case) a very strong overrise appears beginning with point 7, similarly to the magnetotelluric field measurements in the Alps as shown in Fig. 1.

The 2.5-D FRS position (that is nearer to the realistic MT case) also shows this effect, but its amplitude is much weaker because of the absence of the direct transmitter effect.

This “overrise” effect is the strongest in points 8 and 9 lying just over the edge of the dyke in accordance with the theoretical field distortion due to charges or with the adjustment distance expressing the decline of the effect of the charges, respectively.

5. Comparison of the calculated and modeled adjustment distances

Rangayanaki and Madden (1980) and Dawson et al. (1982) made thin sheet numerical modelings to clear how the anomaly of a lateral inhomogeneity is modified by a lower layer of finite resistivity representing the lower crust.

Rangayanaki and Madden gave an approximating formula, while Dawson et al. calculated an exact, analytical one. The conclusion of their calculations was that the horizontal distance in which the EM field sets its values corresponding to the 1-D structure on both sides of the near-surface inhomogeneity increases due to the resistivity of the lower crust.

Although according to Dawson et al. (1982) this "adjustment distance" is a very complicated function of the conductivities and the resistivity of the lower crust, Rangayanaki and Madden's more simple solution:

$$\delta_a = (S_1 R_2)^{1/2} = (\sigma_1 / \sigma_2)^{1/2} (h_1 h_2)^{1/2}$$

can be also applied as it is confirmed by Jones (1983). In the formula h_1 is the thickness of the upper crust, σ_1 is its average conductivity, h_2 and σ_2 are thickness and conductivity of the lower crust, respectively. $S_1 = \sigma_1 \cdot h_1$, $R_2 = h_2 / \sigma_2$.

Applying this formula to our model structures with the conductivity values

$$\sigma_2 = 17 \text{ S m}^{-1}, \quad \sigma_1 \approx 300 \sigma_2, \quad (\sigma_1 / \sigma_2)^{1/2} = 17.32$$

the results are summarized in Table I.

For models 4 and 5 the thin sheet formula cannot be applied.

From the low frequency profile approximating the 2-D magnetotelluric case (Fig. 20) it can be seen that the adjustment distance is approximately 0.40 m for each model. That means that the thin sheet formula of Rangayanaki and Madden gives quite good results in case of the present models in spite of neglecting the thickness and conductivity of the shallow water layer over the graphite models.

Fig. 20 also shows that the adjustment distance of the deep dipping dyke is much greater than that of the thin sheet-like graphite models. Namely, these models perturbate the EM field deeper, and thus, its effect is detectable farther. The adjustment distance is increased by an increase of the model's cross-section perpendicular to the current flow due to a larger quantity of charges. This enhancement is less than linear as

Table I

Model	h_1	h_2	δ_a
1	0.01 m	0.145 m	0.660 m
2-3	0.01 m	0.145 m	0.660 m
4-5	?	?	?
6-7	0.016 m	0.136 m	0.808 m
8	0.04 m	0.116 m	1.180 m

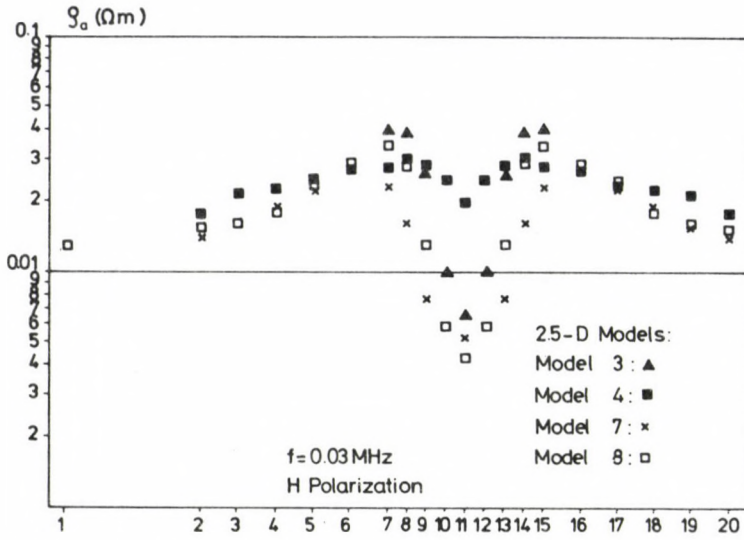


Fig. 20. Profiles ρ_{E_x/H_y} at a frequency $f = 0.03$ MHz to illustrate the adjustment distance of approximately 0.40 m in 2.5-D FRS position

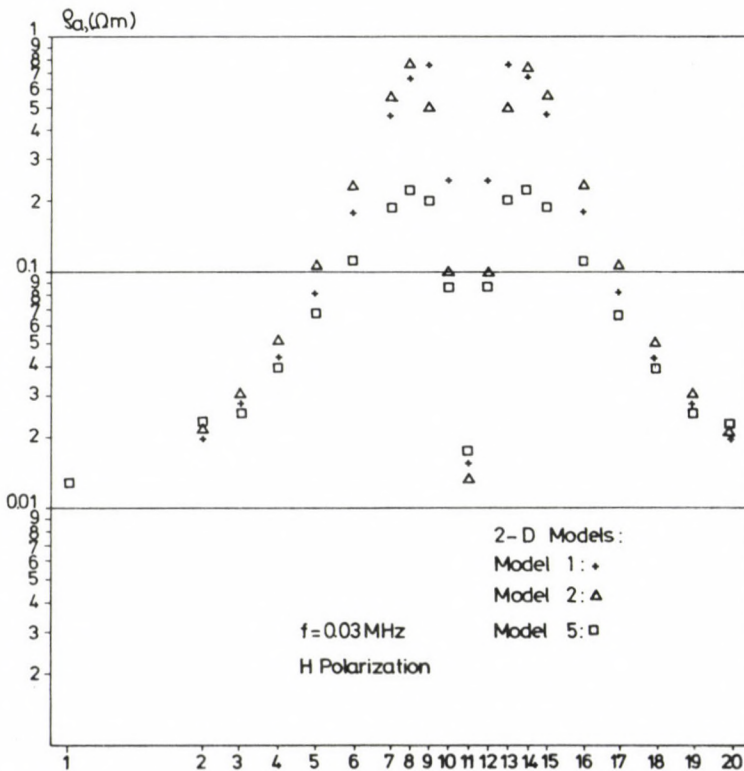


Fig. 21. Profiles ρ_{E_x/H_y} at a frequency $f = 0.03$ MHz in 2-D FRS position

charges in greater depths (h) cause a contribution decreasing as $1/h^2$ to the total electric field. Using the adjustment distance as an interpretation tool, this important effect is to be taken into account.

Similar adjustment distances can be obtained in 2-D FRS positions, too, but the amplitude of the perturbation is much larger than in the MT case (Fig. 21).

6. Interpretation of H_z/H_y FRS anomalies

While the horizontal electric and magnetic field distribution of the 2-D MT case in polarization H can be well approximated by 2.5-D FRS modeling, there remain significant differences in the vertical magnetic fields. This fact is due to a mixture of polarizations H and E in case of horizontal dipole generated EM field. In addition, the E polarization field is antiparallel on the two opposite sides of the dyke causing also significant changes in H_z .

This is why the H_z anomaly of 2.5-D FRS modeling cannot be interpreted as a 2-D MT approximation.

Figures 24 and 25 show sounding curves H_z/H_y for the 2-D model No. 2, and for the 2.5-D model No. 3. The distortion in the 2-D FRS case is much stronger than in the 2.5-D FRS case, showing a significant transmitter effect in H_z/H_y , too. Several low frequency anomaly profiles H_z/H_y over models Nos 2 and 3 are presented in Figs 26 and 27.

7. Transition between DC and AC characteristics of the EM field over conducting dykes

It is important to determine the period range in which MT field over different dyke models can be approximated by a simple DC field distribution.

Figures 22 and 23 show profiles $\rho(E_x/H_y)$ in 2-D FRS and 2.5-D FRS (2-D MT) positions for different periods.

The field distribution can be regarded as a DC one, when the period increases the shape of the anomaly does not change, hence the ρ profiles are only parallelly shifted. In case of our model structures the shape of the anomalies changes both in 2-D and 2.5-D FRS situations depending on frequency.

The periode range of the DC field character begins at much longer periods than the longest period used for analogue modeling. (See Appendix.)

8. Summary

As it has been proved by physical modeling of natural- (MT) and artificial electromagnetic soundings (FRS), in polarization H that the "adjustment distance" is a basic and important parameter in the MT interpretation and in the study of "current channeling".

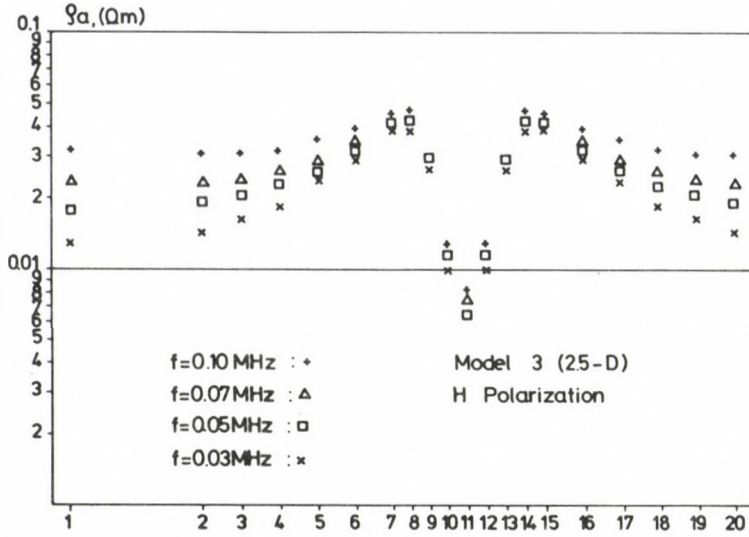


Fig. 22. Effect of frequency decrease over model No. 3 on ρ_{E_x/H_y} in case of large periods (in case of less distorted 2-D MT position)

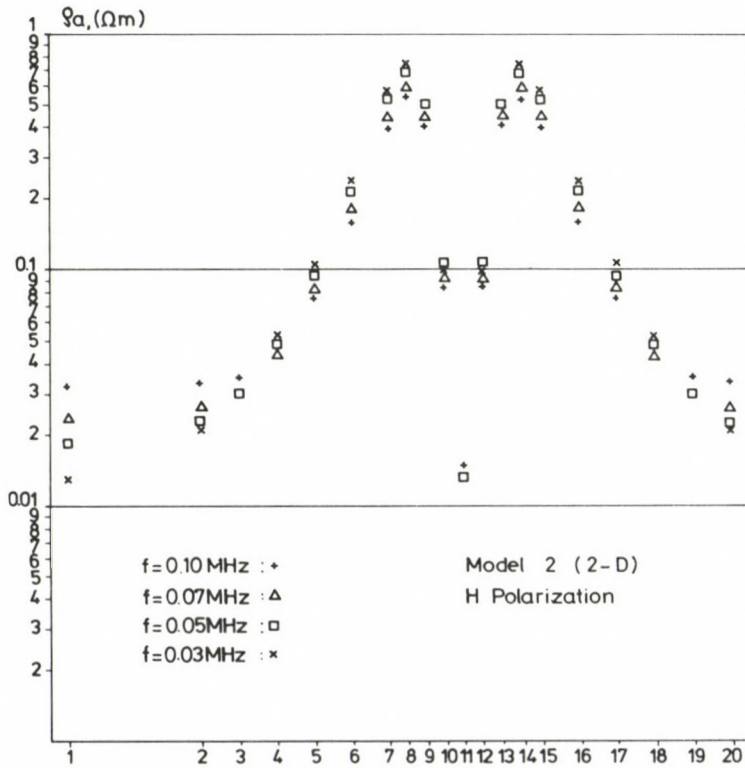


Fig. 23. Effect of the frequency decrease in profiles over model No. 2 on ρ_{E_x/H_y} at large periods (in case of 2-D FRS position)

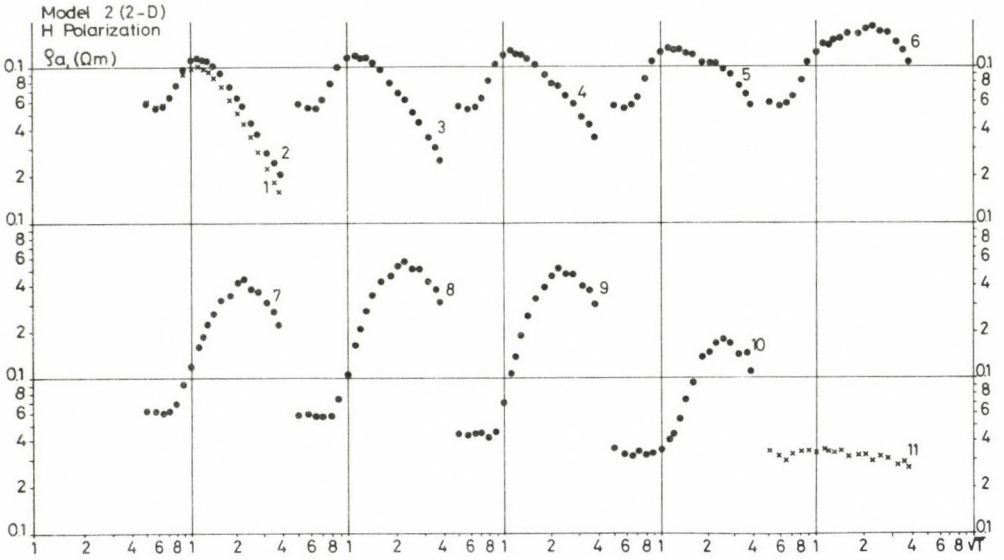


Fig. 24. Sounding curves ρ_{H_z/H_y} over model No. 2 (in case of 2-D FRS position) in points 1—11

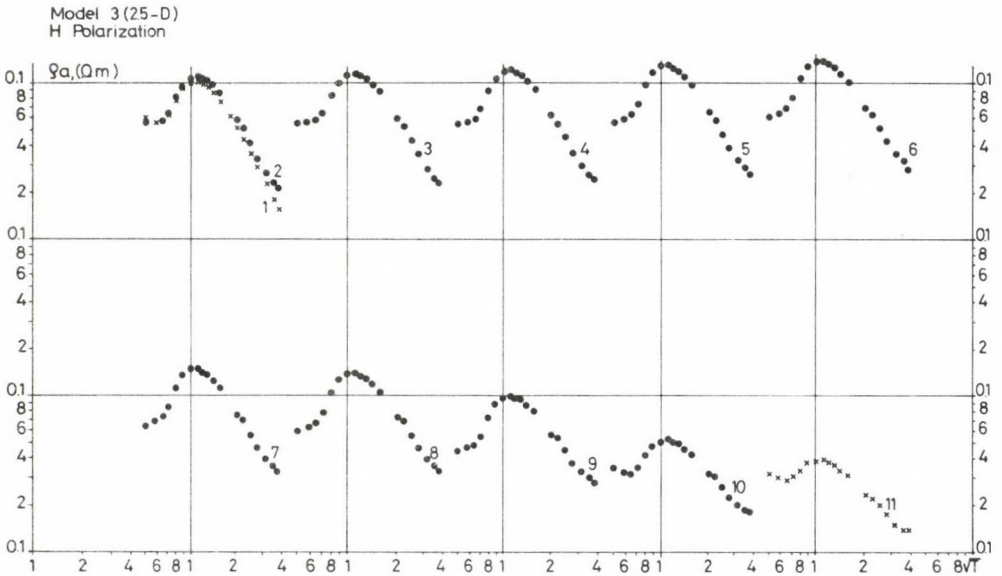


Fig. 25. Sounding curves ρ_{H_z/H_y} over model No. 3 (in case of 2.5-D FRS position) in point 1—11

The adjustment distances have been studied only for one value of σ_2/σ_1 but for several model geometries in the component ratios E_x/H_y and H_z/H_y .

A continuation of the studies for other conductivity contrasts and different structures seems to be necessary.

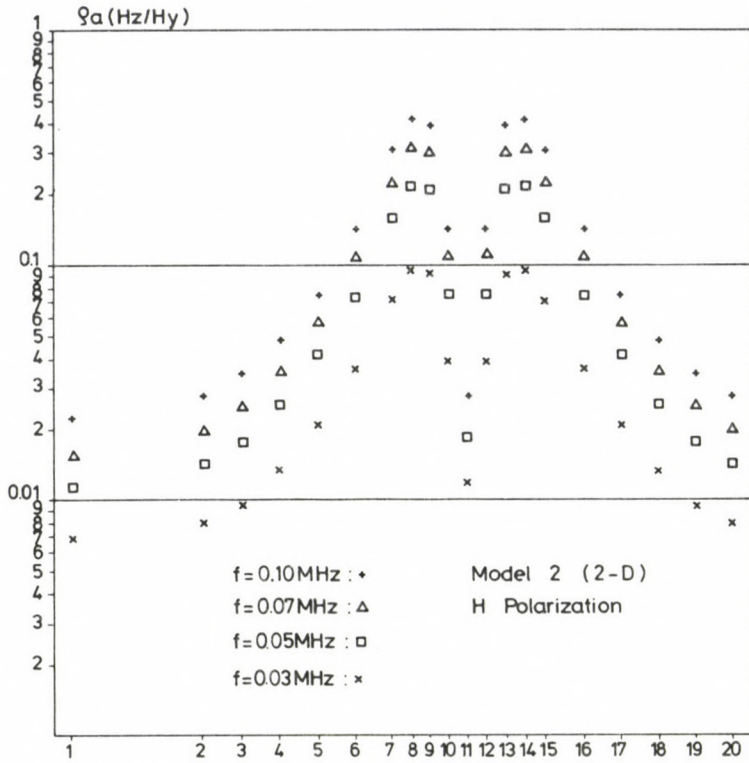


Fig. 26. Low frequency profiles of ρ_{H_z/H_y} in dip direction over model No. 2 (2-D FRS position)

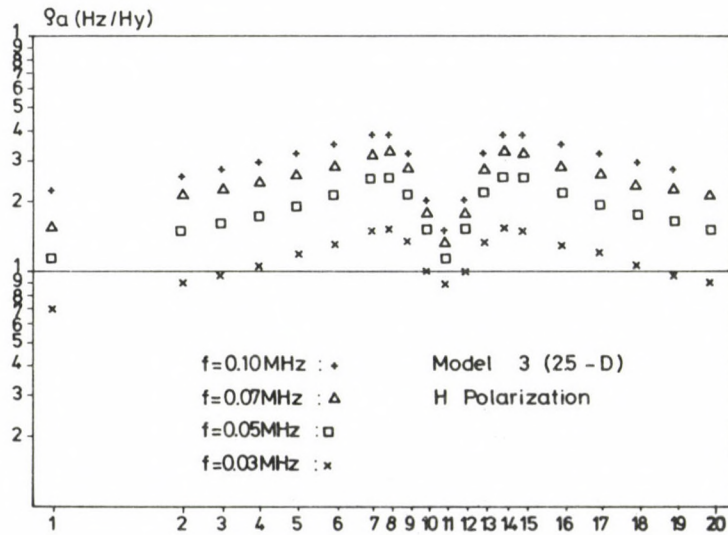


Fig. 27. Low frequency profile of ρ_{H_z/H_y} in dip direction over model No. 3 (2.5-D FRS position)

Appendix

By substituting field values (f) for modeling parameters (m) using the scaling law one gets:

$$\frac{\sigma_m L_m^2}{T_m} = \frac{\sigma_f L_f^2}{T_f}.$$

The period of the DC approximation is

$$T_f > \sigma_f L_f^2 \frac{T_m}{\sigma_m L_m^2}.$$

$$\sigma_m = 1/0.06 \text{ S/m}, \quad L_m = 0.185 \text{ m}, \quad T_m = 1/3 \cdot 10^4 \text{ s}$$

$$T_f > \sigma_f L_f^2 \cdot 5.8 \cdot 10^5.$$

If $\sigma_f = 10^{-2} \text{ S/m}$, $L_f = 10^4 \text{ m}$ (and the conductivity of the dyke is 300 times greater than that of the host rock):

$$T_f > 58 \text{ s.}$$

$$\text{If } \sigma_f = 10^{-2} \text{ S/m}, \quad L_f = 10^5 \text{ m,}$$

$$T_f > 5800 \text{ s.}$$

According to these relations and the modeling results, the electromagnetic field distribution at the calculated periods cannot be regarded as a DC one. Induction effect will disappear only at longer periods.

References

- Ádám A, Pongrácz J, Szarka L, Kardeván P, Szabadváry L, Nagy Z, Zimányi I, Kormos I, Régeni P 1981: Analogue model for studying geoelectric methods in the Geodetic and Geophysical Research Institute of the Hungarian Academy of Sciences. *Acta Geod. Geoph. Mont. Hung.*, 16, 359—380.
- Ádám A, Szarka L, Varga M 1983: Physical and mathematical modeling of crustal conductivity anomalies in the Pannonian basin. *Acta Geod. Geoph. Mont. Hung.*, 18, 467—488.
- Ádám A, Verő J, Wallner Á, Duma G, Gutdeutsch R 1984: Study of the Periadriatic lineament in the Alps by magnetotellurics (in Hungarian). *Magyar Geofizika*, 25, 136—150.
- Dawson T W, Weaver J T, Raval U 1982: B-polarization induction in two generalized thin sheets at the surface of a conducting half space. *Geophys. J. R. astr. Soc.*, 69, 209—234.
- Fischer G 1984: The North Pyrenean magnetic anomaly re-examined. *Annales Geophysicae*, 2, 181—186.
- Flores G, Kurtz R D, DeLaurier J M 1985: Magnetotelluric exploration in the Meager Mountain geothermal area, Canada. *Acta Geod. Geoph. Mont. Hung.*, 20, 165—171.
- Jones A G 1983: The problem of current channelling: A critical review. *Geophysical Survey*, 6, 079—122.
- Le Mouél J L, Menvielle M 1982: Geomagnetic variation anomalies and deflection of telluric currents. *Geophys. J. R. astr. Soc.*, 68, 575—587.
- Márcz Gy, Pongrácz J, Szarka L 1985: Electromagnetic scale modeling instrument for geophysical prospecting (submitted to Scientific Instrumentation).
- McKirdy D McA, Weaver J T 1983: Numerical studies of the channelling of induced currents between two oceans. *J. Geomagn. Geol.*, 35, 623—643.
- Moroz I P 1984: Technical principles of physical modeling in geoelectrics. *Acta Geod. Geoph. Mont. Hung.*, 19, 257—266.
- Moroz I P, Kobzova V M, Timosin B V 1975: Modeling of electromagnetic processes in inhomogeneous media (in Russian). Kiev, Naukova Dumka
- Praus O 1976: Numerical solutions of the MT field in inhomogeneous structures. In: *Geoelectric and Geothermal Studies*. A Ádám ed. Akadémiai Kiadó, Budapest, 231—245.
- Price A T 1973: The theory of geomagnetic induction. *Phys. Earth Planet. Inter.*, 7, 227—233.

- Rangayanaki R P, Madden T R 1980: Generalized thin sheet analysis in magnetotellurics: and extensions of Price's analysis. *Geophys. J. R. astr. Soc.*, 60, 445—457.
- Tátrallyay M 1977: Determination of alternating electromagnetic fields in 2-D structures by finite difference method (in Hungarian). Dissertation, Sopron
- Thera A L, Dupis A 1983: Geomagnetic soundings in Northern Pyrénées: an exploration of the anomalous geomagnetic field by local geology. *J. Geomagn. Geol.*, 35, 643—653.

THREE PHASES OF POST-STORM EVENTS IN IONOSPHERIC ABSORPTION

F MÄRCZ¹

[Manuscript received February 20, 1985]

Intervals with increased ionospheric absorption of radio waves after selected geomagnetic disturbances may be divided into three different consecutive sections, as shown by Lauter et al. (1977) mostly on the basis of case studies. Present investigations using the superposed epoch technique have confirmed the appearance of the three phases at different middle latitudes. For the study of the individual phases, the use of sunset absorption seems to be favourable at higher latitudes, while night absorption may be a more convenient indicator at lower latitudes.

Keywords: geomagnetic disturbances; ionospheric absorption; post-storm event

Introduction

The increased ionospheric absorption of radio waves at mid-latitudes following certain geomagnetic storms is generally called an "after-effect". Lauter et al. (1977) identified the whole period of enhanced absorption as a "post-storm event" (PSE) in the lower ionosphere. Moreover, three consecutive phases of such events have been distinguished, especially on the basis of case studies.

The three phases of PSE are the following as defined by Lauter et al. (1977):

- PSE I: the first phase of enhanced absorption during the main phase of the magnetic storm, the primary effect;
- PSE II: the real after-effect of a magnetic disturbance, well after the maximum of magnetic activity and preferably with larger ionization enhancement than in PSE I;
- PSE III: the very late traces of PSE, small but significant ionization enhancements up to a fortnight after the triggering storm, often reamplified by new magnetic activity.

The main features of the three phases could also be found by means of statistical analyses using the superposed epoch method. Nevertheless, the statistical PSE-trend depended somewhat on the selection of key days. Lauter et al. (1977) have shown that the trend seems to be representative if the occurrence of D_{st} -maximum was used for selecting key days. When accepting the A_p -maximum as key day, the statistical evidence for a separation between PSE I- and PSE II-phases might be rather poor.

¹ Geodetic and Geophysical Research Institute of the Hungarian Academy of Sciences, Sopron, Hungary H-9401, P.O.B. 5

Method of investigation

In the present study, we try to find the three phases of PSE in ionospheric absorption by using two combined criteria for selecting key days, and the selection has been based on daily ΣKp -values. Night and sunset absorption data determined at three l.f. transmission paths are used. Table I contains the description of these paths and the intervals covered by the data applied for investigations.

Table I. Measuring paths for ionospheric absorption

Receiver	Transmitter	Frequency (kHz)	Geogr. latitude of refl. point	Data coverage
Kühlungsborn	Kalundborg	245	54.9° N	1964—74
Průhonice	Československo	272	49.6° N	1965—74
Nagyecenk	Československo	272	48.4° N	1967—73

It is known from earlier studies that the PSE does not appear after each geomagnetic disturbance (Lauter and Knuth 1967, März 1973). Additionally, the absorption enhancement is not always straightforward correlated with the intensity of the geomagnetic disturbance. Nevertheless, the occurrence of PSE can only be expected after an increased level of geomagnetic activity. Because of these somewhat inconsistent experiences, it is highly important what kind of criteria are applied for the selection of key days.

Based on previous results and considerations, a long term average of daily ΣKp has been accepted as the level representing mean geomagnetic activity, and days with ΣKp -values by at least 75 percent above it are chosen as key days for the present analyses. An additional criterion has also been used for the selection, *viz.* it is required that on two out of the three days preceding the key day the daily sum of Kp should not surpass the average value of ΣKp determined for the corresponding year. This additional criterion ensures the elimination of disturbances closely following each other, furthermore the key days are preceded by relatively quiet periods. The two criteria together should result in a selection of well separated disturbances reaching distinct peak values.

Actually, $\Sigma Kp = 17$ was the long term average. It is determined from data of the interval 1964—1974 for which continuous observations of ionospheric absorption (at Kühlungsborn) have been available (cf. Table I). The choice of this interval was reasonable as it covered almost a whole sunspot cycle. According to our first criterion, disturbed days with $\Sigma Kp \geq 30$ were accepted as 0-days for superposed epoch analyses, if the additional criterion was also fulfilled. This occurred in 120 cases for the whole 1964—1974 interval. The absorption data determined at Průhonice and Nagyecenk covered a somewhat shorter period (cf. Table I), thus the number of key days was 111 in

the former and 74 in the latter case. Departures of ionospheric absorption from corresponding monthly medians were determined (and expressed as percentages) for each day of the investigated intervals around the selected key days.

Results

By using the superposed epoch technique, Fig. 1 bottom shows the mean departures of absorption (around geomagnetic storms) derived from both the night (N) and the sunset (SS) data of Kühlungsborn. In Fig. 1 top, the mean variation of ΣKp is indicated. Influenced somewhat by the selection criteria, magnetic activity preceding the key day is rather low, then it rises to a maximum on 0-day. Simultaneously, there is also a maximum in the night and the sunset absorption. Both geomagnetic activity and ionospheric absorption successively decrease following the storm for about three days. After this interval, further enhancements appear in ionospheric absorption while geomagnetic activity remains at a quite stable mean level for about a fortnight.

The sudden increase of ionospheric absorption around the geomagnetic storm can be identified with the first phase of PSE i.e. the primary storm effect. As mentioned

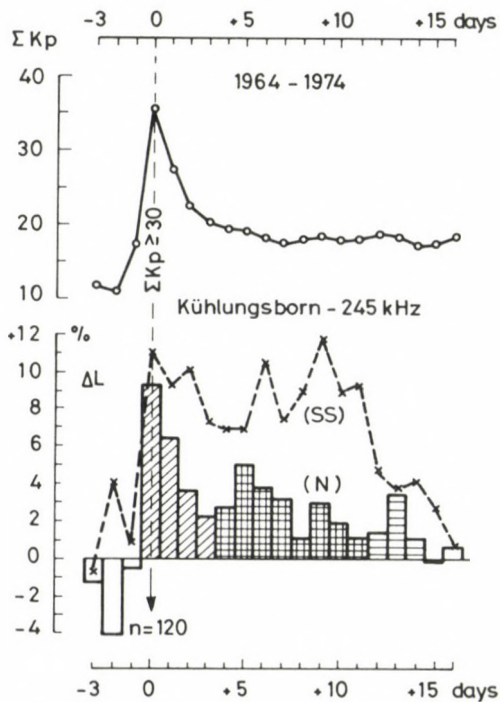


Fig. 1. Top: Mean variation of geomagnetic activity around 120 selected disturbances in 1964–1974. Bottom: Mean departures (ΔL) of ionospheric night absorption (N) from corresponding monthly medians (the three PSE phases are distinguished by different hatchings) and the same for sunset absorption (SS) determined at Kühlungsborn for the same interval as in the top part.

by Lauter et al. (1977), the second phase of PSE appears well after the maximum of the geomagnetic activity. In Fig. 1 bottom, this can be seen in the interval from day +4 to day +11 in both types (N and SS) of absorption. According to Lauter et al. (1977), the enhancement during PSE II should be larger than in case of PSE I. On the basis of Fig. 1 bottom, this is partly true for sunset absorption, while the night absorption has a smaller surplus in PSE II. The third phase of PSE can be traced from day +12 to day +16. Regarding the differences between the mean departures, the PSE III is well separated from PSE II in case of sunset absorption. (The three phases are distinguished by different hatchings in case of night absorption.)

The significance of the results (in Fig. 1 bottom) has been checked by χ^2 -test. Since the statistical treatment was based on departures from monthly medians, a random distribution consisting of equal number of positive and negative departures

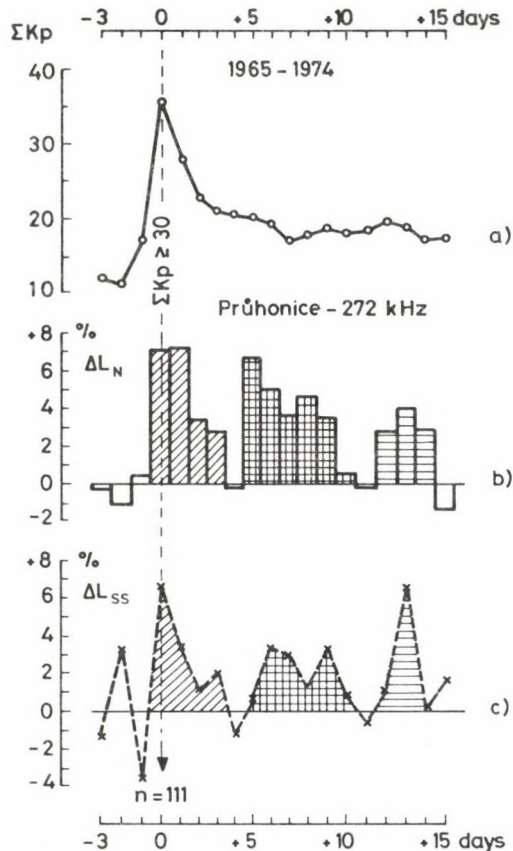


Fig. 2. a) Mean variation of geomagnetic activity around 111 selected disturbances in 1965—1974. b) Mean departures of ionospheric night absorption (ΔL_N) from corresponding monthly medians determined at Průhonice for the interval indicated in a. c) The same as in b, but for sunset absorption (ΔL_{SS}). (The three PSE phases are distinguished by different hatchings.)

has been accepted as null-hypothesis for the χ^2 -test. The real distributions in the individual PSE phases have been compared with this random distribution. Due to a predominance of positive departures in the PSE I-phase (from day 0 to day +3), the χ^2 -test confirmed that the actual distribution differs at a high level of significance from the distribution of the null-hypothesis. (The difference is significant at a 99.9% level in case of night absorption and at a 98% level in case of sunset absorption.) For the PSE II-phase (between day +4 and day +11) a significance at a 95% level was found for both types of absorption (N and SS). According to the χ^2 -test, the PSE III-phase cannot be accepted as significant.

Night and sunset absorption was determined at Průhonice roughly for the same period as at Kühlungsborn. (This material made possible an analysis around 111 key days.) The results presented in Fig. 2 clearly show the three phases of PSE. Moreover, another analysis carried out with the data series of Nagycenk (74 key days) has revealed the occurrence of the three PSE phases at a rather low latitude (Fig. 3).

The significances of these results (in Figs 2 and 3) have also been checked by χ^2 -tests. The detailed confidence values together with the main characteristics of the individual PSE phases (start, end, duration and average amplitude determined as the average of mean departures during the corresponding phase) are presented in Table II

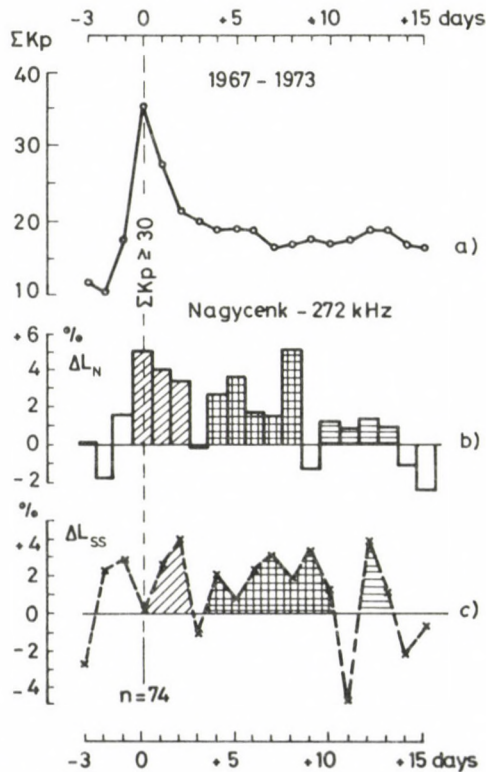


Fig. 3. The same as in Fig. 2, but for Nagycenk and around 74 selected disturbances in 1967—1973.

Table II. PSE parameters for night absorption

Receiver Transmitter	PSE I			PSE II			PSE III		
	Start/End Duration	Av. ampl. (percent)	Signi- ficance	Start/End Duration	Av. ampl. (percent)	Signi- ficance	Start/End Duration	Av. ampl. (percent)	Signi- ficance
Kühlungsborn Kalundborg	0/+3 4 days	+5.4	99.9%	+4/+11 8 days	+2.7	95.0%	+12/+14 3 days	+2.0	no
Průhonice Československo	0/+3 4 days	+5.1	90.0%	+5/+10 6 days	+3.9	80.0%	+12/+14 3 days	+3.1	no
Nagyecnk Československo	0/+2 3 days	+4.2	99.0%	+4/+8 5 days	+2.9	98.0%	+10/+13 4 days	+1.1	no

Table III. PSE parameters for sunset absorption

Receiver Transmitter	PSE I			PSE II			PSE III		
	Start/End Duration	Av. ampl. (percent)	Signi- ficance	Start/End Duration	Av. ampl. (percent)	Signi- ficance	Start/End Duration	Av. ampl. (percent)	Signi- ficance
Kühlungsborn Kalundborg	0/+3 4 days	+9.4	98.0%	+4/+11 8 days	+8.9	95.0%	+12/+16 5 days	+3.2	no
Průhonice Československo	0/+3 4 days	+3.2	95.0%	+5/+10 6 days	+2.0	no	+12/+15 4 days	+2.6	90.0%
Nagyecnk Československo	+1/+2 2 days	+3.3	no	+4/+10 7 days	+2.2	no	+12/+13 2 days	+2.6	no

for night and in Table III for sunset absorption, in case of all the three transmission paths. (A significance below the 80 percent level was not accepted, it is indicated by "no" in the Tables II and III.)

Discussion

A comparison of the appropriate night-time results (Table II) shows that duration and average amplitude of certain PSE phases depend on the latitude of the reflection point. The durations of PSE I-phase and especially those of PSE II-phase become shorter with decreasing latitude, however, for the PSE III durations no characteristic change is evident. The average amplitudes determined for PSE I-phase also decrease towards the lower latitudes, but the picture is rather mixed in case of PSE II and PSE III.

The enhancements of night absorption during PSE I- and PSE II-phases are clearly significant at the Kühlungsborn and the Nagycenk transmission paths, and their confidence is acceptable in case of Průhonice. The average amplitudes in the PSE III-phase are also positive, however, their significances remain below the 80% confidence level.

Table III containing the parameters for sunset absorption shows absorption enhancements significant both in PSE I- and PSE II-phases for the Kühlungsborn-Kalundborg transmission path. These absorption enhancements are quite similar to each other and they are well above those of corresponding phases given for night absorption in Table II. The sunset absorption enhancements (in Table III) are rather small in each phase of PSE at the remaining two transmission paths situated at lower latitudes. These enhancements generally remain even below the corresponding values shown for night absorption in Table II, and their confidence is also poor.

Actually, the present results confirm that the three phases of PSE appear at each of the investigated middle latitudes. Nevertheless, the PSE phases at the highest latitude are more clearly expressed in case of sunset absorption. On the other hand, night absorption can be more convenient for monitoring the occurrence of PSE phases at lower latitudes.

References

- Lauter E A, Knuth R 1967: Precipitation of high energy particles into the upper atmosphere at medium latitudes after magnetic storms. *J. Atmos. Terr. Phys.*, 29, 411—417.
- Lauter E A, Bremer J, Grafe A, Deters I, Evers K 1977: The post-storm ionisation enhancements in the mid-latitude D-region and related electron precipitation from the magnetosphere. *HHI—STP—Report*, No 9, 1—86.
- März F 1973: Further studies on ionospheric absorption and geomagnetic activity. *Acta Geod. Geoph. Mont. Hung.*, 8, 297—311.

SEISMIC ACTIVITY IN HUNGARY

T ZSIROS¹ and P MÓNUS¹

[Manuscript received March 3, 1985]

The present study deals with statistical investigations of Hungarian earthquakes. A seismic activity map is also compiled.

Keywords: earthquake intensity; historical earthquakes; Hungary; seismicity

Introduction

In this paper only the earthquakes originated from the present territory of Hungary which are not regarded as fore- or aftershocks are discussed. For the estimation of the annual frequency of intensities and for the compilation of a seismic activity map we relied on the earthquakes with epicentral intensities $I_0 \geq 4^\circ$ (MSK) occurring between 1859 and 1984, while every events ($I_0 \geq 2^\circ$) were used to construct the distribution of the cumulative numbers covering the period of 1500 to 1984. During the demonstration of the number of the earthquakes in terms of 10 years from 1859 to 1984 different intensity intervals were used.

Data for the statistical investigations have been taken from the work of Zsiros and Tóth (1984) for the period of 1859 to 1984 and from that of Réthly (1952) for the period preceding 1859.

The latest statistical analyses of Hungarian earthquakes were prepared by Csomor and Kiss (1958), Csomor (1972), Bisztricsány (1974, 1977), and Zsiros (1983). These papers mainly dealt with the frequency of the earthquakes but in the studies of Csomor (1972) and Bisztricsány (1977) the question of the periodicity of the seismic activity of Hungary was also discussed.

Broucek et al. (1977) have compiled a version of the distribution of seismic activity for the territory of Austria, Czechoslovakia and Hungary.

Frequency of the earthquakes

The cumulative number of the earthquakes occurred in the present territory of Hungary is represented in Fig. 1 for the period from 1500 to 1983. This distribution shows two remarkable points:

— The “seismic activity” (the growth rate of the cumulative number of the events) can be regarded as stationary from the fifties of the last century to the late 1960s.

¹ Geodetic and Geophysical Research Institute of the Hungarian Academy of Sciences, Seismological Observatory, Budapest, Mérédek u. 18.

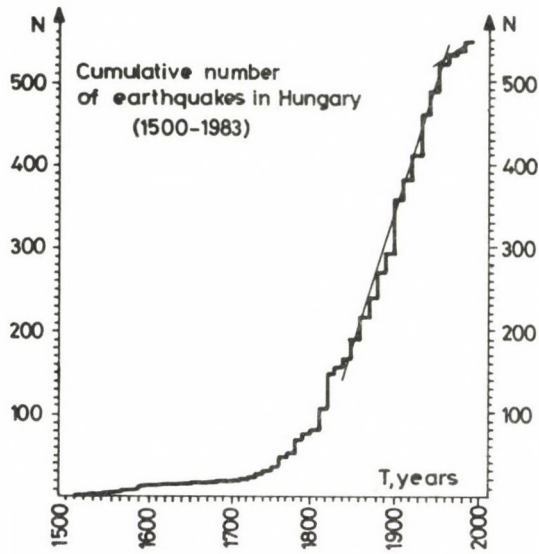


Fig. 1

This feature is unlikely to be due to a radical change in the seismic activity in the middle of the last century, rather to nearly complete observations and even more to recordings of the earthquakes from that time.

— In the last two and a half decades the annual number of earthquakes dropped significantly.

The average annual number of events was 3.2 from 1850 to 1960 while it dropped to 1.1 from 1960 to 1984. In Fig. 2 the number of earthquakes are presented in terms of 10 years for the time period from 1859 to 1984. The lack of events is striking during the last two and a half decades and the first decade of this century is dominant nearly at every intensity level. Concerning the energy release of earthquakes the activity is significantly low between 1959 and 1968 (Zsiros and Tóth 1984).

Because of the incomplete observations of smaller events only earthquakes with epicentral intensities $I_0 \geq 4^\circ$ (MSK) were used for the estimation of the frequency of earthquake intensities for the time period of 1859—1984 (Fig. 3). According to the observations the logarithmic numbers (N) of the events show a linear relation to their sizes, represented here by the epicentral intensities (I_0). Using the conventional least-squares fit the annual frequency relationship is

$$\log N = 1.73 - 0.42 I_0 \quad (1)$$

and the cumulative one is

$$\log N^c = 2.25 - 0.48 I_0. \quad (2)$$

The reciprocal values of N and N^c gave the mean return periods (R and R^c) of the intensities (Table I).

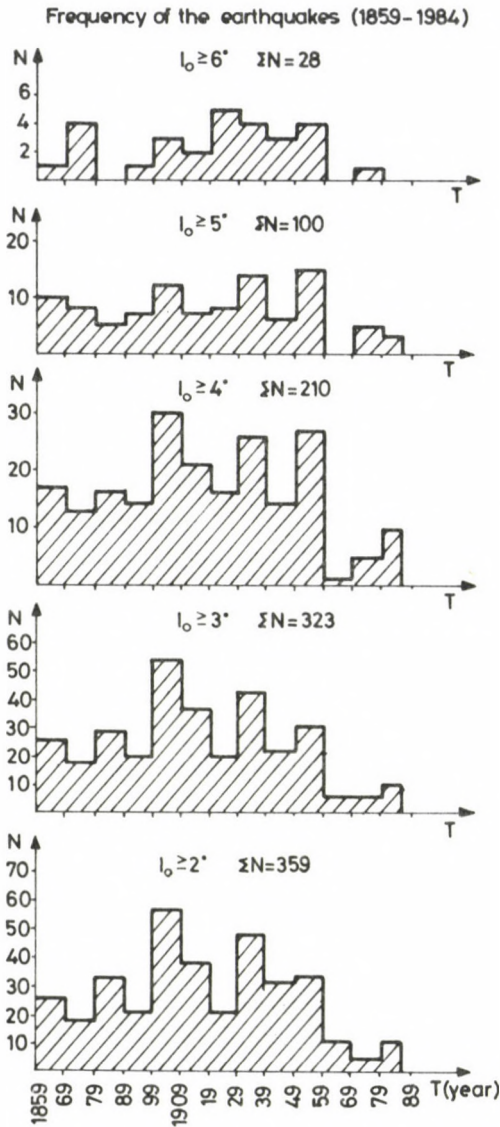


Fig. 2

Assuming that the occurrences of the earthquakes follow a Poisson process and using the relationship

$$\ln \left(1 - P_t(I) \right) = - \frac{t}{R^c(I)} \quad (3)$$

(Lomnitz 1974) the P probability of the occurrence of the earthquakes can be estimated with different epicentral intensities for a given t time interval. The results are summarized in Table II.

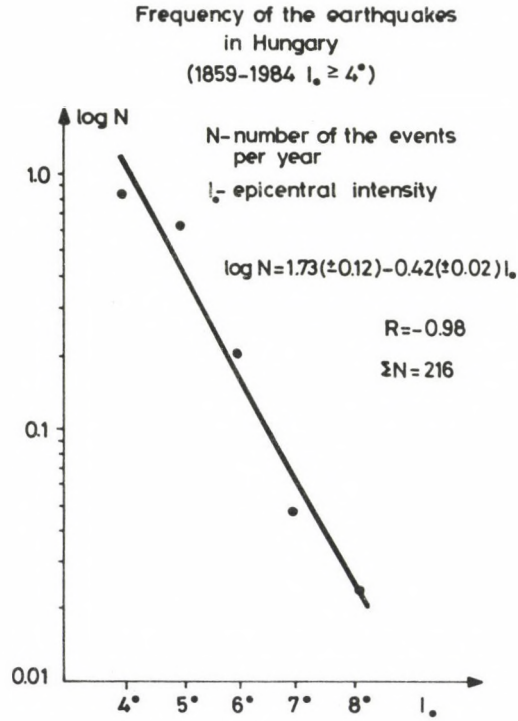


Table I

I_0	R (year)	R^c (year)
4°	0.9	0.5
5°	2.3	1.4
6°	6.2	4.3
7°	16.2	12.9
8°	42.7	38.9

Table II

t (year) \ I_0	5°	6°	7°	8°
1	0.99	0.41	0.16	0.05
5	1.	0.93	0.59	0.25
10	1.	0.99	0.83	0.44
20	1.	1.	0.97	0.69
50	1.	1.	1.	0.95

Activity map

The seismic activity map is intended to characterize the territorial distribution of the seismicity by quantitative values. It has to be based on the distribution of the epicentres and the earthquake frequency relationship. The seismic activity map of Hungary was constructed for the period from 1859 to 1984 using the relation

$$A_{K_0} = \frac{N(1 - 10^{-\alpha})T_N S_N}{10^{-\alpha(K_{\min} - K_0)}T_0 S_0} \quad (4)$$

recommended by Ananiin et al. (1969), where

- A_{K_0} — seismic activity value for K_0 ,
- K_0 — a selected value to which the seismic activity (A) has relation. $K_0 = 10$ (in log joule) is usually chosen for the sake of numerical comparison of different activity maps,
- N — total number of the earthquakes with $K \geq K_{\min}$ in a given area (S_0)
- K_{\min} — minimum energy level above which the earthquakes were taken into account ($K_{\min} = 9.76 \log \text{erg}$).

This estimation is based on the followings:

Using $h = 10$ km average focal depth in the Gutenberg and Richter (1942) relationship, the magnitude, M , is expressed by the epicentral intensity, I_0

$$M = 0.6 I_0 + 0.8. \quad (5)$$

The logarithmic energy, K , of an earthquake with magnitude M is given in joule by the equation

$$K = 4 + 1.8M. \quad (6)$$

From (5) and (6) we obtain

$$K = 5.44 + 1.08 I_0. \quad (7)$$

In our case $I_{\min} = 4^\circ$ therefore K_{\min} is 9.76

α — activity parameter ($\log N(k) = \text{const.} - \alpha K$) ($\alpha = 0.39$).

Using the annual frequency relationship (1) for earthquakes $I_0 \geq 4^\circ$ in equation (7), the result is

$$\log N = 5.92 - 0.39K, \quad (K \geq 9.76). \quad (8)$$

Thus, the activity parameter α is equal to 0.39.

- T_N — time interval for normalization ($T_N = 1$ year)
- S_N — area for normalization ($S_N = 10\,000 \text{ km}^2$)
- T_0 — observational time interval ($T_0 = 126$ years)
- S_0 — observational area ($S_0 = 500 \text{ km}^2$).

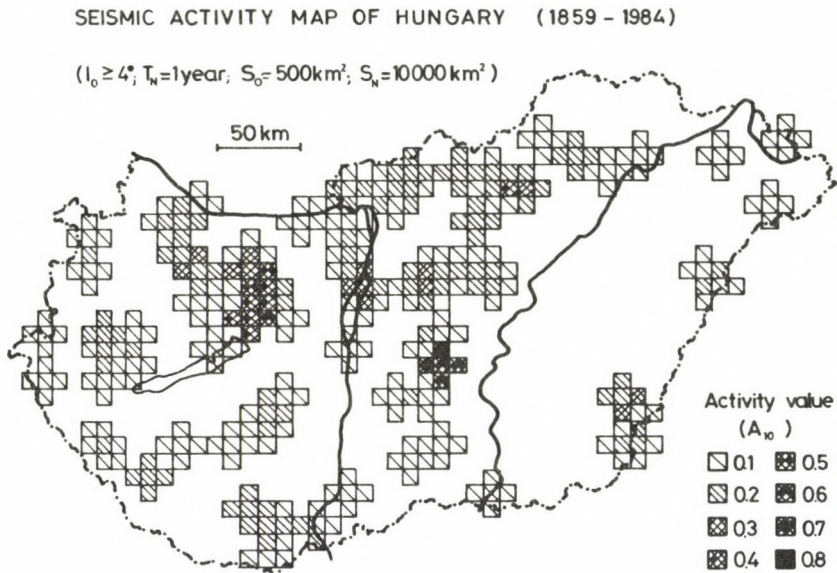


Fig. 4

With these parameters the seismic activity values were calculated in $10 \text{ km} \times 10 \text{ km}$ grids and the result is presented in Fig. 4. This map reflects to the density of earthquake epicentres above the K_0 selected energetic level.

References

- Ananiin I V, Bune V I, Vvedenskaia N A, Kirillova I V, Reisner G I, Sholpov V N 1969: Methods of compiling a map of seismic regionalization on the example of the Caucasus. *VINITI*, Moscow, 57—126.
- Bisztricsány E 1974: Earthquake engineering (in Hungarian). Akadémiai Kiadó, Budapest
- Bisztricsány E 1977: Problems of seismic regionalization for Hungary. In: *Proceeding of the Symposium on the Analysis of Seismicity and on Seismic Risk, Liblice*, 443—450.
- Broucek I, Csomor D, Prochazkova D 1977: First version of the seismic activity map of Czechoslovakia, Hungary and Austria (in Russian). *Acta Geol. Acad. Sci. Hung.*, 21, 297—300.
- Csomor D 1972: Earthquake conditions of Hungary (in Hungarian). Candidate dissertation
- Csomor D, Kiss Z 1958: The seismicity of Hungary (in Hungarian). *Geofizikai Közlemények*, 7, 169—180.
- Gutenberg B, Richter C F 1942: Earthquake magnitude, intensity, energy and acceleration. *Bull. Seism. Soc. Am.*, 32, 163—191.
- Lomnitz C 1974: Global tectonics and earthquake risk. Elsevier
- Réthly A 1952: The earthquakes of the Carpathian Basins (455—1918) (in Hungarian). Akadémiai Kiadó, Budapest
- Zsiros T 1983: Faults and earthquakes in Hungarian territory east of the river Tisza. *Acta Geod., Geoph. Mont. Hung.*, 18, 119—128.
- Zsiros T, Tóth L 1984: Energy release curve and map of Hungary. *Acta Geod., Geoph. Mont. Hung.*, 19, 367—381.

PERSPECTIVES ON ELECTROMAGNETIC DEEP SOUNDING IN ORE PROGNOSTICATION

ÁDÁM A¹, PAARMA H², POSPÍŠIL L³

[Manuscript received May 29, 1985]

The paper is an attempt to relate tectonic data on certain known deep electric conducting zones to aspects of metallogenesis in conformity with the views of V A Bush on Eurasian "transcontinental lineaments".

Keywords: deep fractures; electric conductivity anomaly; metallogenesis; Odra-line; ore prospecting; transcontinental lineament

1. Introduction

Many difficulties lie in the path of ore prospecting in the industrialized countries today. The market prices of many minerals have been falling in recent years, and there are fewer outcrops or other easily identifiable deposits available than there used to be. Thus it has become necessary to develop new prospecting methods, especially with regard to deep-seated ores, and general theories of metallogenesis.

Prognostication of ore deposits (Rundkvist 1978) and the associated classification of ore formations form a new method which has gained currency and which makes use of all the relevant geoscientific data. Both prognostication in general and in particular its application to deep-seated ores involve the need for obtaining information on deep-lying structures. Thus rapid strides are being made in the development of magnetotelluric and magnetovariation investigations (Ádám 1976, Rokityansky 1982, Paarma and Kuosmanen 1982). The suitability of these methods for first-degree prognostication of deep-seated ores (scale 1 : 1 mill.) has nevertheless been discussed relatively little in the literature to date.

2. Aspects of the tectonic setting of ore deposits and zones

In his book "Fundamentals of Metallogenic Analysis", A D Shcheglov (1979) emphasizes the need for *broad-based metallogenic maps* for locating ore-critical zones and draws particular attention to the fact that little mention has been made in the literature of metallogenic theories of autonomic activation, independent of the

¹ Geodetic and Geophysical Research Institute of the Hungarian Academy of Sciences, H-9401 Sopron, POB 5, Hungary

² Jaakonkuja 1F6 90230 Oulu 23, Finland

³ Jos. Fajmanová 16, 62800 Brno, Czechoslovakia

geosynclinal tectonics. The mantle alkaline magmatism in the Baltic Shield, for instance, may be regarded as the product of palaeozoic activation (Vartiainen and Paarma 1979). As it becomes evident that the genesis of many other magmatic intrusions is bound to mantle tectonics, the notion of *automatic magmatic activation* would appear to be gaining strength within metallogenic theory. Deep fracture zones (Bush 1983, von Bauman et al. 1984) are in turn essential for the passage of magmatic and volcanic material into the upper parts of the earth's crust. The most extensive deep fractures, the transcontinental fractures (the 'first-order lineaments' of Bush), constitute approach channels which extend through the lithosphere, and are therefore of considerable significance for mantle magmatism. This helps to explain why it is that many ore-critical regions are linear in their general structure. On the other hand, linear macro-structures of this kind can incorporate a variety of mineral deposits and host rocks differing in type and age (see Khain 1973). Many investigators emphasize that the most ore-critical areas of all are the intersections between deep fracture zones (Kashkai and Tamrazjan 1967, Mayo 1958).

Satellite imagery can provide new, more illustrative information on ore belts of different scales. The tin mineralizations of the palaeozoic and mesozoic ring complexes in the Niger region and Nigeria are a good example of a linear zone some 1000 km in length (Turner and Webb 1974), a zone which stands out clearly on Landsat images and contains tin-bearing granites of two principal ages. Another well-known example is the Great Dyke in Zimbabwe, a Precambrian rift zone possessing numerous mineralizations of various kinds, largely asbestos, copper, nickel, gold and platinum. But this is only part of a larger submeridional structure.

It would thus seem that in Europe, too, we are reaching the stage in metallogenic research at which it would be reasonable to examine both platform areas and old or new geosynclinal areas, or the infra-mantle fracture zones crossing all of these, from the point of view of their metallogeny and activation. The following is an attempt to relate tectonic data on certain known deep electric conducting zones to aspects of metallogenesis in conformity with the views of V A Bush on Eurasian "transcontinental lineaments".

3. Electromagnetic soundings to find ore-bearing structures

In the case of ore prospecting, as with the explorations for other minerals or raw materials, the aim of the geophysical reconnaissance measurements is to find structures which could have been favourable to metallogenesis. As mentioned above, these structures are mainly fractures or faults extended to a great depth by tectonic forces, and hence their crack porosity being higher than that of their surroundings, has allowed the circulation of ore-producing solutions. If the pore volume in the fractures is saturated by conducting electrolytes and/or partly filled by metallic compounds of electronic conduction, these zones can be identified by geoelectric/electromagnetic methods as *Conductivity Anomalies (CA)*.

The electric parameters in the whole section of a deep fracture—primarily the resistivity distribution—can be investigated by geoelectric or electromagnetic methods of great penetration, e.g. magnetotelluric (MTS) or geomagnetic deep soundings (GDS) using the earth's electromagnetic field variations over a very large frequency range (Cagniard 1953). These methods enable one to investigate the earth's lithosphere.

The penetration depth of MTS and GDS is frequency-dependent. One of their variants, the audiomagnetotelluric sounding (AMT) can be used for direct ore prospecting in near-surface structures (Pelkonen et al. 1979) together with the recently favoured technique of spectral induced polarization (Pelton et al. 1978). The latter being an active method which needs an energy supply leading underground imposes depth limits on the exploration.

4. Conductivity anomalies (CA), tectonics and magmatism interrelations

The known conductivity zones are of two characters. The *first type* creates an arc structure. If the positions of the conductivity zones are compared with geological data (Lützner and Vass 1983, Mahel 1974), they correspond to sutures in the foredeep interpreted as a contact zone in the stable East European platforms with Variscan (northern zone) (Jankowski 1972, Porstendorfer et al. 1976) or Alpine (southern zone) folded units (see Fig. 1). The latter forms the so-called Carpathian anomaly (Jankowski et al. 1984). The *second type* creates a linear suture regarded as a significant discontinuity belt. This discontinuity belt represents either an activation zone in the upper mantle, a strike slip zone, or a collision zone (shortening). The conductivity zone in the Rhein graben (Jödicke et al. 1983) and along the Periadriatic and Balaton line (Ádám et al. 1984, Varga 1980) can serve as an example. A special case of this type of anomaly is the so-called Transdanubian anomaly (Ádám 1984).

A combination of the two types can also occur. *The conductivity zone can represent the activation zone of a lineament.* This is of fundamental significance from a metallogenetic point of view. The Odra lineament (Elbe-Zagros lineament in Fig. 2, after Bush 1983) can be considered such an element, regardless of the fact that its "geoelectrical expression" in the platform area is not known at present, although its continuation in the Carpathians is the Carpathian conductivity anomaly referred to above.

In order to show more closely the relationship of the crustal conductivity anomalies to the tectonic lines (lineaments) or zones and their physico-geological features, the conductivity anomalies of East-Central Europe as discovered by MTS and GDS are summarized in Table I together with their geological-geophysical background information. The CA-s are shown in Fig. 1, together with seismicity and Moho depth isolines.

Table I

Electric conductivity anomaly (CA)				Geophysical peculiarities of the CA		
Name	Extension (width)	Depth [km]	Conductance [S]	Seismicity	Heat flow	Is any indication of the CA in the Moho?
Periadriatic-lineaments a) Gail-valley b) Karawanken	linear	16—17 12.5—15	550—2500 2500—3000	Well-known seismotectonic zone (in Villach's earthquakes): in 1348: M=6.5 in 1690: M=6.2 in 1855: M=4.0). In Zell Pfarre und Eisenkappel were also strong earthquakes in Karawanken (Drimmel 1980)	Estimations: 60—80 mWm ⁻² (Čermák and Hurtig's map, 1979)	Moho is here deepest in the Eastern Alps (Kovács 1983)
Balaton-line	linear 8—10 km	7—10	?	Seismically not active (Only in its western part were some earthquakes)	~ 100 mWm ⁻²	No
Transdanubian-Conductivity Anomaly	areal	7 (shallowest: 3) (deepest : 13)	some thousands	Only sparsely. There is seemingly a correlation between the depth of CA and seismicity probably through the fracture tectonics (Ádám 1976)	~ 90—100 mWm ⁻²	Under the Bakony Mts a definite deepening of Moho has been measured (Posgay et al. 1981)
Styrian Alps with Lavanttal in their center	areal	6—9	about 1000	Seismically active (Drimmel 1980)	80—100 mWm ⁻²	Deepening of the Moho westwards (forming the Mts root)
Carpathian CA	linear	15—25 (approximation based on GDS) 7—12 (MT data)		Seismically the most active part of CA is in the Transcarpathian depression (in the continuation of the Odra line) and near to the Peripieninien Klippen belt (Lineament)	50—70 mWm ⁻² but at the eastern part structural peculiarities can cause local temperature enhancements (Čermák and Hurtig 1979)	Great step downward in the Moho discontinuity to the East-European Platform

Table I (contd.)

Magnetic anomaly	Tectonic structure	Magmatism	Ore deposites	Reference with respect to the CA
?	Narrow tectonic zones: Periadriatic and Insubric lineaments. The latter separates the Southern and Eastern Alps	Along the lineaments there are magmatites to the very ends, e.g. Late Variscan granites, Paleogene tonalites, andesites, etc. deformed into lamellae of only 2 km width	Fe, Pb, Zn, Cu	Ádám et al. (1984)
In the Velencei Mts there is large positive anomaly due to the magmatism	Southern boundary of the Balaton—Velence Late Variscan Granite Belt	Paleogene andezites in Hahót—Pusztaszentlászló, in the Velence Mts, Mátra Mts (Recsk)	Au, Pb, Zn, Cu	Varga (1980) Ádám and Pospíšil (1984)
Anomalies due to basaltic volcanism	Longitudinal and transversal fracture system with definite connection to CA (Ádám 1984)	Pliocene and Quaternary basalt volcanism		Ádám and Verő (1964) Ádám (1981)
?	Seismoactive fracture zones	?	?	Ádám et al. (1981)
	Strongly deformed tectonic zone separating different great tectonic units. Suture zone between East European Platform and Carpathians	At the boundary of the CA there are Pliocene calc-alkaline volcanites in the East Carpathians	Pb, Zn, Hg, As, Mn in connection with neovolcanites in the East Carpathians	Jankowski et al. (1977) Jankowski et al. (1984) Ádám and Pospíšil (1984)

The *conclusions* to be drawn from the comparison of all the data in Table I and Figs 1 and 2 are as follows:

- Crustal conductivity anomalies are generally connected with major tectonic structures (deep fractures, faults, suture zone of subductions, boundaries between different terrain patterns, lineaments, *etc.*) which have been reactivated many times in the past which can be traced to a Moho discontinuity representing a disturbed zone. Although the conductive parts of major tectonic lineaments are often shorter than the whole fracture system, they can enable inframantle lineaments to be located.

- These tectonic zones are often accompanied by (recent) seismicity with hypocentres generally lying outside the conductive layers.
- The heat flow, which is increased by convective heat transport along the fractures, also plays an important role in the formation of CA-s. An empirical relation exists between depth of CA-s and regional surface heat flow (Ádám 1978).
- Magmatic bodies with ore deposits are scattered close to a CA. The ore deposits are in many cases well developed in the area of intersection of two or more tectonic zones.

On the basis of these features it can be stated that crustal electric conductivity structures, principally those having linear features, with their magmatites or volcanites, deserve attention as prospective areas for ore prognostication. From this point of view the Odra line (OL) (or Elbe-Zagros lineament after Bush 1983) will be described in more detail in the following, taking into account its possible continuation to the SE in the Carpathians, in order to acquire more general ideas about these relations.

5. The Odra fracture — a detailed analysis

5.1 General tectonic views

The Odra lineament was defined by Tietz in 1916 under the designation of the Hamburg-Tulcza line (Motyl-Rakowska and Slaczka 1984). *Teisseyre in 1936* and later Dvorák (1968) proved its significance for the evolution of the Variscides. Grocholski (1981), Oberc (1972) and Sawicki (1972) referred to it as “the Middle Odra Faults System” (MOFS), and this was later confirmed by seismic profile DSS VII (Guterch et al. 1977).

The Odra fault system, sometimes also termed the Odra line (OL), has some specific properties (Oberc 1972). It has no continuation upwards in the late Tertiary rocks, which means that it can be studied only by means of boreholes, or to a certain extent by certain geophysical methods.

No proof has been produced so far to suggest that the Middle Odra Fault System is compressive in nature. Two faults en échelon near the town of Lubin seem to belong to the Middle Odra Fault System, which is best known in the Lubin-Sizroszovice copper-bearing area.

It is necessary to emphasize that apart from the “MOFS” the next significant faults active in the Tertiary period exist near the area investigated, e.g.—the Silesia—Lubusza fault, the Marginal Sudetic fault and others. Most of these faults run northwest-southeast, and some approximately east-west.

Many faults in Upper Silesia and the Cracow area follow similar directions. Oberc (1972) and others consider that the faults in both areas belong to the same cycle of deformations, suggesting that in recent times these two areas have developed tectonically in the same way. This also suggests a common cause for these instances of deformation and activation in the Carpathians.

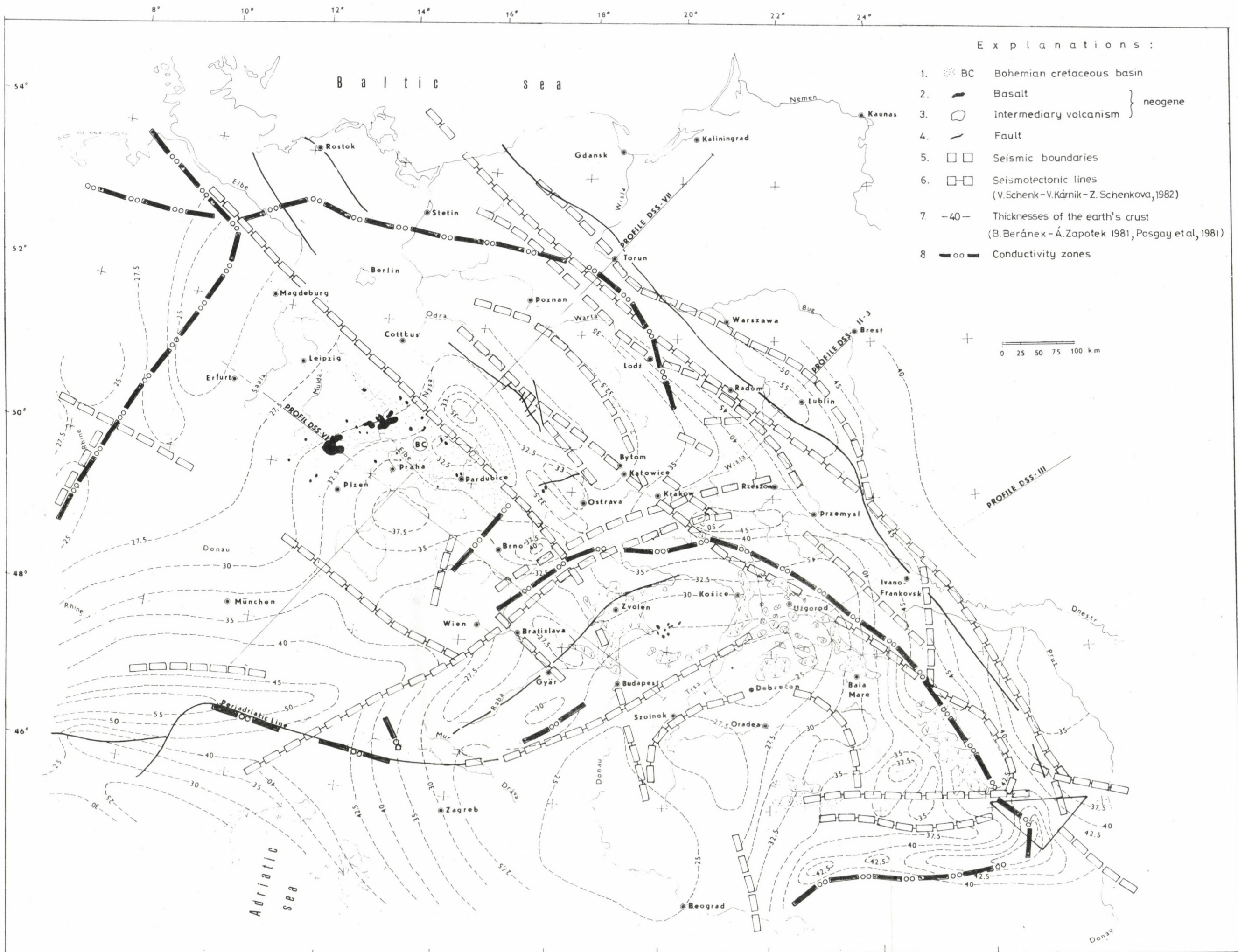


Fig. 1. Geophysical, tectonic and volcanological map of part of Northern, Central and East Central Europe (see key)

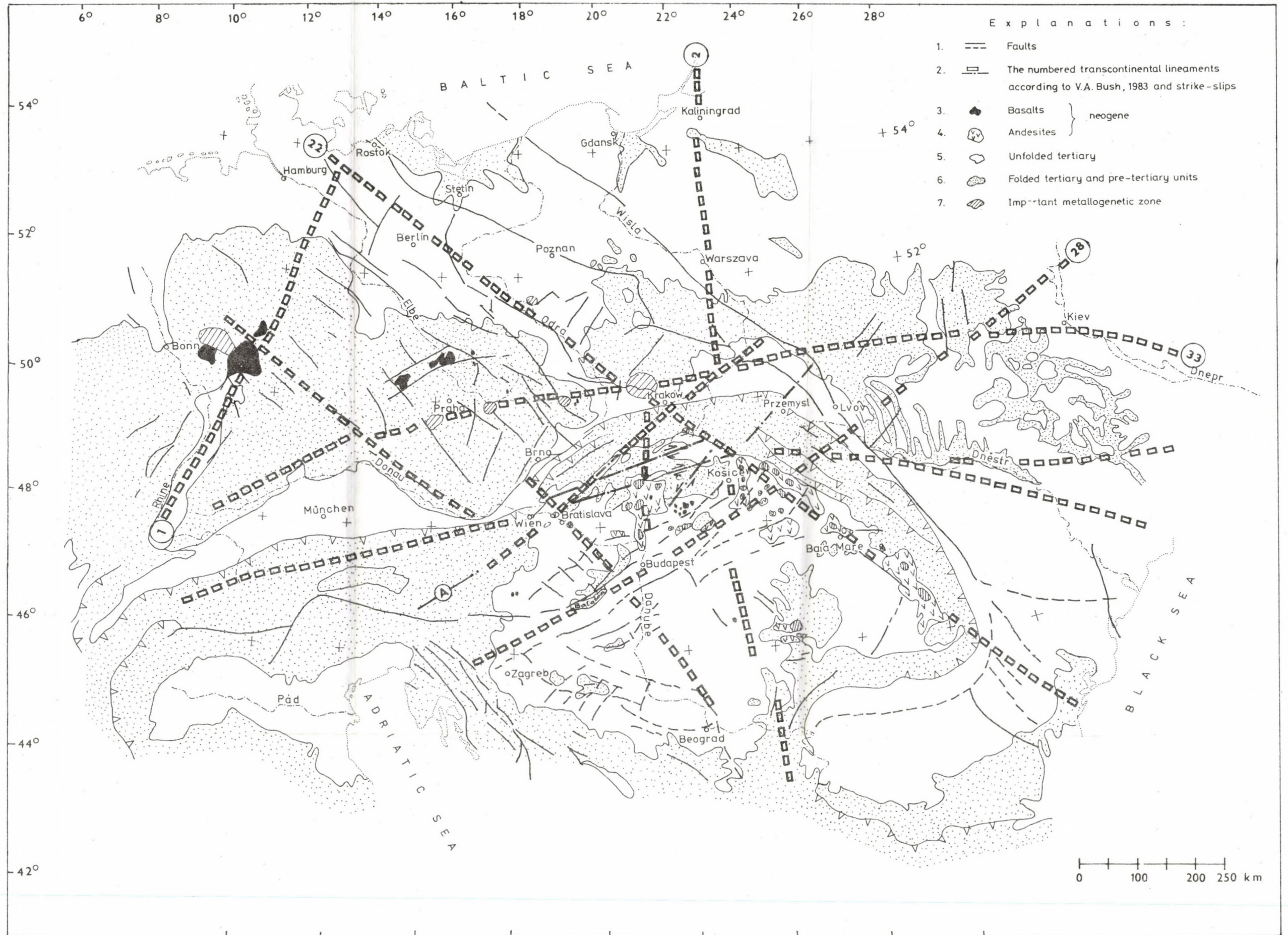


Fig. 2. Linear structures, volcanites and metallogenetic zones of part of Northern, Central and East Central Europe (see key)

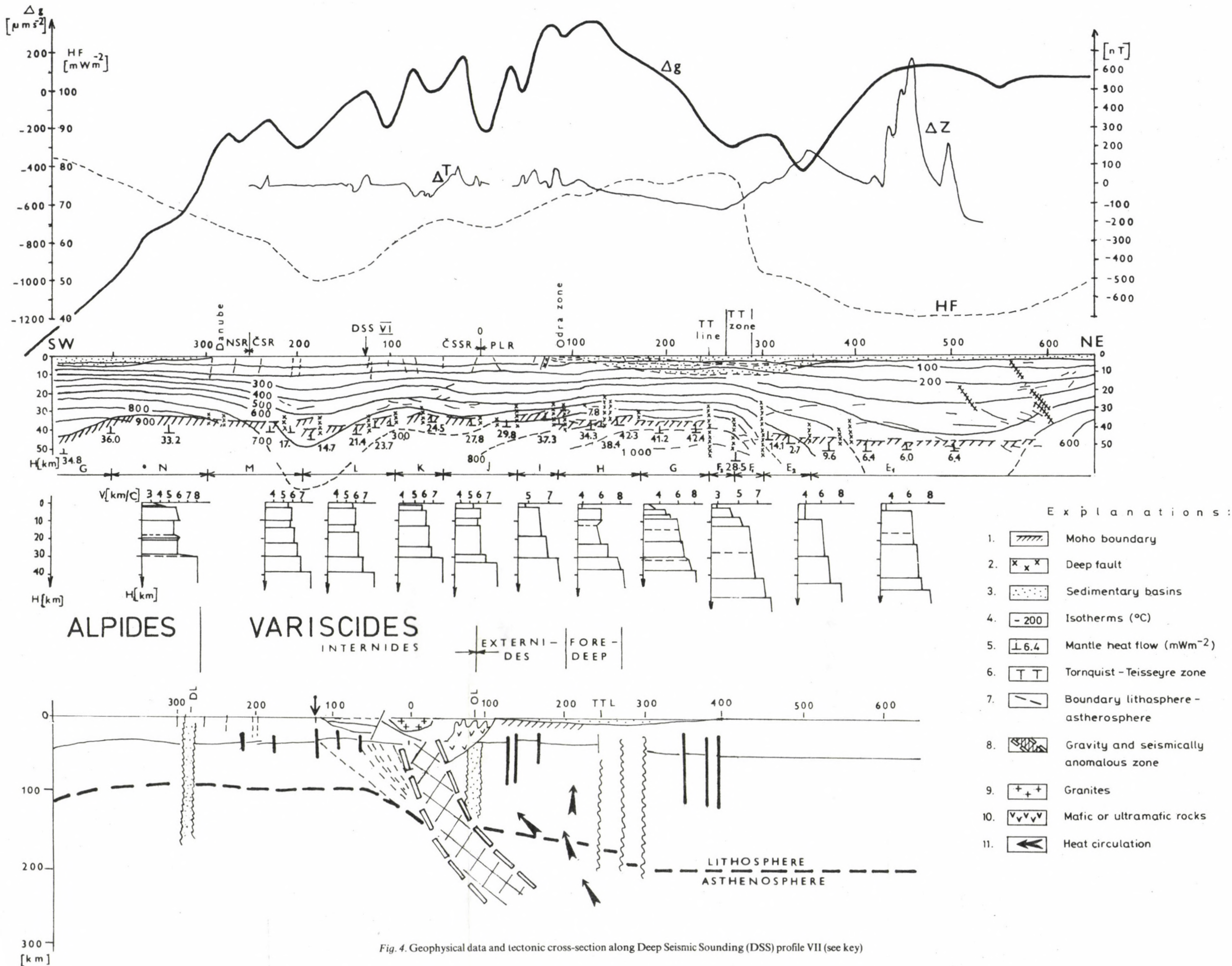


Fig. 4. Geophysical data and tectonic cross-section along Deep Seismic Sounding (DSS) profile VII (see key)



Fig. 3. NOAA 6 satellite image, near-infrared channel. Received by the Finnish Meteorological Institute, August 4, 1984 at 06^h 24' G. M. T. Greytone contrasts have been sharpened by the National Board of Survey, Photogrammetric Division, Finland. OL with arrows = Odra line

Below the Carpathians the course of the Odra lineament is indistinct, although it can still be followed using geophysical data and space images (Fig. 3). More concrete information on its continuation to the southeast has been given by the seismic profil DSS III (Sollogub and Chekunov 1977), in which significant interfaces in the earth's crust and the Moho were identified on the course of the Odra line. The authors cited named the whole system the "Odra-Caucasus lineament".

5.2 Geophysical analyses

The territory between the Odra line and the Teisseyre-Tornquist (TT) line is a tectonic transition zone from the ancient East-European Platform to the younger Mid-European one (Caledonides and Variscides). The Teisseyre-Tornquist zone representing an aulacogen structure is attributed by many authors to the ancient intra-continental rift. The transition zone may be distinguished on geological and geophysical evidence (Figs 1, 2).

A detailed treatment of the crustal structure in Poland is given by Guterch et al. (1977). On the whole, the transition from the ancient blocks to the young platform is indicated by the lateral heterogeneity of the Moho with respect to velocity characteristics. The crust in the territory of Poland is divided into *blocks* reaching the base of the crust (Fig. 4) and bounded by deep faults (Fig. 1).

The Odra zone, a well-defined *gravity* height according to the map of Ibrmajer (1979), continues into the Transcarpathian and Transilvanian depressions in the southeast (Pospíšil and Vass 1984), and similar tendencies towards the northwest through Iceland to the Atlantic Ocean appear in the gravity anomaly map.

The position of the main lineaments is also illustrated on the international profile DSS VII (Fig. 4) which extends from the Baltic Sea to the Northern Alps (Beránek et al. 1977, Guterch et al. 1977). The profile supplies the main geophysical information (temperature and heat flow—Milanovsky 1984, gravity data—Ibrmajer 1979, magnetic anomalies are compiled data).

The *temperature* at the Moho in the *OL-TT area*, according Milanovsky (1984), is between 800 °C to 650 °C, and the mantle heat flow ranges from 40 to 42 mWm⁻² (Fig. 4).

One important feature of the OL-TT transition zone is the rise in the asthenosphere from the East European Platform towards the younger platform (Kovtun and Chicherina 1976, Pěčová et al. 1979). The TT zone is also distinguished by an electric crustal anomaly, determined by means of induction arrows (Jankowski 1972). This crustal anomaly, as already mentioned, is of the arc type and is mainly due to the thick sediments in this rift area and their high fluid content. The deeper root of this CA in the crust is not known at present.

5.3 Metallogenetic features

There are two well-known ore fields along the Middle Odra Fault System, i.e. along the northern segment of lineament No. 22 after V. A. Bush (Fig. 2). These are

1. the Zechstein copper deposit near Lubin and Sizroszowice, and
2. the Neogene Silesian Cracovian zinc-lead ore field.

Galkiewicz' characterizes the *Silesian-Cracovian zinc—lead deposits*, economically the most important in the area under study, in the following way (Galkiewicz 1967):

1. The ore mineralization is connected with the Devonian-Jurassic strata.
2. The deposits with more intensive mineralization follow the WNW disjunctive fracture.
3. There is great variability in form and content between the ore bodies.
4. The mineralization has vertical zonality.
5. There are large haloes around the ore bodies.
6. The temperature corresponds to that of the sphalerite formation (120 °C), and
7. the isotropic composition of lead indicates the *neogene age* of the ore mineralization.



Fig. 5. NOAA 6 satellite image, near-infrared channel. Received by the Finnish Meteorological Institute August 5, 1984 at 06^h 00' G. M. T. KL = transcontinental lineament 33, after Bush (1983). Karpinski line. ✓ ✓ = continuation of the Bratislava—Cracow activation zone in South Poland

Most probably there is a relation among these deposits, i.e. the basic alkaline magmatism of the stable zone of the Alpine cycle and the great Elbe-Zagros transcontinental lineament, including the Odra zone.

The genesis of the *Zechstein copper deposit* is unclear (Rydzewski 1976) but it is connected in its position and distribution with the Odra line.

The same metallogenetic features are valid for other volcanic and ore prospecting regions, primarily the Transcarpathian depression, the Gutai Mts, and the Calimani-Harghita Mts, which are located along the continuation of the Odra zone, and at their intersections with other large perpendicular tectonic dislocations.

As these represent the eastern part of the Carpathian conductivity anomaly, we may assume that a conductivity zone can be found near the Middle Odra Fault System, and in this way the connection between the conductive zones with the ore mineralization and activation zones can be proved for this part of the earth's crust.

6. Future aspects

If we look the attached tectonic maps (Figs 1 and 2) we can see that some Middle European transcontinental lineaments (Bush 1983) have conductive parts, e.g. lineament 28 (Fig. 2) contains a CA near Lake Balaton. Although no CA has been detected along lineaments 2 and 33 (Karpinski Line, Fig. 5), it is true that relatively little deep magnetotelluric or magnetovariation sounding has yet taken place in the area concerned. It is evident that some at present still unknown first-order transcontinental lineaments may still exist, e.g. between the Bohemian massif and the West Carpathians (Khain 1973) striking in a NE-SW direction and continuing into the area of Fennosarmatia (cf. Cosmogeological Map of the USSR, 1 : 5 million). If the above is correct, the Silesian-Cracovian zinc-lead ore district and the ore zones located in the



Fig. 6. NOAA 7 satellite image (channel 4=thermal image). Received by the Finnish Meteorological Institute April 20, 1984 at 02^h 50' G. M. T. 28=Kotlas-Baleares transcontinental lineament (after Bush) corresponding to the Balaton line

border area between Czechoslovakia, USSR and Romania must both be situated in areas where three mantle structures intersect. It is an open question as to how we can connect the western part of the Carpathian CA with the possible NE-SW deep structure mentioned above (e.g. line A in Fig. 2). Several authors have interpreted the zone between line A and the flank of the Bohemian Massif as an aulacogene (Pliva 1980).

Deep electromagnetic sounding may prove to be an effective method for locating important mantle and crustal inhomogeneities, and it is therefore a matter of great value for small-scale metallogenetic prognostication that research work should continue in the realm of deep tectonics. The authors have observed how promisingly the part of lineament 28 (Fig. 6) located in Hungary and the southwestern USSR can be interpreted from small-scale satellite images using the thermal channel (night image). It will be important in the future to combine remote sensing and image processing with other geoscientific methods, especially with the MTS and GDS.

Since considerable ore occurrences of different ages are encountered along the Odra zone, the processes of activation and ore genesis must be complex phenomena. It is difficult, for instance, to understand why there should be such an enormous amount of copper in the Polish Zechstein ore deposit without a knowledge of the tectonic phases to which the genesis of this unique ore deposit is related. The MTS and GDS methods combined with deep drillings can probably also mark a fundamentally new achievement from a purely scientific point of view, and we cannot forget the observations made in connection with ultra-deep drilling in the Kola Peninsula.

Acknowledgements

We wish to thank the Finnish Academy for a grant to enable Prof. Paarma to travel to meet the co-authors and to Rautarukki Oy, Department of Ore Prospecting, for its continuous support. Thanks are also due to the Hungarian Academy of Sciences and the Geophysical Enterprise in Brno for help in our work. The Finnish Meteorological Institute is acknowledged for supplying NOAA images. We thank Mr Malcolm Hicks for the throughgoing English correction in our manuscript.

References

- Ádám A 1976: Distribution of the electrical conductivity in seismic (deep) fractures in Transdanubia. *Acta Geod. Geoph. Mont. Hung.*, 11, 277—285.
- Ádám A 1978: Geothermal effects in the formation of electrically conducting zones and temperature distribution in the Earth. *Phys. Earth Planet. Inter.*, 17, 21—28.
- Ádám A 1981: Statistische Zusammenhänge zwischen elektrischer Leitfähigkeitsverteilung und Bruchtektonik in Transdanubien (Westungarn). *Acta Geod. Geoph. Mont. Hung.*, 16, 97—113.
- Ádám A 1984: Fractures as conducting dykes and corresponding 2-D models. *Geophysical Prospecting*, 32, 543—554.
- Ádám A, Pospíšil L 1984: Crustal conductivity anomalies in the Carpathian region. *Acta Geod. Geoph. Mont. Hung.*, 19, 19—34.
- Ádám A, Verő J 1964: Ergebnisse der regionalen tellurischen Messungen in Ungarn. *Acta Technica*, 47, 63—77.

- Ádám A, Márcz F, Verő J, Wallner Á, Duma G, Gutdeutsch R 1981: Magnetotelluric sounding in the transitional zone between the Eastern Alps and Pannonian Basin. *J. Geophys.*, 50, 37—44.
- Ádám A, Duma G, Gutdeutsch R, Verő J, Wallner Á 1984: Periadriatic line in the Alps studied by magnetotellurics (in Hungarian). *Magyar Geofizika*, 25, 136—150.
- Beránek B, Konírová L, Mayerová M, Zouňková M 1977: DSS results HSS on the international Profile VII (in Czech.). *Applied Geophysics*, 14, 99—117.
- Bush V A 1983: Systems of Transcontinental Lineaments of Eurasia (in Russian). *Geotektonika*, 3, 15—32.
- Cagniard L 1953: Basic theory of the magneto-telluric method of geophysical prospecting. *Geophysics*, 18, 605—635.
- Čermák V and Hurtig E 1979: Heat Flow Map of Europe. Enclosure for Terrestrial Heat Flow in Europe. Ed. by V Čermák and L Rybach. Springer-Verlag, Berlin, Heidelberg
- Chekunov V B, Sollogub V B 1979: Crust of the earth — questions of structure and evolution (in Russian). *Geofizicheskij zhurnal*, 1, 19—35.
- Drimmel J 1980: 4. Rezent Seismizität und Seismotektonik des Ostalpenraumes. In: *Der Geologische Aufbau Österreichs*, R Oberhauser ed., Springer Verlag, Wien, New York
- Dvorák J 1968: Tectogenesis of the Central European Variscides. *Vestník Ústr. Ústavu geolog.*, 5, XLIII.
- Galkiewicz T 1967: Genesis of Silesian—Cracovian Zinc-Lead deposits. *Economic Geology Monograph*, 3, 156—167.
- Grocholski W 1981: Variscan basement structures of Poland (in Polish). Proceedings of conference "Geodynamic investigations in Poland". Yablonna, 1981.
- Guterch A, Materzok P, Paykhel J, Perkuc E 1977: Earth's Crustal Structure along 7th International DSS Profile in the Territory of Poland (in Russian). In: *Earth's Crust and Mantle Structures on the Basis of Seismic Investigations*, V B Sollogub ed. Naukova Dumka, Kiev, 148—158.
- Ibrmajer J 1979: Gravity maps of the ČSSR and their geological interpretations (in Czech.). Doctor thesis. Manuscript, PrFUK, Praha
- Jankowski J 1972: Techniques and results of magnetotelluric and geomagnetic deep soundings. In: *Publications of the Institutes of Geophys. Polish Academy of Sciences*, Warszawa, 54, pp. 135.
- Jankowski J, Petr V, Pěčová J, Praus O 1977: The Carpathian geoelectric anomaly and its relation to independent geophysical information. *Acta Geologica Acad. Sci. Hung.*, 21, 337—349.
- Jankowski J, Petr V, Pěčová J, Praus O 1984: Geoelectric anomaly in the Czechoslovak Polish section of the Carpathians on the basis of geomagnetic and magnetotelluric soundings. *Acta Geod. Geop. Mont. Hung.*, 19, 81—91.
- Jödicke H, Untiedt J, Olgemann W, Schulte L, Wegenitz V 1983: Electrical conductivity structure of the crust and upper mantle beneath the Rhenish Massif. In: *Plateau Uplift. The Rhenish Shield — a case history*, K Fuchs ed., Springer Verlag, Heidelberg, 288—302.
- Kakkuri J 1984: The Changing Faces of the Earth (in Finnish). *Ursa, Publ. no.*, 25, 22—31.
- Kashkai M A, Tamrazjan G P 1967: Crofolds (Anticaucasian) of the Crimea-Caucasus Region, their Effect on the Magmatism and Regularities in Useful Minerals Distribution (in Russian). Nedra, Moscow, pp. 75.
- Khain V E 1973: General Geotectonics (in Russian). Nedra, Moscow, pp. 510.
- Kovács S 1983: A tectonic review of the Alps (in Hungarian). *Általános Földtani Szemle*, 18, 77—155.
- Kovtun A A, Chicherina N D 1976: Deep magnetotelluric surveys in the northwestern part of the Russian Platform. In: *Geoelectric and Geothermal Studies (East-Central Europe, Soviet Asia)*. A Ádám ed., Akadémiai Kiadó, Budapest, 517—537.
- Lütznér H, Vass D 1983: Subdivision and stages of development of Variscan and Alpine molasses (on the base of the example of Central European Variscides and West Carpathians). *Veröff. Zentralinst. Physik Erde*, Potsdam, 77, 11—34.
- Mahel M ed. 1974: Tectonics of the Carpathian Balcan mountain system. Explanation of the Tectonic map Carpatho-Balcan mountain system and adjacent areas 1 : 1 000 000. Bratislava, pp. 453.
- Mayo E B 1958: Lineament tectonics and some ore districts of the southwest. *Mining Eng.*, 10, 1169—1175.
- Milanovsky S Y 1984: Deep geothermal structure and mantle heat flow along the Barents sea — East Alps geotraverse. *Tectonophysics*, 103, 175—192.
- Motyl-Rakowska J, Slaczka A 1984: The most important lineaments of the Carpathians and their relationship to the known faults. *Przegląd Geolog.* 2, 72—77.
- Oberc J 1972: Geological structures of Poland. Tectonics III, part 2 — Sudetes and surrounding areas. *Wyd. Geol.*, 464—475.

- Paarma H, Kuosmanen V 1982: Some remarks on the origin and localization of "syngenetic" ore deposits. In: *Sedimentary Geology of Highly Metamorphosed Precambrian Complexes*, A V Sidorenko ed., Nauka, Moscow, 200—210.
- Pěčová J, Petr V, Praus O 1979: Internal electrical conductivity distribution on Czechoslovak territory. Geodynamic Investigations in Czechoslovakia. Final report, VEDA Bratislava, 119—127.
- Pelkonen R, Hjelt S E, Kaikkonen P, Pernu T, Ruotsalainen A 1979: On the applicability of the audiomagnetotelluric (AMT) method for ore prospecting in Finland. Department of Geophysics, Univ. of Oulu, Contribution No. 94, 1—25.
- Pelton W H, Ward S H, Hallof P G, Sill W R, Nelson P K 1978: Mineral discrimination and removal of inductive coupling with multifrequency IP. *Geophysics*, 43, 588—610.
- Pliva G 1980: Contribution to the deep structure of the SE slope of the Bohemian massif (in Czech.). Proceedings of the 7th National Geophysical Conference, Section SI-Seismic, Gottwaldov, 89—94.
- Porstendorfer G, Göthe K, Lengning K, Oelsner Ch, Tanzer R, Ritter E 1976: Nature and possible causes of the anomalous behaviour of electric conductivity in the north of the GDR, Poland and the FRG. In: *Geoelectric and Geothermal Studies, KAPG Geophys. Monograph*, Ádám A ed., Akadémiai Kiadó, Budapest, 487—501.
- Posgay K, Albu I, Petrovics I, Ráner G 1981: Character of the Earth's crust and upper mantle on the basins of seismic reflection measurements in Hungary. *Earth Evolution Sciences*, 1 (3—4), 272—280.
- Pospišil L, Vass D 1984: Influence of the structure of the lithosphere on the formation and development of intramontane and back molasse basins of the Carpathian Mountains. *Geophys. Transaction*, 30, 355—371.
- Rokityansky I I 1982: Geoelectromagnetic investigation of the earth crust and mantle. Springer Verlag, Berlin
- Rundkvist D V ed. 1978: Criteria of the Prognostication of Ore Deposits (in Russian). Nedra, Leningrad, pp. 607.
- Sawicki L 1972: Remarks on Odra lineament. *Kwart. Geol.* 2.
- Shcheglov A D 1979: Fundamentals of Metallogenic Analysis (in Russian). MIR Publishers, Moscow, pp. 335.
- Sollogub V B, Chekunov A V (Editor in Chief) 1977: The structure of the Earth's Crust and Upper Mantle from Seismological Investigations. Collected Papers. Izd. Naukova Dumka, Kiev
- Turner D C, Webb P K 1974: The Daura igneous complex, N. Nigeria: a link between the Younger Granite district of Nigeria and S. Niger. *J. geol. Soc. Long.*, 130, 71—77.
- Varga G 1980: Geophysical investigation of geological basic profiles I. Report on the telluric and magnetotelluric measurements in 1979 (in Hungarian). MÁELGI Report. Manuscript
- Vartiainen H, Paarma H 1979: Geological characteristics of the Sokli carbonatite complex, Finland. *Econ. Geol.*, 74, 1296—1306.
- von Bauman L, Leeder O, Weber W 1984: On the metallogeny and minerogeny of the Postvariscan Platform Stage in Central Europe. *Zeitschrift für Geol. Wissenschaften*, 12, 3, 297—304.



PROFESSOR ISTVÁN HAZAY — 85 YEARS

The community of Hungarian geoscientists congratulate Professor István Hazay, ordinary member of the Hungarian Academy of Sciences at his 85th birthday.

His person is for us living history being closely connected to the last 60 years of Hungarian geodesy, to its theoretical and practical achievements. He became known before the World War as a surveying engineer with wide scientific interest and with an excellent practical sense. Accordingly his career raised from field triangulation works through the publication of his "Adjustment calculations" and the professorship of the Budapest Technical University to the State Prize he obtained.

After the World War he shared his forces between scientific investigations and the training of surveying engineers, a new branch at the university at this time. He reached prominent results in both fields. (A detailed biography and a list of his publications is found in Vol. 16, pp. 3—4 of this journal, where his 80th birthday was celebrated). A professor, a scientist and a human being is in a seldom seen harmony in him. His beloved and esteemed character is a model for the younger generation, equally exemplifying devotion to his field of science, indefatigable readiness to work and noble humanity. His person is closely connected to 37 years of the training of Hungarian surveyors and there are hardly any surveyors in Hungary who did not learn from him

immediately or indirectly either as his student or his associate. This process is being continued as his excellent health, his spiritual and physical fitness allow him to lecture at the university and also to continue scientific investigations. We wish him further good health and working ability to enjoy the well-deserved results of his productive activity together with his family, his colleagues and students.

P Biró

Book Reviews

E HURTIG and H STILLER eds: *Erdbeben und Erdbebengefährdung* (Earthquakes and Earthquake Risk). Akademie-Verlag, Berlin, 1984, 328 p

The present book contains a comprehensive basic review on seismology with a view to deal with many aspects of earthquake risk in the second part. The physical background is emphasized without lengthy mathematical deductions, and a possible best coverage within the given extent is striven at. Thus it is very likely that those interested in certain data or graphs about these problems, will find it here or at least a hint where to look for it.

After an introduction (Chapter 1), the history of seismology is reviewed (Chapter 2), followed by Chapters on seismic waves and instruments (3 and 4), localization of earthquake hypocentres and magnitude determination (5). The treatment on seismic risk starts in Chapter 6 (Seismicity and Tectonics), then Chapter 7 deals with source mechanisms and parameters, Chapter 8 with seismic risk in a restricted sense, Chapter 9 with induced seismicity and Chapter 10 with earthquake forecasting. This summary of the contents may indicate that the book is really thoroughly edited, well balanced and easy to understand.

A historical note to the first isoseist-map constructed: The map of the Mór Earthquake, in 1810 by Pál Kitaibel was published in 1814 and is reproduced in the Proceedings of the Seventeenth Assembly of the European Seismological Commission, Budapest, 1980.

The book can be recommended not only to seismologists, but also to all who have to do anything with seismic risk, be it from an architectural-constructional or from an engineering or governmental point of view.

J Verő

J O NRIAGU and P B MOORE eds: *Phosphate Minerals*. Springer-Verlag Berlin, Heidelberg, New York, Tokyo, 1984

As to the aims of the editors this volume should appeal to geologists, geochemists, lithologists, environmental scientists and engineers, as well as che-

mists and biochemists dealing with the complicated world of phosphorus. In this respect one may say that this book supplies a great want. Phosphate minerals forming one of the most complex and variegated group of the entire mineral kingdom as well as their physico-chemical and thermochemical properties should be of interest not only for geologists in wide sense, but also for experts of other sciences, e.g. medical, environmental, ecological etc. sciences.

Having read the book I had the feeling that nothing more can be said about phosphate minerals either from the mineralogical or from geological-ecological-environmental points of view. More than three hundred minerals are listed in alphabetical order supplied with the remarks concerning the most up-to-date physico-chemical and mineralogical data. Nevertheless, it would be useful to supplement an appendix in which a short comprehension of the mineralogical classification of phosphate minerals would be given.

The sequence of chapters reflects a logic thinking of how to be acquainted with different properties of phosphate minerals. In addition to the traditional chapters, i.e. mineralogy and geochemistry of phosphorites, the formation of phosphate minerals and deposits etc., to my great delight the phosphate minerals in human tissues, the phosphate minerals in waste water treatment systems and the environmental problems of phosphorus are also discussed (Chapters 12—14).

Concerning the phosphate minerals in human tissues, the discussion of the formation and transformation of different minerals in vivo and in vitro may be of greatest interest and the electron and scanning electron micrographs may provide useful information for physicians be they either practitioners or scientific researchers.

From the environmental points of view it is extraordinarily important to know the phosphate phases in waste waters. In Chapter 13 not only the form of the precipitates but also the chemical equilibria of different phases as well as the solubility properties of the solid phases are discussed. In light of these data the possibilities and difficulties of waste water treatment systems, the possibilities of primary, secondary and tertiary removal of phosphorus from waste waters are discussed. This

Chapter is strongly related to the subsequent one (Chapter 14) which deals with the phosphorus content and so-called phosphorus-cycle in the biosphere, with the phosphorus transfer among different ecosystems, as well as the seasonal changes of the phosphorus budget. Especially this latter problem may be important for agronomists, limnologists and forest scientists. The unsolved questions are also listed in order to call the attention of the experts that the behavior of phosphorus should be better understood for more efficient management of the agricultural and forest systems where phosphorus has been and will be used as a fertilizer.

The lists of references subsequent to each chapter, containing altogether more than thousand entries, unequivocally stresses the importance of phosphate minerals and their role not only in the inorganic world of rocks and minerals but also in the life of the human society.

The presentation of the book, the editors' efforts to prepare a really useful manual on phosphate minerals, the form and quality of figures etc. satisfy also the most fastidious tastes. I have only two remarks concerning the principles of data representation. First it would be better to give the constants of the compounds in the same units; e.g. the Gibbs free energy of formation is given in kJ mol^{-1} (Chapter 4, Table IV) and in kcal mol^{-1} (Chapter 10, Table I). The same is valid of the Log K (solubility product). I think that in Chapter 10, Table I there is a misprint, i.e. the term pyromorphite is assigned to two chemical formulae (the lead-chloro-phosphate and the copper-hydroxy-phosphate), though this term concerns only the $\text{Pb}_5(\text{PO}_4)_3\text{Cl}$.

In spite of these smaller errors in printing it is my conviction that having published this book, Springer provided us a very useful manual which I believe to be of interest for the scholars not only of the individual but also of the interdisciplinary sciences.

O Tomschey

H MILLITZER and F WEBER eds: *Angewandte Geophysik. Band I, Gravimetrie und Magnetik*. Akademie-Verlag, Berlin und Springer-Verlag, Wien—New York, 1984, 353 pp. figs 226

This is the first volume of a series planned for three volumes where the following parts will deal with geoelectricity, geothermics, radiometry, nuclear geophysics and aerogeophysics (Vol. II) and seismics (Vol. III). It is based on a cooperation between the Mining Academies in Freiberg (GDR) and Leoben (Austria), with some contributions from the geophysical firm VEB Geophysik in Leipzig and

from the Technical University Vienna. The participation of authors from GDR and Austria enables to deal with exploration practices in East and West, as it is best reflected in Sections 5 and 6 where the problems of processing and interpretation of gravity and magnetic data are discussed from the point of view of the anomalous bodies explored. This double treatment is a clear advantage of the book, as different points of view help to elucidate methods and results.

The theoretical basis for the magnetic and gravimetric methods are outlined in Section 1 of the book (Prof. Rösler, Freiberg, GDR) where ample information can be found on the effect of different anomalous bodies in both fields, mostly without lengthy deductions but with clear indication of the physical content and of the geophysical meaning of the formulae.

Sections 2 and 3 cover applied gravimetry and magnetism (Prof. H Millitzer, Freiberg, Drs. Lindner, Walach, Leoben, Prof. Seiberl, Vienna, Austria and R Scheibe, Leipzig). Instruments, field work, corrections and the necessary complimentary measurements, and some special applications, e.g. sea- and airborne measurements, measurements in mines etc. are discussed. In Section 4, Prof. Mauritsch of Leoben gives a comprehensive review of paleo- and archeomagnetism, outlining the most important facts and methods necessary for exploration geophysicists. The already mentioned last two Sections, 5 and 6, deal with Processing and Interpretation of gravimetric and magnetic measurements (Lindner, Millitzer, Rösler, Scheibe) including a rather wide variety of applications, as e.g. exploration of cavities, archeological use, use in earthquake and landslide prediction etc. The methods discussed range also widely from exact methods to statistical ones.

Section 6 (Walach and Weber) gives examples for the complex interpretation of gravimetric and magnetic measurements for hydrocarbon, coal, ore exploration and for some special geologic problems, e.g. of buried valleys and the serpentinite in Kraubath (Austria).

The book is excellent for the purpose studying but it can be used as well as reference for practical geophysicists.

J Verö

Bibliographie der in der DDR 1977—1982 zur Geschichte der Geologie, Mineralogie, Geophysik und Paläontologie vorgelegten Arbeiten. Veröffentlichungen des Wissenschaftlichen Informationszentrums der Bergakademie Freiberg, No. 106, Bergakademie Freiberg, 1984. 165 pages

This volume includes a bibliography of geology, mineralogy, geophysics and paleontology on books and papers published in the GDR 1977—1982. With a total of 1271 titles it shows that both the interest in the history of the corresponding fields and the covering of geological literature by this bibliography is very intensive. Peter Schmidt from the Bergakademie Freiberg who compiled this booklet can report on a series of sessions devoted to the history and philosophy of geology in the reported period including one on the history of seismology, seismics and tidal research. The background for this sessions and also for the bibliography is a working group consisting of 110 members on the "History and Philosophy of Geological Sciences" within the "Society of Geological Sciences in the GDR". The amount of the work can be estimated from the 400 portraits of geologists listed in an appendix. It is to be hoped that the bibliography will be continued.

J Verő

K FUCHS, K VON GEHLEN, H MÄLZER, H MURAWSKI, A SEMMEL eds: *Plateau Uplift*. The Rhenish Shield—A Case History. Springer Verlag Berlin—Heidelberg—New York—Tokyo; ISBN 3-540-12577-9
1983. 185 figs. XVII, 411 pages. 1300 g Cloth DM 104,—; approx. US\$ 40.40

This volume offers an account of the scientific outcome of a Priority Programme "Vertical movements and their causes using, as example, the Rhenish Massif" which was promoted by the Deutsche Forschungsgemeinschaft for 6 years, from 1976 to 1982. Professor Henning Illies, Karlsruhe, as the Coordinator of the programme—supported by a coordinating committee—brought together geodesists, geologists, geomorphologists, geophysicists, and petrologists at international basis to solve questions regarding epirogenesis in the time when "geological discussions centered around plate tectonics". This joint research in Earth Sciences is a significant contribution to the International Lithosphere Program.

The results of the multi-disciplinary investigations of the plateau uplift of the Rhenish Massif presented in this book provide an excellent opportunity—as told by Fuchs and Wedepohl—to compare geophysical and petrological models of structure, composition and dynamics of the upper mantle.

The chapters of the book are as follows:

1. Plateau Uplift of the Rhenish Massif—Introductory Remarks

2. Regional Tectonic Setting and Geological Structure of the Rhenish Massif
3. Pre-Quaternary Uplift in the Central Part of the Rhenish Massif
4. Plateau Uplift During Pleistocene Time
5. Volcanic Activity
6. Present-Day Features of the Rhenish Massif
7. Crust and Mantle Structure, Physical Properties and Composition
8. Attempts to Model Plateau Uplift
9. Epilogue: Mode and Mechanism of Rhenish Plateau Uplift

As a summary of these outstanding research works we can quote from the Epilogue "An uprise of less dense material from the lithosphere-aesthenosphere boundary seems to be the most likely of the modeled mechanisms" ... but "it must be admitted that the process of uplift is not yet fully understood" and so the efforts should continue. I think this summary qualifies the objective scientific attitude represented in the whole book which is warmly recommended to all geoscientists.

A Ádám

A MESKÓ: *Digital Filtering*. Applications in Geophysical Exploration for Oil. Akadémiai Kiadó, Budapest, Pitman Publishing Ltd., London, Halsted Press, New York, 1984. 635 pp

Professor Meskó's book discusses from the specific point of view of applied geophysics the wide range of digital filtering and spectrum computing methods. Time series occur in many branches of modern science, and one of the basic operations when treating them is just filtering (and spectrum computation). The emphasis is, however, in each branch on different aspects, therefore it is welcome in each field to have own books on the topic. Not only the examples, but the structure and relative importance of parts in the book show the specific point of view chosen. It contains a very great number of procedures, methods and formulas, it gives the most important deductions, is well illustrated with many composite and a number of practical examples; concrete computational algorithms and computer programs are, however, not included. It would be worth to compile a second book on the same topic containing algorithms and programs of the methods treated here. The reader is sometimes curious how the examples have been produced, and this side of the problem is not tackled in the present book.

Part 1 deals with digital filtering generally, including sections on Fourier- and Hilbert trans-

forms, Convolution and correlation, Digital signals, Discrete and Fast Fourier transform, z-transformation and Recursive filtering.

Part 2 is already geophysics-oriented, dealing with optimum filters and their application. The part commences with short, but comprehensive summaries on probability theory and statistics, the next sections are devoted to stochastic processes, Digital Wiener filters and Optimum filters for signal-to-noise ratio enhancement.

Part 3 is then purely geophysical, presenting examples from field practice, from seismics as well as from gravity and magnetic prospecting. Here the latter part is the more voluminous one reflecting the author's main field of interest, too.

The production of the book is generally of a high quality, only the titles of parts and sections are to inconspicuous and therefore it is somewhat difficult to find them.

It is characteristic for this book that it yields a wealth of information about many questions hardly to find elsewhere. Thus it can be recommended to all students and practitioners of applied geophysics, but even experts of other fields may find stimuli in it to their own work.

J Verő

G V FISHER, H U SCHMINCKE: *Pyroclastic Rocks*. Springer Verlag 1984, 472 pages, 339 figs

R V Fisher, Professor at the Geological Department, University of California, USA and H U Schmincke, Professor of Petrology, Ruhr University Bochum, F. R.G. used a new approach of treatment in their hand-book which can be regarded as a high standard university compendium, too.

The greatest merit of the book is the common treatment of the petrology and volcanology of pyroclastites and of the very up-to-date problems of extent structures and tectonics. This method of approach is the reason why the book is not only valuable for petrologists and volcanologists, but also for geologists and geophysicists dealing with the study of extent and crustal structures.

Special value has the data amount of local occurrences of pyroclastites having been collected in many cases by the authors themselves at different places of the Earth. This material of knowledge has been brought near to the reader by an excellent photo material helping hereby the work of specialists.

In the first chapter basic information is outlined about volcanic activity, about the characteristics of spread volcanic materials and accretion of tuffs and their formation into rocks. A special chapter deals

with types of magma-chambers. Chapter 3 gives useful informations especially for volcanologists about the volatile contents of magma and the rheological conditions of silicate melts.

In Chapter 4 the types of formation of pyroclastites are considered in the light of the best known volcanic formations of the Earth. In Chapter 5 the material composition and the structure of pyroclastites are summarized by means of excellent microphotos. In the next six chapters petrology, genetics and description of the main occurrences of the different pyroclastite formations are given including the detailed description of special pyroclastites as tuff-lavas, ignimbrites, lahars, etc.

A special chapter deals with the alteration of volcanic rock-glasses constituting a great part of tuffs during the rock-formation, as it can be concluded from their study to the origin of pyroclastites and to their later geological history.

Chapter 13 sums up the stratigraphy, the tephrochronological importance of pyroclastites of the Earth and discusses the classification of pyroclastic facies.

As a summary as well as the culmination of the work one can learn the relation between the different types of pyroclastites with the conditions of great tectonics on the basis of the theory of plate-tectonics.

The reference list on 38 pages lists the most important papers of the topic published in English and German till 1983.

Specialists can use this book to the systematization and genetic interpretation of the paleogene pyroclastite formations having a stratigraphic importance, an importance in the structural development and sometimes even for industry, but it is useful for geologists and geophysicists as well as for any students of these disciplines.

T Póka

J R HOLTON and T MATSUNO eds: *Dynamics of the Middle Atmosphere. Advances in Earth and Planetary Sciences*. Terra Scientific Publishing Company, Tokyo and D Reidel Publishing Company, Dordrecht (Boston) Lancaster, 1984, 543 pp, 263 figs

The volume contains proceedings of a U.S.—Japan Seminar on the Dynamics of the Middle Atmosphere, held at the East-West Center of the University of Hawaii, Honolulu, Hawaii 8—12 November 1982. The papers, partly overview articles, partly original contributions presented at the Seminar are grouped according to their subject into six groups. These six topics include all important areas of middle atmosphere dynamics from large

scale motions to gravity waves. The discussion of these topics is completed by studies on the role of dynamics in aeronomical processes, in radiative processes and tracer transport. Concerning middle atmosphere dynamics, the most important unresolved problems are considered, problems to be solved are shown and the methods of solution are investigated. Thus, this volume is very useful for all those research workers who want to form an up-to-date picture on middle atmosphere dynamics.

The section devoted to atmospheric gravity waves is introduced by R S Lindzen's article on gravity waves in the mesosphere. This study is followed by R L Walterscheid's papers on gravity wave attenuation and the evolution of the mean state following wave breakdown, by M R Schoeberl and D J Strobel's study on nonzonal gravity wave breaking in the winter mesosphere, by L Hirota's article on the climatology of gravity waves in the middle atmosphere, by B B Balsley, W L Ecklund and D C Fritts's paper on VHF echoes from the arctic mesosphere and lower thermosphere, by M Yamanaka and H Tanaka's study on multiple "gust layers" observed in the middle stratosphere and by a contribution from Y Hayashi and T Matsuno on internal gravity wave enhancement by the chemical heat release due to oxygen recombination.

The section of tides and free oscillations includes an overview on tidal observation by S Kato, T Aso and R A Vincent, linearized steady calculations of semidiurnal tides in the middle atmosphere by T Aso and S Kato, a paper by S Miyahara on zonal mean winds induced by solar diurnal tides in the lower thermosphere and an article by I Hirota and T Hirooka on normal mode Rossby waves observed in the upper stratosphere.

In the section dealing with large scale waves and wave-mean flow interaction questions as the quasi-biennial oscillation, a 2-dimensional numerical model of the semi-annual zonal wind oscillation, numerical simulation of the zonal mean circulation of the middle atmosphere, wave-mean flow interactions during winter, observed sudden warmings diagnosed by the Eliassen-Palm flux and refractive index and the dynamics of minor stratospheric warmings are discussed by R A Plumb, M Takahashi, S Miyahara, J C Gille, L V Lyjak, H Kanzawa and T Matsuno.

In further sections problems connected with radiation, transport of tracers and modeling are reviewed and studied in papers by C B Leovy, J R Holton, J D Mahlman, D G Andrews, D L Hartman, T Matsuno and R G Murgatroyd, K K

Tung, F Hasabe, as well as by M A Geller, J D Mahlman and L J Umscheid, T Tokioka and I Yagai.

P Bencze

J FÜLÖP: *Ásványi nyersanyagok története Magyarországon (History of mineral resources in Hungary)*. Műszaki Könyvkiadó, 1984, 180 pp. 102 figures + X color plates

It is somewhat exceptional that a book in Hungarian should be reviewed on the pages of this journal, but in this case both the topic and the quality of the book motivates such a review.

Emerging from an introductory chapter to a planned Geology of Hungary, the present volume undertakes an effort to trace the mineral resources of artefacts in the Carpathian Basin from earliest times till present. Pebble tools of the Lower Paleozoic men (B.C. 350 000) stand at the beginning of a long series of objects used for the most different purposes made of stone, clay, later ores and metals. A rich choice of objects of arts illustrate this process, including pottery, earliest tools of metal processing, coins, jewelry etc. The geologic background is given by tracing back the possible sources of the raw material for the different uses. Thus prehistoric trade routes can be traced, too.

In medieval times (13th century), Hungary produced more than 80 percent of Europe's gold, and about 25 percent of its silver. In the heydays during the reign of the Anjou-dynasty, the output of gold reached yearly 2500 kg, that of silver 10 000 kg. Thus it is not surprising that Hungarian coins were well known throughout Europe. At the beginning of the 16th century, copper production in Upper Hungary (present Slovakia) reached an unprecedented 3000 t yearly level. But this was the evening of this medieval flourishing, the concurrence of precious metals from the New World was too hard. And the Turkish occupation put an end to the medieval empire, too.

A story of success starts again in the 17th century. The first use of explosives in mine, later the first Mining Academy, the first higher education in technics were the milestones in this way.

The second half of the book describes the development of mineral resources in Hungary in the 20th century. Many color plates—maps, diagrams—illustrate the development in a country, where according to general belief, resources are

scarce. Some coal, oil, gas is well supplemented by bauxite being presently the most important mineral in Hungary—barely mentioned at the end of the last century in a Hungarian book on minerals as occurring only in France. It should not be forgotten, that first geophysical exploration for oil was made at Egbel by H Böckh at the beginning of this century by Eötvös pendulum. These facts and many others help to make this book an excellent reading, and also in many respects a help to all dealing with minerals in Hungary, or even outside its boundaries, and historians will also find interesting facts in it.

J Verő

W WITTKÉ: *Rock Mechanics. Fundamentals of Economic Construction of Underground Excavations. (Felsmechanik. Grundlagen für wirtschaftliches Bauen im Fels.)* Springer-Verlag, Berlin, Heidelberg, New York, Tokyo. 1984. DM 184, US \$ 72.2

The book deals with theoretical and practical aspects of rock mechanics in great detail on its 1050 pages and in its 27 chapters. 798 figures contribute to the understanding of the problems and 305 references enable the reader to find further reading material on special questions.

Four chapters of Part A analyze models of homogeneous and stratified rock structures, stress-induced and heaving-caused deformation and filtration in rocks.

Part B deals with calculation methods in the following five chapters:

- Calculation of stresses and deformations in rocks using the finite element method.
- Taking into account stresses and deformations caused by heaving by the finite element calculation method. Slope stability analysis.
- Calculation of water flow using a non-continuous model.
- Calculation of three-dimensional water flow in rocks using the finite element method and homogeneous rock models.

Part C illustrates the application of the calculation methods for tunnels and adits, extremely large underground excavations (machine rooms), pressure tunnels of hydroelectric stations, foundation of barrages and slopes.

Part D deals with rockmechanical investigations. After defining the aims of the investigations, the book turns to geological prospecting and exploration aimed at determining the rockmechanical parameters. The following chapters describe laboratory analyses of rock samples, shearing investigation of separating surfaces, determination of

deformation parameters, primary stresses, measurement and interpretation of deformations and stresses caused by outbursts, ground water conditions and permeability. The investigation methods described in these chapters are illustrated through practical examples in Chapter 24.

Part E describes the design and construction of underground excavations and illustrates it with examples.

The appendix gives an introduction to vector and matrix calculation, as well as probability theory and mathematical statistics. Handling of the book is made easy by a name and subject index.

The language of the book is easy to understand, it is free of theoretical considerations superfluous for the practical engineer. The book will, therefore, obviously become a useful handbook for mining and civil engineers working on the design or construction of underground excavations.

J Janositz

H J SCHNEIDER ed.: *Mineral Deposits of the Alps and the Alpine Epoch in Europe. Proceedings of the IV. ISMIDA, Berchtesgaden, October 4—10, 1981. Special Publication No. 3 of the Society of Geology Applied to Mineral Deposits.* Springer-Verlag, Berlin—Heidelberg—New York—Tokyo, 1983, 402 pp. 184 figs. DM 98—; US \$ 39.00

This book contains the material of the papers presented at the IV. ISMIDA (International Symposium on Mineral Deposits of the Alps). As the subtitle indicates, the papers are not limited exclusively to the Alpine area, but they cover neighbouring regions, too (there is, however, no paper about Hungary).

The disadvantage of such kind of books is that their material within the given field cannot be complete and well-balanced (some of the areas or occurrences are completely lacking, while others have multiple coverage, sometimes even in overlapping discussions), further the presentation is mosaicslike and only loosely ordered. In the contrary their advantage is—and it is very likely that their popularity is due to this fact—that they present actual results (even if in a not completely finished and closed form) and therefore they inform about current ideas and tendencies.

May be that the Alps do not contain presently mineral resources of global importance, but the occurrences here had played an eminent role in the general history of the discovery and exploration of resources, and that this significance is true even today, should at least partly attributed to the quite

recently created and more and more popular ISMIDA-conferences.

In the systematics of the material, the first part (26 papers) contains "Alpine" occurrences in a narrower sense of the word, followed by 13 papers about extra-Alpine (mostly European, but even two North-African) occurrences. Subdivision is only made in the first part, where 3 papers are of a general character, 14 papers describe single Alpine occurrences or groups of occurrences with a detailed survey of the sites, and 9 papers deal with the geochemistry of Alpine mineral deposits.

Among Alpine deposits, most space is devoted to Permian-Triassic, strata-bound Pb—Zn- (F—Ba) deposits, but some papers deal—among others—with tungsten (mostly scheelite), Fe—Ni—Cu-sulphide, magnesite, halite, and even with Eocene iron ore and hydraulic lime occurrences. Papers on geochemistry survey in addition to the general or special problems of single deposits isotope composition and genetic conclusions drawn from it.

Some deposits or greater groups of deposits are treated from the following extra-Alpine countries, Spain, France, Algeria, German Federal Republic, Greece. Here also Pb—Zn- (F—Ba) deposits are discussed most frequently, but some papers completely differing from the previous ones are also included here (one of the papers summarizes e.g. every known mineral deposit of the German Federal Republic).

P Kisházi

D G BROOKINS: *Geochemical Aspects of Radioactive Waste Disposal*. Springer Verlag, New York—Berlin—Heidelberg—Tokyo (347 pages, 53 figures, 78 tables, 331 references, subject index)

In the 15 chapters the urging problems of the disposal of radioactive wastes of different dangerous effects are discussed and the optimal and real possibilities of burying these wastes in different rock types of the earth crust are dealt with.

Based on the analogies of natural radioactive decay an approach is given to the possibilities of protection and to transplant the theoretical studies in the practical life.

If mankind will realize that recently "nuclear power plants are operating in 35 countries of the world", and radioactive raw materials are mined, processed and used for industrial, experimental, scientific and military purposes, it is unequivocal that the potential danger is increasing and the accumulation of the remaining radioactive wastes becomes ever more dangerous as radioactive infection for the human environment.

The utilization and enrichment of radioactive materials are sources of danger for people living in our days, the inappropriate isolation of wastes will be a heritable source of danger of our successors.

This is why the topic of this book is worthy of interest and numerous countries of the world meet the problem: how to preserve the accumulating masses of radioactive wastes for long times and under isolated conditions.

Having studied the types of radioactive wastes, the environmental effects of natural radioactive materials, the results of geological, hydrological and geochemical researches carried out on different types of rocks as radioactive waste disposal sites of the US (salt deposits, schists, igneous and volcanic rocks etc.) are discussed.

The scale of values among the alternatives of disposal sites is affected by the rentability in addition to the protection of the environment.

The book correctly and objectively illustrates that the complex mode of disposal is the most suitable one.

In the course of studying the investigated and expected disposal sites from the geological points of view it is to be noted that other possibilities, e.g. rejuvenating igneous activity, tectonic movements, etc. that are less emphasized in the book, play also important role when selecting the disposal sites.

This book is a worthy and useful source for experts who have or will have to meet the problems to allocate or select the sites suitable to the isolated disposal of radioactive wastes.

É Pécsi-Donáth

L R LYONS, D J WILLIAMS: *Quantitative Aspects of Magnetospheric Physics. Geophysics and Astrophysics Monographs*. D. Reidel Publishing Company, Dordrecht (Boston) Lancaster

The present book is a most welcome survey on selected important theoretical—quantitative topics of magnetospheric physics. In the past years the field of magnetospheric physics has developed and widened so quickly that it got impossible to follow each of its parts with equal attention. Therefore it became urgent to have reviews on special topics to enable researchers working in neighbouring fields a quick overview. In the present case two eminent representants of magnetospheric physics with a long record of activity have summarized facts and in a few cases views about quantitative aspects of the processes in the magnetosphere in a rather concise form. Topics should be anyway selected as the immense field of the magnetosphere is no more summarizable in a single volume, even not from a

special point of view. So e.g. magnetohydrodynamic waves and field line resonance do not appear in the present book.

The material is distributed to an introduction, to a Chapter on basic principles (charged particle motion in the magnetosphere), and three chapters devoted to special problems. Here the "problem" is organized not from a magnetospheric, but from a physical point of view, being correct in the present case. The first one deals with trapped particles and ring current generation and decay, being important for many magnetospheric processes. The Chapter on Electric Fields has three sections, on convective electric fields, on plasma energization in the tail and auroras (parallel electric fields). All the three fields are very rapidly developing, therefore such a review is more important than ever. The last Chapter deals with Wave-Particle Interactions, and these difficult problems are mastered by the authors elegantly and easy to understand for the reader. Auroral kilometric radiation, whistler-mode waves, ion-cyclotron waves and electrostatic waves outside the plasmopause are the main types treated, including a number of basic concepts and consequences.

The greatest advantage of the book is that a correct equilibrium was found between too few and too much formulas and mathematics. The reader can follow the line of thought without being overburdened with mathematics of secondary importance. Therefore the book can be really recommended to all dealing with magnetospheric physics.

J Verő

W SCHRÖDER ed: *Historical Events and People in Geosciences*. Peter Lang, Frankfurt/M.. Berne, New York, 1985. 220 pp. US \$ 20,85 European University Studies: Series 39, Interdepartmental Congress Reports. Vol. 2.

This series of papers presented at the Hamburg IUGG General Assembly is a very interesting collection on the history of various fields of geophysics. One of the impressive traits of these accounts is a certain heroic devotion being evident in the daily climbing in bad weather to the top of Ben Nevis (E G Formes), in the efforts to establish a high latitude mountain observatory to observe auroras in Haldde (A Brekke), and also in the better known polar research expeditions (K Bretterbauer on the Austro-Hungarian and K H Wiederkehr on the Ross expedition), prominent exponents, or even initiators of certain disciplines report on the history of their achievements (e.g. W Dieminger on Radio-wave propagation and solar-terrestrial physics, L

Biermann on the discovery of the solar wind). There are also papers dealing with the use of historic data, e.g. by J Bloxham and D R Barraclough on the use of historical geomagnetic data in studies of the earth's core, or by M P Pavese and G P Gregori on historical geophysical records in Italy. Biographical notes can be found on several prominent persons (Lamont, Payer, Weyprecht, Wilczek, Regener, Currie, Gauss, Halley), and on outstanding events, as e.g. the twilight phenomena in 1883/84 after the Krakatoa eruption (W Schröder), the first hourly geomagnetic observations in Japan (N Fukushima), the earliest observations of noctilucent clouds (M Gadsden) and an eyewitness's account on the Krakatoa eruption (B M Hamilton) are treated as well in this book. It is a very interesting reading, and it should be emphasized that the series of similar historical publications should be followed. W Schröder, the editor did a service to all interested in the history of geophysics by making these papers accessible.

J Verő

J E COSTA—P JAY FLEISCHER eds.: *Developments and Applications of Geomorphology*. Springer Verlag, Berlin, Heidelberg, 1984. 372 p.

The title of this recent collection of papers is broad enough to refer to any fields in geomorphology and to a wide range of topics in the related geosciences. The number of subjects presented, however, is not too great since each of them are treated in proper detail and in a comprehensive way. Applied geomorphology as conceived by editors and contributors tends to mean physical geography in our interpretation of the term. Firm evidence is given to the long suspected truth that no 'pure' science exists without a great variety of possible as well as useful applications. When applications are demonstrated, the reader is recurrently reminded of the main points in theory and, thus, applied fields are easily linked with basic knowledge.

Let us first consider the paper written by the 'biggest' name among contributors, D R COATES, who has the reputation of being an environmentally minded geomorphologist. Throwing light on the relationships between geomorphology and public policy (pursuing the seemingly odd idea of connecting a natural science with law!), he touches upon one of the vital issues of environmental studies (also arising interest in Hungary), i.e. the assessment of land capability and potential and the optimization of land use. The principles formulated by him are supported by case studies of claims before the law. They are not mere anecdotes of lawsuits but point to

the need of definite and unambiguous judgements (founded by circumspective analyses) on the phenomena and processes of the physical environment. Nevertheless, in the case of an incident when the cause of lowered groundwater table had to be decided (p. 121), author's argumentation is not sufficient to explain why the court decreed the State of New York (investors of a highway) 'not guilty'. The effluent flow of groundwater observed by author (the official expert in the suit) do not contradict to the close correlation between reduced streamflow and lowered groundwater table.

Comprehensive information is contained in *J Toy's* paper on open cast mines in the western United States. The geomorphic processes active before, during and after resource extraction are surveyed. (For us the presentation of the geographical setting is also valuable since the characteristics of natural provinces are tabulated in a succinct form.) His example of the surface-mining of uranium is somewhat 'exotic' for us.

It is to be noted that some of the topics are unfortunately beyond the research interest and expertise of Hungarian geomorphologists. They include coastal features, to which two chapters are devoted: one covers the applications of computer survey and the other is concerned with the detection of changes in the coastal environments.

"The applications of geomorphology are heavily dependent upon the effective use of maps," claims one of the editors, P. JAY FLEISCHER, as he reviews the types of applied geomorphological maps. (Some attention is devoted here to East European cartography represented by the system of symbols by M Klimaszewski regarded as minutely elaborated but too complicated.) It is emphasized that not only specialized applied geomorphological, engineering geological or land use maps are found useful in practice, but the use of maps for 'academic' purposes, such as that of Quaternary materials and landforms, is also demonstrated. The cited suitability maps based on rating are very similar to Hungarian maps of environmental assessment for special purposes.

Further selecting between the topics, recent methods in remote sensing and geochronology—neotectonics are summarized in separate chapters with abundant references. The latter chapter is supplemented with the estimation perspectives of earthquake hazard from geomorphological evidence (dislocation rates and the frequency of seismic events reconstructed from land features). Examples are cited from areas where this is a vital problem (the San Andreas fault zone and the associated fault systems). To extend the scope of case studies outside the mid-latitudes, a paper on the impact of urbanization on the physical environment

of the tropics is also included. Although the conclusions drawn from research mainly in South-east Asian cities (first of all in Singapore) are of not much novelty, the information given fills in a gap in the knowledge of most geomorphologists in Europe.

Another type of environmental hazard is dealt with in the chapter on debris flows. This rather heterogeneous family of mass movements is capable of the dislocation of vast amounts of material with embedded boulders of several tonnes. Based on measured data, the mechanisms of this transport are analyzed in order to judge their relative significance.

In the final chapter the complete literature on the mathematical approaches to river channel parameters is compiled and evaluated. Although numerous equations exist, there is still much to do to increase their levels of accuracy.

D Lóczy

H D HOLLAND and A F TRENDALL eds.: *Patterns of Change in Earth Evolution*. Dahlem Konferenzen, Springer Verlag, Berlin—Heidelberg—New York—Tokyo, 1984. pp. 431. 4 photographs, 48 figures and 12 tables

This book publishes the material of a Dahlem Conference organized by the Stifterverband für Deutsche Wissenschaft. Each year four workshops are organized there with a limited number of participants. The work is done in four interdisciplinary discussion groups. In the present case they are: Possible influences of sudden events on biological radiations and extinctions, Short-term changes affecting atmosphere, oceans and sediments during the Phanerozoics, Events on a time-scale of 10^7 to 10^9 years controlled by tectonism or volcanism, Long term evolution of the crust and mantle. Each topic contains 3—7 contributions and a Group Report on the discussions in the respective study group summarizing the opinions presented at the sessions. To mention a few interesting themes just from the beginning, D M Raup reviews on radiations and extinctions in geologic times with a special emphasis on the reality of these events. E M Shoemaker discusses the effects of large body impacts and presents calculations on the probability of encounters with asteroids and comets. A most important item for the future of mankind is "Sudden changes in atmospheric composition and climate", due to volcanic eruptions, collisions with galactic dust lanes or meteorites (O B Toon). K J Hsü summarizes our knowledge on geochemical markers of impact.

Perhaps the four papers belonging to the first study group can illustrate the wide and important topics covered by each group. The book visualized

the great change in our knowledge about the past history of the Earth which proved not to be as uniform as it was believed some decades ago.

J Verő

W. SCHRÖDER: *Das Phänomen des Polarlichts*. Erträge der Forschung, Bd. 218. Wissenschaftliche Buchgesellschaft, Darmstadt, 1984 159 pages, 29 figures, 7 tables

The aurora is one of the not too numerous natural phenomena which mean something exceptional for men. Such are also lightning and thunderstorm, earthquake, volcanic eruptions, to mention only a few of them. From oldest times they met anxiety and alarm in men, as they were occurring seldom enough to mean something menacing in addition to the immediate dangers they brought. Moreover, for the aurora Germany (and Central Europe) are the correct places to provoke a strong effect, as further to the North it is too often present, further to the South it is too seldom. Thus many reports from the ancient Greek and Roman chronics till late medieval descriptions exist in many coun-

tries. In this book, emphasis is laid on German sources and efforts on this exciting field of science. It is very interesting to compare the story of the phenomenon from different points of view, e.g. from a recent publication from Norway (A. Brekke) and in this book. The Wunderzeychen (miraculous signal) belief is more emphasized in Germany where it was less seen, while in Scandinavia it did not signalize necessarily something bad. Perhaps the most important part of the book is the description of the transition from these early ideas to a well-founded descriptive science in the 18th and 19th centuries, then to a physical interpretation of the phenomenon beginning with the First Polar Year in 1882—83. It is characteristic that the participation of German scientists was decisive mainly in the first half of the 19th century (Gauss, Humboldt, later Fritz, Goldstein, Wiechert).

Schröder's book is worth reading for all interested in solar-terrestrial physics, mainly for those who want to know more on the roots of this branch of science or who want to use data of earlier observations.

J Verő

- treble underlining: bold-face italics
- red underlining: Greek letters
- green underlining: script letters.

Rules for mathematical-physical notations:

- trigonometric, logarithmic, analytic symbols, symbols for units and functions are in roman type (not underlined)
- letter symbols in mathematical and physical formulas, scalars, and subscripts of algebraic and physical quantities are in italics (underlined)
- vectors, matrices, operators in probability theory are in bold-face roman type (double underlining)
- tensors, operators and some special functions are in script letters (green underlining). These cannot be bold.
- Greek letters (red underlining) cannot be bold or extra bold type (thus they cannot be used for vectors or tensors)
- void upper lines e.g. for vectors
- avoid possible confusion between o (letter) and 0 (zero), l (letter) and 1 (one), ν (Greek nu) and v , u (letters) etc.
- explain ambiguous or uncommon symbols by making marginal notes in pencil
- be careful about superscripts and subscripts
- formulae must be numbered consecutively with the number in parentheses to the right of the formula. References in text to the equations may then usually be made by the number in parenthesis. When the word equation is used with a number, it is to be abbreviated, Eq. or Eqs in the plural
- the International System of Units (SI) should be used.

Authors are liable for the cost of alteration in the *proofs*. It is, therefore, the responsibility of the author to check the text for errors of facts before submitting the paper for publication.

3. *References* are accepted only in the Harvard system. Citations in the text should be as:

- ... (Bomford 1971) ... or Bomford (1971)
- ... (Brosche and Sündermann 1976) ...
- ... (Gibbs et al. 1976b) ...

The list of references should contain names and initials of all authors (the abbreviation et al. is not accepted here); for *journal articles* year of publication, the title of the paper, title of the journal abbreviated, volume number, first and last page.

For *books* or *chapters in books*, the title is followed by the publisher and place of publication. All items must appear both in the text and references.

Examples:

Bomford G 1971: Geodesy. Clarendon Press, Oxford

Brosche P, Sündermann J 1976: Effects of oceanic tides on the rotation of the earth. Manuscript. Univ. of Bonn

Buntebarth G 1976: Temperature calculations on the Hungarian seismic profile-section NP-2. In: *Geoelectric and Geothermal Studies (East-Central Europe, Soviet Asia)*, KAPG Geophysical Monograph. Akadémiai Kiadó, Budapest, 561–566.

Gibbs N E, Poole W G, Stockmeyer P K 1976a: An algorithm for reducing the bandwidth and profile of a sparse matrix. *SIAM J. Numer. Anal.*, 13, 236–250.

Gibbs N E, Poole W G, Stockmeyer P K 1976b: A comparison of several bandwidth and profile reduction algorithms. *ACM Trans. on Math. Software*, 2, 322–330.

Szarka L 1980: Potenciáltérképezés analóg modellezéssel (Analogue modeling of potential mapping). *Magyar Geofizika*, 21, 193–200.

4. *Footnotes* should be typed on separate sheets.

5. *Legends* should be short and clear. The place of the tables and figures should be indicated in the text, on the margin.

6. *Tables* should be numbered serially with Roman numerals. Vertical lines are not used.

All the illustrations should contain the figure number and author's name in pencil on the reverse.

Figures will be redrawn. Therefore the most important point is clearness of the figures, even pencil-drawings are accepted (with a duplicate).

Photographs and *half-tone* illustrations should be sharp and well contrasted.

If a specific reduction or enlargement is required, please indicate this in blue pencil on the figure.

The editors will send information to the first author about the *arrival* and acceptance of the papers. A galley proof is also sent to the first author for *correction*. Hundred *offprints* are supplied free of charge.

Periodicals of the Hungarian Academy of Sciences are obtainable
at the following addresses:

AUSTRALIA

C.B.D. LIBRARY AND SUBSCRIPTION SERVICE
Box 4886, G.P.O., Sydney N.S.W. 2001
COSMOS BOOKSHOP, 145 Ackland Street
St. Kilda (Melbourne), Victoria 3182

AUSTRIA

GLOBUS, Höchstädtplatz 3, 1206 Wien XX

BELGIUM

OFFICE INTERNATIONAL DE LIBRAIRIE
30 Avenue Marnix, 1050 Bruxelles
LIBRAIRIE DU MONDE ENTIER
162 rue du Midi, 1000 Bruxelles

BULGARIA

HEMUS, Bulvar Ruszki 6, Sofia

CANADA

PANNONIA BOOKS, P.O. Box 1017
Postal Station "B", Toronto, Ontario M5T 2T8

CHINA

CNPICOR, Periodical Department, P.O. Box 50
Peking

CZECHOSLOVAKIA

MAD'ARSKÁ KULTURA, Národní třída 22
115 66 Praha
PNS DOVOZ TISKU, Vinohradská 46, Praha 2
PNS DOVOZ TLACE, Bratislava 2

DENMARK

EJNAR MUNKSGAARD, Norregade 6
1165 Copenhagen K

FEDERAL REPUBLIC OF GERMANY

KUNST UND WISSEN ERICH BIEBER
Postfach 46, 7000 Stuttgart 1

FINLAND

AKATEEMINEN KIRJAKAUPPA, P.O. Box 128 SF-00101
Helsinki 10

FRANCE

DAWSON-FRANCE S. A., B. P. 40, 91121 Palaiseau
EUROPÉRIODIQUES S. A., 31 Avenue de Versailles, 78170
La Celle St. Cloud
OFFICE INTERNATIONAL DE DOCUMENTATION ET
LIBRAIRIE, 48 rue Gay-Lussac
75240 Paris Cedex 05

GERMAN DEMOCRATIC REPUBLIC

HAUS DER UNGARISCHEN KULTUR
Karl Liebknecht-Straße 9, DDR-102 Berlin
DEUTSCHE POST ZEITUNGSVERTRIEBSAMT Straße der
Pariser Kommüne 3-4, DDR-104 Berlin

GREAT BRITAIN

BLACKWELL'S PERIODICALS DIVISION
Hythe Bridge Street, Oxford OX1 2ET
BUMPUS, HALDANE AND MAXWELL LTD.
Cowper Works, Olney, Bucks MK46 4BN
COLLET'S HOLDINGS LTD., Denington Estate Wellingbo-
rough, Northants NN8 2QT
WM. DAWSON AND SONS LTD., Cannon House Folkstone,
Kent CT19 5EE
H. K. LEWIS AND CO., 136 Gower Street
London WC1E 6BS

GREECE

KOSTARAKIS BROTHERS INTERNATIONAL
BOOKSELLERS, 2 Hippokratous Street, Athens-143

HOLLAND

MEULENHOF-BRUNA B. V., Beulingstraat 2,
Amsterdam
MARTINUS NIJHOFF B.V.
Lange Voorhout 9-11, Den Haag

SWETS SUBSCRIPTION SERVICE

347b Heereweg, Lisse

INDIA

ALLIED PUBLISHING PRIVATE LTD., 13/14
Asaf Ali Road, New Delhi 110001
150 B-6 Mount Road, Madras 600002
INTERNATIONAL BOOK HOUSE PVT. LTD.
Madame Cama Road, Bombay 400039
THE STATE TRADING CORPORATION OF INDIA LTD.,
Books Import Division, Chandralok 36 Janpath, New Delhi
110001

ITALY

INTERSCIENTIA, Via Mazzè 28, 10149 Torino
LIBRERIA COMMISSIONARIA SANSONI, Via Lamarmora 45,
50121 Firenze
SANTO VANASIA, Via M. Macchi 58
20124 Milano
D. E. A., Via Lima 28, 00198 Roma

JAPAN

KINOKUNIYA BOOK-STORE CO. LTD.
17-7 Shinjuku 3 chome, Shinjuku-ku, Tokyo 160-91
MARUZEN COMPANY LTD., Book Department, P.O. Box
5050 Tokyo International, Tokyo 100-31
NAUKA LTD. IMPORT DEPARTMENT
2-30-19 Minami Ikebukuro, Toshima-ku, Tokyo 171

KOREA

CHULPANMUL, Phenjan

NORWAY

TANUM-TIDSKRIFT-SENTRALEN A.S., Karl Johansgatan
41-43, 1000 Oslo

POLAND

WĘGIERSKI INSTYTUT KULTURY, Marszałkowska 80,
00-517 Warszawa
CKP-I W, ul. Towarowa 28, 00-958 Warszawa

ROUMANIA

D. E. P., Bucuresti
ILEXIM, Calea Grivitei 64-66, Bucuresti

SOVIET UNION

SOJUZPECHAT — IMPORT, Moscow
and the post offices in each town
MEZHDUNARODNAYA KNIGA, Moscow G-200

SPAIN

DIAZ DE SANTOS, Lagasca 95, Madrid 6

SWEDEN

GUMPERTS UNIVERSITETSBOKHANDEL AB
Box 346, 401 25 Göteborg 1

SWITZERLAND

KARGER LIBRI AG, Petersgraben 31, 4011 Basel

USA

EBSCO SUBSCRIPTION SERVICES
P.O. Box 1943, Birmingham, Alabama 35201
F. W. FAXON COMPANY, INC.
15 Southwest Park, Westwood Mass. 02090
READ-MORE PUBLICATIONS, INC.
140 Cedar Street, New York, N. Y. 10006

YUGOSLAVIA

JUGOSLOVENSKA KNJIGA, Terazije 27, Beograd
FORUM, Vojvode Mišića 1, 21000 Novi Sad

Acta Geodaetica, Geophysica et Montanistica Hungarica

VOLUME 21, NUMBER 3, 1986

EDITOR-IN-CHIEF

F MARTOS

ASSOCIATE EDITOR

J SOMOGYI

EDITOR

J VERŐ

EDITORIAL BOARD

**A ÁDÁM, GY BARTA, P BIRÓ, S DOLESCHALL,
L KAPOLYI, F KOVÁCS, A MESKÓ, F STEINER,
J ZÁMBÓ**



Akadémiai Kiadó, Budapest

AGGM 21 (3) 241—403 (1986) HU ISSN 0236-5758

ACTA GEODAETICA, GEOPHYSICA et MONTANISTICA HUNGARICA

A Quarterly Journal of the Hungarian Academy of Sciences

Acta Geodaetica, Geophysica et Montanistica (AGGM) publishes original reports on geodesy, geophysics and minings in English.

AGGM is published in yearly volumes of four numbers by

AKADÉMIAI KIADÓ

Publishing House of the Hungarian Academy of Sciences
H-1054 Budapest, Alkotmány u. 21.

Manuscripts and editorial correspondence should be addressed to

AGGM Editorial Office
H-9401 Sopron P.O. Box 5

Subscription information

Orders should be addressed to

KULTURA Foreign Trading Company
H-1389 Budapest P.O. Box 149

INSTRUCTIONS TO AUTHORS

Manuscripts should be sent to the editors (MTA Geodéziai és Geofizikai Kutató Intézet, AGGM Editorial Office, H-9401 Sopron, P.O.Box 5, HUNGARY). Only articles not submitted for publication elsewhere are accepted.

Manuscripts should be typewritten in duplicate, double-spaced, 25 lines with 50 letters each.

The papers generally include the following components, which should be presented in the order listed.

1. Title, name of author(s), affiliation, dateline, abstract, keywords
2. Text, acknowledgements
3. References
4. Footnotes
5. Legends
6. Tables and illustrations

1. The *affiliation* should be as concise as possible and should include the complete mailing address of the authors. The *date of receipt* of the manuscript will be supplied by the editors. The abstract should not exceed 250 words and should clearly and simply summarize the most important methods and results. 5–10 significant expressions describing the content are used as *keywords*. Authors may recommend these keywords.

2. The *text* should be generally in English and as short and clear as possible. From Hungarian authors papers are also accepted in Hungarian.

The section heading should *not* be underlined or in capitals.

Please note that underlining denotes special types:

- single underlining: italics
- double underlining: bold-face roman

CONTENTS

Equations of motion of vertically thrown and falling particles for Newton's drag law — <i>Pethő Sz</i>	241
Some questions of the economic evaluation of natural resources — <i>Faller G</i> and <i>Tóth M</i>	259
On the statistical resonance in vibratory screens and conveyors — <i>Pethő Sz</i>	265
Energy of fluid-bearing porous systems — <i>Zoltán Gy</i>	297
Energy value of changes of mass and state in porous reservoirs — <i>Zoltán Gy</i>	315
Rock model based on pore structure — <i>Bauer K</i> and <i>Balla L</i>	345
Flocculation of the Visonta lignite sludges by polyacrylamides — <i>Mrs. Lakatos Szabó J</i> and <i>Lakatos I</i>	355
A new method to calculate heat- and vapour absorption of mine air — <i>Janositz J</i>	367
Frequency of endogen mine fires as a function of coal loss and rate of advance — <i>Kovács F</i> . . .	389

PRINTED IN HUNGARY
Akadémiai Kiadó és Nyomda, Budapest

EQUATIONS OF MOTION OF VERTICALLY THROWN AND FALLING PARTICLES FOR NEWTON'S DRAG LAW

SZ PETHŐ¹

[Manuscript received September 17, 1983]

The functions distance-time, velocity-time and acceleration-time of vertically thrown solid particles in media are discussed in the paper. The effect of the medium (air or water) is analyzed in great detail. The behaviour of particles classified beforehand with respect to particle size, density and terminal settling velocity is also investigated as a function of initial velocity.

Keywords: drag force; equations of motion; Finkey's constant; initial velocity; kinematic parameters; Newton's drag law; particle size; ratio of co-sedimentation; terminal settling velocity; vertically thrown particles

Symbols

a	acceleration
c	drag coefficient
F	drag force
g	acceleration due to gravity
g_0	Finkey's constant
h	height
m	mass
s	distance
t	time
v	velocity
v_0	terminal settling velocity
V	initial velocity
x	sphere diameter
δ	solids density
γ	medium density

Subscripts

a	ascending, ascent
s	settling
t	total

¹ Technical University for Heavy Industry, Department of Mineral Dressing, H-3515 Miskolc, Hungary

1. Introduction

In theoretical investigations of mineral processing operations, terminal settling velocities have only been taken into account in the analysis of particle motion. In sedimentation and sieving, however, particles are periodically thrown by the equipment and they fall back without ever achieving their terminal settling velocities. Equations of motion of vertically thrown and upward moving particles will first be analysed in the paper, then those for the full period, i.e. for particles thrown up and falling back, will be derived. The established equations of motion enable us to investigate the effect of the medium and the behaviour of particles selected according to particle size, density and terminal settling velocity.

2. Equations of motion of particles thrown up vertically

The differential equation of the motion of a solid particle with mass m thrown in a gaseous or fluid medium with initial velocity $-V$ in the instant $t=0$ can be written (Pethő 1974, Pethő 1976)

$$m \frac{dv}{dt} = mg_0 + F, \quad (1)$$

whereas Finkey's constant depends not only on acceleration due to gravity g , but also on the density of solids δ and medium density γ (Finkey 1924):

$$g_0 = g \frac{\delta - \gamma}{\delta}. \quad (2)$$

Drag force F can be expressed for particles of spherical shape with diameter x and with drag coefficient c (Tarján 1954) as

$$F = c \frac{v^2}{2g} \frac{x^2 \pi}{4}. \quad (3)$$

In the differential equation the direction of the gravitational force has been considered positive; thus the initial velocity of the particle is $-V$.

Substituting drag force F in Eq. (1) and assuming the solid body of mass m to have a spherical shape, differential equation (1) can also be written in the form

$$\frac{dv}{dt} = g_0 \left[1 + \left(\frac{v}{v_0} \right)^2 \right]. \quad (4)$$

In differential equation (4) terminal settling velocity v_0 is (Tarján 1954)

$$v_0 = \sqrt{\frac{4g}{3c}} \sqrt{\frac{x(\delta - \gamma)}{\gamma}}. \quad (5)$$

Drag coefficient c equals 0.43 if Newton's drag law holds; thus (Tarján 1954)

$$\sqrt{\frac{4g}{3c}} = 55.$$

The solution of the differential equation gives instantaneous velocity v by taking into account the initial condition $v = -V$ at $t=0$:

$$v = v_0 \frac{v_0 \tan \frac{g_0 t}{v_0} - V}{V \tan \frac{g_0 t}{v_0} + v_0}. \quad (6)$$

At the highest point of the trajectory of the ascending solid particle we have $v=0$ and by substituting in Eq. (6), the time of ascent t_a can be calculated:

$$t_a = \frac{v_0}{g_0} \tan^{-1} \frac{V}{v_0}. \quad (7)$$

The distance travelled is

$$s = \int_0^{t_a} v dt = \frac{v_0^2}{2g_0} \ln \left(\frac{v_0}{v_0 \cos \frac{g_0 t}{v_0} + V \sin \frac{g_0 t}{v_0}} \right)^2. \quad (8)$$

Substituting (7) in Eq. (8), height of ascent s_a can be calculated:

$$s_a = \frac{v_0^2}{2g} \ln \frac{v_0^2}{v_0^2 + V^2}. \quad (9)$$

Instantaneous acceleration a becomes

$$a = \frac{dv}{dt} = g_0 \frac{v_0^2 + V^2}{\left(v_0 \cos \frac{g_0 t}{v_0} + V \sin \frac{g_0 t}{v_0} \right)^2} \quad (10)$$

and initial acceleration a_0 at instant $t=0$ is:

$$a_0 = g_0 \frac{v_0^2 + V^2}{v_0^2}. \quad (11)$$

Acceleration a_0 at the highest point of the trajectory can be calculated by substituting (7) in Eq. (10):

$$a_0 = g_0. \quad (12)$$

3. Equations of motion of vertically downward moving solid particles

After reaching the highest point of its trajectory, where the instantaneous velocity is 0, the particle starts moving downwards owing to an initial acceleration g_0 . For the downward motion instantaneous velocity v , acceleration a and distance travelled s can be written as

$$v = v_0 \tanh \frac{g_0 t}{v_0} = v_0 \left(1 - \frac{2}{e^{\frac{2g_0 t}{v_0}} + 1} \right) \quad (13)$$

$$a = \frac{g_0}{\cosh^2 \frac{g_0 t}{v_0}} = \frac{4g_0}{\left(e^{\frac{g_0 t}{v_0}} + e^{-\frac{g_0 t}{v_0}} \right)^2} \quad (14)$$

and

$$s = \frac{v_0^2}{g_0} \ln \cosh \frac{g_0 t}{v_0} = \frac{v_0^2}{g_0} \ln \frac{e^{\frac{g_0 t}{v_0}} + e^{-\frac{g_0 t}{v_0}}}{2}. \quad (15)$$

The functions distance-time, velocity-time and acceleration-time are partly given as formulated by Finkey (1924) and partly in a form more suitable for calculations. The reason for this rearrangement is that hyperbolic functions are usually not stored in pocket calculators, therefore they have to be calculated using their logarithmic expressions.

The falling particle travels the same distance, i.e. s_a until it returns to its starting position. The settling time of the particle moving in the direction of gravitational force can be calculated by making Eqs (9) and (15) equal:

$$-\frac{v_0^2}{g_0} \ln \left(\frac{v_0^2}{v_0^2 + V^2} \right)^{1/2} = \frac{v_0^2}{g_0} \ln \cosh \frac{g_0 t}{v_0}. \quad (16)$$

The negative sign is needed because the distance s_a is now travelled downwards. On rearranging the equation we have

$$t_s = \frac{v_0}{g_0} \cosh^{-1} \sqrt{1 + \left(\frac{V}{v_0} \right)^2} = \frac{v_0}{g_0} \cosh^{-1} \frac{V}{v_0} \quad (17)$$

and the same expression given by logarithmic terms

$$t_s = \frac{v_0}{g_0} \ln \left[\frac{V}{v_0} + \sqrt{1 + \left(\frac{V}{v_0} \right)^2} \right]. \quad (18)$$

The total time the particle remains in the medium can be calculated as the sum of t_a given by Eq. (7) and t_s given by Eq. (17).

The velocity v_s and acceleration a_s of the particle reaching its original position after time t_s become

$$v_s = v_0 \tanh\left(\sinh^{-1} \frac{v}{v_0}\right) = \frac{V}{\cosh\left(\sinh^{-1} \frac{V}{v_0}\right)} \quad (19)$$

and

$$a_s = \frac{g_0}{\cosh^2\left(\sinh^{-1} \frac{V}{v_0}\right)}. \quad (20)$$

The velocity of the particle falling back to its original position is smaller than both its terminal settling velocity and the velocity at which it is thrown up, while its acceleration is always smaller than g_0 . These statements can be seen and proved by Eqs (19) and (20) since it holds for the hyperbolic functions that $\tanh x < 1$ and $\cosh x > 1$ if $x > 0$.

We find from the derived equations that though the instantaneous velocity, acceleration and distance travelled according to Eqs (13), (14) and (15) are independent of initial velocity V , but the time t_s , velocity v_s and acceleration a_s of the falling particle regaining its original position according to Eqs (17), (18), (19) and (20) depend also on initial velocity.

Figure 1 illustrates $\tan^{-1} \frac{V}{v_0}$ being directly proportional to the time of ascent t_a and $\sinh^{-1} \frac{V}{v_0}$ directly proportional to the settling time t_s as functions of velocity ratio V/v_0 in the interval 0 to 5. The sum of the two functions is proportional to the total time the particle remains in the medium. Figure 1 also contains the function of this sum. The diagram indicates that the time of descent is always greater than that of the rise because the velocity of the settling particle is always below the terminal settling velocity.

Figure 2 illustrates the functions

$$\ln \frac{v_0^2 + V^2}{v_0^2}$$

proportional to the height of ascent s_a and

$$\frac{v_0^2 + V^2}{v_0^2}$$

proportional to the initial acceleration a_0 as functions of velocity ratio V/v_0 in the interval 0 to 5.

The two functions are plotted in the same diagram because there is a functional connection between the initial acceleration and the height of ascent. Comparing Eqs (9) and (11) correlation

$$s_a = \frac{v_0^2}{2g_0} \ln \frac{g_0}{a_0} \tag{21}$$

can be obtained for the height of ascent. According to the expression in Eq. (21) the correlation between the height of ascent and the initial acceleration is given by a logarithmic function.

Figure 2 shows the parabolic change of expression $1 + \left(\frac{V}{v_0}\right)^2$ proportional to the initial acceleration as a function of V/v_0 . The logarithmic function directly proportional to the height of ascent has an inflexion at $V/v_0 = 1$, i.e. if the particle is thrown at the terminal settling velocity. The function is convex from above for velocities greater than v_0 and concave for smaller velocities.

Since the logarithmic function

$$\ln \left[1 + \left(\frac{V}{v_0} \right)^2 \right]$$

proportional to the height of ascent has an inflexion at $V/v_0 = 1$, the equations of motion of a particle thrown at the terminal settling velocity will be dealt with in great detail.

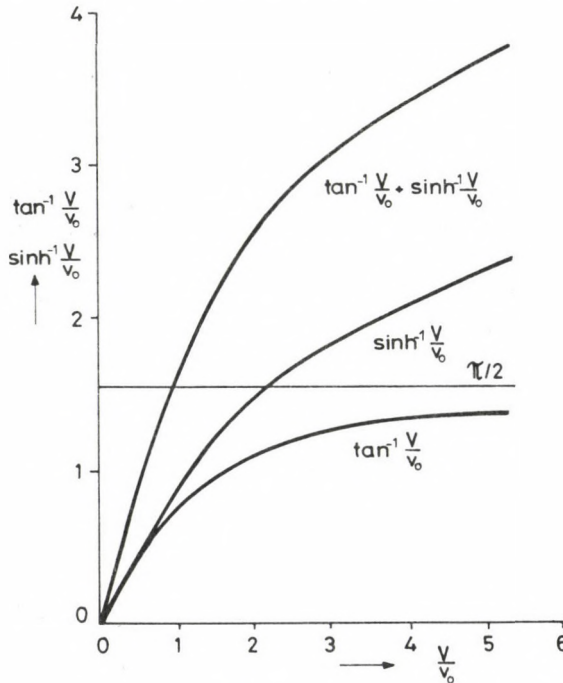


Fig. 1. Functions $\tan^{-1} \frac{V}{v_0}$ and $\sinh^{-1} \frac{V}{v_0}$ as functions of $\frac{V}{v_0}$

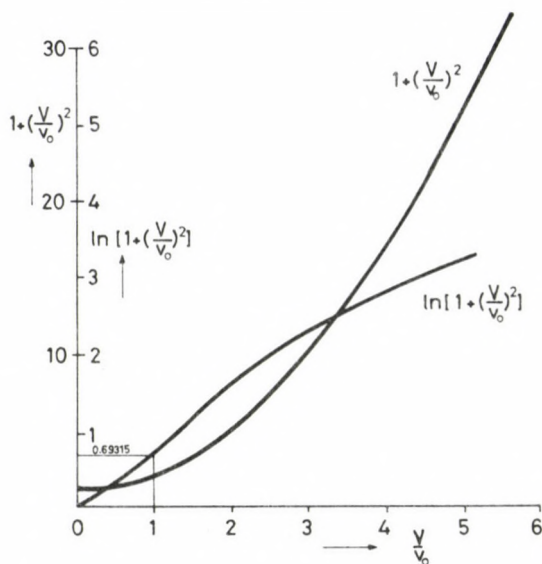


Fig. 2. Functions $1 + \left(\frac{V}{v_0}\right)^2$ and $\ln \left[1 + \left(\frac{V}{v_0}\right)^2\right]$ as functions of $\frac{V}{v_0}$

4. Equations of motion of a particle thrown at the terminal settling velocity

If $V = v_0$, i.e. the initial velocity and the terminal settling velocity are the same, the time of ascent t_a , the height of ascent s_a , the initial acceleration a_0 and the time of fall or settling t_s are

$$t_a = \frac{\pi}{4} \frac{v_0}{g_0} = 0.78540 \frac{v_0}{g_0} \quad (22)$$

$$s_a = -\frac{\ln 2}{2} \frac{v_0^2}{g_0} = -0.346575 \frac{v_0^2}{g_0} \quad (23)$$

$$a_0 = 2g_0 \quad (24)$$

$$t_s = 0.88137 \frac{v_0}{g_0} \quad (25)$$

Expressing hyperbolic functions and their inverses with exponential and logarithmic formulae, it can be proved that the velocity and acceleration of the returning particle become

$$v_s = \frac{v_0}{\sqrt{2}} = \frac{V}{\sqrt{2}} \quad (26)$$

and

$$a_s = \frac{g_0}{2}, \quad (27)$$

respectively.

5. Equations of motion as functions of medium and particle parameters

Equations of motion of vertically thrown solid particles in a medium differ from those which hold for a vacuum. The equations of motion of a rising and falling particle in a vacuum depend on initial velocity V only. The motion of a particle in a medium is affected, apart from the initial velocity, by the properties of the medium, *viz.* by its density and viscosity, by the parameters of the particle, *viz.* by its size, density and shape and finally by the drag coefficient depending on both medium and particle parameters. The parameters of the medium and of the particle have been represented in our previous equations by constants g_0 , v_0 and c . In the following discussion the equations of particle motion will be analyzed as functions of the aforementioned parameters of the medium and the particle.

On substituting Eqs (2) and (5) in Eq. (9) the height of ascent s_a can be calculated as

$$s_a = -\frac{2}{3} \frac{x\delta}{c\gamma} \ln \left[1 + \left(\frac{V}{v_0} \right)^2 \right]. \quad (28)$$

According to Eq. (28) the height of ascent is linearly proportional to the size and density of the particle and inversely to drag coefficient and the density of the medium. It is also proportional to the natural logarithm of the squared relative initial velocity. The denominator of the relative initial velocity is the terminal settling velocity expressed in terms of the aforementioned parameters x , δ , c and γ (s. Eq. 5) which modifies direct linear and inverse proportionalities found in Eq. (28).

Ratio v_0/g_0 can be found both in Eq. (7) of ascent and in Eq. (17) of settlement. The reciprocal of this ratio is also contained in several expressions. On substituting v_0 and g_0 we have

$$\frac{v_0}{g_0} = \delta \sqrt{\frac{4x}{3cg(\delta-\gamma)\gamma}}. \quad (29)$$

Thus it can be seen that the time of ascent t_a and that of settlement t_s depends on the parameters of the particle and of the medium according to Eq. (29). Apart from that, the time of ascent depends on the \tan^{-1} function of the relative initial velocity and the time of settlement depends on the \sinh^{-1} function of the relative initial velocity.

6. Some parameters of particles thrown at small initial velocity in air and water

The effect of the density of the medium on the particle motion can be investigated in accordance with initial velocity V (Káplár 1983). Our investigations—without going into details here—show that for initial velocities smaller than terminal settling velocities applied at sieving and sedimentation, the height of ascent and the length of stay generally increase with increasing density of medium. For great initial velocities, however, these parameters of particle motion decrease with increasing density of medium (Káplár 1983) and the height of ascent has a maximum as a function of density of medium.

In our following analysis the main parameters of the motion of solid particles thrown at small initial velocity V in air and water will be investigated and compared with the values obtained for a vacuum.

Table I displays the parameters of motion of galena and quartz particles thrown at an initial velocity $V=92.9455$ cm/s in air. The parameters refer to two galena and two quartz particles with densities 7.5 and 2.65 g/cm³. Particle sizes are 4 and 11.32 cm. Their ratio $11.32/4=2.83$ corresponds to that of co-settlement. This selection of densities and particle sizes enables us to investigate the motion of particles with the same densities but different particle sizes, of those with identical sizes but various densities and finally of those with equal terminal settling velocities and with various sizes and densities.

Initial velocity 92.9455 cm/s occurs in the sieving and sedimentation of coarse particles. If the amplitude of the circular motion of the sieve is 1.5 cm and the speed 10/s, the particles are thrown at initial velocity V from the sieve (Pethő and Veres 1983).

Table I illustrates terminal settling velocities v_0 , accelerations g_0 , heights of ascent s_a , times of ascent and settlement t_a and t_s , and the total length of stay t_t (being the sum of t_a and t_s) and the velocity of settlement v_s as the particle regains its original position in air.

The height of ascent of solid particles thrown at an initial velocity 92.9455 cm/s is 4.40309 cm in a vacuum, the time of ascent equals 0.094746 s, and that of settlement is

Table I. Parameters of the trajectories of vertically thrown particles in air

Parameters	Particle sizes and densities			
	$x = 4$ cm, $\delta = 7.5$ g/cm ³	$x = 11.32$ cm, $\delta = 7.5$ g/cm ³	$x = 4$ cm, $\delta = 2.65$ g/cm ³	$x = 11.32$ cm, $\delta = 2.65$ g/cm ³
v_0 , cm/s	8377.61	14093.79	4979.02	8377.61
g_0 , cm/s ²	980.83	980.83	980.52	980.52
s_a , cm	4.40358	4.40376	4.40448	4.40497
t_a , s	0.094758	0.094761	0.094781	0.094788
t_s , s	0.094760	0.097461	0.094787	0.094790
t_t , s	0.189518	0.192222	0.189568	0.189578

the same. As Table I indicates the particle with $x = 4$ cm and $\delta = 7.5$ g/cm³ reaches the shortest height of ascent, i.e. 4.40358 cm. The times of ascent and of settlement of this particle are also minimum, with 0.094578 and 0.094760 s. Maximum height and time of ascent ($s_a = 4.40497$ cm, $t_a = 0.094788$ s, $t_s = 0.094790$ s) are those of the particle with 11.32 cm and 2.65 g/cm³ and with terminal settling velocity identical with that of the previous one. The results prove that the kinematic parameters of particles moving in air and having a small initial velocity (e.g. in sieving) hardly differ from those holding in a vacuum. Further, the parameters of particles with various sizes, densities and terminal settling velocities also show only negligible differences.

The heights and times of ascent in water and for small initial velocities V (Káplár 1983), however, substantially exceed those for a vacuum. We can thus find wide differences in these parameters of the particles classified with respect to their sizes, densities and terminal settling velocities, enabling us to draw appropriate conclusions.

Table II also displays kinematic parameters of two galena and two quartz particles, but for water. Particle sizes equal 15.75 and 4 cm given the ratio of co-sedimentation

$$\frac{7.5 - 1}{2.65 - 1} = \frac{15.75}{4} = 3.93.$$

Table II contains initial accelerations a_0 , heights of ascent s_a , times t_a , t_s and t_t and returning velocities to the starting position v_s for four different initial velocities. The four initial velocities are: 92.9455 cm/s; 141.298 cm/s, corresponding to the terminal settling velocity of a quartz particle with 4 cm diameter and 2.65 g/cm³ density; 280.446 cm/s, being the terminal settling velocity of a galena particle with 4 cm diameter and 7.5 g/cm³ density or that of a quartz particle with 15.75 cm diameter and 2.65 g/cm³ density; and finally 556.627 cm/s giving the terminal settling velocity of a galena particle of 15.75 cm size and 7.5 g/cm³ density.

Using the data in Table II, the heights of ascent s_a and the lengths of stay in the medium t_t are plotted as functions of initial velocities V in Fig. 3.

Particles thrown at the same small initial velocity ascend higher in water than in air and their length of stay also exceeds that in air. Galena and quartz particles of 4 cm in diameter thrown at an initial velocity of 92.9455 cm/s ascend to a height of 4.820 cm and 5.876 cm, while they would reach a height of ascent of 4.40358 cm and 4.40497 cm in air with ratios of 1.095 and 1.334. The length of stay of the same particles in water is 0.2130 s and 0.2775 s while it is only 0.189518 s and 0.189578 s in air with ratios 1.124 and 1.464 for the lengths of stay. (The same particles, however, thrown at great initial velocities ascend higher in air than in water.)

As the data in Table II indicate, the height of ascent, the length of stay, and other kinematic parameters of the particle are strongly affected by the particle size, density and terminal settling velocity; therefore the effect of these parameters on the particle motion will be dealt with separately in great detail in the next section.

Table II. Parameters of the trajectories of vertically thrown particles in water for various initial velocities

$V,$ cm/s	$x = 4$ cm,			$\delta = 2.65$ g/cm ³			$x = 4$ cm,			$\delta = 7.5$ g/cm ³		
	$v_0 = 141.298$ cm/s,			$g_0 = 610.811$ cm/s ²			$v_0 = 280.446$ cm/s,			$g_0 = 850.2$ cm/s ²		
	a_0	s_a	t_a	t_s	t_t	v_s	a_0	s_a	t_a	t_s	t_t	v_s
92.9455	875.1	5.876	0.1346	0.1429	0.2775	77.650	943.6	4.820	0.1056	0.1074	0.2130	88.218
141.298	1221.6	11.328	0.1817	0.2039	0.3857	99.913	1066.0	10.463	0.1539	0.1599	0.3138	126.187
280.446	3017.0	26.104	0.2554	0.3324	0.5878	126.187	1700.4	32.061	0.2591	0.2907	0.5498	198.305
556.627	10089.8	45.834	0.3059	0.4811	0.7870	136.954	4199.5	73.878	0.3642	0.4739	0.8381	250.453

$V,$ cm/s	$x = 15.75$ cm,			$\delta = 2.65$ g/cm ³			$x = 15.75$ cm,			$\delta = 7.5$ g/cm ³		
	$v_0 = 280.446$ cm/s,			$g_0 = 610.811$ cm/s ²			$v_0 = 556.627$ cm/s,			$g_0 = 850.2$ cm/s ²		
	a_0	s_a	t_a	t_s	t_t	v_s	a_0	s_a	t_a	t_s	t_t	v_s
92.9455	677.9	6.710	0.1469	0.1495	0.2964	88.218	873.9	5.011	0.1083	0.1088	0.2171	91.676
141.298	765.9	14.564	0.2143	0.2225	0.4368	126.187	905.0	11.379	0.1629	0.1645	0.3272	136.954
280.446	1221.6	44.626	0.3606	0.4047	0.7653	198.305	1066.0	41.219	0.3056	0.3173	0.6228	250.454
556.627	3017.0	102.833	0.5069	0.6597	1.1666	250.453	1700.4	126.300	0.5142	0.5770	1.0912	393.595

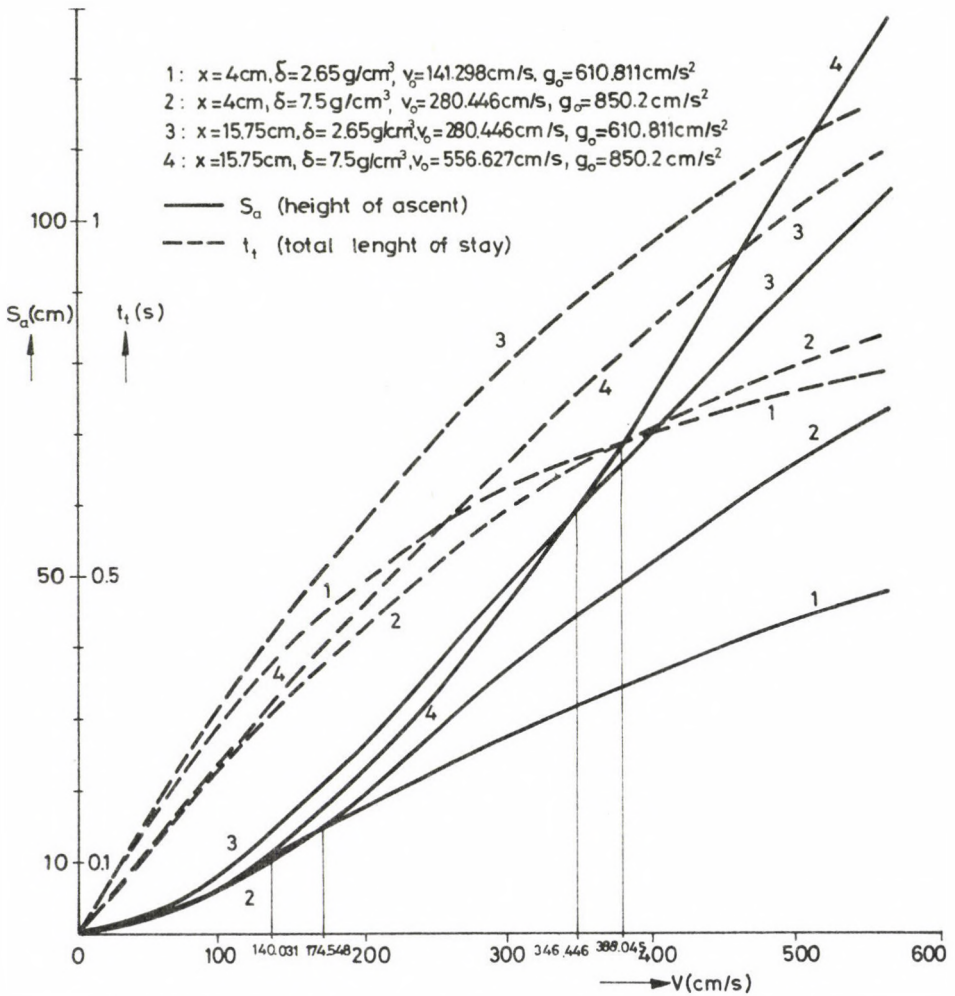


Fig. 3. Heights of ascent and lengths of stay as functions of the initial velocity

7. Comparative analysis of the motion of particles with identical size, density and terminal settling velocity

Our following analysis will focus on the comparison of the equations of motion in water of particles with identical size but different density, of those with identical density but different size and of those with identical terminal settling velocity but with different size and density. For the sake of the investigation, the ratios of the heights of ascent and of the lengths of stay will be calculated.

Let the terminal settling velocity of one particle be v_{01} , its Finkey's constant g_{01} , those of another v_{02} and g_{02} . Both particles will be thrown at the same initial velocity V . The ratios of heights of ascent r_a and of the lengths of stay in the medium r_t become

$$r_a = \frac{v_{01}^2 g_{02}}{v_{02}^2 g_{01}} \frac{\ln \frac{v_{01}^2}{v_{01}^2 + V^2}}{\ln \frac{v_{02}^2}{v_{02}^2 + V^2}} = \frac{x_1 \delta_1}{x_2 \delta_2} \frac{\ln \frac{v_{01}^2}{v_{01}^2 + V^2}}{\ln \frac{v_{02}^2}{v_{02}^2 + V^2}} \quad (30)$$

and

$$r_t = \frac{v_{01} g_{02}}{v_{02} g_{01}} \frac{\tan^{-1} \frac{V}{v_{01}} + \sinh^{-1} \frac{V}{v_{01}}}{\tan^{-1} \frac{V}{v_{02}} + \sinh^{-1} \frac{V}{v_{02}}} = \frac{\delta_1 \sqrt{x_1(\delta_2 - \gamma)}}{\delta_2 \sqrt{x_2(\delta_1 - \gamma)}} \frac{\tan^{-1} \frac{V}{v_{01}} + \sinh^{-1} \frac{V}{v_{01}}}{\tan^{-1} \frac{V}{v_{02}} + \sinh^{-1} \frac{V}{v_{02}}} \quad (31)$$

7.1 Comparative analysis of the motion of particles with identical size and different densities

The ratios of the heights of ascent r_a and of lengths of stay in the medium r_t for two particles with identical size and different densities will be

$$r_a = \frac{\delta_1}{\delta_2} \frac{\ln \frac{v_{01}^2}{v_{01}^2 + V^2}}{\ln \frac{v_{02}^2}{v_{02}^2 + V^2}} \quad (32)$$

and

$$r_t = \frac{\delta_1 \sqrt{\delta_2 - \gamma}}{\delta_2 \sqrt{\delta_1 - \gamma}} \frac{\tan^{-1} \frac{V}{v_{01}} + \sinh^{-1} \frac{V}{v_{01}}}{\tan^{-1} \frac{V}{v_{02}} + \sinh^{-1} \frac{V}{v_{02}}} \quad (33)$$

The equations and Table II enable us to draw some conclusions. Particles of greater density thrown at smaller initial velocity fail to reach the same height of ascent and length of stay in the medium as those of smaller density. Throwing the same particles at greater initial velocity, those of greater density ascend higher and stay longer in the medium. Applying, e.g. an initial velocity of 141.298 cm/s to particles of

4 cm in diameter, that of 2.65 g/cm³ density reaches a height of ascent of 11.328 cm while that of 7.5 g/cm³ density only 10.463 cm, with their ratio $r_a = 1.083$. The ratio of the lengths of stay of the same particles is $r_t = 0.3857/0.3138 = 1.229$. If the initial velocity equals 280.446 cm/s, the ratios of heights of ascent and of lengths of stay become $r_a = 26.104/32.061 = 0.814$ and $r_t = 0.5878/0.5498 = 1.069$. The ratios are identical for particles of 15.75 cm diameter if they are thrown at initial velocities of 280.446 cm/s and 556.627 cm/s. In the case of a smaller initial velocity we have $r_a = 44.626/41.219 = 1.083$ and $r_t = 0.7653/0.6228 = 1.229$, while for a greater initial velocity $r_a = 102.833/126.3 = 0.814$ and $r_t = 1.1666/1.0912 = 1.069$ hold. The ratios differ for smaller and greater particles since the initial velocity V equals the terminal settling velocity of one of the particles.

There exists an initial velocity V for which the heights of ascent of the two particles with varying densities are identical, and there is another initial velocity V for which the lengths of stay in the medium are the same. The ratios r_a and r_t now equal unity. If particles of 4 cm diameter with densities 7.5 g/cm³ and 2.65 g/cm³ are thrown at the velocity of 174.548 cm/s, the height of ascent equals 30.299 cm for both particles, while applying an initial velocity of 388.045 cm/s the lengths of stay are identical, at 0.6839 s. Throwing the two particles of 15.75 cm in diameter at an initial velocity $V = 346.446$ cm/s, they ascend to the same height of 119.320 cm.

Since particles of greater density have greater terminal settling velocities than particles of the same size but of smaller density, the velocity at which they return to the initial position v_s is also greater for particles of greater density.

7.2 Comparative analysis of the motion of particles with identical density and different sizes

Of particles with identical density and different sizes that of greater size always ascends higher and its length of stay, including the times of ascent and of settling, is also greater.

The ratios of the heights of ascent and the lengths of stay are

$$r_a = \frac{x_1}{x_2} \frac{\ln \frac{v_{01}^2}{v_{01}^2 + V^2}}{\ln \frac{v_{02}^2}{v_{02}^2 + V^2}} \quad (34)$$

and

$$r_t = \left(\frac{x_1}{x_2} \right)^{1/2} \frac{\tan^{-1} \frac{V}{v_{01}} + \sinh^{-1} \frac{V}{v_{02}}}{\tan^{-1} \frac{V}{v_{02}} + \sinh^{-1} \frac{V}{v_{01}}} \quad (35)$$

Equations (34) and (35) prove that the ratios become greater with increasing initial velocity but they approach x_1/x_2 or $(x_1/x_2)^{1/2}$ only for very great initial velocities. Ratio r_a always exceeds r_t . The data displayed in Table II also show that these ratios for particles with greater densities are smaller under otherwise identical circumstances, since the terminal settling velocities of these particles are greater.

Throwing quartz particles of 2.65 g/cm^3 density at an initial velocity of 141.298 cm/s , the ratios of the heights of ascent and of the lengths of stay for particles of 15.75 cm and 4 cm become $r_a = 14.564/11.328 = 1.286$ and $r_t = 0.4368/0.3857 = 1.133$. Applying an initial velocity of 280.446 cm/s , we have $r_a = 44.626/26.104 = 1.710$ and $r_t = 0.7653/0.5878 = 1.302$. Ratios r_a and r_t are precisely the same for galena particles of 7.5 g/cm^3 density and 15.75 cm and 4 cm diameter if the initial velocity is 280.446 cm/s and 556.627 cm/s .

Coarser particles regain their starting positions at greater velocities v_s due to their greater heights of ascent and greater terminal settling velocities.

7.3 Comparative analysis of the motion of particles with identical terminal settling velocity

Throwing particles of identical terminal settling velocity at the same initial velocity V , that of the smallest density, i.e. of greatest size, reaches the greatest height of ascent and stays for the longest time in the medium. Both the ratio of the heights of ascent and that of the lengths of stay in the medium for two particles with equal terminal settling velocity become

$$r_a = r_t = \frac{g_{02}}{g_{01}} = \frac{(\delta_2 - \gamma)\delta_1}{(\delta_1 - \gamma)\delta_2} \quad (36)$$

which means that they are equal to the ratio of Finkey's constants for the particles. Throwing a quartz and a galena particle of identical terminal settling velocity at the same initial velocity V , the height of ascent and length of stay in the medium for the quartz particle are also $850.2/610.811 = 1.392$ times those of the galena particle. The ratio of the initial accelerations a_0 of these particles is also 1.392 .

Particles of identical terminal settling velocity regain their starting position at the same velocity v_s .

8. Heights of ascent and lengths of stay as functions of the initial velocity

We have seen in the previous section that the heights of ascent and lengths of the particles investigated depend variously on their initial velocities.

As Fig. 3 indicates for initial velocities below 140.031 cm/s , a galena particle of 4 cm diameter reaches the smallest height, the coarser galena particle of 15.75 cm

diameter ascends higher than that of 4 cm, while the quartz particle of 4 cm ascends even higher and the greatest height of ascent is reached by the quartz particle of 15.75 cm. Between initial velocities 140.037 cm/s and 174.548 cm/s the sequence of the heights of ascent is: galena particle of 4 cm, quartz of 4 cm, galena of 15.75 cm and quartz of 15.75 cm. The sequence for the range 174.548 cm/s and 346.446 cm/s becomes: quartz of 4 cm, galena of 4 cm, galena of 15.75 cm and quartz of 15.75 cm. For initial velocities greater than 346.446 cm/s, we have the heights of ascent in the following sequence: quartz of 4 cm, galena of 4 cm, quartz of 15.75 cm and galena of 15.75 cm. The changes of sequence can be explained by the points of inflection or by the convex shapes in the range $V > v_0$ and by the concave ones for $V < v_0$ of the curves s_a in Fig. 3 as looked at from above. Therefore the curves in Fig. 3 intersect each other where the initial velocities equal the terminal settling velocities. Of the particles investigated, the quartz particle of 4 cm has the smallest terminal settling velocity with 141.298 cm/s. Applying small initial velocities, this quartz particle ascends higher than the two galena particles. Its curve of s_a intersects the curves of the two galena particles at the abovementioned values with increasing V . The tangent of inclination of the function becomes smaller for greater initial velocities and the quartz particle ascends less high than the two galena particles.—The curves of s_a for the galena and quartz particles with identical terminal settling velocity have their points of inflection at same place, i.e. at $V = v_0 = 280.446$ cm/s; therefore the two curves fail to intersect each other.

The curves of the length of stay are also plotted in Fig. 3 as functions of the initial velocity V . They are convex if looked at from above, and similarly to those of functions s_a , they intersect each other. As regards the relationships of the lengths of stay, there are also four sections with identical sequences for the four particles in each of the sections as they were for the heights of ascent. The only difference is in the limits of the sections for the lengths of stay which are higher than those of the sections for the heights of ascent.

Initial velocity values of the points of intersection are also indicated in Fig. 3.

Applying small initial velocities, particles of great density ascend less high and their length of stay is also shorter than that of particles with small density, irrespective of the particle size if a previous classification took place using a sieve series corresponding to the ratio of co-sedimentation. Therefore small initial velocities below the smallest terminal velocity of the various particles in the feed (in our present investigation 141.298 cm/s) are advantageous from the point of view of sedimentation. In sieving, however, greater initial velocities are required. Smaller particles now ascend less high irrespective of their densities, and reach the sieve plate more quickly; thus a stratification advantageous for sieving is achieved within the stratum of materials. A great initial velocity is also required if surface moisture is high and particles are prone to stick together.

Figure 4 illustrates the instantaneous heights of ascent and accelerations of the four particles investigated for an initial velocity of 92.9455 cm/s within a given period.

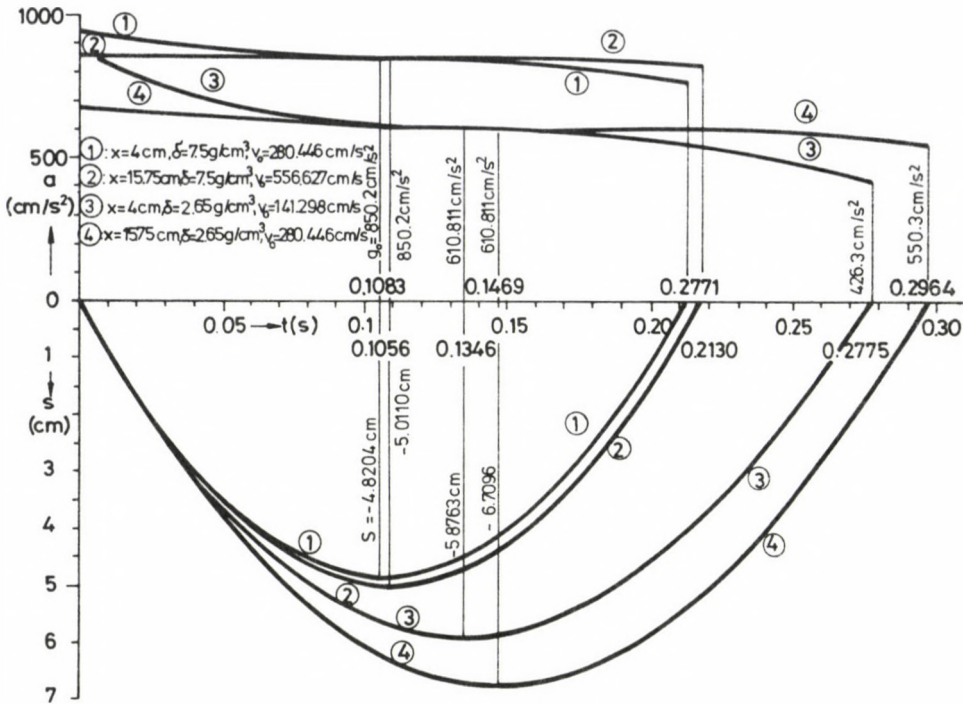


Fig. 4. Acceleration-time and distance-time functions of vertically thrown solid particles for initial velocity $V=92.9455\text{ cm/s}$

The instantaneous velocities are the tangents of inclination of the distance functions. The curves can, consequently, be regarded as the acceleration-time functions of four particles thrown by a sieve-settling machine. The figure gives the times of ascent and full lengths of stay (their differences giving the time of settlement), distances travelled and accelerations.—The figure also indicates that the curves of the two galena particles of great density run rather closely to each other; therefore there is hardly any difference in the heights of ascent and in the lengths of stay. Particles of small density have greater instantaneous velocities, heights and times of ascent and lengths of stay in the medium than those of great density. The curves of the particles with small density differ from each other more distinctly, with a greater difference in the heights of ascent, viz. $6.7096 - 5.8763 = 0.8333\text{ cm}$.

Acknowledgements

The author wishes to express his gratitude to I Raisz for carrying out the calculations and to Zs Káplár for his referee's opinion utilized in the paper.

References

- Finkey J 1924: Die wissenschaftlichen Grundlagen der nassen Erzaufbereitung. (Scientific principles of wet ore processing). Springer Verlag, Berlin
- Káplár Zs 1983: Opinion about Sz Pethő's paper "Laws of motion of vertically thrown and falling particles in medium". (In Hungarian) Manuscript
- Pethő Sz 1974: Über die statistische Resonanz. (On the statistic resonance). *Acta Geod., Geoph., Mont. Hung.*, 9, 371–382.
- Pethő Sz 1976: Remarks on the theory of the statistic resonance. (In Hungarian) *Bányászati és Kohászati Lapok—Bányászat* 109, 123–127.
- Pethő Sz, Veres Gy 1983: Principles and equipment of classification at great particle size. (In Hungarian) *Építőanyag*, 35, 161–167.
- Tarján G 1954: Ore processing. (In Hungarian) Tankönyvkiadó, Budapest

SOME QUESTIONS OF THE ECONOMIC EVALUATION OF NATURAL RESOURCES

G FALLER¹ and M TÓTH²

[Manuscript received July 18, 1984]

Natural resources of limited availability should be exploited by taking into account both their efficiency of utilization and *in-situ* national value. A method is presented to determine the optimum production value of domestic raw materials, depending on the specific costs and expenditures.

Keywords: economic evaluation; expenditure; mineral resources; optimum production; specific costs

Natural resources—among them non renewable mineral sources and renewable soils—are generally characterized by being at disposal in limited quantities, meaning that the quantity of products made from them is limited, too.

Besides, the sources have different natural properties and, as a consequence, their utilization is of different economy even by applying technology of the same level. On the other hand, the products of the processing industry can be manufactured in virtually unlimited quantities and independently of the natural conditions.

It follows from the different features of the natural resources and their limited availability that compared to the price of products of the processing industry, established generally at the level of average production costs, the movement of the costs of natural resources is different. The prices may reveal a permanent deviation from these costs. (The indispensable natural resources with less favourable properties which are necessary for the satisfaction of demands are determined today by the mass marginal costs.) Compared to that, the resources with more favourable properties may be characterized through marginal costs, being independent of technological and economic conditions, offering a significant advantage and a good basis for the economic evaluation of natural resources.

The efficiency of the utilization of certain natural resources at the level of the national economy is the proportion of the prospective production value of the product (the cost limit determined by marginal costs) and the production costs expectable on the basis of optimum technology, while the *in-situ* national value is a discounted summarized value of the production values and costs at the time of evaluation.

The high number, mansidedness and interrelated character of the factors influencing the value of natural resources at the level of the national economy including

¹ Ministry of Industry, Budapest, Mártírok útja 85, 1024, Hungary

² Union of Mining, Budapest, Arany J. u. 10. 1051, Hungary

the effects of the modernization of production and application technologies and those of the economic environment make it obvious that a constant evaluation of the natural resources may be realized within a system, integrated into the national economy as a whole, interrelated with the optimization of the whole production structure, considering the infrastructural and social implications.

When ranking the resources of the different new materials and those of the processing industry according to the specific input and on integrating the resource-elements according to resource groups, the results may be presented in a system where the abscissa is the possible produced quantity at a future date and the ordinate is the specific expenditure. As a result, we generally obtain a related steep curve for the natural resources and a flat one for the products of the processing industry.

An absolutely simplified and merely symbolic model of this consideration is demonstrated in Fig. 1, where curve *a* represents domestic mineral resources, curve *b* domestic agricultural raw materials, curve *c* the products of the processing industry and curve *d* the integrated production possibilities of all aforementioned at the future date in question.

When considering with a preliminary character the possibilities of social resources and the purposes of economic policies, designating the total planned material requirements of the country at the future date in question and projecting this point into the curve integrating possible resources and placing the crossing point at the ordinate, the horizontal projecting line intersects the optimum production volumes of the individual resource-groups from their integrated curves and defines the specific cost-limits for the individual sources on the ordinate.

The difference between optimum production volume and domestic requirements for the individual groups of resources with a positive sign gives the advisable volume of exports and with a negative sign that of imports. For products not figuring in international trade—like water—the level of domestic production is determined by the domestic requirements as a programme level.

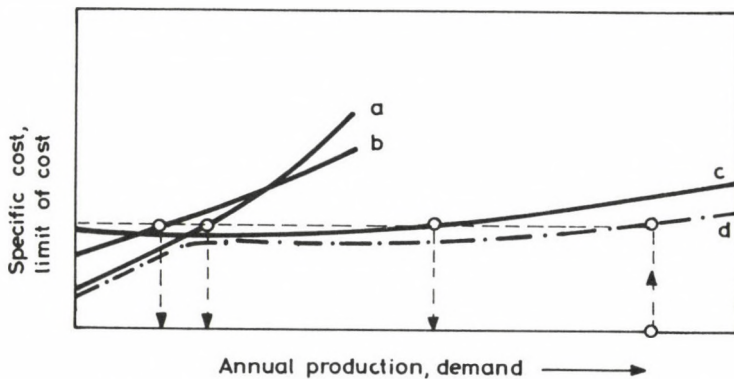


Fig. 1. Simplified model for optimization of production structure

The optimum volume of the individual groups of sources, calculated in the described manner may be modified by other factors or limits, missing from the function to a higher or lower extent in some cases even significantly. The prospective production structure of a country, its optimization and definition of the optimum utilization of the natural resources represent a very complicated iteration programming task with the purpose of achieving the most efficient allocation of the social resources for the total verticuum rendered complex by interrelations.

Interrelated with this highly complicated task the described model demonstrates only the methodological basic principle of programming, the very thought that the optimum of the utilization of natural resources with different properties is to be determined by the crossing point of the resources classified on the basis of specific costs—depending on its level and steepness through the nearly horizontal line of expenditures for the products of processing industry.

By scheduling curves *a* and *b* of Fig. 1 which integrate the import sources calculated on the basis of specific costs referred to product unit of identic utilization value, we may plot the model according to Fig. 2.

The continuous curve of Fig. 2 (the curve of resources) may be gained from the resources at the period in question, it shows the resources integrated as a function of the specific expenditures referred to the similar utilization value and the vertical noncontinuous line represents the demand at the period in question. The crossing point of the resource-curve and demand reveals the marginal costs of the natural resources involved on the ordinate, determining the cost limit at the period (the vertical distances between the line projecting the cost limit on the ordinate and the resource's curve represent the added value of the individual resources).

The level and steepness of the continuous line and, as a consequence, the marginal costs defined by the crossing point of the two lines, the limits of costs depend on the following factors:

- possible scale and expenditures of the expansion of the production of natural resources and putting the new ones into production
- possible scale and expenditures of replacing the products of resources with other domestic ones or imported ones in an equivalent way

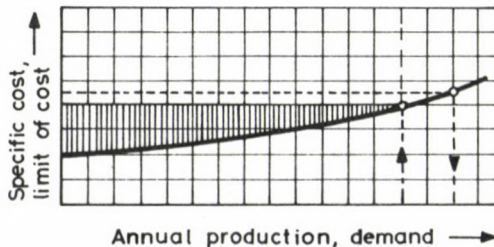


Fig. 2. Cost limit of natural resources production at a given time

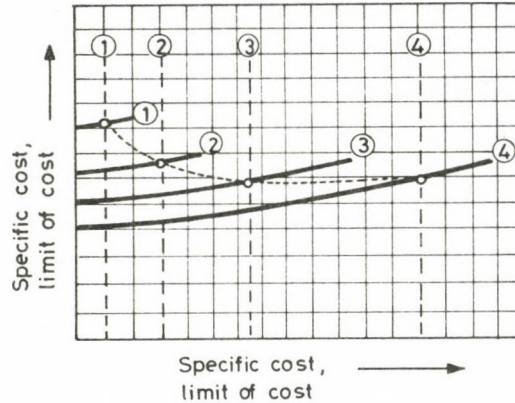


Fig. 3. Temporal changes of the cost limit of natural resources

- re-utilization of the products of the resources, the expected rate and expenditures
- possible modification of the increment of requirements.

A decreasing level of the curve of resources in the sequence of periods is obvious because of the expansion of the quantity of resources as a result of the previously described possibilities and the decrease in specific expenditures, expressed at unchanged value of money, resulting from the increasing economic efficiency of the production value of the processing industry. At the same time, we may observe an increasing demand generally at an accelerating pace.

When plotting the curves of resources and related demands for certain periods on this basis (for example half centuries) we obtain Fig. 3.

On the basis of the previous considerations this hypothetical model which may be considered more or less typical and the expenditure levels are signalized by the connecting dotted curve revealing initially a decreasing trend for the expenditure level at certain periods, being followed by a moderate decrease and increase.

When considering the non-replaceable products of natural resources (like water) the rise after the deepest point of the expenditure is steeper and with the possibility of a high volume replacement, as a result of the technological development with related favourable costs, the curve connecting the expenditure volumes does not show any rise but a further decrease. This may be the case for the replacement of expensive coal, of expensive hydrocarbons by fissioning materials or fusion energy.

The costs' limit of smaller periods within bigger time intervals may naturally differ from those, demonstrated on the levelled off model in Fig. 3. So, e.g. after an especially successful geological and industrial R and D period—as it was the case in the middle of century on the field of the energy-carriers on account of the ample supply of hydrocarbons—we may observe a significant decrease of the curve of sources and consequently that of the world market price, corresponding to the costs'

limits, so as an effect—as it happened in the 1960-s concerning the coal and nuclear energy—the rhythm of $R + D$ is more moderate. This is the reason for moderate decrease of the level of the curve of sources in the following period, on the other hand there is an exaggerated increase of the requirement, determined by a higher demand as a result of lower prices. Thus the level of the costs' limit (the world market price), defined as the crossing point of the two lines—as it happened in the 1970-s—shows an increase because of two reasons. This circumstance—as it may be experienced for example in the present days, too—has its effect in the opposite direction because of speeding up the rhythm of $R + D$ and lowering the scale of the increase of demand. So—in a more moderate way—we may reckon with a period of decrease of prices. The equalized generatrix of the periodical changes, transformed up in certain cases with monopolistic and political factors in the theoretical model, demonstrated in Fig. 3, respectively the slight continuous decrease of prices, characterized with dotted line. (The prices are significantly influenced by the very fact, too, that the existing consumers may “bear” higher prices than the new ones, applicable for replacement, consumption of raw materials; but requiring investments.)

It was previously mentioned that the properties of the natural resources basically determine the requirements for exploitation and processing and, for that matter, the economic parameters of the production of the endproduct of the production verticuum of the raw materials to be considered as homogeneous.

In the course of the correlation and heuristic functions revealing numerical connections between the *in-situ* natural properties of primary raw materials and ultimate raw materials, we have to avail ourselves of a great many abstractional simplifications and abstractions in order to ensure identical bases and comparability. So we assume for example, a processing factory on the natural resource, similarly up-to-date technologies, prices and wages, the same bank rate and currency of a steady value.

Quite rough estimates of the investigation on this basis are shown on the nomogram of Fig. 4 representing the expenditures for the production of the endproduct as electric energy and metal in dollars at the 1982 rate with a lot of simplification as a function of the proportion of depth and thickness of coal-mines, the degree of the tectonic effects, primary danger, specific weight and heating value of the products and the metal content.

The application of the nomogram is shown by the dotted lines and arrows.

According to the nomogram the costs of the production of 1 kWh electric energy on the basis of a coal mine, situated at a depth of 100 meters, being 10 meter thick, not very tectonic with a heating value of 20000 kJ/kg, amount to 2 cents. If an other coal mine is situated at a depth of 500 meters, strongly tectonized and the heating value is only 10000 kJ/kg, the costs of the produced electric energy will be close to 5 cents/kWh.

In a similar way, we may learn from the figure the costs for metals produced from ores with different properties.

When knowing the natural properties of the mines, which are recently established, being in the phase of building or planned to be established in other countries, we may state on the basis of the knowledge of costs, calculated with the nomogram the relationship of our own projects for establishing mines with the mines of the same destination all over the world and check in an indirect way the economic advisability of our own consideration related to establishing mines.

In the knowledge of the exploitation costs determined by the natural properties of the prospective sources and the transport costs which may be easily calculated as the function of the distances between the different countries by the aid of the nomogram, the extent to which an international integration or the exports and imports of raw materials is possible, can also be determined.

The examinations carried out on the basis of the described methodological principles may thus promote the optimum exploitation and utilization of the natural resources including the mineral ones—both on international and domestic levels.

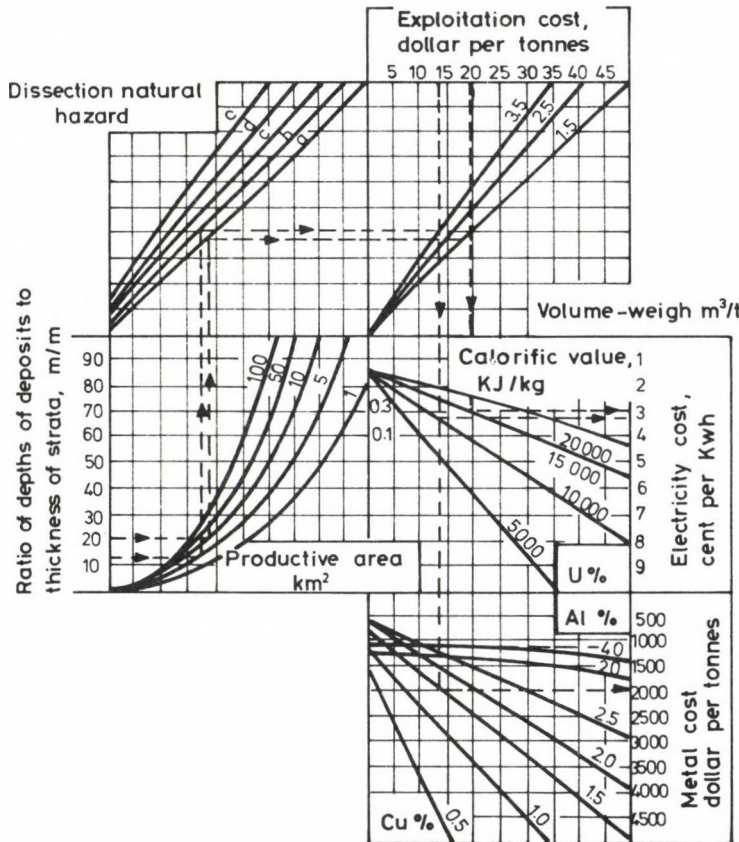


Fig. 4. Ultimate product cost in function of the natural endowments of sites

ON THE STATISTICAL RESONANCE IN VIBRATORY SCREENS AND CONVEYORS

SZ PETHŐ¹

[Manuscript received May 23, 1984]

If screens, vibratory conveyors, jig washers are operated according to the laws of statistical resonance, the time of one stroke of the machines (or its integer multiples) and the time spent in the medium by the thrown particle are exactly the same. The paper deals with the characteristic parameters of the statistical resonance. Following parameters are analyzed: ratio of the acceleration of the equipment to the acceleration due to gravity, the angle of the mechanism at the instant of throw, the distance travelled by the particle during one stroke, its velocity and the inclination of the path when the particle hits the screen panel. These parameters were investigated as functions of the dip of the screen panel, angle of the throw of the particle and its initial velocity.

By applying the equations deduced here the capacity of the equipment and the sharpness of separation of the screens can be influenced, thus present formulas can be used both in planning and operation.

Keywords: angle of impact; angle of throw; initial velocity; length of stay; relative acceleration; statistical resonance; vibratory conveyor; vibratory screen

Symbols

c	centrifugal force acting on a particle of unit mass
g	acceleration due to gravity, gravitational force acting on a particle of unit mass
$K = r\omega^2/g$	relative acceleration
v_s	velocity of the particle in the plane of the screen
O	origin
y	varying part of the relative acceleration; ordinate
S_{\perp}	distance travelled per stroke at normal throw
r	radius in circular motion
Q	impact point of the particle on the screen
s_s	distance travelled per stroke in the plane of screen
T_s	time of stroke
T_p	length of stay
t_1	time at which the particle is thrown from the screen
V	initial velocity
V_Q	impact velocity
$V_{Q\perp}$	normal component of the impact velocity
α	angle of screen dip
β	angle of throw
γ	angle of tangent to the particle path in the point of impact
δ	angle of impact
ω	angular velocity
x	horizontal coordinate
y_1	ordinate of the path of the particle
y_2	ordinate of the straight line representing the screen panel

¹ Technical University for Heavy Industry, Miskolc, H-3515, Hungary

Indices

<i>as</i>	ascent
<i>max</i>	maximum
<i>n</i>	negative
<i>p</i>	positive
<i>Q</i>	referring to impact
\perp	normal
<i>i</i>	intersection
<i>infl</i>	inflexion
<i>min</i>	minimum
<i>c</i>	collision
<i>o</i>	referring to throw at $\beta=0^\circ$

1. Introduction

If screen equipment, vibratory conveyors, jig washers are operated according to the laws of statistical resonance, the time of one stroke of the machine (or its integer multiple) corresponds exactly to the time spent in the medium by the thrown particle, therefore in the moment of the impact, the particle is thrown again up. The capacity of machines operated so is a maximum, their wear is the possible minimum, and the separation sharpness of the screens is optimum (Schubert 1975).

The phenomenon studied here, namely the equality of the period of the equipment with the period of the particles' motion, is called statistical resonance in theory and practice of mineral dressing. This name is evidently incorrect (Káplár, personal communication, 1984).

In the deduction of the laws of statistical resonance, a vacuum is supposed. The laws can be, however, applied also for air, since for the relatively short distances the particles need about equal times in a vacuum and in air (Tarján 1954, Pethő 1974, Pethő 1984).

For the value of the basic quantity of the statistical resonance, i.e. the ratio of the acceleration of the equipment to the acceleration due to gravity, a value of $(\pi^2 + 1)^{1/2} \approx 3.3$ was given (Tarján 1954, Schubert 1975). To obtain this value, a horizontal screen panel and a vertical throw of the particle is assumed, therefore it has a limited validity only. The necessary relative acceleration may deviate from 3.3 significantly in both directions if either the dip of the screen panel or the angle of the particle's throw differs from the mentioned values. Other parameters of the statistical resonance, i.e. the angle of the driving mechanism at the instant of throwing the particle, the distance travelled by the particle during one stroke, its velocity and impact angle of the path of the particle when hitting the screen panel, influence significantly the capacity of the equipment, and in case of screens, the sharpness of separation. All these considerations require thorough and detailed analyses.

The formulas deduced in the paper can also be used with minor modifications if the equipment is operated outside of the validity of the statistical resonance.

In the following the parameters of the statistical resonance are deduced separately for equipment with positive and negative dips, then the parameters will be investigated as functions of the screen dip, and the angle and initial velocity at the instant of throwing the particles.

**2. Parameters of the statistical resonance
in equipment with negative dip**

In Fig. 1, the screen panel or conveyor with a dip α is denoted by an oblique straight line. The particle is thrown from this panel at an angle of β with an initial velocity V . The origin of the system of coordinates O is in the point of the throw on the panel. The figure also shows the path and the impact point Q of the thrown particle. According to the basic condition of the statistical resonance, the throw and the impact occurs in identical positions of the screen panel, therefore the screen panel of a dip α can be represented by a single oblique straight line. Figure 2 contains the forces acting on the thrown particle and their components normal to the screen panel. The force $c = r\omega^2 \cos \omega t$ acting on a particle with unit mass is transmitted by the driving mechanism of the screen. g is the acceleration due to gravity. The components of c and g normal to the screen panel are c_{\perp} and g_{\perp} , respectively. The particle leaves the panel at the moment t_1 in an angle ωt_1 ,

$\alpha = 30^\circ$	$y_a = -1.8214 \text{ cm}$	$\bar{\tau} = 114.8961^\circ$
$\beta = 45^\circ$	$x_a = 3.1547 \text{ cm}$	$\delta = 35.1039^\circ$
$\frac{V^2}{2g} = 1 \text{ cm}$	$OQ = 3.6427 \text{ cm}$	$T = 0.1007 \text{ s}$
$V = 44.2945 \text{ cm/s}$	$y_{as} = 0.5000 \text{ cm}$	

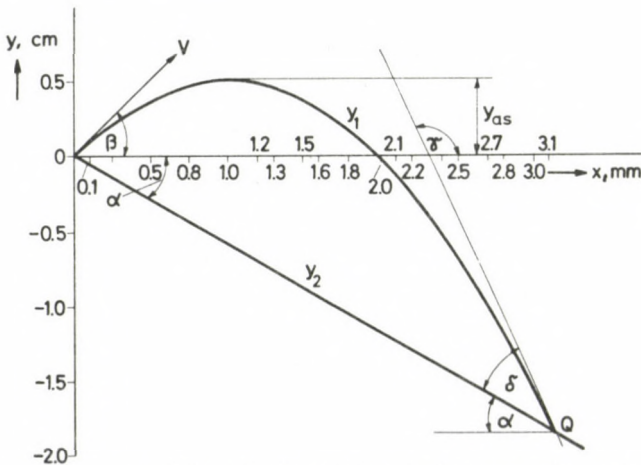


Fig. 1. Parameters of the path of a particle and of a screen with negative dip

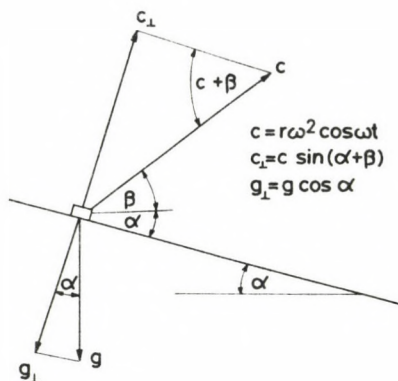


Fig. 2. Forces acting on a particle of unit mass on the equipment with a dip of α

$$\cos \omega t_1 = \frac{g}{r\omega^2} \frac{\cos \alpha}{\sin(\beta + \alpha)} = \frac{1}{K} \frac{\cos \alpha}{\sin(\beta + \alpha)}. \quad (1)$$

In that moment the initial velocity V is equal to the velocity of the equipment:

$$V = r\omega \sin \omega t_1. \quad (2)$$

The equations of the path of the particle and that of the straight line with a dip of α are:

$$y_1 = \tan \beta x - \frac{g}{2V^2 \cos^2 \beta} x^2 \quad (3)$$

and

$$y_2 = (-\tan \alpha)x \quad (4)$$

respectively.

The straight line has a negative tangent as seen in Fig. 1. The angle in the figure is namely in the fourth quadrant, and as $\tan(360^\circ - \alpha) = -\tan \alpha$, thus the equation of the straight line is that in Eq. (4). Due to this negative sign, screening or conveying in the direction of the dip, as shown in the figure will be called in the following screening or conveying with a negative dip. (The direction in the figure indicates the general situation.)

Using the two previous equations, the coordinates of the impact point Q , x_Q and y_Q can be calculated from the condition $y_1 = y_2$:

$$x_Q = \frac{2V^2}{g} (\tan \beta + \tan \alpha) \cos^2 \beta \quad (5)$$

and

$$y_Q = -\frac{2V^2}{g} (\tan \beta + \tan \alpha) \tan \alpha \cos^2 \beta. \quad (6)$$

The distance $\overline{OQ} = s_s$ in the plane of the screen panel travelled in one stroke, is:

$$s_s = \frac{x_Q}{\cos \alpha} = \frac{2V^2}{g} \frac{\tan \beta + \tan \alpha}{\cos \alpha} \cos^2 \beta. \tag{7}$$

The time T_p necessary for this path can be determined if the coordinate y_Q is also expressed from the law of free fall:

$$y_Q = V \sin \beta T_p - \frac{g}{2} T_p^2. \tag{8}$$

By making Eqs (6) and (8) equal, the time T_p is found from a quadratic equation. Only one of its roots is positive, thus the length of stay for the path T_p becomes

$$\begin{aligned} T_p &= \frac{V \sin \beta}{g} \left[1 + \sqrt{1 + 4(\tan \beta + \tan \alpha) \tan \alpha \cot^2 \beta} \right] = \\ &= \frac{2V}{g} \cos \beta (\tan \beta + \tan \alpha). \end{aligned} \tag{9}$$

In the point of impact Q , the tangent of the path is $\tan \gamma$. This tangent can be calculated from the following equation:

$$\tan \gamma = \frac{\left(\frac{dy}{dt}\right)_Q}{\left(\frac{dx}{dt}\right)_Q} = \frac{V \sin \beta - g T_p}{V \cos \beta} = \tan \beta - \frac{g}{V \cos \beta} T_p. \tag{10}$$

By substituting length of stay T_p one gets:

$$\begin{aligned} \tan \gamma &= -\tan \beta \sqrt{1 + 4(\tan \beta + \tan \alpha) \tan \alpha \cot^2 \beta} = \\ &= -(\tan \beta + 2 \tan \alpha). \end{aligned} \tag{11}$$

According to this equation, the angle γ is in case of screening with a negative dip always obtuse. Its value does not depend on the initial velocity V , it depends only on the dip of the screen α and on the angle β of the throw of the particle.

From the point of view of screening technology, the impact angle δ is of special importance. δ is the angle between the plane of the screen panel and the tangent of the path of the particle in the impact point.

According to Fig. 1 $\delta = 180^\circ - \alpha - \gamma$. Taking into account the previous formula for $\tan \gamma$, one gets:

$$\tan \delta = \tan [(180^\circ - \alpha) - \gamma] = \frac{\tan \beta + \tan \alpha}{1 + \tan \beta \tan \alpha + 2 \tan^2 \alpha}. \tag{12}$$

An analysis of this function shows that the impact angle is less than 90° . $\delta = 90^\circ$ is valid only for a horizontal screen panel and for $\beta = 90^\circ$. This function will be analyzed in more detail in the following as the impact angle has great significance.

For the deduction of the basic formulas of the statistical resonance, the time of one stroke of the screen equipment is written as

$$T_{st} = \frac{2\pi}{\omega}. \quad (13)$$

By substituting the initial velocity V from Eq. (2) into Eq. (9) of the travel time and putting T_i and T_p equal, we obtain

$$\frac{2\pi}{\omega} = \frac{r\omega}{g} \sin \omega t_1 \sin \beta [1 + \sqrt{1 + 4(\tan \beta + \tan \alpha) \tan \alpha \cot^2 \beta}] \quad (14)$$

and

$$\sin \omega t_1 = \frac{1}{K} \frac{2\pi}{\sin \beta [1 + \sqrt{1 + 4(\tan \beta + \tan \alpha) \tan \alpha \cot^2 \beta}]} \quad (15)$$

By using $\sin^2 \omega t_1 + \cos^2 \omega t_1 = 1$, parameter K can be obtained from Eqs (1) and (15) ($K = r\omega^2/g$):

$$K = \sqrt{\frac{(2\pi)^2}{\sin^2 \beta [1 + \sqrt{1 + 4(\tan \beta + \tan \alpha) \tan \alpha \cot^2 \beta}]^2} + \frac{\cos^2 \alpha}{\sin^2(\alpha + \beta)}} \quad (16)$$

Calculating $\tan \omega t_1 = \sin \omega t_1 / \cos \omega t_1$ and taking into account Eqs (1) and (15), the tangent of the angle at the instant of throw can be calculated as

$$\tan \omega t_1 = \frac{2\pi \sin(\alpha + \beta)}{\sin \beta \cos \alpha [1 + \sqrt{1 + 4(\tan \beta + \tan \alpha) \tan \alpha \cot^2 \beta}]} \quad (17)$$

Both these equations can be written in simpler forms. By carrying out the operations in the denominator of the first term of Eq. (16):

$$\frac{1}{\sin^2 \beta [1 + \sqrt{1 + 4(\tan \beta + \tan \alpha) \tan \alpha \cot^2 \beta}]^2} = \frac{1}{4} \frac{\cos^2 \alpha}{\sin^2(\beta + \alpha)} \quad (18)$$

By expanding $\sin(\alpha + \beta)$ in the numerator of Eq. (17), and carrying out the operations, one has:

$$\frac{2 \sin(\alpha + \beta)}{\sin \beta \cos \alpha [1 + \sqrt{1 + 4(\tan \beta + \tan \alpha) \tan \alpha \cot^2 \beta}]} = 1 \quad (19)$$

On substituting Eq. (18) into Eq. (16), and Eq. (19) into Eq. (17), the value of K becomes

$$K = \frac{\cos \alpha}{\sin(\beta + \alpha)} \sqrt{\pi^2 + 1} \quad (20)$$

and

$$\tan \omega t_1 = \pi \quad (21)$$

Thus the angle of the driving mechanism in the moment of the throw is:

$$\omega t_1 = \tan^{-1} \pi = 72.3432^\circ . \tag{22}$$

According to these basic formulas of the statistical resonance, the relative acceleration K according to Eq. (20) is the product of the constant $(\pi^2 + 1)^{1/2} \cong 3.3$, and a variable quantity $\cos \alpha / \sin (\beta + \alpha)$, depending on the dip of the screen and on the angle of throw. The angle ωt_1 of the driving mechanism when the throw occurs, is according to Eq. (22) a constant value, $\tan^{-1} \pi$.

The initial velocity V is in case of statistical resonance:

$$V = r\omega \frac{\pi}{\sqrt{1 + \pi^2}} = 0.9529 r\omega . \tag{23}$$

This equation shows the initial velocity V to be the product of the constant containing π and $r\omega$. The initial velocity does not depend on the dip α of the screen panel and on the angle β of the throw of the particle.

The velocity V_Q of the particle in the impact point Q can be obtained from the equation

$$V_Q^2 = (V \cos \beta)^2 + (V \sin \beta - g T_p)^2 . \tag{24}$$

According to Eq. (9), the impact velocity V_Q is by substituting T_p :

$$\begin{aligned} V_Q &= V \sqrt{\cos^2 \beta + [\sin \beta - 2(\tan \beta + \tan \alpha) \cos \beta]^2} = \\ &= V \cos \beta \sqrt{1 + (\tan \beta + 2 \tan \alpha)^2} . \end{aligned} \tag{25}$$

The component $V_{Q\perp}$ of this velocity normal to the screen panel becomes

$$V_{Q\perp} = V_Q \cos (90^\circ - \delta) = V_Q \sin \delta = V_Q \sin (\gamma + \alpha) . \tag{26}$$

2.1 Parameters of screening with negative dip in case of normal throw

The excitation of electromagnetic vibrators with angle of dip α is normal to the screen panel. The particles are also thrown in the direction of the excitation, i.e. perpendicularly to the screen panel. Vibratory conveyors are often operated similarly.

In the special case investigated $\beta = 90^\circ - \alpha$. Accordingly, the throw happens at an angle of the driving mechanism:

$$\cos \omega t_1 = \frac{g}{r\omega^2} . \tag{27}$$

The thrown particle is displaced in the plane of the screen panel by a distance of

$$s_s = \frac{2V^2}{g} \frac{\sin \alpha}{\cos^2 \alpha} . \tag{28}$$

The time T_p of the flight is:

$$T_p = \frac{V \cos \alpha}{g} [1 + \sqrt{1 + 4(1 + \tan^2 \alpha) \tan^2 \alpha}] = \frac{2V}{g \cos \alpha}. \quad (29)$$

In the impact point the tangent of the path $\tan \gamma$ and that of the impact $\tan \delta$ are:

$$\tan \gamma = -\cot \alpha \sqrt{1 + 4(1 + \tan^2 \alpha) \tan^2 \alpha} = -\left(\frac{1}{\tan \alpha} + 2 \tan \alpha\right) \quad (30)$$

$$\tan \delta = \frac{1}{2 \tan \alpha}. \quad (31)$$

The relative acceleration K and the angle of the throw ωt_1 , characterizing statistical resonance, are

$$K = \cos \alpha \sqrt{\pi^2 + 1} \quad (32)$$

and

$$\omega t_1 = \tan^{-1} \pi = 72.3432^\circ. \quad (33)$$

According to Eq. (32), parameter K is solely a function of $\cos \alpha$, neglecting constant $(\pi^2 + 1)^{1/2}$. The impact velocity V_Q is:

$$V_Q = V \cos \alpha \sqrt{\tan^2 \alpha + (1 + 2 \tan \alpha)^2}. \quad (34)$$

3. The parameters of the statistical resonance in case of equipment with positive dip

The straight line in Fig. 3 denoting the screen panel makes an acute angle with the horizontal axis of the system of coordinates. The origin of the coordinate system is also here in the point of the throw of the particle. The figure shows that the particle can leave the screen panel only if $\beta > \alpha$.

The angle ωt_1 of the driving mechanism at the instant of throwing the particle can be obtained from the equality $c_\perp = g_\perp$

$$\cos \omega t_1 = \frac{g}{r\omega^2} \frac{\cos \alpha}{\sin(\beta - \alpha)} = \frac{1}{K} \frac{\cos \alpha}{\sin(\beta - \alpha)}. \quad (35)$$

In the case investigated the equation of the straight line is $y = \tan \alpha x$, i.e. the tangent is positive. The equation of the flight path has already been given by Eq. (3). Due to the positive tangent, screening and conveying indicated in Fig. 3 is of positive dip.

The displacement of the particle in the plane of the screen panel $\overline{OQ} = s_s$ is:

$$s_s = \frac{2V^2}{g} \frac{\tan \beta - \tan \alpha}{\cos \alpha} \cos^2 \beta. \quad (36)$$

$\alpha = 15^\circ$ $y_a = 0.3929 \text{ cm}$ $\gamma = 129.8961^\circ$
 $\beta = 60^\circ$ $x_a = 1.4641 \text{ cm}$ $\delta = 54.8961^\circ$
 $\frac{V^2}{2g} = 1 \text{ cm}$ $OQ = 1.5158 \text{ cm}$ $T = 0.0480 \text{ s}$
 $V = 44.2945 \text{ cm/s}$ $y_{as} = 0.7500 \text{ cm}$

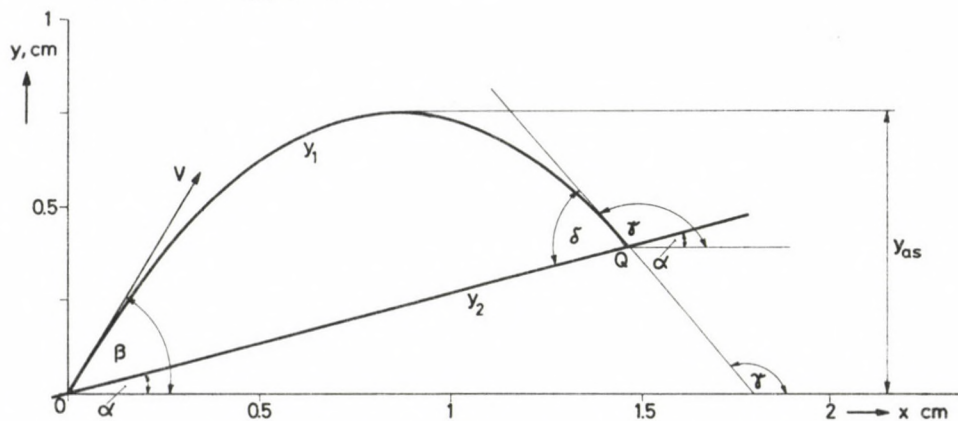


Fig. 3. Parameters of the path of a particle and of a screen with positive dip

The time between throw and impact, i.e. the time of flight T_p is:

$$\begin{aligned}
 T_p &= \frac{V \sin \beta}{g} [1 + \sqrt{1 - 4 \tan \alpha (\tan \beta - \tan \alpha) \cot^2 \beta}] = \\
 &= \frac{2V}{g} \cos \beta (\tan \beta - \tan \alpha).
 \end{aligned}
 \tag{37}$$

In the point of impact the tangent of the path of the particle $\tan \gamma$ and that of impact $\tan \delta$ are:

$$\tan \gamma = -\tan \beta \sqrt{1 - 4 \tan \alpha (\tan \beta - \tan \alpha) \cot^2 \beta} = -(\tan \beta \pm 2 \tan \alpha) \tag{38}$$

and

$$\tan \delta = \tan [(180 + \alpha) - \gamma] = \frac{\tan \beta - \tan \alpha}{1 - \tan \beta \tan \alpha + 2 \tan^2 \alpha} \tag{39}$$

Parameter K characterizing statistical resonance and angle ωt_1 will also be determined here by using the values of $\sin \omega t_1$ and $\cos \omega t_1$. The value of K can be obtained from the condition of the throw of the particle (Eq. 35). The latter can be calculated from the equality of the times T_p , given by Eq. (37), and T_{st} , given by Eq. (13).

$$\sin \omega t_1 = \frac{1}{K} \frac{2\pi}{\sin \beta [1 + \sqrt{1 - 4 \tan \alpha (\tan \beta - \tan \alpha) \cot^2 \beta}]} \tag{40}$$

The sum of the squares of Eqs (35) and (40) yields the relative acceleration K :

$$K = \sqrt{\frac{(2\pi)^2}{\sin^2 \beta [1 + \sqrt{1 - 4 \tan \alpha (\tan \beta - \tan \alpha) \cot^2 \beta}]^2}} + \frac{\cos^2 \alpha}{\sin^2 (\beta - \alpha)}. \quad (41)$$

The denominator of the first term is:

$$\frac{1}{\sin^2 \beta [1 + \sqrt{1 - 4 \tan \alpha (\tan \beta - \tan \alpha) \cot^2 \beta}]^2} = \frac{1}{4} \frac{\cos^2 \alpha}{\sin^2 (\beta - \alpha)}. \quad (42)$$

By substituting, the relative acceleration K becomes

$$K = \frac{\cos \alpha}{\sin (\beta - \alpha)} \sqrt{\pi^2 + 1}. \quad (43)$$

According to this equation, the relative acceleration is the product of the constant $(\pi^2 + 1)^{1/2}$ and the variable factor $\cos \alpha / \sin (\beta - \alpha)$.

By dividing Eq. (40) by Eq. (35) one gets:

$$\tan \omega t_1 = \frac{2\pi \sin (\beta - \alpha)}{\sin \beta \cos \alpha [1 + \sqrt{1 - 4 \tan \alpha (\tan \beta - \tan \alpha) \cot^2 \beta}]}. \quad (44)$$

After some mathematics we have from the previous equation

$$\tan \omega t_1 = \pi; \quad \omega t_1 = \tan^{-1} \pi = 72.3432^\circ. \quad (45)$$

Equation (45) shows that the throw from the screen panel happens in case of screening with positive dip, independently of the angle of dip α and the angle of throw β , at an angle $\tan^{-1} \pi$.

The impact velocity of the particle in point Q is:

$$\begin{aligned} V_Q &= V \sqrt{\cos^2 \beta + [\sin \beta - 2(\tan \beta - \tan \alpha) \cos \beta]^2} = \\ &= V \cos \beta \sqrt{1 + (-\tan \beta + 2 \tan \alpha)^2}. \end{aligned} \quad (46)$$

The component $V_{Q\perp}$ normal to the screen panel of velocity V_Q is according to Fig. 3:

$$V_{Q\perp} = V_Q \cos(90^\circ - \delta) = V_Q \sin \delta = V_Q \sin(\gamma - \alpha). \quad (47)$$

4. Analysis of the parameters moving on the screen panel

In the following the distances travelled by the particles on the screen panel or conveyor during one stroke, their lengths of stay, velocity, impact angle and relative acceleration K characteristic of the statistical resonance are analyzed. All these values influence the capacity of the equipment, further in case of screening, also the sharpness of selection. Due to their importance, the impact angle and the relative acceleration are analyzed in special sections.

4.1 Analysis of the path during one stroke

The distance travelled by the particles during one stroke s_s and through it, the dependence of the capacity on the initial velocity V and dip α of the equipment is unambiguous. In the following the relationship between the distance travelled during one stroke and the angle of throw β , will be analyzed.

Equations (7) and (36) for the distance travelled can also be written as

$$s_s = \frac{2V^2}{g} \frac{\tan \beta \pm \tan \alpha}{\cos \alpha} \cos^2 \beta = \frac{V^2}{g \cos \alpha} [\sin 2\beta \pm \tan \alpha (1 + \cos 2\beta)]. \quad (48)$$

In this equation the trigonometrical identity $2 \cos^2 \beta = 1 + \cos 2\beta$ has been applied. A transformation of Eq. (48) yields

$$\begin{aligned} s_s &= \frac{V^2}{g \cos \alpha} (\sin 2\beta \pm \tan \alpha \cos \beta) \pm \frac{V^2}{g \cos \alpha} \tan \alpha = \\ &= \frac{V^2}{g \cos^2 \alpha} [\sin(2\beta \pm \alpha) \pm \sin \alpha]. \end{aligned} \quad (49)$$

According to Eq. (49), the distance travelled during one stroke changes as a function of the sine function of the angle of throw periodically.

The maximum distance per stroke can be obtained by equating the first derivative to zero

$$\frac{\partial s_s}{\partial \beta} = \frac{2V^2}{g \cos^2 \alpha} \cos(2\beta \pm \alpha) = 0. \quad (50)$$

The location of the maximum is:

$$2\beta \pm \alpha = \frac{\pi}{2} + n\pi; \quad n = 0, \pm 1, \pm 2, \dots \quad (51)$$

That means that the greatest distance is travelled during one stroke by the particle in the plane of the screen panel with a dip of α at the same initial velocity V , if

$$\beta = \frac{90^\circ \mp \alpha}{2}. \quad (52)$$

The maximum distance s_{\max} is:

$$s_{\max} = \frac{V^2}{g \cos^2 \alpha} (1 \pm \sin \alpha). \quad (53)$$

If $\beta = \mp \alpha$, or $\beta = 90^\circ$, then $s_s = 0$, and if $\beta = (180^\circ \mp \alpha)/2$, then

$$s_s = \pm \frac{V^2 \sin \alpha}{g \cos^2 \alpha}. \quad (54)$$

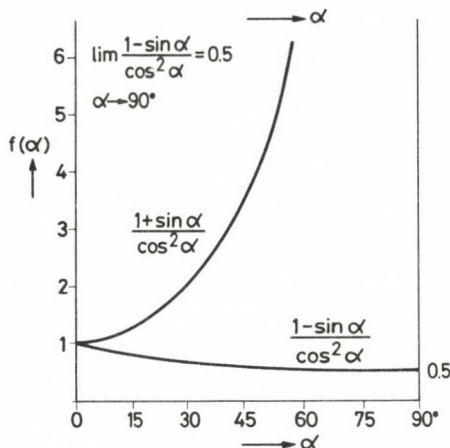


Fig. 4. The functions $\frac{1 \pm \sin \alpha}{\cos^2 \alpha}$ vs. α

The functions $(1 + \sin \alpha)/\cos^2 \alpha$ and $(1 - \sin \alpha)/\cos^2 \alpha$ are shown in Fig. 4. At $\alpha = 0^\circ$ both functions have the value of unity. At a screen dip 90° the former function approaches infinity, that of the latter has the limit of 0.5. The two functions represented in the figure as functions of screen dip, are proportional to the maximum distances per stroke occurring at angles of throw of $\beta = (90^\circ - \alpha)/2$.

4.2 Analysis of the length of stay

The thrown particle has a length of stay T_p changing periodically according to the sine function of angle β . To show this, the times in Eqs (9) and (37) are transformed as

$$T_p = \frac{2V}{g} \cos \beta (\tan \beta \pm \tan \alpha) = \frac{2V}{g \cos \alpha} \sin(\beta \pm \alpha). \quad (55)$$

Equation 55 shows that the length of stay is the longest, if $\sin(\beta \pm \alpha) = 1$, i.e. if the particle is thrown perpendicularly to the screen panel:

$$\beta = 90^\circ \mp \alpha. \quad (56)$$

The maximum length of stay can be expressed by substituting Eq. (56) into Eq. (55)

$$T_{p \max} = \frac{2V}{g \cos \alpha}. \quad (57)$$

If $\beta \pm \alpha = 0^\circ$, and 180° , respectively, then the particle fails to be thrown away, and the length of stay is zero.

By substituting $\beta = 90^\circ - \alpha$ into Eq. (49), the distance travelled by the particle s_\perp during one stroke of the screen with negative dip in case of a normal throw, can be found as

$$\frac{s_\perp}{s_{\max}} = \frac{2 \sin \alpha}{1 + \sin \alpha} \quad (59)$$

This equation is the same as Eq. (28).

The ratio of s_\perp to the maximum distance according to Eq. (53) becomes

$$\frac{s_\perp}{s_{\max}} = \frac{2 \sin \alpha}{1 + \sin \alpha} \quad (59)$$

Comparing Eqs (54) and (58) it can be seen that applying a normal throw, i.e. $\beta = 90^\circ - \alpha$, the particle is thrown twice as far as in the case of throwing at an angle of $\beta = (180^\circ - \alpha)/2 = 90^\circ - \alpha/2$.

4.3 Analysis of the particle velocity

The distance travelled per divided by the length of stay yields the velocity of the particle. Thus, dividing Eq. (48) or (49), by Eq. (55) we have

$$v_s = V \frac{\cos \beta}{\cos \alpha} = \frac{V}{2 \cos \alpha} \frac{\sin(2\beta \pm \alpha) \pm \sin \alpha}{\sin(\beta \pm \alpha)} \quad (60)$$

This function shows that the velocity changes periodically as a function of the angle of throw. It shows further that in case of equal angles β and α , the velocities are equal at negative and positive dip screens. The maximum velocity is obtained in case of horizontally throwing the particle: $\beta = 0^\circ$ (or 180° , respectively), when $\cos \beta = 1$. The maximum velocity now is:

$$v_{s \max} = \frac{V}{\cos \alpha} \quad (61)$$

At $\beta = 90^\circ$, the velocity is zero.

If $\beta = (90^\circ - \alpha)/2$, or $\beta = 90^\circ - \alpha$, then the velocity of the particles becomes

$$v_s = V \frac{\cos\left(45 - \frac{\alpha}{2}\right)}{\cos \alpha} = \frac{1}{2} V \frac{\sqrt{1 + \cos \alpha} + \sqrt{1 - \cos \alpha}}{\cos \alpha} \quad (62)$$

or

$$v_s = V \tan \alpha \quad (63)$$

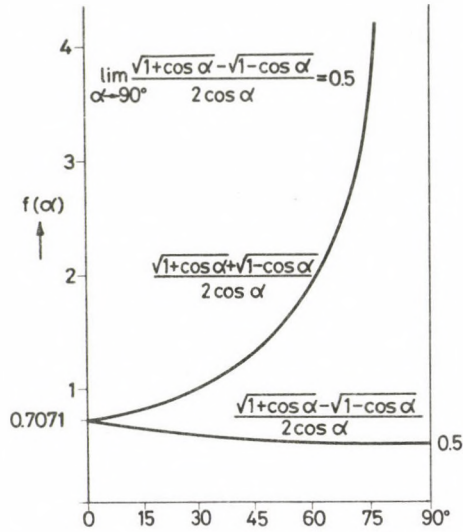


Fig. 5. The functions $\frac{\sqrt{1+\cos \alpha} \pm \sqrt{1-\cos \alpha}}{2 \cos \alpha}$ vs. α

Figure 5 shows in the interval $0^\circ \leq \alpha \leq 90^\circ$ the functions

$$\begin{aligned} &(\sqrt{1+\cos \alpha} + \sqrt{1-\cos \alpha}) / 2 \cos \alpha \quad \text{and} \\ &(\sqrt{1+\cos \alpha} - \sqrt{1-\cos \alpha}) / 2 \cos \alpha. \end{aligned}$$

At $\alpha = 0^\circ$, both functions have the value $\sqrt{2}/2$. At 90° the functions have no substitution value, the former approaches infinity while the latter's limit is $1/\sqrt{2}$. Multiplying the values read from these graphs by initial velocity V , particle velocities for the angle of throw $\beta = (90^\circ - \alpha)/2$ are obtained.

4.4 Analysis of the impact and collision velocities of the particles

The impact velocity V_Q , according to Eqs (25) and (46) can also be expressed as

$$\begin{aligned} V_Q &= V \sqrt{\cos^2 \beta + [\sin \beta - 2(\tan \beta \pm \tan \alpha) \cos \beta]^2} = \\ &= V \sqrt{\cos^2 \beta + (\mp 2 \tan \alpha \cos \beta - \sin \beta)^2} = \\ &= V \sqrt{1 + 2 \tan^2 \alpha \left[1 \pm \frac{\sin(2\beta \pm \alpha)}{\sin \alpha} \right]}. \end{aligned} \tag{64}$$

On a screen with negative dip, the impact velocity is maximum, if $\sin(2\beta + \alpha) = 1$, i.e. at an angle of throw

$$\beta = \frac{90^\circ - \alpha}{2}. \tag{65}$$

(At that angle of throw also the distance per stroke has a maximum.) In case of $\sin(2\beta + \alpha) = -1$, i.e. at $2\beta + \alpha = 270^\circ$, the velocity would be a minimum, but the angle of throw corresponding to this value has no physical sense.

On a screen with negative dip the maximum impact velocity $V_{Q_{\max}}$ is by taking Eq. (55) into account:

$$V_{Q_{\max}} = V \sqrt{1 + 2 \frac{\sin \alpha (1 + \sin \alpha)}{\cos^2 \alpha}}. \tag{66}$$

On a screen panel with positive dip, the impact angle would be maximum at $\sin(2\beta - \alpha) = -1$, i.e. $2\beta - \alpha = 270^\circ$. The angle of throw $\beta = (270^\circ + \alpha)/2$ is, however, impossible. But velocity V_Q is the higher the better β approaches 90° . Further if $\sin(2\beta - \alpha) = 1$, then the impact velocity of the particle is minimum. The impact angle is now

$$\beta = \frac{90^\circ + \alpha}{2} \tag{67}$$

and the impact velocity V_Q is equal to the initial velocity V , i.e. $V_Q = V$.

The component of the velocity V_Q normal to the screen panel, $V_{Q\perp}$ is

$$\begin{aligned} V_{Q\perp} &= V_Q \sin(\gamma \pm \alpha) = V_Q (\sin \gamma \cos \alpha \pm \cos \gamma \sin \alpha) = \\ &= V_Q \left(\frac{\tan \gamma}{\sqrt{1 + \tan^2 \gamma}} \cos \alpha \pm \frac{1}{\sqrt{1 + \tan^2 \gamma}} \sin \alpha \right). \end{aligned} \tag{68}$$

By substituting here $\tan \gamma$ from Eqs (11) and (38), one gets

$$V_{Q\perp} = V_Q \frac{\mp \sin \alpha \cos \beta - \cos \alpha \sin \beta}{\sqrt{\cos^2 \beta + (\mp 2 \tan \alpha \cos \beta - \sin \beta)^2}}. \tag{69}$$

A comparison of Eq. (64) and (69) shows that

$$V_{Q\perp} = -V \sin(\beta \pm \alpha) = V |\sin(\beta \pm \alpha)|. \tag{70}$$

Equation (70) shows that the absolute value of the component of the impact velocity normal to the screen panel has a maximum if $\beta = 90^\circ \mp \alpha$, i.e. in case of throwing perpendicularly to the screen panel.

The component of the impact velocity normal to the screen panel v_c is the sum of the initial velocity in Eq. (23) and the velocity $V_{Q\perp}$ in Eq. (70):

$$v_c = V [1 + |\sin(\beta \pm \alpha)|] = 0.9529 r\omega [1 + |\sin(\beta \pm \alpha)|]. \tag{71}$$

It can be seen from here that the collision velocity also has a maximum in case of a throw normal to the screen panel. Equation (71) shows further that the collision velocity depends in addition on angles α and β , also on the product $r\omega$ (on the peripheral velocity of the driving mechanism).

4.5 Numerical example for the study of the parameters of the particle motion

Table I contains the values of the parameters studied previously as functions of the angle of throw β . On a screen having a dip of $\alpha = 30^\circ$, for an initial velocity $V = 44.2945$ cm/s ($V^2/2g = 1$ cm) the distance travelled per stroke has been calculated using Eq. (49), the length of stay using Eq. (55), the velocity by Eq. (60), and the impact velocity of the particle by Eq. (60) for angles of throw $\beta = -30, -15, 0, 15, \dots, 165, 180^\circ$. The values listed have been determined for screen panels having both negative and positive dips (the corresponding values have the indices n and p , respectively).

On a screen panel with negative slope the maxima of the distance travelled per stroke (4 cm) and the velocity of the particle at impact on the panel (76.7203 cm/s) occur at an angle of throw $\beta = (90^\circ - 30^\circ)/2 = 30^\circ$, and the corresponding length of stay is 0.09030 s, the velocity on the screen panel is 44.294 cm/s. The maximum of the length of stay occurs at an angle of throw $\beta = 90^\circ - 30^\circ = 60^\circ$, with a value of 0.10427 s (the throw is normal to the screen panel), the distance travelled per stroke is 2.6 cm, the velocity of the particle 25.573 cm/s, and the velocity of the particle at impact equals 67.6609 cm/s. At an angle of throw $\beta = 0^\circ$, the velocity has a maximum with 51.147 cm/s.—These

Table I. Distance, length of stay and velocity of the particles as functions of the angle of throw for a screen panel with a dip of 30° ($V^2/2g = 1$ cm)

β	s_{sn} [cm]	s_{sp} [cm]	τ_{pn} [s]	τ_{pp} [s]	v_s [cm/s]	[cm/s] v_{Qn}	v_{Qp} [cm/s]
-30	0	-4	0	-0.09030	44.294	44.294	76.720
-15	1.3333	-3.6427	0.02699	-0.07373	49.404	57.184	74.401
0	2.6667	-2.6667	0.05214	-0.05214	51.147	67.661	67.661
15	3.6247	-1.3333	0.0737	-0.02699	49.404	74.401	57.184
30	4	0	0.09030	0	44.294	76.720	44.294
45	3.6427	0.9761	0.10072	0.02699	36.166	74.401	31.693
60	2.6667	1.3333	0.10427	0.05214	25.573	67.661	25.573
75	1.3333	0.9761	0.10072	0.07373	13.238	57.184	31.693
90	0	0	0.09030	0.09030	0	44.294	44.294
105	-0.9761	-1.3333	0.07373	0.10072	-13.238	31.693	57.184
120	-1.3333	-2.6667	0.05214	0.10427	-25.573	25.573	67.661
135	-0.9761	-3.6427	0.02699	0.10072	-36.166	31.693	74.401
150	0	-4	0	0.09030	-44.29	44.293	76.720
165	1.3333	-3.6427	-0.02699	0.07373	-49.404	57.184	74.401
180	2.6667	-2.6667	-0.05214	0.05214	-51.147	67.661	67.661

values show that the different parameters, e.g. the velocity change significantly as a function of the angle of throw. Therefore, the technical parameters of screens and conveyor systems (amplitude, revolutions, angle of dip, angle of throw *etc.*) have to be determined with utmost care.

The numerical values of the parameters of the particle motion in case of a screen panel with positive dip can be found in Table I, including maxima and minima. In case of the same angle of throw the distances travelled per stroke and lengths of stay are less on a screen with positive dip than with a negative one, but the velocities are the same as for negative dip (this last remark has already been made in connection with Eq. 60).

5. Analysis of the angle of impact

From the point of view of screening technology, the value of the angle of impact δ , is of an utmost importance. The angle of impact should be as great as possible as in such a case the particle size of the separation approximates well the size of the screen's mesh, and the separation is most effective. The most advantageous case is when particles fall perpendicularly on the screen panel. In the following analysis, the influence of the angle of throw β and of the dip of the screen panel α will be investigated on the angle of impact in great detail.

The tangent of the angle of impact δ may be written in a general form, i.e. for both positive and negative dips on the basis of Eqs (12) and (39)

$$\tan \delta = \frac{\tan \beta \pm \tan \alpha}{1 \pm \tan \beta \tan \alpha + 2 \tan^2 \alpha} \quad (72)$$

The angle of impact will be first analyzed at a fixed value of the screen's dip, for different values of the angle of throw, then assuming a constant angle of throw, the influence of the screen's dip will be studied.

5.1 *The angle of impact at a fixed value of the screen's dip as a function of the angle of throw*

The angle of impact is first analyzed for the values of the angle of throw $\beta = 0^\circ$, $(90^\circ \mp \alpha)/2$ and $(90^\circ \mp \alpha)$ investigated so far, then for fixed values of the screen's dip, the two functions δ of Eq. (72) will be plotted and using them, the regularities of the angle of impact will be summarized.

The velocity of the particles is a maximum at $\beta = 0^\circ$. By substituting $\beta = 0^\circ$ into Eq. (72), the angle of impact for this case is obtained

$$\tan \delta_0 = \pm \frac{\tan \alpha}{1 + 2 \tan^2 \alpha} \quad (73)$$

This function shows that at a horizontal throw, the angle δ_0 is always smaller than α . The angle of impact has further a maximum as a function of the angle of screen dip. From Eq. (73) we have for the location of this maximum of δ_0

$$\alpha = \tan^{-1} \frac{1}{\sqrt{2}} = 35.2644^\circ. \quad (74)$$

The maximum angle of impact δ_{0max} is

$$\delta_{0max} = \tan^{-1} \frac{\sqrt{2}}{4} = 19.4712^\circ. \quad (75)$$

The maximum angle of impact is thus less than 20° . In order to obtain high velocities of the particles, and consequently, a high capacity of conveyors angles of throw near the horizontal are advantageous. In screening, a horizontal throw ($\beta = 0^\circ$) is disadvantageous due to the small angles of impact be the dip of the screen of any value.

In case of throwing at an angle of throw of $\beta = (90^\circ \mp \alpha)/2$, the distance travelled by the particle in the plane of the screen panel has a maximum. One gets by substituting β into Eq. (72) and by taking into account relationships

$$\tan \left(45^\circ \mp \frac{\alpha}{2} \right) = \frac{1 \mp \tan \frac{\alpha}{2}}{1 \pm \tan \frac{\alpha}{2}}$$

and

$$\tan \alpha = \frac{2 \tan \frac{\alpha}{2}}{1 - \tan^2 \frac{\alpha}{2}}$$

that the tangent of the angle of impact $\delta_a/2$ is

$$\tan \frac{\delta_a}{2} = \tan \left(\frac{90^\circ \mp \alpha}{2} \right). \quad (76)$$

The angle of impact is thus the same as the angle of throw and both have the value $(90^\circ \mp \alpha)/2$. In case of an angle of throw $(90^\circ - \alpha)/2$, great screen dips are not recommended due to the resulting small angles of impact. For example in case of a screen with a dip of 30° , the angle of impact is also 30° , but on a screen with a 45° dip, it is only 22.5° .

If the throw of the particle is normal to the screen panel, i.e. if $\beta = 90^\circ \mp \alpha$, then according to Eq. (31) the tangent of the angle δ_\perp is

$$\tan \delta_\perp = \frac{1}{2 \tan \alpha}. \quad (77)$$

This equation shows that in case of great screen dips the angle of impact is small. In case of a screen with a dip of 15° , the angle of impact is 61.2499° , at $\alpha = 30^\circ$, it is only 40.8934° and at 45° it becomes as small as 26.5651° . These values are, however, more advantageous, than the angles of impact in case of a throw at $(90^\circ \mp \alpha)/2$. Due to the more advantageous angles of impact the throw of the particles should be normal on screens with greater dips, e.g. 30° .

Figure 6 shows the values of the angle of impact assuming a screen panel with a dip of 15° as a function of the angle of throw β according to Eq. (72). There are two functions on the figure, one for negative, and the other for positive dips.

Each function in Fig. 6 has a point of inflexion. In order to find these points of inflexion, the first and second derivatives of the angle of impact, expressed from Eq. (72):

$$\delta = \tan^{-1} \frac{\tan \beta \pm \tan \alpha}{1 \pm \tan \beta \tan \alpha + 2 \tan^2 \alpha}$$

should be calculated and the latter equated to zero:

$$\frac{\partial \delta}{\partial \beta} = \frac{1 + \tan^2 \beta}{1 + (\tan \beta \pm 2 \tan \alpha)^2} \tag{78}$$

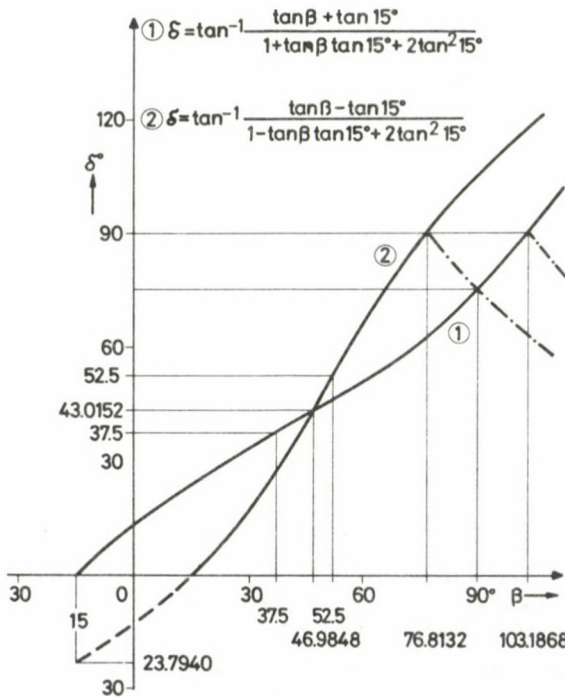


Fig. 6. The angle of impact vs. angle of throw on a screen panel with a dip of 15°

$$\frac{\partial^2 \delta}{\partial \beta^2} = \frac{4 \tan^2 \alpha \sin 2\beta \mp 4 \tan \alpha \cos 2\beta}{[1 + 2 \tan^2 \alpha (1 + \cos 2\beta) \pm 2 \tan \alpha \sin 2\beta]^2} = 0. \quad (79)$$

The latter expression is zero, if:

$$\tan 2\beta_{\text{infl}} = \pm \frac{1}{\tan \alpha} = \pm \cot \alpha = \pm \tan \left(\frac{\pi}{2} - \alpha \right) \quad (80)$$

whence

$$\beta_{\text{infl}} = \frac{90^\circ \mp \alpha}{2}. \quad (81)$$

In case of such an angle of throw, as has been already seen in connection with Eq. (76), the angle of impact equals the angle of throw: $\delta_{\text{infl}} = \beta_{\text{infl}} = (90^\circ \mp \alpha)/2$. In Fig. 6 the points of inflexion and their coordinates are indicated. On a screen with a negative dip of 15° , the angles of throw and impact are both 37.5° , on a screen with positive dip, the same angles are 52.5° . The function δ corresponding to screens with negative dips (1 in Fig. 6) is concave down at angles of throw less than that of the point of inflexion and concave up at greater angles of throw. In case of screening with positive dips (curve 2, in Fig. 6), the situation is just opposite.

Figure 6 shows that the two functions intersect each other. Thus there is a certain angle of throw at which the angles of impact are equal both at screens with negative and positive dips. The angle of throw β_i for this case is calculated from

$$\frac{\tan \beta + \tan \alpha}{1 + \tan \beta \tan \alpha + 2 \tan^2 \alpha} = \frac{\tan \beta - \tan \alpha}{1 - \tan \beta \tan \alpha + 2 \tan^2 \alpha}$$

as:

$$\tan \beta_i = \sqrt{1 + 2 \tan^2 \alpha}. \quad (82)$$

By substituting this value in any side of the previous equation the tangent of the angle of impact δ_i is obtained:

$$\tan \delta_i = \frac{1}{\sqrt{1 + 2 \tan^2 \alpha}}. \quad (83)$$

By comparing Eqs (82) and (83) one finds that

$$\tan \beta_i = \frac{1}{\tan \delta_i} = \cot \delta_i = \cot(90^\circ - \beta_i). \quad (84)$$

Therefore $\delta_i = 90^\circ - \beta_i$, i.e. in the present case the angle of throw and impact are complements of each other. In case of the screen panel with a dip of 15° , $\beta_i = 46.9205^\circ$ and $\delta_i = 43.0795^\circ$ according to Fig. 6. On a screen with a dip of 30° , the corresponding values are: $\beta_i = 52.2388^\circ$ and $\delta_i = 37.7612^\circ$. Figure 6 shows further that at angles of throw greater than β_i , the angle of impact is greater for a screen with positive dip, and at angles of throw less than β_i , the angle is greater for screens with negative dips.

Figure 7 shows that on a screen panel with positive dip, the normal impact of the particles can also be ensured. In such a case $\delta = 90^\circ$, and from Fig. 7, $\gamma = 90^\circ + \alpha$. Using Eq. (38), the angle of throw β_\perp corresponding to a normal impact is obtained as:

$$\tan \beta_\perp = 2 \tan \alpha - \tan(90^\circ + \alpha) = \frac{1 + 2 \tan^2 \alpha}{\tan \alpha}. \tag{85}$$

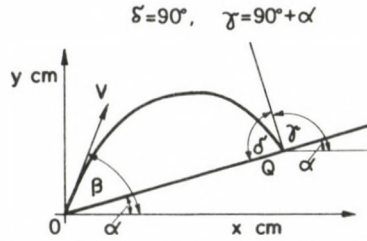


Fig. 7. Normal impact of the particles on a screen panel with positive dip

This equation has a minimum as a function of the angle of dip α . The minimum value $\beta_{\perp \min}$ corresponds to an angle of dip

$$\alpha = \tan^{-1} \frac{1}{\sqrt{2}} = 35.2644^\circ \tag{86}$$

and the minimum angle of throw is:

$$\beta_{\perp \min} = \tan^{-1} \frac{4}{\sqrt{2}} = 70.5288^\circ. \tag{87}$$

The angle of throw is thus exactly twice the dip of the screen panel. The value of angle γ is 125.2644° .

It is found from Eq. (85) for $\alpha = 15^\circ$ that $\beta_\perp = 76.8132^\circ$, also indicated in Fig. 6 ($\gamma = 105^\circ$). These values show that normal impact can only be reached with great angles of throw. According to Eq. (87) the minimum of the angle of throw is 70.5288° , but the dip of the screen is now too great, 35.2644° .

In case of an angle of throw $\beta = 90^\circ$, the limit of the angle of impact can be determined by a simple rearrangement of Eq. (72):

$$\lim_{\beta \rightarrow 90^\circ} \tan \delta = \lim_{\beta \rightarrow 90^\circ} \frac{1 \pm \frac{\tan \alpha}{\tan \beta}}{\frac{1}{\tan \beta} \pm \tan \alpha + 2 \frac{\tan^2 \alpha}{\tan \beta}} = \pm \frac{1}{\tan \alpha} = \pm \cot \alpha. \tag{88}$$

The angles of throw and impact as functions of the dip of the screen are presented in Table II. The dips of the screen panels in the first column of the table are 0, 5, 15, 30,

Table II. Some characteristic angles of throw and impact vs. dip of the screen panel

α	$\beta_{\text{infl},n}$	$\beta_{\text{infl},p}$	β_i	δ_i	δ_{\perp}	β_{\perp}
0	45. —	45. —	45. —	45. —	90. —	90. —
5	42.5	47.5	45.2176	44.7824	80.0750	85.0750
15	37.5	52.5	46.9205	43.0795	61.8132	76.8132
30	30. —	60. —	52.2388	37.7612	40.8934	70.8934
35.2644	27.3678	62.6322	54.7356	35.2644	35.2644	70.5288
45	22.5	67.5	60. —	30. —	26.5651	71.5651
60	15. —	75. —	69.2952	20.7048	16.1021	76.1021
75	7.5	82.5	79.4547	10.5453	7.6307	82.6307
85	2.5	87.5	86.4667	3.5333	2.5048	87.5048
90	0. —	90. —	90. —	0. —	0. —	90. —

35.2644, 45, 60, 75, 85 and 90°. The next two columns of the table indicate according to Eq. (81) the angles of throw $\beta_{\text{infl},n} = (90^\circ - \alpha)/2$ for screen panels with negative dips, and $\beta_{\text{infl},p} = (90^\circ + \alpha)/2$ for positive dips. In case of throwing at these angles the angles of impact are the same. The next columns of the table contain the angles β_i according to Eq. (82) and δ_i according to Eq. (83). It has been shown by Eq. (84) that for any screen dip $\beta_i + \delta_i = 90^\circ$. δ_{\perp} is the angle of impact calculated with Eq. (77), i.e. that in case of throwing perpendicularly to the screen panel. With this normal throw, the particle travels in the direction of the screen's dip, therefore perpendicular throw is only possible on screens with negative dips. The last column of the table shows the angles of throw β_{\perp} calculated with Eq. (85) at which a thrown particle reaches the screen panel of positive dip in normal direction.

For screen panels with negative dips the angle $\beta_{\text{infl},n}$ decreases with increasing dip α , while $\beta_{\text{infl},p}$ increases with increasing α , and the corresponding angles of impact change similarly. The sum of $\beta_{\text{infl},n}$ and $\beta_{\text{infl},p}$ is 90°. With increasing screen dip, β_i is increasing, and δ_i is decreasing. δ_{\perp} is also decreasing with increasing screen dip. On a screen panel with a dip of 35.2644°, δ_i and δ_{\perp} have also the value 35.2644°, in case of smaller dips, δ_{\perp} , in case of greater dips, δ_i is greater. Otherwise both δ_i and naturally δ_{\perp} are greater than $\beta_{\text{infl},n}$ for any dip. The values of β_{\perp} indicate that normal impact can be ensured by great angles of throws.

Table III shows the angles of impact for screens with negative and positive dips of 5, 15, 30, 35.2644 and 45°, and for angles of throw 0, 5, 15, 30, 45, 60, 75, 85 and 90°, further for $\beta_{\text{infl},n}$, $\beta_{\text{infl},p}$ and β_{\perp} .

In case of a horizontal throw, i.e. for $\beta = 0^\circ$, the angles of impact are so small that they decrease the falling through probability of grains with sizes less than the mesh diameter. It has already been shown by Eqs (74) and (75) that the angle of impact has a maximum with 19.4712° at a screen dip of 35.2644°. Table III shows that the angle of impact is 13.1868, 19.1066 and 18.4349° on screens with dips of 15, 30 and 45°. But the velocity the particles travel with is maximum at $\beta = 0^\circ$, and the distance travelled per

Table III. Dependence of the angle of impact δ on the screen's dip α and the angle of throw β

	$\beta^\circ \tan^{-1} \frac{\tan \beta \pm \tan 5}{1 \pm \tan \beta \tan 5 + 2 \tan^2 5}$			$\beta^\circ \tan^{-1} \frac{\tan \beta \pm \tan 15}{1 \pm \tan \beta \tan 15 + 2 \tan^2 15}$			$\beta^\circ \tan^{-1} \frac{\tan \beta \pm \tan 30}{1 \pm \tan \beta \tan 30 + 2 \tan^2 30}$			$\beta^\circ \tan^{-1} \frac{\tan \beta \pm \frac{1}{\sqrt{2}}}{2 \pm \frac{1}{\sqrt{2}} \tan \beta}$			$\beta^\circ \tan^{-1} \frac{\tan \beta \pm \tan 45^\circ}{1 \pm \tan \beta \tan 45 + 2 \tan^2 45}$		
	1		2		3		4		5		6		7		
0	4.9251	—	0	13.1868	—	0	19.1066	—	0	19.4712	—	0	18.4349	—	
5	9.7066	0.—	5	16.9389	—	5	21.1649	—	5	21.0755	—	5	19.4035	—	
15	18.8899	10.3116	15	23.7940	0.—	15	24.8961	—	15	24.0053	—	15	21.2068	—	
30	31.9552	26.9184	30	33.0675	17.3737	30	30.—	0.—	27.3678	27.3678	—	22.5	22.5	—	
42.5	42.5	41.5515	37.5	37.5	28.0305	45	35.1039	21.2060	30	28.0736	—	30	23.7940	—	
									35.2644	29.4962	0.—				
45	44.5995	44.5234	45	41.9325	39.8961	60	40.8934	60.—	45	32.2356	12.7644	45	26.5651	0.—	
47.5	46.7015	47.5	52.5	46.4654	52.5	70.8934	46.1021	90.—	60	37.1034	52.8966	60	30.—	30.—	
60	57.3285	62.2902	60	51.2060	65.1039	75	48.4349	81.2060	62.6322	38.0964	62.6322	67.5	32.2356	67.5	
75	70.6433	79.2978	75	61.8132	87.6263	85	55.4568	65.5585	70.5288	41.4729	90.—	71.5651	33.6901	90.—	
85	80.0749	89.9227	76.8132	63.2409	90.—	90	60.—	60.—	75.—	43.7392	78.0727	75	35.1039	75.—	
85.0750	80.1478	90.—	85	70.2229	80.2446				85	50.2838	60.4372	85	40.7416	51.0532	
90	85.—	85.—	90	75.—	75.—				90	54.7356	54.7356	90	45.—	45.—	

stroke is maximum at $\beta_{\text{infl},n}$ therefore the recommended dips of vibratory conveyors are between 0° and $\beta_{\text{infl},n} = (90^\circ - \alpha)/2$.

On a screen panel with given dip the increase of the angle of throw increases the impact angle. This increase, however, differs on screen panels with positive and negative dips. This was already mentioned in connection with Eq. (84) and Fig. 6. At angles of throw less than β_i , the angle of impact is greater on screens with negative dips, but at angles of throw greater than β_i , the angle of impact is greater on screens with positive dips. If the particle is thrown on a screen panel with a dip of 15° at an angle of throw of 46.9205° , then the angle of impact is, corresponding to Table II, independently of the sign of the dip, 43.0795° . If the angle of throw is $\beta_{\text{infl},n} = 37.5^\circ$, i.e. less than the former value, then the angle of impact is on a screen with negative dip again 37.5° and on a screen with positive dip according to Table III, 28.0305° . At an angle of throw of 45° , the same values are 41.9325 and 39.8961° . If the angle of throw is $\beta_{\text{infl},p} = 52.5^\circ$, then the two angles of impact are 46.4654 and 52.5° . At even greater angles of throw the angle of impact is even greater on screens with positive dips. With an angle of throw 76.8132° (calculated from Eq. 85) the screen panel of positive dip is reached by the particles normally, while at the same angle of throw the angle of impact is only 63.2409° on a screen panel with negative dip.

For vibratory conveyors the angle of impact has no special significance, the aim is the greatest possible transport capacity. Therefore the angle of throw of conveyors with greater dips should be 0° or a value near it, as the velocity the particles travel with has a maximum at 0° . In horizontal or nearly horizontal conveyors this angle should be $\beta_{\text{infl},n} = (90^\circ - \alpha)/2$ since the distance travelled per stroke is in this case a maximum. At screens the greatest possible impact angle should be striven at to achieve high sharpness of separation. Therefore the most advantageous solution is the normal throw for great screen dips, and $\beta_{\text{infl},n}$ or an angle of throw near it for screens with small dips.

On the basis of the angles of impact in Tables II and III the advantages of the screen with positive dip are apparent. It has been shown that on a screen with positive dip, the nearly normal impact of the particles can be ensured. Due to the great angles of throw and to the positive dip, the distance travelled by the particles per stroke is small, therefore the positive dip is only recommended for medium or small grain sizes.

5.2 Angle of impact as a function of the screen dip at fixed values of the angle of throw

Table IV presents data of the angle of impact at fixed values of the angle of throw (30 and 60°) at different positive and negative dips of the screen panel. The first column contains the angles of throw, viz. $0, 5, 15, 30, 45, 60, 75, 85$ and 90° .

In case of screening with negative dip at an angle of throw of 30° , the angle of impact has a maximum as a function of the dip of the screen, because the angles of

Table IV. Impact angles of fixed angles of throw vs. screen's dip

α	$\delta = \tan^{-1} \frac{\tan \beta + \tan \alpha}{1 + \tan \beta \tan \alpha + 2 \tan^2 \alpha}$		$\delta = \tan^{-1} \frac{\tan \beta - \tan \alpha}{1 - \tan \beta \tan \alpha + 2 \tan^2 \alpha}$	
	$\beta = 30^\circ$	$\beta = 60^\circ$	$\beta = 30^\circ$	$\beta = 60^\circ$
0	30. —	60. —	30. —	60. —
5	31.9551	57.3286	26.9185	62.2902
15	33.0675	51.2060	17.3737	65.1039
30	30. —	40.8934	0. —	60. —
45	23.7940	30. —	- 9.8961	30. —
60	16.1021	19.1066	- 10.8934	0. —
75	7.9113	8.7940	- 6.7380	- 5.1039
85	2.6210	2.6714	- 2.4304	- 2.2902
90	0. —	0. —	0. —	0. —
	$\delta_{\max} = 33.1010$ $\alpha_1 = 13.4490$		$\delta_{\min} = - 11.1101$ $\alpha_1 = 50.6560$	$\delta_{\max} = 65.2644$ $\alpha_2 = 17.6322$ $\delta_{\min} = - 5.2644$ $\alpha_1 = 72.3678$

impact corresponding to screen dips of 0, 15 and 30° are 30, 33.0675 and 30°, respectively. If the dip of the screen panel is further increased, the angle of impact decreases, thus the maximum should lie between the mentioned values. If the particle is thrown at an angle of 60°, the angle of impact decreases from 60 to 0° if the screen's dip increases from 0 to 90°.

On a screen panel with positive dip, if the particles are thrown at angles of 30°, the impact angle decreases with the increase of the dip. If the dip of the screen is greater than 30°, the angle of impact has negative values. In this negative range, the angle of impact has a minimum. If the angle of throw is 60°, the angle of impact has a maximum between screen dips 0 and 90°, then a minimum of negative sign. Between the maximum and minimum, there is an angle of impact of 0° at 60° dip, and similarly the angle of impact is 0° at $\alpha = 90^\circ$.

It is seen from the data of the table that at a fixed angle of throw the angle of impact has both maxima and minima as a function of the screen dip. In the following, these screen dips and angles of impact are determined separately for negative and positive screen dips.

In case of a screen panel of negative dip the angle of impact δ is given by Eq. (12). By taking the angles β as constant the function is differentiated with respect to α

$$\frac{\partial \tan \delta}{\partial \alpha} = \frac{-(1 + \tan^2 \alpha)(2 \tan^2 \alpha + 4 \tan \beta \tan \alpha + \tan^2 \beta - 1)}{(1 + \tan \beta \tan \alpha + 2 \tan^2 \alpha)^2} = 0. \tag{89}$$

The derivative is zero if one of the factors in the numerator is zero, i.e.:

$$2 \tan^2 \alpha + 4 \tan \beta \tan \alpha + (\tan^2 \beta - 1) = 0. \tag{90}$$

This quadratic equation has two solutions, namely

$$\tan \alpha_{1,2} = \pm \sqrt{\frac{1}{2}(1 + \tan^2 \beta) - \tan \beta} \quad (91)$$

yielding screen dips on which the particles thrown at equal angles, the maximum and minimum of the angle of impact are obtained. For the calculation of the maximum and minimum the latter equation should be substituted into Eq. (12). If the upper, positive sign is taken in Eq. (91), the angle of impact has a maximum:

$$\tan \delta_{\max} = \frac{1}{2\sqrt{2(1 + \tan^2 \beta) - 3 \tan \beta}} = \frac{\cos \beta}{2\sqrt{2} - 3 \sin \beta}. \quad (92)$$

If the lower, negative sign is taken, the substitution into Eq. (12) yields the minimum angle of impact.

$$\tan \delta_{\min} = \frac{-1}{2\sqrt{2(1 + \tan^2 \beta) + 3 \tan \beta}} = \frac{-\cos \beta}{2\sqrt{2} + 3 \sin \beta}. \quad (93)$$

In case of screening with positive dip, the same method should be followed. By differentiating Eq. (39) with respect to α and equating the derivative with zero, the screen dips of the maximum and minimum are

$$\tan \alpha_{1,2} = \pm \sqrt{\frac{1}{2}(1 + \tan^2 \beta) + \tan \beta}. \quad (94)$$

The upper, positive sign yields the minimum of the angle of impact. This minimum is the same, as given in Eq. (93). With the lower, negative sign one obtains the maximum of the angle of impact and it is given by Eq. (92).

Figure 8 shows the values of

$$\tan \alpha_1 = \left[\frac{1}{2}(1 + \tan^2 \beta) \right]^{1/2} - \tan \beta$$

from Eq. (91) and those of

$$\tan \delta_{\max} = \cos \beta / (2\sqrt{2} - 3 \sin \beta)$$

according to Eq. (92) as functions of the angle β . At $\beta = 0^\circ$, $\tan \alpha_1 = (1/2)^{1/2}$, $\alpha_1 = 35.2644^\circ$, and $\tan \delta_{\max} = 1/(2\sqrt{2})$, $\delta_{\max} = 19.4712^\circ$. These values have already been obtained from Eqs (74) and (75). If the angle of throw is 45° , the necessary screen dip is 0° , and the angle of impact also 45° . These values can be found from Fig. 8.

The function $\tan \delta_{\max}$ (Eq. 92) has a discontinuity at

$$\sin \beta = \frac{2\sqrt{2}}{3}, \quad (95)$$

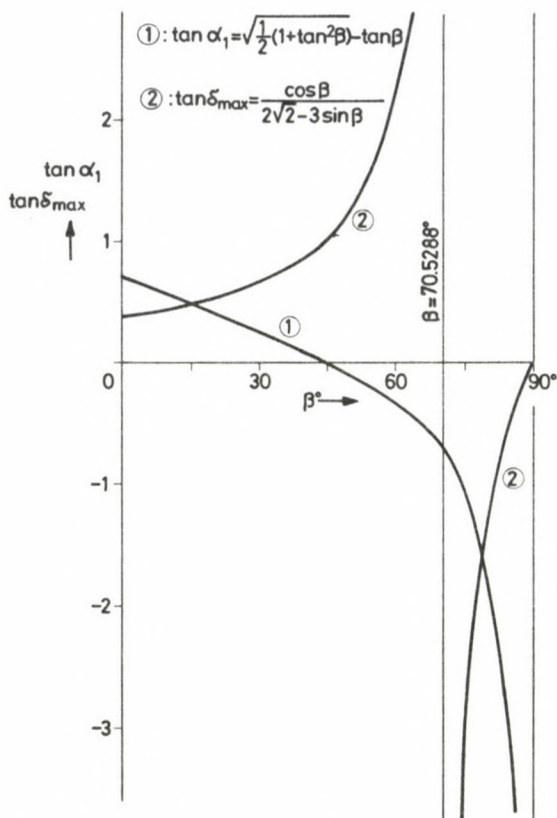


Fig. 8. Functions $\tan \alpha_1$ and $\tan \delta_{\max}$ vs. the angle β

i.e. at $\beta = 70.5288^\circ$. In that case the tangent of the screen's dip is $-1/\sqrt{2}$, indicating screening with a positive dip of 35.2644° . It was already shown with Eqs (86) and (87) that in case of a dip of 35.2644° and an angle of throw of 70.5288° , the impact is normal. The same can be shown using Eq. (92), if Eq. (95) is substituted. The discontinuity of the function $\tan \delta_{\max}$ at $\beta = 70.5288^\circ$ is indicated in Fig. 8 by a vertical line.

The last column of Table IV shows the maximum and minimum calculated from the previous equations. For example on a screen with a positive dip of 17.6322° and at an angle of throw of 60° , the angle of impact has a maximum with 65.2644° . At the same angle of throw, the angle of impact has a minimum with -5.2644° on a screen with a dip of $\alpha = 72.3678^\circ$. $\delta = 5.2644^\circ$, if the particle is thrown at -60° on a screen with a negative dip of 72.3678° .

6. The relative acceleration characterizing the statistical resonance

The relative acceleration K necessary for the statistical resonance is according to Eqs (20) and (43):

$$K = \frac{\cos \alpha}{\sin(\beta \pm \alpha)} \sqrt{\pi^2 + 1}. \quad (96)$$

A value of $(\pi^2 + 1)^{1/2} = 3.2969$ is given for K (Tarján 1954, Schubert 1975). According to the present investigations, K strongly depends both on the dip of the screen and the angle of throw. Therefore, our following analysis will focus on the effect of the dip α and of the angle of throw β on parameter K .

The coefficient of $(\pi^2 + 1)^{1/2}$ is:

$$y = \frac{\cos \alpha}{\sin(\beta \pm \alpha)} = \frac{1}{\sin \beta \pm \cos \beta \tan \alpha}. \quad (97)$$

To study the parameter K , it is sufficient to analyse this function. The value of y in Eq. (97) is studied first at a fixed value of α , at $\beta = 0^\circ$, $(90^\circ \mp \alpha)/2$ and $(90^\circ \mp \alpha)$, then the maxima and minima of this function will be investigated.

If the throw is horizontal, i.e. $\beta = 0^\circ$, we have

$$y = \pm \frac{1}{\tan \alpha}. \quad (98)$$

According to Eq. (74), the maximum of the angle of impact δ occurs at a dip of $\alpha = 35.2644^\circ$. In that case $y = \sqrt{2}$.

With an angle of throw $\beta = (90^\circ \mp \alpha)/2$ the angle of impact is $(90^\circ \mp \alpha)/2$, and the distance travelled per stroke has a maximum. By substituting into Eq. (97) one has

$$y = \frac{\cos \alpha}{\sin \left(45 \pm \frac{\alpha}{2} \right)} = \frac{2 \cos \alpha}{\sqrt{1 + \cos \alpha} \pm \sqrt{1 - \cos \alpha}}. \quad (99)$$

If $\beta = 90^\circ \mp \alpha$, the length of stay of the particle is a maximum, and the function y is

$$y = \cos \alpha. \quad (100)$$

For a screen with positive dip, normal impact can be ensured by β_\perp ; $\tan \beta_\perp$ has been already given in Eq. (85). By expressing $\sin \beta$ and $\cos \beta$ from it, and putting into Eq. (97) the function y becomes

$$y = \frac{\sqrt{(1 + 2 \tan^2 \alpha)^2 + \tan^2 \alpha}}{1 + \tan^2 \alpha} \quad (101)$$

$y = 1$ if $\cos \alpha = \sin(\beta \pm \alpha)$. It follows from this equation that independently of the screen's dip, $y = 1$ at $\beta = 90^\circ$ (i.e. vertical throw) and

$$\sin \beta = \cos 2 \alpha \tag{102}$$

thus $K = (\pi^2 + 1)^{1/2}$.

Finally, it can be shown by calculating the first derivative that with constant dip the function y in Eq. 97 (and also K) has a minimum as a function of the angle of throw at

$$\frac{\partial y}{\partial \beta} = \cos \beta \mp \sin \beta \tan \alpha = 0. \tag{103}$$

This function is zero, if $\beta = 90^\circ \mp \alpha$, i.e. in case of normal throw. This is obvious since if the throw is normal the length of stay of the particle in air or a vacuum is the greatest. In such a case the function y is according to Eq. (100) $y = \cos \alpha$.

Figure 9 shows the function $y = \cos \alpha / \sin(\beta \mp \alpha)$ characterizing the statistical resonance as a function of the angle of throw β , if $\alpha = 75, 60, 45, 30, 15$ and 0° . The functions bear serial numbers. Curves 1, 2, 3, 4 and 5 refer to screening with negative

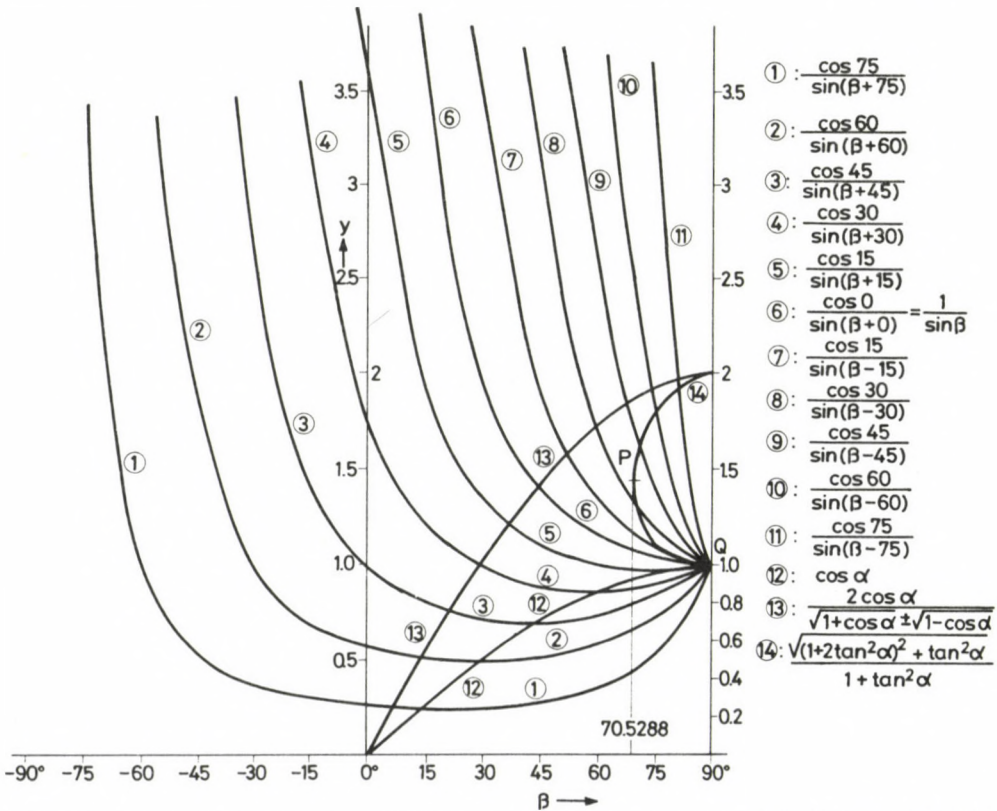


Fig. 9. The characteristic function of the statistical resonance $y = \cos \alpha / \sin(\beta \pm \alpha)$ vs. β , for different values of α

dip, curve 1 stands for a screen panel with a dip of 75° , curve 5 for that with a dip of 15° . Curve 6 is the function $1/\sin \beta$, referring to a horizontal screen panel. Further curves indicate screening with positive dip; curve 7 stands for a dip of 15° , curve 11 for a screen dip of 75° . (The formulae of the functions are also indicated in the figure).

The set of curves shows firstly that the value of the function is very great if the angle β approaches the dip α : in case of $\beta \rightarrow \pm \alpha$, one has $\cos \alpha / \sin(\beta \pm \alpha) \rightarrow \infty$.

Another finding is that for $\beta = 90^\circ$, both functions equal unity. (Now, we have $K = (\pi^2 + 1)^{1/2}$). This has been proven earlier. The figure shows further that for a screen with negative dip, according to Eq. (102), y also equals unity at angles of throw $\beta = \sin^{-1}(\cos 2\alpha)$. (E.g. in case of a screen panel with a dip of 15° , at $\beta = 60^\circ$). Between these angles of throw the functions have minima according to Eq. (103) at a throw normal to the screen panel). The minima are connected in Fig. 9 by the function $y = \cos \alpha$ (curve 12), i.e. $y_{\min} \leq 1$. In case of an angle of throw $\beta = 0^\circ$, the function studied has the form $1/\tan \alpha$ according to Eq. (98). The values of $1/\tan \alpha$ are given in case of the representation used in Fig. 9 by the abscissae of the points of intersection of the ordinate axis with curves $\cos \alpha / \sin(\beta + \alpha)$.

Relying on these considerations it is found that the values of y and K are less than unity and 3.3, respectively in a range being the wider, the greater the dip of the screen is. For example, on a screen with a dip of 45° , y is less than unity within the limits 0 and 90° , while for a screen with a dip of 15° , the range of β angles, where y is less than unity, is only between 60° and 90° .

Figure 9 contains further the function of Eq. (99) being valid for angles of throw $\beta = (90^\circ \mp \alpha)/2$. This function is denoted in the figure by 13 and it intersects all curves of the set, even those corresponding to screening with positive dip. At $\alpha = 60^\circ$ and $\alpha = 0^\circ$, we have $\beta = 45^\circ$, thus at such screen dips and such an angle of throw the function 13, intersects the function $1/\sin \beta$ denoted by 6. At angles of throw $0^\circ \leq \beta < 45^\circ$, function 13 intersects the functions of screening with negative dips, and at $45^\circ < \beta \leq 90^\circ$ those with positive dips. At $\beta = 90^\circ$, i.e. at $\alpha = 90^\circ$ the limit of function (99) is simultaneously its maximum with

$$\lim_{\alpha \rightarrow 90^\circ} \frac{2 \cos \alpha}{\sqrt{1 + \cos \alpha} - \sqrt{1 - \cos \alpha}} = 2. \quad (104)$$

Thus the value of function y denoted by 13 in Fig. 9, and calculated from Eq. (99), lies between 0 and $\sqrt{2}$ for angles of throw between 0 and 45° , i.e. for screening with negative dips, and between $\sqrt{2}$ and 2 for screening with positive dips.

The value of all functions referring to a screening with positive dips equals unity at $\beta = 90^\circ$. With angles of throw less than 90° , the value of y is always greater than 1: the decrease of the angle of throw is accompanied with a monotonous increase of y . y also depends on the dips of the screen: with increasing dip, y also increases.

The functions referring to screening with positive dips are also intersected by function 14 corresponding to Eq. (101), referring to normal impact. On a horizontal screen panel, the condition for the normal impact is $\beta = 90^\circ$; the numerical value of the function is 1. The angles of throw β_\perp necessary to ensure normal impact for different screen dips were given in Table II. All these facts explain the peculiar trend of curve 14. If the screen's dip is 35.2644° , $\tan \alpha = 1/\sqrt{2}$, the angle of throw is a minimum, 70.5288° , and the value of function 14 is $y = \sqrt{2}$. This minimum angle of throw is indicated in the figure together with the corresponding point P . The limit of the function is simultaneously the maximum, and it occurs at $\alpha = 90^\circ$ and $\beta = 90^\circ$, respectively:

$$\lim_{\alpha \rightarrow 90^\circ} \frac{\sqrt{(1 + 2 \tan^2 \alpha)^2 + \tan^2 \alpha}}{1 + \tan^2 \alpha} = 2. \quad (105)$$

The limit of the functions in Eqs (104) and (105) is 2, therefore these functions have a common point at $\alpha = 90^\circ$ in Fig. 9. Thus, the function y referring to normal impact (Eq. 101) has a minimum of 1 and a maximum of 2, the corresponding relative acceleration K is between 3.3 and 6.6.

7. Some conclusions about screening technique using the laws of statistical resonance

The exact knowledge of y and the relative acceleration K , respectively, is necessary when planning vibratory conveyors. The curves presented in Fig. 9 prove that the value of K changes within wide limits if the screen's dip and the angle of throw change. Having great K values, both the driving mechanism and the equipment itself are exposed to high loads, necessitating high stability parts and robust construction. These factors increase production costs.

In the previous section it has already been mentioned that in order to achieve high capacity of the vibratory conveyors, impact angles between 0° and $(90^\circ - \alpha)/2$ are most advantageous. In such a case the values of function y lie in the area limited by the vertical axis and curves 13 and 8. Depending on the angles α and β , there are very different values in this area. E.g. on a machine with a 45° dip, the value of y equals unity and 0.732 for angles of throw 0 and 30° while they are 3.732 and 1.218 at a dip of 15° for angles of throw 0 and 37.5° . Thus the parameter of the relative acceleration K is an optimum in small dip equipment at angles of throw of $(90^\circ - \alpha)/2$, and in equipment with higher dips at angles of throw 0° or near 0° .

Screening equipment should have possibly greatest impact angles. To reach them, in horizontal screens angles of throw $(90^\circ - \alpha)/2$, at higher dips $90^\circ - \alpha$ should be used. In this case the values of y lie in the area limited by curves 6, 12 and 13 in Fig. 9.

The values of y and K are here not so much differing than in the area characterizing vibratory conveyors. On a horizontal screen panel e.g. and at a throw under 45° (biaxial screening) $y = \sqrt{2}$ (being the highest value in the area), and for a screen dip of 15° (rotary screens) the y values are 1.218 and 0.966 for angles of throw 37.5° and 75° , and for a screen panel of 30° (electromagnetic vibrators) the values are 1 and 0.866 for angles of throw 30° and 60° . These values suggest that the advantages of the normal throw are more evident on screen panels with greater dips. On a horizontal screen panel, the angle of throw 45° is recommended mainly to ensure suitable transport of the material. The relative acceleration K is now $\sqrt{2} \cdot 3.3 = 4.667$ necessitating a robust construction.

For equipment with positive dip, the value of y lies in the area limited by curves 6, 13 and 14. The minimum of y is in this area 1, the maximum 2. In order to ensure the normal impact of the particles, curve 14 is recommended, as it has already been mentioned. Point P on this curve refers to a screen panel with a dip of 35.2644° , the ordinate of the point being $y = \sqrt{2}$.

Screening with positive dip is to be used if the normal impact of the particles is ensured. The distance travelled per stroke is however, now small. Thus, screens with positive dips are to be used for the separation of hardly screenable materials in the medium range.

References

- Finkey J 1924: Scientific fundamentals of wet ore processing (in German). Verlag von Julius Springer, Berlin
 Káplár Zs 1984: Referee's opinion on the paper "On the statistical resonance".
 Pethő Sz 1974: On the statistical resonance (in German). *Acta Geod., Geoph. Mont. Hung.*, 9, 371–382.
 Pethő Sz 1984: Laws of motion of vertically thrown and falling back particles in a medium. *Építőanyag*, 36, No 2, 48–56.
 Schubert 1975: Mineral dressing (in German). Vol. I. VEB Deutscher Verlag für Grundstoffindustrie, Leipzig
 Tarján G 1954: Ore dressing. Tankönyvkiadó, Budapest

ENERGY OF FLUID-BEARING POROUS SYSTEMS

GY ZOLTÁN¹ †

[Manuscript received September 12, 1984]

Basic statement of this study is that the mass and state of a porous reservoir is decisive concerning the energy content of the system. However, thermodynamics teaches that the absolute value of the energy content of a system cannot be determined, changes of the mass and state of a system can characterize the change of energy content only, according to the direction and rate of the change. This principle has been used in the study to determine the change of interfacial energy accompanying changes in the mass and state of the system. An attempt has also been made at determining the ratio of the change in interfacial energy to that in total energy content of the system.

Keywords: capillary pressure; change of state; fluid-bearing reservoir; interfacial energy; interfacial tension; phase exchange; porous system; underground gas storage; wettability

Symbols

A	Surface area, interfacial area
A_c	capillary cross-section
A_{sg}	solid-gas interfacial area
d	capillary diameter
F	force
F_c	capillary resistance
g	acceleration due to gravity
h	height
i	number of observation (subscript)
J	$J(S_g) = p_g/Z$
K	$K(S_g) = \frac{p_g}{Z} S_g$
n	mole number
p	pressure
p_g	gas pressure = $p_w + P_c$
p_w	water pressure, constant (= 2, 4, 6, 8, 10 MPa)
P_c	capillary pressure = $P_c(S_g) = P'_c(S_w)$
r	capillary radius
R	gas constant
S	saturation
S_g	gas saturation
S_w	water saturation
S_{wres}	residual water saturation
S_{gl}	gas saturation at the inflexion point of function $P_c(S_g)$
T	temperature
T_{norm}	normal temperature
V	volume
V_k	volume, non-variable
V_v	volume, variable
V_g	gas volume

¹ Chemical Research Laboratory for Mining of the Hungarian Academy of Sciences, Miskolc, P.O.B. 2, H-3515

V_w	water volume
V_{gk}	gas volume, constant in laboratory (= 14 700.0 cm ³)
V_{gv}	gas volume, variable
V_m	mole volume
V_p	pore volume
V_{pk}	pore volume, in laboratory (= 147.7475 cm ³)
V_{gkr}	gas volume, non-variable, in reservoir
V_{pkt}	pore volume, in reservoir
W	energy (work)
W_{stg}	storing energy
W_{std}	stored energy
Z	$Z(S_g) = Z[p_g; T; \varepsilon]$ compressibility
ε	factor relating to composition of natural gas
ρ	density
σ	interfacial tension
Θ	contact angle
β	elastic compressibility of water

Introduction

The author is convinced that energy will become the most valuable product for society in the near future and public view will change about the role of energy. Mankind will regard the conditions of survival of civilization in a way that they will be deeply affected by the changes of energy balance. Consequently, interest will also be focussed on small amounts of energy that have been previously neglected because of uncertainties in their determination or because their role have been regarded as unimportant. A radical change of view can be expected in the coming years since some kind of energy is attached to all aspects of life—either energy is generated or energy consumption takes place. Phenomena accompanying energy changes will not be regarded primary or secondary and civilization will rely more and more on energy generated and used since it is indispensable for life.

This study is aimed at providing a synthesis on theoretical and experimental work to analyse and determine the energy yield produced by changes of mass and state in fluid-bearing reservoirs to emphasize the energetical importance of natural states. We intend to investigate energy contents bound to various states of phase in porous reservoirs. The modification in these states of phase are combined with changes of the energy bearing importance for every-day-life, partly, because work is done by these states in certain cases at the expense of their energy content, partly, because in other cases the natural states of the reservoirs have to be changed for practical purposes requiring work to alter the energy of the system.

All components of energy of the fluid-bearing reservoirs have a definite function which have their effects simultaneously to our intentions—they either help the changes intended or act against them. The study will analyse the role and quantity of these energy components and investigate their effects on technical procedures aimed at meeting energy requirements of every-day-life.

Changes of energy content accompanied with interface phenomena

Interfacial energy is the most general energy component in the energy balance of porous reservoirs saturated with fluids. All changes of state having any effect on the interface are accompanied by certain change of energy which is the most important at the interface of the phases composing the porous reservoir, i.e. the rock and the fluids saturating the pores. Experts have never doubted that changes of state at interfaces have energetical consequences, but no attempt has been made to determine quantitatively the changes of energy content in connection with transformation of state. This fact was one of the reasons for selecting the analysis of energetical changes of interfacial phenomena as the topic of this study. It is also expected that by finding numerical correlations between the parameters of state and energy content, conclusions can be drawn from the changes of reservoir energy for the parameters of state. This would establish a new view in reservoir mechanics: the direction and amount of changes in the latent energy bound to interfacial phenomena could provide a useful tool for determining the character of the reservoir.

To avoid purely theoretical considerations, our investigation of the changes of energy content in connection with changes of state at interfaces will be focussed on problems of underground gas storage being one of the most important practical fields of energetics, essentially nothing but a complex physico-chemical phenomenon. Our considerations will emphasise the importance of theoretical analysis on physico-chemical phenomena in the every-day-practice.

1. Energy requirement of changes at interfaces in natural reservoirs

Underground gas storage—one of the great technical achievements of the latest decades—has been created partly by economical necessity, partly by the gaps between gas production and the interests of the consumer. A buffer is needed between the producer and consumer to solve the contradiction of interests and create a suitable balance of production and consumption. To operate this buffer the basic technical feature is that the compressor station produces the necessary injection pressure while compressing gas into the underground reservoir.

Under gas storage, multiple work is done whose components are usually not distinguished from each other and even they are not separately analysed.

Porous structures of underground geological formations suitable for gas storage—either exhausted gas reservoirs or non-gas-bearing geological structures—are never empty, but they always contain the possible formation fluids. This is mainly formation water which can be accompanied by residual gas content left behind after the primary production. Oil, even if it had been present in considerable amount, has

been usually displaced, thus practically there are only two phases: formation water and residual gas content with injected gas to be stored in the reservoir. These fluids and the porous rock form a rather complex thermodynamical system because of their interactions which is further complicated by the continuous change of the parameters of state. The partial phase exchange in the pores is the most general and most interesting of the possible changes. In this process the interfacial states are reorganized in the whole system and this reorganisation brings about a change in the energy of the system to an extent which bears great importance on the factors causing this change.

Multiple work required from the injection system, as indicated previously, is composed of the following elements:

a) Drainage of the wetting phase filling partly or fully the pores from the surface of the wetted solid phase. Since formation water can only be considered as a wetting phase if gas and water fill the pores of the reservoir, this condition means the drainage of formation water from the rock surface.

b) Transportation of the fluid phase separated from the rock surface to a farther part of the geological structure.

c) Compression of the gas to be stored to the required pressure in the pores free of formation water.

The injection system is expected to perform all these tasks simultaneously and continuously from the beginning to the end of the injection period and produce the required amount of stored gas at the required pressure to meet consumption's need. This part of the investigation is aimed at analysing the drainage of the wetting phase from the solid phase and determining the energy requirement of this process. Determining compression work under c) is expected the most simple task while the work needed for transportation of the wetting phase can only be calculated if the real geological structure is known since this work depends on the geometry of the flow channels.

Draining the wetting phase from the rock surface forms new interfaces. The change of the interfacial states brings about a change in energy of the system which can be indirectly followed through the change of the parameters characterizing interfaces. The cyclic operation of the reservoir consisting of injection and production of gas into and from the reservoir brings about the most general change of state, i.e. the change of the saturation in the pores. Work required to perform this periodic process can be characteristic of the interface. The basic physical phenomenon forming the main line of our investigations will be analysed on the simplest element of the porous system: physical and mathematical modelling of water displacement and gas injection will be carried out for a single capillary of arbitrary shape and size. Let us consider two of the basic equations of physics

$$F = Ap \quad (1)$$

and

$$dW = f(h) dh. \quad (2)$$

These equations containing functions between the quantities force, surface and pressure, as well as work, force and displacement will lead to mathematically formulating our general problem.

Let us consider a porous rock perfectly saturated with water from which a non-wetting phase, i.e. gas displaces formation water wetting the rock. Whatever is the geometry of the capillary composed of communicating pores, certain pressure difference is needed to displace the wetting fluid by a less or non-wetting phase from the pores. Capillary pressure being the maximum pressure difference between the phases and belonging to a steady state, can be regarded as the resistance of the wetting phase against the non-wetting one to be overcome by the second phase to fill the pores. Physically thinking the work is done by the non-wetting phase while its pressure overcomes the capillary resistance of the wetting phase.

The capillary composed of the pores among rock particles cannot be modelled mathematically, its shape and size is complicated thus the pore geometry cannot be taken into account in physico-chemical equations. Regardless of shape variations, to every capillary length dh an unknown cross-section A_c belongs yielding resistance force

$$F_c = A_c P_c \tag{3}$$

where P_c is the capillary pressure. This force is not constant because capillary pressure depends not only on interfacial tension and wettability considered constant but also on the geometry of the capillary changing continuously along its length. Overcomes, however, the second phase the resistance of the wetting phase and moves interface A_c between them by length dh against force F_c , then the displacement and the unknown capillary cross-section give expression

$$A_c dh = dV_g \tag{4}$$

However, change of volume and capillary pressure representing resistance, can be measured. Since capillary pressure changes as a function of pore geometry, thus capillary pressure is a function of the volume of one of the phases in the pores. Because the work required by the change of gas volume has to be determined, it is suitable for the mathematically precise formulation to regard capillary pressure as a function of gas volume:

$$P_c = P_c(V_g) \tag{5}$$

For work required by the displacement of gas-fluid interface, using Eqs (1)–(5)

$$dW = P_c(V_g) dV_g$$

can be written, whence

$$W = \int_{V_{g1}}^{V_{g2}} P_c(V_g) dV_g \tag{6}$$

Equation (6) expresses that the integral of the products of the resistances and the corresponding volumetric changes yields the volumetric work of the expanding gas while its volume changes from V_{g1} to V_{g2} .

This equation requires to measure both capillary pressure and change of gas volume in pore volume V_{pk} . Because this measurement is difficult to perform and needs special equipment, let us rearrange our equation to remove the gas volume of the pores. Accepting that the pores of the laboratory core sample are saturated with two phases only, i.e. natural gas and formation water, we have

$$V_g + V_w = V_{pk}$$

or

$$V_g = V_{pk} - V_w, \quad (7)$$

and for dV_g

$$dV_g = -dV_w.$$

Substituting into Eq. (6)

$$W = - \int_{\alpha_1}^{\alpha_2} P_c(V_{pk} - V_w) dV_w \quad (8)$$

while the limits of integration are

$$\alpha_1 = V_{pk} - V_{g1} = V_{w1}$$

and

$$\alpha_2 = V_{pk} - V_{g2} = V_{w2}.$$

In Eq. (8) only the change of water content V_w in the pores has to be determined which is much more easier to measure than the change of gas volume. Disadvantageous feature of the equation is however that it gives the work with respect to the total pore volume V_{pk} of the sample. Since the volume of the rock sample is limited, numerical results are less comprehensive for practice, they need certain reappraisal. To avoid this drawback, let us rearrange Eq. (7)

$$V_g = V_{pk} - V_w = V_{pk} \left[1 - \frac{V_w}{V_{pk}} \right].$$

Since

$$\frac{V_w}{V_{pk}} = S_w,$$

we have

$$V_g = V_{pk}[1 - S_w],$$

whence

$$dV_g = d[V_{pk} - V_{pk}S_w] = -V_{pk} dS_w$$

and the new limits of integration

$$\alpha_1 = \frac{V_{pk} - V_{g1}}{V_{pk}} = 1 - S_{g1} = S_{w1}$$

and

$$\alpha_2 = \frac{V_{pk} - V_{g2}}{V_{pk}} = 1 - S_{g2} = S_{w2}.$$

The final form of our equation becomes

$$W = -V_{pk} \int_{S_{w1}}^{S_{w2}} P_c [V_{pk}(1 - S_w)] dS_w. \tag{9}$$

Equation (9) enables us to limit the information required on measuring capillary pressure—saturation function only. No special laboratory technique is needed in this method, because the capillary pressure—saturation relationship can be measured in all reservoirmechanical laboratories. On the other hand, with

$$dS_w = d \left[\frac{V_w}{V_{pk}} \right],$$

V_{pk} constant and V_w changing only, Eq. (9) without coefficient V_{pk} before the integral gives work referred to unit pore volume. This result is more plausible and using V_{pk} it can be calculated for pore volume V_{pt} of the real reservoir. Work needed to the phase exchange in the whole reservoir is obtained by using the proper sign: volumetric work done by the system is negative and it is positive if it is done by an outside source of energy. R.H.S. of Eq. (9) indicates reduction in saturation, i.e. the volume of gas is increased while the volume of water is reduced in the pore, *viz.* work is done in the system.

In the view of our results, energy requirement of changes of interface has been calculated from data obtained by measurements on a laboratory experimental reservoir. Phases of the experimental reservoir, *viz.* rock, formation water and natural gas, originate from an actual gas reservoir. Their physical, chemical and physico-chemical properties have been maintained as far as it was possible. To minimize the effect of circumstances on results, our laboratory experiments have been carried out under reservoir conditions, i.e. high pressure and temperature. Thus, the difference between energy requirement of changes of state calculated from laboratory measurements and that of the actual reservoir can be expected small enough to eliminate any uncertainty in the final conclusions.

Measured data and calculated values of energy are omitted, instead, graphs of functions are shown in the figures enabling us to determine the direction and rate of change of energy content in connection with changes in interfacial states.

Figure 1 illustrates capillary pressure as a function of saturation. Curves I to IV belong to formation pressure 2 MPa while curves V and VI have been determined at formation pressures 4 and 6 MPa. Formation temperature was 348.16 K i.e. 75 °C in all experiments.

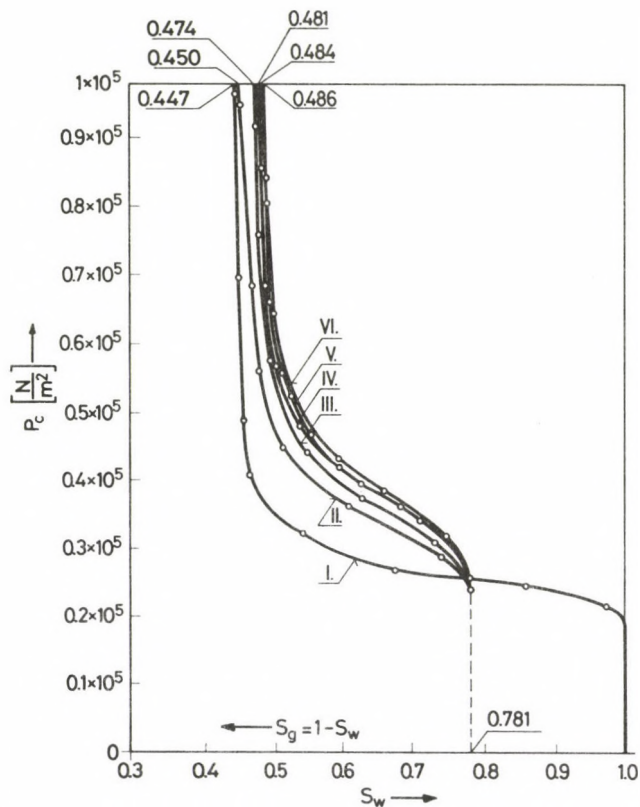


Fig. 1. Fundamental $P_c(S_w)$ function based on laboratory measurements

Measurement series were considered necessary to check the reliability of data measured under identical conditions and to decide whether there was any difference between data obtained under different conditions. As Fig. 1 indicates, only the first measurement series starts from saturation value $S_w = 1$, the starting water saturation has been selected for residual water saturation $S_{wr} = 0.781$ in all other measurement series. This helped to compare the results calculated from the measurement series because the same pressure differential viz. 10^5 Pa between the phases was characteristic of all cases and the difference between water saturations corresponding to this same pressure difference varied between 0.447 and 0.486 as indicated at the curves of Fig. 1.

Figure 2 illustrates energy requirement of changes of the interface as a function of mass change in the reservoir. Gas injected to the pores, displaces formation water primarily saturating the reservoir, and occupies it at the given reservoir pressure. Meanwhile the mass in the investigated part of the reservoir continuously changes because water is gradually displaced and its place is occupied by gas of increasing mass. However, this most general change in the state of the pores is not characterized by the

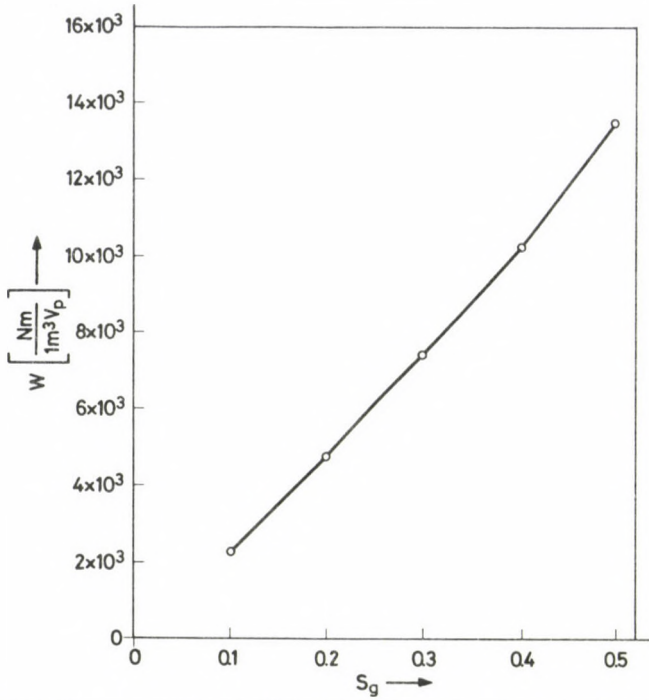


Fig. 2. Energy requirement of interfacial changes in unit pore volume V_{pkt}

instantaneous mass of the phases in practice, instead, energy requirement of the changes of interfaces is expressed in terms of a more plausible parameter, viz. instantaneous saturation. Therefore, energy requirement has been illustrated as a function of saturation in our diagrams, too.

Since

$$S_g = 1 - S_w$$

always holds, any of the two phases playing any role in the change of saturation can be considered an independent variable. Energy requirement of the change of saturation in 1 m^3 pores can be illustrated either as a function of the continuously increasing saturation of natural gas or the continuously decreasing saturation of formation water, both of them are plausible for practice. But since the aim of the change of phases in the pores is gas storage, it is suitable to regard gas saturation as independent variable because in this way the most important characteristic of the reservoir is properly emphasized from the practical point of view.

2. Energy requirement of interfacial changes in an ideal reservoir

Figure 2 shows that energy requirement of interfacial changes of 1 m³ pore volume is very high, much higher than it could have been expected before analysing the results of the experiments. This energy or work has to be done if saturation is intended to be changed against the energy represented by the interfacial properties. Numerical values are listed in Table I.

Table I

S_g	0.1	0.2	0.3	0.4	0.5
W N m	2247	4752	7387	10180	13407

Considering values in Table I, the total energy requirement of gas storage might seem extraordinarily high. The values in Table I represent energy needed to separate phases only, and it will be increased by the compression work of gas. This work further increases if the part of the reservoir affected by gas injection increases and this work has to be done every time when gas is injected into the reservoir and formation water is moved in the pores. During this process new interfacial structures are formed and a major part of specific energy requirement of phase exchange seems to be realized in this work. To avoid any error, theoretical considerations of our previous chapter have to be checked by a method differing in its details from those to be checked. Since other authors failed to analyse this problem, there were no data available to be used for comparison. Therefore some of the basic principles of physical chemistry and thermodynamics shall be used as means of control.

The physical phenomenon will be related to the most simple porous medium, *viz.* a cylindrical capillary of constant cross-section. Let us now carry out the following experiment; the porous system shall be brought into contact with an arbitrary fluid wetting the solid phase. This fluid will rise in the pores as long as the weight of the fluid column achieves a balance with the molecular forces resulting from the interactions of the molecules of the solid, fluid and gaseous phases. For equilibrium the following equation holds:

$$r^2\pi h \Delta\rho g = 2\pi r\sigma \cos\theta = F_c,$$

whereas molecular forces acting along perimeter $2\pi r$ of the capillary are replaced by resulting force F_c .

In this equation we can write

$$r^2\pi = A_c$$

and in case of equilibrium, at the state of rest of the meniscus

$$h\Delta\rho g = P_c.$$

Our equation can now be written as

$$P_c A_c = 2\pi r \sigma \cos \theta = F_c$$

expressing that the force calculated as the product of capillary pressure P_c and cross-section A_c belonging to this pressure is in equilibrium with resultant F_c of the molecular forces.

Let us expand the gas above the meniscus to push the interface by length dh against force F_c . The overcome constant resistance calculated by dh

$$dW = P_c A_c dh = \sigma \cos \theta 2\pi r dh,$$

whereas

$$A_c dh = dV_g$$

and

$$2\pi r dh = dA_{sg}.$$

With these values

$$dW = P_c dV_g = \sigma \cos \theta dA_{sg}$$

and because in a capillary of constant cross-section capillary pressure is independent of the place of the meniscus

$$W = -P_c \int_{V_{g1}}^{V_{g2}} dV_g = -\sigma \cos \theta \int_{A_{sg1}}^{A_{sg2}} dA_{sg}. \tag{10}$$

This "porous system" is one of the possible thermodynamic systems and the mathematical equation expressing an elementary experiment gives the volumetric work of gas expansion—according to a strict thermodynamic view. This work, similarly to the measurements on sandstone samples from natural reservoirs, is the integral of the products of differential changes of volume and the corresponding resistances to overcome. If only the solid-gas interface changes with the volume dV_g in our experiment, we can state that W is nothing but the work of separation of the solid-fluid interface or, what is essentially the same, that of creating the gas-solid interface. This is expressed by the R.H.S. of Eq. (10) giving the total work done in terms of the product of energy needed to produce unit surface and the change of the total solid-gas interfacial area $[A_{sg2} - A_{sg1}]$. This is proved in our porous system of cylindrical capillary not only by the mathematical equation, but by experimental consideration, too. Capillary pressure is namely correlated to the form of the meniscus, i.e. gas-liquid interface, and since P_c is everywhere the same in a capillary of constant radius, necessarily gas-liquid interface does not change either, therefore work done fully refers to the energy required by the change on the solid-liquid interface. If the change in the

pore does not occur in this way but the gas-liquid interface also changes instead of or beside the change of the solid-liquid interface, our equation gives the work needed for the interfacial changes even now whose total value is furnished by the integral of products $P_c dV_g$. This work, however, does not fully refer to the change of the solid-liquid interface, one part of it is required by the change of the liquid-gas interface. All this promotes the intention of our experiment: to prove or deny the correctness of the results obtained for real reservoirs.

Let us return to Eq. (10) and continue our experiment but in a porous system suitable for storage and consisting of cylindrical capillaries of the same size and shape as previously but of infinite number. Force and energy conditions of a single capillary are valid for each of these capillary systems. If the pores of this system are also saturated with two phases, *viz.* formation water and gas only, correlation

$$V_g + V_w = V_{pk}$$

of natural rock samples is also valid. Hence

$$dV_g = -dV_w$$

and with the new limits of integration

$$W = -P_c \int_{V_{w1}}^{V_{w2}} dV_w. \quad (11)$$

This equation is suitable for control but from the calculation point of view it is more advantageous to introduce changes of saturation instead of changes of volume:

$$V_w = V_{pk} S_w,$$

$$dV_w = V_{pk} dS_w.$$

The limits of integration will be

$$S_w = \frac{V_{w1}}{V_{pk}} = S_{w1}$$

and

$$S_w = \frac{V_{w2}}{V_{pk}} = S_{w2}.$$

Our equation becomes

$$W = -V_{pk} P_c \int_{S_{w1}}^{S_{w2}} dS_w. \quad (12)$$

Work requirement of the phase exchange in a porous system of arbitrary extension V_{pk} can be calculated with this equation if capillary pressure given by capillary dimension, interfacial tension and wettability as well as the change of saturation are known. For convenience, a porous system of 1 m^3 has been chosen for

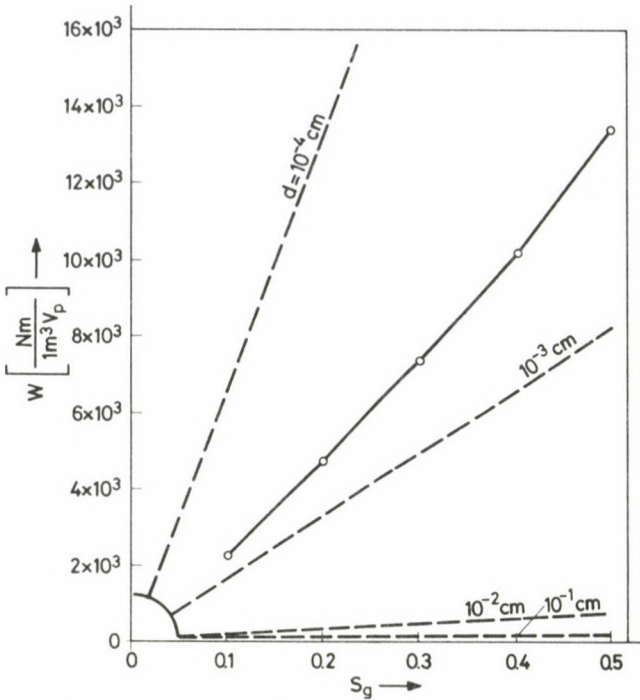


Fig. 3. Energy requirement of the phase exchange in an ideal pore space of cylindrical capillaries as a function of S_g

the purposes of the control investigation, the interfacial tension of the fluid phases has been arbitrarily taken for $72 \cdot 10^{-3} N/m$ and the system has been perfectly water wet i.e. $\cos \theta = 1$.

To allow conclusions, the results of our theoretical control experiment are illustrated in Fig. 3 for various capillary diameters in a way that energy data referring to each two capillary diameters intercept data obtained for the pore volume of $1 m^3$ of the real reservoir.

Energy values obtained for the capillary porous system are probably reduced by the simplicity of the pore structure while wettability and interfacial tension tend to exert an effect towards increasing the energy requirement of the phase exchange because the possible maximum values have been assumed.

In spite of all that Fig. 3 furnishes a satisfying argument for our method. The data about the energy of interfacial properties within energy requirement of the phase exchange can be accepted and they provide a good orientation concerning the partial energy consumption of underground gas storage. This will enable us to determine the total energy requirement of underground gas storage with a good approximation.

3. Dependence of changes of the interfaces on the pore volume

Equation (9) shows that expression

$$- \int_{S_{w1}}^{S_{w2}} P_c [V_{pk}(1 - S_w)] dS_w$$

furnishes energy equivalence of interfacial changes in the pore volume V_{pk} referred to unit pore volume. For a pore volume of arbitrary magnitude, e.g. the size of a real reservoir, this energy value has to be multiplied by the volume V_{pt} of the reservoir to obtain the total energy requirement of the change of saturation in the reservoir. If the effective work requirement of the change of gas saturation from $S_g=0$ to $S_g=0.5$ (s. Table I) is calculated for a reservoir of 10^6 m^3 pore volume, it seems that solely the work of separating the wetting and wetted phases requires very great energy. Numerical values are contained in Table II.

Table II

S_g	Nm
0.1	2 246 791 794
0.2	4 752 425 331
0.3	7 387 313 200
0.4	10 180 432 460
0.5	13 407 139 900

A reservoir with a pore volume of 10^6 m^3 cannot be considered a large one, nevertheless the work requirement seems to be very high. Taking the values expressed in Nm, it cannot be decided whether this work is really great and where does it lie among the other energy constituents of the total energy requirement of the full change of state. To answer this question, this work will be compared with the volumetric work of the change of gas volume accompanied with the change of state in the reservoir. This comparison will, however, give an orientation about the order of magnitude of the energy or energy equivalence of the interfacial changes only.

4. Energy requirement of interfacial changes in terms of volumetric work of the system

Every value of the parameters of state of the system i.e. pore volume and the fluids saturating it, determines a certain state of energy whose changes can be reflected by the instantaneous values of the parameters of state. In the instant before the less wetting phase enters the pore volume, equation

$$p_g V_g = n Z RT \tag{13}$$

expresses this state. This state can be represented by capillary pressure measurement equipment (Fig. 4) whereas gas volume V_g is that above semipermeable diaphragm and the total gas volume connected to it. By overcoming the resistance of the aqueous

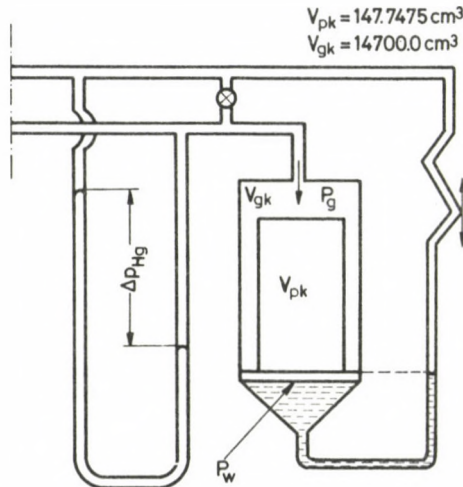


Fig. 4. Principal layout of apparatus enabling changes of mass and state in a porous fluid reservoir

phase, gas takes the place of displaced water in the pore volume. It can easily be seen that the state of the gaseous phase continuously changes during displacement and if the process is strictly isotherm, gas pressure and volume change only. For this most simple case approximating reality only, the change of the state of energy of the gas can be described by equation

$$d[p_g V_g] = n RT dZ . \tag{14}$$

Expressing V_g from Eq. (13), we have

$$V_g = n RT \frac{Z}{p_g}$$

and considering the signs of the terms in Eq. (14) with a systems-centric approach, the differential equation to be solved becomes

$$-p_g dV_g = n RT Z \ln p_g - n RT dZ \quad (15)$$

and the solution is

$$- \int_{V_{g0}}^{V_g} p_g dV_g = n RT \int_{\ln p_{g0}}^{\ln p_g} Z \ln p_g - n RT \int_{Z_0}^Z dZ. \quad (16)$$

Boundary conditions of the differential equation are given by the parameters of state of the system or they can be calculated for arbitrary i -th state from parameters p_{g0} , V_{g0} and Z_0 of the initial state

$$\frac{p_{gi}}{Z_i} V_{gi} = \frac{p_{gi-1}}{Z_{i-1}} V_{gi-1}, \quad (17)$$

hence

$$p_{gi} = \frac{p_{gi-1}}{Z_{i-1}} V_{gi-1} \frac{Z_i}{V_{gi}}. \quad (18)$$

But since p_g and Z are in mutual interaction throughout the whole process, p_{gi} of the i -th state can only be determined by compressibility

$$Z_i = Z[p_{gi}; T; \varepsilon].$$

There are two possible ways, the first of them can only be expected to furnish an approximative solution of Eq. (16). In Eq. (18) Z_i is required to determine p_{gi} . Because of the above reason, for an approximative solution let us take compressibility Z_{i-1} already known instead of Z_i and calculate p_{gi} . The solution is obviously approximative and differs from the correct value of p_{gi} to that extent as Z_{i-1} differs from Z_i . Equation (18) has now to be written emphasizing Boyle's equation and the approximation applied as

$$p_{gi} = \frac{p_{g0}}{Z_0} \frac{V_{g0}}{V_{gi}} Z_{i-1}. \quad (19)$$

Equation (19) enables us to calculate the approximate value of

$$p_g = p_g(S_g)$$

and from each p_g the corresponding Z . V_g is obtained from measurement, thus everything is available for the solution of Eq. (16). But since our aim is to decide whether energy component due to the interfacial properties and its change with the mass and state can be regarded great or it cannot, let us compare this energy

component to the volumetric work of the expanding gas. Taking into account L.H.S. of Eq. (16) and the fact that all correlations refer to a state of equilibrium of the system,

$$p_g = p_w + P_c$$

holds and we can write

$$- \int_{V_{g0}}^{V_g} p_g dV_g = - \int_{V_{g0}}^{V_g} (p_w + P_c) dV_g. \tag{20}$$

By solving Eq. (20) one can answer the question whether energy needed to overcome capillary forces can really be regarded great since ratio

$$\frac{\int_{V_{g0}}^{V_g} p_g dV_g}{\int_{V_{g0}}^{V_g} P_c dV_g}$$

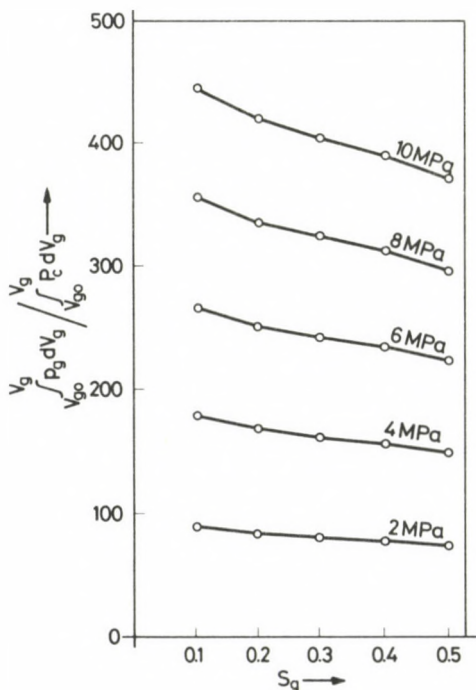


Fig. 5. Ratio of the volumetric work of the gas and the energy requirement of interfacial changes as a function of the state of reservoir in pore volume V_p

can be calculated as a function of the state of the system. Figure 5 illustrating numerical values of this ratio shows that the change of the total energy of storage amounts to several hundredfold of that due to interfacial properties with increasing formation pressure representing reservoir resistance. The decline of the ratio of these energy components with increasing saturation follows from the fact that capillary resistance increases more rapidly with increasing gas content in the pore volume than the total energy requirement of the change in the pore volume.

Another method to determine the relative magnitude of the energy requirement of interfacial changes is not of approximative character since it relies on the determination of parameters p_{gi} and Z_i applying Boyle's equation. The method will be discussed in our next paper in detail because theoretical considerations to be analysed there will promote its understanding. The two methods will then be compared and an attempt will be made at deciding their reliability and their advantages and disadvantages from practical point of view.

ENERGY VALUE OF CHANGES OF MASS AND STATE IN POROUS RESERVOIRS

GY ZOLTÁN¹ †

[Manuscript received September 12, 1984]

The study deals with energy components of porous reservoirs in connection with changes in saturation and elastic energy of formation water. These energy components, similarly to that connected with changes in interfacial energy, are determined by changes of mass and state of the system.

Keywords: capillary pressure; compressibility; formation pressure; interfacial tension; porous reservoir; saturation; wettability

Symbols

A	surface area, interfacial area
A_c	capillary cross-section
A_{sg}	solid-gas interfacial area
d	capillary diameter
F	force
F_c	capillary resistance
g	acceleration due to gravity
h	height
i	number of observation (subscript)
J	$J(S_g) = p_g/Z$
K	$K(S_g) = \frac{p_g}{Z} S_g$
n	mole number
p	pressure
p_g	gas pressure = $p_w + P_c$
p_w	water pressure, constant (= 2, 4, 6, 8, 10 MPa)
P_c	capillary pressure = $P_c(S_g) = P_c'(S_w)$
r	capillary radius
R	gas constant
S	saturation
S_g	gas saturation
S_w	water saturation
S_{wres}	residual water saturation
S_{gl}	gas saturation at the inflexion point of function $P_c(S_g)$
T	temperature
T_{norm}	normal temperature
V	volume
V_k	volume, non-variable

¹ Chemical Research Laboratory for Mining of the Hungarian Academy of Sciences, Miskolc, P.O.B. 2, H-3515

V_v	volume, variable
V_g	gas volume
V_w	water volume
V_{gk}	gas volume, constant, in laboratory (= 14 700.0 cm ³)
V_{gv}	gas volume, variable
V_{mol}	mole volume
V_p	pore volume
V_{pk}	pore volume, in laboratory (= 147.7475 cm ³)
V_{gkt}	gas volume, non-variable, in reservoir
V_{pkt}	pore volume, in reservoir
W	energy (work)
W_{stg}	storing energy
W_{std}	stored energy
Z	$Z(S_g) = Z[p_g; T; \varepsilon]$ compressibility
ε	factor relating to composition of natural gas
ρ	density
θ	contact angle
β	elastic compressibility of water
σ	interfacial tension

1. Energy of an experimental reservoir in laboratory

Regardless of the technical conditions of the experimental system, according to the principles to be followed, a constant gas volume V_{gk} is attached to pore volume V_{pk} of the core sample saturated with water (Zoltán 1986). Gas pressure at the instant of beginning equals the pressure of aqueous phase saturating pore volume V_{pk} , i.e.

$$p_{g0} = p_w.$$

Instantaneous state of n moles of the gas in the system is described by equation

$$p_g V_g = n Z_0 R T. \quad (1)$$

If gas mass in volume V_{gk} steadily increases, gas pressure also increases keeping gas volume constant until gas pressure reaches the resistance resulting from the sum of formation pressure and threshold capillary pressure. Equilibrium at this point becomes

$$p_g = p_w + P_{ck}.$$

With a further increase of gas mass, its pressure exceeds the above value corresponding to a state of equilibrium and water is displaced from pore space V_{pk} until gas pressure

$$p_g = p_w + P_c$$

calculated from

$$P_c = p_g - p_w$$

reaches equilibrium with the resistance represented by the sum of formation pressure and capillary pressure, the latter depending on the interfacial properties of the porous

reservoir. Since the interfacial properties *viz.* wettability, interfacial tension and specific surface area jointly determine the state of saturation as a measurable parameter, P_c can always be expressed as a function of the saturation of one of the saturating phases:

$$P_c(S_g) = P'_c(S_w).$$

Saturation of one of the phases can always be calculated from that of the other because for two phases, *viz.* water and gas

$$S_g + S_w = 1.$$

For convenience, independent variables indicating the state of saturation will only be denoted if omitting it would cause ambiguity. Consequently, instead of

$$p_g(S_g) = p_w + P_c(S_g)$$

we will use

$$p_g = p_w + P_c.$$

The basic equation of the change of state belonging to the differential change of gas mass, can be written as

$$p_g dV_g + V_g dp_g = RT d[nZ]. \tag{2}$$

If we start observing the energy content of the system at the instant when

$$p_g = p_w$$

i.e.

$$P_c = 0,$$

the change of energy content of the system through arbitrary change of state will be obtained from differential equation (2) as

$$\int_{V_{g0}}^{V_g} p_g dV_g + \int_{p_{g0}}^{p_g} V_g dp_g = RT \int_{Z_0}^Z n dZ + RT \int_{n_0}^n Z dn \tag{3}$$

whereas the lower limits of integration indicate parameters of state, compressibility and gas mass expressed in mole number corresponding to $P_c = 0$. Equation (3) describes the change of energy accompanying the physical phenomenon as accurately as the parameters of state of the phenomenon, *viz.* pressure, volume and mass of gas and compressibility depending on gas pressure and temperature as well as their changes, can be observed. Gas temperature will be regarded constant according to Eq. (2) and it will equal the temperature of the experimental system or formation temperature.

For the parameters of state

$$p_g = p_w + P_c,$$

$$V_g = V_{gk} + V_{gv},$$

$$n = n_I + n_{II}$$

and

$$Z = Z_I = Z_{II}, \quad (4)$$

always hold where I indicates parameters characterizing changes in gas space V_{gk} attached to pore space while II denotes mass and compressibility of the gas with changing volume in the pore volume. Z is the same in the pore space and in the free gas space attached to it because the pressure, temperature and composition is considered identical in both volumes. Consequently, function

$$Z = Z[p_g; T; \varepsilon]$$

can only change with gas pressure. Substituting Eqs (4) into Eq. (2), we obtain with the new limits of integration

$$\begin{aligned} & \int_{V_{g0}}^{V_g} p_w dV_g + \int_{V_{g0}}^{V_g} P_c dV_g + \int_{p_{g0}}^{p_g} V_{gk} dp_g + \int_{p_{g0}}^{p_g} V_{gv} dp_g = \\ & = RT \int_{Z_0}^Z n_I dZ + RT \int_{Z_0}^Z n_{II} dZ + RT \int_{n_{I0}}^{n_I} Z dn_I + RT \int_{n_{II0}}^{n_{II}} Z dn_{II}. \end{aligned} \quad (5)$$

Equation (5) gives the components of the change of energy content initiated by the mass change of the system as follows:

- volumetric work of the expanding gas against formation pressure represented by constant water pressure;
- volumetric work of the expanding gas against capillary pressure depending on saturation;
- compression work in constant gas space V_{gk} outside pore space;
- compression work in variable gas volume V_{gv} in the pore space;
- change of the internal energy of the gas in gas volume V_{gk} outside pore space;
- change of the internal energy of the gas in variable gas volume V_{gv} in pore space;
- energy required by the increase of gas mass in constant gas volume;
- energy required by the increase of gas mass in variable gas volume of the pore space.

Last two terms of R.H.S. of Eq. (5)

$$RT \int_{n_{I0}}^{n_I} Z dn_I + RT \int_{n_{II0}}^{n_{II}} Z dn_{II} = RT \int_{n_0}^n Z dn, \quad (6)$$

i.e energy equivalent to the change of mass in the reservoir can also be considered as the work done by an external system to alter mass and state of the reservoir to the extent and direction expressed by Eq. (6).

Equation (5) describes the rate of energy change of the system at conditions fixed by itself. Though these conditions do not make difficulties in the application, Eq. (5) fails to really be suitable. On the one hand it is not practical enough for engineers because it expresses gas mass in terms of mole numbers instead of pressure and volume, and on the other hand it contains an excessively large number of parameters hampering assessment of the essence of the physical process. Equations (5) and (6) will be, therefore, rewritten in a way that at keeping its accuracy, geometrical volumes and pressure values obtained from laboratory experiments will be used. From among the possible ways the simplest one will be selected. Let us consider identities

$$n_I = \frac{n_I V_{\text{mol}}}{V_{\text{mol}}}$$

and

$$n_{II} = \frac{n_{II} V_{\text{mol}}}{V_{\text{mol}}}$$

which will be used to eliminate mole number. First, products $n_I V_{\text{mol}}$ and $n_{II} V_{\text{mol}}$ will be determined.

For a gas mass containing n moles in an arbitrary state we can write

$$p_g V_g = n Z R T.$$

Let us transform our system into another state with parameters T_{norm} and p_{g0} keeping the gas mass constant. Gas volume will be expressed by mole volume. For the new state we get

$$p_{g0} n V_{\text{mol}} = n Z_0 R T_{\text{norm}}.$$

From latter two equations we obtain

$$n V_{\text{mol}} = \frac{Z_0 T_{\text{norm}}}{p_{g0} T} \frac{p_g}{Z} V_g.$$

Since the volume of the gas outside pore space is

$$V_{gk},$$

and gas volume inside pore space can be expressed by product

$$V_{pk} S_g$$

in any state of the pore space, thus mole numbers of gas masses in each of the volumes can be written as

$$n_I = \frac{Z_0 T_{\text{norm}}}{p_{g0} V_{\text{mol}}} \frac{V_{gk}}{T} \frac{p_g}{Z}$$

and

$$n_{II} = \frac{Z_0 T_{\text{norm}}}{p_{g0} V_{\text{mol}}} \frac{V_{pk}}{T} \frac{p_g}{Z} S_g.$$

Introducing expressions

$$\frac{p_g}{Z} = J$$

and

$$\frac{p_g}{Z} S_g = K,$$

and taking into account that for a gas mass of a single mole

$$\frac{Z_0 T_{\text{norm}}}{p_{g0} V_{\text{mol}}} = \frac{1}{R}$$

holds, we have for mole numbers n_I and n_{II}

$$n_I = \frac{V_{gk}}{RT} J$$

and

$$n_{II} = \frac{V_{pk}}{RT} K.$$

Hence the changes in mole number are

$$dn_I = \frac{V_{gk}}{RT} dJ$$

and

$$dn_{II} = \frac{V_{pk}}{RT} dK.$$

Substituting expressions n and dn into Eqs (5) and (6) and rewriting the limits of integrations according to the substitutions, our equations become more plausible and easier to handle:

$$\begin{aligned} & \int_{V_{g0}}^{V_g} p_w dV_g + \int_{V_{g0}}^{V_g} P_c dV_g + \int_{p_{g0}}^{p_g} V_{gk} dp_g + \int_{p_{g0}}^{p_g} V_{gv} dp_g = \\ & = V_{gk} \int_{Z_0}^Z J dZ + V_{pk} \int_{Z_0}^Z K dZ + V_{gk} \int_{J_0}^J Z dJ + V_{pk} \int_{K_0}^K Z dK, \end{aligned} \quad (7)$$

and

$$RT \int_{n_0}^n Z \, dn = V_{gk} \int_{J_0}^J Z \, dJ + V_{pk} \int_{K_0}^K Z \, dK . \tag{8}$$

Since

$$V_g = V_{pk} S_g$$

holds for every state of the system, Eq. (7) can also be written so as to contain geometric volumes in which the change of energy content represented by terms of Eq. (7) takes place:

$$\begin{aligned} & V_{gk} \int_{p_{g0}}^{p_g} dp_g - \int_{Z_0}^Z J \, dZ + V_{pk} \int_{S_{g0}}^{S_g} p_w \, dS_g + \int_{S_{g0}}^{S_g} P_c \, dS_g + \\ & + \int_{p_{g0}}^{p_g} S_g \, dp_g - \int_{Z_0}^Z K \, dZ = V_{gk} \int_{J_0}^J Z \, dJ + V_{pk} \int_{K_0}^K Z \, dK . \end{aligned} \tag{9}$$

From our previous discussions it follows that in Eq. (7)

$$V_{gk} \int_{J_0}^J Z \, dJ = \int_{p_{g0}}^{p_g} V_{gk} \, dp_g - V_{gk} \int_{Z_0}^Z J \, dZ \tag{10}$$

and

$$\begin{aligned} & V_{pk} \int_{K_0}^K Z \, dK = \int_{V_{g0}}^{V_g} p_w \, dV_g + \int_{V_{g0}}^{V_g} P_c \, dV_g + \\ & + \int_{p_g}^{p_{g0}} V_{gv} \, dp_g - V_{pk} \int_{Z_0}^Z K \, dZ \end{aligned} \tag{11}$$

must hold which is obviously true.

Considering Eqs (7)–(11) it can be observed that the components of the change of total energy content being equivalent to the changes of mass and state in the pore space of the fluid-bearing reservoir, are strictly local and functional, i.e. energy elements are used for distinct tasks and in distinct places. This observation can be utilized when we intend to change the mass and state of a reservoir. Knowing the volumetric elements of the reservoir structure, the quantities of their parameters of state and the changes of energy given by the rates and directions of parameter changes, we can influence the system according to our purposes to control the technical processes energetically suitably.

2. Minimum in the specific energy of the change of saturation

True reflexion of the physical phenomena in the laboratory experimental reservoir by Eqs (3), (5) and (7) to (11) inspires to investigate analytically the change of energy in the system—with a view on practical use in the future.

Equations (10) and (11) contain changes of energy content accompanying changes of state of the system according to their original place and further investigations also seem suitable to be conveyed so as to separate rates and directions of changes according to geometric volumes V_{gk} and V_{pk} .

From Eqs (10) and (11) we have

$$dW_I(S_g) = V_{gk}Z dJ = V_{gk} dp_g - V_{gk}J dZ \quad (12)$$

and

$$dW_{II}(S_g) = V_{pk}Z dK = p_w dV_g + P_c dV_g + V_{gv} dp_g - V_{pk}K dZ, \quad (13)$$

whence

$$dW_I(S_g) + dW_{II}(S_g) = dW(S_g) = RTZ dn. \quad (14)$$

Substituting

$$\frac{p_g}{Z} = J$$

into Eq. (12) and rearranging, we have

$$dW_I(S_{gi}) \simeq \Delta W(S_{gi}) = V_{gk} \left\{ p_{gi} - p_{gi-1} - \frac{\Delta Z_i}{2} \left[\frac{p_{gi}}{Z_i} + \frac{p_{gi-1}}{Z_i - 1} \right] \right\}. \quad (15)$$

Equation (15) shows that energy elements ΔW_I change as the state of the system changes and $\Delta W_I(S_g)$ has a definite minimum whose place is determined by the point of inflexion of function $p_g(S_g)$ because where

$$p_{gi} - p_{gi-1} = \text{Min}$$

holds, there

$$\frac{dp_g(S_g)}{dS_g}$$

has a minimum. At this minimum

$$\frac{d^2 p_g(S_g)}{dS_g^2} = 0$$

also holds. Furthermore, where

$$p_g - p_{gi-1} = \text{Min}$$

holds, there from

$$Z = Z[p_g(S_g); T; \varepsilon]$$

we have

$$Z_i = Z_i - Z_{i-1} = \text{Min}.$$

Summing up, we have found that energy elements in V_{gk} determined by Eq. (15) change in the range of saturation investigated in a way that consecutive values of ΔW_I have a minimum at a certain saturation. This minimum can be found at the place of inflexion of function $p_g(S_g)$.

The other component of $dW(S_g)$ can similarly be obtained from Eq. (13):

$$dW_{II}(S_{gi}) \simeq \Delta W_{II}(S_{gi}) = V_{pk} \left\{ p_{gi} S_{gi} - p_{gi-1} S_{gi-1} - \frac{\Delta Z_i}{2} \left[\frac{p_{gi}}{Z_i} S_{gi} + \frac{p_{gi-1}}{Z_{i-1}} S_{gi-1} \right] \right\}. \tag{16}$$

Knowing that function $p_g(S_g)$ is strictly monotonously increasing and has an inflexion, Eq. (15) gave an immediate idea about the relative change of energy elements ΔW_I in the range of saturation investigated. However, Eq. (16) fails to furnish similar orientation about the change of term ΔW_{II} . Equation (16) reveals only as much as that $\Delta W_{II}(S_g)$ cannot be zero even if

$$p_{gi-1} = p_{gi} = p_{gi+1}$$

holds but it does not inform us unambiguously about changes in energy elements ΔW_{II} contributing to the changes of energy content required by the change of state of the system.

Since Eq. (15) proves the existence of a minimum and determines its place in connection with

$$dW_I(S_g),$$

it seems suitable to look for similar information concerning term

$$dW_{II}(S_g).$$

Elementary energy values $dW_I(S_g)$ and $dW_{II}(S_g)$ compose the change of energy content required by unit change of saturation according to Eq. (14) which can be important if we intend to rationalize the changes of state in a reservoir energetically. Thus the question is how do energy elements

$$dW_{II}(S_g)$$

change in the range of saturation investigated, i.e.

$$dW_{II}(S_{gi}) \cong dW(S_{gi+1}) \quad ? \tag{17}$$

From Eqs (13) and (16) we obtain without any approximation or neglection

$$\frac{\Delta p_{gi}}{\Delta p_{gi+1}} \cong \frac{\frac{S_{gi}}{Z_i} + \frac{S_{gi+1}}{Z_{i+1}} + \Delta S_{gi+1}}{\frac{S_{gi}}{Z_i} + \frac{S_{gi-1}}{Z_{i-1}} - \Delta S_{gi}}. \quad (18)$$

For convenience we will write Eq. (18) in a simpler form

$$\text{L.H.S.} \cong \text{R.H.S.}$$

It can be easily proved that

$$\text{L.H.S.} = \frac{\Delta p_{gi}}{\Delta p_{gi+1}} \simeq \frac{\left(\frac{\partial p_g}{\partial S_g}\right)_{S_g = \frac{S_{gi} + S_{gi-1}}{2}}}{\left(\frac{\partial p_g}{\partial S_g}\right)_{S_g = \frac{S_{gi} + S_{gi+1}}{2}}},$$

i.e. L.H.S. is nothing but a good approximation of the ratio of derivatives calculated from consecutive terms S_{gi-1} , S_{gi} and S_{gi+1} . And since

$$p_g(S_g) - p_w = P_c(S_g)$$

holds for every state of saturation of the reservoir, we can write

$$\left(\frac{\partial p_g}{\partial S_g}\right)_{S_g = \frac{S_{gi} + S_{gi-1}}{2}} = \left(\frac{\partial P_c}{\partial S_g}\right)_{S_g = \frac{S_{gi} + S_{gi-1}}{2}} \quad (19)$$

and, similarly,

$$\left(\frac{\partial p_g}{\partial S_g}\right)_{S_g = \frac{S_{gi} + S_{gi+1}}{2}} = \left(\frac{\partial P_c}{\partial S_g}\right)_{S_g = \frac{S_{gi} + S_{gi+1}}{2}} \quad (20)$$

And now it can be seen that L.H.S is the ratio of derivatives of function

$$P_c = P_c(S_g).$$

From the character of $P_c(S_g)$ it can easily be proved that P_c strictly monotonously increases as a function of S_g towards P_{ci} at inflexion point while ratio L.H.S. calculated from derivatives strictly monotonously decreases approaching unity with the closest approximation in the differential proximity of S_{g1} . With a further increase of S_g , in the range of saturation

$$S_g > S_{g1}$$

L.H.S. continues to strictly monotonously decrease towards a value less than unity achieving it at saturation

$$S_g = 1 - S_{wres}.$$

Concerning L.H.S. we can sum up the following statements. In the range of saturation

$$S_g < S_{gl}$$

$$\text{L.H.S.} > 1$$

always holds, while for

$$S_g > S_{gl}$$

we have

$$\text{L.H.S.} < 1 .$$

Let us now consider R.H.S. of Eq. (18). From the changes of S_g and the character of function

$$Z = Z(S_g)$$

it is easy to realize that R.H.S. (S_g) strictly monotonously decreases but its value always exceeds unity even at

$$S_g = 1 - S_{wres} .$$

Analysing now the whole Eq. (18) we see that R.H.S. exceeds unity over the whole range of saturation from $S_g = 0$ to $S_g = 1 - S_{wres}$, while L.H.S. remains below unity in the range

$$S_g > S_{gl} ,$$

and exceeds it in the range

$$S_g < S_{gl} .$$

However, our results obtained so far fail to give precise explanation about the relative magnitude of L.H.S. and R.H.S. of Eq. (18). A calculation of numerical values furnishes data listed in Table I for $p_w = 2$ MPa and 10 MPa using Eq. (18).

In Table I numerical values of R.H.S. follow the theoretical considerations only, i.e. R.H.S. strictly monotonously decreases but exceeds unity. L.H.S., however, also exhibits values differing from those to be expected by the analytical results.

Although these anomalies can be explained by obvious irregularities of function

$$P_c = P_c(S_g)$$

determined experimentally, it seems nevertheless justifiable to elucidate theoretically our basic question

$$dW_{II}(S_{gi}) \cong dW_{II}(S_{gi+1})$$

because the change of energy content of the porous reservoir could not be determined otherwise with sufficient accuracy. Equation (14) has indicated already that

$$dW_I(S_g) + dW_{II}(S_g) = dW(S_g)$$

Table 1. Calculated values of L.H.S. and R.H.S. of Eq. (18) for $p_w = 2$ MPa and 10 MPa

i	S_g	L.H.S.	R.H.S.	
			2 MPa	10 MPa
0	0.000	0.000	0/0	0/0
1	0.000	7.540	+	+
2	0.005	5.640	224.545	47.095
3	0.010	1.273	2.965	2.840
4	0.015	1.500	1.987	1.939
5	0.020	1.100	1.659	1.630
6	0.025	1.333	1.494	1.474
7	0.030	1.000	1.396	1.380
8	0.035	0.882	1.330	1.317
9	0.040	0.944	1.283	1.272
10	0.045	1.385	1.248	1.238
11	0.050	0.813	1.220	1.212
12	0.055	1.143	1.198	1.191
13	0.060	0.933	1.180	1.174
14	0.065	1.000	1.165	1.159
15	0.070	1.000	1.152	1.147
16	0.075	1.000	1.142	1.137
17	0.080	1.071	1.132	1.127
18	0.085	1.076	1.124	1.120
19	0.090	1.083	1.117	1.112
20	0.095	0.923	1.110	1.108
21	0.100	1.083	1.104	1.101

elementary change of energy content furnished energy equivalent of change of mass and phase in the system referring to an arbitrary independent variable. If the terms of above summation are known, technical processes may be controlled in such a way that their sum has the most advantageous value.

Let us choose an indirect way for the determination of

$$dW_{II}(S_g).$$

From our previous discussions we know that in the range of saturation

$$S_g > S_{g1}$$

we have

$$\text{L.H.S.} < \text{R.H.S.}$$

Therefore for these saturation values

$$dW_{II}(S_{gi}) < dW_{II}(S_{gi+1})$$

always holds, i.e. in this range of saturation energy elements $dW_{II}(S_g)$ exhibit a strictly monotonous increase as a function of S_g .

For the range of saturation

$$S_g < S_{g1}$$

we have

$$\text{L.H.S.} > 1.$$

But because we also know that numerical values of R.H.S. can only be those exceeding unity over the whole range of saturation investigated, our question

$$dW_{II}(S_{gi}) \cong dW_{II}(S_{gi+1})$$

remained unanswered for saturation values

$$S_g < S_{g1}.$$

Let us now, therefore, apply the following method to determine the relative magnitude of energy elements for the range of saturation

$$S_g < S_{g1}.$$

It follows from elementary geometric considerations that theoretically there is an infinitely great number of functions

$$P_c = P_c(S_g)$$

and

$$p_g = p_g(S_g)$$

in this range of saturation that can be characterized by Eqs (19) and (20). Among these infinitely many pressure profiles there must exist one and only one for which

$$p_g^* = p_g^*(S_g)$$

will modify Eq. (17) so that equality dominates, i.e.

$$dW_{II}(S_{gi}) = dW_{II}(S_{gi+1}). \tag{21}$$

Function

$$p^*(S_g)$$

will be determined by starting from point

$$P_1(S_{g1}; p_{g1})$$

of inflexion and solving equation

$$a \cdot \{[p_{gi-1}]^*\}^2 + b[p_{gi-1}]^* + c = 0 \tag{22}$$

in the range of saturation

$$S_g < S_{g1}.$$

Our first equation to be solved is

$$a \cdot \{[p_{g1-1}]^*\}^2 + b \cdot [p_{g1-1}]^* + c = 0$$

whence co-ordinate p_{gi-1} of point P_{1-1} preceding p_i will be obtained while the other co-ordinate will be the corresponding value $S_{g(i-1)}$ of independent variable. Our further procedure is suggested by Eq. (22): every unknown quantity $[p_{gi-1}]^*$ will be calculated by using

$$p_g^*(S_{gi}),$$

$$p_g^*(S_{gi+1})$$

and their functions. Consequently, coefficients of the unknown $[p_{gi-1}]^*$ and the pure term of equation, i.e. values a , b and c will be determined from expressions

$$p_{gi}^* = p_g^*(S_{gi}),$$

$$p_{gi+1}^* = p_g^*(S_{gi+1}),$$

$$Z_i^* = Z^*[p_g^*(S_{gi}); T; \varepsilon]$$

and

$$Z_{i+1}^* = Z^*[p_g^*(S_{gi+1}); T; \varepsilon].$$

Full form of Eq. (22) for any $[p_{gi-1}]^*$ depending on S_{gi-1} will then become

$$\begin{aligned} & \left[[p_{gi-1}]^* \right]^2 \left\{ - \left[\frac{Z'-1}{p'_g} \right] S_{gi-1} + \left[\frac{Z'-1}{p'_g} \right]^2 \frac{p_{gi} S_{gi}}{2 Z_i} + \right. \\ & \left. + \left[\frac{Z'-1}{p'_g} \right] \frac{S_{gi-1}}{2} \right\} + [p_{gi-1}]^* \left\{ - \left[\frac{Z'-1}{p'_g} \right] \frac{p_{gi} S_{gi-1}}{2} - \right. \\ & \left. - \left[\frac{Z'-1}{p'_g} \right] p_{gi+1} S_{gi+1} + \left[\frac{Z'-1}{p'_g} \right] \Delta Z_{i+1} \frac{p_{gi+1} S_{gi+1}}{2 Z_{i+1}} + \right. \\ & \left. + \left[\frac{Z'-1}{p'_g} \right] \Delta Z_{i+1} \frac{p_{gi} S_{gi}}{2 Z_i} - S_{gi-1} - \left[\frac{Z'-1}{p'_g} \right]^2 \frac{p_{gi}^2 S_{gi}}{2 Z_i} + \right. \\ & \left. + \left[\frac{Z'-1}{p'_g} \right] \frac{p_{gi} S_{gi}}{2 Z_i} + 2 \left[\frac{Z'-1}{p'_g} \right] p_{gi} S_{gi} \right\} + \\ & \left. + \left\{ 2 p_{gi} S_{gi} - \left[\frac{Z'-1}{p'_g} \right] \frac{p_{gi}^2 S_{gi}}{2 Z_i} - p_{gi+1} S_{gi+1} + \right. \right. \\ & \left. \left. + \Delta Z_{i+1} \frac{p_{gi+1} S_{gi+1}}{2 Z_{i+1}} + \Delta Z_{i+1} \frac{p_{gi} S_{gi}}{2 Z_i} \right\} = 0. \end{aligned}$$

Solutions of Eq. (22) belonging to all S_g furnish function

$$p_g^* = p_g^*(S_g)$$

for which equality holds between every

$$dW_{II}(S_{gi})$$

and

$$dW_{II}(S_{gi+1})$$

in Eq. (21).

However, numerical values of equation

$$p_g^* = p_g^*(S_{gi})$$

suggest that the mathematical condition implied by Eq. (21) requires a physical state that would be impossible in nature (Fig. 1). Consequently, the change of

$$dW_{II}(S_{gi})$$

can only be increasing, thus referring to our original question we have

$$dW_{II}(S_{gi}) < dW_{II}(S_{gi+1}) .$$

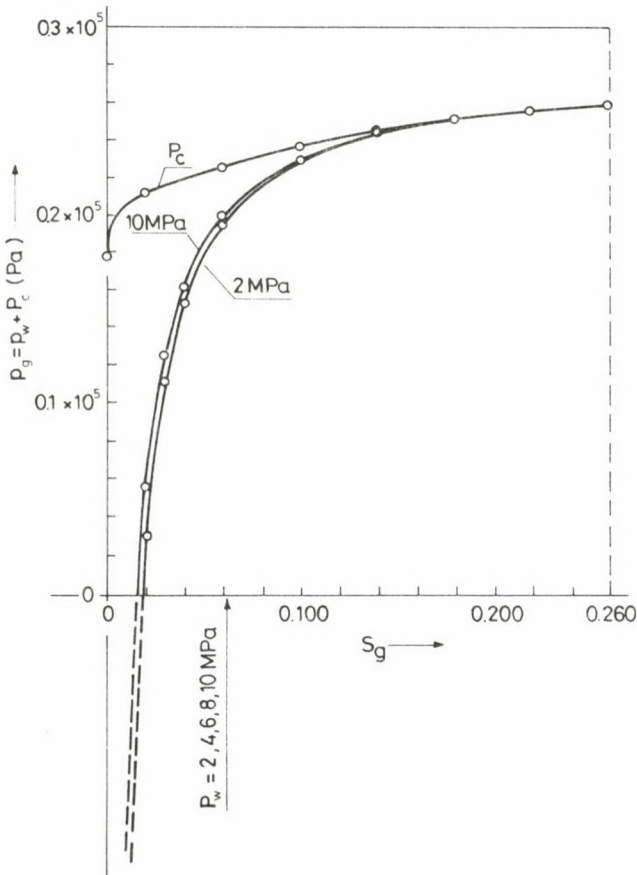


Fig. 1. Functions $p_g(S_g)$ meeting condition $dW_{II}(S_{gi}) = dW_{II}(S_{gi+1})$ at function $P_c(S_g)$ characteristic of the system

Let us now consider the change of energy content always accompanying elementary changes of mass and state of our system by taking into account equations

$$V_{gk}Z dJ + V_{pk}Z dK = RTZ dn$$

following from Eq. (8) and

$$dW_I(S_g) + dW_{II}(S_g) = dW(S_g) = RTZ dn$$

based on Eq. (14).

Equation

$$dW(S_g) = RTZ dn$$

expresses changes of elementary energy components depending on saturation for the whole laboratory system, i.e. totality of volumes V_{gk} and V_{pk} . Plotting values for formation pressures 2, 4, 6, 8 and 10 MPa, we obtain a set of curves displaying functions

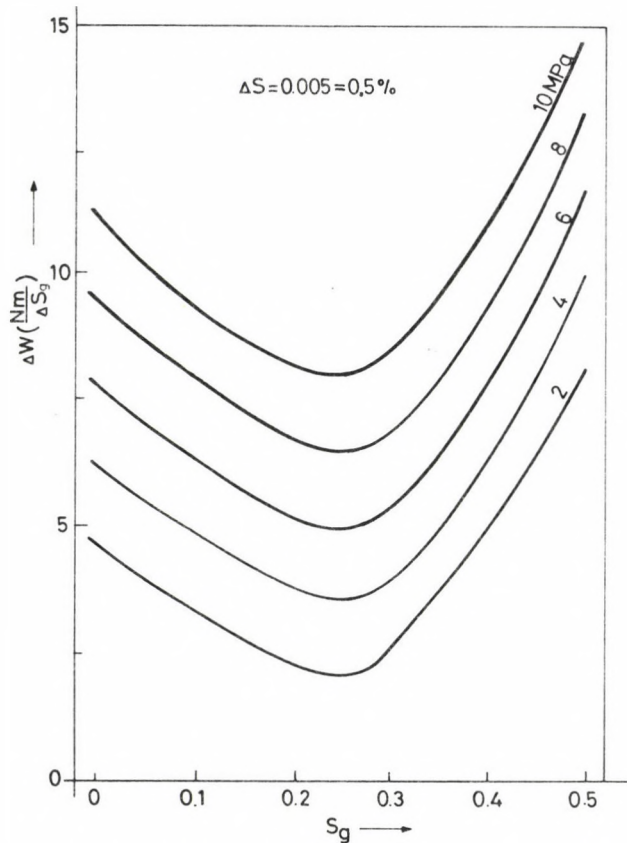


Fig. 2. $dW(S_g)$ as a function of reservoir state

$dW(S_g)$ exhibiting definite minima (Fig. 2). Our latter equations showed that all function values

$$dW(S_g)$$

consisted of two terms representing changes of energy content in volume V_{gk} and V_{pk} attached to the previous one but still separable. However, since this set of curves reflects changes of total energy content, it is also necessary to determine the changes of energy contents in the two spaces separately. This has led to the recognition of a minimum in

$$dW_I(S_g)$$

and monotonous increase of

$$dW_{II}(S_g).$$

In Fig. 2 values of function $dW(S_g)$ referring to unit volume have been plotted to ensure a clearer picture. Since their character remained unchanged for unit volumes, it became obvious that the change of energy content of a natural reservoir also depends on its being divided into V_{gk} and V_{gv} . Translated that into every day practice this means that advantageous states can also be achieved in the energetics of a porous reservoir by suitably selecting geometric dimensions of the volumes while taking into account other natural properties, too.

As a summary, we can state that specific energy requirement of the change of saturation, i.e. work needed to produce unit change of saturation possesses a definite minimum whose place is determined by the point of inflexion of function $P_c(S_g)$ depending on the interfacial properties of the system. Minimum work is needed around this value of saturation if the state of saturation and mass and state of the system are intended to be changed or this is the state of saturation that can be maintained at the cost of minimum energy.

It is also important for the energetics of the system that question

$$dW_I(S_{gi}) \cong dW_{II}(S_{gi}) \tag{23}$$

referring to volumes composing total reservoir volume can be answered for the range of saturation bearing practical importance by inequality

$$\frac{Z_i + Z_{i-1}}{Z_i} p_{gi} S_{wi} < \frac{Z_i + Z_{i-1}}{Z_{i-1}} p_{gi-1} S_{wi-1} \tag{24}$$

thus we have

$$dW_I(S_{gi}) < dW_{II}(S_{gi}). \tag{25}$$

Comparing any pair of values from Eqs (12), (13) and (16) or expressions

$$\begin{aligned} dW_I(S_g) &= V_{gk} Z dJ = V_{gk} dp_g - V_{gk} J dZ \simeq \\ &\simeq V_{gk} \left\{ p_{gi} - p_{gi-1} - \frac{\Delta Z_i}{2} \left[\frac{p_{gi}}{Z_i} + \frac{p_{gi-1}}{Z_{i-1}} \right] \right\} \end{aligned}$$

and

$$\begin{aligned} dW_{II}(S_g) &= V_{pk} Z dK = p_w dV_g + P_c dV_g + \\ &+ V_{gv} dp_g - V_{pk} K dZ \simeq \\ &\simeq V_{pk} \left\{ p_{gi} S_{gi} - p_{gi-1} S_{gi-1} - \frac{\Delta Z_i}{2} \left[\frac{p_{gi}}{Z_i} S_{gi} + \frac{p_{gi-1}}{Z_{i-1}} S_{gi-1} \right] \right\} \end{aligned}$$

in the sense of Eq. (23), we have Eq. (24). On rearranging we obtain

$$0 \cong 1 - \frac{S_{wi}}{S_{wi-1}} \left[1 - \frac{\Delta Z_i}{Z_i} + \frac{\Delta P_{ci}}{p_{gi-1}} - \frac{\Delta Z_i}{Z_i} \frac{\Delta P_{ci}}{p_{gi-1}} \right]$$

which answers the question in Eq. (23). Here, if

$$\begin{aligned} i \leq 0, & \quad \text{then } dW_I(S_{gi}) = dW_{II}(S_{gi}), \\ i = 1, & \quad \text{then } dW_I(S_{gi}) > dW_{II}(S_{gi}), \\ i > 1, & \quad \text{then } dW_I(S_{gi}) < dW_{II}(S_{gi}). \end{aligned}$$

States corresponding to $i=0$ bear no importance because they indicate steadiness reflected by

$$dW_I(S_{gi}) = dW_{II}(S_{gi}).$$

If $i > 1$, in the proximity of

$$S_g = 1 - S_{wr}$$

energetical character of the system can change again and we may have

$$dW_I(S_{gi}) > dW_{II}(S_{gi})$$

because values of saturation approach an other possible limit of variation. Beyond this limit no change of saturation can be brought about, and the energy of system exhibits the same phenomenon as observed at

$$i = 1,$$

thus, necessarily, inequality

$$dW_I(S_{gi}) > dW_{II}(S_{gi})$$

reflects really the physical meaning of the phenomenon.

Practical importance of the theoretical considerations carried out so far will be enlightened by the following analysis of the energy balance of an arbitrary reservoir.

3. High energy reservoirs

Our earlier analyses made an attempt to investigate the effect of the interfacial properties on the energetic character of porous reservoirs especially those implying technical and scientific problems in their every-day operation. The author is convinced that the results of the investigation contribute to performing changes of phase in reservoirs under optimum conditions through acquiring knowledge about the components characterizing the reservoir.

Engineers will find beneficial the conclusion that the change of energy content possesses a minimum as a function of the change of state and the place of the minimum, i.e. the state the minimum corresponds to, can be determined. To acquire a general view it is necessary to know whether this phenomenon can be observed in all reservoirs and has the same character or there may be exceptions and what are the causes and symptoms of them.

Based on the considerations concerning the inflexion of function $P_c(S_g)$, let us perform an analysis of Eqs (14), (15) and (16) for capillary pressure-saturation functions $P_c(S_g)$ lacking inflexion. Since

$$\dots \Delta p_{gi-1} < \Delta p_{gi} < \Delta p_{gi+1} \dots$$

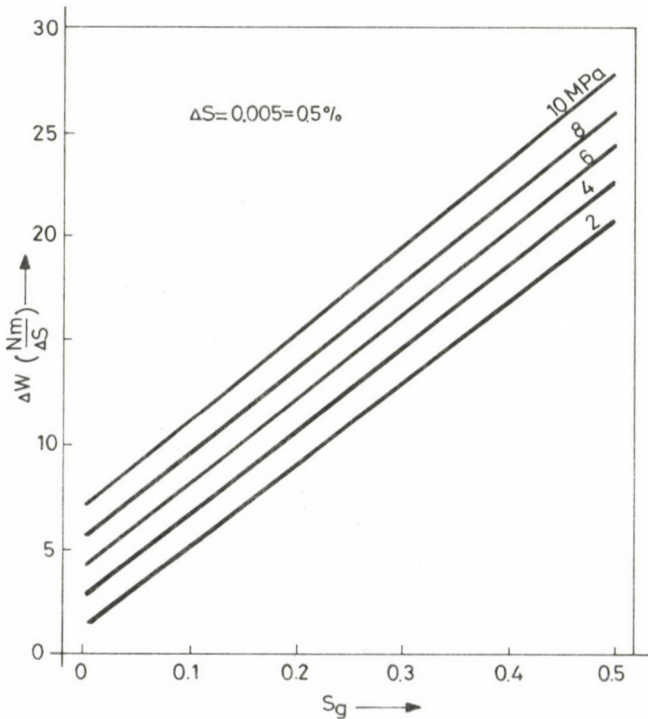


Fig. 3. $dW(S_g)$ as a function of reservoir state in a "high energy" system

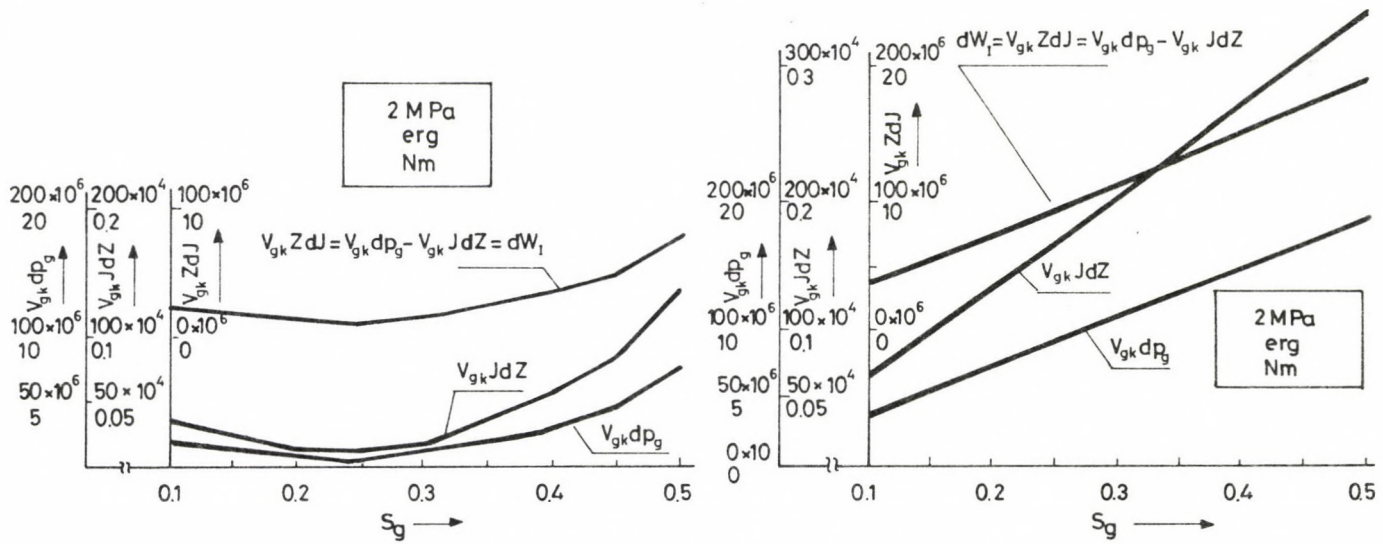


Fig. 4. $dW_1(S_g)$ and its components as a function of reservoir state at 2 MPa formation pressure

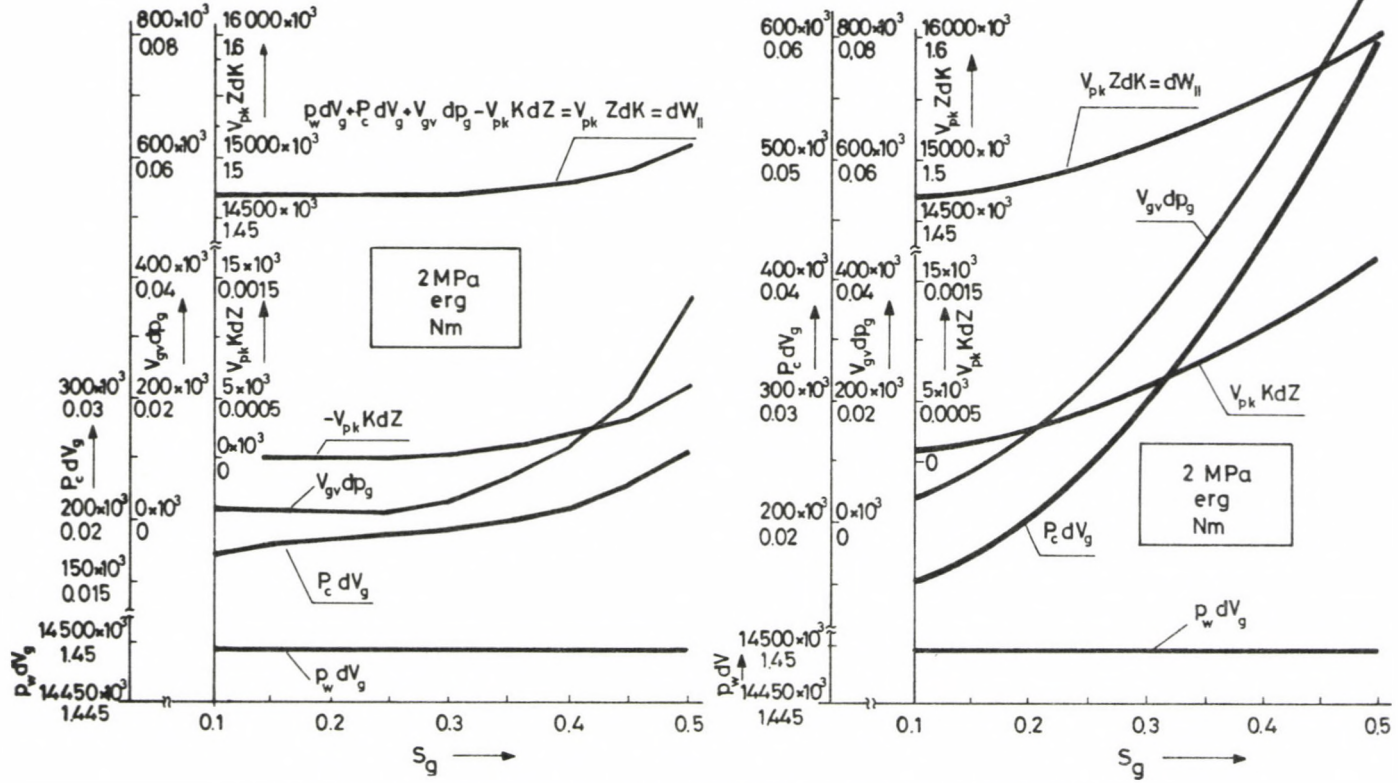


Fig. 5. $dW_{II}(S_g)$ and its components as a function of reservoir state at 2 MPa formation pressure

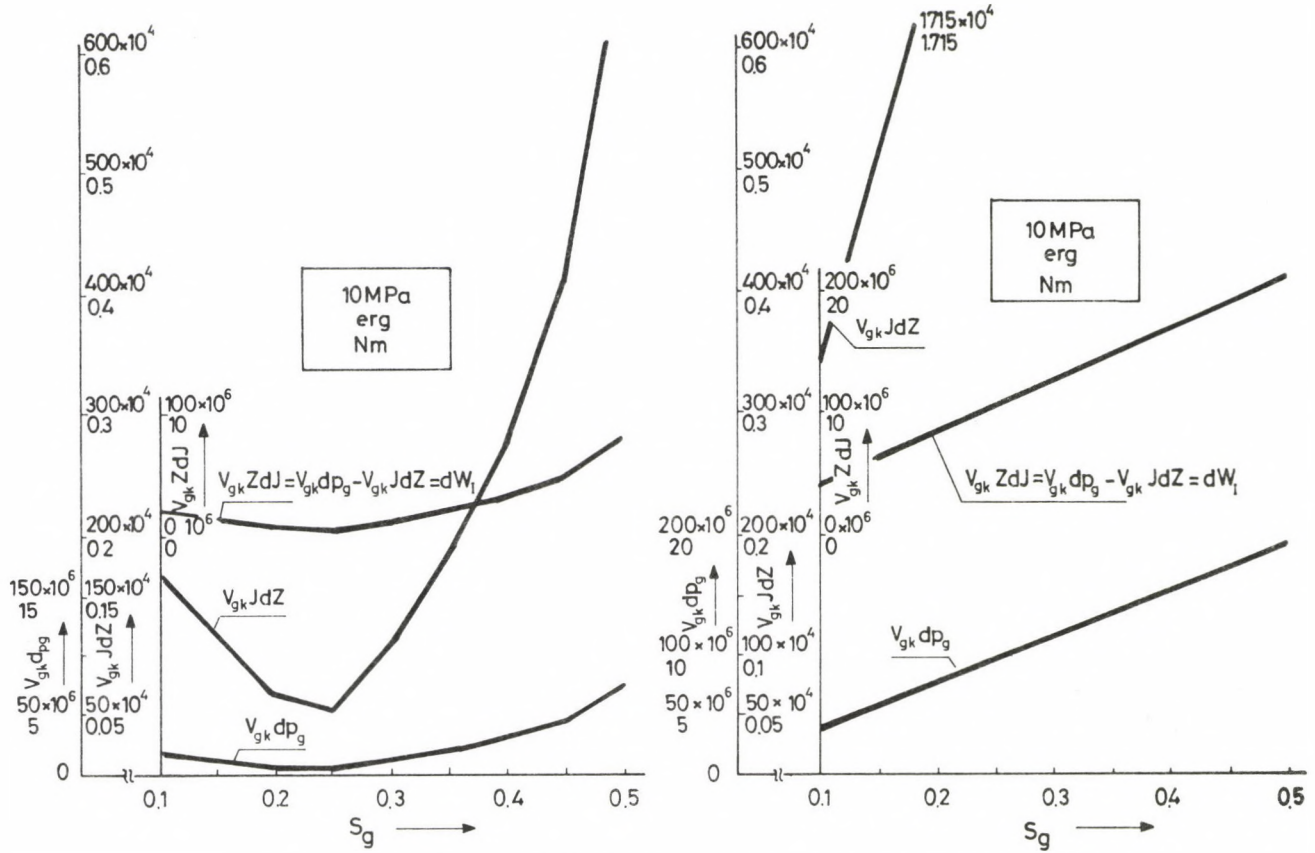


Fig. 6. $dW_1(S_g)$ and its components as a function of reservoir state at 10 MPa formation pressure

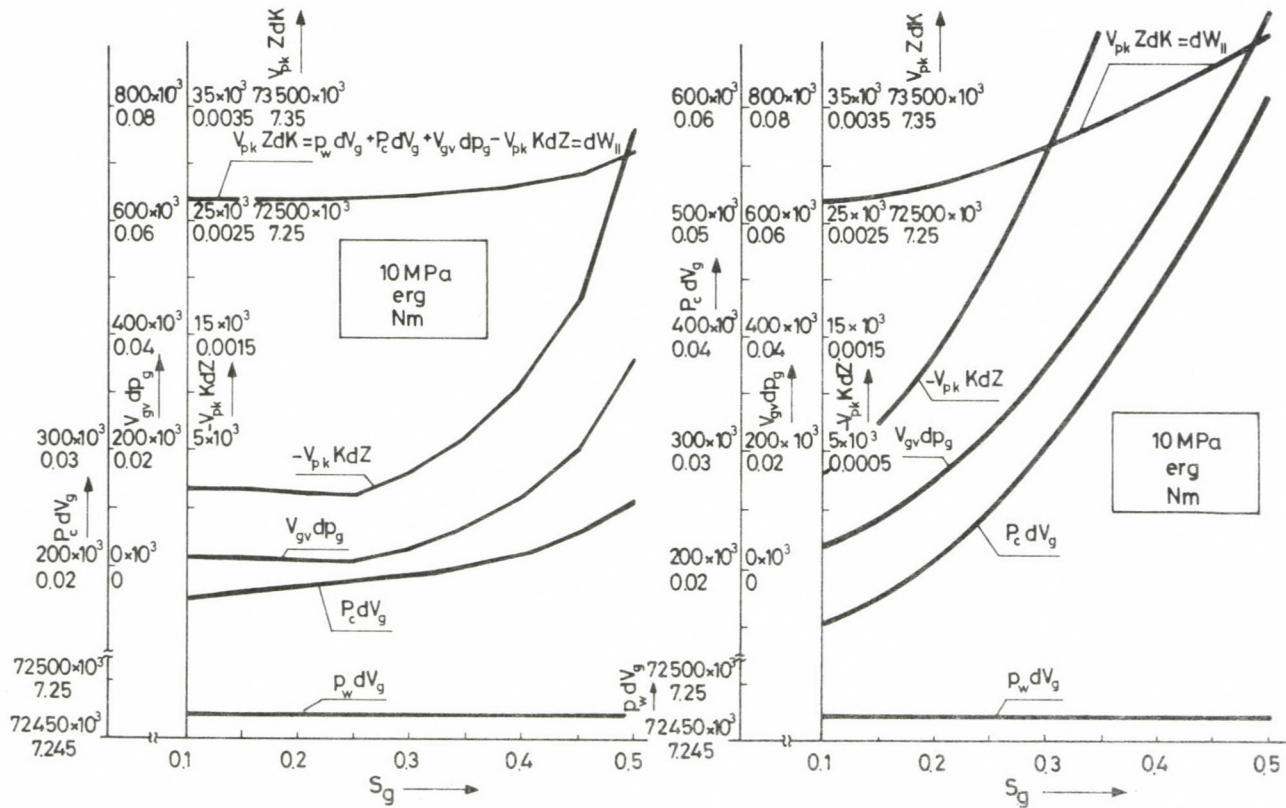


Fig. 7. $dW_{II}(S_g)$ and its components as a function of reservoir state at 10 MPa formation pressure

and

$$Z_{i-1} > Z_i > Z_{i+1},$$

function $dW_I(S_g)$ exhibits a strictly monotonous increase, so does also $dW_{II}(S_g)$. Consequently, the graph of function given by Eq. (14) must have the same characteristic since energy elements

$$dW(S_g)$$

show a strictly monotonous increase as a function of saturation (Fig. 3).

To illustrate our considerations, a set of figures will be demonstrated—omitting the presentation of calculated values. Figures 4 to 7 prove that elementary changes of energy content differ considerably for the changes of state of the two capillary systems. Differences can be observed on the curves illustrating energy components and their sum expressed as

$$dW(S_g) = dW_I(S_g) + dW_{II}(S_g).$$

A function $P_c(S_g)$ with a characteristic inflexion indicates a state in the energetical system of the porous reservoir which always exhibits the minimum we have already concluded to. While in porous reservoirs characterized by capillary pressure-saturation functions without any inflexion, the change of energy content has a strictly monotonous tendency: it is either increasing or decreasing depending on the change of the mass being the most general independent variable of the system.

Since the properties of the pore structure and the interfacial state in the reservoir usually produce a function $P_c(S_g)$ with an inflexion (a reservoir character contrary to that can hardly be met), it can be expected that energetical conditions of the reservoir disadvantageously influence the technical-economic enterprise of underground gas storage. This problem will also be referred to in analysing energy balance.

4. Elastic energy of formation water in porous reservoirs

For every state of a fluid-bearing reservoir

$$V_g + V_w = V_{pk}$$

holds and, consequently

$$dV_g + dV_w = 0.$$

In our previous analyses, volumetric changes of phases saturating the pores were considered to be brought about in a way that the less wetting phase of higher pressure displaces the wetting one of lower pressure from the pores, but the amounts of volumetric changes are equal:

$$dV_g = -dV_w.$$

It is obvious that this kind of interpretation of changes in the reservoir is somewhat simplified because a change of the mass of the system is accompanied with more complex phenomena. If parallelly to a change of the pressure from p_{gi-1} to p_{gi} , the volume occupied by the wetting phase changes from V_{gi-1} to V_{gi} , the change of the volume of the wetting phase between the two states of equilibrium will be:

$$V_{wi} - V_{wi-1} = dV_{wi}. \tag{26}$$

This total volumetric change takes place in a way that the volume dV'_{wki} of water volume V_{gi-1} at state $(i-1)$ is displaced from the pores and water volume V'_{wi} is elastically compressed and takes up volume V_{wi} belonging to the following state of equilibrium. Thus, we have

$$\begin{aligned} V_{wi-1} + dV'_{wki} &= V'_{vi} \\ V'_{wi} + dV_{w\beta i} &= V_{wi}, \end{aligned}$$

and hence with respect to Eq. (26)

$$dV_{wi} = V_{wi} - V_{wi-1} = dV'_{wki} + dV_{w\beta i}.$$

Volumetric change dV_{wi} of the wetting phase and its components are regarded as formation conditions. However, we can only observe volume dV'_{wki} having left the reservoir i.e. not at formation state. But with the physical parameters from the volume $\Delta V'_{wki}$ observed outside the reservoir, its value at formation conditions and elastic volumetric change

$$dV_{w\beta}$$

of the residual wetting phase reduced by that, can be calculated. Using expression

$$-\beta = \frac{1}{V} \frac{dV}{dp},$$

we have

$$dV'_{wki} = \Delta V_{wki} [1 - \beta(p_{gi} - p_{g0})]$$

and

$$dV_{w\beta i} = -\beta V'_{wi} (p_{gi} - p_{gi-1}),$$

whereas V'_{wi} already has been determined.

The sum of volumetric changes of the wetting phase calculated in this way gives the total volumetric change of the gaseous phase from which change of energy content accompanying changes of mass and state can also be calculated. From Eq. (4) we have

$$V_g = V_{gk} + V_{gv}$$

and

$$dV_g = -dV_w = -dV'_{wk} - dV_{w\beta},$$

further, using

$$P_c = p_g - p_w$$

we can write

$$-p_w dV'_{wk} - P_c dV'_{wk} - p_g dV_{w\beta} + V_{gk} dp_g + V_{gv} dp_g = RT d[nZ],$$

where

$$V_{gv} = - \int_{V_{w0}}^{V_w} dV_w,$$

and finally

$$\begin{aligned} & - \int_{V'_{wk0}}^{V'_{wk}} p_w dV'_{wk} - \int_{V'_{wk0}}^{V'_{wk}} P_c dV'_{wk} - \int_{V_{w\beta0}}^{V_{w\beta}} p_g dV_{w\beta} + \int_{p_{g0}}^{p_g} V_{gk} dp_g + \int_{p_g}^{p_{g0}} V_{gv} dp_g = \\ & = RT \left[\int_{Z_0}^Z n dZ + \int_{n_0}^n Z dn \right]. \end{aligned}$$

The last equation expresses the change of energy content brought about as a change between the parameters of state implied by the limits of integration. The change of gas mass expressed by mole numbers in R.H.S. of the equation can be similarly eliminated as it was done in connection with Eqs (5) to (7). However, here we also take into account the elastic volumetric change of the formation water, i.e. instead of S_w and S_g used previously, $S_{w\text{eff}}$ and $S_{g\text{eff}}$ are applied to characterize the state of saturation.

5. Remarks on the order of magnitude of energy requirement of interfacial changes

In Chapter 4 of Zoltán (1986) the question of the order of magnitude concerning changes of energy content accompanying interfacial changes has already been discussed: calculated figures of Tables I and II (Zoltán 1986) largely exceeded those expected. However, to decide whether these values are really great or not within the total energy of the system, one has to compare these changes with other changes of energy characteristic of the system. So values of ratio

$$\frac{\int_{p_{g0}}^{p_g} p_g dV_g}{\int_{p_{g0}}^P P_c dV_g}$$

have been determined as a function of the state of saturation. However, this method has only been regarded approximative because gas pressure values after gas expansion calculated by Boyle's law failed to accurately comply with the actual values. The question concerning the reliability of this method remained thus somewhat unanswered.

Another method to assess the orders of magnitude of changes in the energy component $p_g dV_g/P_c dV_g$ can be outlined as follows. Let us consider mole number n in Eq. (2) obtained from Eq. (1) constant and write as

$$n = n_I + n_{II} .$$

Our differential equation becomes

$$p_g dV_g + V_g dp_g = n_I RT dZ + n_{II} RT dZ .$$

n_I and n_{II} will be determined as we have done previously and the change of energy content of the system will be obtained as

$$\begin{aligned} \int_{V_{g0}}^{V_g} p_w dV_g + \int_{V_{g0}}^{V_g} P_c dV_g + \int_{p_{g0}}^{p_g} V_{gk} dp_g + \int_{p_{g0}}^{p_g} V_{gv} dp_g = \\ = V_{gk} \int_{Z_0}^Z J dZ + V_{pk} \int_{Z_0}^Z K dZ . \end{aligned} \tag{26}$$

Limits of the solution are given by the parameters of state of the system, they can be calculated from the initial P_{g0} and V_{g0} for any i -th state. As we already have used

$$\frac{P_{gi}}{Z_i} V_{gi} = \frac{P_{gi-1}}{Z_{i-1}} V_{gi-1}$$

whence

$$p_{gi} = p_{gi-1} \frac{V_{gi-1}}{V_{gi}} \frac{Z_i}{Z_{i-1}} .$$

In this equation, as compared with the $(i-1)$ -th state, measured value V_{gi} is new, while p_{gi-1} and Z_{i-1} are already known from the previous, $(i-1)$ -th state. The value p'_{gi} approximating p_{gi} will be determined by Z_{i-1} instead of Z_i depending on p_{gi} and not yet known:

$$p'_{gi} = p_{gi-1} \frac{V_{gi-1}}{Z_{i-1}} \frac{Z_{i-1}}{V_{gi}} .$$

With p'_{gi} approximating p_{gi} only, the corresponding value of Z'_i will be calculated:

$$Z'_i = Z' [p'_{gi}; T; \varepsilon]$$

and that will be used to determine p''_{gi} :

$$p''_{gi} = \frac{p_{gi-1} V_{gi-1}}{Z_{i-1}} \frac{Z'_i}{V_{gi}}.$$

Using p''_{gi}

$$Z''_i = Z' [p''_{gi}; T; \varepsilon]$$

and the third step of approximation yields

$$p'''_{gi} = \frac{p_{gi-1} V_{gi-1}}{Z_{i-1}} \frac{Z''_i}{V_{gi}}.$$

Since expression

$$\frac{p_{gi-1} V_{gi-1}}{Z_{i-1}}$$

is used in every step, by denoting it by N_{i-1} we can write

$$p'''_{gi} = N_{i-1} \frac{Z''_i}{V_{gi}}$$

and

$$p^{IV}_{gi} = N_{i-1} \frac{Z'''_i}{V_{gi}}.$$

The approximation procedure will be continued until differences between consecutive values of p_g and Z remain below an arbitrarily small value. Using last values of p_g and Z , expression

$$\frac{p_{gi-1}}{Z_{i-1}} V_{gi-1} = \frac{p_{gi}}{Z_i} V_{gi}$$

satisfies Boyle's law and p_g and Z found thus steady will be substituted into Eq. (26). Substituting

$$p_g = P_c + p_w$$

again, we have

$$- \int_{V_{g0}}^{V_g} p_g dV_g = - \left[\int_{V_{g0}}^{V_g} P_c dV_g + \int_{V_{g0}}^{V_g} p_w dV_g \right].$$

We can now calculate the ratio of the full volumetric work of expansion to energy requirement of interfacial changes.

In applying the method of approximation, the consecutive steps were continued until the 12th one and Eq. (26) was solved with last values

$$p_{gi}^{XII}; Z_i^{XII}$$

Table II. Ratio of the volumetric work of the gas to energy requirement of interfacial changes for two values of formation pressure

$$\int_{V_{g0}}^{V_g} p_g dV_g \quad / \quad \int_{V_{g0}}^{V_g} P_c dV_g$$

i	S _{gi}	2 MPa		10 MPa	
		p _{gi} ^{XII} ; Z _i ^{XII}	p' _{gi} ; Z' _i	p _{gi} ^{XII} ; Z _i ^{XII}	p' _{gi} ; Z' _i
0	0.000	0/0	0/0	0/0	0/0
1	0.000	0/0	0/0	0/0	0/0
6	0.025	97.368	97.363	486.844	486.820
11	0.050	94.472	94.474	472.368	472.374
16	0.075	92.434	92.432	462.182	462.169
21	0.100	90.695	90.693	453.490	453.480
26	0.125	89.192	89.193	445.980	445.983
31	0.150	87.874	87.874	439.392	439.392
36	0.175	86.721	86.722	433.632	433.634
41	0.200	85.713	85.714	428.594	428.596
46	0.225	84.828	84.828	424.173	424.173
51	0.250	84.043	84.042	420.250	420.245
56	0.275	83.333	83.333	416.704	416.703
61	0.300	82.671	82.675	413.396	413.396
66	0.325	82.031	82.031	410.198	410.198
71	0.350	81.387	81.386	406.979	406.977
76	0.375	80.670	80.699	403.548	403.544
81	0.400	79.948	79.948	399.794	399.790
86	0.425	79.105	79.105	395.581	395.579
91	0.450	78.153	78.153	390.824	390.821
96	0.475	77.076	77.076	385.442	385.439
101	0.500	75.848	75.848	379.300	379.298
106	0.525	74.417	74.417	372.151	372.150
111	0.550	72.137	72.137	360.752	360.751
112	0.553	71.349	71.349	356.810	356.808

and first ones

$$p'_{gi}; Z'_i.$$

The ratio of the full volumetric work and energy requirement of interfacial changes calculated for the two extreme values 2 and 10 MPa differed so little that the difference could not be grafically illustrated, it was rather listed in Table II.

Reference

Zoltán Gy 1986: Energy of fluid-bearing porous systems. *Acta Geod., Geoph. Mont. Hung.* 21, 297—315

ROCK MODEL BASED ON PORE STRUCTURE

K BAUER¹ and L BALLA¹

[Manuscript received November 5, 1984]

For the exploitation of reservoirs of fluids, beyond the reservoir-mechanical fundamental parameters: permeability and porosity, diffusion parameters, calculated from the measurements of the physical modelling are frequently needed, however, the rock model cannot be assembled if the permeabilities and porosities are known.

The relationship between the permeability and porosity is more complicated than that a general unambiguous correlation could exist between them, by knowing the one parameter the numerical value of the other cannot be determined.

For this, the knowledge of one or more further parameters characterizing the pore structure is needed.

In case of simpler systems, the parameters, characterizing the pore structure can be deduced from the Navier-Stokes equation, using the negligations taken according to the structure of the porous medium and the character of the flow.

Keywords: permeability; pore structure; porosity; rock model

Symbols

<i>a</i>	formation-factor parameter
<i>A</i>	specific surface, m^{-1}
<i>b</i>	factor Klinkenberg, bar
<i>c</i>	concentration
<i>D_d</i>	dispersion factor, $m^2 s^{-1}$
<i>D₀</i>	free-molecular diffusion factor, $m^2 s^{-1}$
<i>F</i>	formation factor
<i>h</i>	length of core
<i>H</i>	horizontal
<i>k₀</i>	shape factor
<i>K</i>	permeability, μm^2
<i>l</i>	length of way
<i>m</i>	formation factor parameter
<i>p</i>	pressure, bar
<i>r</i>	ratio of lengths of way
<i>t</i>	time, s
<i>T</i>	tortuosity
<i>v</i>	velocity, ms^{-1}
<i>V</i>	vertical
<i>z</i>	distance, m
α	pore structure parameter
φ	porosity
Φ	diameter

¹ Chemical Research Laboratory for Mining of the Hungarian Academy of Sciences, Miskolc-Egyetemváros, P.O.B. 2. Hungary, H-3515

Indices

<i>a</i>	mean value
<i>e</i>	real
<i>i</i>	serial number
∞	extrapolated

Introduction

Based on more than 100 analysing papers published in this topic, beginning from the investigations of Emersleben (1925) referring to fibrous-stringy materials, through the relationships, deduced by Kozeny (1927) for the unsettled grain-assemblies, by taking into consideration the work done by Adzumi (1939), Klinkenberg (1941) in field of the low pressure gas flow, too, as well as the results of Millington and Quirk (1961) respecting also the pore size classes, or the analyses of Azzam and Dullien (1976), based on the double pore size distribution, respectively, it can be stated that for a more precise reflection of the connection between $K-\varphi$ minimum 2, but maximum 5 further parameters are necessary characterizing the pore structure.

Of course, there are more parameters than given above, characterizing the pore structure from any side, and according to the analysis of Greenkorn (1981)—made also in this field—the most widely used ones are the following: tortuosity; pore coordination number; shape factor, characterizing the cross section of the arterial drainage, grain coordination number; characteristical pore dimension; various specific surfaces; according to the nature of the flow, by the low pressure gas flow: the additional module, by turbulent flow: the turbulence factor the reciprocal value of which is the length measure in the microscopical Pecklet number.

Aim of our investigation is to enable to group the available rock material for the convective-conductive gas-diffusion experiments in such a way that the one-dimension long rock models can be possibly assembled from pore structure samples being equivalents with each other. For this, beyond the knowledge of the numerical values of K and φ of the rock material, a more detailed information is needed regarding the rock-pore space, and this can be suitably done by means of the determination of the gas permeability curves according to Klinkenberg. Over and about that in some cases grain size analysis and rock permeability measurements for bed water can be also done for the further interpretation of the permeability-porosity data of the sample assembly or for the control of the compatibility of rock-bed water.

Rock processing and its results

The processed rock material originates from the bench drilling No. Hsz. 80 from a depth of 1025–1065 m, and it is a core sample of not full recovery, in a parting of 1025–1043 m, 1043–1060 m, 1043–1065 m, however, within this intervals, the proper place of

Table I. Distribution of rock test pieces originating from the core drilling No. Hsz. 80. according to the depth, quantity

Depth, m	1025 – 1043	Sign of the sample
Total number, pieces	4	
Φ , mm	80	
h , mm	65	1
	240	2
	110	3
	50	4
Depth, m	1043 – 1060	
Total number, pieces	3	
Φ , mm	80	
h , mm	50	5
	50	6
	80	7
Depth, m	1043 – 1065	
Total number, pieces	5	
Φ , mm	80	
h , mm	70	8
	110	9
	50	10
	60	11
	50	12

the individual rock pieces is not signed, or the order of these relating to each other was not decidable. In Table I the samples were signed with a number from 1-till 12, for the identification of our investigation results, and this is the reference number by the denomination of test pieces cut out from these in horizontal and vertical direction, machined to a cylindrical shape, shown in detail in Table II.

The gas permeability was determined by a vacuum method in a reciprocal pressure interval of $1.5 \text{ bar}^{-1} < P_a^{-1} < 30 \text{ bar}^{-1}$, and the K gas permeability, extrapolated to an infinite pressure was determined from the linear regression of the measured ($K_i; P_{ai}^{-1}$) data, or the factor "b", according to Klinkenberg. One part of the characteristic curves, $K(P_a^{-1})$ is shown on Fig. 1, and the K_∞ , determined for the sample assembly in this way, and the rock porosity values determined by means of distilled water are included in Table III.

Table II. Test pieces and their macroscopical structure

Sign	Test piece		Note
	number	av. length cm	
1	1 V	2.5	
	1 H	2.5	
2	3 V	2.5	heterogeneous, with coal-strips of 0.5–1 mm and clay-strips
	+1	8 pieces cut into slices of 2 cm	
3	1 V	2.5	heterogeneous with clay, 2 samples came apart
	5 H	8.0	
4	1 V	2.5	in horizontal direction claystrip in 10%
	1 H	6.0	
5	1 V	2.5	1 is homogeneous, other heterogeneous
	3 H	7.0	
7	1 V	2.5	horizontally with clay strips 1 sample is deteriorated
	4 H	6.0	
8	1 V	2.5	homogeneous
	3 H	6.0	
11	1 H	8.0	in the middle of the axis there is a coaly strip of 4 mm
12	1 V	2.5	in the direction of the axis there is a coaly strip
	1 H	2.5	

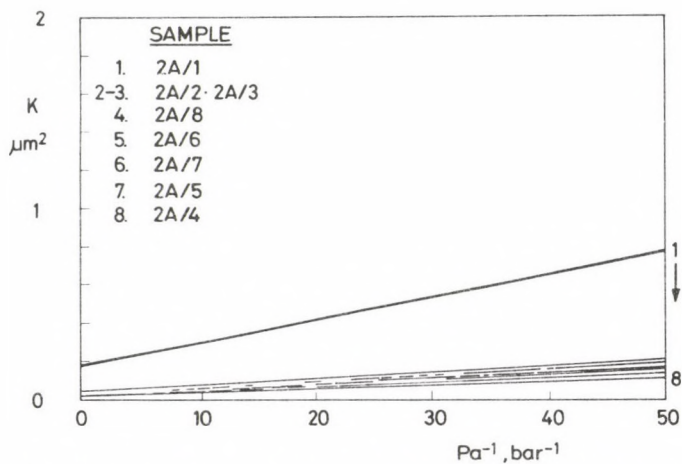
**Fig. 1.** Change of gas permeability in dependence of average pressure

Table III. Physical characters of the test pieces

Sample		K_{∞} μm^2	φ	b bar	$K_{r, \text{water}}$ μm^2	Fraction of grain size			
Sign	Orien- tation					0-45 μ	45-90 μ	90-135 μ	135-180 μ
						frequency in dependence of percentage of the total grain number			
1/A	H	0.660	0.302	0.0494	0.601				
1/B	V	0.1038	0.298	0.1283	0.032	43	29	21	7
2A/1	V	0.178		0.0667	—				
2A/2	V	0.040		0.0811	0.018				
2A/3	V	0.041		0.0796	0.015				
2A/4	V	0.020	0.215	0.0860	0.005				
2A/5	V	0.021		0.1132	—				
2A/6	V	0.027		0.1034	—				
2A/7	V	0.023		0.1178	0.006				
2A/8	V	0.032		0.1009	0.010				
3A	H	0.439	0.299	0.0599	—				
3B	H	0.324	0.299	0.0436	—				
3D	H	0.342	0.294	0.0553	—				
3F	V	0.308	0.297	0.0563	—				
4A	H	0.216	0.293	0.0554	—				
4B	H	0.390	0.327	0.0635	—				
5A	H	0.670	0.320	0.0462	—				
5B	H	0.204	0.308	0.0676	—				
5C	H	0.225	0.313	0.0662	—				
5D	V	0.107	0.299	0.0895	—	41	34	15	10
7A	V	0.173	0.311	0.0521	—				
7B	H	0.530	0.315	0.0500	—				
7C	H	0.512	0.314	0.0475	—				
7E	V	0.148	0.313	0.0815	—	32	33	25	10
8A	H	0.436	0.273	0.0422	—				
8B	H	0.409	0.270	0.0406	—				
8C	H	0.687	0.289	0.0436	—	26	12	23	39
8D	V	0.712	0.284	0.0424	—				
11A	H	1.434	0.336	0.0410	—				
12	H	1.037	0.303	0.0139	0.985				
12B	V	0.852	0.300	0.0440	0.702				

Aspects of sorting of test pieces for the rock model of the diffusion experiments

The whole of the test pieces investigated can be regarded as an assembly with not continuous filling, its elements are the individual test pieces which can be denoted by the symbol $d \in H$. The elements of this assembly differ in their characteristic features.

Two such characteristic features, x and y , can be composed as a pair ordered on basis of a number double:

$$H = \{(x_i, y_i)\}$$

and the number of its elements agrees with that of elements H . Within H , further real part-assemblies can be formed:

$$H_i \subseteq H$$

which can be generated by giving any function f_i .

An assembly of the ordered pairs

$$X \xrightarrow{f_i} Y$$

represents a function only in the case, if $(x, y) \in Y$, $x \in X$ and $y = f_i(x)$.

In interest of the simplicity of function connection, it can be written also for characteristic features x, y , submitted to a proper function transformation.

Further on, the pairs of rock characteristic features K_∞ and $K_\infty b$, ordered according to φ are formed. For both characteristic features a logarithmical function transformation, and within this for N a power transformation according to N are applied, where N can be $\{1, 2, 3, 4, 5, \dots\}$.

The gas permeability K_∞ can be interpreted according to the relationship of Kozeny:

$$K_\infty = \frac{\varphi^3}{k_0 T A^2} \quad (1)$$

For the not consolidated systems, $k_0 T$ is about 5, where T is the tortuosity interpreted by Carman (1937) according to the principle of Dupuit, or $T = (l_e/l)^2$ respectively, where $l_e/l = r$, which is the ratio of the real and virtual ways.

In case of loose assemblies depending on the porosity of the rock, too, it holds: $1.33 \leq r \leq 1.7$, if the interval is $0.72 \geq \varphi \geq 0.36$. In average: $\varphi_a \simeq 0.47$ and $r_a \simeq 1.41$, and corresponding to this $k_0 \simeq 2.5$. By a more complicated assembly where the pore space of the frame grains (φ_1) is filled by assembly of grains (φ_2) being significantly less than these, the porosity is $\varphi \simeq \varphi_1 \cdot \varphi_2$, and according to values r_1 and r_2 , depending on φ_1 and φ_2 , it exists the relationship $r \simeq r_1 \cdot r_2$.

In general, for a multiple assembled heterogeneous grain assembly it holds $\varphi \simeq \varphi_1 \cdot \varphi_2 \cdot \varphi_3 \dots \varphi_n$, $r \simeq r_1 \cdot r_2 \cdot r_3 \dots r_n$, i.e. the tortuous way length increases by

decreasing porosity, while tortuosity T changes with the second power of the increase, and the value k_0 changes also in smaller-bigger measure.

For a heterogeneous, complicated clay-sand rock, Jacquin (1965) considers as justified the relationship $T=(F\varphi)^2$, while the formation factor can be characterized by the empirical relationship $F=a\varphi^{-m}$, in this way the tortuosity can be written as

$$T=a^2 \cdot \varphi^{2-2m} \quad (2)$$

by means of which the relationship (1) can be transformed to

$$K_\infty = \frac{\varphi^{1+2m}}{k_0 \cdot a^2 \cdot A^2} \quad (3)$$

and further on, by applying an approximation, where $a=1$; $m=2$, the approximation

$$K_\infty \simeq \alpha_1 \cdot \varphi^5, \quad \alpha_1 \sim A^{-2} \quad (4)$$

was found as very useful by Jacquin for the characterization of the change of permeability according to the porosity, if in the original grain assembly, only the quantity of the cement material, consequently the measure of the cementation changes.

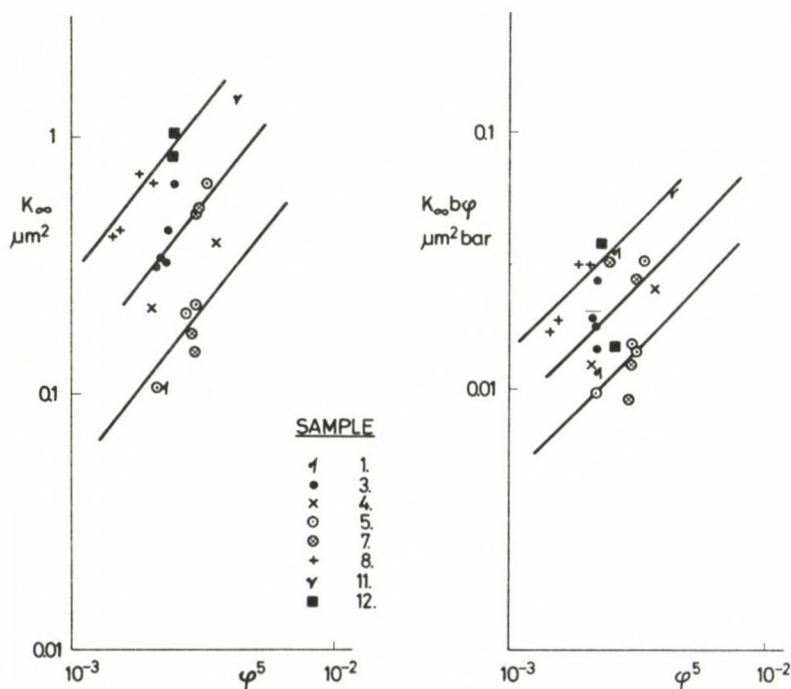


Fig. 2 Change of the characteristic parameters of the test pieces according to the porosity in a transformed form

On basis of investigations of Adzumi (1939), Klinkenberg (1941) and Carman (1956) it can be detected that for the change of the product $K_{\infty}b$, according to the porosity, a relationship like (4) can be deduced, if the form $T=(F\varphi)^2$ and the approximation $a=1, m=2$ is accepted:

$$K_{\infty} \cdot b\varphi \simeq \alpha_2 \cdot \varphi^5, \quad \alpha_2 \sim A^{-1}. \quad (5)$$

By taking these into consideration, if the assemblies of the ordered pairs $(\log K_{\infty}, \log \varphi^5)$ and $(\log(K_{\infty}b\varphi)_i, \log \varphi_i^5)$ are formed—see Fig. 2—within this assembly, by means of straight lines with slope 1, such part-assemblies can be formed that for the rock sample individuals ordered along these the values α_1 and α_2 are approximately constant. At the same time it can be observed that by all the three assemblies along the straight the arrangement is not homogeneous and mutually unambiguous. This fact can be explained by the macroscopical heterogeneity of the test samples. E.g. by the heterogeneity types according to Fig. 3, the above mutual unambiguity cannot be fulfilled, because the macroscopical heterogeneity, which is from the point of view of the mass transport determining K_{∞} , or of the mol mass reflection expressed in $K_{\infty} \cdot b$ identical, cannot imply the same boundary condition. In this way, based on the arrangement within the assembly, the faulty test pieces can be filtered out from these they can be built up to a linear rock model however, for the remainders, the constants α_1 and α_2 can be determined, too. For the whole of the assemblies the coordinates of the centre of gravity are characteristic with the corresponding $K_{\infty \min}, K_{\infty \max}, (K_{\infty}b\varphi)_{\min}, (K_{\infty}b\varphi)_{\max}$ and φ_{\min} , with φ_{\max} greatest error.

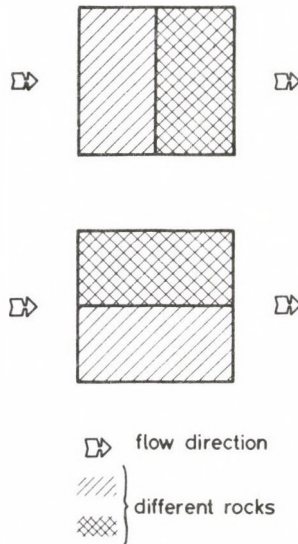


Fig. 3 Rock test piece with length- or cross- heterogeneity with faulty structure

Criterion for the physical modelling

The criterium for the physical modelling can be originated on basis of mathematical modelling describing the process of convective-conductive gas diffusion:

$$\frac{\partial c}{\partial t} = -v \frac{\partial c}{\partial z} + \frac{\partial}{\partial z} \left(D_d \frac{\partial c}{\partial z} \right). \quad (6)$$

The ratio of D_d gas dispersion factor in relationship (6) and D_0 free-molecular gas-diffusion factor can be interpreted in the following way:

$$\frac{D_d}{D_0} = \frac{1}{(\varphi F)^2} + a_1 \cdot \frac{v}{D_0 A} + a_2 \cdot \frac{v^2}{D_0 A} \quad (7)$$

where a_1 and a_2 are constant.

Using the relationship $F \simeq \varphi^{-2}$, $\alpha_1 \sim A^{-2}$, $\alpha_2 \sim A^{-1}$, we obtain:

$$\frac{D_d}{D_0} = \varphi^2 + a_1 \cdot \frac{v}{D_0} \alpha_2 + a_2 \cdot \frac{v^2}{D_0^2} \alpha_1 \quad (8)$$

where a_1 and a_2 are including the used proportionality factors.

On basis of relationship (8) it can be stated that if the experimental determination of the values D_d/D_0 is wanted on a rock model depending on the velocity v , then for the formation of the rock model, the test pieces can be selected for which the characteristic features (α_1 and α_2)—within the tolerated limits—are identical.

Summary

In generalized case, for the selection of rock models corresponding to the laws of physical modelling, the values of permeability and porosity are not sufficient.

Parameters characterizing the pore structure being more detailed must be taken also into consideration to fulfill the model laws. By the physical modelling of convective-conductive gas-diffusion processes, these parameters are suitably the parameters α_1 and α_2 .

On basis of identity of values α_1 and α_2 it is possible to form the corresponding rock models.

References

- Adzumi H 1939: Bull. Chem. Soc. Japan, 14, 343.
Azzam M J S and Dullien F A L 1976: Ind. Eng. Chem. Fundam., 15, 281.
Carman P C 1937: Trans. Inst. Chem. Engrs., London, 15, 150.
Carman P C 1956: Flow of Gases through Porous Media, Butterworths Co. London
Emersleben O 1925: Phys. Z., 26, 601.
Greenkorn R A 1981: AIChE J., 27, 529.
Jacquin C 1965: Rev. de l'Inst. Frans. Petr. 4.
Klinkenberg L J 1941: API. Drill. Prod. Pract., 200.
Kozeny J S B 1927: Akad. Wiss. Wien, 136, abt 11a, 271.
Millington R J and Quirk J P 1961: Trans. of Far. Soc. 57, 1200.

FLOCCULATION OF THE VISONTA LIGNITE SLUDGES BY POLYACRYLAMIDES

MRS. LAKATOS J SZABÓ¹ and I LAKATOS¹

[Manuscript received January 17, 1985]

The study deals with the flocculation of Visonta clay-lignite sludges by polyelectrolytes. Laboratory tests have proved that the highly stable heterodisperse suspension, hardly sedimentable by itself and unfilterable by conventional methods, can be dewatered by anionic polyacrylamides, yielding a final slurry concentration of 350 to 500 g dm⁻³. The formation of loose-structured and large-sized flocs allows troublefree filtration and dewatering. The flocs are mainly formed by a bridging mechanism, while the role of the agglomeration mechanism based on charge neutralization can be neglected. The specific flocculant consumption of dewatering is 1 to 2 kg/t solid, which is presently equivalent to 200 to 500 Ft/t (3–6 \$/t) within the costs of the preparation technology of the lignite.

Keywords: anionic polymers; bridging mechanism; coagulate; degree of hydrolysis; dewatering; floc; flocculation; lignite sludge; polyacrylamide; polyelectrolyte; sedimentation; sorption; suspension

Introduction

Both the literature data and the industrial practice prove the economic necessity of an ever increasing portion of energetical coals to be subjected to mineral processing which, by the use of various coal beneficiation techniques, can provide more valuable solid energy carriers of higher heating value for power plant operators (Gimpl 1979, Pethő 1980). This endeavour can also be recognized in connection with the Visonta lignite (Szabó and Csizmadia 1982, Szabó and Csizmadia 1984). In recent years a number of wet technologies have been developed for this purpose, but certain technological steps have led to lively controversies among experts (Tarján 1981, Pethő and Tompos 1982). One of the main problems in this field is the dewatering of large quantities of difficult-to-handle sludges with high clay content produced by waste materials and reduction of ash content desired from both economic and environmental point of view.

The aim of the laboratory investigations was to solve the dewatering problems of sludges, produced by waste handling of the Visonta lignite. Since literature suggests that sedimentation of stable suspensions containing various sorts of coal could be successfully solved by polyelectrolytes (Alexandrova et al. 1976, Clarke and Bagster 1982, Yokoyama et al. 1977, Kaminski et al. 1976, Lakatos and Mrs Lakatos Szabó

¹ Chemical Research Laboratory for Mining of the Hungarian Academy of Sciences, Miskolc-Egyetemváros, P.O.B. 2. Hungary, H-3515

1980, Schwoyer 1981, Singh et al. 1982) polyacrylamides of Hungarian and foreign made were used to solve the task. The investigations were aimed at determining the effect of the type, molecular mass, concentration and degree of hydrolysis of the polymer, salt content and pH of the medium, and mechanical mixing and dual (anionic-cationic) polymer system on the efficiency of flocculation and at assessing the filterability of the concentrated sludge.

Experimental

A sludge containing clay and lignite with a slurry concentration of 40 g dm^{-3} and a dissolved salt content of 1.22 g dm^{-3} was investigated. According to the microscopic particle size analysis, 60 percent of the solid in suspension had grain sizes less than $10 \mu\text{m}$, and the specific surface area was about $2500 \text{ cm}^2 \text{ g}^{-1}$. Ash content of the solid is 71.7%, but it increases with decreasing particle size, according to the Central Institute for Mining Development (KBFI). The waste present besides the combustible material, as regards its mineral composition, contained mainly quartz and montmorillonite (above 60 percent).

The electrokinetic (zeta) potential characteristic of the sludge is -0.020 V , determined by a Micromeritics Zeta Potential Analyser. Though this value can be regarded small, the dispersed system has proved very stable, hardly inclined to any settling by itself. Owing to the particle size of the dispersed solid, dewatering cannot be solved using conventional filters because of the very low permeability of the secondary filter cake.

To destabilize sludges containing waste, partially hydrolyzed polyacrylamides were used as flocculants. Of the polymers used in the test program, the principal data for those to be discussed in the study are listed in Table I.

Table I. Characteristics of flocculant polyacrylamides

Name	Ionic character	Average molecular mass $\times 10^6$	Degree of hydrolysis %	Manufacturer
Separan MG-205	anionic	7.2	1–2	Dow Chemical Co., USA
Separan AP-45	anionic	6.5	12–15	Dow Chemical Co., USA
Separan AP-30	anionic	3.5	30	Dow Chemical Co., USA
Separan AP-273	anionic	5.2	32	Dow Chemical Co., USA
Separan AP-269	anionic	0.8	40	Dow Chemical Co., USA
Separan XD-30207	anionic	8.0	35	Dow Chemical Co., USA
Separan XD-8467	cationic	2.0	5–10	Dow Chemical Co., USA
Separan XD-8494	cationic	2.0	35	Dow Chemical Co., USA
NIKE 61/80	anionic	4.0	5	Nitrochemical Works, Hungary
NIKE 42/80	anionic	5.2	15	Nitrochemical Works, Hungary
NIKE 77/80	anionic	6.5	30	Nitrochemical Works, Hungary

The sedimentation tests were carried out at room temperature, using conventional methods. Upon adding the required amount of solution containing the flocculant and after normal mixing, sedimentation volume (V_{sed}) was measured as a function of time and slurry concentration (c_{sed}) was calculated in sedimentation volume. In the figures showing the process kinetics, the volume of the slurry-free liquid containing only traces of solid ($V - V_{\text{sed}}$) and the relative slurry concentration (c_{sed}/c_0) are plotted as functions of time or polymer concentration.

Sorption properties of the polymer were determined under dynamic conditions (Lakatos and Mrs Lakatos Szabó 1980). Filterability of both initial and flocculated slurry was checked by laboratory vacuum filtration, under application, as a primary filter bed, of glass frits of various pore sizes.

Results and discussion

From a colloid chemical point of view, the waste-containing sludge being investigated forms a heterodisperse suspension, the kinetic stability of which is due to its extremely high distribution and aggregative stability. In general, stability is determined by the resultant electrokinetic potential. High zeta potential prevents the colloidal solid particles in dispersion from getting coagulated by collision. If we wish to modify the stability of such a system, the zeta potential has to be influenced so as to reduce surface potential and/or the thickness of the diffuse layer in the electric double layer. In industrial practice, this problem can usually be solved by the use of inorganic salts of multivalent cations as primary coagulants. Coagulation mechanism, however, based on neutralisation of surface charge failed to prove successful for Visonta lignite sludges.

Schwoyer (1981) suggests that dewatering of stable systems with a low zeta potential is possible only by bridging mechanism, though an action of complex mechanisms cannot be excluded either. Singh et al. (1982) have shown that on adding polyelectrolytes to coal suspensions, a charge neutralization first takes place, to be followed by bridge-formation. Thus, it is a process based on agglomeration and flocculation that may actually lead to dewatering of suspension. Alexandrova et al. (1976) have solved with success the sedimentation of anthracite suspensions, using cationic polyacrylamides. With a negative zeta potential it is possible that here, too, the determinant process for dewatering was provided by the surface charge neutralization. Therefore, although effective flocculation was expected from anionic and nonionic polymers, the cationic polymers could not be excluded from the test program either, because of the negative zeta potential. So the laboratory tests were started by studying the effect of the structure (ionic character) and concentration of the polymer on flocculation kinetics. In Fig. 1 sedimentation volume obtained during the flocculation with different polymers is illustrated as a function of time at constant polymer

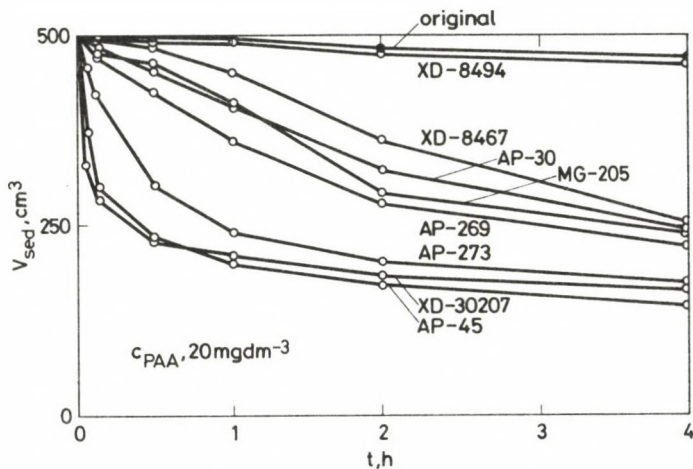


Fig. 1. Sedimentation volume as a function of time

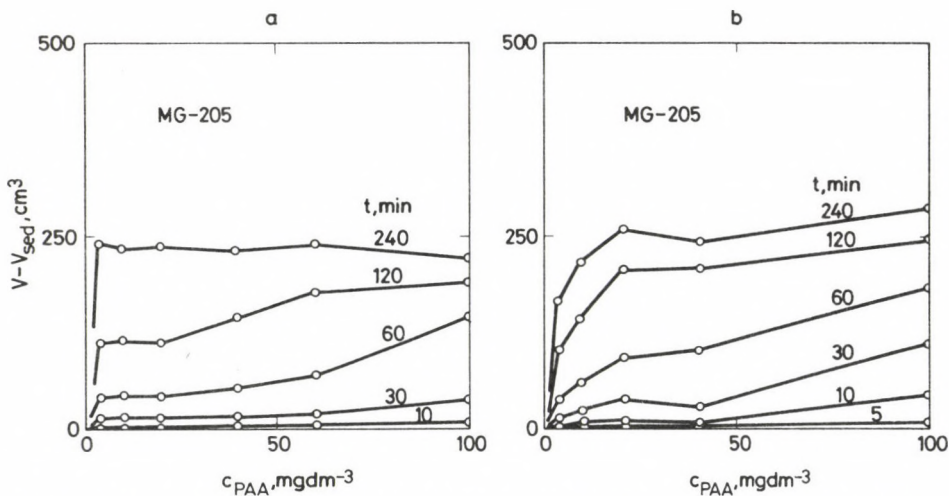


Fig. 2. Sedimentation effect of Separan MG-205 polymer (a) following vigorous stirring of the suspension; (b) without stirring

concentration. Figures 2 and 3 in turn show the flocculating effect of two anionic polyacrylamides with different degrees of hydrolysis as a function of polymer concentration, (a) after 1 hour of intensive mixing of the slurry and (b) for conventional case.

Figures 1–3 prove that effective sedimentation of the Visonta lignite sludges can only be achieved by hydrolyzed polyacrylamides of anionic character. The flocculating effect of slightly hydrolyzed, essentially nonionic polymers will approach that of ionic

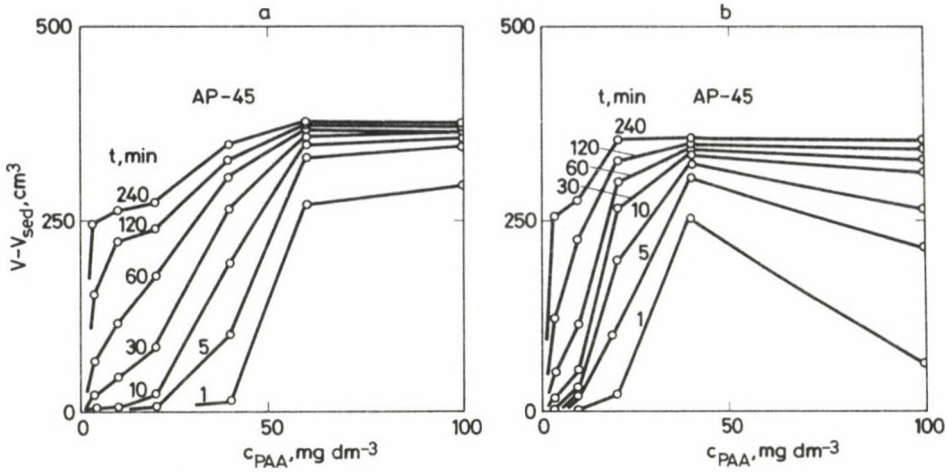


Fig. 3. Sedimentation effect of Separan AP-45 polymer (a) following vigorous stirring of the suspension; (b) without stirring

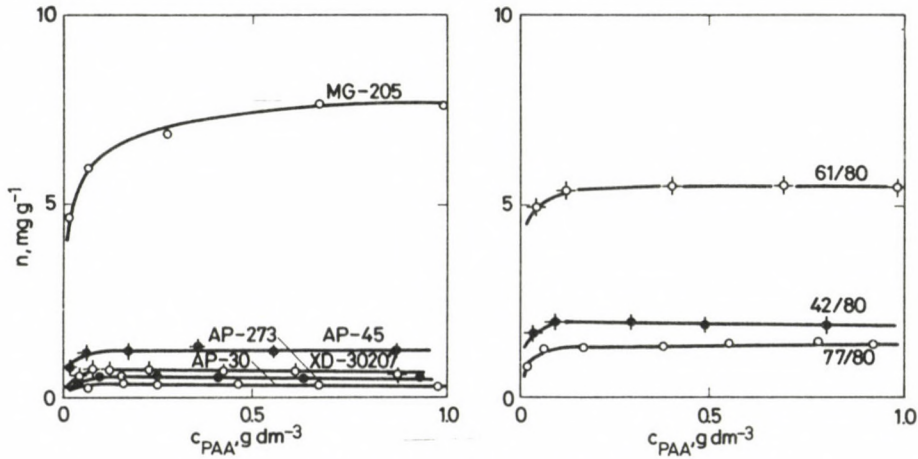


Fig. 4. Specific sorption loss of polyacrylamides on the Visonta lignite

ones only after a long time. On the other hand, no sedimentation effect can be registered with the cationic polymers.

The experimental findings do come up to expectations, and the explanation of the phenomenon lies with the sorption interaction between polymer and solid. It has been shown in our earlier investigations (Lakatos and Mrs Lakatos Szabó 1980, Lakatos et al. 1981) that the polyacrylamide is bound to the natural rocks also containing clay minerals first of all by chemisorption. The chemical bond is established between multivalent cations on the rock surface and the polymer's carboxyl groups,

and due to the inadequately dissociating bond, the sorption can practically be regarded irreversible. Sorption interaction of nonionic polymers is of physical character hence the process is reversible in most cases. With cationic polymers, however, no sorption interaction in the above sense takes place. According to Fig. 4, the specific sorption loss of foreign and Hungarian anionic polymers on clay-lignite solids varies between 0.2 and 8.0 mg g⁻¹, and, owing to molecular structural reasons, its amount is the greater the less the degree of hydrolysis of polymers. Curves with isotherm character suggest among other things, that flocculants for economic industrial application should be looked for mainly among polymers exhibiting small amounts sorbed (<2 mg g⁻¹), i.e. low specific flocculant consumption.

Experience proves that the sedimentation effect increases with the degree of hydrolysis, this change being not linear, though. At the same time the effect of the relative molecular mass of the polymer can be neglected within the range investigated, although it is desirable for the polymer's molecular mass to be above 10⁶. According to the experimental results, sedimentation rate and dewatering efficiency markedly increase as polymer concentration increases. However, in some cases signs of chemical overdosing become apparent (e.g. right hand side, Fig. 3) which may be relative and effective in character. In our case the former is concerned, and can be regarded local. That is, without intensive stirring the concentrated solution of the flocculant added to the sludge, because of solution structural reasons, will not mix entirely and instantaneously with the suspension. On the other hand, a part of the flocculant will not take part in bridging. Under our test conditions, a polymer concentration of about 50 mg dm⁻³ can be considered optimal.

Several authors (e.g. Singh et al. 1982, Schlauch 1981) attach a decisive importance to the manner of mixing in the sedimentation of concentrated disperse systems, using polyelectrolytes. Besides preventing local overdosing of chemicals, intensive stirring is also instrumental in the primarily formed, loosely built-up flocs being subjected to structural rearrangement due to mechanical forces. This may result in an important amount of water being forced out of the aggregates and a further increase in sedimentation efficiency. In a few instances we had similar experience, however, the difference between the 4-hour sedimentation curves is negligible, moreover, for short settling time sedimentation without intensive stirring showed greater rate than that with stirring.

In our subsequent investigations an attempt was made at deciding whether the Visonta lignite could be settled with Hungarian polyacrylamides developed by the Nitrokémiai Ipartelep (Nitrochemical Works) and the Chemical Research Laboratory for Mining of the Hungarian Academy of Sciences. From among the experimentally produced polymers, the flocculating effect of three acrylamide-acrylic acid copolymers of similar molecular mass but different degree of hydrolysis is shown in Fig. 5 as a function of concentration. Experience gained thus far proves that the sedimentation effect of polymers hydrolyzed to 5 percent is weak while that of polymers

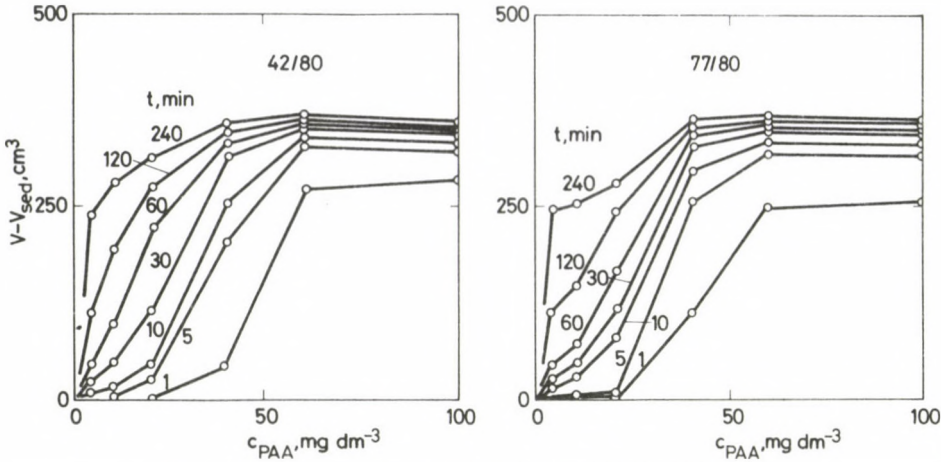


Fig. 5. Sedimentation effect of NIKE 42/80 and NIKE 77/80 polymers

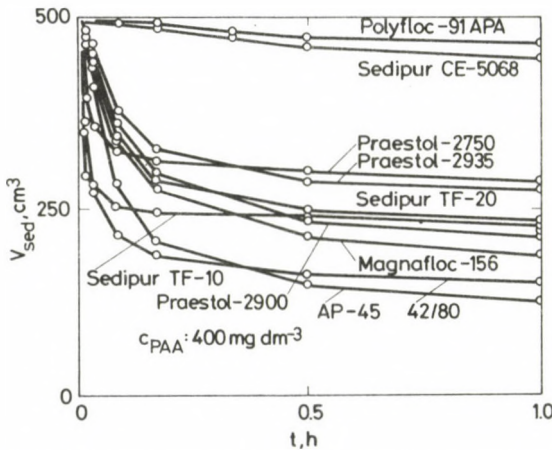


Fig. 6. Sedimentation volume as a function time for various flocculants

hydrolyzed to 15 and 30 percent is satisfactory in every respect. The latter substance, for short settling times and long ones alike, rivals the best foreign product named Separan. In fact, its effectiveness is not inferior to that of other western products currently used for flocculating coal sludges either, as is evident from Fig. 6. It should be noted in connection with the latter figure that the comparative measurement data were also obtained with a Visonta lignite sludge but of different composition and slurry concentration.

Natural and industrial disperse systems always contain smaller or greater amounts of inorganic salts, and though the effect of inorganic salts on the

sedimentation of stable sludges based on coagulation is small, it is not negligible either. The salt effect manifests itself principally by influencing the dissociation state of the macromolecule and its conformation in solution, which naturally can also be brought in direct relation with the tendency for bridging.

Figure 7 illustrates relative slurry concentration as a function of polymer concentration for two polymers at changing salt content. Experience suggests that the dewatering of a lignite sludge is made conveniently in a system with a low salt content if instantaneous settling is required. On the other hand, the concentration of dissolved salts is advantageous to increase above 10 g dm^{-3} if at least 30 minutes are available for settling, because in this manner a concentrate of somewhat greater slurry concentration can be produced, although the advantages achieved by salt content control are not very great.

The adjustment of pH of the disperse system to be settled involves theoretical and practical problems similar to those connected with the salt content control because in the majority of cases, buffering requires a considerable amount of inorganic salts to be dissolved. The Visonta lignite sludge was in the pH range of 6.0 to 6.2. By using a sufficient amount of buffer (alkali-phosphates), the pH was shifted in the acidic and basic directions ($\text{pH}=3.58$ and $\text{pH}=9.10$) and stabilized at the neutral point ($\text{pH}=6.95$), respectively. Results show that the sedimentation efficiency was considerably decreased by the chemicals added to adjust the pH. The rate of sedimentation,

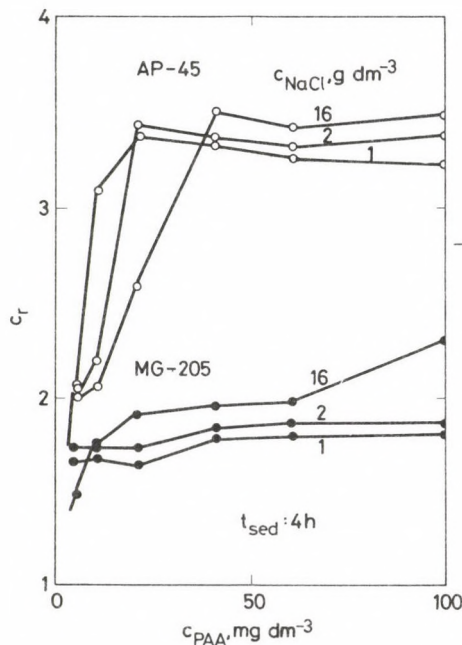


Fig. 7. Effect of salt content on relative slurry concentration

especially at the beginning was much less than in the reference case, and the final sedimentation volume was also greater.

Finally, the possibility of a two-step sedimentation or that using a dual polymer system was investigated. In our case, the theoretical basis for employing a dual polymer system is that, according to the sedimentation tests, the surface recharging takes place at an electrolyte concentration of 50 to 100 mg dm⁻³. Using an anionic polymer in this concentration range, the solid particles and the aggregates also containing free polymer segments, will have temporarily a negative surplus charge. As long as this surplus charge exists a further increase in aggregation is possible by adding a cationic macromolecule to the system which neutralizes the free surplus charge. A surplus amount of anionic polymer is first added to the suspension, then, following primary aggregation a cationic polymer is introduced in a suitable concentration.

In our experiments, negative surcharging in the first step was performed with anionic polymers; the sludge had a polymer concentration of 100 mg dm⁻³. Upon normal mixing, an aqueous solution of cationic polyacrylamides XD-8467 and XD-8494 were added to the sludge starting to settle. After repeated mixing, and measuring in usual manner the sedimentation rate, the curves of Fig. 8 were obtained showing the amount of the solid-free aqueous phase as a function of concentration of the cationic polymers.

It is clear from the figure that sedimentation rate of the sludge can be considerably increased by using a dual polymer system. The sedimentation rate at the beginning of flocculation, is well above the former values. The final volume of sedimentation is, however, in both cases less than that of the system flocculated with anionic polymer only. Sedimentation efficiency is affected by the structural state of both cationic and anionic polymer. The minimum of the curves indicates that, in the

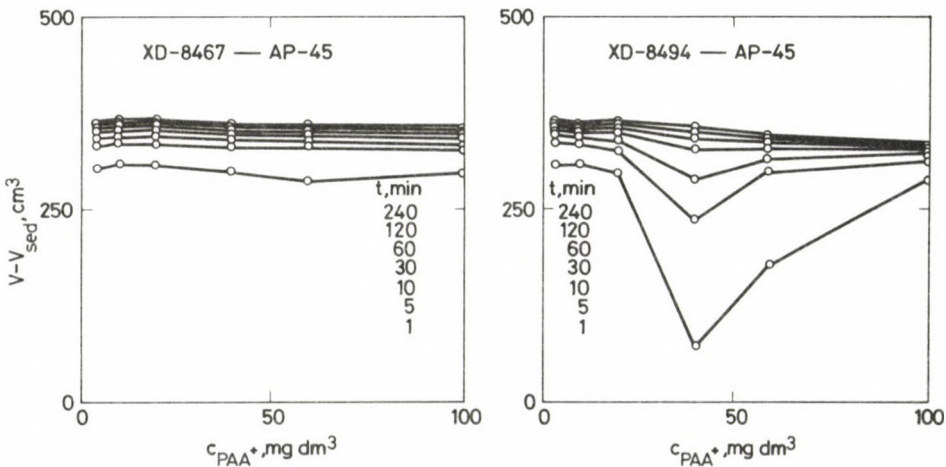


Fig. 8. $V - V_{sed}$ curves characteristic of the flocculation with a dual (anionic-cationic) polymer

dual polymer system, complicated recharging, bridging, and chemical bond-forming processes take place, which may be optimized only by thorough laboratory investigations. Their control, on the other hand, in the industrial application, lays a burden well above the average on the experts.

In each case, sedimentation tests were supplemented by filtration tests, performed in conventional and standard equipment. Glass frits of varying pore sizes and glass fibre-reinforced Whattman paper filters were used as a primary filter bed. In filtering the initial and the diluted lignite sludge, the rate of filtration slowed down to 10^{-3} to 10^{-4} cm min⁻¹ after obtaining a filtrate of 2–3 cm³ and became rapidly zero. A solid-free filtrate could only be obtained by filters with pore sizes less than 1 µm. The flocculated sludge, however, could be filtered without any difficulty also with filters of pore size above 15–20 µm, and the rate of filtration was practically determined by the permeability of the primary filter bed. One of the most important advantages of dewatering based on bridging is, perhaps, the formation of loose-structured giant flocs which according to experience may also be filtered out on a 63 to 100 µm bronze sieve. Even in such a case, permeability change of the filter cake was responsible for a reduction of 50% at the most of the initial rate of filtration, which results in a low solid-content filtrate even with the use of continuous vacuum drum filters. This advantage largely compensates for the certainly existing drawback that polyelectrolytes could not raise final slurry concentration above 350–500 g dm⁻³. Viewed from the angle of the technology to be applied, this means that water is suitable to be recovered from the flocculated sludge by filtration instead of sedimentation. Summing up, dewatering the Visonta lignite sludge poses no technical problems, the consumption of 1–2 mg g⁻¹ (1–2 kg/t) flocculant, however, implies a chemicals cost of Ft 200–500 (\$ 3–6) per ton of solid obtained, representing an important item within the preparation technology of the Visonta lignite.

Summary

Laboratory dewatering tests on the Visonta lignite sludge, using polyelectrolytes, have proved that the heterodisperse suspension, which has a high distribution and aggregate stability in its initial state and is unfilterable by conventional methods, can be flocculated if anionic polyacrylamides are used. Most efficient sedimentation can be obtained by the use of polyacrylamides having a medium molecular mass (1 to $3 \cdot 10^6$) and degree of hydrolysis. The efficiency of polymers developed in Hungary and experimentally produced by the Nitrochemical Works is in no way inferior to the best flocculants of foreign origin. The salt content and pH of the suspension play no decisive part in the sedimentation phenomenon. By intensive stirring of the system containing the flocculant and by using a dual anionic-cationic polymer system, the rate of settling at the initial stage of dewatering may be considerably influenced. Using polyelectrolytes, a sludge of a final slurry concentration of from 350 to 500 g dm⁻³ is formed,

whose excellent filterability is ensured by the loose-arranged giant flocs. According to test experiences, the sedimentation process is mainly due to a bridging mechanism, while the role of the agglomeration mechanism based on charge neutralization can be neglected.

References

- Alexandrova L D, Borts M A, Stepanova D I 1976: O flokuliruemosti antracitovih shlamov (in Russian). *Chimia tverdovo topliva*, 3, 57–64.
- Clarke M C and Bagster D F 1982: The recovery of coal values from colliery rejects by selective flocculation. CHEMECA 82', 10th Chem. Eng. Conf., Barton, Australia, 208.
- Gimpl E 1979: Coal preparation (in Hungarian). *BKL Bányászat*, 112, 819–829
- Kaminski V S, Sokolova M S, Safranova K I 1976: Mechanizm flokulyacji ugotynih chastic polyoxietilenom (in Russian). *Chimia tverdovo topliva*, 4, 46–50.
- Lakatos I and Mrs Lakatos Szabó J 1980: Investigation of the sorption phenomena of polyacrylamides in porous media under dynamic condition. *Acta Chim. Hung.*, 105, 57–72.
- Lakatos I, Mrs Lakatos Szabó J, Tóth J 1981: Factors influencing polyacrylamide adsorption in porous media and their effect on flow behaviour. In: Shah D O: *Surface phenomena in enhanced oil recovery*. Plenum Press, New York, 821–842.
- Pethő Sz 1980: Suggestions for preparation of Hungarian energetical coals to improve energy production (in Hungarian). *BKL Bányászat*, 113, 688–692.
- Pethő Sz and Tompos E 1982: Contribution to Possibilities of the Visonta lignite preparation' of Szabó I and Csizmadia L (in Hungarian). *BKL Bányászat*, 115, 41–42.
- Singh J, Singh N N, Tripathy P S M, Rao S K 1982: On the mechanism of flocculation of coal slurries. *J. Mines, Met. Fuels*, 30, 586–588.
- Schlauch R M 1981: Coagulation for gravity type clarification and thickening. In: Schwoyer W L K: *Polyelectrolytes for water and wastewater treatment*. CRC Press, Inc., Boca Raton, Florida, 91–145.
- Schwoyer W L K 1981: Sludge dewatering. In: Schwoyer W L K: *Polyelectrolytes for water and wastewater treatment*. CRC Press, Inc., Boca Raton, Florida, 159–211.
- Szabó I and Csizmadia L 1982: Possibilities of the Visonta lignite preparation (in Hungarian). *BKL Bányászat*, 115, 35–40.
- Szabó I and Csizmadia L 1984: Preparation of the Visonta lignite waste (in Hungarian). *BKL Bányászat*, 117, 181–187.
- Tarján G 1981: Remarks and suggestions on lignite preparation (in Hungarian). *BKL Bányászat*, 114, 730–745.
- Yokoyama Y, Yoshiaki N, Misuno H 1977: Effect of cationic polymers on flocculation of suspensions of fine coal particles. *Sviyo Kaishy*, 18, 532–536.

A NEW METHOD TO CALCULATE HEAT- AND VAPOUR ABSORPTION OF MINE AIR

J JANOSITZ¹

[Manuscript received February 21, 1985]

Calculation methods of the heat transfer of the rocks surrounding a mine opening are analysed in the paper. Equations suggested for different conditions in the literature are discussed.

Measurements showed that the ratio of heat- and vapour absorption of mine air is constant while flowing through mine openings of identical vapour content. Based on this finding a new calculation method of simultaneous heat- and vapour-absorption is presented in the paper.

Autocompression, friction and other heat can also be taken into account by the calculations if their flow into the mine air is constant along the total length Δl of an airway section.

Keywords: heat absorption; mine air; Ruhr coal mines; vapour absorption

Symbols

α	Heat-transfer coefficient,	W/m ² K
a	Ratio between vapour absorption and enthalpy increase,	g/kJ
a_r	Coefficient of temperature conductivity of rocks	m ² /s
$\begin{cases} A(p) \\ B(p) \end{cases}$	Constants of the general solution of Bessel's differential equation	
Bi	Biot number	
C	Constant characterizing the increment between heat-transfer coefficients of humid and dry surfaces	
c_{pa}	Specific heat of air at constant pressure,	1.005 kJ/kg K
d	Equivalent diameter of mine openings,	m
$D_{\Delta(x)}$	Estimated standard deviation of the estimation based on regression function $\Delta x = a\Delta h$,	g/kg
ϑ	Transformed value of rock temperature	
Θ	Laplace transform of ϑ	
E	Constant introduced in the deductions	
ε	Roughness characteristic of the surface of mine openings	
η	Dynamic viscosity,	Ns/m ²
F	Cross-section of the mine opening,	m ²
Fo	Fourier number	
$h, \Delta h, dh$	Enthalpy, enthalpy increment and elementary increment of enthalpy of mine air,	kJ/kg
$l, \Delta l, dl$	Length, partial length, elementary length of airway,	m
M	Mass flow rate of air,	kg/s
λ	Coefficient of thermal conductivity,	W/m K
N	Number of measured data used in the calculation of regression function $\Delta x = a\Delta h$,	
ν	Kinematic viscosity,	m ² /s
p	Symbol of time after Laplace-transformation	
p	Part of heat-absorption of mine air expended to temperature increase	

¹ University of Heavy Industry, Institute of Mining, Miskolc-Egyetemváros H-3515

\dot{q}	Heat flux,	W/m^2
Q	Heat flow in unit time,	W
r	Radial distance from the axis of the mine opening,	m
r_v	Heat of vaporization of water,	2486 kJ/kg
R	Heat radius, the equivalent radius of mine opening,	m
Re	Reynolds number	
R_a	Gas constant of air,	$287 \frac{J}{kg K}$
ρ	Density,	kg/m^3
$\rho(z)$	König's constant for calculating the heat radius	
$s_1, s_2 (s_1 < s_2)$	Sides of a mine opening of rectangular cross-section,	m
t	Temperature,	$^{\circ}C$
$T=273.15+t$	Absolute temperature,	K
τ	Time,	s
U	Perimeter of the section perpendicular to air flow,	m
v	Average flow velocity of air,	m/s
\dot{V}	Flow rate of air,	m^3/s
$x, \Delta x, dx$	Vapour content, increment, elementary increment of vapour content of the air,	g/kg
y, y_0	Constants introduced in the deductions,	$^{\circ}C$
$z = s_1/s_2$	Ratio of sides of mine openings of rectangular cross-sections	

Indices

e	else
eff	effective
s	surface
r	rock
a	air
ao	air in the initial section of the airway
pa	air at constant pressure
p	primary
t	part expended to temperature increase
v	vapour
x	part expended to increase of vapour content

*Constants and dimensionless numbers applied or introduced
in the deductions*

$$P = \frac{Q_0}{\dot{V} \rho_a c_{pa}}$$

$$Pr = \frac{c_{pa} \eta}{\lambda}$$

$$Re = \frac{v \cdot d}{\nu}$$

$$y = t_p - t_a$$

$$y_0 = t_p - t_{ao}$$

$$Y = P/E$$

$$Nu = \frac{\alpha d}{\lambda}$$

$$Bi = \frac{\alpha R}{\lambda}$$

$$E = \frac{\lambda_r K (Bi, Fo) U}{R(\dot{V}) \rho_a c_{pa}}$$

$$Fo = \frac{a_r \tau}{R^2}$$

$$D = E \Delta l$$

$$\mathfrak{G} = \frac{t_p - t}{t_p - t_a}$$

**Mathematical analysis of the heat flow perpendicular to the axis
of a mine opening of circular cross-section**

A great number of papers have been published in this field during the last two decades (Batzel 1952, Boldizsár 1957, Esztó 1983, Frycz 1981, Knechtel et al. 1975, König 1952, Scherban et al. 1959, Starfield 1966, Voss 1969, Vost 1982) therefore only the most important initial conditions and equations of the most frequently used method are dealt with.

The following assumptions are made in most papers analysing the problem:

- heat conductivity of the rocks surrounding the mine opening is the same everywhere,
- before drifting a roadway the rock temperature t_p is everywhere the same,
- temperature t_a and flow rate \dot{V} of the air flowing into the mine opening are constant,
- axial heat flow in the rock can be neglected in comparison to the radial heat flow,
- heat flow into the air from the rock wall by heat radiation is negligible to convective heat transfer ($v > 1$ m/s).

The partial differential equation of heat conduction

$$\Delta t = \frac{\rho c}{\lambda} t' \quad (1)$$

can be written above in cylindrical coordinates for the above conditions as:

$$\frac{\partial t}{\partial \tau} = a_r \left[\frac{\partial^2 t}{\partial r^2} + \frac{1}{r} \frac{\partial t}{\partial r} \right]. \quad (2)$$

Introducing variable

$$\vartheta = \frac{t_p - t}{t_p - t_a} = \frac{t_p - t}{\Delta t}, \quad (3)$$

where $\Delta t = t_p - t_a$, Eq. (2) becomes

$$\frac{\partial \vartheta}{\partial \tau} = a_r \left[\frac{\partial^2 \vartheta}{\partial r^2} + \frac{1}{r} \frac{\partial \vartheta}{\partial r} \right]. \quad (4)$$

Let Θ be the Laplace transform of $\vartheta(\tau, r)$, i.e.:

$$\mathcal{L}\vartheta(\tau, r) \sim \Theta(p, r). \quad (5)$$

Thus the Laplace transform of Eq. (4) can be written as (Scherban et al. 1959)

$$\frac{d^2 \Theta}{dr^2} + \frac{1}{r} \frac{d\Theta}{dr} - \frac{p}{a_r} \Theta = 0. \quad (6)$$

Equation (6) is a modified zero-order Bessel's differential equation whose general solution is (Korn and Korn 1975):

$$\Theta(p, r) = A(p)I_0(sr) + B(p)K_0(sr),$$

where

$$s = \sqrt{\frac{p}{a_r}}. \quad (7)$$

In Eq. (7) I_0 and K_0 denote the modified zero-order Bessel and Hankel functions. Following boundary conditions can here be considered to determine constants A and B :

— Heat flux at the surface of the mine opening from the rock into the opening is equal to the heat absorbed by the mine air, i.e.:

$$\dot{q} = \lambda \left[\frac{\partial t}{\partial r} \right]_{r=R} = \alpha [t - t_a]_{r=R} \quad (8)$$

— Heat lacking in the surrounding rock of a mine opening of radius R and unit length after time τ is equal to the heat absorbed by the mine air at a surface of unit length of the mine opening during this time. In other form:

$$c \cdot \rho \int_{r=R}^{\infty} (t_p - t) 2r\pi \cdot 1 \cdot dr = \alpha \int_{\tau=0}^{\tau} (t - t_a)_{r=R} 2R\pi \cdot 1 \cdot d\tau. \quad (9)$$

Using Eq. (3), we have for Eqs (8) and (9)

$$\dot{q} = -\lambda \left[\frac{\partial \vartheta}{\partial r} \right]_{r=R} \cdot \Delta t = \alpha [1 - \vartheta]_{r=R} \cdot \Delta t, \quad (10)$$

and

$$\Delta t \rho c \cdot \int_{r=R}^{\infty} \vartheta \cdot r \cdot dr = \alpha R \cdot \Delta T_0 \int_{\tau=0}^{\tau} [1 - \vartheta]_{r=R} \cdot d\tau. \quad (11)$$

Using the formulae of Bessel and Hankel functions (Korn and Korn 1975)

$$\frac{dI_0(x)}{dx} = I_1(x),$$

$$\frac{dK_0(x)}{dx} = -K_1(x) \quad (12)$$

$$x^m I_{m-1}(x) dx = x^m I_m(x)$$

and

$$x^m K_{m-1}(x) dx = -x^m K_m(x),$$

the Laplace transforms of Eqs (10) and (11) become:

$$-\lambda[AI_1(sR) - BK_1(sR)] \cdot s = \alpha \left[\frac{1}{p} - AI_0(sR) - BK_0(sR) \right], \quad (13)$$

and

$$\frac{\rho c}{s^2} \{sr[AI_1(sr) - BK_1(sr)]\}_{r=R} = \frac{\alpha R}{p} \left[\frac{1}{p} - AI_0(sR) - BK_0(sR) \right]. \quad (14)$$

R.H.S. of Eq. (14) is finite, but L.H.S. can only have finite value if $A=0$. In this way the same expression is obtained for B from both Eq. (13) and Eq. (14):

$$B = \frac{\alpha}{p[\alpha K_0(sR) + K_1(sR)]}. \quad (15)$$

In the analysis of the influence of rock heat on the mine air, dimensionless Fourier (Fo) and Biot (Bi) numbers are preferred to the parameters applied previously. Using these numbers, we have from Eq. (15):

$$\Theta(p, r) = \frac{K_0(sr)}{p \left[K_0(sR) + \frac{sR}{Bi} K_1(sR) \right]}. \quad (16)$$

Calculating the expected temperature and humidity conditions in the mine the expression

$$-R \left[\frac{\partial \Theta}{\partial r} \right]_{r=R} = K(Fo, Bi) \quad (17)$$

is called age factor. It can be determined by the nomograph in Fig. 1 (Scherban et al. 1959). Hence $K(Fo, Bi)$ equals the inverse Laplace transform of the function

$$F(p) = -R \left[\frac{\partial \Theta}{\partial r} \right]_{r=R} = \frac{R^2}{a} \frac{K_1(sR)}{sR \left[K_0(sR) + \frac{1}{Bi} K_1(sR) \right]}. \quad (18)$$

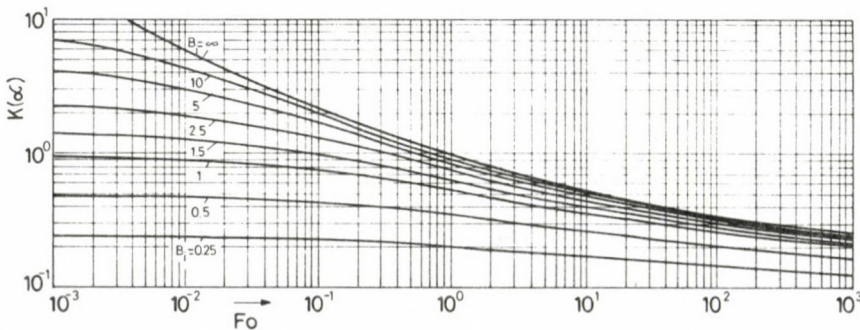


Fig. 1. Nomograph for determining age factor $K(\alpha) = f(Fo, Bi)$

It can be proved that function (18) has only at $p=0$ singularity and at the same time this is also the forking point of this function. In such a case, for the retransformation the integrating path of the applied inverse integral must be supplemented to form a closed curve so that it does not contain the forking point.

If $p = ve^{j\varphi}$, it can be proved by Jordan's-lemma that:

$$K(Bi, Fo) = \frac{R}{a_r} \frac{1}{2\pi j} \int_0^{\infty} [F(ve^{-j\pi}) - F(ve^{j\pi})] e^{-v\tau} dv. \quad (19)$$

Marzilger and Wagener (1972) published a method to determine the integral in Eq. (19). With slight modifications we have for the heat flux entering the mine opening of circular cross-section through its wall

$$\dot{q} = \frac{\Delta t}{R} K(Bi, Fo). \quad (20)$$

With \dot{q} the enthalpy increment of the air in a circular cross-section of elementary length dl is:

$$dh = \frac{\dot{q}U}{V\rho_a} dl. \quad (21)$$

If there is no vapour absorbed by the air in the mine opening, it holds for the temperature increase of the air dt_a flowing through the mine opening of length dl

$$dh = c_{pa} \cdot dt_a. \quad (22)$$

Introducing variables y , y_0 , E and D , Eq. (22) can be transformed:

$$Ey dl = -dy, \quad (23)$$

whence

$$\frac{dy}{y} = -E dl. \quad (24)$$

Assuming that $K(Bi, Fo)$ is constant within the length dl , in Eq. (24) E can be taken as constant. In other words, if the dry temperature is t_{ao} at the beginning of the airway of length Δl and the dry temperature is t_a at the end, it holds from Eq. (24) for the temperature increase $t_a - t_{ao}$

$$t_a - t_{ao} = y_0(1 - e^{-D}). \quad (25)$$

At time τ after opening a mining excavation the effect of rock heat on mine air can be calculated under the given conditions. For this purpose, however, the variables in the equations have to be known.

Calculation of the heat radius R for airways with non-circular cross-sections

In our previous analysis it has been assumed that the airways have circular cross-sections. Such roadways, however, are rare in mining, therefore it will be analysed what value can substitute R for airways with non-circular cross-sections.

The problem was investigated by König (1952) in detail. According to his paper the "equivalent" radius R for roadways with rectangular cross-sections can be calculated as

$$R = \frac{U}{\rho(z)}, \quad (26)$$

where function $\rho(z)$ depends on the ratio $s_1/s_2 = z$ ($s_2 \geq s_1$) between the sides of the cross-section of the airway. The diagram in Fig. 2 shows the change of $\rho(z)$ as a function of the ratio of sides. The following values have been determined for $\rho(z)$ of regular geometric figures by König (1952):

For triangle: 7.108; for quadrilateral: 6.778; for hexagon 6.521; for octagon 6.421; for decagon: 6.374 and for circle: $6.283 = 2\pi$. In case of a rectangle Eq. (27) can be used for the approximation of $\rho(z)$ (Fig. 2):

$$\rho(x) = \begin{cases} -13.62 z^3 + 15.07z^2 - 6.24z + 7.89, & \text{if } 0 < z < 0.5 \\ -0.139z + 6.91 & \text{if } 0.5 < z < 1. \end{cases} \quad (27)$$

$z = s_1/s_2$.

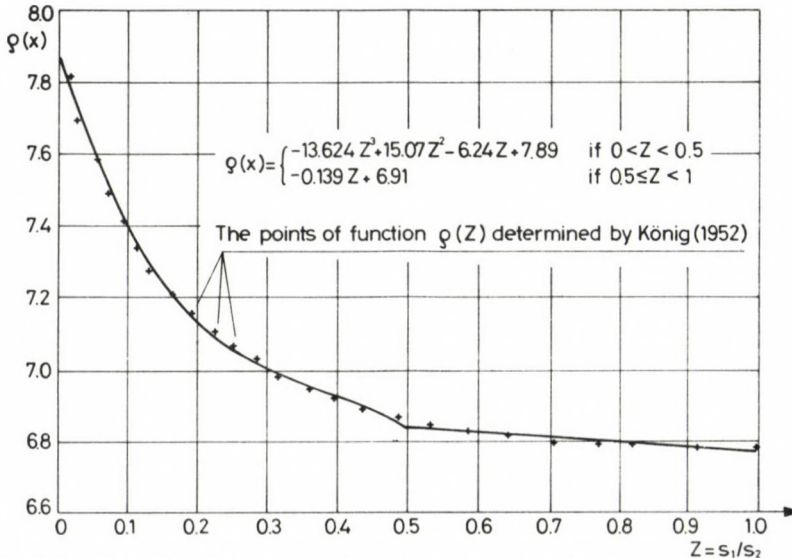


Fig. 2. König's function $\rho(x)$ as a function of the ratio of sides s_1/s_2 of roadways with rectangular cross-section

If the cross-section differs from each of the geometric figures mentioned, then it is approximated by the most similar geometric figure. Contours of the approximation figure

- should enclose the same cross-sectional area, and
- should have a deviation from the original contour as small as possible.

By $\rho(x)$ of the approximate geometric figure and the original U the approximate heat radius can be determined.

Esztó (1983) suggests the following equation for the calculation of R :

$$R = \frac{1}{2} \left[\frac{U}{2\pi} + \sqrt{\frac{F}{\pi}} \right]. \quad (28)$$

Selecting the coefficient of heat conductivity λ

The coefficient of heat conductivity of the rocks surrounding airway depends on the rock type and other physical characteristics of the rock. Plenty of data can be found in the literature for the different rocks and conditions. Some of them are listed in Table I.

The coefficient of temperature conductivity a_r , given in Table I can be calculated from λ_r , c_a and ρ_r as:

$$a_r = \frac{\lambda_r}{c_a \cdot \rho_r}. \quad (29)$$

According to Mücke (1964) the humidity content of rocks affects λ only very slightly.

Calculation of the heat-transfer coefficient α

Air flow in mine openings is practically always turbulent. In turbulent flow heat flow takes place in the form of mixing within the air. In developed turbulent flow ($Re > 10^4$) an intensive mixing takes place producing constant air temperature in the cross-section of core. A sudden temperature change can only be observed within the boundary layer. Nusselt and many other researchers developed usable equations on the basis of similitude theory by processing the experimental data of the heat transfer in turbulent flows. The most accurate equation is published by Miheyev (1953) on page 84 of his book:

$$Nu = 0.023 Re_s^{0.8} Pr^{0.4}. \quad (30)$$

Table I. Physical-thermal characteristics of rocks after K Chumra (Knechtel et al. 1975)

Rocks	ρ_r Density 10^3 kg/m^3	c_r Specific heat $\text{kJ/kg} \cdot \text{K}$	λ_r Coefficient of thermal conductivity $\text{W/m} \cdot \text{K}$	a_r Coefficient of temperature conductivity $10^{-6} \text{ m}^2/\text{s}$
Peridotite	2.68–3.12	0.831	2.31–4.14	1.04–1.60
Pyroxenite	2.65–3.09	0.840	2.09–3.93	0.93–1.52
Gabbro	2.61–3.01	0.957	2.01–3.51	0.80–1.37
Diorite	2.61–2.90	1.007	2.15–3.60	0.76–1.20
Syenite	2.60–2.81	0.882	1.91–4.61	0.83–1.81
Granite	2.61–2.68	0.815	2.23–3.61	1.05–1.65
Diabase	2.36–2.62	0.719	1.98–4.53	1.17–2.40
Basalt	2.90–3.09	0.715	1.67–5.56	0.78–2.42
Porphyry	2.58–2.88	0.710	1.67–5.59	0.82–2.74
Andesite	2.58–2.82	0.530	1.64–4.43	1.12–2.98
Trachyte	2.48–2.78	0.573	1.51–3.07	1.14–1.90
Gneiss	2.62–2.71	0.465	1.28–2.56	1.05–2.03
Serpentine	2.66–3.04	0.830	1.91–2.79	1.87–1.10
Crystalline slate	2.30–2.90	0.773	1.26–2.63	1.70–1.73
Marble	2.61–2.72	0.874	2.26–3.67	0.99–1.50
Limestone	1.40–1.97	0.831	0.85–2.79	0.71–1.70
Dolomite	2.65–2.75	0.840	2.08–5.23	0.93–2.25
Gravel	2.59–2.69	0.552	1.51–4.52	1.06–2.98
Quartzitic sandstone	2.39–2.64	0.809	1.72–4.14	0.91–1.99
Quartzite	2.56–2.70	0.830	1.98–6.05	0.90–2.70
Quartzitic slate	2.48–2.63	0.756	1.55–3.80	0.81–1.91
Slay slate	2.15–2.66	1.208	0.93–2.88	0.36–0.89
Sludge	2.24–2.63	1.062	1.51–3.36	0.63–1.09
Weakly bound clay slate	2.11–2.25	0.815	1.25–2.33	0.79–1.27
Weakly bound clay	2.31–2.48	0.692	0.95–1.163	0.59–0.67
Clayey sand	2.56–2.51	0.806	0.35–3.31	0.17–1.80
Bituminous coal	1.09–1.47	0.782	0.09–0.70	0.10–0.60
Lignite	0.81–1.23	0.502	0.03–0.31	0.07–0.50
Salt	2.39–2.82	0.465	3.88–7.21	3.50–5.40

In Eq. (30) the logarithmic average temperature t_s within the cross-section must be used, while the equivalent diameter of the mine opening has to be taken as a characteristic dimension. Equation (30) can be applied if for air

$$2 \cdot 10^6 > Re > 10^4$$

and if

$$2500 > Pr > 0.7$$

(31)

hold. Nu and Re must be calculated here with the average values over the cross-section of air flow!

Expressing α from Eq. (30), we have

$$\alpha = 0.023 \frac{\lambda_a}{d} \left(\frac{w \cdot d}{v_a} \right)^{0.8} Pr^{0.4}. \quad (32)$$

Vost (1982, 1973) also applies the same formula. For gases with uniform atomic structure Pr is constant and depends neither on pressure, nor on temperature. For monatomic gases $Pr = 0.67$, for diatomic gases $Pr = 0.72$, for triatomic gases $Pr = 0.8$ and for four- or more atomic gases $Pr = 1$. Thus, if the amount of other gases besides O_2 and N_2 in air (CO_2 , H_2O , CH_4 etc.) is negligible, we have $Pr = 0.72$.

λ_a and v_a also depend on temperature. According to Fekete and Menyhárt (1975, page 10)

$$\lambda_a = (243 + 0.7t_a) \cdot 10^{-4} \quad (33)$$

holds within the temperature range $-20^\circ C < t_a < 100^\circ C$.

Kinematic viscosity can be calculated from dynamic viscosity

$$v_a = \frac{\eta_a}{\rho_a}. \quad (34)$$

According to Fekete and Menyhárt (1975, page 18)

$$\eta_a = (12.55 \sqrt{T_a} - 33.94) \cdot 10^{-7} \quad (35)$$

holds within temperature limits $0 < t_a < +85^\circ C$;

and

$$\eta_a = (0.05639t_a + 17.279) \cdot 10^{-6}$$

within temperature limits $-50 \leq t_a \leq 35^\circ C$.

Air density can be calculated by Eq. (36):

$$\rho_a = \frac{p_a}{R_a T_a} \quad (36)$$

in other words α can be determined from Eq. (32).

According to Batzel (1952), in roadways without support

$$\alpha = 4.07 + 8.14v^{0.8} \quad (37)$$

holds and if steel arches with lagging are used, we have

$$\alpha = 2.91 + 7.56v^{0.6}. \quad (38)$$

König (1952) uses the value 26.8 for roadways and 25.6 for shafts (page 13).

Voss (1967) proposes equation

$$\alpha = 4.42 \varepsilon \frac{v^{2/3}}{d^{1/3}} \quad (39)$$

where ε denotes the mean roughness factor of the wall. According to Ufer $\varepsilon=2.7$ in workings, $\varepsilon=1.7$ in roadways with uneven walls (with support), $\varepsilon=1.35$ in roadways without support and $\varepsilon=1$ in roadways with exceptionally even walls. Shcerban obtained for ε values between 2.4 and 3.0 in workings with high prop density (Voss 1967).

This equation gives good result for $v \geq 1$ m/s. For lower air velocities the fraction of free convection also increases. Shcerban et al. (1959) use equation

$$\alpha = 2.71(1 + 5\sqrt{v}). \quad (40)$$

Vost (1982) also uses an equation similar to Eq. (32) to calculate α . The specific heat of the air depends on the vapour content (Barenbrug 1974), i.e.

$$c_{pa} = 1.005 + 1.893x \cdot 10^{-3} \text{ kJ/kg K} \quad (41)$$

where x denotes vapour content.

Hence the warming up of the flowing air by the dry rock surface can be calculated.

If the mine openings are humid, material transfer is to be also taken into account together with heat transfer. In other words one has to calculate with the vapour absorption of the air. As well known, wet (perspiring) human skin has higher "heat-transfer" ability than the dry one.

Equation (8) had a very important role in our earlier discussions. It is, however, only correct for dry heat transfer. Its material transfer also takes place besides heat transfer, validity of Eq. (8) and all other equations derived from it must be checked. L.H.S. of Eq. (8) gives heat flux leaving the surface of the mine opening while R.H.S. contains heat flux absorbed by the air. If term \dot{q}^* for material transfer is added to the convective heat transport on R.H.S., Eq. (8) is modified as

$$\lambda \left(\frac{\partial t}{\partial r} \right)_{r=R} = \alpha(t - t_a) + \dot{q}^*. \quad (42)$$

If

$$\dot{q}^* = \alpha^*(t - t_a), \quad (43)$$

Equation (42) can be re-written as

$$\lambda \left[\frac{\partial t}{\partial r} \right]_{r=R} = \alpha_{\text{eff}}(t - t_a) \quad (44)$$

with

$$\alpha_{\text{eff}} = \alpha(1 + C), \quad \text{and} \quad \alpha^* = C\alpha.$$

Equation (21) can be applied by using age factor determined by α_{eff} . In such cases Δh consists of two parts: from fraction Δh_t increasing air temperature and fraction Δh_x increasing vapour content.

$$\frac{\alpha}{\alpha^*} = \frac{\Delta h_t}{\Delta h_x} \quad (45)$$

$$(\Delta h = \Delta h_t + \Delta h_x).$$

It has to be emphasized that condition (44) must hold for parts of and the whole surface of mine opening.

It can be proved that a linear correlation exists between the measured values of enthalpy Δh and vapour absorption Δx (Janositz 1979)

$$\Delta x = a \Delta h \quad (46)$$

(Figs 3–15).

If temperature and humidity conditions of a mine opening should be planned, whose humidity can be characterized by coefficient a in Eq. (46), the value of C necessary to calculate α_{eff} can be obtained by using Eqs (42) and (43) from the formula

$$C \cong \frac{ar_v}{1 - ar_v}. \quad (47)$$

In each of Figs 3–15 measured data fit surprisingly well to Eq. (46). In the measured results beside the rock heat, machine heat plays also a role. That means that

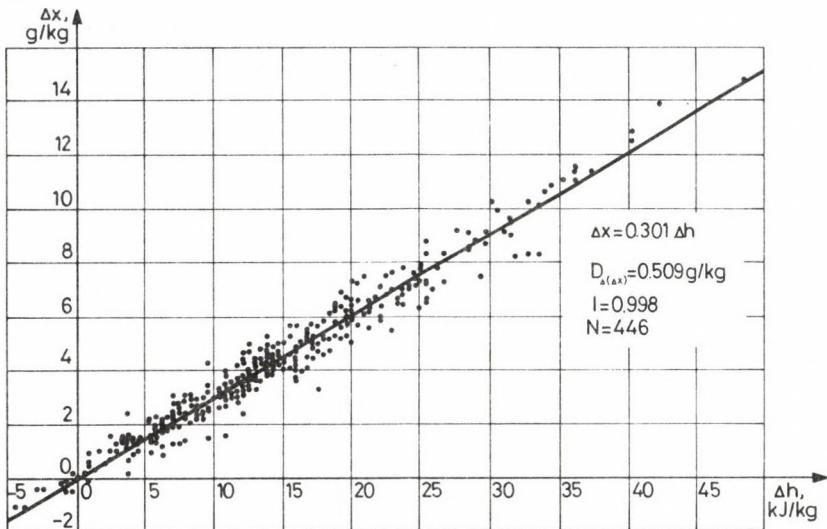


Fig. 3. Vapour absorption of mine air vs. enthalpy increase in the mines of the Ruhr district, measured in 1966 (Janositz 1979)

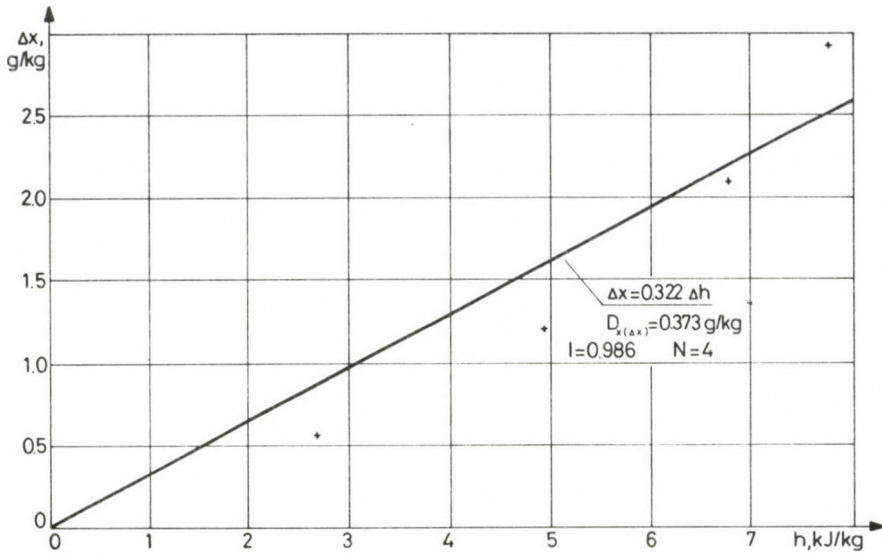


Fig. 4. Vapour absorption vs. enthalpy increase of mine air in the intakes of flush workings of the Ruhr district, measured in 1971 (Janositz 1979)

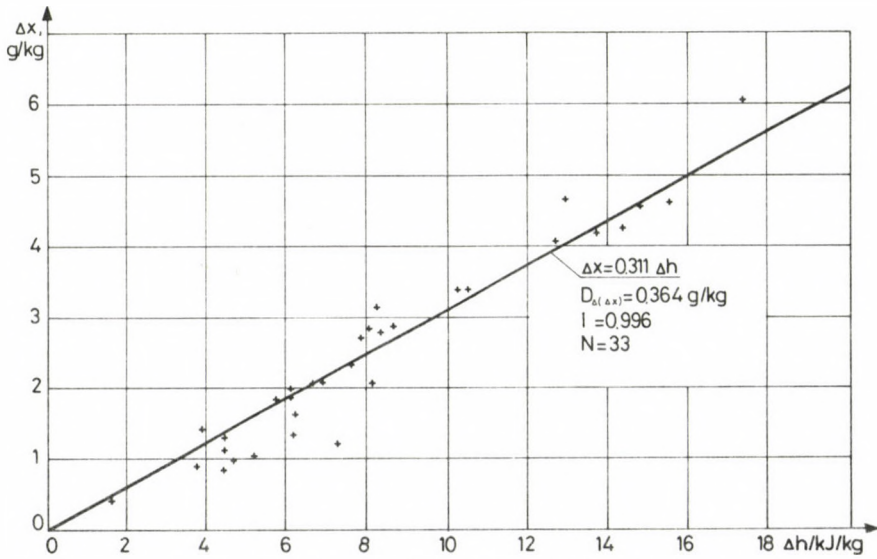


Fig. 5. Vapour absorption vs. enthalpy increase of mine air in the intakes of caving longwall workings in the Ruhr district, measured in 1971 (Janositz 1979)

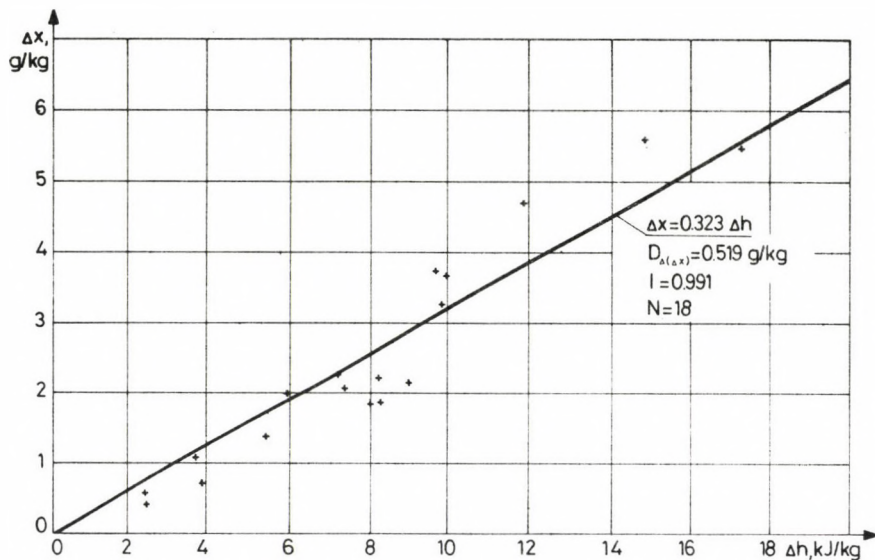


Fig. 6. Vapour absorption vs. enthalpy increase of mine air in the return airways of caving longwall workings in the Ruhr district, measured in 1971 (Janositz 1979)

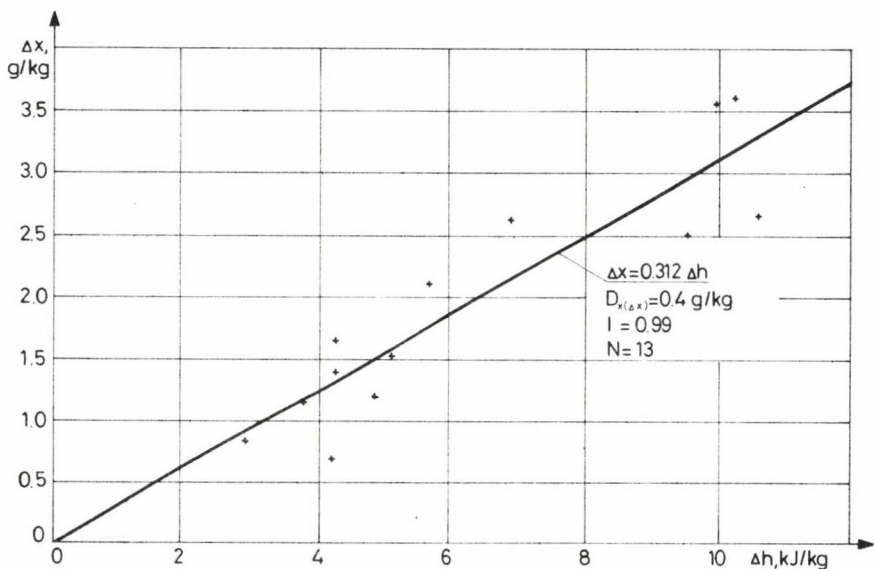


Fig. 7. Vapour absorption vs. enthalpy increase of mine air in the workings with pneumatic stowing in the Ruhr district, measured in 1971 (Janositz 1979)

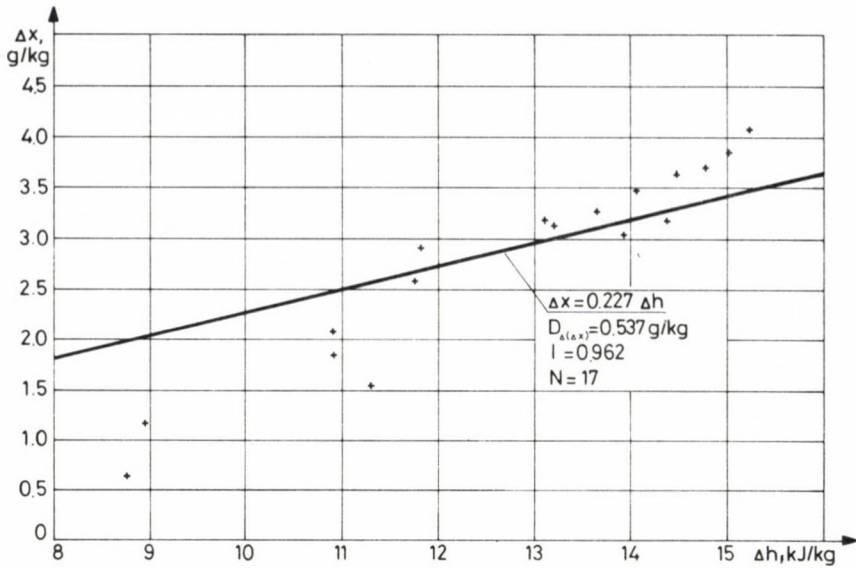


Fig. 8. Vapour absorption vs. enthalpy increase of mine air in the intake of working 94/A of Mine XX of Oroszlány Coal Mines, measured by M Barabás

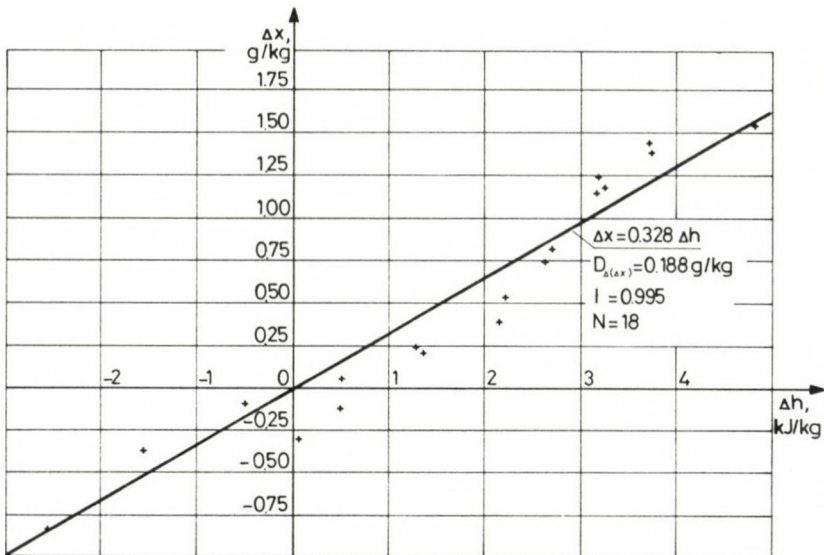


Fig. 9. Vapour absorption vs. enthalpy increase of mine air in the longwall working 101/F of Mine XX of the Oroszlány Coal Mines, measured by M Barabás

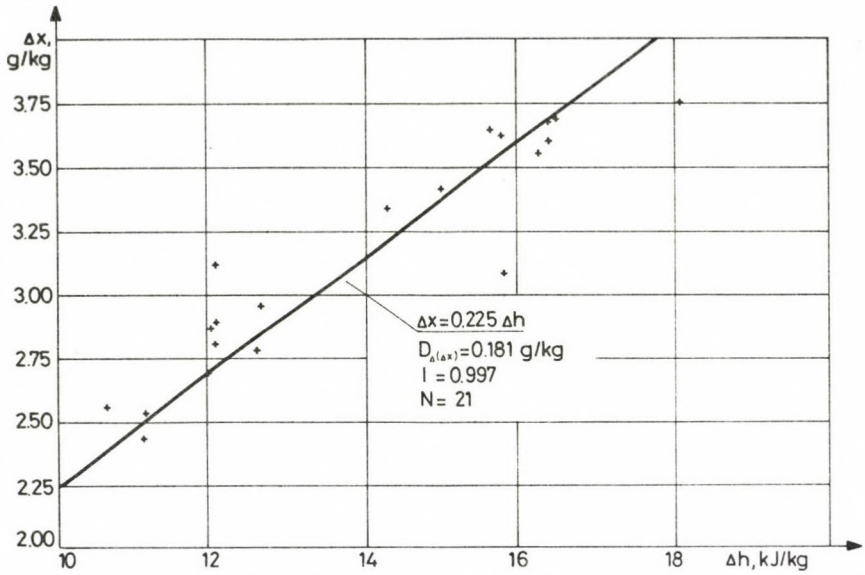


Fig. 10. Vapour absorption vs. enthalpy increase of mine air in the intake of the longwall working in the Mine XXII of the Oroszlány Coal Mines measured by M Barabás

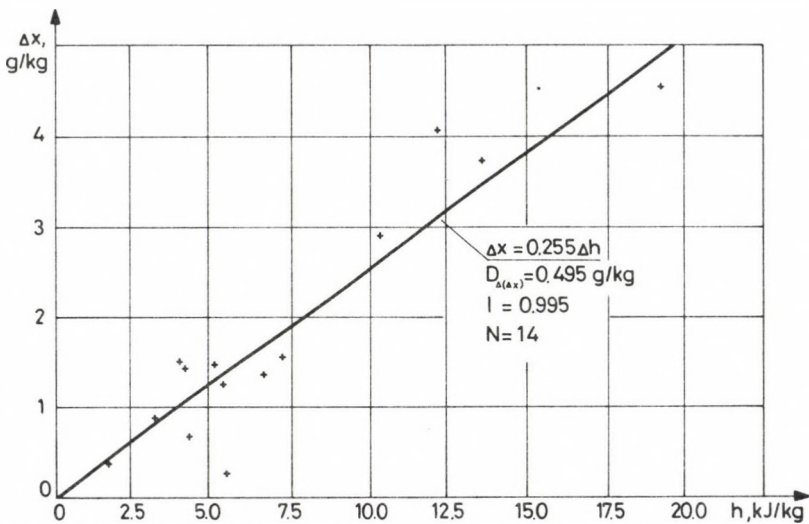


Fig. 11. Vapour absorption vs. enthalpy increase in the development roadways of the Mine IV of the Mecsek Ore Mines, measured by M Selmec

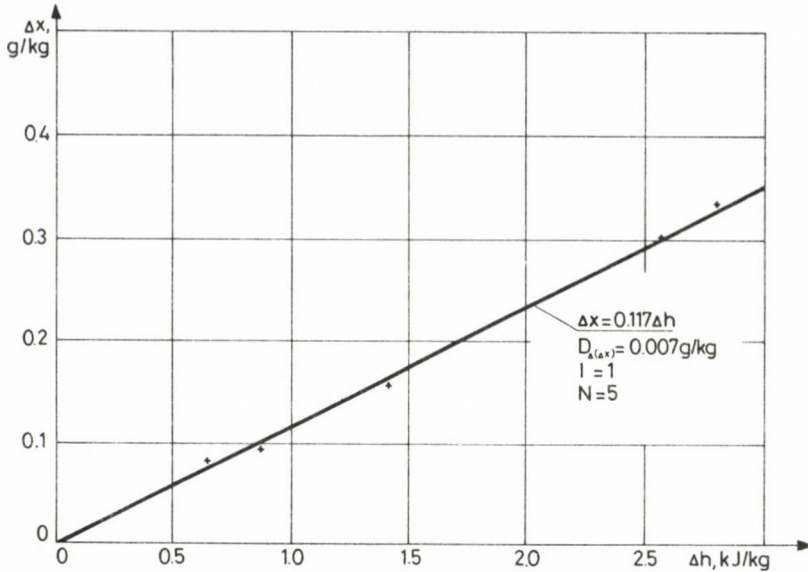


Fig. 12. Vapour absorption vs. enthalpy increase of mine air in the main gallery in the 700 m level of the Recsk Ore Mine, measured by I Cifka (Central Institute for Mining Development, 1983)

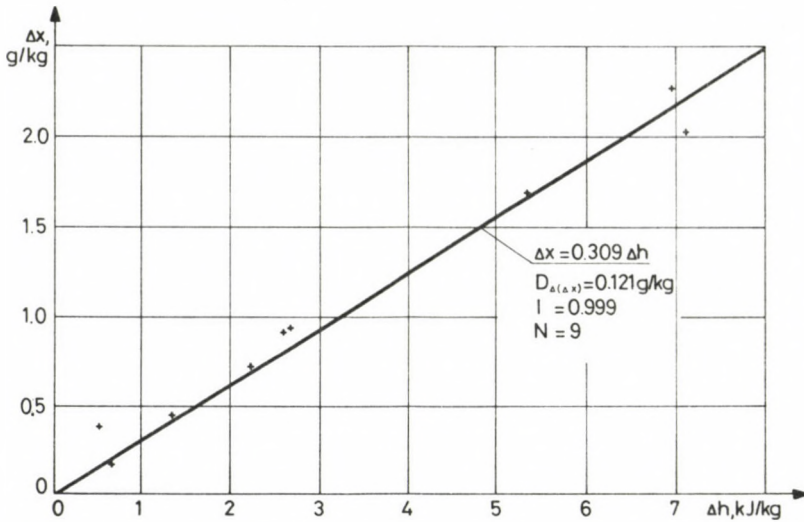


Fig. 13. Vapour absorption vs. enthalpy increase of mine air in the main haulage roads of Mine IV of the Mecsek Ore Mines, measured by I Cifka (Central Institute for Mining Development, 1983)

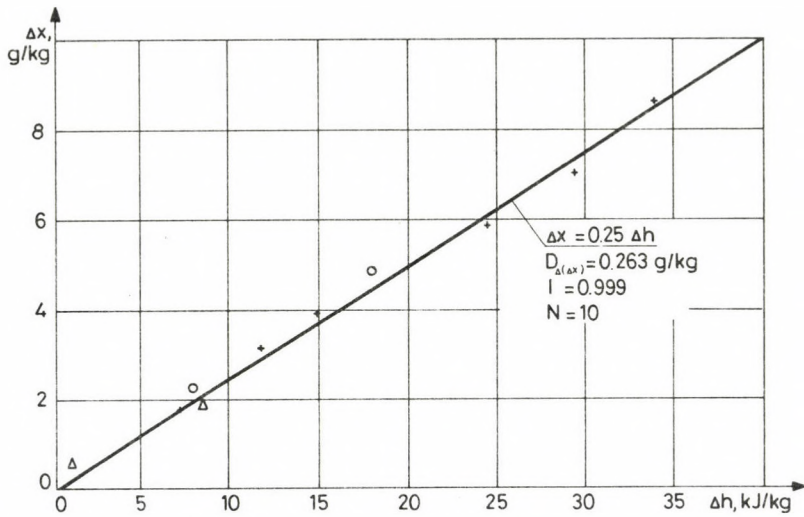


Fig. 14. Vapour absorption vs. enthalpy increase of mine air in different airways of the Mines Lyukó and Feketevölgy of the Borsod Coal Mines according to the measurements of L Rem. Legend: + advance heading with machine; o working; Δ heading with drilling and blasting

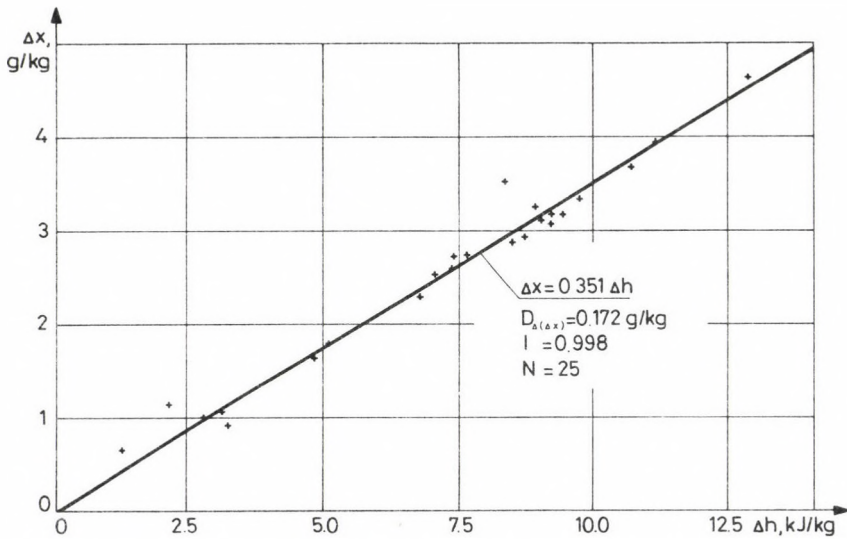


Fig. 15. Vapour absorption vs. enthalpy increase of mine air in a very wet roadway section in the level -900 m in the Reesk Ore Mine measured by I Cifka (Central Institute for Mining Development, 1983)

in mine openings with high humidity there is a very close connection between material transfer and heat transfer while rock and machine heats are transferred by air circulation. In the papers dealing with air conditioning in mines the intensity of vaporization is considered proportional to the difference between the vapour contents of the evaporating surface and the air absorbing vapour. It is further assumed that the air on the evaporating surface is saturated. Thus the ratio of Δh to Δx depends besides the degree of humidity of the surface also on the vapour content of the air.

Equation (46) contradicts this assumption. In Eq. (46), namely, the amount of vapour absorbed by the mine air is independent of the vapour content of the air and depends only on the heat absorption.

The contradiction can be explained by the determinant role of vortices at the contours of the flow cross-section in the heat and vapour absorption of the mine air. They

- “dilute” the warmer and more vapour-saturated near-surface air layers by the colder and less humid air of the main stream, and they
- transport into the main air flow the warmer and more humid air volumes “torn away” from the wall environment.

In this process it is of great importance that, at the surface of a mine opening of any length, a part of the air mass M_s taking part directly in the air- and vapour-transfer processes remains in the cavities of the uneven surface, i.e. in the macro- and micro-fissures sheltered from the air circulation. If air mass M_s of the air near the wall and of vapour content x_s and enthalpy h_s is exchanged with the air of vapour content x_a and enthalpy h_a of the main air flow and the main air flow transports a mass flow rate M_a into the mine opening, the enthalpy increment becomes

$$\Delta h = \frac{M_s h_s + (M_a + M_s) h_a}{M_a} - h_a = \frac{M_s}{M_a} (h_s - h_a) \quad (48)$$

$$\Delta h = \frac{M_s}{M_a} (h_s - h_a) \quad (49)$$

and the vapour content increment is:

$$\Delta x = \frac{M_s}{M_a} (x_s - x_a). \quad (50)$$

That means that according to Eq. (46):

$$a = \frac{h_s - h_a}{x_s - x_a}. \quad (51)$$

Thus, as measurement data suggest, if the vapour content x_a of the circulating air decreases in a mine opening, vapour content x_s of the air layers near the walls decreases at the same rate.

Summing up, it can be seen that besides air velocity v_a , air temperature t_a and vapour content x_a in the mine openings, the intensity of vapour absorption of the air depends essentially only on the material, roughness and humidity of the wall surface, air velocity v_a and temperature difference $t_s - t_a$, while the value of a in Eqs (46) and (51), is practically not influenced by x_a .

Using this law the simultaneous heat- and vapour-absorption of the mine air circulating through a mine opening can be calculated. For this purpose it is necessary to know the humidity of the mine opening and the value a in Eq. (46) characterizing evaporating ability. Hence C can be calculated from Eq. (47), and α_{eff} from Eq. (44). Age factor $K(\alpha_{\text{eff}})$ can now be obtained by making use of α_{eff} . According to Eq. (45) the heat warming the air is the p -th fraction of total heat absorbed by the air:

$$p = \frac{1}{1 + C}. \quad (52)$$

With this ratio, temperature t_a of the air at the end of the airway of length Δl with an initial temperature t_{a0} becomes

$$t_a = t_p - (t_p - t_{a0})e^{-pD}. \quad (53)$$

Enthalpy increase Δh of the air can be calculated as

$$\Delta h = \frac{c_{pa}}{p}(t_p - t_{a0})1 - e^{-pD} \quad (54)$$

and the increase of vapour content Δx is calculated from Eq. (46). The allowable length Δl of the airway sections can be chosen on the basis of the change of age factor K along the airway. Δl can only be as long an airway section as keeping the change of K negligible, e.g. in a longwall advancing in its total length simultaneously, Δl can be the total face length. In headings, however, near the face only the length reached during one cutting cycle or, in case of continuous advance, the length reached within 1–2 hours can be taken as Δl ; for sections farther from the face lengths have to be chosen for Δl , within which the age of the roadway differs from the average age only by maximum 1–2 percents. In all such cases, where other heat, e.g. autocompression, friction, cooling or machine heat has also a role besides rock heat in the change of temperature and vapour content of the air, it is advisable to choose Δl for small, i.e. not longer than 1–2 m. In such cases the enthalpy increase of the air is calculated so that the heat Q_e of other heat sources is also taken into account. If the air absorbs heat Q_e uniformly along the airway, it can be written that

$$dQ_e = Q_0 dl. \quad (55)$$

Hence the enthalpy increase of the air along an elementary airway length dl is

$$dh = \frac{dQ_r + dQ_e}{\dot{V}\rho_a} = (Ey + P) dl. \quad (56)$$

The heat flow in rocks dQ_r can be calculated from Eqs (21) and (24). Equations (22), (51), (55) and (56) furnish

$$-dl = \frac{dy}{Ey + P}. \quad (57)$$

Having integrated both sides of Eq. (57) the air temperature increase along Δl is in case of dry heat absorption

$$t_a - t_{ao} = (y_0 + Y)(1 - e^{-D}). \quad (58)$$

If p -th fraction of the heat absorption is used for the temperature increase of the air and the remaining fraction for the increase of the vapour content, then

$$t_a - t_{ao} = (y_0 + Y)(1 - e^{-pD}) \quad (59)$$

holds.

If the p_r -th fraction of rock heat Q_r and p_e -th part of other heat Q_e is used for the increase of the air temperature and the remaining part increases vapour content, then the temperature increase along airway length Δl is

$$t_a - t_{ao} = \left(y_0 + \frac{p_e}{p_r} Y \right) (1 - e^{-p_r D}). \quad (60)$$

References

- Analysis of ventilation and air conditioning in deep mines. Part I. Research report of the Central Institute for Mining Development.
- Barenbrug A W T 1974: Psychrometry and psychrometric Charts. Chamber of Mines of South Africa
- Batzel S 1952: Die Ermittlung thermischer Werte in Grubenbauen und ihre Verwendung für die mathematische Lösung klimatischer Probleme. *Bergbau-Archiv* 13, No. 3/4, 15–34.
- Bende I, Cifka I 1974: Ventilation of mines. Measurement checking methods (in Hungarian). Műszaki Könyvkiadó, Budapest.
- Boldizsár T 1957: Calculation of the temperature increase of humid mine air by numerical and graphic method (in Hungarian).
- Esztó M 1983: A simple and reliable method for predicting air conditions in mines (in Hungarian). BKL Bányászat, 116, 241–244.
- Fekete I, Menyhárt I 1975: Theoretical principles of ventilation technics (in Hungarian). Műszaki Könyvkiadó, Budapest.
- Fodor Gy 1962: Engineering application of the Laplace transformation (in Hungarian). Műszaki Könyvkiadó, Budapest.
- Frycz A 1981: Klimatyzacja kopalni Wydawn. "Slask" Air conditioning in mines (in Polish).
- Janositz J 1979: Statistische Auswertung von Klimamessungen. *Glückauf-F.H.* 40, No. 6, 258–263.
- Jávor A 1977: Mining engineering. Ventilation of mines (in Hungarian). Műszaki Könyvkiadó, Budapest.
- Knechtel I, Maciejewska, Soltys W 1975: Możliwość stosowania w polskich kopalniach węgla radwanickiej metody prognozowania temperatury powietrza w wyrobiskach ślepych. *Przegląd Górniczy*, No. 6, 243–252.
- Korn G A, Korn T M 1975: Handbook of mathematics for engineers (in Hungarian). Műszaki Könyvkiadó, Budapest.

- König H 1952: Mathematische Untersuchungen über das Grubenklima. *Bergbau-Archiv*, 13, No. 3/4, 1–14.
- Marzilger B, Wagener B 1972: Eine numerische Lösung zur Berechnung des Wärmetechnischen Altersbeiwertes mit Fehlerabschätzung. *Glückauf, F. H.*, 33, No. 4, 134–143.
- Miheyev M A 1953: Fundamentals of heat transfer calculation in the practice (in Hungarian). Tankönyvkiadó, Budapest.
- Mücke G 1964: Die Wärmeleitfähigkeit von Karbongesteinen und ihr Einfluss auf das Grubenklima. *Bergbau-Archiv*, 25, No. 1/2, 35–58.
- Perry I H 1968: Handbook of chemical engineers (in Hungarian). Műszaki Könyvkiadó, Budapest.
- Shcerban A N, Kremnav O A, Zhuravlenko V I 1959: Náucsnyie osznovü roszcseta i regulirovania teplovovo rezsima glubokih saht. Izd. akad. nauk. Ukr. SSR, Kiev
- Starfield A M 1966: The computation of temperature increases in wet and dry airways. I. *Mine Vent. Soc. S. Africa*, 19, 157–165.
- Ufer W 1961: Untersuchungen über die Abhängigkeit der Wärmeübergangszahl von der Widerstandszahl in rechteckigen Kanälen und ihre Bedeutung für den Einfluss der Gebirgswärme auf die Wettertemperatur. Thesis, Aachen
- Voss I 1965: Beitrag zur Vorausberechnung der Erwärmung und der Wasserdampfaufnahme der Wetter in Steinkohlenbergwerken. *Glückauf, F.H.*, 26, No. 4, 187–198.
- Voss I 1967: Die Bestimmung thermischer Kenngrößen aus Messungen über die Wärmeaufnahme der Wetter und die Auskühlung des Gebirges um einziehende Wetterwege. *Glückauf, F.h.* 28, No. 2, 67–80.
- Voss I 1969: Ein neues Verfahren zur Klimavorausberechnung in Steinkohlenbergwerken. *Glückauf F. H.*, 30, No. 6, 321–331.
- Voss I 1981: Grubenklima Glückauf-Betriebsbücher Band 27. Verlag Glückauf GmbH, Essen
- Vost K R 1973: In-situ measurements of the surface heat transfer coefficient in underground airways. *J. S. Afr. Inst. Min. Metall.*, 73, 269–272.
- Vost K R 1982: The prediction of air temperatures in intake haulages in mines. *J. S. Afr. Inst. Min, Metall.*, 82, 316–328.

FREQUENCY OF ENDOGEN MINE FIRES AS A FUNCTION OF COAL LOSS AND RATE OF ADVANCE

F KOVÁCS¹

[Manuscript received February 21, 1985]

From general considerations on endogenic mine fires and by processing the data of longwalls of the Mecsek Coal Mines, the author found fire hazard increasing considerably with the increase of stopping losses. Frequency and specific number of fires suddenly increase above 10 to 15 percent coal loss.

When increasing the rate of advance of the working face, the frequency and specific number of endogenic fires decreases considerably. No fires occur above a rate of advance of 1.6 to 2.0 m/d.

In workings with top coal caving coal loss is considerably higher and the rate of advance lower than with slicing method. Therefore, the potential of fire hazard increases if coal caving is applied. The frequency of warmings and fires for top coal caving is about three times higher in average than those with slicing method. As a result of the high production concentration, however, the number of fires per unit production is less for top coal caving than with slicing method.

To increase safety and rentability of the top coal caving method, special development work is needed for improving protection methods, because the potential of fire hazard is greater than with slicing method.

Keywords: coal loss; endogen mine fires; fire hazard; longwalls; Mecsek coal mines; rate of advance

Endogenic mine fires and the hazards caused by them are among the most important elementary hazards jeopardizing mining activity. Poisonous gases produced by the fire represent a direct danger to the miners while the fire can initiate a fire-damp explosion in the presence of methane. Fires also considerably jeopardize production safety and material goods.

Fire hazard and its degree in connection with endogenic mine fires is determined by three basic conditions: the simultaneous presence of *pyrophorous material* and *oxygen* for a suitably long *time*.

The analysis of the natural and technical parameters determining the degree of fire hazard has to be primarily aimed at their effects in maintaining the conditions of ignition and burning. The effects of the parameters of working can only be characterized in an acceptable way for the practice if an absolute or at least relative parameter can be given characterizing fire hazard. An absolute parameter is practically impossible to formulate, therefore, even relative parameters quantifying the effects of the natural and technical parameters represent an acceptable result.

¹ Technical University for Heavy Industry, H-3515 Miskolc, Hungary

The paper will analyse the effects of parameters of working having a considerable influence on the degree of fire hazard according to data about longwalls in coal mines published by Lindeau (1977), Veselovsky (1975) and the Department of Mining Engineering (1984).

Soviet and Czechoslovak data also indicate an unambiguous, definite connection between the frequency of endogenic mine fires (number of fires for one working) and the *amount of coal loss* in workings. Data from the coal-field Prokofyevsk-Kiselyovsk were used to illustrate the connection between coal loss and frequency in Fig. 1. The frequency shows an especially sharp increase above a loss of 15 to 20 percent. A 2 to 3 times increase of the loss increases fire hazard 50 to 60 times. A decrease of the loss to the half (e.g. from 30 to 35 percent to 15 to 20 percent) reduces the frequency of fires to its one fifth.

Both practice and theoretical considerations suggest that the *rate of advance* of the workings is another determinant parameter of fire hazards. The rate of advance exerts its effect on fire hazard through the incubation time (self-heating time) of the caved coal and oxygen supplied by the air flowing through the gob. If oxygen supply to pyrophorous coal is ceased within the incubation time, spontaneous ignition takes place. The rate of advance of the working face versus average frequency of fires is plotted in Fig. 2 on the basis of Soviet data. In the given natural conditions, 35 to 40 m/month is the rate of advance that keeps the frequency of fires at a minimum of 2 percent. 3 to 4 times increase of the rate of advance in workings reduces fire hazard to its 1/15th.

Statistical data show that the third group of parameters determining fire hazard refers to the ventilation, *viz. method of ventilation, air volume and air velocity*. Experience suggests that at an O_2 content of 12 to 15 percent no spontaneous ignition takes place and in case of 8 to 10 percent O_2 even warming stops. If oxygen content of

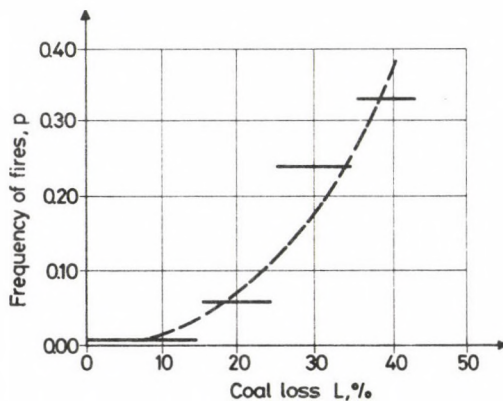


Fig. 1. Frequency of fires vs. coal loss (Soviet data)

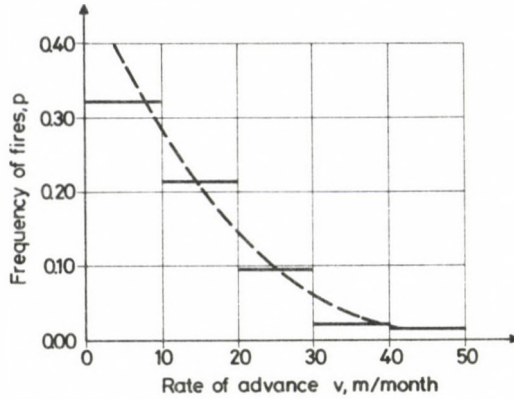


Fig. 2. Frequency of fires vs. rate of advance (Soviet data)

the air in the gob decreases below 5 to 8 percent the flame goes out, at 3 to 5 percent the glow ceases, and at 0 to 3 percent O_2 content the fire is fully extinguished.

The extension of the working panel in the pitch being practically the *face length* of the longwall in case of working along the strike, also influences frequency of fires. According to Soviet data, an increase of the face length by 50 percent increases fire hazard as much as 27 percent.

The extension of the working panel along the strike, i.e. practically the *run-out length* of the longwall in case of working along the strike, influences fire hazard due to changes of ventilation conditions, increase of the lengths of roadways, decay of maintenance conditions and reduction of the rate of advance.

According to investigations, the retreating or advancing direction of the workings and the heights of sublevels have an additional influence on the fire hazard.

From among the parameters influencing fire hazard the effect of coal loss and rate of advance will be analysed here on the basis of data of longwalls in the Mecsek Coal Mines between 1979 and 1983, including data of 214 workings in Pécsbánya, Vasas, Kossuth, Zobák and Béta mines (Department of Mining Engineering 1985). 103 of them worked in thin beds, 60 were slicings in thick beds and 51 applied top coal caving. 29 percent of the workings were in advancing and 63 percent in retreating direction. There were 16 workings where the direction was partially advancing and partially retreating. It has been assumed for the investigations that the coal beds worked by these workings did not differ in their pyrophorous character. Detailed results of the analysis are not presented here, only results showing general characteristics are given. No difference was made concerning the angles of inclination of the beds. For sake of expressivity the results are presented in diagrams.

From the results of analysing the effect of *coal loss*, the working loss L in percent is plotted against relative frequency p of fires (warming + fire). The diagrams show the relative frequencies belonging to the different intervals.

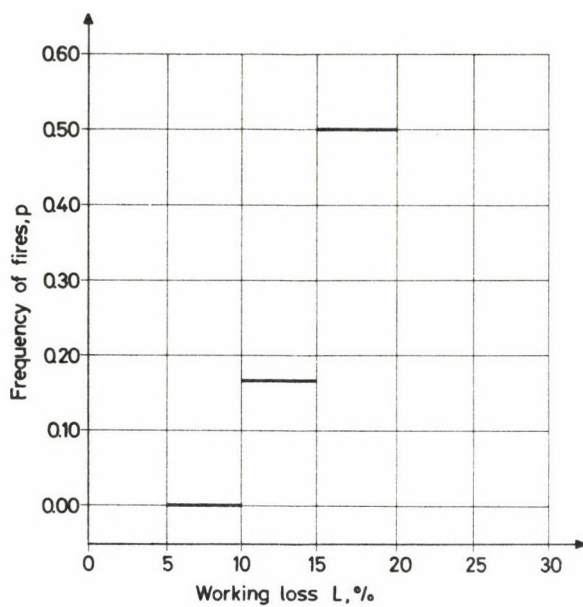


Fig. 3. Frequency of fires as a function of coal loss in the longwalls of Vasas mine (slicing + top coal caving)

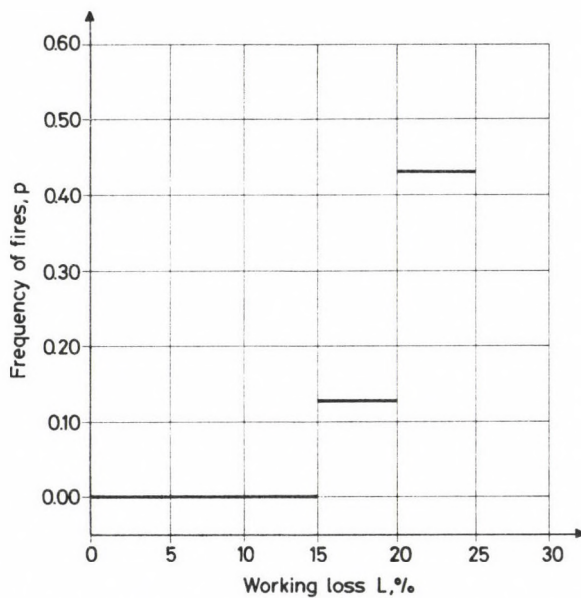


Fig. 4. Frequency of fires as a function of coal loss in the longwalls Kossuth mine (slicing + top coal caving)

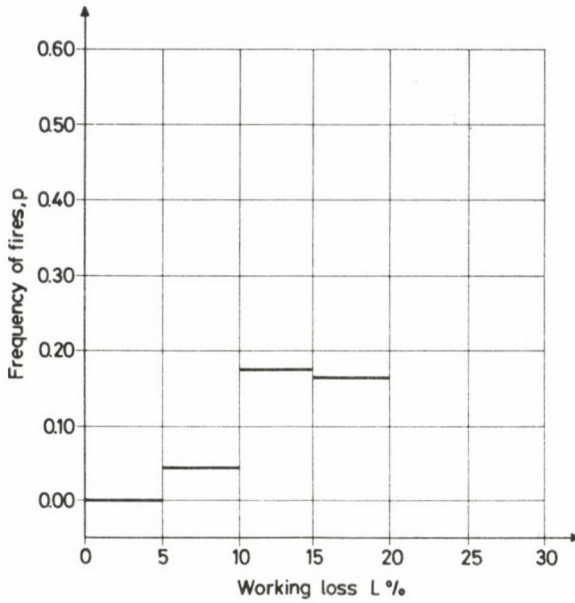


Fig. 5. Frequency of fires as a function of coal loss in longwalls with slicing (Vasas, Zobák, Kossuth mines)

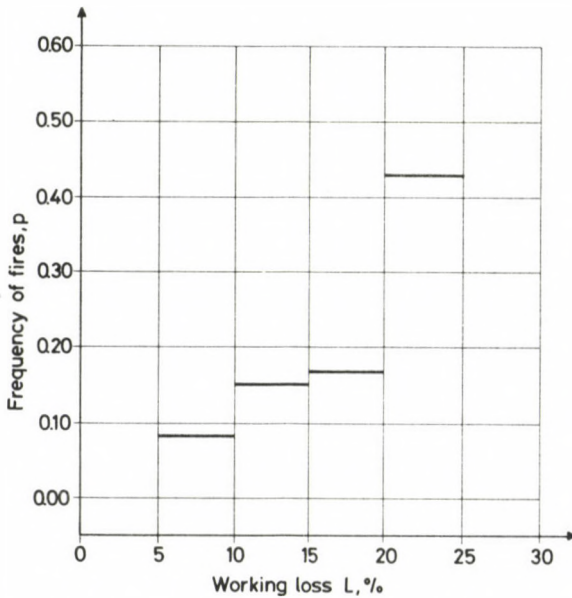


Fig. 6. Frequency of fires as a function of coal loss in workings with top coal caving

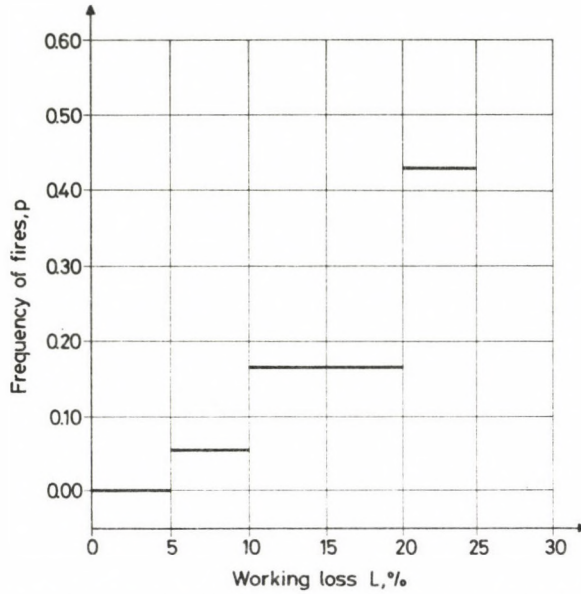


Fig. 7. Frequency of fires as a function of coal loss in longwalls displaying data of slicing and top coal caving together (Vasas, Kossuth, Zobák mines)

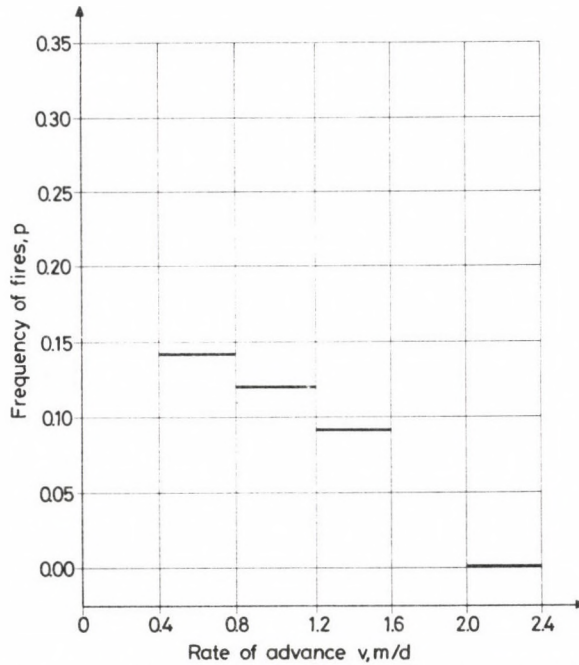


Fig. 8. Frequency of fires as a function of rate of advance in longwalls with slicing (Pécsbánya, Vasas, Kossuth, Zobák mines)

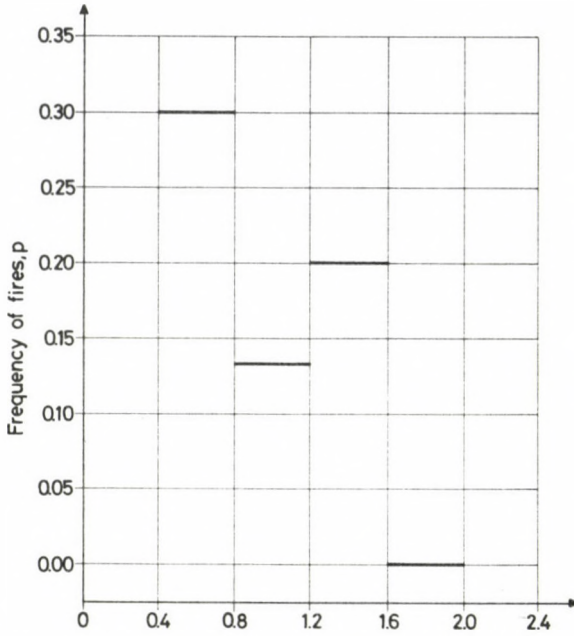


Fig. 9. Frequency of fires as a function of rate of advance in longwalls with top coal caving (Vasas, Kossuth, Zobák mines)

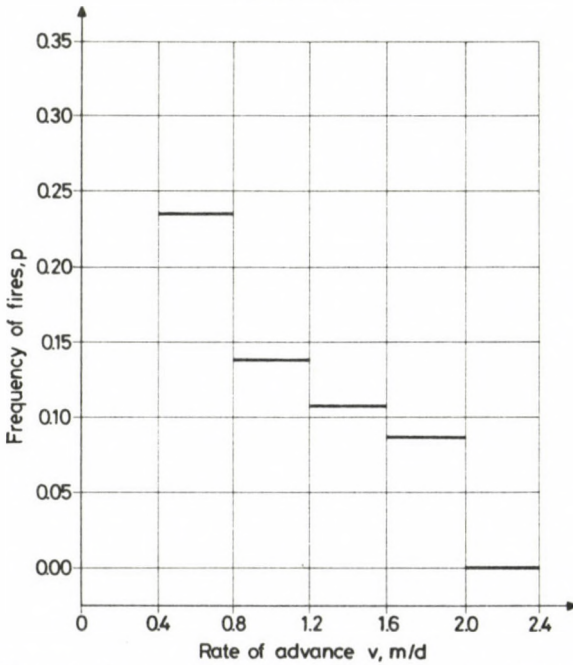


Fig. 10. Frequency of fires as a function of rate of advance. Combined data of slicing and top coal caving methods (Pécsbánya, Vasas, Kossuth, Zobák mines)

Figure 3 illustrates for Vasas mine and Fig. 4 for Kossuth mine the data referring to workings with slicing and top coal caving. In Fig. 5 the data of slicings while in Fig. 6 those of the workings with top coal caving are shown for Vasas, Kossuth and Zobák mines. Figure 7 displays the combined data of workings with slicing and top coal caving. The effect of working loss can be unambiguously detected in the figures: an increase of the coal loss considerably increases the frequency of fires. There is a sudden increase in the rate of danger in the range of 10 to 15 percent of working loss.

Analysing the effect of the rate of advance the relative frequency of fires is plotted against the average rate of advance day v m/d in the following figures. Figure 8 shows data of workings with slicing, Fig. 9 data of those with top coal caving, while Fig. 10 illustrates all data referring to both method of working. The effect of the rate of advance is clearly visible. If the rate of advance of the face increases, the expected frequency of fires considerably decreases: no warning or fire occurred at a rate of advance over 2 m/d.

Frequency parameters analysed above refer to all workings regardless their dimensions or outputs. Frequency parameters defined in such a way may distort fire hazard, especially in cases where the data of workings with slicing and top coal caving were taken into one category, because the frequency of fires fails to reflect coal output.

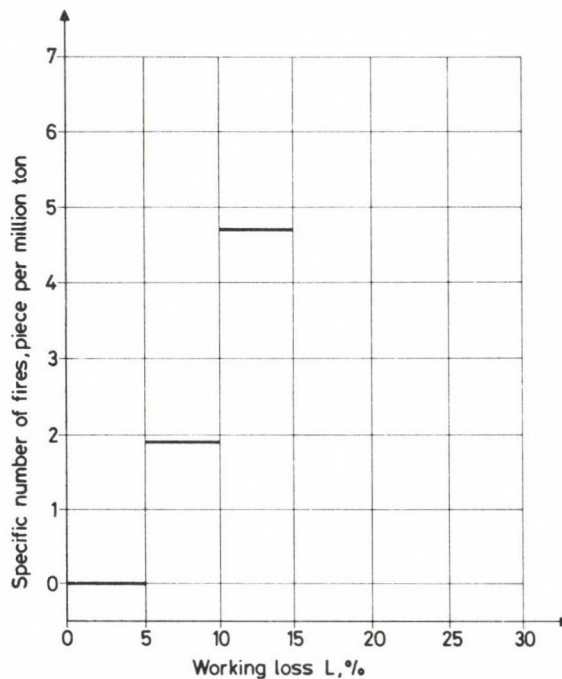


Fig. 11. Specific number of fires as a function of coal loss in longwalls with slicing (Vasas, Kossuth, Zobák mines)

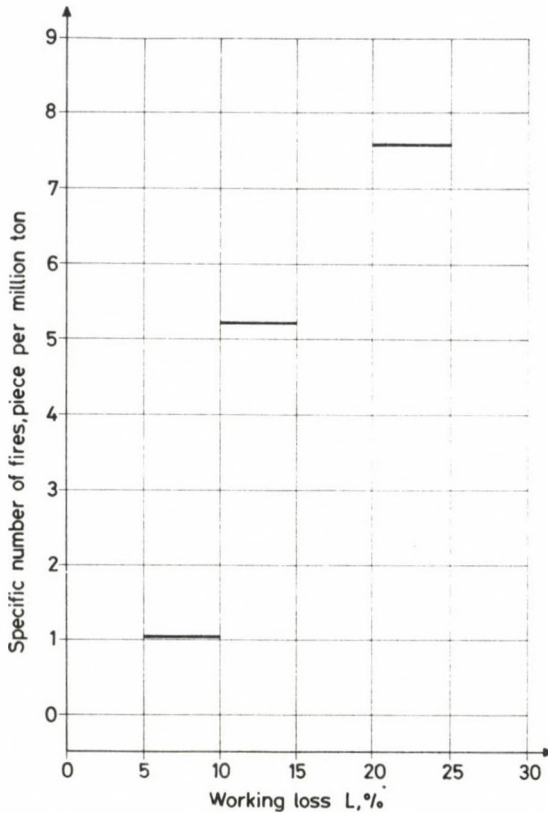


Fig. 12. Specific number of fires as a function of coal loss in longwalls with top coal caving (Vasas, Kossuth, Zobák mines)

The distortion may be considerable since workings with slicing yield in general a few times 10 thousand tons of coal, while the output of top coal caving can amount to several 100 thousand tons.

To characterize the degree of fire hazard more really, the specific number of fires in piece per million ton (warmings + fires) have also been investigated as functions of working loss and rate of advance.

Figures 11 and 12 show the specific number of fires as a function of coal loss for workings with slicing and top coal caving, respectively. Figure 13 illustrates combined data for both types of workings. Working loss considerably increases the degree of fire hazard, there is a sudden increase in the range of 10 to 15 percent loss.

The connection between the specific number of fires and the rate of advance is shown in Figs 14 and 15. The degree of fire hazard considerably decreases with increasing rate of advance: a sudden increase can be observed in the range of 1.6 to 2.0 m/d.

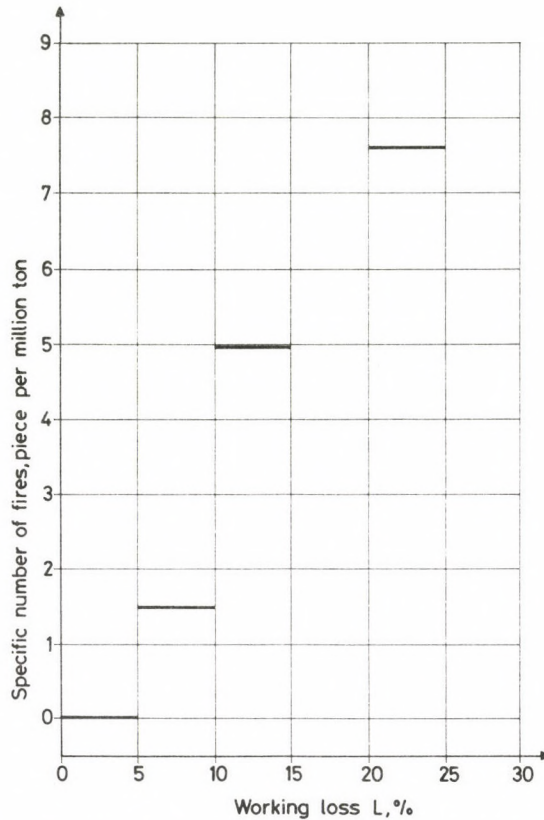


Fig. 13. Specific number of fires as a function of coal loss in longwalls with slicing and top coal caving (Vasas, Kossuth, Zobák mines)

The data presented show that increasing working loss increases the degree of fire hazard, while the increase of the rate of advance of the face considerably reduces frequency and specific number of fires.

Special attention has been paid to analysing the data of the top coal caving method, because due to its character it is accompanied with high working losses and, in the majority of the cases with low rates of advance.

The data about the workings of the Mecsek Coal Mines showed that the coal loss was in average 6.55 percent in thin beds and 7.92 percent in thick beds. For top coal caving, however, the coal loss amounted to 16.02 percent, i.e. 2.2 times that in slicings. Thus, the potential degree of fire hazard is higher in case of top coal caving than in workings applying slicing method. This conclusion is supported by the fact that in workings with de facto fires the average coal loss was 14.4 percent, while in workings without fires, the average coal loss was only 10.2 percent, indicating 1.41 times higher working losses in workings affected by fires.

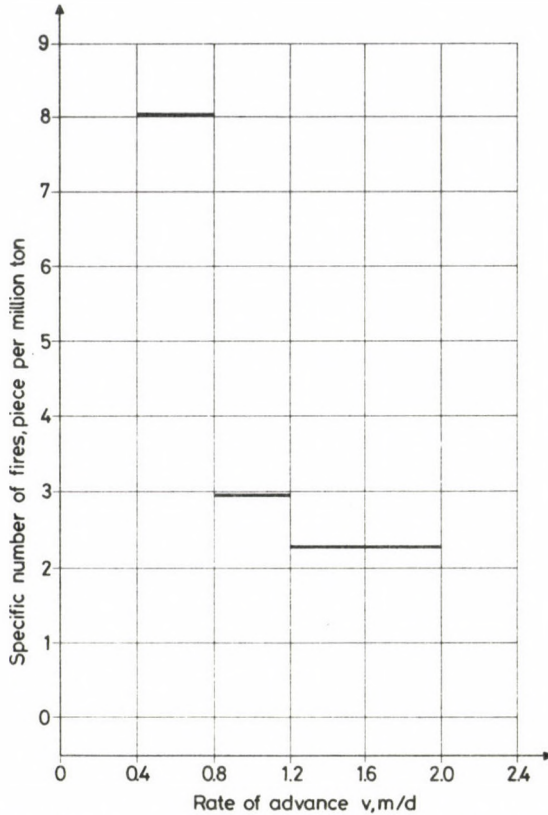


Fig. 14. Specific number of fires as a function of rate of advance longwalls with top coal caving (Kossuth, Zobák mines)

Analysing the data referring to the rate of advance showed that the average speed amounted to 1.39 m/d in slicings in thick beds, at the same time it was as low as 1.07 m/d in workings with top coal caving. This indicates again a higher potential fire hazard for top coal caving. The same conclusion is suggested by the rates of advance averaging in 1.14 m/d in workings with fires and 1.23 m/d without.

Obviously, the parameters of top coal caving (loss, rate, output) are strongly affected by the worked seam thickness ($M = M_0 + M'$) and within that by the face height M_0 and the thickness of the caved top coal M' . The analysis of the Mecsek data illustrated this effect. In Fig. 16 the data of Zobák mine are presented indicating a characteristic increase of coal loss and decrease of rate of advance as a function of the thickness of caved coal.

Overall data of the four mines of the Mecsek Coal Mines (Pécsbánya, Vasas, Kossuth, Zobák) are listed in Table I displaying numbers of warmings, fires and totals

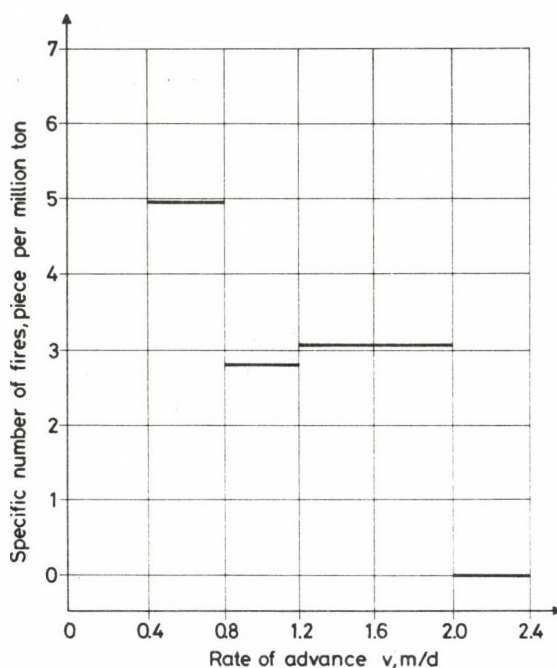


Fig. 15. Specific number of fires as a function of rate of advance speed. Combined data for slicing and top coal caving methods (Pécsbánya, Kossuth, Zobák mines)

(warmings + fires), the number and outputs of all workings frequencies p (piece per piece) and specific numbers (piece per million tons).

The data suggest that the *frequency of warmings* in slicings in both thin and thick beds is practically *equal* ($p = 0.1020$ and $p = 0.0847$, the average being 0.0955), while in workings with top coal caving the frequency of warming is about twice as high as that of slicing ($p = 0.1765$). The *frequency of fires* is again nearly *the same* in workings with slicing both in thick and thin beds ($p = 0.0202$ and $p = 0.0339$, the average is 0.0255), but for top coal caving it is six times that of slicings, with $p = 0.1569$. The frequency of *all fires* (warmings + fires) is $p = 0.3333$ in workings with top coal caving, i.e. about three times that of workings with slicing ($p = 0.1210$).

When comparing the frequencies of workings with slicing in thin and thick beds with the frequencies of workings with top coal caving, it can be concluded that only each fourth or fifth warming develops into a fire in workings with slicing (as seen from the ratio of the corresponding frequencies), but in workings with top coal caving only one warming can be suppressed out of ten, while the other nine warmings developed into fires. The comparison of the two ratios (1 : 4 to 5, and 9 : 10, respectively) indicates that in workings with top coal caving the successful protection against fires is a considerably more difficult task than in slicings in thin or thick beds. Hence it seems

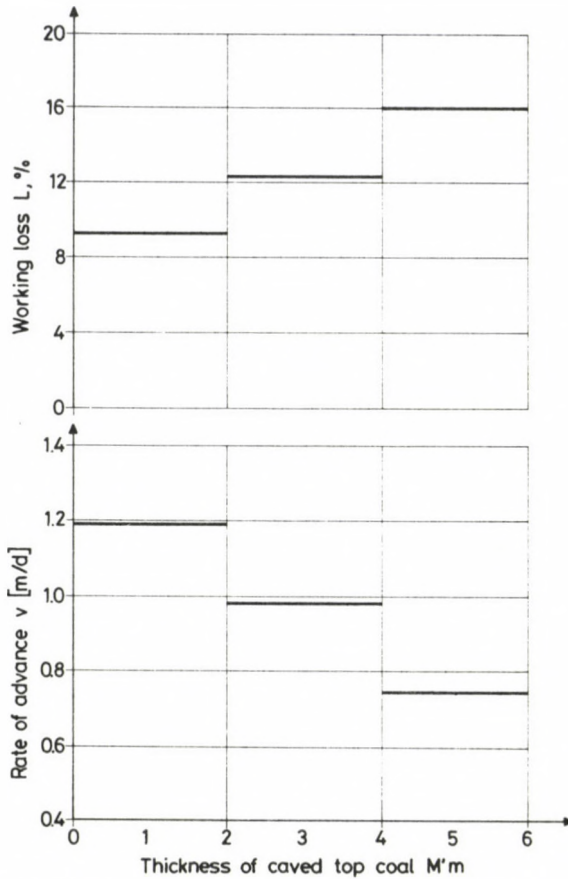


Fig. 16. Average values of rate of advance and working loss versus thickness of caved top coal (Zobák mine)

from the comparison of the *frequencies* that the fire hazard is much higher in workings with top coal caving, namely the frequency of warmings is twice, that of fires 5 to 6 times and that of all events including fires and warmings three times higher than in slicings in thin or thick beds.

The frequency as a parameter, however, is controversial in certain respect. All workings are taken with the same weight, the production capacity and the total quantity extracted from the different workings is not taken into account. The assessment of fire hazard by the frequency for workings with top coal caving is controversial as the main advantage of top coal caving lies in the higher working concentration (less preparation, higher capacity) and higher productivity. For the sake of a more real comparison and a more complex consideration from several aspects, let us analyse the specific numbers of warmings, fires and total events. (Specific number is the number of events per 1 million ton coal).

Table I. Frequency and specific numbers of warmings and fires in longwalls of the Mecsek Coal Mines

Characteristic indices	Thin bed workings	Thick bed workings with slicing	Total of workings with slicing	Workings with top coal caving	Total of workings
Number of workings [piece]	98	59	157	51	208
Total output of workings [t]	3902623	2820606	6723229	7466601	14079070
Number of warmings [piece]	10	5	15	9	24
Frequency of warmings [piece per piece]	0.1020	0.0847	0.0955	0.1765	0.1154
Specific number of warmings [piece per million tons]	2.5486	1.7727	2.2311	1.2054	1.7047
Number of fires [piece]	2	2	4	8	12
Frequency of fires [piece per piece]	0.0202	0.0339	0.0255	0.1569	0.0577
Specific number of fires [piece per million tons]	0.5124	0.7091	0.5950	1.0714	0.8523
Number of all fires [piece] (warming + fire)	12	7	19	17	36
Frequency of all fires [piece per piece]	0.1224	0.1186	0.1210	0.3333	0.1731
Specific number of all fires [piece per million tons]	3.0749	2.4817	2.8260	2.2427	2.5169

The specific number of *warmings* differs only slightly in case of workings with slicing in thin and in thick beds (2.55 and 1.77, respectively, in average: 2.23), while for top coal caving this specific number is practically half that found in slicings: 1.21 event per 1 million ton. The specific number of fires for slicings is 0.60 event per 1 million ton, while in workings with top coal caving, however, 1.07 event per 1 million ton. The specific number of all events is in case of slicing 2.83, but for top coal cavings only 2.24 event/10⁶ t, i.e. 80 percent of the former.

The comparison of the frequencies p and the specific numbers yielded different results in certain respect for the fire hazard assessment for slicings and workings with top coal caving. While the frequency for workings with top coal caving ($p=0.3333$) is about three times of that for slicings ($p=0.1210$), the specific number of events in workings with top coal caving (2.24) is *only 80 percent* of the specific number of slicings (2.83). The application of the specific numbers yields a much better assessment about the fire hazard of workings with top coal caving due to the **significantly higher** production of this method. A similar change may be observed in the parameters of warmings and fires if analysed separately. While the frequency of warmings in workings with top coal caving is twice that found in slicings, the specific number of the former (1.21) is only about half of that of slicings (2.23). The frequency of fires in workings with

top coal caving ($p = 0.16$) is six times higher than that in slicings (0.026), but the specific number of the former ($p = 1.07$) is only about twice that calculated for slicings (0.60).

The increase of production in workings with top coal caving achieved mostly by a 2 to 4 times increase of the worked seam thickness—is substantially higher than the increase of fire hazard, thus the specific parameters of the fires changed advantageously.

The localization of warmings is, however, more difficult in workings with top coal caving than in slicings. Obviously, the potential of fire hazard is higher in case of top coal caving due to the higher coal loss and the slower advance, therefore enhanced protection measures have to be taken against fires. To increase both production and the miners' safety, working loss has to be primarily reduced and the rate of advance has to be increased by developing technology and machinery of top coal caving. To reduce fire hazard, effectivity of fire protection methods and equipment also has to be improved. In the operation of high capacity workings with complex mechanization, the possibility of quick air circulation cutoff must be ensured. Those methods are suitable for this purpose, that ensure the protection of equipment and the possibility of a rapid reopening and continuing of production.

References

- Department of Mining Engineering, Technical University for Heavy Industry 1984: Critical analysis of top coal caving mining techniques and damp-proof blasts in the Mecsek Coal Mines and suggestions to increase safety (in Hungarian). Research Report for the Ministry of Industry, Miskolc
- Department of Mining Engineering, Technical University for Heavy Industry 1985: Connection between the danger of fire and the natural and technical parameters of longwalls in the Mecsek Coal Mines (in Hungarian). Research Report for the Mecsek Coal Mines, Miskolc
- Lindeau N I 1977: Origin, prevention and extinguishment of endogenic fires in coal mines (in Russian). Izd. "Nedra", Moscow 1977, 312.
- Veselovsky V S 1975: Forecast and prevention of endogeneous fires (in Russian). Izd. "Nauka", Moscow 1975, 159.

INTRODUCTION TO THE PALYNOLOGY OF PRE-QUATERNARY DEPOSITS

By

Miklós Kedves

Vols 1–2.

Studia Biologica Academiae Scientiarum Hungaricae 19–20.

*In English. Approx. 240 pages. 72 figures. 81 electromicrographs in 20 plates.
17 × 25 cm. Paperback. Approx. \$ 18.00
ISBN 963 05 3975 6*

The work contains a synthesis of fundamental knowledge necessary for pre-Quaternary spore- and pollen studies. The knowledge of the sporomorph composition of pre-Quaternary deposits is important even from the practical (mineral exploration) point of view.

The first volume gives an overview of the subject at large. The chapters dealing with problems of spore and pollen chemistry, degradation, corrosion and preservation are informative as to the extremely resistant properties of the palynomorphs, accounting for their sensitivity to some influences as well (e.g. alkaline medium, oxidation, etc.). In the chapter discussing sporomorph stratification a historical review of the problem, including a description of the most important concepts, is given. The ontogeny of the exine and its evolutionary significance on the submicroscopic level are called to reveal the origin of the individual components of the wall of a sporomorph and to call attention to their geohistorical value. In the chapter on the surface sculptural elements the fundamentals of the matter are dealt with. A comprehensive review of transmission electron microscopic results concerning now-living and fossil sporomorphs is given and, eventually, the basic morphological characteristics of spores and pollen grains are discussed. From among the remaining chapters devoted to methodology is worthy of being quoted, for it encompasses all the essential preparation processes.

The second volume is focussed, in its introductory part, on the general knowledge of fossil spore-pollen studies, primarily as far as practical needs (mineral exploration) are concerned, the problems of production, dispersion and selective fossilization being discussed. Next to follow are the most essential characteristics, the variations and the paleophytogeographical data of sporomorph spectra listed according to geological time units. The individual chapters are closed in both volumes by a list of fundamental bibliography.



AKADÉMIAI KIADÓ · BUDAPEST

PALEOGENE FOSSIL SPOROMORPHS OF THE BAKONY MOUNTAINS

By

Miklós Kedves

Studia Biologica Academiae Scientiarum Hungaricae 21.

In English. Approx. 160 pages. 17 × 25 cm

Paperback. Approx. \$ 14.00

ISBN 963 05 4066 5

The taxonomical results of investigations into the fossil sporomorphs of Paleogene deposits from the Bakony Mountains were discussed in three fascicles of the *Studia Biologica* serial (1973: I. — Spores, 1974: II. Gymnospermatophyta and Angiospermatophyta Brevaxones pollen grains, 1978: III. — Angiospermatophyta Longaxones, tetrad and polyad pollen grains). The present volume, the closing fascicle of the communication, deals with an evaluation of the results. Main chapters:

Addendum to the review of the literature of Paleogene spore-pollen studies.

Evaluation of sporomorphs from the Paleogene deposits of the Bakony Mountains (I. Stratigraphic value of Paleogene sporomorphs from the Bakony Mountains, II. Sporomorph spectra of Paleogene profiles in the Bakony Mountains; 1. Bakony, 1.1. Northern (Old) Bakony 1.1.1. Dudar 1.1.2. Zirc 1.1.3. Olaszfalu 1.1.4. Pénteszgyőr 1.1.5. Hárskút 1.1.6. Balinka 1.2. Southern Bakony 1.2.1. Nyirád 1.2.2. Nyirád Basin 1.2.3. Halimba 1.2.4. Úrkút 1.2.5. Kolontár 2. Mór Graben 2.1. Mór 2.2. Rákhegy 2.3. Fehérvárcsurgó 2.4. Moharakodó 3. Vértes 3.1. Csákberény, III. Present state of Paleogene spore-pollen studies in Hungary). The sporomorph composition of the Paleogene deposits of the Bakony Mountains differs by several characteristic features from the case of the coeval deposits of other parts of Europe: 1. Some of the characteristic Lower Eocene taxa of the Normapolles group are absent from the Hungarian localities. 2. The tri- and subtriporate pollen grains recovered from the Lower Eocene of Hungary include different form-species, too. 3. In the Lower Eocene deposits of Western Europe the fossil sporomorphs of the genus *Platycarya* are locally abundant, while in Hungary it is pollen grains of the form-genus *Plicatopollis* that often predominate.



AKADÉMIAI KIADÓ · BUDAPEST

Mid-Tertiary Stratigraphy and Palaeogeographic Evolution of Hungary

By

T. BÁLDI

In English, 1986, approx. 240 pages, 17 × 25 cm

Hardcover approx. \$24.00

ISBN 963 05 3945 4

The first part of the book discusses important Late Eocene through Early Miocene formations of Hungary. Beside the description of sedimentologic and other geological features, the fauna, especially the mollusc-fauna is treated in detail. Special attention is paid to the palaeoenvironments (facies) of these formations.

In the second part the author tries to summarize the palaeogeographic and tectonic evolution of the Late Eocene through Early Miocene basins of Hungary. The interdependence is stressed between the evolution of these basins and the crustal shortenings in the outer Carpathian flysch troughs.

In the Appendix the capital mollusc taxa of the Tard and Kiscell Clays are presented and documented by the help of more than 130 photos. This epibathyal fauna is a valuable contribution to present knowledge of deep-marine, Tertiary mollusc-faunas.



AKADÉMIAI KIADÓ · BUDAPEST

Distributors:

KULTURA Hungarian Foreign Trading Co.

P.O.B. 149

H-1389 Budapest

Hungary

- treble underlining: bold-face italics
- red underlining: Greek letters
- green underlining: script letters.

Rules for mathematical-physical notations:

- trigonometric, logarithmic, analytic symbols, symbols for units and functions are in roman type (not underlined)
- letter symbols in mathematical and physical formulas, scalars, and subscripts of algebraic and physical quantities are in italics (underlined)
- vectors, matrices, operators in probability theory are in bold-face roman type (double underlining)
- tensors, operators and some special functions are in script letters (green underlining). These cannot be bold.
- Greek letters (red underlining) cannot be bold or extra bold type (thus they cannot be used for vectors or tensors)
- void upper lines e.g. for vectors
- avoid possible confusion between o (letter) and 0 (zero), l (letter) and 1 (one), ν (Greek nu) and v , u (letters) etc.
- explain ambiguous or uncommon symbols by making marginal notes in pencil
- be careful about superscripts and subscripts
- formulae must be numbered consecutively with the number in parentheses to the right of the formula. References in text to the equations may then usually be made by the number in parenthesis. When the word equation is used with a number, it is to be abbreviated, Eq. or Eqs in the plural
- the International System of Units (SI) should be used.

Authors are liable for the cost of alteration in the *proofs*. It is, therefore, the responsibility of the author to check the text for errors of facts before submitting the paper for publication.

3. *References* are accepted only in the Harvard system. Citations in the text should be as:

- ... (Bomford 1971) ... or Bomford (1971)
- ... (Brosche and Sündermann 1976) ...
- ... (Gibbs et al. 1976b) ...

The list of references should contain names and initials of all authors (the abbreviation et al. is not accepted here); for *journal articles* year of publication, the title of the paper, title of the journal abbreviated, volume number, first and last page.

For *books* or *chapters in books*, the title is followed by the publisher and place of publication. All items must appear both in the text and references.

Examples:

Bomford G 1971: *Geodesy*. Clarendon Press, Oxford

Brosche P, Sündermann J 1976: Effects of oceanic tides on the rotation of the earth. Manuscript. Univ. of Bonn

Buntebarth G 1976: Temperature calculations on the Hungarian seismic profile-section NP-2. In: *Geoelectric and Geothermal Studies (East-Central Europe, Soviet Asia)*, KAPG Geophysical Monograph. Akadémiai Kiadó, Budapest, 561–566.

Gibbs N E, Poole W G, Stockmeyer P K 1976a: An algorithm for reducing the bandwidth and profile of a sparse matrix. *SIAM J. Numer. Anal.*, 13, 236–250.

Gibbs N E, Poole W G, Stockmeyer P K 1976b: A comparison of several bandwidth and profile reduction algorithms. *ACM Trans. on Math. Software*, 2, 322–330.

Szarka L 1980: Potenciálértékepezés analóg modellezéssel (Analogue modeling of potential mapping). *Magyar Geofizika*, 21, 193–200.

4. *Footnotes* should be typed on separate sheets.

5. *Legends* should be short and clear. The place of the tables and figures should be indicated in the text, on the margin.

6. *Tables* should be numbered serially with Roman numerals. Vertical lines are not used.

All the illustrations should contain the figure number and author's name in pencil on the reverse.

Figures will be redrawn. Therefore the most important point is clearness of the figures, even pencil-drawings are accepted (with a duplicate).

Photographs and *half-tone* illustrations should be sharp and well contrasted.

If a specific reduction or enlargement is required, please indicate this in blue pencil on the figure.

The editors will send information to the first author about the *arrival* and acceptance of the papers. A galley proof is also sent to the first author for *correction*. Hundred *offprints* are supplied free of charge.

Periodicals of the Hungarian Academy of Sciences are obtainable
at the following addresses:

AUSTRALIA

C B D LIBRARY AND SUBSCRIPTION SERVICE
Box 4886, G.P.O., Sydney N.S.W. 2001
COSMOS BOOKSHOP, 145 Ackland Street
St. Kilda (Melbourne), Victoria 3182

AUSTRIA

GLOBUS, Hochstadtplatz 3, 1206 Wien XX

BELGIUM

OFFICE INTERNATIONAL DE LIBRAIRIE
30 Avenue Marnix, 1050 Bruxelles
LIBRAIRIE DU MONDE ENTIER
162 rue du Midi, 1000 Bruxelles

BULGARIA

HEMUS, Bulvar Ruszki 6, Sofia

CANADA

PANNONIA BOOKS, P.O. Box 1017
Postal Station "B", Toronto, Ontario M5T 2T8

CHINA

CNPICOR, Periodical Department, P.O. Box 50
Peking

CZECHOSLOVAKIA

MAD'ARSKÁ KULTURA, Národní třída 22
115 66 Praha
PNS DOVOZ TISKU, Vinohradská 46, Praha 2
PNS DOVOZ TLÁČE, Bratislava 2

DENMARK

EJNAR MUNKSGAARD, Norregade 6
1165 Copenhagen K

FEDERAL REPUBLIC OF GERMANY

KUNST UND WISSEN ERICH BIEBER
Postfach 46, 7000 Stuttgart 1

FINLAND

AKATEEMINEN KIRJAKAUPPA, P.O. Box 128 SF-00101
Helsinki 10

FRANCE

DAWSON-FRANCE S. A., B. P. 40, 91121 Palaiseau
EUROPÉRIODIQUES S. A., 31 Avenue de Versailles, 78170
La Celle St. Cloud
OFFICE INTERNATIONAL DE DOCUMENTATION ET
LIBRAIRIE, 48 rue Gay-Lussac
75240 Paris Cedex 05

GERMAN DEMOCRATIC REPUBLIC

HAUS DER UNGARISCHEN KULTUR
Karl Liebknecht-Straße 9, DDR-102 Berlin
DEUTSCHE POST ZEITUNGSVERTRIEBSAMT Straße der
Pariser Kommune 3-4, DDR-104 Berlin

GREAT BRITAIN

BLACKWELL'S PERIODICALS DIVISION
Hythe Bridge Street, Oxford OX1 2ET
BUMPUS, HALDANE AND MAXWELL LTD.
Cowper Works, Olney, Bucks MK46 4BN
COLLET'S HOLDINGS LTD., Denington Estate Wellingbo-
rough, Northants NN8 2QT
WM. DAWSON AND SONS LTD., Cannon House Folkstone,
Kent CT19 5EE
H. K. LEWIS AND CO., 136 Gower Street
London WC1E 6BS

GREECE

KOSTARAKIS BROTHERS INTERNATIONAL
BOOKSELLERS, 2 Hippokratous Street, Athens-143

HOLLAND

MEULENHOF-BRUNA B. V., Beulingstraat 2,
Amsterdam
MARTINUS NIJHOFF B.V.
Lange Voorhout 9-11, Den Haag

SWETS SUBSCRIPTION SERVICE

347b Heereweg, Lisse

INDIA

ALLIED PUBLISHING PRIVATE LTD., 13/14
Asaf Ali Road, New Delhi 110001
150 B-6 Mount Road, Madras 600002
INTERNATIONAL BOOK HOUSE PVT. LTD.
Madame Cama Road, Bombay 400039
THE STATE TRADING CORPORATION OF INDIA LTD.,
Books Import Division, Chandralok 36 Janpath, New Delhi
110001

ITALY

INTERSCIENTIA, Via Mazzè 28, 10149 Torino
LIBRERIA COMMISSIONARIA SANSONI, Via Lamarmora 45,
50121 Firenze
SANTO VANASIA, Via M. Macchi 58
20124 Milano
D. E. A., Via Lima 28, 00198 Roma

JAPAN

KINOKUNIYA BOOK-STORE CO. LTD.
17-7 Shinjuku 3 chome, Shinjuku-ku, Tokyo 160-91
MARUZEN COMPANY LTD., Book Department, P.O. Box
5050 Tokyo International, Tokyo 100-31
NAUKA LTD. IMPORT DEPARTMENT
2-30-19 Minami Ikebukuro, Toshima-ku, Tokyo 171

KOREA

CHULPANMUL, Phenjan

NORWAY

TANUM-TIDSKRIFT-SENTRALEN A.S., Karl Johansgatan
41-43, 1000 Oslo

POLAND

WĘGIERSKI INSTYTUT KULTURY, Marszałkowska 80,
00-517 Warszawa
CKP-I W, ul. Towarowa 28, 00-958 Warszawa

ROUMANIA

D. E. P., Bucuresti
ILEXIM, Calea Grivitei 64-66, Bucuresti

SOVIET UNION

SOJUZPECHAT — IMPORT, Moscow
and the post offices in each town
MEZHDUNARODNAYA KNIGA, Moscow G-200

SPAIN

DIAZ DE SANTOS, Lagasca 95, Madrid 6

SWEDEN

GUMPRTS UNIVERSITETSBOKHANDEL AB
Box 346, 401 25 Goteborg 1

SWITZERLAND

KARGER LIBRI AG, Petersgraben 31, 4011 Basel

USA

EBSCO SUBSCRIPTION SERVICES
P.O. Box 1943, Birmingham, Alabama 35201
F. W. FAXON COMPANY, INC.
15 Southwest Park, Westwood Mass. 02090
READ-MORE PUBLICATIONS, INC.
140 Cedar Street, New York, N. Y. 10006

YUGOSLAVIA

JUGOSLOVENSKA KNJIGA, Terazije 27, Beograd
FORUM, Vojvode Mišića 1, 21000 Novi Sad

2

Acta Geodaetica, Geophysica et Montanistica Hungarica

VOLUME 21, NUMBER 4, 1986

EDITOR-IN-CHIEF

F MARTOS

ASSOCIATE EDITOR

J SOMOGYI

EDITOR

J VERŐ

EDITORIAL BOARD

**A ÁDÁM, GY BARTA, P BIRÓ, S DOLESCHALL,
L KAPOLYI, F KOVÁCS, A MESKÓ, F STEINER,
J ZÁMBÓ**



Akadémiai Kiadó, Budapest

AGGM 21 (4) 405—465 (1986) HU ISSN 0236-5758

ACTA GEODAETICA, GEOPHYSICA et MONTANISTICA HUNGARICA

A Quarterly Journal of the Hungarian Academy of Sciences

Acta Geodaetica, Geophysica et Montanistica (AGGM) publishes original reports on geodesy, geophysics and minings in English.

AGGM is published in yearly volumes of four numbers by

AKADÉMIAI KIADÓ

Publishing House of the Hungarian Academy of Sciences
H-1054 Budapest, Alkotmány u. 21.

Manuscripts and editorial correspondence should be addressed to

AGGM Editorial Office
H-9401 Sopron P.O. Box 5

Subscription information

Orders should be addressed to

KULTURA Foreign Trading Company
H-1389 Budapest P.O. Box 149

INSTRUCTIONS TO AUTHORS

Manuscripts should be sent to the editors (MTA Geodéziai és Geofizikai Kutató Intézete, AGGM Editorial Office, H-9401 Sopron, P.O.Box 5, HUNGARY). Only articles not submitted for publication elsewhere are accepted.

Manuscripts should be typewritten in duplicate, double-spaced, 25 lines with 50 letters each. The papers generally include the following components, which should be presented in the order listed.

1. Title, name of author(s), affiliation, dateline, abstract, keywords
2. Text, acknowledgements
3. References
4. Footnotes
5. Legends
6. Tables and illustrations

1. The *affiliation* should be as concise as possible and should include the complete mailing address of the authors. The *date of receipt* of the manuscript will be supplied by the editors. The abstract should not exceed 250 words and should clearly and simply summarize the most important methods and results. 5-10 significant expressions describing the content are used as *keywords*. Authors may recommend these keywords.

2. The *text* should be generally in English and as short and clear as possible. From Hungarian authors papers are also accepted in Hungarian.

The section heading should *not* be underlined or in capitals.

Please note that underlining denotes special types:

- single underlining: italics
- double underlining: bold-face roman

CONTENTS

On the deep electrical conductivity of the central part of Caucasus Minor on base of MTS data — <i>Demidova T A</i>	405
High-pressure elastic wave velocities in Armenian granitoids of different age and origin — <i>Volarovich M P, Yefimova G A, Balasanyan V S</i>	415
High-pressure changes of remanent rock magnetization — <i>Lebedev T S, Savenko B Ya</i>	423
Zonality of the elastic parameter distribution under regional PT conditions in the Earth's crust — <i>Lebedev T S, Korchin V A, Burtny P A</i>	431
Change of acoustic rock properties due to deformation under complex states of stress — <i>Bayuk E I, Dyaur N I</i>	449
<i>Book reviews</i>	
Angewandte Geophysik. Band II. Geoelektrik — Geothermik — Radiometrie — Aerogeophysik, Militzer H and Weber F eds — <i>Verõ J</i>	457
Fundamentals of mining engineering, Zambó J — <i>Martos F</i>	457
Principles of sedimentary basin analysis, Miall A D — <i>Ádám A</i>	459
Introduction to potential theory, Sigl R — <i>Somogyi J</i>	459
Optimization and design of geodetic networks, Grafarend E W and Sanso F eds — <i>Somogyi J</i>	460
The geometry of geodetic inverse linear mapping and non-linear adjustment, Teunissen P J G — <i>Somogyi J</i>	461
In memoriam Professor Antal Tárczy-Hornoch — <i>Somogyi J</i>	463

PRINTED IN HUNGARY
Akadémiai Kiadó és Nyomda, Budapest

ON THE DEEP ELECTRICAL CONDUCTIVITY OF THE CENTRAL PART OF CAUCASUS MINOR ON BASE OF MTS DATA

T A DEMIDOVA¹

[Manuscript received October 22, 1984]

The basic points of the interpretation approach and the conclusions about the electrical conductivity in the Earth interior of Caucasus Minor are summarized on the base of a comprehensive analysis of the results of 70 MTS in the interval 4—400 s using numerical thin-sheet modelling.

Keywords: Caucasus Minor; electrical conductivity; magnetotelluric sounding

1. The investigated territory belongs to one of the most active regions of the Earth and is characterized by both a high seismicity and a wide extension of the thermal phenomena. A nearly E-W striking zone with increased gradients of the temperature and heat flow (Fig. 1) was separated on the basis of geothermic investigations (Avetisyants et al. 1975) at the boundaries of the arch part of the Armenian meganticlinal. The results of 70 MTS (in the interval 4—400 s) were used to investigate the deep electrical structure of this region (Fig. 2).

Demidova et al. (1985), Debadov et al. (1984) and Vanyan et al. (1987) examined in detail the results of the joint analysis of field and model data. Here we summarize the basic points of the interpretation approach and the conclusions about the electrical conductivity in the Earth's interior.

2. The modern methods for deep interpretation of the MTS data inevitably requires the analysis of the distortion effects of surface conductivity inhomogeneities and the use of a procedure to decrease this effect for the concrete territory. In the present case the most significant part of the distortion is caused by changes in the thickness of the sedimentary-volcanic layers (from 0 to 3000 m), and in its water saturation, by the extremely inhomogeneous character of the highly resistive lava flows *etc.* Actually it is obvious from the map of the summarized longitudinal conductivity (S) of Armenia (Demidova et al. 1985) and of the Caucasus region (Fig. 1) that the upper layer is characterized by the presence of isometric conductivity inhomogeneities of complex forms and different sizes with an S -value ranging from 50 to 2000 Ohm^{-1} .

3. Numerical modelling of the electromagnetic fields for the thin-sheet model proved to be an effective tool for the investigation of these distortions. The model reflects the conductivity distribution within boundaries of the investigated sedimentary-volcanic cover corresponding to the S map. Two classes of models were

¹ Shirshov Institute of Oceanology, USSR Academy of Sciences (Laboratory of Geophysical Fields), Moscow

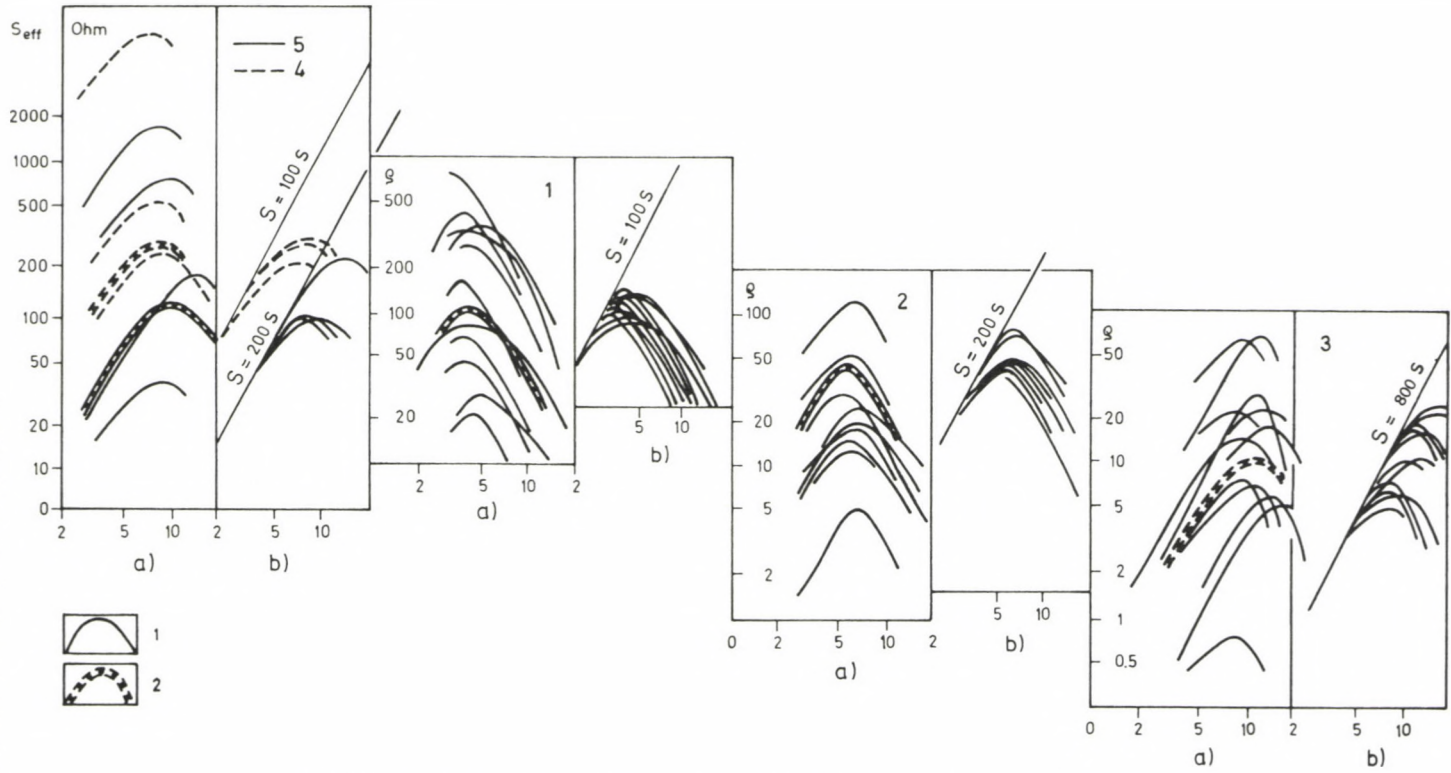


Fig. 2. a) experimental curves of the zones 1-5; b) reduction to a common S_1 ; 1— ρ_{eff} ; 2—average curves $\bar{\rho}_{\text{eff}}$

frequency range. On the basis of the modelling (Demidova et al. 1985), maps were constructed representing the directions and the amplitudes A and B of major axes of the telluric polarization ellipses. One can see in Fig. 3 (a and b) the maps of A and B axes in accordance with a large-scale map of Armenia. The results of another calculation (Debadov et al. 1984) are presented in the form of theoretical MTS curves for a set of field stations.

The results of the modelling obtained with the two different programmes are similar to each other in the low frequency part and confirm a significant distortion of the MTS curves in the whole territory investigated. These distortions influence in a similar way the response of different deep profiles; they are mainly caused by the galvanic effects and lead to the displacement of both the oriented and the effective curves along the axis ρ_a ; at $T > 10\text{--}20$ s they are practically of identical forms. At $T \approx 10\text{--}400$ s they are characterized by the same peculiarities as the field curves presented in Fig. 2a: one can see a clear ascending branch, a maximum and a descending branch. At long periods ($T > 400$ s) the rightside branches of the model curves are significantly different for the different deep profiles in case of the conditions studied. The similarity of the oriented and the effective curves being confirmed by the modelling allows to use only the effective curves in the later analysis.

4. It is shown by a joint analysis of the field and model curves that: a) on the basis of the shape of ρ_a curves in the interval $T = 4\text{--}400$ a (similar to the K -type curves) the presence or absence of the conductive layer in Armenia cannot be ruled out unambiguously because these curves like K -type can characterize in certain surface conditions the so-called "cold" standard deep profile with continuously decreasing of resistivity with depth; b) that is why separate field MTS curves cannot be used for the estimation of the type of any deep profile, because they differ only slightly from curves of the standard deep profile; c) to clear up the character of the deep section and to determine the depth of the conductive layer (if it is not absent) gets possible (when the regional background of the conductivity is realistically selected) having introduced appropriate corrections, characterizing the field of the inhomogeneities (according to the calculations on base of the S map) in values of "apparent depth" of the conductor obtained on the basis of average curves or by means of a comparison of average field curves and model ones.

5. A certain elimination of the distortion effects due to local small inhomogeneities, not reflected on the S map, is done by means of an averaging of the effective curves within 5 zones. These zones differ in the conductivity distribution of the volcanic-sedimentary layer, in consequence of the different structures and are separated as a result of the segmentation of the territory on the basis of the form of MTS curves, (more exactly of the location of the maximum on the effective curves with respect to T). This averaging (Fig. 2) is carried out after displacing at first the high frequency branch of the curves along the axis ρ_a to the S_1 line corresponding to the mean surface conductivity of the respective zone according to the S map. A comparison of the average curves with

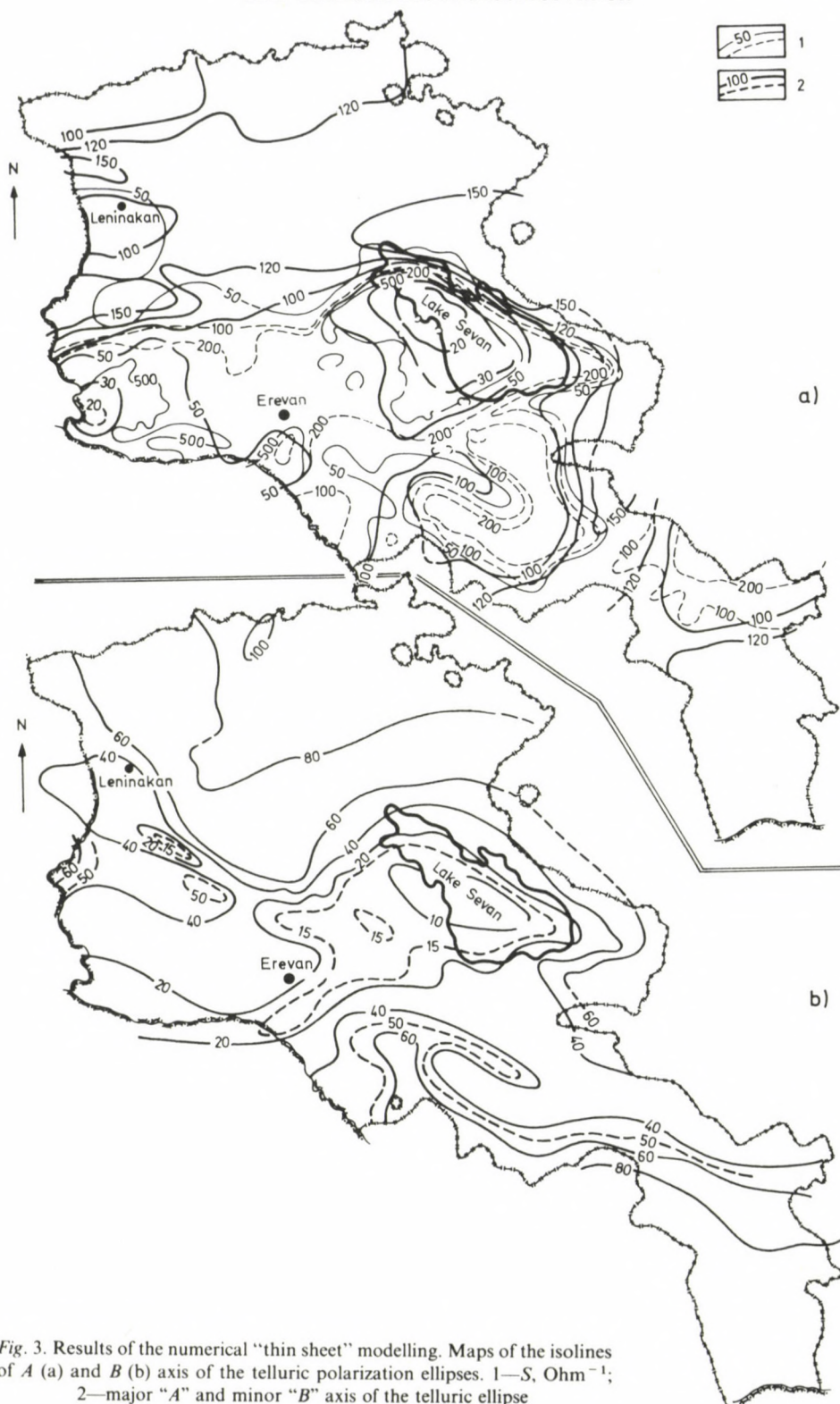


Fig. 3. Results of the numerical "thin sheet" modelling. Maps of the isolines of *A* (a) and *B* (b) axis of the telluric polarization ellipses. 1—*S*, Ohm⁻¹; 2—major "A" and minor "B" axis of the telluric ellipse

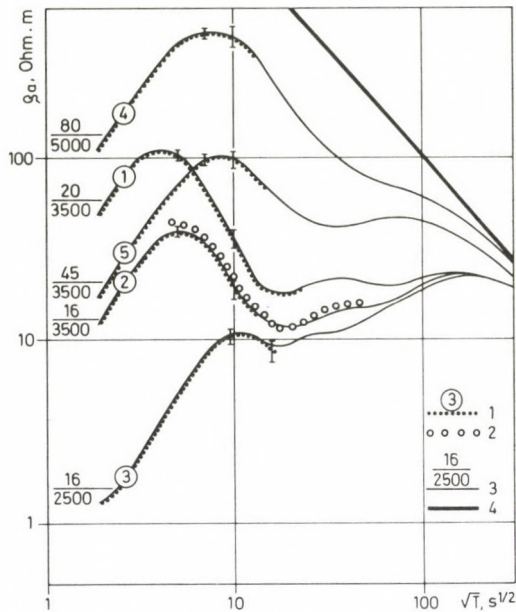


Fig. 4. Results of the comparison of experimental and theoretical data: a) the average and 1-D curves: 1—field curves $\bar{\rho}_{\text{eff}}$ averaged along the zones; numbers denote zones; 2—long period curve ρ_{eff} on the basis of material by Grigoryan and Shakunazaryan (1982), reduced to S_1 in the second zone; 3—collection of 1-D curves; in the numerator: the depth to the first conductive layer; in the denominator: its summarized conductivity Ohm^{-1} ; 4—the global “standard” curve

the 1-D ones hints at the presence of a conductive layer on the background of a gradient resistivity decreasing with depth. The top of the layer is lying South of Sevan at depths of 20 km (Zone 1), 16 km (Zones 2 and 3) and -NW of it at depths of 80 km (Zone 4) and 45 km (Zone 5) (Fig. 4 and Table I) (Variant 1).

6. Some evaluations carried out demonstrate that current penetration from the upper layer to the lower conductive ones is insignificant. It gets necessary to take into account the influence of the regional effect by introducing improvements, mentioned in Section 4. For the relative correction of the depths in different zones, the values of the calculated effective fields $E = \sqrt{A \cdot B}$ are used. These are averaged along the zones (Demidova et al. 1985), and related to the unit value of the mean field in Zone 2. The corrected value is equal to the mean value of H in the respective zone, divided by this coefficient. The values of the respective parameters are presented in Table I — Variant II.

The correction was also done taking into account the relative distortions in the different points by means of a similar coefficient (Variant III).

Figure 5 shows a comparison of the depth in the zones with the zone-average model curves (Variant IV). The ρ_a curve of zone 2 sharply differs in its position from the

“standard” model curve having the same surface S -distribution and it is similar to the corresponding curve for the “hot” crustal section with a conducting layer at a depth of 20 km.

The curves in the 5th zone do not differ significantly from the standard ones (Variant IV).

Thus the following approaches were used for the estimation of the geoelectrical deep profile on the basis of the MTS data at periods $T=4-400$ s: 1. study of average curves for each zone; 2. correction of the obtained average values H_a using the field calculation according to Demidova et al. (1985); 3. a similar correction for individual curves along the profile; 4) comparison of average model curves and average field ones according to Debadov et al. (1984). The results of each approximation give evidence of a high conductivity at the deep section South of Sevan and of the evolution of a crustal layer there at a depth of 15–20 km, further of the general increase of the resistivity (and a possible change in the temperature) N and W of it, where the depth of the crustal layer exceeds 2–4-times the depth in the southern parts. However, there are only a few MTS results in the zones 4 and 5 and more detailed field works are needed here yet. The results are significantly diverging only for the most conductive zone 3. Using *a priori* informations (geothermic data, geological position) it is possible to consider a more reasonable conclusion about the presence of a crustal layer in the zone 3 at the same depth as in zones 1 and 2 — first variant, i.e. it is to be admitted that a significant penetration is present in this zone 3 (e.g. by means of deep fractures), leading to the smoothing out of the S -effect.

7. The longer period curve (Fig. 4) constructed by the author according to the results by Grigoryan and Shakhnazaryan (1982) and shifted to the same average value of S for the zone 2, where it was observed, certifies that besides the crustal layer at a depth of 16 km, an asthenospheric layer is also expected at a depth below 70 km.

8. The position of the conductive surface layer is on the basis of the known profiles near to the position of the 400–500 °C isotherm as calculated from heat flow by Miridzhanyan (1979). It is probable that the nature of the discovered conductive layer is connected with the saturation of the rocks with high temperature fluids during regressive metamorphism, accompanied by dehydration and development of a layer

Table I

Parameters	No. of zones	1	2	3	4	5
S_{av} , S (Ohm^{-1})		100	200	800	50	200
H_y , km (variant I)		20	16	16	80	45
E , % (averaging)		60	70	25	140	115
H_y , km (variant II)		23	16	45	40	29
H , relative (variant III)		—	1	3	3	—
H_y , km (variant IV)		—	20	—	—	40–50

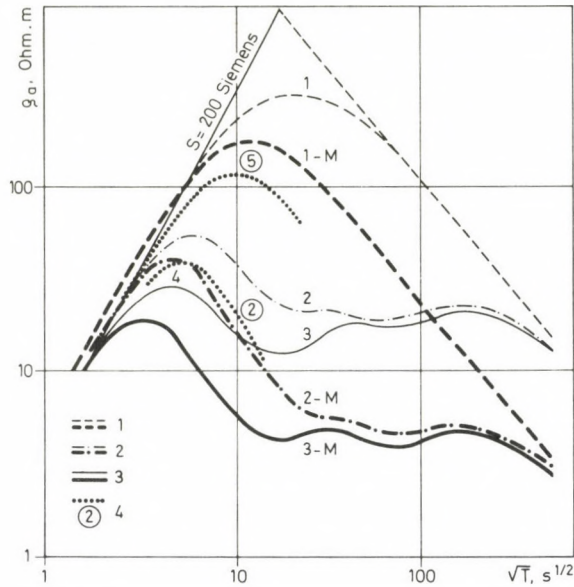


Fig. 5. Average and computed (Debadov et al. 1984) curves for different profiles in case of an inhomogeneous upper layer: 1—"cold" (gradient) section; thin line — 1-D curve, thick line — curve according to modelling; 2—the above mentioned curves for a profile having a conductive layer with $H=20$ km; 3—the same for $H=10$ km; 4—field curves, the same as in Fig. 4 but for the zones 2 and 5

with high porosity and being separated from upper rocks by an impenetrable shell in the sediments (Bryksin and Khlestov 1980). Another explanation of evolution of high porosity, small cracks and connected features of metamorphism is suggested by Nikolayevski and Sharov (1985) on the basis of the results of brittle failure of deep rocks in condition of dynamic stress.

It is possible to increase the accuracy of the determination of the depth of the conductive layer by active sources.

Acknowledgement

The author sincerely thanks Prof. Vanyan for very fruitful discussions.

References

- Avetisyants A A, Makarenko F A, Sergienko S I, 1975: Heat flow in Zakavkazye. *DAN*, 222, 3, 222.
 Bryksin A V, Khlestov V V, 1980: Nature of the intracrustal wave guide in the continental rift zone and areas of current activation, *Geologiya i geofizika*, 8, 87-95.

- Debadov A S, Demidova T A, Yanikyan V O 1984: Spectral iteration modeling of the Armenian magnetotelluric field. *Fizika Zemli*, 7, 101—108.
- Demidova T A, Egorov I V, Yanikyan V O 1985: Galvanic distortion of the magnetotelluric field of Caucasus Minor. *Geomagnetism i aeronomia*, No. 3, 474—481.
- Grigoryan D S, Shakunazaryan A D 1982: Some results of deep magnetotelluric soundings in Armenia. *Isv. Akademii Nauk Arm. SSR. Nauki o Zemle*, 4.
- Miridzhanyan P T 1979: Prognostic estimation of the temperature of the deep layers of the Earth's crust in the territory of Armenia. *Isv. Akademii Nauk Arm. SSR. Nauki o Zemle*, 5, 58—63.
- Nikolayevski V N, Sharov V I 1985: Faults and rheological rock lamination of the Earth crust. *Fizika Zemli*, No. 1, 16—28.
- Vanyan L L, Demidova T A, Yanikyan V O, Chernyavsky G A 1987: Preliminary geoelectrical model of the crust in Armenia. *Fizika Zemli*, No 1

HIGH-PRESSURE ELASTIC WAVE VELOCITIES IN ARMENIAN GRANITOIDS OF DIFFERENT AGE AND ORIGIN

M P VOLAROVICH¹, G A YEFIMOVA¹, V S BALASANYAN¹

[Manuscript received May 3, 1985]

The paper looks into the influence of coloured minerals on the elastic behaviour of Armenian granitoids. In these rocks elastic wave velocities are determined by the coloured minerals, the proportion of which depends on age and genesis of rocks.

Keywords: Armenia; coloured minerals; elastic properties; granitoids

Introduction

Regularities in the changes of elastic mineral characteristics in the depth of the Earth are in a close connection with the mineral-forming geological processes (Volarovich et al. 1974, Belikov 1972, Rac 1968, Rezanov and Gaddin, 1967). In this sense an appropriate study of rocks from certain regions gives possibility to establish some connections between the physical properties of rocks and their geological past. In this paper some results for rocks from the Armenian granitoid complex (which has a significant importance in the geological structure of the region) are shown.

Experimental

The analysis of experimental studies has shown differences in the elastic wave velocity depending on the age of the granitoid complexes, as each of them has its own individual mineral composition, structure, texture and evolutionary conditions (genesis) as basic factors which have some influence on the elastic and other properties of rocks. On the other hand, these characteristic features made it possible to determine the velocity, as a random function of these or other factors for different thermodynamic parameters.

The general diagram in Fig. 1 indicates that the zones of the longitudinal wave velocity curves as functions of the pressure and the temperature (determined by the well

¹ Institute of Physics of the Earth, Gruzinskaya 10, 123810 Moscow, USSR

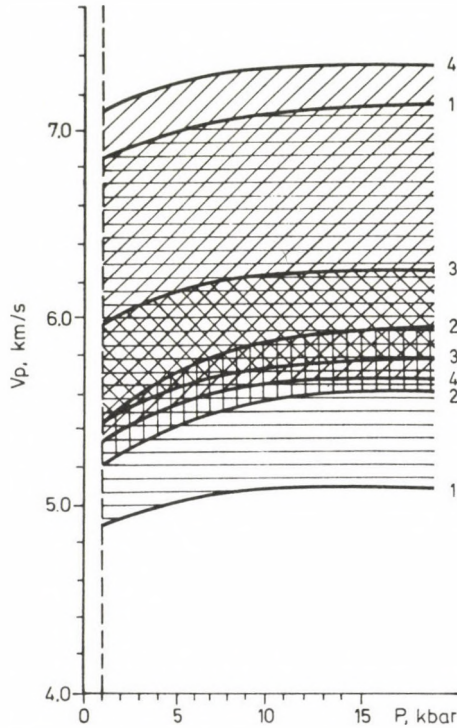


Fig. 1. Zones of longitudinal wave velocity curves as functions of the PT conditions for granitoids of different age. 1-1 Paleozoic rocks; 2-2 Middle Jurassic granitoids; 3-3 Lower Cretaceous granitoids; 4-4 Tertiary granitoids

known method described by Volarovich et al. 1977, 1978) are different for granitoids of different origin. The greatest differences in velocities (5.0–7.2 km/s at 1500 MPa) can be observed for granitoids from the Paleozoic complex which can be explained by their mineral composition, compound structure and metamorphic processes. The longitudinal wave velocity zone as a function of the pressure and the temperature is also wide (5.64–7.32 km/s at 1500 MPa) for Tertiary metamorphic granites. This complex has been formed by multiple magmatic intrusions into the folded structures and strain slips, and as a consequence, it has a large variety in its petrographic composition (Balasanyan 1968, Bagdasaryan 1966, Adamyan 1970, Gulyan and Tatevosyan 1970). Among the rocks there may be leucocratic ones with a minimal coloured mineral content and granitoids which are rich in coloured minerals. A simultaneous occurrence of three coloured minerals (pyroxene, amphibole and biotite) is characteristic of the majority of rocks. A large fluctuation in composition of these three high-velocity minerals results in a strong dispersion in the longitudinal wave velocities of the Tertiary granitoids in each

pressure and temperature range. Figure 1 shows that the longitudinal wave velocity values lie in a narrow zone for Low Cretaceous (5.76–6.24 km/s at 1500 MPa) and especially for Middle Jurassic granitoids (5.6–5.93 km/s at 1500 MPa) due to their homogeneous petrographic composition, *viz.* the high proportion of coloured minerals, without any significant fluctuation of composition (especially for Middle Jurassic granitoids).

On the basis of the longitudinal wave velocities, granitoids of different genesis can be distinguished. Taking into account that thermodynamic conditions leave their marks on the composition and the structure (which are the basic factors of elastic rock properties), this statement becomes evident. Therefore granitoids which have been formed by metamorphic processes and granitization, have the highest variability in the elastic wave velocity. The hybrid granitoids differ from similar rocks of magmatic origin in their high longitudinal wave velocities which is connected to an increase of coloured mineral content (due to fusion of the host rocks of basic composition with the silicious magma).

On the basis of the longitudinal wave velocity values it is possible to estimate the degree of pollution (assimilation) of the granitoid magma by auxiliary rocks. For example the hybridization processes in the Tertiary granitoid complex are more expressed than in the Lower Cretaceous granitoids (Balasanyan 1968, Bagdasaryan 1966), therefore Tertiary rocks having high longitudinal wave velocities (7.25–7.58 km/s at 1500 MPa) strongly differ from similar Lower Cretaceous rocks (6.51–6.53 km/s at 1500 MPa).

It is remarkable that the zones of the velocity curves as functions of pressure in Paleozoic and Jurassic plagiogranites of similar composition strongly differ from each other in their investigated physical parameters as indicated by Fig. 2. Nevertheless, their ages and geological conditions are different what is the reason of their higher longitudinal wave velocities and densities compared with the similar Jurassic rocks.

Vein rocks (aprites, pegmatites) which developed considerably later and under other thermodynamic conditions have lower elastic wave velocities.

A significant decrease in elastic wave velocities can be observed in granitoids influenced by a cataclastic process (Paleozoic), Na and K somatism (Jurassic and Tertiary in turn), hydrothermal solutions and mineralization.

A velocity decrease in rocks of metasomatic origin and in hydrothermally altered granitoids is in good correlation with the change of the mineral composition of rocks due to postmagmatic solutions. According to microscopic studies this change means a loss of dark minerals (Fe, Mg, Ca) and a growth of light minerals (Si, Na, K). This process results in a rarefaction of rocks which is the reason of a decrease in the elastic rock parameters. It has been observed that an increasing ore minerals content (e. g. sphalerite and galenite) results in a velocity decrease.

Some special feature of the Armenian granitoid complexes of different age make it possible to clear up the dependence of the longitudinal wave velocity on other factors.

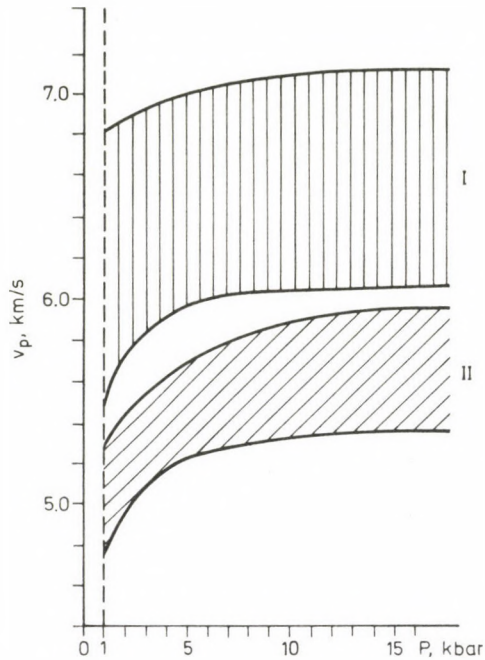


Fig. 2. The zones of longitudinal wave velocity curves as functions of the pressure and the temperature for plagiogranites of Paleozoic and Middle Jurassic ages; I Paleozoic plagiogranites, II Middle Jurassic plagiogranites

Our laboratory studies have indicated strong correlation between longitudinal wave velocities and the coloured mineral content, since the elastic wave velocities for the majority of the afore-mentioned petrographic types are predetermined by coloured minerals.

Figure 3 shows that the longitudinal wave velocity curves for the main types of Tertiary granitoids are in different zones completely corresponding to the proportion of the dark minerals. Thus at 1500 MPa these zones have velocities 5.66–6.1; 5.69–6.36; 6.56–7.03 and 6.4–7.32 km/s corresponding to granites having coloured mineral contents of 1–11 percent; to granitoids of 9–18 percent; to quartz diorites of 20–25 percent and to monsonite rocks of 18–30 percent. In Fig. 3 two velocity zones can be distinguished, where the petrographic types of Tertiary granitoids are brought together in twos as a function of the coloured mineral content, namely 5.66–6.36 km/s for granites and granodiorites, and 6.4–7.32 km/s for quartz diorites and monsonites.

In Fig. 4 the zones of curves for quartz diorites from the Cretaceous and Tertiary granitoid complexes strongly differ from each other due to the high proportion of dark minerals (20–25 percent) in Tertiary rocks.

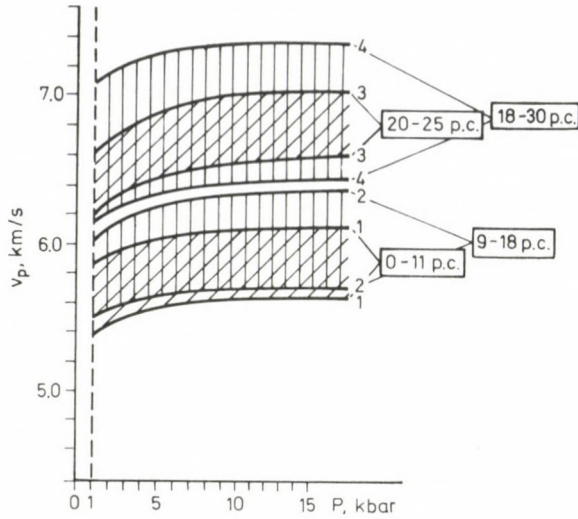


Fig. 3. Zones of longitudinal wave velocity curves under high PT conditions for the main rock-constituents of the tertiary granitoid complex and their dependence on the proportion of dark minerals. 1-1 granites; 2-2 granodiorites; 3-3 quartz diorites; 4-4 quartz monzonites. Percentages mean proportions of coloured minerals

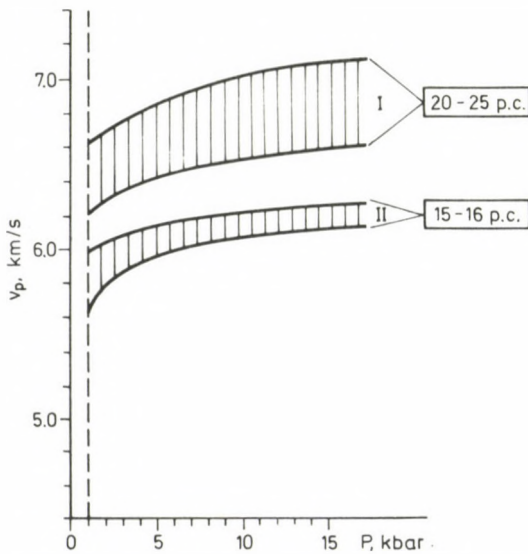


Fig. 4. Zones of longitudinal wave velocity curves and high PT conditions for uniform quartz diorites of Lower Cretaceous and Tertiary ages and their dependence on the proportion of dark minerals

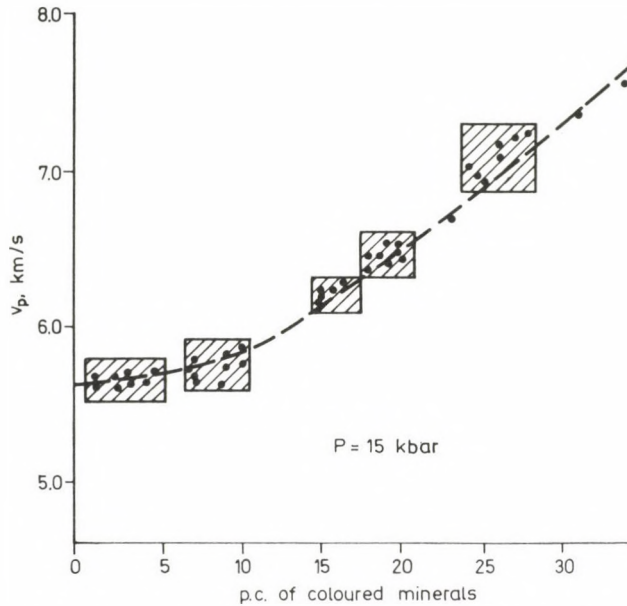


Fig. 5. Correlation between longitudinal wave velocity and proportion of dark minerals in Armenian granitoids at 1500 MPa

The longitudinal wave velocity dependence on the coloured mineral content in granitoids calculated from the average values is illustrated in Fig. 5. An increase in the proportion of dark minerals results in a strong velocity increases, especially over 10 percent.

Conclusions

The decisive effect of coloured minerals on the elastic wave velocity is demonstrated by the following two factors:

1. granitoids which are almost uniform in the proportion of coloured minerals, and different in the quantity of other rock-forming minerals, have almost equal longitudinal values (Lower Cretaceous complex),
2. hybrid granitoids have high velocity values, but the vein and postmagmatic altered rocks have low velocity values in direct connection with their coloured mineral contents.

In general, Armenian granitoids have high longitudinal wave velocity values which is not characteristic of silicious rocks. The main reason of that is their Tertiary age. According to Dely these rocks differ from other main types of similar rocks in their proportion of coloured minerals, having enhanced MgO , $FeO + Fe_2O_3$, CaO and

reduced SiO_2 ($\text{Na}_2\text{O} + \text{K}_2\text{O}$) contents. This is the reason of their increased dark mineral content and their increased longitudinal wave velocity values.

Thus on the example of Armenian granitoids the influence of coloured minerals on the elastic behaviour of rocks has been shown. In these rocks the elastic wave velocity values are determined by coloured minerals, the proportion of which depends on the age and genesis of rocks. Accordingly, the proportion of coloured minerals divides these rocks on the basis of physical properties into groups, representing their ages and mineral types.

References

- Adamyán A I 1970: The Megrinsk group of intrusives (in Russian). In: *Geology of the Soviet Union*, Moscow, Nedra, 43, 323–333.
- Bagdasaryán G P 1966: Intrusive rocks of the Barzum-Pambak region. In: *Geology of Armenia* (petrography, intrusive rocks) (in Russian). Yerevan, Armenian Academy of Sciences, 3, 256–323.
- Balasanýan S I 1968: Basic features of magmatism in Armenia (in Russian). Yerevan, Mitk.
- Belikov B P 1972: Effect of petrographic composition and development history of rocks on their physical-mechanical (with emphasis on elastic) properties (in Russian). In: *Magmatism, formation of crystalline rocks in the depth of the Earth*. Papers of the 4th petrographic all-Union meeting. Nauka, 2, 66–96.
- Gulyán E H, Tatevosyan T Sh 1970: The Bargushatsk group of intrusives (in Russian). In: *Geology of the Soviet Union* (Armenia). Nedra, 43, 311–323.
- Rac M V 1968: Inhomogeneity of rocks and their physical properties. Nauka
- Rezanov I A, Gaddin N E 1967: On the geological meaning of seismic velocity anisotropy in the Earth's crust (in Russian). *Izvestiya, Ser. geol.* 4, 10–16.
- Volarovich M P, Bayuk E I, Levikin A I, Tomashevskaya I S 1974: Physical-mechanical properties of rocks at high pressures and temperatures (in Russian). Nauka
- Volarovich M P, Bayuk E I, Efimova G A 1975: Elastic properties of minerals at high pressure (in Russian). Nauka
- Volarovich M P, Bayuk E I, Shaginyan G Sh 1977: Investigation of velocities and alternation of P-waves in rocks and minerals at pressures to 1500 MPa at temperatures to 600 °C (in Russian). *Izvestiya, Fizika Zemli* 7, 82–90.
- Volarovich M P, Bayuk E I, Shaginyan G Sh 1978: Investigation of velocity and attenuation of longitudinal waves in rocks and minerals at high pressures internal heating (in Russian). In: *Physical properties of rocks and minerals at high pressures and temperatures*. Nauka, 8–18.

HIGH-PRESSURE CHANGES OF REMANENT ROCK MAGNETIZATION

T S LEBEDEV¹ and B YA SAVENKO¹

[Manuscript received May 3, 1985]

In this paper a comparative analysis of the changes of remanent rock magnetization at hydrostatic and uniaxial pressures is reported on. The role of reversible and irreversible processes in the general demagnetization due to pressure-effects is estimated.

On the basis of experimental data obtained at high hydrostatic pressures, the changes of remanent magnetization of several crystalline rocks from different Ukrainian geological regions have been considered. A close relation between the magnetic changes of the minerals and their genetic characteristics is emphasized.

Keywords: hydrostatic pressure; magnetic changes of rocks; remanent rock magnetization; Ukrainian rocks; uniaxial pressure

Introduction

In order to investigate the structure and the development of the Earth's crust and the composition and the state of minerals, it is necessary to have data about the magnetic properties of rocks as a function of depth. The pressure, which has a certain depth-determined distribution, plays an important part in the change of physical (among them magnetic) properties. The change of the remanent rock magnetization at high hydrostatic pressure and uniaxial compression can serve as a qualitative characteristic of the elastic stresses modelled by laboratory experiments. The resultant effect of pressure on the remanent magnetization is determined by the sum of changes of irreversible and reversible magnetization, while their relations indicate the state of loading. Irreversible changes usually are results of a constant pressure (e. g. lithostatic) reversible changes on the other hand, are indirectly related to temporary mechanical loadings.

Experimental

Experimental investigations of the remanent magnetization (I_{rs}) at uniaxial compression were carried out by a hydraulic press ensuring recording the loading force (Kapichka and Savenko 1979). To produce hydrostatic pressure a special high-

¹ Institute of Geophysics of the Ukrainian Academy of Sciences, 252164 Kiev — 164, Palladin ave. 32, USSR

pressure equipment was used (Lebedev et al. 1972). The maximum pressure of 260 MPa was chosen to be in the elastic range of deformation. In the experiments, using different types of mechanical loading the same samples were always used since in this pressure range there are no irreversible structural destructions (Mineralogical thermometrics and barometrics 1965). In general, magnetic changes were recorded at $P = P_i$, while the irreversible ones at $P = 0$. The value of the change of I_{rs} was determined by the difference of these values during the reversible process.

The relation between the irreversible and reversible components of the remanent magnetic change depends on a number of factors. Load transfer has an important role. The results of experiments carried out on basalts (Kapichka and Savenko 1979) indicate that higher gradients of $I_{rs} = f(P)$ were found at uniaxial pressure. For each of the investigated samples the following regularity was found. The greatest changes of I_{rs} were observed at low pressures while increasing the pressure to its maximum these changes are insignificant. The converse was observed for hydrostatic pressure: at small pressures changes of I_{rs} are insignificant and the highest changes are in the high-pressure region. For combined loads when constant hydrostatic pressure and uniaxial stress are superposed (these experiments are very close to the real pressure distribution in the crust), the curves representing the magnetic changes are between the maxima and minima corresponding to the above-mentioned pressure conditions (Lebedev et al. 1977). It should also be emphasized that for each of the samples the irreversible changes caused by uniaxial compression are greater than the resultant changes of I_{rs} at hydrostatic pressures.

Thus magnetic changes of rocks are determined first of all by irreversible processes and the effect of reversible processes is relatively small.

At hydrostatic pressure the increment of irreversible changes in I_{rs} is determined to a considerable extent by the pressure. They achieve their highest values in the pressure range below 500 MPa. A further increase in the load brings about only small magnetic changes. For the investigated basalt samples the irreversible changes resulting in the destruction of I_{rs} have been found to amount to 30–95 p. c. of the initial remanent magnetization.

The measure of irreversible changes in the general demagnetization effect strongly depends on the type of the load. In case of a hydrostatic pressure below 200 MPa the maxima of the reversible components are about 14 p. c. of the summarized change (6 p. c. in average). For uniaxial compression the role of reversible processes is far more significant. At 200 MPa their maxima may achieve 38 p. c. of the final changes (24 p. c. in average).

The differences in the remanent magnetic stability due to the effect of pressure are also due to physical processes producing a certain magnetic state of the ferromagnetites, i. e. a certain value and character of the remanent magnetization. Therefore I_{rs} has not been chosen as a basic magnetic parameter of the high-pressure rock magnetic change. The remanent magnetization was obtained in strong magnetic

fields. The magnetization process was the same for each of the investigated samples. Thus the different characters of functions $I_{rs} = f(P)$ will be determined to a lesser degree by the composition of magnetic minerals than by grain-sizes and structural properties but first of all by the frequency and pattern of internal defects and dislocations as well as their mobility during external pressure.

The grain size plays an important part in the destruction process of I_{rs} caused by the pressure. According to data published by Elenska and Savenko (1978) only grains larger than 0.03μ participate in the remanent magnetic changes. This is the critical grain size in the transition between one-domain and multi-domain structures. For basalts the grain-size fluctuation is in the range of 2–200 μ , being practically a multi-domain structure, which is characteristic of ferrimagnetic minerals.

For average chemical composition the coercive force H_c of the magnetic minerals is determined by the grain size and its structural properties.

Similarly to the remanent magnetization, the value of H_c is in a close connection with the internal stresses, determining the equilibrium state of energy of the ferrimagnetites. Therefore the relations of the reversible and irreversible parts of the change of I_{rs} at high pressures are directly related to the distribution of soft and hard magnetic domains in the spectrum of micro-coercive forces of ferrimagnetites. Multiple pressure-actions and cessations (cycles) result in the dissemination of the reversible part of the change of I_{rs} and in the stabilization of internal stresses. A similar result can also be obtained by compression considerably over the liquid-limit. After a previous compression the reaction of samples to subsequent external pressure is far weaker, and in such cases their remanent magnetization seems to be more stable.

The reconstruction mechanism of the remanent rock magnetization after multiple compression is connected with the internal state of stress and can be explained by mutual magnetostatic effects between the domains with crystalline anisotropy. At uniaxial compression the conversion of the domain structure takes place perpendicularly to the direction of the acting pressure. The internal stress is suppressed by the hydrostatic pressure, though the orientation of the spontaneous magnetic vectors is affected by the laboratory magnetic field. As the movements of the domain boundaries are retarded, especially in the dislocation accumulation zones, a different reconstruction degree of the reversible part of the remanent magnetic changes in the samples can be observed.

The source of the internal stresses is the imperfect crystalline structure of the ferrimagnetic grains. They are first of all due to the presence of dislocations, point defects and their accumulation. The effect of these factors on the degree of the change of I_{rs} depends on the character of the dislocation distribution, on their types and also on the type of the domain boundaries. Under external load, the ferrimagnetite changes its size corresponding to the magnetostriction constant. At the same time on the domain boundaries a local magnetic change takes place which always depends on the acting stresses. The mutual effect of these internal stresses with the stress field due to

dislocations causes a holdback of the domain boundaries during their movement, determining the value of the retarding (coercive) force. Arriving at the external load a discrete displacement of the domain structure takes place from a certain potential minimum to another one, resulting in a remanent magnetic change. According to the experiments these processes can be either irreversible or reversible. The irreversible changes of I_{rs} are connected with additional energy consumptions (hysteresis loss).

The reversible processes take place in an opposite direction on the domain boundaries as compared with the irreversible processes. The processes on the boundaries do not affect the internal stress-fields. According to the experimental results the irreversible changes of the remanent magnetization are mainly due to irreversible movements of the domain boundaries, while for the reversible changes the rotation process of the spontaneous magnetic vectors is the most characteristic factor.

Using a laboratory magnetic field, there are two types of boundaries in the ferrimagnetite. In the first type an external magnetic force increases the domain volumes magnetized by this field. In the second one there is a force which decreases the domain volumes magnetized against the field. Equalization of energy barriers caused by dislocations during an external magnetic field effect, results in an additional boundary displacement. Depending on the connections between the first and the second types of domain boundaries an increase or decrease of the remanent magnetization can be observed. All ferrimagnetite domains are oriented in the fixed direction by the strong magnetic field, in which the initial value of I_{rs} was obtained. Therefore in the investigation of $I_{rs}=f(P)$ only a decrease of the remanent magnetisation can be observed.

High-pressure magnetic properties of rocks from the Ukrainian shield

On the basis of a generalization of experimental data a comparative analysis was made to look into the changes of the remanent magnetization as a function of depth H in crystalline rocks from a number of geological regions of Ukraine. The experimental results at high hydrostatic pressures are summarized in Table I. The numerators contain the differences of maxima and minima of $I_{rs}(H)$ and the denominators the mean values — all in percentage.

The data obtained indicate that all investigated rock types are characterized by a decreased remanent magnetization. At a maximum pressure of 250 MPa (corresponding to a depth of 10 km) the rock can preserve about 47–60 p. c. of its initial magnetization (neglecting the effect of temperature). Disregarding the closeness of intervals and characters of the $I_{rs}(H)$ in these values significant differences can be observed. They are especially conspicuous if we compare composition, structural and genetic features of ferrimagnetite minerals of these rocks.

The basic factors, determining the stability of $I_{rs}(P)$ are the thermodynamic rock-forming conditions. Ferrimagnetite minerals are developed under different thermody-

Table I

Rocks, regions	Remanent magnetization I_{rs} (P) at different depths				
	2 km	4 km	6 km	8 km	10 km
Crystalline basement rocks from the Dneprovsk-Donets depression	95—70	95—60	90—50	85—45	80—35
	82	78	70	65	57
Effusive rocks from the Dneprovsk-Donets depression	90—65	90—50	85—45	80—35	75—25
	82	70	65	57	50
Intrusive rocks from the Ukrainian Shield	95—45	95—65	95—45	95—30	95—15
	85	80	70	62	55
Effusive rocks from the Ukrainian Shield	95—80	95—40	90—35	85—30	85—25
	87	67	62	57	55
Metamorphic rocks from Krivoy Rog	95—80	90—50	80—40	70—30	65—30
	87	70	60	50	47
Intrusive rocks from the Krim Mountains	93—70	85—55	80—45	80—40	75—40
	82	65	62	60	57
Volcanogenic formations from the Trans-Carpathians	98—75	95—60	90—50	90—40	90—30
	88	77	70	65	60

namic conditions. Therefore they excel in their typomorphic features appearing in the internal structure of the grains, in the presence of inclusions and isomorphic contaminations. This fact ensures wide ranges of the acting pressure within which the magnetism remains stable.

An investigation of the pressure-affected changes of I_{rs} of ferrous quartzites from different metamorphic facies made it possible to obtain additional information on the investigated mutual effects of high pressures and temperatures (Lebedev et al. 1977). In the experimental process, in the low-pressure range, where the magnetite was associated with high-temperature minerals, I_{rs} of the samples proved to be extremely stable. When the pressure increases, they are characterized by a sudden magnetic decrease in the interval up to 100 MPa. At higher pressures the gradient of the decreasing function becomes smaller and the curve $I_{rs}=f(P)$ has an asymptotic behaviour, i. e. I_{rs} becomes stable. Such changes of the remanent magnetization of ferrous quartzite samples can be caused by long-term effects of high thermodynamic parameters. A sudden decrease of I_{rs} in the initial pressure-interval (up to 100 MPa) can also be associated with some specialities of development of the magnetites, the grains of which are almost free from visible inclusions.

The remanent magnetization of medium-temperature and ferrous quartzite samples is less sensitive to the pressure, which can be explained by weaker pressure and temperature effects during the development of these rocks under conditions typical for the amphibolite facies. An increased stability of I_{rs} to the high-pressure effects also informs on the presence of oriented inclusions of amphibole, biotite and magnetite. The

remanent magnetization of ferrous quartzites of the greenschist facies proved to be the most stable to the high-pressure effect, especially in the first interval (up to 100 MPa) and a further increase of P results in an insignificant decrease of I_{rs} , which may be caused by different inclusions of nonmetallic minerals.

As in the high-pressure investigation of the remanent magnetization changes of approximately the same magnetic state of the magnetite domain structure were investigated for different ferrous quartzites, the obtained data can be used as an additional information of the composition as well as as on the structural and genetic properties of these rocks. If the pressure and temperature distributions are known in the deep zones for a certain part of the Earth's crust, the experimental and theoretical investigations of the remanent magnetization make it possible to describe precisely the character of the changes of magnetite-ferrous rocks with the depth.

Magnetoferrous rocks of the Ukrainian shield at hydrostatic pressures of 500–800 MPa (corresponding to a depth interval of 20–30 km) preserve in average 20–30 p.c. of their magnetization. According to our investigations these depths represent the lower boundary of the effect of pressure on the remanent magnetization, as the temperature here can be as high as 200–300 °C and our data suggest that with increasing temperature, the rock magnetization will be destroyed (Elenska and Savenko 1978).

The stability of $I_{rs}(P)$ is determined in a significant degree by the level of metasomatic processes in the rocks. The influence of this factor on the stability of rocks under the effect of pressure can be seen from the results obtained for intrusive rocks from the Krim Mountains (Lebedev et al. 1976).

In tectonical structures with which the intrusions are in accordance, the allometasomatic processes of the Na-branch are well developed. Their intensity — due to the heterogeneous structure of meganodes — is different in different sections, and as a consequence these rocks were affected by different metasomatic processes.

It should be noted that in the investigated samples there are epigenetic forms of finely dispersed magnetites together with syngenetic titanomagnetite crystals which were developed as a result of Na-metasomatism in paramagnetic minerals. Although it is the magnetite which has the main influence on the magnetic properties of rocks in the stability of its magnetization to the pressure effect, the different degree of metasomatic processes is also reflected.

The rocks containing minerals from the titanomagnetite series especially at pressures 1500 MPa preserve 42 p.c. of the initial I_{rs} in average. I_{rs} varies within a wide range as a function of pressure. Among ferromagnetites, the titanomagnetites are the most difficult investigation objects at high pressures, first of all because of the changeable and various chemical composition and structural-textural properties. Naturally, it is difficult to consider at once all factors which influence the internal stress distribution and determine the change of I_{rs} for titanomagnetites under the effect of pressure. Therefore only a few aspects of the relation between the composition of

titanomagnetites and their stability affected by the pressure were investigated (Savenko et al. 1976).

For basalts of the Ukrainian Shield, which, according to geological, petrographical and petrochemical data, are typical representatives of the trap formation, a clear relation was found between the character of the remanent magnetization at high pressures, and the value of the Curie temperature. Magnetic minerals of basalts are represented by homogeneous titanomagnetites which were least affected by oxidation processes. Pressure-stability of rocks increases with decreasing Curie temperature almost linearly according to the function of the decreasing proportion of magnetic components in the system $x \text{TiFe}_2\text{O}_4(1-x)\text{Fe}_3\text{O}_4$. Finally, the equal degree of oxidization and other factors result in an increment of the inhomogeneity in the magnetic minerals, having a strong effect on the size and form of magnetic grains, on their mutual positions, and as a consequence on the distribution of internal stresses, resulting, as a whole in increase of the stability of the sample under the effect of pressure.

A quite different picture can be observed for effusive rocks from the Dnieper-Donets depression, which — in terms of their structural features — belongs to the hypabyssic facies. Disregarding the fact that, as a result of wearing-away and oxidization of titanomagnetite minerals, some minerals were formed which are identical on the basis of minerographic investigations, the essence of these processes is their degradation and therefore the influence of the reaction products in the general rock magnetization effect can be different in each individual case. This does not allow to set up an unambiguous relation between the degree of the change of remanent magnetization of the samples at high pressures and the Curie temperature of ferromagnetites.

These magnetic properties of effusive rocks may be due to the degree of conservation of the initial ferromagnetite material till the moment of investigation. Disregarding the fact that the samples contain the same mineral (titanomagnetite), the degree of development of secondary superposed processes can be so different that they cause variations of the magnetic parameters under the effect of pressure. The value of this latter factor can be calculated by extrapolating the data of experimental investigations of remanent magnetic changes at high pressures.

Thus relation the results of these investigations show a close connection between the remanent magnetization of the investigated rocks as a function of depth, and their genetic properties. The further investigations, which are aimed at setting up a relationship between the magnetic characteristics of the minerals and the degree of their destruction at high pressures and temperatures, will make it possible to characterize the thermodynamic circumstances, having acted in the formation of different rocks.

References

- Elenska M B, Savenko V Ya 1978: Experimental investigation of the destruction process of the remanent magnetization in simultaneous effects of pressure and temperature (in Russian). In: *Physical properties of rocks at high thermodynamic parameters*. Proceedings of the All-Union Meeting, 1978, Baku, 218—219.
- Kapichka A, Savenko B Ya 1979: A comparison of the changes of remanent magnetization in basalts at hydrostatic pressure and uniaxial stress (in Russian). *Geofizichesky Zhournal of the Ukrainian Academy of Sciences*, Kiev, 1, 57—61.
- Lebedev T S, Savenko B Ya, Shapoval V I, Korchin V A 1972: An equipment to investigate the magnetic properties of rocks at hydrostatic pressures of maximum 250 MPa (in Russian). *Geofizichesky Sbornik of the Ukrainian Academy of Sciences*, Kiev, 46, 85—87.
- Lebedev T S, Savenko B Ya, Poznanskaya N F 1976: Magnetic properties of rocks at high hydrostatic pressures (in Russian). In: *Petrophysical characteristics of the Soviet part of the Baltic Shield*. Proceedings of the Kola filiation of the Academy of Sciences of the Soviet Union, Apatiti, 132—137.
- Lebedev T S, Savenko B Ya, Poznanskaya N F, Stebnovskaya Yu M 1977: Magnetic properties of ferrous quartzites of the Ukrainian Shield at high pressures and temperatures (in Russian). *Geofizichesky Sbornik of the Ukrainian Academy of Sciences*, Kiev, 79, 34—44.
- Mineralogical thermometrics and barometrics (in Russian). 1965. Moscow, Nauka
- Savenko B Ya, Poznanskaya N F, Karzanova A Ya 1976: Investigation of effusive rocks of the Ukrainian Shield and the Dneprovsk-Donets depression at high pressures and temperatures (in Russian). In: *Paleomagnetism, magnetism, geomagnetic field*. Proceedings of the All-Union Meeting "The main geomagnetic field and the problems of geomagnetism", 1976, Moscow. Kiev, Naukova Dumka, 61—68.

ZONALITY OF THE ELASTIC PARAMETER DISTRIBUTION UNDER REGIONAL PT CONDITIONS IN THE EARTH'S CRUST

T S LEBEDEV¹, V A KORCHIN¹, P A BURTNÝ¹

[Manuscript received May 3, 1985]

In this paper the elastic properties of rock samples extracted from a deep borehole in the central part of the Ukrainian pre-Cambrian shield are studied by laboratory experiments under different thermobaric conditions.

At first the distribution of the elastic properties and the density of the minerals are discussed along the whole depth of the borehole (3.5 km), and their possible changes in the Earth's crust in depths of 25 km were also prognosed. The relations determined exhibit several extreme zones associated mainly with some specific features of the given mineral composition and with the real thermobaric conditions in the deep.

In this part of the Ukrainian shield on the basis of experimental data, some separated low velocity crustal blocks of thermodynamic origin are assumed to exist in the depth interval of 5–25 km. If the rocks in these zones have relatively low values of v_p and v_s , the velocities will further decrease due to a simultaneous effect of a certain coupling of P and T .

Our studies on the elastic parameters of magmatic and metamorphic rocks of the Ukrainian shield and other regions revealed the general behaviour of the minerals in the lithosphere: a thermobaric zonality of elastic properties with the depth which appears in forms of high and low velocity zones. The thickness of zones, their position, the intensity of the change of the elastic parameters and other properties depend to a great extent on the regional vertical distribution of pressure and temperature. The experimental investigations, however, do not exclude the possibility of an other kind of velocity zonality in the lithosphere related to changes of the mineral composition. Thus, changes in thermodynamic conditions indicate probable places of these zones.

Keywords: elastic properties of rocks; Ukrainian shield; zonality in the crust

General remarks

A complex laboratory study of the physical properties of rocks and minerals under high thermodynamic conditions provides new information about their changes and compositions, and enables the estimation of their states in great depths. Drilling cores from deep and super-deep boreholes are of great importance, since they provide unique information on the distribution of the physical properties of rocks. They enable us to check some experimental and theoretical results, and to improve the regional

¹ Institute of Geophysics of the Ukrainian Academy of Sciences, 252601, Kiev-180, Palladin ave. 32, USSR

*PT*model experiments, etc. (Lebedev 1975, 1977, 1980, 1981, Lebedev and Korchin 1979, Lebedev et al. 1974).

In accordance with the afore-mentioned statements, in this paper the elastic properties of rocks from one of the first deep boreholes in the central part of the Ukrainian shield (Lebedev et al. 1983) are studied and the zonality of the distribution of the elastic parameters under crustal *PT* conditions in this region is shown.

The geological-geophysical basis of applying such experimental laboratory data to the interpretation of the seismic data are the differences in the seismoacoustic properties of rocks in the investigated section and their relationships with the composition, the structural-textural, strength parameters, defects and several other properties (Lebedev 1975, 1977, 1980, 1981, Lebedev and Korchin 1979, 1982, Lebedev et al. 1979, 1981 and others). Elastic parameters of rocks can be determined from their longitudinal and transversal wave velocities v_p and v_s and their density ρ (Landau and Lifschitz 1965).

The state of the minerals under thermodynamic conditions at great depths is determined by Young's modulus E , displacement y , compression K , Poisson's ratio δ , and Lamé's constants λ and μ .

The investigations were carried out at the Department for the Physical Properties of Rocks of the Geophysical Institute of the Ukrainian Academy of Sciences in Kiev. Samples were studied at different pressures (max. 650 MPa) and temperatures (max. 350°C). Equipment and the method applied are described by Lebedev and Korchin (1979), Lebedev et al. (1974, 1976, 1977) and others. In the experiments, the method of programmed modelling was applied in a high pressure apparatus representing the deep zones of the Earth's crust (Lebedev 1975, 1977, 1980, 1981, Lebedev and Korchin 1979, Lebedev et al. 1974).

Elastic rock properties were studied on approximately 200 samples from the whole borehole profile at atmospheric pressure and room temperature. Then the measurement values for a given depth were corrected on the basis of the changes of v_s and v_p of the most characteristic rock samples from the borehole, measured experimentally in the laboratory at high pressure and temperature. Such a method does not only clear up the general relationships of the elastic rock properties under various temperatures and pressures, but it gives a possibility to predict the elastic state of minerals in the deep zones of the crust.

The depth of the borehole (approximately 3500 m core drilling) can be divided, as a first approximation, into two parts. In the upper part (approximately the upper 2900 m) porphyroblast migmatites with subordinate pegmatoid granites (mainly in the upper levels) are predominant. The lower part from 2900 m to almost the bottom, is basically biotite gneiss. In the whole interval small embedded layers of fine- and middle-grained and gneiss-like granites, and scarcely even picrite porphyrites and diabase dykes of totally different composition can be found (Lebedev et al. 1983).

Experimental I. (Atmospheric Pressure and Room Temperature)

For the experiments the core samples of the afore-mentioned rocks were selected in quantities proportional to their occurrences along the borehole. The mineral composition is shown in Table I. In Table II the minima, maxima and averages of the elastic rock properties and densities at atmospheric pressure and room temperature are summarized. The investigated rocks exhibit a low standard deviation ($\bar{\rho} = 2.75 \text{ g/cm}^3$, $\Delta\bar{\rho}/\rho = \pm 9 \text{ p. c.}$) and a wide range in the velocity variation ($\bar{v}_p = 5.55 \text{ km/s}$, $\Delta v_p/\bar{v}_p = \pm 26 \text{ p. c.}$, $v_s = 3.11 \text{ km/s}$, $\Delta v_s/\bar{v}_s = \pm 24 \text{ p. c.}$). The other elastic parameters vary within wider intervals. Yet in more than 70 p. c. of the investigated samples the various elastic parameters are close to the averages of the corresponding groups.

Deviations from the mean values can be due to changes in composition, structural-textural properties and the physical-mechanical state. The highest velocities at atmospheric pressure were measured in coarse-grained samples composed of a few components having significant plagioclase, microcline and quartz content. Secondary alternations of minerals and the dynamic metamorphism result in a decrease of the velocities by 10–15 p. c. Nevertheless, there are some cases, when the mechanic deformation is "healed" by secondary minerals, resulting in extraordinary high velocities. This can be most frequently observed in pegmatoid granites and migmatites. The elastic parameters decrease with decreasing grain size first of all due to an increase of the effective surface of the contacts between the grains. This finding holds especially for middle- and fine-grained granites and low-velocity migmatites. It is the increase of the biotite content that is responsible for the reduction of v_p and v_s because it causes a layering and as a consequence an increase in the acoustic inhomogeneity.

Thus on the basis of velocity properties of rocks it can be assumed that the sections with the higher velocities in the uppermost crust are associated with

Table I

Mineral composition of rocks revealed from the deep borehole in the central part of the Ukrainian shield

Name of rocks (quantity of samples)	Mineral composition (in percents by volume)				
	<i>Pe</i>	<i>Mi</i>	<i>Q</i>	<i>Bi</i>	auxiliaries
porphyroblast migmatites (85)	11–64	2–50	12–40	7–22	1–3 P_x (amphibole)
pegmatoid granites (17)	14–20	57–76	5–25	—	1–3
fine- and middle-grained granites (13)	23–36	28–46	20–37	1–8	1–2 P_x and y_2
gneiss-like granites (19)	29–50	6–32	16–33	4–17	1–5 P_x (amphibole)
biotite gneisses (18) and garnet-biotite gneisses (14)	14–42	0–15	7–53	18–36	— P_x to 5 p. c. y_2 to 4–10 p. c.

Table II

Elastic properties and density of rocks revealed from the deep borehole in the central part of the Ukrainian shield

Physical parameters	Name of rocks (quantity of samples)						
	porphyroblast migmatites (85)	pegmatoid granites (17)	middle- and fine-grained granites (13)	gneiss-like granites (19)	biotite gneisses (18)	biotite gneisses with garnet (14)	dyke rocks (11)
v_p , km/s ⁻¹							
min	4.84	5.37	3.90	4.64	4.23	4.18	5.66
max	6.54	6.83	3.62	6.12	6.18	6.39	6.80
mean	6.12	6.05	5.00	5.35	4.92	5.04	6.38
V_s , km/s ⁻¹							
min	2.65	2.49	2.30	2.65	2.51	2.60	3.22
max	3.80	3.52	3.31	3.66	3.74	3.46	3.66
mean	3.47	3.11	2.78	3.01	2.96	2.95	3.46
E , Mbar							
min	0.49	0.45	0.35	0.48	0.42	0.47	0.78
max	0.95	0.85	0.70	0.86	0.75	0.89	1.05
mean	0.74	0.69	0.51	0.64	0.60	0.62	0.94
G , Mbar							
min	0.19	0.17	0.14	0.19	0.18	0.15	0.31
max	0.35	0.32	0.29	0.35	0.31	0.34	0.41
mean	0.29	0.25	0.20	0.26	0.24	0.25	0.36
σ							
min	0.199	0.249	0.231	0.124	0.089	0.081	0.251
max	0.331	0.387	0.313	0.286	0.272	0.324	0.308
mean	0.266	0.315	0.275	0.249	0.210	0.220	0.289
K , Mbar							
min	0.35	0.40	0.22	0.19	0.22	0.18	0.55
max	0.75	0.78	0.58	0.54	0.49	0.70	0.87
mean	0.52	0.65	0.39	0.42	0.34	0.40	0.74
β , Mbar ⁻¹							
min	1.34	1.33	1.73	1.84	2.04	1.43	1.20
max	2.87	2.53	4.69	5.36	4.64	5.54	1.60
mean	1.92	1.82	2.73	2.49	3.07	2.52	1.39
ρ , g/cm ⁻³							
min	2.66	2.58	2.59	2.63	2.71	2.72	2.97
max	2.81	2.65	2.66	2.71	3.06	2.91	3.15
mean	2.78	2.60	2.63	2.66	2.76	2.81	3.07

porphyroblast migmatite occurrences and partly to dyke-like formations. Low velocity sections (to depths of 3.5 km) are connected to gneisses, middle- and fine-grained granites and rocks having been subjected to dynamic metamorphism.

In Fig. 1 the generalized results for the afore-mentioned parameters at atmospheric pressure and room temperature are indicated by small circles. The averages for different intervals after a correction by the effect of pressure and temperature for a corresponding depth are indicated by solid lines.

Let us consider some main principles of changes in the elastic properties v_p , v_s , δ , σ , E and γ , and the density for the depth interval 250–3500 m. In the whole vertical section of the borehole a general tendency showing their decrease as a function of depth can be observed, which is probably due to an increased loosening of contacts between the grains of common origin, and this loosening is being caused by inhomogeneous internal stresses. This phenomenon is proved by an increase of compressibility with the depth and a decrease of plasticity, and even by an increase of the standard deviation of the elastic parameters. The reason of the observed phenomenon is partly an increased re-layering of rocks having different compositions, their mutual penetrations and the partial contacts between the different formations. These factors result essentially in a decrease of elasticity due to a change of the parameters of the rock. On the other hand, local inhomogeneous stresses decrease the elastic parameters of rocks in a general trend.

The laboratory analysis made it possible to separate five different ranges according to the elastic properties in the following depth intervals: No. 1: 550–800 m, No. 2: 1250–1700 m, No. 3: 2200–2550 m, No. 4: 2550–3000 m and No. 5: 3000–3500 m.

Their description is as follows:

Interval No. 1 seems to be connected to the changes of the mineral composition: in the migmatite block: high-velocity, coarse-grained granites with less density are sandwiched.

This results in constancy of parameters E and γ , and some enhancement of σ .

Intervals No. 2 and No. 3 can be called "real structural". It is interesting to note that in the intervals No. 2 and No. 3 dykes consisting of hard, high velocity rocks are detected. It is evident that their penetration into the host rock causes a deterioration of the elastic parameters of the host rock. They have traces of dynamic metamorphism, their structure is less perfect and evidently in the past they underwent a significant non-hydrostatic stress effect. This is related by the enhancement of the compressibility, by some rarefaction, and by lower values of E and γ .

Region No. 3 is very well expressed. This is characterized by a low velocity. This velocity decrease is probable due to significant inhomogeneous stress effects on the minerals during dyke formation. Furthermore interval No. 3 can be found at a greater depth than the non-elastic interval No. 2 but it is over the interval No. 4, which contains high-elasticity and low-compressibility rocks. This latter interval is represented by well crystallized coarse-grained formations having excellent contacts between the grains. In

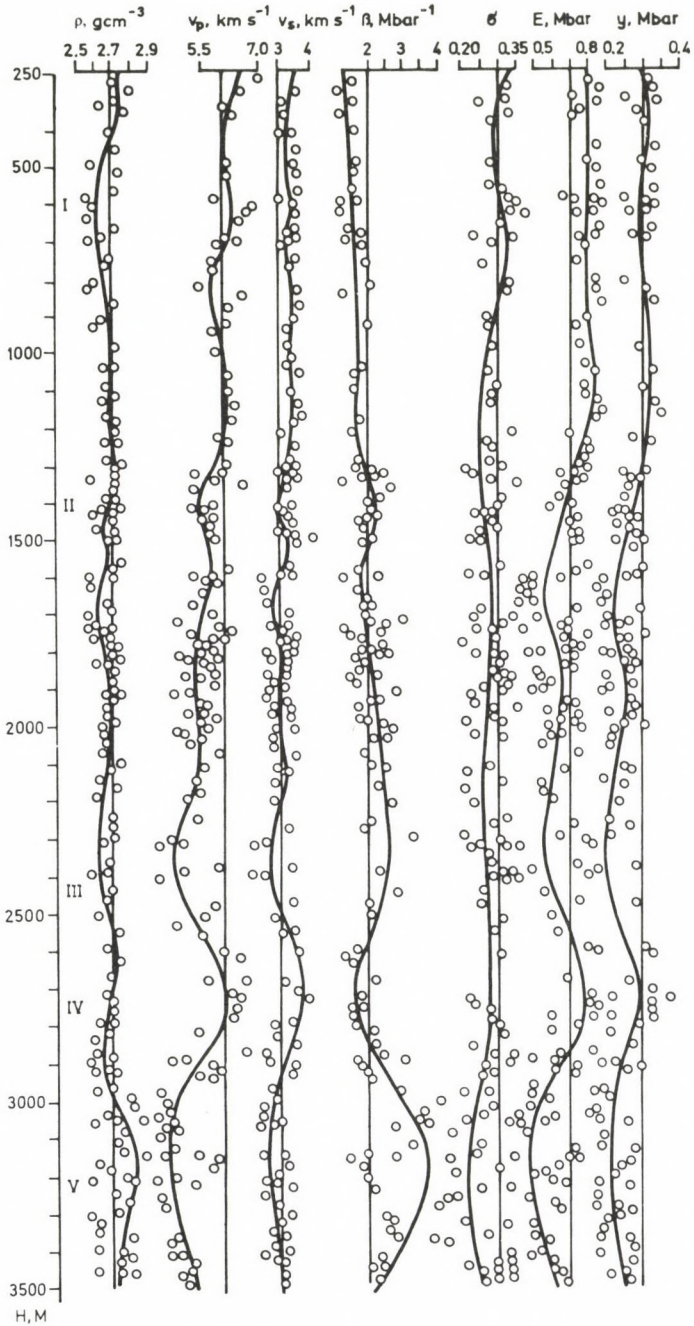


Fig. 1. Elastic parameters and density of rocks (experimental data with real pressure and temperature corrections) from one of the deep drill holes in the central part of the Ukrainian shield

dynamic metamorphic rocks the internal faults usually are "corrected" by secondary minerals.

These intervals are almost inert to the effects of pressure and temperature as they were probably formed under special thermodynamic conditions. It can be assumed that the minerals here and now are under a permanent stress of a preferred orientation.

These features have some effect also on the formation of the underlying region No. 5, which is also a "real structural" one and has the lowest velocity values. Basically this interval is characterized by gneisses, middle, fine-grained and gneiss-like granites with weak contacts between the grains. It is characterized by high mechanic anisotropy and sufficiently strong inhomogeneous residual stresses. It may be assumed that these rocks have been in different thermoelastic fields. It is possible that they were under the effect of significant heat and their structure is very faulty, they show high compressibility, low plasticity and weak elasticity. Several mineral formations in the region No. 5 are already affected by the increasing temperature and pressure with the depth.

Assuming that the general hydrostatic pressure here is reduced by non-hydrostatic stresses, a significant temperature effect must have been present, resulting in a general decrease of the elastic parameters.

It should be noted that this knowledge is not sufficient for the analysis of the elastic parameters and state of rocks at greater depths. For example at a depth of 3.5–4.0 km the pressure can be as high as 100 MPa which undoubtedly influenced the physical-mechanical characteristics of the minerals. This has been supported by experiments carried out at high P and T , corresponding to depths around 25 km.

Experimental II. (Thermodynamic Investigations)

At first the elastic behaviour of the borehole rocks in the experiments carried out at high hydrostatic pressure will be discussed. The results for v_p and $v_s = f(P)$ are shown in Figs 2 and 3. For the majority of porphyroblast migmatites in the pressure interval to 100 MPa (Fig. 2a) an intensive velocity increase (3–4 p. c.) can be observed, then between 1 and 5 kbar the further increase is only some 1.5 p. c. It should be noted that rocks with high initial v_p and v_s usually change only slightly (≤ 1.5 p. c.) with the increasing pressure. At 500 MPa the standard deviation of v_p and v_s is as low as 0.6–0.5 km/s in turn.

The behaviour of migmatites having low v_p and v_s is somewhat different. Up to 100–200 MPa the increase of v_p and v_s in migmatites is insignificant and at higher pressures (max. 500 MPa) they increase smoothly at an almost constant gradient, approximately $7 \cdot 10^{-4}$ km/s MPa.

The high pressure velocity variations in granites have a different character (Fig. 2b). For pegmatoid types a smooth increase can be observed till 400 MPa having an anomalous low dv_p/dp , approximately $4 \cdot 10^{-4}$ km/s MPa.

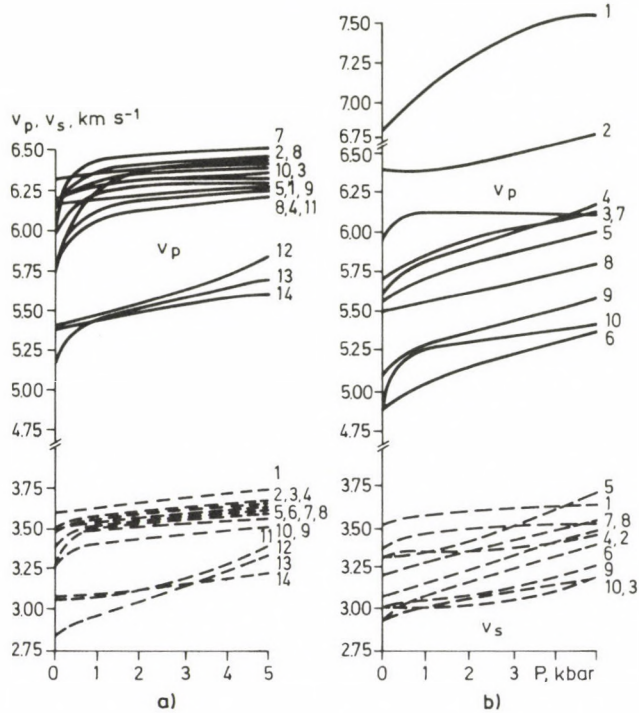


Fig. 2. Curves $v_p, v_s = f(P)$ of samples from different depths. a) porphyroblast migmatites (1–1170 m, 2–2061 m, 3–1250 m, 4–750 m, 5–2781 m, 6–1045 m, 7–416 m, 8–666 m, 9–1035 m, 10–930 m, 11–1505 m, 12–2111 m, 13–1962 m, 14–1594 m); b) pegmatoid granites (1–606 m, 2–695 m, 3–2906 m), middle- and coarse-grained granites (4–3188 m, 5–2855 m, 6–1707 m), gneiss-like granites (7–705 m, 8–1435 m, 9–2191 m, 10–2012 m). Full lines v_p , dotted lines v_s

In the pressure interval 0–100 MPa in fine-grained and middle-grained granites an intensive velocity increase can be seen, which is continued at higher pressures. Velocities in the gneiss-like granites change in different ways (Fig. 2b). The velocity changes in the samples having high initial v_p and v_s are insignificant.

Other granite types exhibit a quite intensive velocity increase at pressures even beyond 100 MPa. For example in the pressure interval 50–500 MPa the values dv_p/dp and dv_s/dp are approximately $6 \cdot 10^{-4}$ km/s MPa. At high pressures the changes of velocity in biotite and garnet-biotite gneisses are almost the same: they are characterized by a wide range of v_p and v_s having a smooth increase (Fig. 3a). Dyke rocks (Fig. 3b) with high velocities at atmospheric pressure change only slightly at higher pressures.

Thus at depths of max. 3.5 km the most intensive changes of v_p and v_s take place in the low-velocity granite types of porphyroblast migmatites and gneiss-like granites while the weakest changes are observed in dyke formations and pegmatoid granites.

The highest deviations from the mean velocities are observed in middle- and fine-grained granites and gneisses. At greater depths these relations exhibit certain modifications due to the increasing temperature effect. Therefore, in order to determine the elastic state of rocks at great depths special experiments have been carried out simultaneously modelling the high quasi-hydrostatic pressure and temperature.

The experimental thermobaric conditions were produced by a regional program, which models the deep PT conditions in the Kirovograd block in the central part of the Ukrainian shield where the borehole is situated. The program of experiments (Fig. 4) was elaborated on the basis of the assumed temperature and density data (Lebedev 1975, 1977, 1980, 1981, Lebedev and Korchin 1979, Lebedev et al. 1974, Kruchenko et al. 1981, Kutas 1978). Many authors state (Lebedev 1975, Lebedev and Korchin 1979, Gzovsky et al. 1973 and others) that in the upper parts of the lithosphere, in the Earth's crust, in the majority of cases a non-hydrostatic pressure distribution can be observed due to several factors (tectonic stresses, temperature variations, hydrothermal processes *etc.*). Thus our model experiments were carried out at quasi-hydrostatic pressures in high-temperature chambers. Some features of the elastic properties for hydrostatic (P_h) and quasi-hydrostatic (P_q) pressures are illustrated in Figs 5 and 7 (curves 1'-4', 1''-4'').

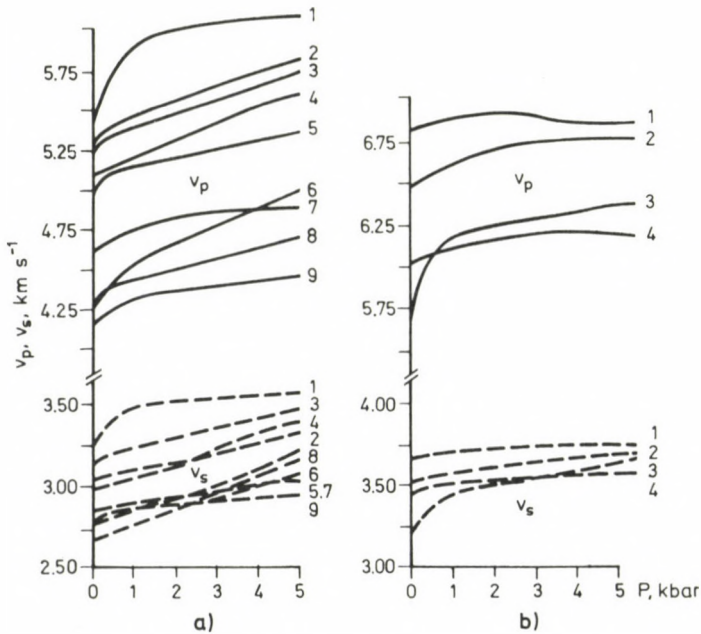


Fig. 3. v_p and v_s in the drill core samples as functions of hydrostatic pressure. a) gneisses (1-1932 m, 2-3479 m, 3-3320 m, 4-3456 m, 5-1804 m, 6-3100 m, 7-2301 m, 8-2980 m, 9-3220 m); b) dyke rocks (1-2063 m, 2-1370 m, 3-3362 m, 4-2131 m) Full lines - v_p , dotted lines - v_s .

A simultaneous effect of high pressure and temperature on the investigated objects results in a special variation of their elastic parameters (Figs 5–8). First of all it should be noted that the complex distribution of v_p , $v_s = f(PT) = f(H)$ is characterized by a series of experimental factors.

The relation for the migmatites is as follows: The lower the velocity at atmospheric pressures and the greater the change of v_p , $v_s = f(P)$, the more strongly expressed are the anomalous regions on the curves v_p , $v_s = f(H)$. The explanation for it is that the low velocity values are characteristic of rocks which are more defected and

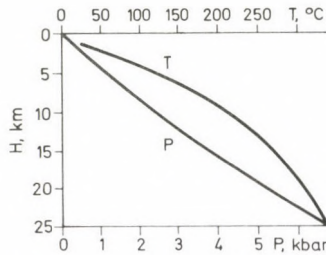


Fig. 4. Program of thermobaric model experiments for rocks from the central part of the Ukrainian Shield

composed of more components. At high temperatures and quasi-hydrostatic pressure the thermodynamic stresses in the samples are only partly compensated by the hydrostatic pressure resulting in additional microfractures in the mineral matter. In rocks of a perfect structure, and of a few components, these effects are slighter. According to the measured elastic parameters under different PT conditions (Fig. 6a, curve 1 and 2), low compressibility β and high plasticity sections (with increasing Poisson's ratio) correspond to the velocity maximum zones. The low-velocity zones are related to the rarefaction of the rocks (β increases) and to the transition towards a more brittle state (σ decreases).

In model conditions simulating simultaneous effects of pressure and temperature, the coarse-grained rocks (pegmatoid granites) show slightly different behaviour (Figs. 5,6). Here the temperature effect is maximum. At 60–80 °C and 100 MPa (corresponding to a depth of 3.5–4 km) a steep decrease of v_p and some moderation of v_s can be observed. At temperatures higher than 100 °C the velocity values are even lower than those of the same rock on the surface. Here at high temperature an anisotropic dilatation effect of rock-forming minerals clearly appears, which is not compensated by the simultaneous pressure increase. For example under thermobaric conditions corresponding to depths greater than 3.5 km, according to the measured Poisson's ratios it can be assumed that these formations lose their plasticity, although according to the initial values of σ they belong to highly plastic rock types. Their compressibility starts to increase due to the microfracturing, during the anisotropic dilatation of coarse-grained rock-forming minerals (Fig. 6, curves 3, 4).

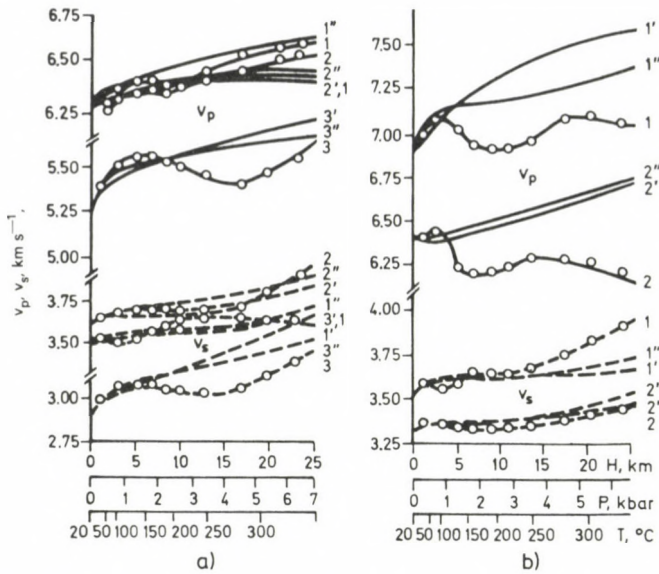


Fig. 5. Materials of PT model experiments. a) porphyroblast migmatites: 1-2781 m, 2-1170 m, 3-1962 m; b) pegmatoid granites: 1-606 m, 2-695 m 1''-3'' — hydrostatic pressure and 1'-3' — quasi-hydrostatic pressure at 20 °C. 1-3 — simultaneous effect of quasi-hydrostatic pressure and temperature

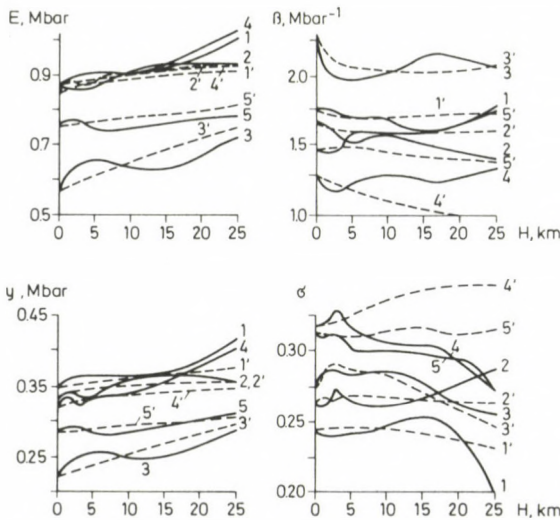


Fig. 6. Graphs of E , γ , β , $\sigma = f(PT) = f(H)$ Porphyroblast migmatites: 1-2781 m, 2-1170 m, 3-1962 m, pegmatoid granites: 4-606 m, 5-695 m. Isotherms 20 °C at P_h are denoted by dotted lines

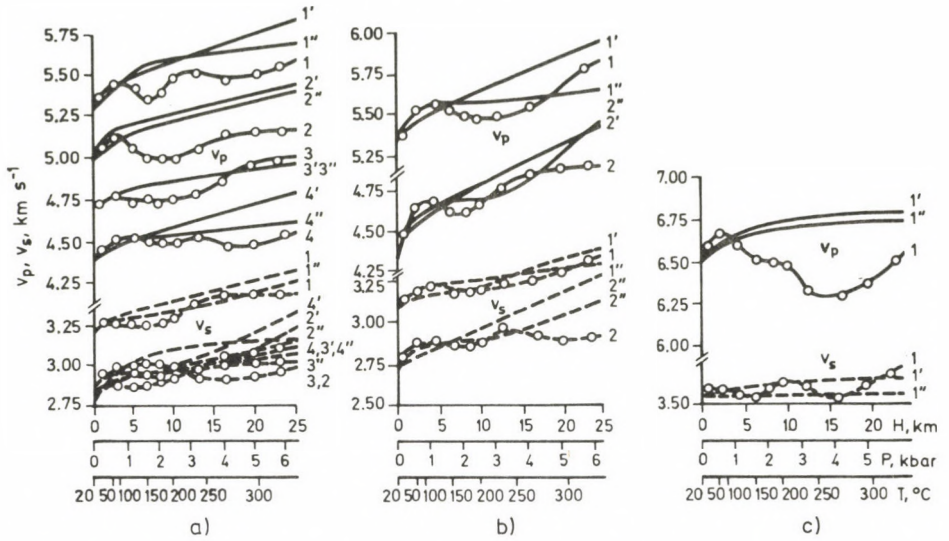


Fig. 7. Results of the programmed experiments: $v_p, v_s = f(PT) = f(H)$. a) biotite gneisses: 1–3320 m, 2–1804 m, 3–2301 m, 4–2980 m, b) biotite gneisses with garnet: 1–3479 m, 2–3100 m, c) picrite porphyrite: 1–1370 m. Other symbols are the same as in Fig. 5

In the high thermodynamic regions (at high pressure and temperature) mainly gneisses from great depths were investigated (Figs 7, 8). According to the atmospheric elastic properties, they belong to mineral formations with weak contacts between the grains due to their high biotite content or to special features of the state of contacts between rock-constituents during the process of their formation at depths greater than 3.0–3.5 km. For each of the investigated gneisses the following general relation has been found: small differences between v_p and v_s in the thermobaric experiments corresponding to depths of 3–5 km. A further “lowering” of the samples, i. e. increasing pressure and temperature corresponding to the program, results in extreme velocity variations (Fig. 7). On the curves some anomalous high- and low-velocity zones can be observed. According to Fig. 7 a decrease of v_p and v_s from their maximum values to their minima are almost the same for all of the gneisses and these values are 100–150 and 75–100 km/s in turn. Depth intervals of the first velocity reductions in gneisses are close to each other (7–10 km). In many cases a second decrease also appears (but already in the interval 15–17 km).

Elastic properties of gneisses under PT conditions corresponding to depths of 3–5 km change more intensively than those under pressure effect alone (Fig. 8). Here with increasing temperature the rocks usually are compressed more intensively. Functions $\beta = f(PT) = f(H)$ prove this effect. A temperature of 60–80 °C and a pressure of about 100 MPa ($H = 3.5$ km) results in plastification. Values of σ also increase. In addition, for a further increase of pressure and temperature, parameters E , γ , β and σ vary in a

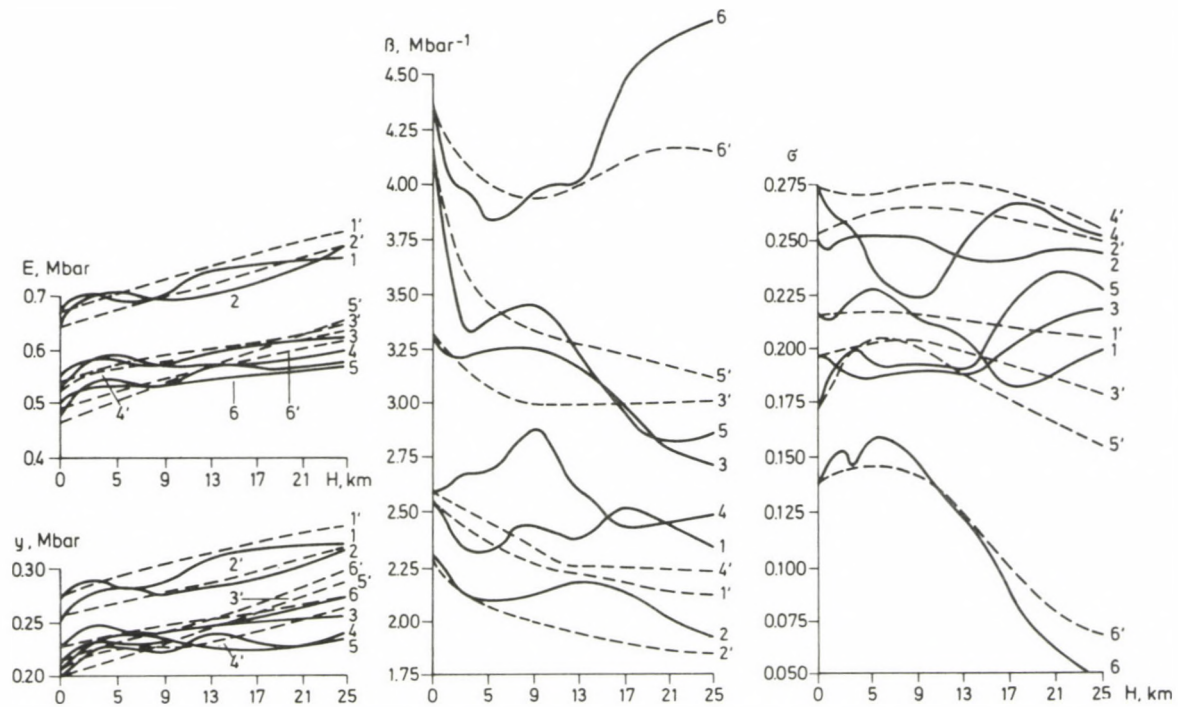


Fig. 8. Graphical functions of $E, y, \beta, \sigma = f(PT) = f(H)$. Biotite gneisses: 1-3320m, 2-1804 m, 3-2301m, 4-2980 m, biotite gneisses with garnet: 5-3479 m, 6-3100 m. Other symbols are the same as in Fig. 6

complex manner (Fig. 8). In the curves showing their relations with depth, maximum and minimum zones can also be observed, similarly to v_p and v_s . In these sections the rocks are more "incompact" (large β) and "brittle" (small δ). For gneisses the rarefaction can be as high as 0.1–0.2 p. c. of ρ_{max} , since $\Delta\beta$ is $0.8\text{--}0.5 \times 10^{-11} \text{ Pa}^{-1}$.

The curves $v_p, v_s = f(PT) = f(H)$ of the dyke rock sample—picrite porphyrite—in case of different PT conditions are also characterized by anomalous sections. The minimum zones can be observed at pressures and temperatures corresponding to depths 6.5 and 16 km, and a maximum can be found at 11 km. Heating of these rocks at high pressure results in their rarefaction and an increase of their brittleness (Fig. 7).

Conclusions and interpretations

On the basis of our experimental data and earlier papers (Lebedev 1975, 1977, Lebedev and Korchin 1979, 1982 and others) a model has been presented describing the crustal distribution of elastic properties in the investigated region for greater depths than that of the borehole. In the upper crust (max. 5 km) the elastic parameters (v_p, v_s, E, γ and K) change only slightly with depth. Their gradients depend first of all on the composition and structural-textural properties of mineral formations, on the character of the increase of pressure and temperature and on the general stress of blocks or rock masses. Maximum gradients are found in faulty fine-grained formations which are rich in high-velocity plastic minerals (plagioclase and amphibole). Elastic properties of unaltered coarse-grained rocks having perfect structure and quartz-rich formations, where significant inhomogeneous stresses are observed, increase more gently. This mineral is usually characterized by high v_p and v_s at atmospheric pressure. In this depth interval the temperature (max. 80 °C) has no significant effect on the elastic parameters. Here the pressure and additional stresses are dominant.

An intensive decrease of compressibility can also be observed due to their compaction (0.3–0.5 p. c.). This effect is the strongest for rocks with high quartz and biotite content and inhomogeneous stresses.

Let us now discuss the information content of Poisson's ratio (Lebedev and Korchin 1979, Lebedev et al. 1981). It can be assumed that in the investigated region (not deeper than 5 km) almost each rock strives at a more plastic state, with the exception of coarse-grained breeds having high proportion of brittle minerals, as quartz and garnet.

Taking into account that at depths greater than 5–6 km the rocks (especially in the separated large blocks with thicknesses of more than 5 km) differ from each other in their mineral composition by some 10–15 p. c. but they are close to each other in their genesis. On the basis of experimental data sections with anomalous changes in elastic property can be assumed. Most frequently these zones excel in their extreme (low or high) elastic wave velocities. They seem to be of thermodynamic nature—a result of

opposite pressure and temperature effects on the physical-mechanical state of the rock. High-velocity sections (also E , γ and K) evidently are due to pressure and low-velocity ones due to temperature. If the mineral has a complex structure, many components and an unequal distribution of internal residual stresses, the critical accumulation of the elastic energy and the following stress relaxation in forms of local microfractures can be repeated with a certain periodicity (Lebedev and Korchin 1979). The recurrence depends on the state of the material and on the regional gradient of the temperature and pressure. Such a fluctuation of the mentioned zones has been experimentally discovered by us and it has been illustrated in form of functions $v_p, v_s = f(PT) = f(H)$.

Therefore, in certain PT conditions which are characteristic of the Earth's crust in this part of the Ukrainian Shield, several low-velocity zones of thermodynamic origin can be separated. Especially, for the region of the borehole, the most likely depth interval is 7–12 km ($\Delta v_p \approx 0.10$ – 0.25 km/s and $\Delta v_s \approx 0.05$ – 0.10 km/s). They are in accordance with coarse-grained granites and migmatites and also with separated gneiss blocks. Low-velocity zones at depths 16–22 km can also be connected to granites, gneiss-like formations, picrite-porphyrites and diabases. Experimental data of samples from this borehole and from other regions of the Ukrainian Shield (Lebedev 1977, Lebedev and Korchin 1979 and others) support our assumption on the low-velocity thermodynamic zones at depths of 6–25 km, including the detectable zones by the seismic method ("Structure of the Earth's crust . . ." 1978, 1980, Kruchenko et al. 1981 and others). In these zones minerals are characterized by low elasticity, density, high brittleness (close to the critical value) and higher plasticity in the internal parts. These zones, whose existence is explained by thermodynamic reasons, could also be produced by changes of the mineral composition (Lebedev et al. 1979), though undoubtedly the effect of pressure and temperature corresponding to given depths represents considerable corrections for their position, size, intensity and contrast.

A complete interpretational approach to the drilling results, geological and geophysical field observations, as well as laboratory investigations of the elastic properties of rocks under different PT conditions furnished a better picture about the crust in the region of the borehole. Here, to the west of the Kirovograd deep fracture the upper part of the section is settled first of all by granitoides of the New Ukrainian Massif. To the east sedimentary-metamorphic formations of terrigenous composition are settled, having significant proportion of volcanogenic rocks in the lower part (Lebedev et al. 1983).

On the basis of the above-mentioned experimental investigations about the elastic properties of the core samples and relying on other papers (Lebedev 1975, 1977, 1980, Lebedev and Korchin 1979 and others), low-velocity seismic zones of thermodynamic origin have been found. According to the differences of composition in the western and eastern parts of the vertical cross section, these zones have to be found in different depths. In the region of the New Ukrainian Massif they are somewhat deeper than to the east. The low-velocity zone in the sedimentary-metamorphic

formations is narrower and broadens only near the deep fracture joining a similar zone (also broadening at the fracture) in the granitoides. The latter is related to the fact that in the region of the Kirovograd deep fracture interbedded migmatites, granites and rests of nongranitized biotite gneisses, altered by different effect can often be observed. In this part of the Earth's crust the low velocity zones are characterized by small Δv_p , and the gradient of the investigated mineral sometimes approaches zero. Such zones in the depth interval of 5–9 km are confirmed by seismic exploration (Kruchenko et al. 1981).

Assuming an Archaic formation of granulite facies at depths greater than 15–17 km, an analogous zone between 16 and 21 km can be expected. Results of our high-pressure and -temperature investigations about elastic properties of charnockites, several granites and middle-grained gneisses with high pyroxene as well as some other rocks of the region, can be used for forecast purposes (Lebedev and Korchin 1979). Depending on their composition and PT conditions the thickness of this zone must vary between 4 and 10 km.

Such extreme regions enable us to describe more exactly the nature of some seismic boundaries. One of them is between the Proterozoic and Archaic rocks associated with a high-velocity zone, confirmed by the functions $v_p = f(PT) = f(H)$ determined by a model for high pressures and temperatures (Lebedev et al. 1983).

Acknowledgements

The authors express their thanks to B V Polovinkin, V A Protsko, V I Shevchenko and V A Kruchenko for their valuable discussions on the experimental results and the geological and geophysical information.

References

- Gzovsky M V, Turchaninov I A, Markov G A et al. 1973: State of stress of the Earth's crust on the basis of data measured in mine openings and of tectonophysical analysis (in Russian). In: *State of stress of the Earth's crust*. Moscow, Nauka, 35–50.
- Kruchenko V A, Polovinkin B V, Tripolsky A A 1981: Deep structure of the Earth's crust in the central part of the Ukrainian Shield along the Deep Seismic Sounding Profile Nikolaev–Kiev (in Russian). *Geofizichesky Zhurnal, Ukrainian Academy of Sciences*, 3, 82–88.
- Kutas R I 1978: Heat flow fields and the thermal model of the Earth's crust (in Russian). Kiev, Naukova Dumka
- Landau, L D, Lifschitz E M 1965: *Theory of elasticity* (in Russian). Moscow, Nauka
- Lebedev T S 1975: Physical properties of rocks in the lithosphere at great depths (in Russian). In: *Problems of the physics of the Earth in the Ukraina*. Kiev, Naukova Dumka, 98–117.
- Lebedev T S 1977: Elastic properties of rocks under experimental conditions of high pressures and temperatures. *High Temperature—High Pressure*, 9, 705–706.
- Lebedev T S 1980: Model studies of physical properties of minerals in high-pressure-temperature experiments. *Physics of the Earth and Planetary Interiors*, 25, 292–303.
- Lebedev T S 1981: Current problems of experimental investigations of physical properties of minerals under thermobaric model conditions of the lithosphere (in Russian). In: *Physical properties of rocks at high*

- pressures and temperatures for the problems of seismology. (Proceedings of the 6th All-Union Meeting), Tashkent, Fan, 23–24.
- Lebedev T S, Korchin V A 1979: Dynamics of changes in elastic properties of rocks under varying P and T-conditions of the Earth's crust. In the International Monograph KAPG: *Theoretical and Experimental Investigations of Physical Properties of Rocks and Minerals under Extreme P and T-conditions*. Berlin, Akademie Verlag, 57–88.
- Lebedev T S, Korchin V A 1982: Connection of elastic rock properties with their mineral composition at high pressure (in Russian). *Geofizichesky Zhurnal, Ukrainian Academy of Sciences*, Kiev, 4, 42–50.
- Lebedev T S, Korchin V A, Shapoval V I, Lahtanov V T 1974: Method and instrument of simultaneous investigations of transverse and longitudinal wave velocities in rocks at high pressures (in Russian). *Geofizichesky Sbornik, Ukrainian Academy of Sciences*, Kiev, 58, 41–49.
- Lebedev T S, Shapoval V I, Korchin V A 1974: Programmed modelling of deep thermodynamic conditions in experimental investigations of elastic properties of minerals. *Gerlands Beiträge zur Geophysik*, Leipzig, 83, 340–346.
- Lebedev T S, Korchin V A, Vasilyaka V T 1976: Investigations of elastic properties of minerals under hydrostatic conditions at high thermodynamic parameters (in Russian). *Geofizichesky Sbornik, Ukrainian Academy of Sciences*, Kiev, 69, 26–34.
- Lebedev T S, Korchin V A, Shapoval V I 1977: Simultaneous investigations of longitudinal and transverse wave velocities in rocks and in minerals under various experimental PT-conditions (in Russian). In: *Investigation of physical properties of the Earth's minerals at high thermodynamic parameters*. Kiev, Naukova Dumka, 18–33.
- Lebedev T S, Korchin V A, Shapoval V I 1981: Poisson's Ratio of Minerals and its Informativity at High PT-regimes. *Gerlands Beiträge zur Geophysik*, Leipzig, 90, 58–64.
- Lebedev T S, Korchin V A, Burtny P A 1982: Elasticity and flexibility constants of several rock-forming minerals at high pressure (in Russian). *Geofizichesky Zhurnal, Ukrainian Academy of Sciences*, Kiev, 4, 18–28.
- Lebedev T S, Orischenko I V, Korchin V A 1979: A multi-variable regression analysis of laboratory data on the elastic rock properties at high PT zones, in connection with the study of the composition of deep zones of the Earth's crust (in Russian). *Geofizichesky Sbornik, Ukrainian Academy of Sciences*, 87, 49–57.
- Lebedev T S, Polovinkin B V, Korchin V A et al. 1983: Elastic properties of rocks from a deep borehole in the central part of the Ukrainian Shield and relationships of their changes under various thermobaric conditions of the Earth's crust (in Russian). *Geofizichesky Zhurnal, Ukrainian Academy of Sciences*, Kiev, 5, 10–25.
- Structure of the Earth's crust and the upper mantle in Central and Eastern Europe (in Russian). Kiev, Naukova Dumka, 1978, 272.
- Structure of the Earth's crust in Central and Eastern Europe on the basis of geophysical data (in Russian). Kiev, Naukova Dumka 1980, 208.

CHANGE OF ACOUSTIC ROCK PROPERTIES DUE TO DEFORMATION UNDER COMPLEX STATES OF STRESS

E I BAYUK¹ and N I DYAU¹

[Manuscript received May 3, 1985]

In this paper velocities and amplitudes of longitudinal elastic waves are studied for sedimentary, metamorphic and volcanic rocks at hydrostatic pressures and deformations due to complex states of stress.

In sedimentary and in metamorphic rocks the velocity and amplitude changes can serve as precursors of the rock fracture.

Keywords: acoustic properties of rocks; amplitude of elastic waves; elastic waves; hydrostatic pressure; rock fracture; velocity of elastic waves

Introduction

The importance of the investigation of velocity and amplitude changes of elastic waves as possible precursors of fracture formation in different states of stress was pointed out many times (Volarovich et al. 1979, Sadovsky 1975 and others). Although the published data on the changes of elastic rock properties, as a result of their deformation, are sometimes contradictory, such contradictions can be explained by the mineral composition and structure of rocks and by the experimental conditions.

In this paper the velocities and the amplitudes of longitudinal elastic waves are studied at hydrostatic pressures and deformations due to complex states of stress. Samples of various rock types were collected for this experiment: sedimentary (sandstone), metamorphic (amphibolites and gneisses) and volcanic rocks (basalts, andesites and dacites). The results for each rock type were generalized and they were compared for rocks of different types. All samples are from depths greater than 4 km, with exception of two sandstones, which were collected in outcrops.

The middle-grained sandstones are composed of detritus of 0.2–0.25 mm with angled-round forms. They are of some 70–75 p. c. of the whole rock mass, hardened by clayey minerals. The detritus is basically quartz, between the grains plagioclase, mica, detritus of microquartzites, micastate and other rocks can be found. The cement is

¹ Institute for Geology and Exploitation of Combustible Raw Materials, 117313, Moscow, Fersmana, 50

porous, with secondary carbonatic, coagulation features or coalescent quartz grains in some places. The texture is irregular.

The biotite-plagioclase gneisses are basically composed of biotite and plagioclase, sometimes of accessory aluminiferous minerals (staurolite, andalusite, sillimanite, granat) and rarely of amphiboles. The gneisses are unequally muscovitized and can be characterized by striation coinciding with the stratification which crosses the axis of samples at an angle of 45–60°. The thickness of the biotite-rich dark stripes is 1 to 4 mm.

The amphibolites are massive, they frequently show schistosity and biotitization and in some cases they are striped or appear in form of lens-like striped rocks. Their striation is due to thin amphibole embeddings in the homogeneous mass of amphibole-feldspar composition. There are also amphibolites of spotted structure, in association with porphyry blastes of granats. For the experiments the most homogeneous schistous amphibolites were selected.

The effusive rock samples were taken from boreholes that penetrated the metamorphic lava and tuff of moderate acidity (dacites) and average (andesites) composition. They are composed of plagioclase inclusions which were substituted to a considerable extent by carbonates, chlorites, sericites and partly of the basic mass of decomposed glass of fluidal structure. The glass in dacites is of acidic composition and the quantity of inclusions decreases to 5–10 p. c. There are more inclusions in andesites and in basalts (25–30 p. c.) and pyroxenes and amphiboles also occur.

Experimental

The complicated stress state experiments were carried out using the modernized UIMK equipment (Pavlova 1975), in which hydrostatic pressures up to 500 MPa and differential stresses up to 1500 MPa can be produced.

Cylinder-like samples of 16-mm diameter and 25-mm length were prepared in such a way that the cylinder axis coincided with the drilling core axis. The samples were hermetically sealed by a thin brass case and by the ultrasonic transducers on the separating surfaces.

The experiments were carried out in two stages: first a hydrostatic pressure was produced which was increased by 10 MPa steps. In the second stage at a given external pressure a compression stress along the axis was produced by means of the power cylinder of the equipment, and the deformation was increased till formation of principal fractures.

In both processes (hydrostatic pressure and complex state of stress) the propagation time of longitudinal waves in the sample and the amplitude of the first arrival were determined. The emitting frequency was 1 MHz and the observation error of the propagation time was less than 0.02 μ s. A complete electric equipment consisted of a G5–15 generator, a US–10 wide-band amplifier and an SI–70 oscillograph.

The deformations due to longitudinal and transversal stresses were measured by strain gauges glued on the samples by elastic adhesives and by recording potentiometers of type PDS-OIM or a digital voltmeter V7-21.

The velocity v in the equipment was determined on the basis of the deformation and the delay of the elastic wave propagation time. The amplitude of the first arrival was determined visually using an oscillograph.

Results

The petrophysical characteristics of the samples *viz.* density, effective porosity and longitudinal wave velocity were studied first under atmospheric conditions. Their intervals are shown in Table I.

Table I shows that the porosity of both the metamorphic and volcanic samples changes in a narrow interval from 0.9 to 3.18 p. c., while the porosity interval of metamorphic rocks is somewhat wider. The highest porosity values can be measured in sedimentary rocks and their K_p intervals are also considerably wide. The density values are typical for each rock (Volarovich 1978), only the higher upper limits for gneisses should be noted, which are related to highly aluminiferous minerals or amphiboles.

In sedimentary rocks high velocity values were observed at atmospheric pressure and at 120 MPa, probably due to the high density and hardness of the selected sandstones.

In metamorphic rocks the P-wave velocity at atmospheric pressure is very low. This is due to the inclination of several rock-constituent minerals to fracture formation during changes in the state of stress caused by external stress increase. The volcanic rocks having high proportion of glass are apparently less cracked and their P-wave velocity at atmospheric pressure is significantly higher and the scattering is less. At high pressures (120 MPa) a sudden velocity increase can be observed in metamorphic rocks

Table I

Density, effective porosity and longitudinal wave velocity of sedimentary, metamorphic and volcanic rocks under atmospheric conditions and at 120 MPa

Rock	Density ρ , g/cm ³		Porosity K_p , p.c.		Velocity v , km/s	
	ρ_{\min} — ρ_{\max}	ρ_{av}	$K_{p\min}$ — $K_{p\max}$	K_p	v_{\min} — v_{\max} 1 atm	v_{\min} — v_{\max} 120 MPa
Sandstones	2.36—2.66	2.59	3.4—11	6.4	3.4—4.4	4—5.6
Gneisses	2.63—2.83	2.70	1.7—3.2	2.3	2.5—4.9	5.8—6.5
Amphibolites	2.93—2.97	2.95	2.4—2.5	2.5	2.3—4	6.4—7.1
Basalts	2.76—2.78	2.77	1.0—1.4	1.2	5.9—6.1	6.1—6.4
Andesites, dacites	2.68—2.72	2.70	0.9—2	1.6	4.9—5.8	5.6—6.2

due to the closure of microfractures while the velocity increase is moderate in sedimentary rocks and volcanites. The velocity intervals at 120 MPa correspond to their mineral compositions.

The characteristics of the longitudinal wave velocity changes as a function of pressure can be clearly seen in Fig. 1, where typical curves for some metamorphic, volcanic and sedimentary rock samples are shown. A furcation of curves can be observed at high pressures as a function of basicity: the curve for amphibolite lies at the top, followed by curves representing the gneisses and volcanic rocks and the curve for sedimentary rocks is at the bottom. For volcanic rocks from top to bottom the curves for basalt, andesite, andesite-dacite and dacite are situated.

The sedimentary rocks are characterized by a non-monotonic velocity change as a function of pressure. The curves consist of an initial steep part and a consecutive section of moderate increase. This is due to the inhomogeneity of rocks, where the places of highly elastic minerals are filled with a soft, high-plasticity material.

In the metamorphic rocks the sudden velocity increase (30–170 p. c.) in the first section becomes slower in the interval 50–180 MPa. The slope of curves for amphibolites is usually greater than for gneisses what can be explained by some specialities of the longitudinal wave velocity change with pressure in the rock-constituent minerals — amphiboles and biotite (Bayuk 1981, Lebedev, Korchin 1983).

In this way, in case of hydrostatic pressure, significant differences in the longitudinal wave velocity change with pressure can be observed between sedimentary, metamorphic and volcanic rocks.

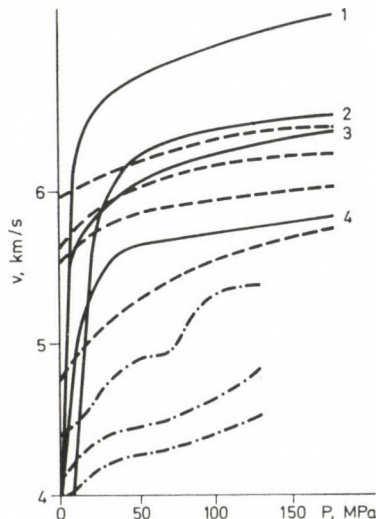


Fig. 1. Longitudinal wave velocity v as a function of the hydrostatic P for amphibolite (1), for biotite-plagioclase gneisses (2, 3, 4), for volcanic rocks (dots) and for sedimentary rocks (dash-and-dot line)

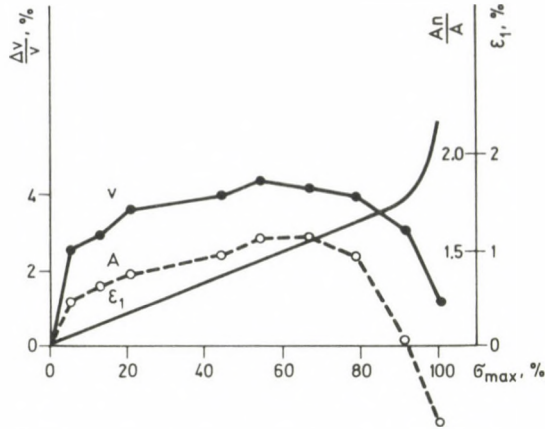


Fig. 2. The relative longitudinal wave velocity change $\Delta v/v$, the amplitude of the first arrival A_p/A and the deformation ε_1 as functions of the loading stress expressed in percentage of the maximal stress σ_{max} for a biotite-plagioclase gneiss

The effect of irreversible rock deformations on the acoustic properties were studied at 100–120 MPa external pressures.

In the investigated sedimentary rock samples the longitudinal deformation—due to pressures corresponding to the strength limit—changes from 2.5 to 8 p. c. and the irreversible (plastic) deformation—from 1.7 to 4.5 p. c. The longitudinal deformation of metamorphic rocks under these conditions was between 1.9 and 2.3 p. c., and that of volcanic rocks between 1.3 and 2.4 p. c. The irreversible deformation for metamorphic rocks proved to be somewhat greater (0.8–1 p. c.) than for volcanic ones (0.4–0.7 p. c.).

In complex states of stress longitudinal wave velocity and amplitude increments are in the elastic range. A microfracture formation process appears already in the elastic deformation range, preparing a main fracture (Volarovich et al. 1979). The microfracture formation is compensated by the appearance of microfractures, thus both elastic wave velocity and amplitude increase, although the velocity and the amplitude growths are different for different rocks.

The amphibolites and the gneisses have sharp velocity and amplitude increments already in the early stress state (5–15 p. c. of σ_{max}). The longitudinal wave velocity increases by 3–6 p. c. and the amplitude by 40–80 p. c. These values are higher in amphibolites than in gneisses (see Figs 2 and 3). The acoustic parameters continue to increase in the elastic range but in a more moderate manner.

In the transition toward the plastic deformation range, in metamorphic rocks a velocity decrease and in most cases an amplitude decrease occurs at stresses corresponding to 70–80 p. c. of σ_{max} . The intensity of the acoustic parameter changes increases near the strength limit. The plastic deformation is characterized by a

formation of microfractures not only in the crystals but between the grains too, when the separate fractures, spreading from crystal to crystal join. In the end a main fracture begins to form.

In sedimentary rocks, similarly to the metamorphic ones, a sharp velocity increase can be observed at the beginning of the deformation. A velocity maximum was obtained at 30–50 p. c. of σ_{max} , then, in the non-elastic range the velocity decreases

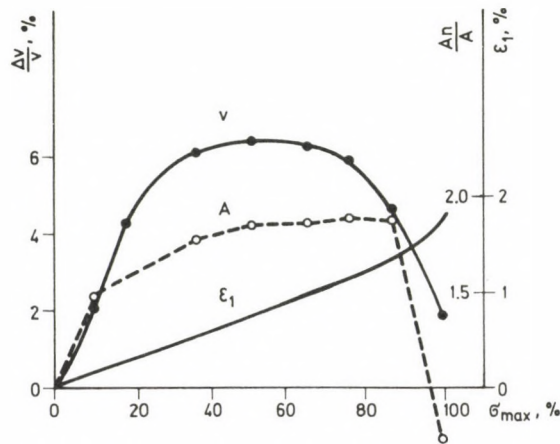


Fig. 3. The relative longitudinal wave velocity change $\Delta v/v$, the amplitude of the first arrival A_p/A and the deformation ϵ_1 as functions of the loading stress expressed in percentage of the maximal stress σ_{max} for an amphibolite

intensively. For several rocks the maximal-stress velocity was even less than its initial value. The longitudinal wave amplitudes always increased during the deformation process and this increase was more significant than in metamorphic rocks (see Fig. 4).

The volcanic rocks have some special features during the deformation process. First of all the velocity change is continuous and significantly weaker than in the other rock types, it has its maxima at stresses of 30–40 p. c. of σ_{max} (Fig. 5). A continuous change of the P-wave amplitude can be observed but its increase can be as significant as in the metamorphic rocks (Table II). In stress interval 40–80 p. c. of σ_{max} the volcanites are characterized by constant velocity and amplitude values. Frequently, the amplitude does not change or even increases before fracture. The velocity decreases at stresses corresponding to 80–90 p. c. of σ_{max} by 1.5–2.5 p. c. In Table II the intervals of longitudinal wave velocity and amplitude changes are shown for each of the investigated rocks at several fixed stress values, expressed in percentage of the maximal stresses i. e. the strength limit. Emphasizing the differences in the changes of the acoustic parameters for the three rock types, it should be noted that the anomalous velocity and amplitude changes can serve as precursors of rock fractures. In

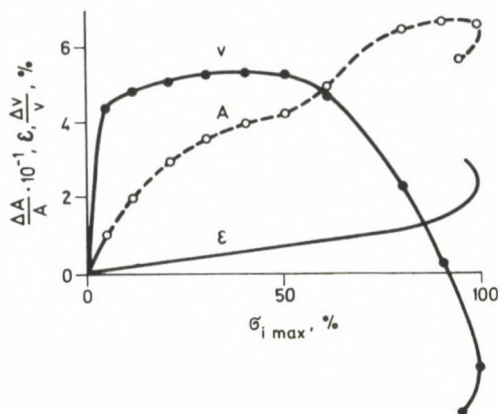


Fig. 4. The relative longitudinal wave velocity change $\Delta v/v$, the amplitude of the first arrival A_p/A and the deformation ε_1 as functions of the loading stress expressed in percentage of the maximal stress σ_{max} for a sandstone

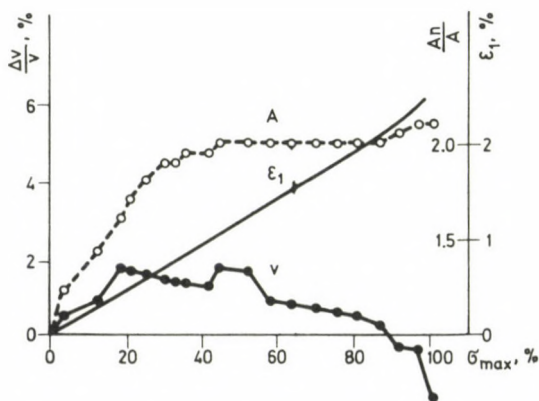


Fig. 5. The relative longitudinal wave velocity change $\Delta v/v$, the amplitude of the first arrival A_p/A and the deformation ε_1 as functions of the loading stress expressed in percentage of the maximal stress σ_{max} for a porphyry basalt

sedimentary and metamorphic rocks the precursors are more effective, as in sedimentary rocks the velocity has a drastic change before fracture and in metamorphic rocks both the velocity and the amplitude suddenly decrease. In addition, the longitudinal wave velocity change of 3–8 p. c. (in sedimentary and in metamorphic rocks) and the amplitude change of 30–70 p. c. (in metamorphic rocks) are considerably greater than the corresponding changes of 1.5–2.5 p. c. and of max. 20 p. c. in volcanic rocks.

Table II

Intervals $\Delta v/v$ and A_p/A in sedimentary metamorphic and volcanic rocks for different stress values expressed in percentage of ρ_{\max} at 120 MPa external pressure

Rocks	Parameter	20% σ_{\max}	40% σ_{\max}	60% σ_{\max}	80% σ_{\max}	100% σ_{\max}
Sandstones	$\Delta v/v, \%$	5—7	6—8	5—6	2—4	1—(-3)
	A_p/A	1.3—1.4	2—2.1	2.5—2.8	3—3.3	3.5—4
Gneisses	$\Delta v/v, \%$	3.6—5.5	4—7	4.3—8	4—7.5	1—5
	A_p/A	1.4—1.7	1.5—2.2	1.6—2.4	1.2—2.7	0.6—2
Amphibolites	$\Delta v/v, \%$	3.5—6.5	6—7	6.5—8	5.5—8	2—4
	A_p/A	1.6—1.9	1.8—2.3	1.9—2.5	1.9—2.3	0.7—2
Basalts, andesites	$\Delta v/v, \%$	1—2	2—2.5	1—2.5	0.5—2.5	1—(-1)
	A_p/A	1.1—1.7	1.2—2	1.2—2	1.2—2	1.2—2.1
Dacites	$\Delta v/v, \%$	3—4.5	4.5—5.5	4—5.5	4—5.5	2.5—4.5
	A_p/A	1.6—2.2	1.7—2.2	1.8—2.3	1.8—2.4	1.8—2.6

Conclusions

1. Under hydrostatic pressure with a maximum of 120 MPa the metamorphic rocks (amphibolites, gneisses) are characterized by a significant and drastic longitudinal wave velocity increase of 30–170 p. c. The increments of these parameters in sedimentary rocks are less (18–25 p. c.), and those in volcanic rocks even less (5–20 p. c.) in accordance with the composition and structure of these rocks.

2. Rock deformations under external pressures of 120 MPa result in additional longitudinal wave velocity and amplitude increments in the elastic range. The smallest increments were measured in basalts and andesites.

3. In the nonelastic deformation range, in metamorphic rock sudden velocity and amplitude decreases can be observed (3–5 p. c. and 30–70 p. c. in turn), while the sedimentary rocks have a velocity decrease of 5–8 p. c. These phenomena can serve as promising precursors of rock fracture.

References

- Bayuk E I 1981: Elastizitätseigenschaften der Minerale bei hohen Drucken. *Gerlands Beiträge zur Geophysik*, 90, 363–372.
- Lebedev T S, Korchin V A et al. 1979: Elastic properties of some rock-forming minerals and mineral matter deformations at high hydrostatic pressure. In: *Physical properties of rocks and minerals under extreme PT conditions*. Akademie Verlag, Berlin, 31–41.
- Pavlova N N 1975: Deformation and reservoir properties of rocks (in Russian). Moscow, Nauka
- Sadovsky M A 1975: Physics of the epicentre of earthquakes (in Russian). Edited by Sadovsky M A, Moscow, Nauka
- Volarovich M P, Tomashevskaya I S, Budnikov V A 1979: Rock mechanics at high pressure (in Russian). Moscow, Nauka
- Volarovich M P 1978: Handbook of physical properties of minerals and rocks at high pressure (in Russian). Edited by Volarovich M P, Moscow, Nedra

Book reviews

H MILLITZER and F WEBER eds: *Angewandte Geophysik Band II. Geoelektrik-Geothermik-Radiometrie-Aerogeophysik*. Akademie Verlag Berlin, Springer Verlag Wien-New York 372 pp, 208 figs, 44 tables

In the series of textbooks published by the staffs of universities in the GDR (Freiberg) and in Austria (Leoben, Wien) this is the second volume dealing with geoelectricity, geothermics, radiometry and aerogeophysics. The main emphasis is laid on geoelectricity in accordance with its role in geophysical prospecting. The first half of the book covers topics under this heading. The next two sections on geothermics and radiometry are included into roughly one fifth of the volume each and aerogeophysics is represented by some selected chapters in a short closing section.

The great development in the interpretation of geoelectric methods with the advance of computerization is well reflected. Traditional processing is only mentioned to illustrate the possibilities of the different methods. There is a wide range of instruments and methods available for specific purposes which are described in this textbook. It is, however, to be noted that just the selection of the most powerful and therefore the best fitted method for any purpose is not promoted for the students to enable the best choice. Practical examples are given to help such a selection, but some discussion about the capacities of the different methods would be more helpful. This could be realized by omitting some methods in order to enable a detailed description of others as e.g. the two and a half pages devoted to magnetotellurics including more than half page of a table on the spectrum of electromagnetic waves in the Earth's environment is hardly sufficient to understand the point of the method and just here nothing is said about computerized processing. Anyway, the introductory theoretical discussion is very clear and comprehensive.

Geothermics and radiometry are treated apparently in more details than geoelectric methods and there are straightforward descriptions of the main points of their use in applied geophysics including again well selected practical examples both from the GDR and Austria together with case histories from the corresponding literature. The aerogeophysical section includes some examples for several possible airborne methods.

There are not to many misprints in the book. Some of them are already corrected on correction sheets in the book.

The common textbook series of Akademie Verlag and Springer will be supposedly for a rather long time the basic source of information for German-speaking students of applied geophysics.

J Verő

J ZAMBÓ: *Fundamentals of mining engineering*. (A bányaművelés alapjai.) Akadémiai Kiadó. Budapest. 1985. P. 162.

Following the Analysis of mining location (Bányászati telepítések analitikája) published by the Műszaki Könyvkiadó in 1966 and the Optimum location of mining facilities published by the Akadémiai Kiadó in 1968 — just to mention his books published by Hungarian publishers and in this field only — Professor J Zambó, ordinary member of the Hungarian Academy of Sciences contributed with a new book to the thesaurus of Hungarian technical literature. The Author is the founder of the school of the analytical mining engineering and his latest book can be regarded as a summing and synthesizing work of the results of his investigations in this field.

The book deals with the spatially and economically most suitable and effective, or, optimum

location of — primarily underground — facilities indispensable for the extraction of minerals, i.e. for mining. In doing that, it takes into account the conditions of the environment where these facilities have to be located and, for a fairly long period of time, safely and economically operated.

These “environmental properties” are much more complicated and complex, and are subject to more restrictions in mining than in any other producing branch of industry, and, in addition, they are mainly unknown when opening and development begin. Location of mineral deposits in the Earth's crust was determined during geological times by an “unpredictable” co-effect of genesis, transport and metamorphism of minerals influenced by various factors. Thus every deposit represents an individual case and apart from types grouped on the basis of a few common characteristics, we may come across numerous deposits belonging to none of the groups. The effective working of these deposits with widely varying geometry and physical properties can be carried out on the basis of the principles and their practical application laid down by the Author in his book which can be used as objective tool in designing opening, development and working. Basically, there are four such principles, *viz.*

(i) the cost of material and personnel transport be minimum;

(ii) production capacity and the extension of the mine panel — if they can be freely selected — be optimum, expressed by the minimum of the correlated costs;

(iii) the main underground routes taking into account the physical-mechanical properties of the rocks, have to be arranged in such a way as to ensure minimum construction and maintenance costs;

(iiii) the underground opening and development — level height, place and distance of cross-cuts etc. — be optimum.

To the most general principles formulated in points (i) to (iiii), further, similarly important theorems can be added. Thus alternative solutions can often be considered from among which the person or institution in charge of making decisions can select by taking into account other, less quantifiable circumstances.

The book deals with the theme in six chapters.

Chapter I. looks at the collection of spatially distributed masses movable on freely selected or forced trajectories — to ensure an optimum point of collection by minimizing work of mass transport. The numerical-graphical method of solution is easy to “mechanize”.

Chapter II. deals with the optimum location of shafts and panels, as well as main cross-cuts and

main haulageways. Cases of free selection and various restrictions can be found in this chapter too.

Chapter III. analyzes the mining cost function, the return of investment and the coefficient of economic efficiency.

In Chapter IV. the Author investigates the optimum production capacity of mines and coal-burning electrical power plants. Special consideration is given to the problem of interests and simple interest is recommended since in his previous work the Author has proved that the principle of the interest does not hold in practice.

Chapter V. contains the planning of opening and development, and deals with thick and multiple seams in a separate subchapter.

Chapter VI. investigates some of the special problems of mine ventilation: ventilation systems and — probably for the first time in technical literature — air escapes. Harmony between mechanical cutting and transport at faces is investigated in great detail for complexly mechanized workings. Finally, some problems concerning roof control in drifts are analyzed.

It seems suitable to start the general evaluation of the book by stating that it justifiably bears the title “Fundamentals of mining engineering” since, undoubtedly, physical and economic principles of mining engineering are amalgamated into a unified and homogeneous system in it. Whatever method of extraction is adopted to a mineral deposit (deep mining, open pit mining or borehole mining), materials have to be transported in underground roadways and on attached surface roads, *viz.* useful products, waste, water, slurry, air electric current, personnel etc. Spatially distributed mass and the set produced by concentrating it in various distinguished points can be regarded as one (or more) density fields. The model is, therefore physical and by no means geometrical, as it used to be regarded so often and by so many. This gives the physical principles of mining engineering.

Another side of the “fundamentals” which cannot be separated from the first one is obviously the cost or price of work of transporting masses. Therefore, the other projection of the “fundamentals” is the economy of mining engineering. On the one hand, mining is materials producing process and on the other, and just for that, it is an economic activity too. Minimizing or optimizing work results at the same time in optimizing efficiency and economy.

The book is not an easy reading: some places require concentrated attention, but its clean logic and the precise drafting make studying it enjoyable. Like all of Zambó's papers and books, this one also

analyzes each problem by starting from the simplest case and gradually approaching more complicated systems. The initial thoughts of each topic (chapter) seem natural and even axiomatic: consecutive analyses are developed from them. Numerical examples and, especially, the great amount of figures (144 of them on 162 pages!) provide a tremendous help. Figures have a special function: they not only illustrate the text, but also supplement or, in some cases, replace it. This contributes to making the book so elegantly concise.

Since transport of great amounts of masses on freely selected or fixed routes is no speciality of mining only, all researchers and designers concerned with problems of various fields of science and branches of industry can benefit from studying the book, who have the task of selecting the optimum solution for the transport of great amounts of masses in cases when the transport routes can be freely selected or when the optimum solution has to be determined by taking into account restricting conditions.

F Martos

A D MIALI: *Principles of Sedimentary Basin Analysis*. 1984. 387 figs XII, 490 pages. 1415 g
Cloth DM 120,—; approx. US \$ 44.80 Berlin—Heidelberg—New York—Tokyo: Springer—Verlag ISBN 3—540—90941—9

The principal aim of this book is to outline the elements of a completely new stratigraphy which is nowadays far from being a descriptive art. It represents a *mature science* "based on the most fundamental understanding of global sedimentary and tectonic processes". This modern stratigraphy is strongly supported by five revolutionary changes in sedimentary geology beginning gradually in about 1960, such as "facies models", "depositional systems" method, "seismic stratigraphic techniques", "plate tectonic theory" and "chronostratigraphy" including radiometric dating technique and magnetic reversal stratigraphy.

The author, coming from "the fertile academic climate of University of Toronto" lays the emphasis on "what a geologist can actually see in outcrops, well records and cores, and what can be obtained using geophysical techniques".

The book consists of the following chapters:

- Chapter 1 Introduction
2 Collecting the data
3 Stratigraphic correlation
4 Facies analysis

- 5 Basin mapping method
6 Depositional systems
7 Burial history
8 Regional and global stratigraphic cycles
9 Sedimentation and plate tectonics
10 Conclusions

In the conclusion Miall reviews *the structure of the book* and reemphasizes some of his ideas. "The organization of the chapters is intended to reflect on increasing complexity of information". There is an enormous variety of combination of plate setting, stratigraphic architecture and depositional system. The author is able to touch only on a few but very important details about many basins around the world (chapters 8 and 9).

As is written in the Preface "It is intended that the book be used throughout a student's training and professional employment, and it should provide an important reference for graduate and undergraduate courses in stratigraphy, sedimentology, basin analysis, petroleum geology and mineral exploration".

This excellent work with its quality of high level is warmly recommended to those mentioned above.

A Ádám

R SIGL: *Introduction to potential theory*. Abacus Press in association with Herbert Wichmann Verlag 1985. 229 pages, 101 figures, 5 tables.

The book is a translation of German edition published in 1973. This valuable and very clearly written book presents the fundamental mathematical and physical topics necessary for studying physical geodesy, the determination of the earth's shape and the gravitational field.

In Part I the author discusses vectors which are an important and much used aid in forming and presenting geometrical and physical relations, as well as performing a valuable service in potential theory and physical geodesy. Elementary operations with vectors are presumed to be known and consequently receive brief treatment. The section therefore centres around a detailed study of vector analysis. This comprises vector differentiation and integration as well as the operators derived from them. Integral theorems by Gauss and Stokes are dealt with in detail and a section on curvilinear coordinates has been added.

In Part II the attraction and potential of finite masses is discussed, whereby, in accordance with geodetic application, spatially bounded masses and surface distribution are emphasised. There is also a

very detailed treatment of integral theorems. A further section deals with the behaviour of the potential and its derivatives within the field-producing mass.

In Part III spherical harmonics are looked at through the power series development of the reciprocal distance of two points or of their potentials of attraction. One chapter deals with the important application of series development in spherical harmonics. The ellipsoidal harmonic functions in the last section are not identical to Lamé's functions; on the contrary, they are special harmonic ellipsoidal functions adapted to geodetic requirements.

In Part IV the author derives first uniqueness theorems and solutions of the three boundary value problems. Later Fredholm's linear inhomogeneous integral equations of the second type are presented as a means of providing a general solution.

The translation of the book into English was a very good idea. It will help all students and research workers of geodesy acquire more easily the theoretical basis of physical geodesy.

J Somogyi

E W GRAFAREND and F SANSONO eds: *Optimization and Design of Geodetic Networks*. Springer—Verlag, Berlin—Heidelberg—New York—Tokyo, 1985, 606 pages, 13 figures

The book reviews the current status of the use of mathematical optimization and statistics in the design of geodetic networks, based on lectures delivered by international experts for the Third Course of the International School of Advanced Geodesy, Erice, Italy. It deals with geodetic optimization in terms of different order design problems.

Chapter A (G Schmitt) gives a review on network designs including criteria, risk functions, design ordering.

Chapter B (P J G Teunissen) deals with zero order design. It presents the basic theory of generalized inverses which is necessary for solving systems of linear equations of arbitrary size. The datum problem is discussed and a general expression derived for S-transformations which allows one to transform from one datum to another. The relation with the theory of generalized inverses is also shown.

Chapter C (K R Koch) is devoted to first order design. It is focussed on free networks only, i. e. networks for which the datum has to be defined. Thus the properties of these networks, especially the

dependence of the covariance matrix of the estimated coordinates on the choice of the datum are reviewed. Estimable coordinates for the free nets are obtained by means of projected parameters and it is shown that these projections also give the transformations between different datums.

Chapter D (G Schmitt) deals with second order design. It is focussed on the problem of the choice of the weights to be given to the various possible observations in the network in order that the estimates of the coordinates exhibit prefixed statistical properties. Since the weights of the observations can be considered to be largely dependent on the number of repetitions, the second order design techniques can also be used to solve that part of the first order design problem concerned with the existence of certain connections between nodes.

Chapter E (G Schmitt) gives a review of third order design. The third order design has been defined as the problem of improving, extending or densifying an existing network in an optimal way by introducing additional points and additional observations.

Chapter F (P A Cross) deals with numerical methods in network design. The economy of any design procedure is largely dependent upon the numerical methods employed. Some more important numerical methods are reviewed.

Chapter G (D Fritsch) gives some additional information about the capacity of the linear complementarity algorithm. Practical applications complete theoretical insights for better understanding how to use the algorithm not only in optimization problems but also from a more general point of view coming from approximation theory.

Chapter H (W D Schuh) deals with quick computation of geodetic networks using special properties of eigenvalues. The principle of the iterative methods is shown. Especially the conjugate gradient method is described. Afterwards a method is presented which enables a quicker and more reliable computation.

Chapter I (D Delikaraoglou) is focussed on estimability analyses of the free networks of differential range observations to GPS satellites. Rank defect situations are reviewed here for the geometric mode. Rank deficiencies in the differential GPS observational equations have also been analyzed.

Chapter J (A Dermanis) deals with optimization problems in geodetic networks with signals. The presence of signals in the adjustment of geodetic observations, in connection with the problem of how to treat them in the adjustment, does not allow the direct formulation of the standard optimization problems which have been developed for geodetic

networks without signals. In this part an attempt is made to look into the problems of network optimization arising from the presence of signals.

In Chapter K (H Sünkel) deals with Fourier analysis of geodetic networks. It consists of two parts. The first part provides a smooth introduction into spectral methods by investigating various interpolation methods, the second part is almost entirely the work of P Meissl.

Chapter L (E W Grafarend and F W Krumm) is focussed on Continuous networks I. Criterion matrices are constructed from continuous networks being observed by signal derivatives of first and second order. The method of constrained least squares leads to differential equations up to fourth order, to characteristic boundary values and constraints according to the datum choice. In detail the transformation of a criterion matrix into a network datum and its comparison with the variance-covariance matrix is presented.

Chapter M (B Benciolini) deals with Continuous networks II. The theory of continuous geodetic networks is a powerful tool to study the error propagation. The discrete least square principle must be interpreted as a discrete approximation of a continuous variational principle.

Chapter N (E W Grafarend) reviews the deformation measures and their finite element approximation, the datum problem in estimating deformation measures, the criterion matrices for deforming networks and the datum transformation of a criterion matrix.

Chapter O (F Crosilla) deals with an original method for constructing a criterion matrix for deforming networks. This consists of the contraction of the eigenvalue spectrum and the rotation of the eigenvectors of a covariance matrix relating to a displacement point coordinate vector.

Chapter P (F Sanso) is focussed on the analysis of time series with applications to geodetic control problems. The problems related to the estimation of the covariance and spectral density functions are discussed. The classical theory of forecasting is presented by using a more update mathematical language. It shows the construction of a particular class of stochastic models, namely the autoregressive-moving average models.

Chapter Q (P J G Teunissen) deals with the quality control in geodetic networks. Generally one can consider the quality of a network design to be made up of three factors: economy, precision and reliability. Economy expresses the costs of observation; precision as expressed by the posteriori covariance matrix of the coordinates, is the measure of the network characteristics in propagating

random errors and reliability describes the ability of the redundant observations to check model errors.

Chapter R (B Schaffrin) deals with aspects of network design. Several aspects of network design are investigated in more detail, among them the datum problem for criterion matrices, the additional consideration of reliability constraints, the solution of design problems via the complementary algorithm, and the transformation of the third order design problem for Gauss-Markov models into a second order design problem for mixed models.

The book is well illustrated with numerous figures and tables. A list of references is given at the end of each chapter. As a handbook this work may be useful to students and research workers and it is a welcome addition to the literature.

J Somogyi

P J G TEUNISSEN: *The geometry of geodetic inverse linear mapping and non-linear adjustment*. Netherlands Geodetic Commission, Publications on geodesy, volume 8, number 1, 1985, VII + 177 pages, 33 figures.

This publication gives a contribution to the theory of geodetic adjustment. In geodesy it is very common to use geometric reasoning. In fact, geodesy benefited considerably from the development of the study of differential geometry. At the present differential geometry can be said to constitute an essential part of both mathematical and physical geodesy. Also in geodetic adjustment theory, adjustment was soon considered as a geometrical problem. More recently we witness a renewed interest in the geometrization of adjustment theory (e. g. introduction into geodesy of the modern theory of Hilbert spaces).

The two main topics discussed are:

1. the problem of inverse linear mapping
2. the problem of non-linear adjustment.

After introduction, Chapter II deals with the theory of inverse linear mapping. Many problems in physical science involve the estimation or computation of a number of unknown parameters which bear a linear relationship to a set of data. The data may be influenced by random and systematic errors. That is the case in geodesy too. The fact that data are generally only measured at discrete points, leaves one in geodesy with the problem of determining a continuous unknown function from a finite set of data. This problem is described in terms of a possible inconsistent and undetermined linear system. It is shown that every inverse of a given linear map can

be uniquely characterized through the choice of three linear subspaces.

Chapter III elaborates the consequences of the linear mapping problem for planar, ellipsoidal and three-dimensional geodetic networks. For various situations there are constructed sets of base vectors for the nullspace of the designmap. The chapter is concluded with a discussion on the problem of connecting geodetic networks. Three alternative methods of connection are discussed under fairly general assumptions concerning the admitted degrees of freedom of the network involved.

Chapter IV treats the problem of non-linear adjustment. After a general problem statement and a brief introduction into Riemannian geometry, the

local convergence behaviour of the Gauss iteration method (GM) is discussed. A differential geometric approach is used throughout. It is shown that the local behaviour of GM is asymptotically linear. Next some conditions are discussed which assure the global convergence of GM. The remaining part of the chapter gives some suggestions as how to estimate the extrinsic curvatures in practice. The chapter is concluded with a brief discussion on some problems which are still open for future research.

The publication is very clearly written, it deals with interesting and up-to-date problems and so will be useful to research scientists.

J Somogyi

In memoriam Professor ANTAL TÁRCZY-HORNOCH,
Member of the Hungarian Academy of Sciences

It had been just three months ago that we celebrated Professor Tarczy-Hornoch on his 85th birthday. Now we have the grievous task to announce his death on January 16, 1986. In him, we have lost an outstanding personality of geosciences in Hungary and abroad. He was well known all over the world. His scientific activity covered the fields of mine surveying, geodesy and geophysics, and he published important results from the history of these scientific fields, too.

Professor Tarczy-Hornoch was born on October 13, 1900 in Oroszvég, in county Bereg of the then Upper-Hungary. After the primary schools there, he continued the studies in the grammar school of Munkács. Afterwards he spent one year with the signal corps in St. Pölten. In 1919 he started to study at the Bergakademie in Leoben, and got his diploma as mining engineer in 1932. In 1924, he obtained his Dr. techn. with a thesis entitled "Neue Gesichtspunkte zur rechnerischen Lösung der Markscheideraufgaben". He worked with Professor Aubell as assistant, and presented his habilitation thesis "Das Verwerferproblem im Lichte des Markscheiders". Prior to this procedure he was appointed to the chair of surveying and mine surveying at the high school of mining, metallurgy and forestry in Sopron, Hungary. He married in 1928 Irén Tarczy and supplemented his original name Hornoch to Tarczy-Hornoch.

He started his educational activity at the high school in Sopron with great competence and at a high level. He proposed the publication of a foreign language journal, "Aus den Mitteilungen der Berg- und Hüttenmännischen Abteilung an der kgl. ung. Palatin-Joseph-Universität für technische und Wirtschaftswissenschaften Sopron, Ungarn". The first number was issued in 1929 with him as editor. He presented many of his results in this journal. The same journal has enabled that the high school, (from 1934 a Technical University) could carry out an international exchange of publications in all parts of the world, including the Soviet Union, too, already at the beginning of the thirties. The success of the Mitteilungen has shown that the Sopron University is worthy of the traditions of the world famous Selmec Mining Academy, and the name of Sopron got known in the world of mining, too. The Soviet connections of the university contributed to the fact that the buildings were only very shortly requisitioned by Soviet military organs in 1945, and education and research could be started already in autumn of the same year.

Professor Tárczy-Hornoch's activity developed to the highest level in the years following World War II. He was elected corresponding, and in the same year (1946) ordinary member of the Hungarian Academy of Sciences for his work in mining survey, geodesy and geophysics. He initiated the education of surveying engineers in 1949, then that of engineers in geophysics in 1951. It was also his proposal to create in Sopron the Geodetical and Geophysical Research Laboratories of the Hungarian Academy of Sciences for basic research in these fields, and he was the first director of the Geodetical Laboratory. In 1957 he took over the Geophysical Laboratory, too. He led the university chair till 1959, when the university was transferred to Miskolc (mining) and Budapest (surveying), respectively. He was the director of the two laboratories till retirement in 1972.

He was awarded several times for his educational and research activities, including the golden Kossuth-prize, the 1st class of State Prize, the Golden class of the Work Order etc. He was awarded also by foreign countries; in Bulgaria, he obtained the 1st class of the Cyrill and Method Order, he was a member of the World Academy, corresponding member of the Austrian, Bulgarian, French and Polish Academies of Sciences, honorary doctor of the Freiberg, Graz, Leoben, Miskolc, Sopron and Vienna universities. He played a significant role in the international scientific community as chairman of the Hungarian IUGG Commission where he represented the interests of his discipline and of his country at a very high level. He brought several scientific meetings to Hungary. He played a leading role in Hungarian technical life; he was awarded by the highest medals of the Hungarian geophysical, surveying, mining and measurement technical societies.

He was very fond of the town Sopron; it was his second home after the birthplace. The local leaders appreciated his achievements, and in addition to the Pro Urbe-medal, he got the highest award of the city: he was elected a Honorary Citizen.

He was Editor in Chief of *Acta Geodaetica, Geophysica et Montanistica* for twenty years, and a member of the editorial board of journals like *Geoexploration* (Amsterdam), *Gerlands Beiträge zur Geophysik* (Leipzig), *Pure and Applied Geophysics* (Basel and Stuttgart) and *Monographs on Terrestrial, Solar and Cosmic Physics* (Leipzig).

His scientific publications cover the fields of geodesy and surveying, mine surveying, geophysics and history of these branches; he is author of six books (one of them together with Professor Hristov of Bulgaria, another with Professor Hazay). The number of his scientific papers in books, journals and other publications is above 300 in more than 50 journals of 15 countries, and he is referred to in several hundred books and other publications.

As a teacher he was hard to please, nevertheless he educated to enthusiasm for the profession. He promoted the help to poor students in the difficult times after the war to enable them university studies. He had chosen his staff with a good hand, many of them reached later leading positions. The school he created at the university became

known everywhere. He gave a good example in national and international cooperation. He was led by the idea that the language of science is capable to surmount all difficulties and it is a link between peoples and countries, irrespective of nationality, ethnic groups and political ideas. He demanded the same arduous and diligent work from his staff as from himself. He meant that on the long run only honest work can bring fruits. Geodetic and geophysical researches initiated by him developed to a research centre in Sopron with a wide net of observatories. Many of his coworkers are in his former institute and try to educate a new generation to be fond of geosciences. His connections to the institute were close till his very last days.

Two generations of Hungarian geoscientists commemorate Professor Tarczy-Hornoch, the internationally known scientist, the excellent teacher. We shall preserve his memory and transmit his ideas to future generations.

J Somogyi

Chronostratigraphie und Neostratotypen Band VII Miozän der Zentralen Paratethys

Wissenschaftlicher Redakteur:

Prof. Dr. A. PAPP

Rezensent:

Prof. Dr. G. HÁMOR

In deutscher Sprache. 1985. 636 Seiten. 17×25 cm

Gebunden \$49.00/DM 137,—/£35.00

ISBN 963 05 3949 7

Die Stratigraphie gilt als das vielleicht wichtigste Systematisierungsgrundprinzip der geologischen Forschung und machte in den vergangenen 25 Jahren eine stürmische Entwicklung durch. Die Serie „Chronostratigraphie und Neostratotypen“, die auf Initiative von Ján Seneš (Tschechoslowakei) und Adolf Papp (Österreich) in der Organisation der Subkommission für Neogenstratigraphie der Internationalen Geologischen Union, unter breiter internationaler Zusammenarbeit, im Jahre 1967 begonnen worden ist, enthält die in der Erkennung der Bildungen der einzelnen Miozänstufen erreichten wichtigsten Ergebnisse, eine komplette Revision der Neogenstratigraphie Europas. Es sind bisher sechs Bände dieser Serie in der Edition des Verlages der Slowakischen Akademie der Wissenschaften erschienen.

Die Bildungen von pannonischem (unterpannonischem) Alter befinden sich größtenteils auf dem Gebiet Ungarns. Deshalb wurde dieser Band vom Verlag der Ungarischen Akademie der Wissenschaften in Betreuung genommen.

Der wissenschaftliche Redakteur des Werkes war Prof. A. Papp, Leiter des Lehrstuhls des Paläontologischen Instituts der Universität Wien. An der Arbeit nahmen 12 ungarische, 7 österreichische, 5 tschechoslowakische, 5 jugoslawische und 2 rumänische Fachleute teil. Das Buch behandelt die allgemeinen geologischen, paläogeographischen Kennzeichen, stratigraphischen Grundprofile, Fossilengruppen (Foraminiferen, Mollusken, Nannoplankton, Mikroplankton, Ostracoden, Silicoplaentinen, Diatomeen, Fische, Säugetiere, Palynoflora, Makroflora) der Pannonbildungen, ferner deren stratigraphische Bedeutung. 63 geologische Karten bzw. Profile, 24 Tabellen und 103 Phototafeln ergänzen den Band.

Die industriell-praktische Bedeutung des Werkes liegt darin, daß im Neogen und innerhalb des Neogens hauptsächlich in den pannonischen Entwicklungen bedeutende Rohstoffvorkommen (Kohlenwasserstoffe, Lignit, Wasser usw.) bekannt sind. So kann es außer von den sich mit diesen Bildungen befassenden Forschungsgeologen, Paläontologen und Hochschullehrern auch von Industriefachleuten als Handbuch ausgezeichnet benutzt werden.



AKADÉMIAI KIADÓ · BUDAPEST

- treble underlining: bold-face italics
- red underlining: Greek letters
- green underlining: script letters.

Rules for mathematical-physical notations:

- trigonometric, logarithmic, analytic symbols, symbols for units and functions are in roman type (not underlined)
 - letter symbols in mathematical and physical formulas, scalars, and subscripts of algebraic and physical quantities are in italics (underlined)
 - vectors, matrices, operators in probability theory are in bold-face roman type (double underlining)
 - tensors, operators and some special functions are in script letters (green underlining). These cannot be bold.
 - Greek letters (red underlining) cannot be bold or extra bold type (thus they cannot be used for vectors or tensors)
 - void upper lines e.g. for vectors
 - avoid possible confusion between o (letter) and 0 (zero), l (letter) and 1 (one), ν (Greek nu) and v , u (letters) etc.
 - explain ambiguous or uncommon symbols by making marginal notes in pencil
 - be careful about superscripts and subscripts
 - formulae must be numbered consecutively with the number in parentheses to the right of the formula. References in text to the equations may then usually be made by the number in parenthesis.
- When the word equation is used with a number, it is to be abbreviated, Eq. or Eqs in the plural
- the International System of Units (SI) should be used.

Authors are liable for the cost of alteration in the *proofs*. It is, therefore, the responsibility of the author to check the text for errors of facts before submitting the paper for publication.

3. *References* are accepted only in the Harvard system. Citations in the text should be as:

- ... (Bomford 1971) ... or Bomford (1971)
- ... (Brosche and Sündermann 1976) ...
- ... (Gibbs et al. 1976b) ...

The list of references should contain names and initials of all authors (the abbreviation et al. is not accepted here); for *journal articles* year of publication, the title of the paper, title of the journal abbreviated, volume number, first and last page.

For *books* or *chapters in books*, the title is followed by the publisher and place of publication. All items must appear both in the text and references.

Examples:

- Bomford G 1971: *Geodesy*. Clarendon Press, Oxford
- Brosche P, Sündermann J 1976: Effects of oceanic tides on the rotation of the earth. Manuscript. Univ. of Bonn
- Buntebarth G 1976: Temperature calculations on the Hungarian seismic profile-section NP-2. In: *Geoelectric and Geothermal Studies (East-Central Europe, Soviet Asia)*, KAPG Geophysical Monograph. Akadémiai Kiadó, Budapest, 561–566.
- Gibbs N E, Poole W G, Stockmeyer P K 1976a: An algorithm for reducing the bandwidth and profile of a sparse matrix. *SIAM J. Numer. Anal.*, 13, 236–250.
- Gibbs N E, Poole W G, Stockmeyer P K 1976b: A comparison of several bandwidth and profile reduction algorithms. *ACM Trans. on Math. Software*, 2, 322–330.
- Szarka L 1980: Potenciáltérképezés analóg modellezéssel (Analogue modeling of potential mapping). *Magyar Geofizika*, 21, 193–200.

4. *Footnotes* should be typed on separate sheets.

5. *Legends* should be short and clear. The place of the tables and figures should be indicated in the text, on the margin.

6. *Tables* should be numbered serially with Roman numerals. Vertical lines are not used.

All the illustrations should contain the figure number and author's name in pencil on the reverse.

Figures will be redrawn. Therefore the most important point is clearness of the figures, even pencil-drawings are accepted (with a duplicate).

Photographs and *half-tone* illustrations should be sharp and well contrasted.

If a specific reduction or enlargement is required, please indicate this in blue pencil on the figure.

The editors will send information to the first author about the *arrival* and acceptance of the papers. A galley proof is also sent to the first author for *correction*. Hundred *offprints* are supplied free of charge.

Periodicals of the Hungarian Academy of Sciences are obtainable
at the following addresses:

AUSTRALIA

C. B. D. LIBRARY AND SUBSCRIPTION SERVICE
Box 4886, G.P.O., Sydney N.S.W. 2001
COSMOS BOOKSHOP, 145 Ackland Street
St. Kilda (Melbourne), Victoria 3182

AUSTRIA

GLOBUS, Hochstadtplatz 3, 1206 Wien XX

BELGIUM

OFFICE INTERNATIONAL DE LIBRAIRIE
30 Avenue Marnix, 1050 Bruxelles
LIBRAIRIE DU MONDE ENTIER
162 rue du Midi, 1000 Bruxelles

BULGARIA

HEMUS, Bulvar Ruszki 6, Sofia

CANADA

PANNONIA BOOKS, P.O. Box 1017
Postal Station "B", Toronto, Ontario M5T 2T8

CHINA

CNPICOR, Periodical Department, P.O. Box 50
Peking

CZECHOSLOVAKIA

MAD'ARSKÁ KULTURA, Národní třída 22
115 66 Praha
PNS DOVOZ TISKU, Vinohradská 46, Praha 2
PNS DOVOZ TLAČE, Bratislava 2

DENMARK

EJNAR MUNKSGAARD, Norregade 6
1165 Copenhagen K

FEDERAL REPUBLIC OF GERMANY

KUNST UND WISSEN ERICH BIEBER
Postfach 46, 7000 Stuttgart 1

FINLAND

AKATEMINEN KIRJAKAUPPA, P.O. Box 128 SF-00101
Helsinki 10

FRANCE

DAWSON-FRANCE S. A., B. P. 40, 91121 Palaiseau
EUROPÉRIODIQUES S. A., 31 Avenue de Versailles, 78170
La Celle St. Cloud
OFFICE INTERNATIONAL DE DOCUMENTATION ET
LIBRAIRIE, 48 rue Gay-Lussac
75240 Paris Cedex 05

GERMAN DEMOCRATIC REPUBLIC

HAUS DER UNGARISCHEN KULTUR
Karl Liebknecht-Straße 9, DDR-102 Berlin
DEUTSCHE POST ZEITUNGSVERTRIEBSAMT Straße der
Pariser Kommune 3-4, DDR-104 Berlin

GREAT BRITAIN

BLACKWELL'S PERIODICALS DIVISION
Hythe Bridge Street, Oxford OX1 2ET
BUMPUS, HALDANE AND MAXWELL LTD.
Cowper Works, Olney, Bucks MK46 4BN
COLLET'S HOLDINGS LTD., Denington Estate Wellingbo-
rough, Northants NN8 2QT
WM. DAWSON AND SONS LTD., Cannon House Folkstone,
Kent CT19 5EE
H. K. LEWIS AND CO., 136 Gower Street
London WC1E 6BS

GREECE

KOSTARAKIS BROTHERS INTERNATIONAL
BOOKSELLERS, 2 Hippokratous Street, Athens-143

HOLLAND

MEULENHOF- BRUNA B. V., Beulingstraat 2,
Amsterdam
MARTINUS NIJHOFF B.V.
Lange Voorhout 9-11, Den Haag

SWETS SUBSCRIPTION SERVICE

347b Heereweg, Lisse

INDIA

ALLIED PUBLISHING PRIVATE LTD., 13/14
Asaf Ali Road, New Delhi 110001
150 B-6 Mount Road, Madras 600002
INTERNATIONAL BOOK HOUSE PVT. LTD.
Madame Cama Road, Bombay 400039
THE STATE TRADING CORPORATION OF INDIA LTD.,
Books Import Division, Chandralok 36 Janpath, New Delhi
110001

ITALY

INTERSCIENTIA, Via Mazzè 28, 10149 Torino
LIBRERIA COMMISSIONARIA SANSONI, Via Lamarmora 45,
50121 Firenze
SANTO VANASIA, Via M. Macchi 58
20124 Milano
D. E. A., Via Lima 28, 00198 Roma

JAPAN

KINOKUNIYA BOOK-STORE CO. LTD.
17-7 Shinjuku 3 chome, Shinjuku-ku, Tokyo 160-91
MARUZEN COMPANY LTD., Book Department, P.O. Box
5050 Tokyo International, Tokyo 100-31
NAUKA LTD. IMPORT DEPARTMENT
2-30-19 Minami Ikebukuro, Toshima-ku, Tokyo 171

KOREA

CHULPANMUL, Phenjan

NORWAY

TANUM-TIDSKRIFT-SENTRALEN A.S., Karl Johansgatan
41-43, 1000 Oslo

POLAND

WEGIERSKI INSTYTUT KULTURY, Marszałkowska 80,
00-517 Warszawa
CKP-I W, ul. Towarowa 28, 00-958 Warszawa

ROUMANIA

D. E. P., Bucuresti
ILEXIM, Calea Grivitei 64-66, Bucuresti

SOVIET UNION

SOJUZPECHAT — IMPORT, Moscow
and the post offices in each town
MEZHDUNARODNAYA KNIGA, Moscow G-200

SPAIN

DIAZ DE SANTOS, Lagasca 95, Madrid 6

SWEDEN

GUMPERTS UNIVERSITETSBOKHANDEL AB
Box 346, 401 25 Goteborg 1

SWITZERLAND

KARGER LIBRI AG, Petersgraben 31, 4011 Basel

USA

EBSCO SUBSCRIPTION SERVICES
P.O. Box 1943, Birmingham, Alabama 35201
F. W. FAXON COMPANY, INC.
15 Southwest Park, Westwood Mass. 02090
READ-MORE PUBLICATIONS, INC.
140 Cedar Street, New York, N.Y. 10006

YUGOSLAVIA

JUGOSLOVENSKA KNJIGA, Terazije 27, Beograd
FORUM, Vojvode Mišića 1, 21000 Novi Sad